BERICHTE
aus dem Fachbereich Geowissenschaften
der Universität Bremen

No. 186

Scheibner, C.

ARCHITECTURE OF A CARBONATE PLATFORM-TO-BASIN TRANSITION ON A STRUCTURAL HIGH (CAMPANIAN-EARLY EOCENE, EASTERN DESERT, EGYPT) CLASSICAL AND MODELLING APPROACHES COMBINED

Berichte, Fachbereich Geowissenschaften, Universität Bremen, No. 186,
173 pages, Bremen 2001

ISSN 0931-0800

Architecture of a carbonate platform-to-basin transition on a structural high (Campanian-early Eocene, Eastern Desert, Egypt) - classical and modelling approaches combined

Dissertation
for the doctorate degree
of the Department of Geosciences
at the University of Bremen

submitted by

Christian Scheibner

Bremen, 2001

Tag des Kolloquiums:

21.09.2000

Gutachter:

Prof. Dr. J. Kuss

Prof. Dr. H. Willems

Prüfer:

Prof. Dr. C. Devey

Prof. Dr. O. Brockamp

für Alice Scheibner und Jürgen Friedrich Scheibner

I think that we shall have to get accustomed to the idea that we must not look upon science as a „body of kowledge", but rather as a system of hypotheses; that is to say, as a system of guesses of anticipations which in principle cannot be justified, but with which we work as long as they stand up to tests, and of which we are never justified in saying that we know they are „true" or „more or less certain" or even „probable".

Karl A. Popper, 1934

Preface

The results of this study are documented in five separate papers, which are published or submitted. My own contributions to the individual papers are as follows:

1) Maastrichtian-Early Eocene litho- biostratigraphy and palaeogeography of the northern Gulf of Suez Region, Egypt, CHAPTER 2

Authors: Scheibner, Marzouk, Kuss

Journal: Journal of African Earth Sciences (2001) 32, 223-255

Status: published

Own contributions: field work, all data on planktic foraminifers, interpretation of calcareous nannofossil data, facies analyses, geologic interpretation, graphical presentation

2) Shelf architectures of an isolated Late Cretaceous carbonate platform margin, Galala Mountains (Eastern Desert, Egypt), CHAPTER 3

Authors: Scheibner, Marzouk, Kuss

Journal: Sedimentary Geology (2001) 145, 23-43

Status: published

Own contributions: field work, all data on planktic foraminifers, interpretation of calcareous nannofossil data, facies analyses, geologic interpretation, calculation of slope angles, graphical presentation

3) Slope sediments of a Paleocene Ramp-to-Basin transition in NE-Egypt, CHAPTER 4

Authors: Scheibner, Kuss, Marzouk

Journal: International Journal of Earth Sciences (2000) 88, 708-724

Status: published

Own contributions: field work, all data on planktic foraminifers, interpretation of calcareous nannofossil data, facies analyses, geologic interpretation, graphical presentation

4) Carbonate platform to basin transition along an Upper Cretaceous to Lower Tertiary Syrian Arc Uplift, Galala Plateaus, Eastern Desert, Egypt, CHAPTER 5

Authors: Kuss, Scheibner, Gietl

Journal: GeoArabia (2000) 5, 405-424

Status: published

Own contributions: field work, data on planktic foraminifers, part of geologic interpretation, graphical presentation

5) Stratigraphic modelling of carbonate platform-to-basin sediments (Maastrichtian to Paleocene) in the Eastern Desert, Egypt, CHAPTER 6

Authors: Scheibner, Kuss, Speijer

Journal: Paleogeography, Palaeoclimatology, Palaeoecology

Status: submitted

Own contributions: field work, all data on planktic foraminifers, interpretation of calcareous nannofossil data, geologic interpretation, computer modelling, graphical presentation

Contents

Summary

Thirty Campanian to Early Eocene sections from the carbonate platform of the Galala Mountains, Eastern Desert (Egypt) and the adjacent transitional and basinal settings farther south have been conducted during two campaigns in 1997 and 1998. Approximately 2000 m of section have been measured with a total number of 928 samples (595 soft samples for obtaining washed residues and 333 limestones for thin-section preparation). Microfossil (planktonic foraminifers and calcareous nannoplankton) and microfacies data together with detailed field observations form the basis of this thesis. The main chapters (chapters 2-6) have been or will be published separately.

In the Campanian to Early Eocene of the Eastern Desert three different environmental regimes have been investigated that are reflected by lithostratigaphic and facies units. The results of the facies investigation in combination with numerous isolated local and regional studies from the literature and the different types of hiatuses observed in the area led to a detailed palaeogeography of the Maastrichtian to Early Eocene, documented in 11 palaeo-geographic maps. Special emphasis is put on the interfingering of shallow-water limestones over swells and tectonically induced uplifts and basinal chalks, marls and shales (CHAPTER 2).

In combination with palaeoenvironmental information of basinal sections farther to the south we calculated slope geometries of two principal carbonate platform models for the Campanian to Maastrichtian shallow-water to slope deposits of the carbonate platform in the Southern Galala. Because of the initial structural topography and sedimentary patterns the model of an asymmetrical platform is favoured. This asymmetrical platform margin is formed like a rimmed platform in southeasterly direction and like a ramp in southwesterly direction with slope angles of 5° to 8° for the rimmed part, whereas the ramp part would have an angle of less than 0.1° (CHAPTER 3).

During the late Paleocene, three phases of carbonate ramp progradation and intercalated hemipelagic units were differentiated at St. Paul at the southern rim of the Southern Galala. The three prograding phases are indicated by increased mass-transport deposition of glides, slumps and debris flows. Each subsequent advance of ramp progradation was more pronounced. Microfacies investigations highlight the changing depositional origins from a basinal outer-ramp setting to a middle- to inner ramp setting (CHAPTER 4).

The analyses of the sedimentary facies, sedimentary cycles and changes in sea level of Campanian to Lower Eocene deposits enabled the reconstruction of the evolution of the platform-slope-basin transition. The individual sedimentary cycles of the southward-prograding carbonate platform reveal the changing large-scale depositional geometry. The facies architecture reflects the evolution from a rimmed shelf (Late Cretaceous) to a distally steepened ramp (latest Cretaceous to Paleocene) and eventually to a homoclinal ramp (Early Eocene) (CHAPTER 5).

In two computer simulations with the stratigraphic modelling program PHIL the Maastrichtian and Paleocene of the Galala Mountains have been modelled using geologic parameters obtained in the previous chapters. It is possible to evaluate the depostional processes and their controlling

parameters on and from the platform. The results of the two computer simulations of the Maastrichtian and the Paleocene provide information about areas of the platform that are poorly exposed or eroded in earlier times. The most important parameters that control stratigraphic geometry of carbonate platforms are changes in relative sea-level, sediment flux and initial topography (CHAPTER 6).

Zusammenfassung

Während zweier Geländeaufenthalte in den Galala Bergen, welche Teil der Östlichen Wüste Ägyptens sind, wurden in den Jahren 1997 und 1998 insgesamt 30 Profile mit einer Gesamtmächtigkeit von ca. 2000 m aufgenommen. Die Profile stammen von einer Karbonatplattform und den südlich daran anschließenden Hang- und Beckenbereichen. Insgesamt wurden 928 Proben genommen (595 Lockerproben und 333 Festproben). Die Auswertung von Mikrofossil- (Planktische Foraminiferen und Kalkiges Nannoplankton) und Mikrofaziesdaten bilden zusammen mit detaillierten Geländebeobachtungen das Grundgerüst dieser kumulativen Dissertation. Die 5 Hauptkapitel (Kapitel 2-6) wurden bzw. werden separat veröffentlicht.

Während des Campan bis frühen Eozän wurden in der Östlichen Wüste drei unterschiedliche Faziesbereiche untersucht. Die Ergebnisse dieser Faziesanalysen, zusammen mit einer Vielzahl von lokalen und regionalen Untersuchungen und den dokumentierten Hiatustypen, wurden in 11 paleogeographischen Karten dargestellt. Besondere Beachtung fand dabei der Übergang von Flachwasserkarbonaten, die auf Schwellen und tektonisch bedingten Hochstrukturen abgelagert wurden, zu den Kreiden, Mergeln und Tonen des Beckens (CHAPTER 2).

In Kombination mit Informationen zu Paläoumweltbedingungen aus Beckenprofilen weiter südlich wurden Hangwinkel für zwei Campan-Maastricht Karbonatplattformrandmodelle errechnet. Aufgrund der Ausgangstopographie und den sedimentären Ablagerungsmustern wird das Modell eines asymmetrischen Plattformrandes bevorzugt. Dieser asymmetrische Plattformrand ist in südöstlicher Richtung als „rimmed" Plattform ausgebildet, mit Hangwinkeln von 5° - 8°, während die Rampe in südwestlicher Richtung Hangneigungen von weniger als 0,1° aufweist (CHAPTER 3).

Während des späten Paleozäns konnten beim Kloster St. Paul drei Phasen einer Rampenpro-gradation mit drei zwischengeschalteten hemipelagischen Einheiten dokumentiert werden. Diese drei progradierenden Phasen sind durch verstärkte Massentransportablagerungen wie Gleitungen, Rutschungen und Debris Flows gekennzeichnet. Dabei war jeder nachfolgende Rampenvorstoß stärker ausgebildet als der vorherige. Mikrofaziesuntersuchungen zeigen weiterhin, daß die Herkunft dieser Massentransportablagerungen sich mit der Zeit vom Becken/äußere Rampe zur mittleren/inneren Rampe verlagerte. (CHAPTER 4).

Die Untersuchungen der sedimentären Gesteine und Zyklen und der Meeresspiegelveränderungen ermöglichte für den Zeitraum von Campan bis unteres Eozän die Rekonstruktion der zeitlichen Entwicklung des Plattform-Hang-Becken Überganges. Die einzelnen sedimentären Zyklen dieser südwärts progradierenden Karbonatplattform dokumentieren dabei die sich ändernden Ablagerungsgeometrien. Der Karbonatplattform veränderte sich dabei von einer „rimmed" Plattform in der Oberkreide über eine distal versteilte Rampe in der obersten Kreide und dem Paleozän zu einer homoklinalen Rampe im frühen Eozän (CHAPTER 5).

In zwei Computersimulationen mit dem stratigraphischen Modellierungsprogramm PHIL wurden das Maastricht und das Paleozän mit Hilfe der geologischen Parameter modelliert, die in den vorherigen Kapiteln ermittelt wurden. Dadurch ist es möglich, die Ablagerungsprozesse und ihre steuernden Faktoren auf und von der Plattform zu bewerten. Die Ergebnisse der zwei

Computersimulationen des Maastrichts und des Paleozäns liefern Informationen über die Gebiete der Plattform, die nur schlecht oder gar nicht mehr aufgeschlossen sind. Die wichtigsten Parameter, die die Ablagerungsgeometrien von Karbonatplattformen steuern, sind Veränderungen des relativen Meeresspiegels, der Sedimenteintrag und die Ausgangstopographie (CHAPTER 6).

Acknowledgements

In the first place I have to thank Prof. J. Kuss for setting up the project and its financial support. Furthermore, his input and the fruitful and stimulating discussions greatly improved the quality of the thesis.

Special thanks to Dr. Robert P. Speijer who introduced me to the planktic foraminifers and helped me by various kinds of questions that arise during this study like questions about previous literature, questions about nomenclature, questions about the English language etc. He also critically reviewed all the previous versions of the individual chapters and gave very valuable comments on every topic of the work.

I would like to thank Dr. Akmal M. Marzouk (Tanta University, Egypt) for his detailed calcareous nannoplankton investigation. The results of his investigations improved the results of this study very much.

Prof. A. M. Bassiouni (Ain Shams University, Egypt) is especially thanked for the logistical support and making work in Egypt possible for us (organisation of permits), Dr. A. Mohsen Morsi (Ain Shams Univ.) is equally thanked for logistical support, for providing his room for the washing of samples, and an open ear for all problems encountered during our stay in Egypt. All other colleagues of the Geology Department of Ain Shams University and the monks of the monastery of St. Anthony and St. Paul are thanked for their hospitality.

Anja Scharf, Ralf Bätzel and Markus Brinkmann (all University of Bremen) helped with the sample preparation. The English language in these chapters was significantly improved by Erna Friedel. Erna Friedel also helped with various problems within the department.

The individual chapters benefited much from the thoroughly revision by reviews of Dr J. Grötsch, Prof. T. Bechstedt, Prof. G. Einsele, Dr. S. Lüning, Dr. A. Flexer and 4 anonymous reviewers.

For various kinds of help and encouragement I am indebted to all colleagues (former and present) of our working group: Dr. Peter Luger, Dr. Sebastian Lüning, Dr. Ralf Gietl, Dr. Kristin Schnack, Dr. Martina Bachmann, Dr. Robert. P. Speijer, Dipl. Geol. Frauke Schulze and Dipl. Geol. Jan Bauer.

Several colleages of other working groups of the geosciences department contributed to this thesis with their technical help in questions concerning computer problems. Especially Dr. Tom Wagner is thanked for his technical advice, the reading of parts of the manuscript and some unforgettable fights in the squash-court.

The investigations were funded by the Graduiertenkolleg "Stoff-Flüsse in marinen Geosystemen" of the University of Bremen and the German Science Foundation (DFG). Further financial support came from the University of Bremen (FNK)

Katja Heeschen is thanked for her morally support during the years, especially in the last weeks. Thanks for all the telephone calls and emails.

Last but not least I would like to thank my parents for their morally and financially support.

CHAPTER 1

Introduction

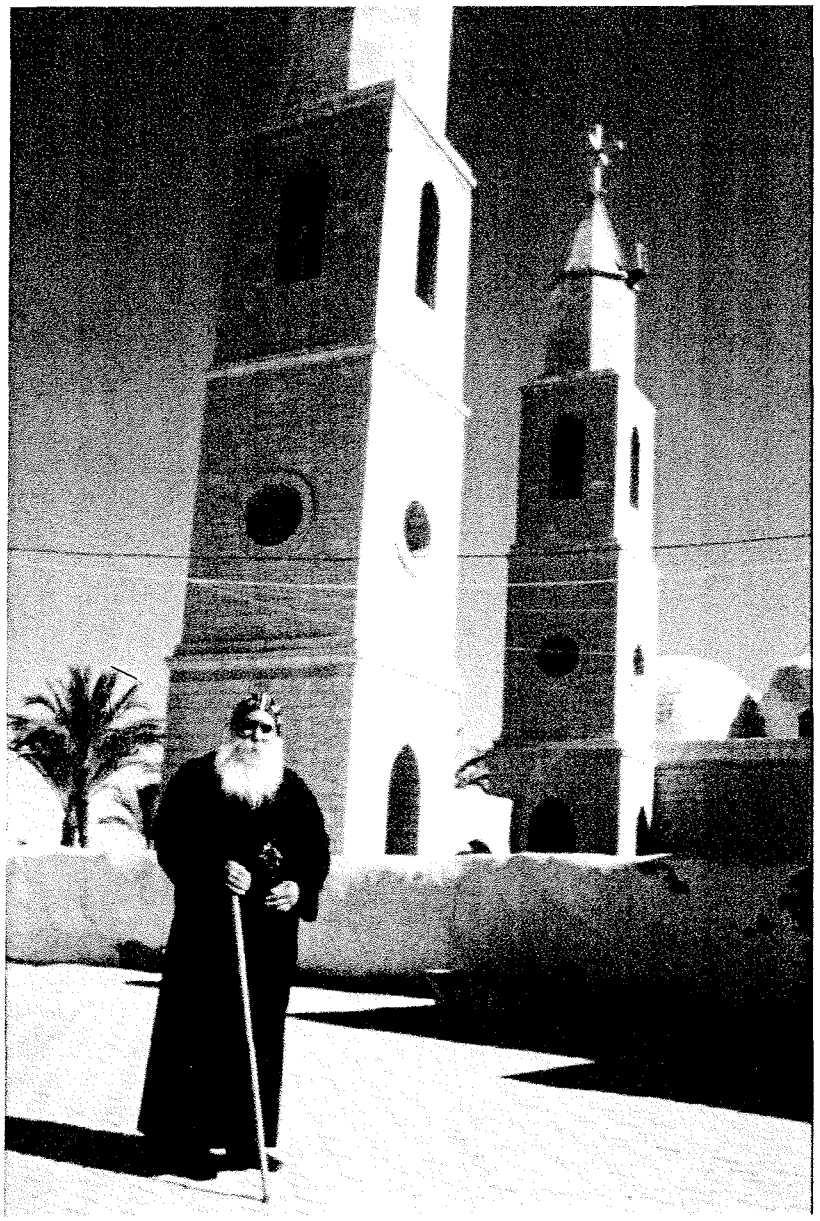

One of the monchs of St. Anthony (in front of the main church)

Photo by Christian Scheibner (1998)

Introduction

Platform-to-basin transitions are key areas for understanding processes that involve both the platform and the adjacent basin. Only here the progradation or retrogradation of the platform can be dated precisely with calcareous nannofossils or planktic foraminifers that live in deep waters and shallow benthic organisms from the platform. This temporal accuracy is necessary to discuss and correlate climatic and environmental processes on the platform with those in the adjacent basin. Furthermore, platform-to-basin settings provide essential information on the type of platform. Until now, the reasons for changes between different platform morphologies are only poorly understood. Possible reasons for morphologic transitions are the lack of framebuilding organisms, large extinctions of the dominating organisms, oceanic (upwelling and eutrophication), climatic, and tectonic factors (Burchette and Wright, 1992). With respect to these fundamental geological aspects the Upper Cretaceous to Lower Paleogene successions of the Galala Mountains in the Eastern Desert of Egyt are of special interest. These sections cover the time span of one of the most severe extinctions in earth history (Sepkoski, 1982) and are involved in tectonic processes that led to the building of Syrian Arc Fold belt.

Until now, Upper Cretaceous to Lower Paleogene carbonate platform-slope-basin transitions in the Tethys have only been studied in Italy (Maiella: Eberli et al., 1994) and Hungary (Bakony: Haas, 1999). The Galala Mountains in the Eastern Desert in Egypt represent another important region in the southern Tethys that has been investigated over the last years by Prof. Kuss and his working group (Kuss, 1986; Bandel and Kuss, 1987; Kuss and Leppig, 1989; Kulbrok 1996; Gietl, 1998). These and numereous Egyptian studies provide the basis for the investigations presented in this PhD thesis. The field work of this project was conducted during two campaigns in 1997 and 1998. Various Campanian to early Eocene sections were studied in detail, representing the carbonate platform of the Galala Mountains and adjacent transitional and basinal settings farther south. Approximately 2000 m of section documenting a total time intervall from 75 to 52 Ma. have been measured with a total number of 928 samples (595 soft samples for obtaining washed residues and 333 limestones for thin-section preparation). Microfossil (planktonic foraminifers and calcareous nannoplankton) and microfacies data together with detailed field observations form the basis of this research.

One of the first comprehensive publications dealing with the Galala Mountains was presented by Zittel (1883) in his work on the Libyan Desert. He described the St. Anthony section (measured by Georg Schweinfurth) nearby the monastery of St. Anthony. Schweinfurth was the most prominent scientist of this episode (Said, 1990) and one of the first Europeans to visit the monasteries of St. Anthony and St. Paul in the late 1870´s. During his stay he drew several sketches of the monasteries that are published in Schweinfurth (1922) and are printed on the covers of the individual chapters of this thesis. The next 3 paragraphs shortly introduces the general topics of carbonate platforms, tectonics and stratigraphic modelling.

Carbonate platforms: Carbonate platforms can be distinguished in rimmed platforms and ramps. Ramps can be further subdivided into distally steepened ramps and homoclinal ramps (Read, 1985). Rimmed carbonate platforms are marked by a pronounced increase in slope. Read (1985) subdivided rimmed carbonate platforms into a) depositional or accretionary margins with aggradation and progradation, generally lacking high marginal escarpments, b) bypass margins, occurring in areas of rapid aggradation, that may be associated with a marginal escarpment and c) erosional margins characterised by high steep escarpments. Many examples of rimmed platforms, ramps or transitions of one type into the other were described from the fossil record (Read, 1985; Burchette & Wright, 1992). It is assumed that ramps „automatically" evolve into rimmed platforms, but numerous examples show that they may maintain their low-gradient profile and thus represent true keep-up depositional systems of their own (Wright & Burchette, 1998).

Tectonic overview: The carbonate platform of the Galala Mountains evolved on a tectonically induced topographic high. This high is part of the Syrian Arc Fold Belt that is composed of the Palmyride and Sinai-Negev Fold belts in Syria and Israel and can be traced to the subsurface of the Western Desert (Ayyad and Darwish, 1996). The domal anticlines of the Syrian Arc Fold belt are related to processes associated with the successive stages in the opening of the Atlantic ocean (Kerdany and Cherif, 1990) and with the opening (Keely, 1994) and closure of the Neo-Tethys (Stampfli et al., 1995). The tectonic evolution of north Sinai indicates that the late Triassic-Liassic separation of the Turkish microplate (opening of the Neo-Tethys) formed east-northeast orientated normal faults. Due to the northward drifting of the Turkish microplate the older Paleo-Tethys was closed in mid-Jurassic time (Sengör and Yilmaz, 1981). From this time on, the movement of Africa towards Eurasia (closing of the Neo-Tethys) generated compressive stresses. The Late Cretaceous (Turonian) opening stage of the Atlantic ocean caused Eurasia to move eastward with respect to Africa, generating a dextral shear (Kerdany and Cherif, 1990). These processes led to a reactivation of the older east-northeast orientated faults and subsequently to formation of the structures of the Syrian Arc belt (Moustafa and Khalil, 1990).

Stratigraphic Modelling: In the first four of the following five chapters, classical geological approaches (e.g. biostratigraphy, facies analysis) are employed to discuss geology of the area. In the fifth chapter these results supplemented by literature data serve as input parameters to run a forward stratigraphic modelling program. In forward stratigraphic models, stratigraphic successions are simulated through time using an initial set of parameters. Calibration with the real world is done by running the simulations repeatedly, comparing the model output with geological data, and modifying the initial parameters to minimize the differences between the model and the reality (Bornholdt et al, 1999).

Aims: The prime goals of this PhD thesis are:

- to improve our understanding of the factors controlling the growth of carbonate platforms (e.g. sea-level changes, sedimentation rates).
- to provide insights into the processes that led to changing platform morphologies (rimmed platform versus ramp).
- to reconstruct the depositional history of the platform-basin transition at the Galala Mountains.
- to obtain information on areas of the carbonate platform that are not or only poorly exposed (through allochthonous sediments and stratigraphic modelling).
- to evaluate the effectiveness of computer simulation programs (here PHIL) in modelling sedimentary sequences.
- to clarify the confusing stratigraphic nomenclature used in the region.

Overview of research: The above mentioned topics are treated in the following five chapters, that have been or will be published as separate papers.

CHAPTER 2: Maastrichtian-Early Eocene litho- and biostratigraphy and palaeogeography of the northern Gulf of Suez Region, Egypt, focuses on the Maastrichtian to Early Eocene environmental regimes in the northern Eastern Desert and in western Sinai. The different environmental regimes are reflected in different lithologies and hence different formations. On the basis of new measured sections and isolated local and regional studies from the literature the individual formations and their synonyms are reviewed. Overall, these lithostratigraphic units reflect three different environmental regimes. The first regime is characterised by uplift and erosion or non-deposition resulting mostly from the uplift of the Northern Galala/Wadi Araba (NGWA) structure. The shallow-water carbonate platform and slope deposits represent the second regime and are found north and south of the NGWA high. The third regime is represented by basinal chalks, marls and shales. Special emphasis is put on the interfingering of shallow-water limestones over swells and tectonically induced uplifts with basinal chalks, marls and shales. This transitional areas are key areas for a) the understanding of the gross architecture of the carbonate platforms and b) are essential for correlating shallow-water (biozonations based mainly on larger foraminifers) with deep-water successions (biozonations based on calcareous nannoplankton and planktic foraminifers). The results of the facies investigation in combination with the different types of hiatuses observed in the area led to a detailed palaeogeography of the Maastrichtian to Early Eocene, documented in 11 maps.

Whereas chapter 2 can be seen as a review of the overall geology of the northern Gulf of Suez region the succeeding two chapters discuss individual aspects of the Campanian to Early Eocene carbonate platform on a very local scope.

CHAPTER 3: Shelf architectures of an isolated Late Cretaceous carbonate platform margin, Galala Mountains (Eastern Desert, Egypt) concentrates on the Campanian to Maastrichtian shallow-water

to slope deposits of the carbonate platform in the Southern Galala. The sedimentary patterns observed in the sections are discussed and have been attributed to individual sedimentary sequences. The identified changes in sea level are at least partly of eustatic origin but a tectonic component can not be ruled out. In combination with palaeoenvironmental informations on the basinal sections farther south we calculated slope geometries of two principal carbonate platform models. Because of the initial structural topography and sedimentary patterns, an asymmetrical platform is postulated. Until now, many examples of rimmed platforms, ramps or transitions of one type into the other were described from the fossil record. A combination of different types of platforms as reconstructed in the Galala Mountains, has not been described before. This asymmetrical platform margin is formed like a rimmed platform towards southeast and like a ramp in southwest direction. The rimmed platform is subdivided into a gentle upper slope and a steep lower slope. The paleowater-depth as approximated from facies and benthic foraminifers data, between the slope sections and the basinal sections change from 100 m (slope) to 300-500 m in the basinal sections. These differences in water-depth lead to angles of the steep slope of the rimmed part of 5° to 8°, whereas the ramp part would have an angle of less than 0.1°.

CHAPTER 4: Slope sediments of a Paleocene Ramp-to-Basin transition in NE-Egypt focuses again on the important transitional zone between shallow-water and basinal environments. This chapter evaluates the sedimentary structures in an excellent, late Paleocene outcrop near the monastery of St. Paul, 360 m wide and 50 m high. Three phases of carbonate ramp progradation and three intercalated hemipelagic units were differentiated at this locality. The three prograding phases are indicated by increased mass-transport deposition of glides, slumps and debris flows. Each subsequent advance of ramp progradation was more pronounced. Microfacies investigations highlight the changing depositional origins from a basinal outer-ramp setting with coraline red algae prevailing in the Selandian to Thanetian to a middle- to inner ramp setting with nummulitids dominating in the late Thanetian. Changes of sea level are a likely trigger for the onset of mass-transport deposition. Comparisons with regional cycle boundary interpretations led to the attribution of at least two mass-transport deposits to lowstands in sea level.

CHAPTER 5: Carbonate platform to basin transition along an Upper Cretaceous to Lower Tertiary Syrian Arc Uplift, Galala Plateaus, Eastern Desert, Egypt again concentrates on the regional geology of the Upper Campanian to Lower Eocene strata. The analyses of the sedimentary facies, sedimentary cycles and changes in sea level enabled the reconstruction of the evolution of the platform-slope-basin transition. The individual sedimentary cycles of the southward-prograding carbonate platform reveal the changing large-scale depositional geometry. The facies architecture reflects the evolution from a rimmed shelf (Late Cretaceous) to a distally steepened ramp (latest Cretaceous to Paleocene) and eventually to a homoclinal ramp (Early Eocene).

While chapter 2 to chapter 5 discuss the various aspects of the Upper Cretaceous to Lower Eocene carbonate platform with regard to „basic" geologic parameters like biostratigraphy, lithostratigraphy, sedimentary patterns and changes in sea level

CHAPTER 6: Stratigraphic modelling of Maastrichtian to Paleocene carbonate platform to basin sediments, Eastern Desert, Egypt, combines the results of the previous chapters with the stratigraphic simulation program PHIL (Process and History Integrated Layers). The aims of using computer modelling are manifold. It is possible to evaluate the depostional processes and their controlling parameters on and from the platform. The results of two computer models of the Maastrichtian and the Paleocene provide information about areas of the platform that are poorly exposed or eroded in earlier times. The most important parameters in our models that control stratigraphic geometry of carbonate or mixed carbonate siliciclastic platforms are changes in relative sea-level, sediment flux and initial topography. The simulated geologic parameters lithology, overall thickness and paleowater-depth resemble very well field and laboratory measurements of the individual sections. The timing of the earlier proposed transition from a Maastrichtian rimmed platform to a Paleocene distally steepened ramp can be improved. The rimmed platform persists at least until the late Paleocene what is documented by the calculated relatively high slope angles of 6°. The slope angles of the Maastrichtian that are calculated earlier with angles of 5°-8° are confirmed by the results of this study which proposes an angle of 8°.

Finally **CHAPTER 7: conclusions and perspectives** summarizes the previous six chapters and announces topics for future studies.

References

Ayyad, M.H. and Darwish, M., 1996. Syrian Arc structures: a unifying model of inverted basins and hydrocarbon occurences in North Egypt. Egyptian General Petroleum Company Seminar. Cairo, pp. 1-19.

Bandel, K. and Kuss, J., 1987. Depositional environment of the pre-rift sediments - Galala Heights (Gulf of Suez, Egypt). Berliner geowiss. Abh. A 78, 1-48.

Bornholdt, S., Nordlund, U. and Westphal, H., 1999. Inverse stratigraphic modeling using genetic algorithms. In: Harbaugh, J.W., Watney, W.L., Rankey, E.C., Slingerland, R., Goldstein, R.H. and Franseen, E.K. (Eds.), Numerical experiments in stratigraphy: Recent advances in stratigraphic and sedimentologic computer simulation. SEPM, Spec. Publ. 62, Tulsa, pp. 85-90.

Burchette, T.P. and Wright, V.P., 1992. Carbonate ramp depositional systems. Sedimentary Geology 79, 3-57.

Eberli, G.P., Bernoulli, D., Sanders, D. and Vecsei, A., 1993. From aggradation to progradation: the Maiella Platform, Abruzzi, Italy. In: Simo, J.A.T., Scott, R.W. and Masse, J.P. (Eds.), Cretaceous carbonate platforms. The American Association of Petroleum Geologists, Tulsa, pp. 213-232.

Gietl, R., 1998. Biostratigraphie und Sedimentationsmuster einer nordostägyptischen Karbonatrampe unter Berücksichtigung der Alveolinen-Faunen. Berichte aus dem Fachbereich Geowissenschaften der Universität Bremen 112, 135.

Haas, J., 1999. Genesis of Late Cretaceous toe-of-slope breccias in the Bakony Mts. Hungary. Sedimentary Geology 128, 51-66.

Keeley, M.L., 1994. Phanerozoic evolution of the basins of Northern Egypt and adjacent areas. Geologische Rundschau 83, 728-742.

Kerdany, M.T. and Sherif, O.H., 1990. Mesozoic. In: Said, R. (Ed.), The geology of Egypt. Balkema, Rotterdam, pp. 407-438.

Kulbrok, F., 1996. Biostratigraphie, Fazies und Sequenzstratigraphie einer Karbonatrampe in den Schichten der Oberkreide und des Alttertiärs NordostÄgyptens (Eastern Desert, N´Golf von Suez, Sinai). Berichte aus dem Fachbereich Geowissenschaften der Universität Bremen 81, 216.

Kuss, J., 1989. Facies and paleogeographic importance of the pre-rift limestones from NE-Egypt/Sinai. Geologische Rundschau 78, 487-498.

Kuss, J., 1986. Facies develpment of Upper Cretaceous-Lower Tertiary sediments from the monastery of St. Anthony/Eastern Desert, Egypt. Facies 15, 177-194.

Moustafa, A.R. and Khalil, M.H., 1990. Structural characteristics and tectonic of north Sinai fold belts. In: Said, R. (Eds.), The geology of Egypt. Balkema, Rotterdam, pp. 382-389.

Read, J.F., 1985. Carbonate platform facies models. AAPG Bulletin 69, 1-21.

Said, R., 1990. History of geological research. In: Said, R. (Ed.), The geology of Egypt. Balkema, Rotterdam, pp. 3-7.

Schweinfurth, G., 1922. Auf unbetretenen Wegen in Aegypten: Aus eigenen verschollenen Abhandlungen und Aufzeichnungen. Hoffmann und Campe, Hamburg.

Sengör, A.M.C. and Yilmaz, Y., 1981. Tethyan evolution of Turkey: A plate tectonic approach. Tectonophysics 75, 181-241.

Sepkoski, J.J.J., 1982. Mass extinctions int the Phanerozoic oceans: a review. In: Silver, L.T. and Schultz, P.H. (Eds.), Geological implications of impacts of large asteroids and comets on the Earth. GSA Spec. Paper 190, Boulder, pp. 283-289.

Stampfli, G., Favre, P., Pillevuit, A. and Vannay, J.C., 1995. The Neotethys-East Mediterranean basin connection. Program 2nd International Symposium: The Geology of the Eastern Mediterranean Region, Jerusalem, 1995, Abstract Volume, p. 17.

Wright, V.P. and Burchette, T.P., 1998. Carbonate Ramps: an introduction. In: Wright, V.P. and Burchette, T.P. (Eds.), Carbonate Ramps. Geological Society, London, London, pp. 1-5.

Zittel, K.A., 1883. Beiträge zur Geologie und Palaeontologie der Lybischen Wüste und der angrenzenden Gebiete von Ägypten. Paleontographica 30,

CHAPTER 2

Maastrichtian-Early Eocene Litho- Biostratigraphy and Palaeogeography of the northern Gulf of Suez Region, Egypt

C. Scheibner, A.M. Marzouk and J. Kuss

published 2001
in Journal of African Earth Sciences
Vol. 32, p. 223-255

Small bell tower of the monastery of St. Anthony
(at the main entrance)

Photo by Christian Scheibner (1998)

Maastrichtian-Early Eocene Litho- Biostratigraphy and Palaeogeography of the Northern Gulf of Suez Region, Egypt

C. Scheibner[a], A. M. Marzouk[b] and J. Kuss[a]

[a] Universität Bremen, FB5, P.O. Box 330440, 28334 Bremen, scheibne@uni-bremen.de, kuss@uni-bremen.de

[b] Geology Department, Faculty of Science, Tanta University, Tanta 31527, Egypt

Keywords

Galala Mountains, western-central Sinai, Maastrichtian, Paleocene, Early Eocene, palaeogeography, biostratigraphy, lithostratigraphy

ABSTRACT

The Maastrichtian-Lower Eocene sediments on both sides of the northern Gulf of Suez can be subdivided into 8 formal formations (including one group) and one informal formation that are described in detail. These lithostratigraphic units reflect three different environmental regimes of deposition or non-deposition. The first regime is characterised by uplift and erosion or non-deposition resulting mostly from the uplift of the Northern Galala/Wadi Araba (NGWA) structure, a branch of the Syrian Arc foldbelt. The shallow-water carbonate platform and slope deposits of the Late Campanian-Maastrichtian St. Anthony Formation and the Paleocene-Lower Eocene Southern Galala Formation and Garra Formation represent the second regime and are found north and south of the NGWA high. The third regime is represented by basinal chalks, marls and shales of the Maastrichtian Sudr Formation and of the Paleocene-Eocene Dakhla, Tarawan, Esna Formations, the Dakhla/Tarawan/Esna informal Formation and the Thebes Group. The distribution and lateral interfingering of the above mentioned environmental regimes reflect different vertical movements, changing basin morphology, sea-level changes and progradation of shallow-water sediments and is illustrated on 11 palaeogeographic maps.

INTRODUCTION

During the last decades many authors investigated the stratigraphic subdivision of the Upper Cretaceous-Palaeogene strata in the Galala Mountains and western-central Sinai (Fig. 1). Most of these studies were focused on the bio- and lithostratigraphic interpretation of isolated sections. Only few authors, like Masters (1984) and Said (1990), concentrated on regional comparisons.

In this work we combine our stratigraphic results from the Galala Mountains and neighbouring areas with literature data from numerous isolated sections (especially in western-central Sinai). We concentrate on questions of lateral facies transitions and their stratigraphic synchroneity or diachroneity. Special emphasis is put on the interfingering of shallow-water limestones over swells and tectonically induced uplifts and basinal marls and shales. The results of the facies investigation in combination with the different types of hiatuses observed in the area led to a detailed palaeogeography of the Maastrichtian to Early Eocene, that is documented in 11 maps.

GEOLOGICAL SETTING:

The investigated area represents a segment of the northern passive margin of the Afro-Arabian Plate. This passive margin formed during the late Triassic/Jurassic opening of the Neotethys. The extensional tectonic processes resulted in the formation of E-W striking, northward deepening half-grabens that were mostly covered by the Late Triassic-Early Cretaceous seas depending, among others, on sea-level fluctuations. Beginning with the initial stages of the collision between the African and European plates during Turonian times, a dextral transpressive reactivating of the half-grabens took place along the North African-Arabian plate boundary (e.g. Moustafa and Khalil, 1995). As a consequence, a system of inverted, uplifted and folded grabens was formed along the Syrian Arc System (Fig. 1). This area is known in Egypt also as "unstable shelf" (Krenkel, 1925; Said, 1960). They contrast with the tectonically unaffected area further south ("stable shelf"). While the latter is characterised by lithologically uniform marine strata, formed on a gently north-dipping shelf, small-scaled facies variations are obvious within the basin-swell-morphologies of the unstable shelf area (Kuss et al., in press). The Galala mountains in the Eastern Desert together with areas on W-Sinai represent a southern branch of the Syrian Arc, called Northern Galala/Wadi Araba high (NGWA) (Kuss et al. in press) (Fig. 2). The Upper Cretaceous-Palaeogene carbonate dominated successions of a south and north-dipping carbonate ramp prograde from the Northern Galala/Wadi Araba high. Facies-transitions between the Paleocene shallow-water ramp carbonates and deeper-water intrashelf marls of the Southern Galala Sub-basin (Fig. 2) farther south have been studied in sections along the dip direction. Mass transport deposits like slides, slumps, and debris-flows occur (Scheibner et al. 2000).

METHODS:

The study area is exposed around the northern parts of the Gulf of Suez. Eight Upper Cretaceous-Palaeogene sections of the Northern and Southern Galala on the western side of the Gulf of Suez were investigated in detail (Fig. 3), including the northern and southern forelands of the Galalas. Additionally, data of western-central Sinai, opposite of the working area, was reviewed.
Facies interpretations are based on fine-scale logging of stratigraphic sections in and along the NGWA high. Studies of 169 thin-sections of the Maastrichtian-Early Eocene interval are

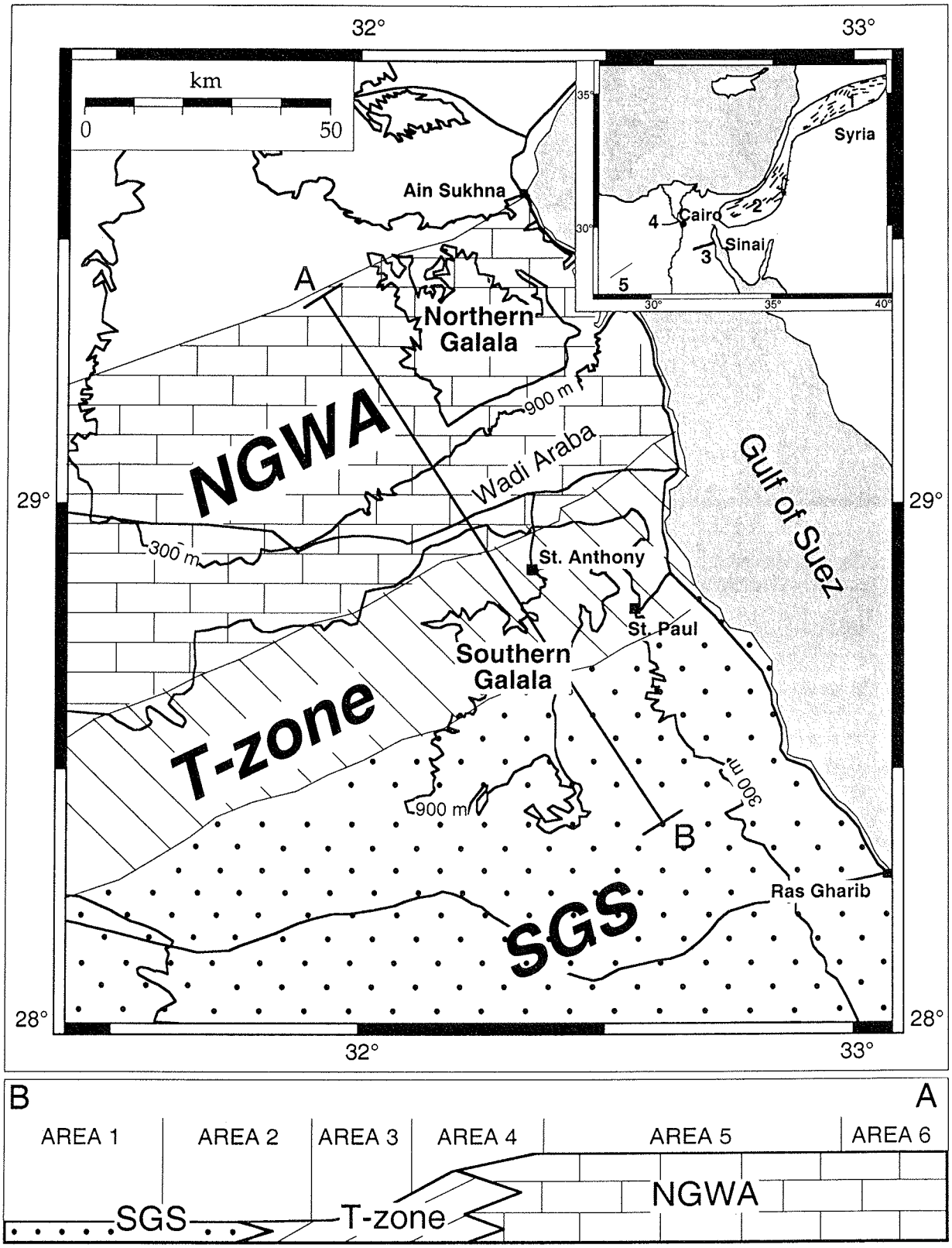

Fig. 1: *The two Galala Plateaus at the western Gulf of Suez forming part of a Syrian Arc fold in the Eastern Desert - see inlay: 1 = Palmyrid Fold Belt; 2 = Negev-Sinai Fold; 3 = Northern Galala/Wadi Araba High; 4 = Abu Roash; 5 = Bahariya Uplift/Western Desert. During Late Cretaceous – Palaeogene times, the platform (NGWA) to basin (SGS) transitions (T-zone) were formed roughly parallel with the strike of the Galalas. In transect A – B (below) the boundaries of areas 1-6 are indicated.*

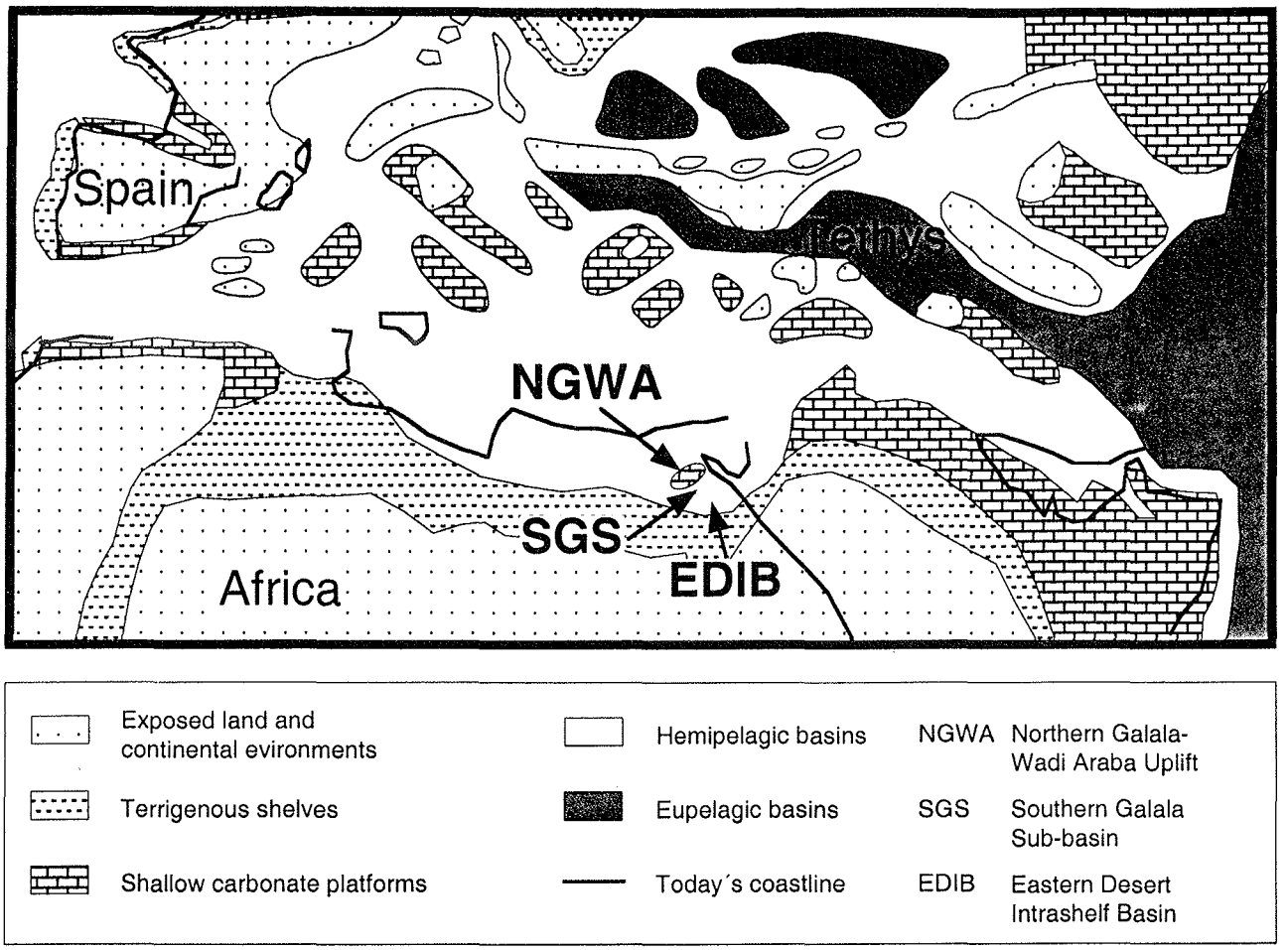

Fig. 2: *Latest Maastrichtian palaeogeographic map of the circum-tethyan realm (modified after Camoin et al. 1993). The area of investigation is around the Northern Galala/Wadi Araba high (NGWA) and reaches to the Southern Galala Sub-basin (SGS) in the south. The SGS is part of the Eastern Desert Intrashelf Basin (EDIB).*

supplemented by 479 marl samples that formed the base for a high-resolution biostratigraphic frame based on planktic and benthic foraminifers and calcareous nannoplankton.

BIOSTRATIGRAPHY

For the Maastrichtian, we followed the biostratigraphic scheme given by Perch-Nielsen (1985) and Norris et al. (1998) (Fig. 4). The biostratigraphic schemes of Berggren et al. (1995) for planktic foraminifers (P-zones), of Martini (1971) for calcareous nannoplankton (NP-zones) and of Serra-Kiel et al. (1998) for shallow benthic foraminifers (SB-zones) are used for the Paleocene and Early Eocene. The calibration of planktic foraminifers and calcareous nannoplankton is from Norris et al. (1998) for the Cretaceous and from Berggren et al. (1995) for the Palaeogene (Fig. 4). In section T2 (Fig. 4a) NP10 could be divided in 4 subzones, named NP10a, NP10b, NP10c and NP10d, following Aubry (1995). In sections T1, D2 and D3 (Fig. 4a) NP10 can only be subdivided into two subzones (NP10a-c and NP10d) because *T. digitalis* could not be found. Faris and Strougo (1998) and Aubry et al. (1999) also used this subdivision in their description of the Esna shales of Egypt. In addition to

Berggren et al. (1995), we follow Speijer et al. (2000) in subdividing the planktic foraminiferal biozone P5 into P5a, P5b and P5c. The very short subzone P5b is characterised by the total range of *M. allisonensis* marking the Late Paleocene thermal maximum.

All sections presented in Fig. 4 were recalibrated to the above mentioned schemes. If planktic foraminifers as well as calcareous nannofossils were used for biostratigraphy we gave the calcareous nannoplankton priority. Which biostratigraphic scheme is used (planktic foraminifers or calcareous nannoplankton) is indicated in the figures.

Luger et al. (1998) presented a new planktic foraminiferal biozonation for the Maastrichtian for those areas, in which the Late Maastrichtian index fossil *A. mayaroensis* is very rare or absent. Marzouk and Lüning (1998) described a strong variability of planktic foraminifers and calcareous nannoplankton correlations on Sinai, especially in the lower Paleocene, whereas in the upper Paleocene the different zonal correlations are in good agreement. Boukhary and Abdelmalik (1983) and El-Dawoody (1992) reviewed the biostratigraphy of the Late Paleocene-Eocene succession in Egypt.

LITHOSTRATIGRAPHY OF MAASTRICHTIAN-EARLY EOCENE STRATA

Ever since the first description of the Maastrichtian to Eocene sediments in the Western Desert by Zittel (1883) (Fig. 5), the lithostratigraphic subdivision of the Upper Cretaceous-Eocene successions in Egypt has been the subject of many discussions, especially during the 1950´-1960´s (Nakkady, 1950; Nakkady, 1957; El-Naggar, 1966a, b; El-Naggar 1968; Sabry 1968). Even today, lithostratigraphic terminology is used non-uniform (Issawi et al., 1999), especially the Esna Formation (Hermina and Lindenberg, 1989). For terminology we used Hermina et al. (1989) as a basis, especially with respect to usage of lithostratigraphic subdivision. In accordance with recommendations of the International Stratigraphic Guide (Salvador, 1994) we describe lithostratigraphic units by a geographic term combined with a unit term instead of a geographic term combined with a lithologic term to allow for lithologic variability, e.g. Esna Formation instead of Esna Shale, as has been used frequently in the past.

In the following paragraph a short summary of the commonly used formations and their regional distribution of the Upper Cretaceous-Palaeogene lithostratigraphic units for northern Egypt and Sinai is given including some additional suggestions (Fig. 5). Detailed historical overview can be found in El-Naggar (1966) and Issawi (1972).

According to Zittel´s (1883) description of the Upper Cretaceous to Lower Eocene sediments in the Western Desert (Farafra, Dakhla and Kharga) (Fig. 5), the following lithostratigraphic units occur from bottom to top: *Overwegi* layers, ash-grey shales („aschgraue Blätterthone"), snow-white layered limestone or chalk with *Ananchytes ovata*, green shales („grünliche Blätterthone") and *Operculina* limestone (Unterlibysche Stufe). Near Esna he miscorrelated the green shales underlying the *Operculina* limestone with the Danian „ash-grey shales" of the Western Desert. With this miscorrelation a long confusion of lithostratigraphic terminology started. Beadnell

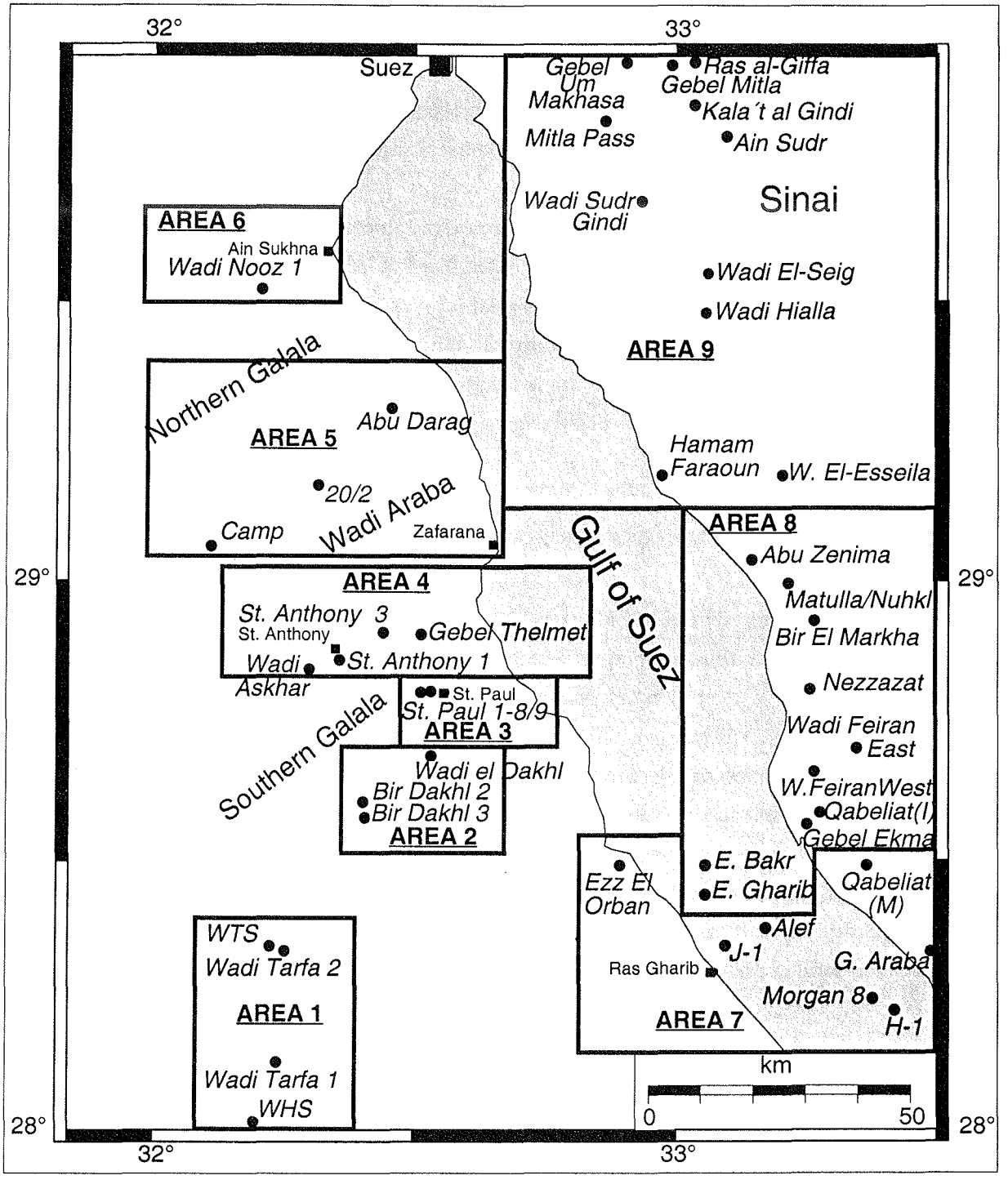

Fig. 3: *Section map of the northern part of the Gulf of Suez. The 9 rectangles represent areas of different depositional history. The sections in areas 1-6 on the western side of the Gulf of Suez (Galala mountains) are based on new and literature data whereas the sections of the areas 7-9 on the eastern side of the Gulf of Suez (Sinai) are based on literature data only.*

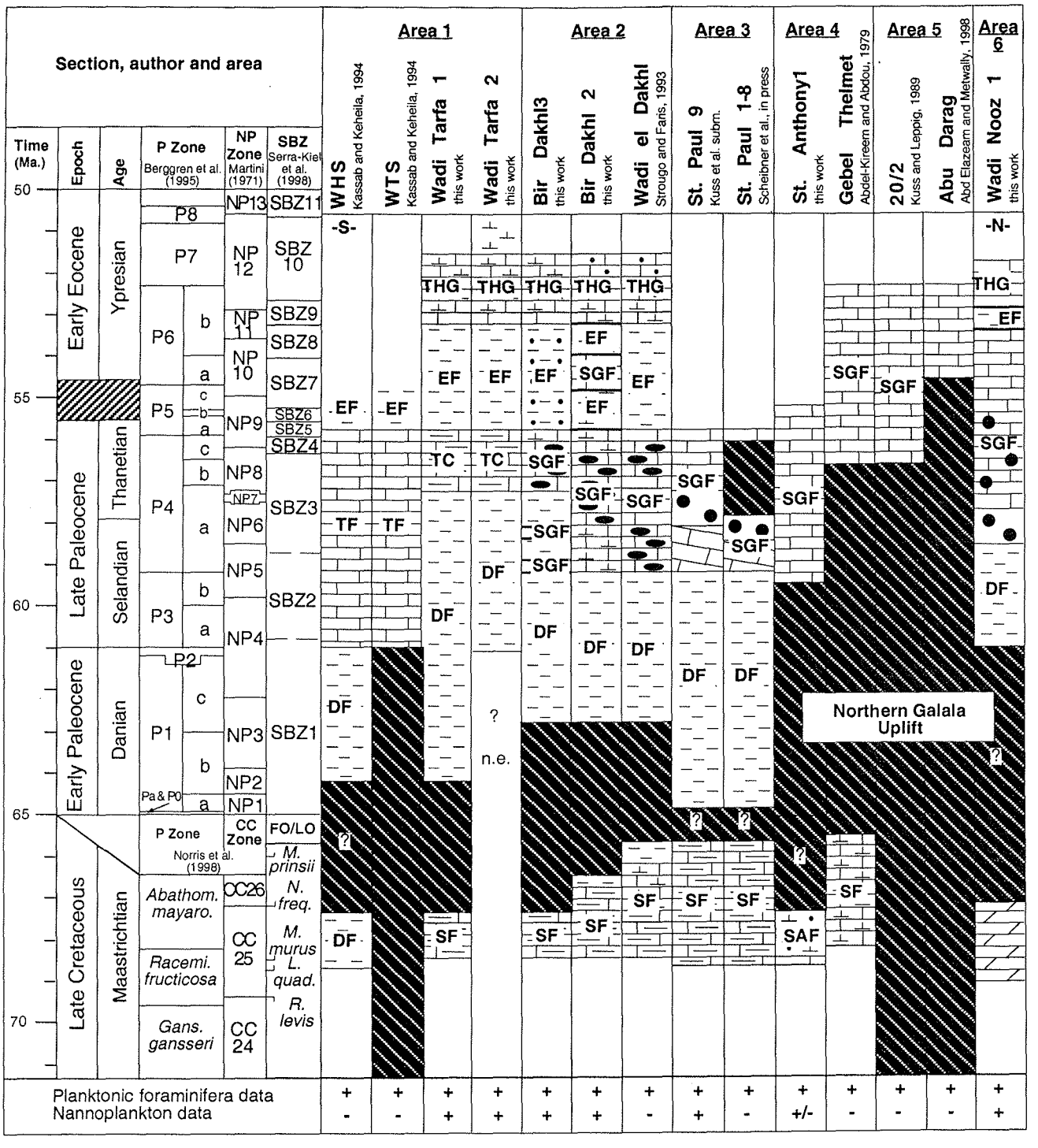

Formations:

THG	Thebes Group
EF	Esna Formation
SGF	Southern Galala Formation
TF	Tarawan Formation
GF	Garra Formation
DF	Dakhla Formation
DTE	Dakhla/Tarawan/Esna Formation
SAF	St. Anthony Formation
SF	Sudr Formation

Lithologies:

chert, hiatus, sandstone, debris flow, slides, marl, shale, limestone, chalk, dolomite

n.e. not exposed

Fig. 4a

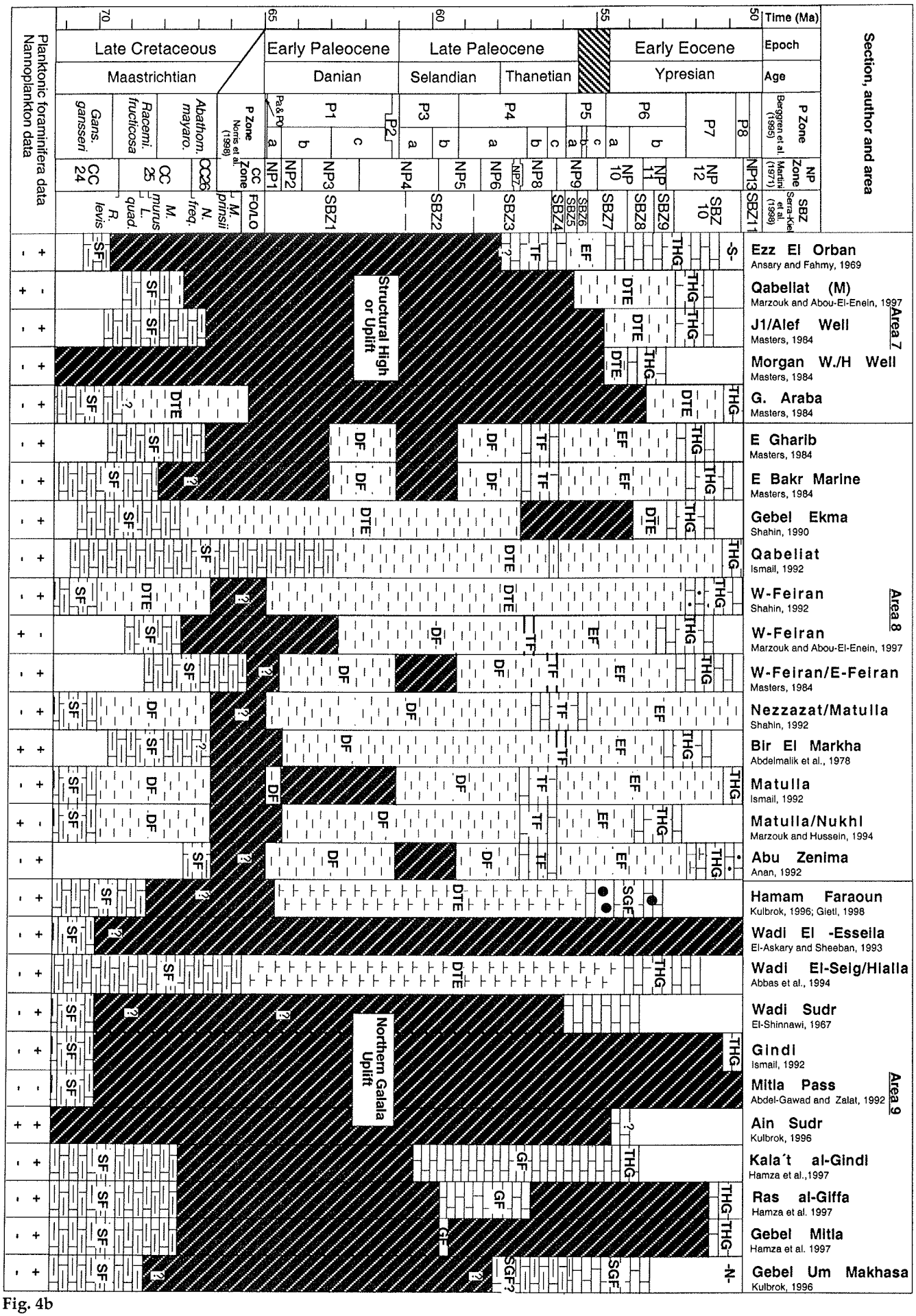
Section, author and area
Time (Ma)
Epoch
Age
P Zone Berggren et al. (1995)
NP Zone Martini (1971)
SBZ Serra-Kiel et al. (1998)
P Zone Norris et al. (1998)
CC Zone FOLO
Planktonic foraminifera data
Nannoplankton data
Late Cretaceous
Maastrichtian
Early Paleocene
Danian
Late Paleocene
Selandian
Thanetian
Early Eocene
Ypresian
Gans. gansseri
Racemi. fructicosa
Abathom. mayaro.
R. levis
M. murus
L. quad.
N. freq.
M. prinsii
Structural High or Uplift
Northern Galala Uplift
Area 7
Area 8
Area 9
Ezz El Orban
Ansary and Fahmy, 1969
Qabeliat (M)
Marzouk and Abou-El-Enein, 1997
J1/Alef Well
Masters, 1984
Morgan W./H Well
Masters, 1984
G. Araba
Masters, 1984
E Gharib
Masters, 1984
E Bakr Marine
Masters, 1984
Gebel Ekma
Shahin, 1990
Qabeliat
Ismail, 1992
W-Feiran
Shahin, 1992
W-Feiran
Marzouk and Abou-El-Enein, 1997
W-Feiran/E-Feiran
Masters, 1984
Nezzazat/Matulla
Shahin, 1992
Bir El Markha
Abdelmalik et al., 1978
Matulla
Ismail, 1992
Matulla/Nukhl
Marzouk and Hussein, 1994
Abu Zenima
Anan, 1992
Hamam Faraoun
Kulbrok, 1996; Gietl, 1998
Wadi El -Esseila
El-Askary and Sheeban, 1993
Wadi El-Selg/Hialla
Abbas et al., 1994
Wadi Sudr
El-Shinnawi, 1967
Gindi
Ismail, 1992
Mitla Pass
Abdel-Gawad and Zalat, 1992
Ain Sudr
Kulbrok, 1996
Kala't al-Gindi
Hamza et al.,1997
Ras al-Giffa
Hamza et al. 1997
Gebel Mitla
Hamza et al. 1997
Gebel Um Makhasa
Kulbrok, 1996

Fig. 4b

Fig. 4: *Biostratigraphy and lithology of newly measured Maastrichtian-Palaeogene sections including sections taken from the literature. The broad grey band reflects the current opinion on the position of the Paleocene-Eocene boundary. The biozonations of planktonic foraminifers (P zones), calcareous nannoplankton (NP zones for Palaeogene and CC zones for Maastrichtian) and shallow benthic foraminifers (SBZ) are listed. In the Maastrichtian the first and last occurences of calcareous nannoplankton index forms are indicated. The different biozonal schemes used are indicated with + (used) and - (not used). Other biozonal schemes such as shallow benthic foraminifers, macrofossils and ammonites are rarely used here and are not listed.*
The black areas indicate hiatuses, due to erosion or non-deposition. The question marks indicate uncertain stratigraphic ranges.
Fig. 4a: *Sections of area 1 to area 6 on the western side of the Gulf of Suez (Galala mountains) are mostly new measured sections together with sections from the literature.* **Fig. 4b:** *Sections of area 7 to area 9 on the eastern side of the Gulf of Suez (Sinai) are entirely from the literature. Unfortunately it is not clear from which part of Gebel Qabeliat Marzouk and Abou-El-Enein (1997) took their section. Because of the hiatus this section was attributed to area 8 whereas the section Gebel Qabeliat of Ismail (1992) belongs to area 7.*

(1905) described for the first time an „Esna Shale" unit above the chalk (Tarawan) and the Danian shales as passage beds between the Cretaceous and the Eocene. Hume (1912) mentioned the Lower and the Upper Esna shales below and above the chalk (Tarawan), respectively, and Said (1961) introduced the Dakhla Shale as a new formation replacing the Danian shales of Beadnell (1905) and the Lower Esna of Hume (1912). The chalk between the Dakhla and Esna Formations was named Tarawan Chalk by Awad and Ghobrial (1965). Since then the terms Dakhla (DF), Tarawan (TF) and Esna Formation (EF) were generally accepted for the lithostratigraphic subdivision in southern and western Egypt (Hermina and Lindenberg, 1989). El-Naggar (1966) introduced the terms Lower Oweina Shale, Middle Oweina Chalk and Upper Oweina Shale for the Tertiary part of the Dakhla, Tarawan and Esna Formations but this lithostratigraphic scheme found little acceptance in the scientific community.

The subdivision of Awad and Ghobrial (1965) cannot be applied to the Late Cretaceous-Palaeogene strata of N Egypt and Sinai, however, because the Tarawan Formation is partly absent or very thin. Although Hermina and Lindenberg (1989) attributed a Late Paleocene to Early Eocene age to the Esna Formation, they mentioned that "the upper part of the Dakhla, the Tarawan and the Esna which range from Paleocene to Early Eocene age in southern Egypt are represented in northern Wadi Qena and on Sinai by the Esna Formation which overlies the Maastrichtian-Paleocene Sudr Formation, and underlies the Lower Eocene limestone (Thebes)." This usage has lead to a stratigraphic miscorrelation of the Esna Formation that ranges in southern and western Egypt only from Upper Paleocene to Lower Eocene whereas in northern Egypt and Sinai it starts as early as latest Maastrichtian (e.g. Said, 1990; Lüning et al., 1998a). Therefore we propose the Dakhla/Tarawan/Esna Formation (DTE) as an informal lithostratigraphic unit for Upper Maastrichtian-Lower Eocene shales and marls in those parts of northern Egypt and Sinai, where the Tarawan Formation cannot be differentiated (Fig. 5).

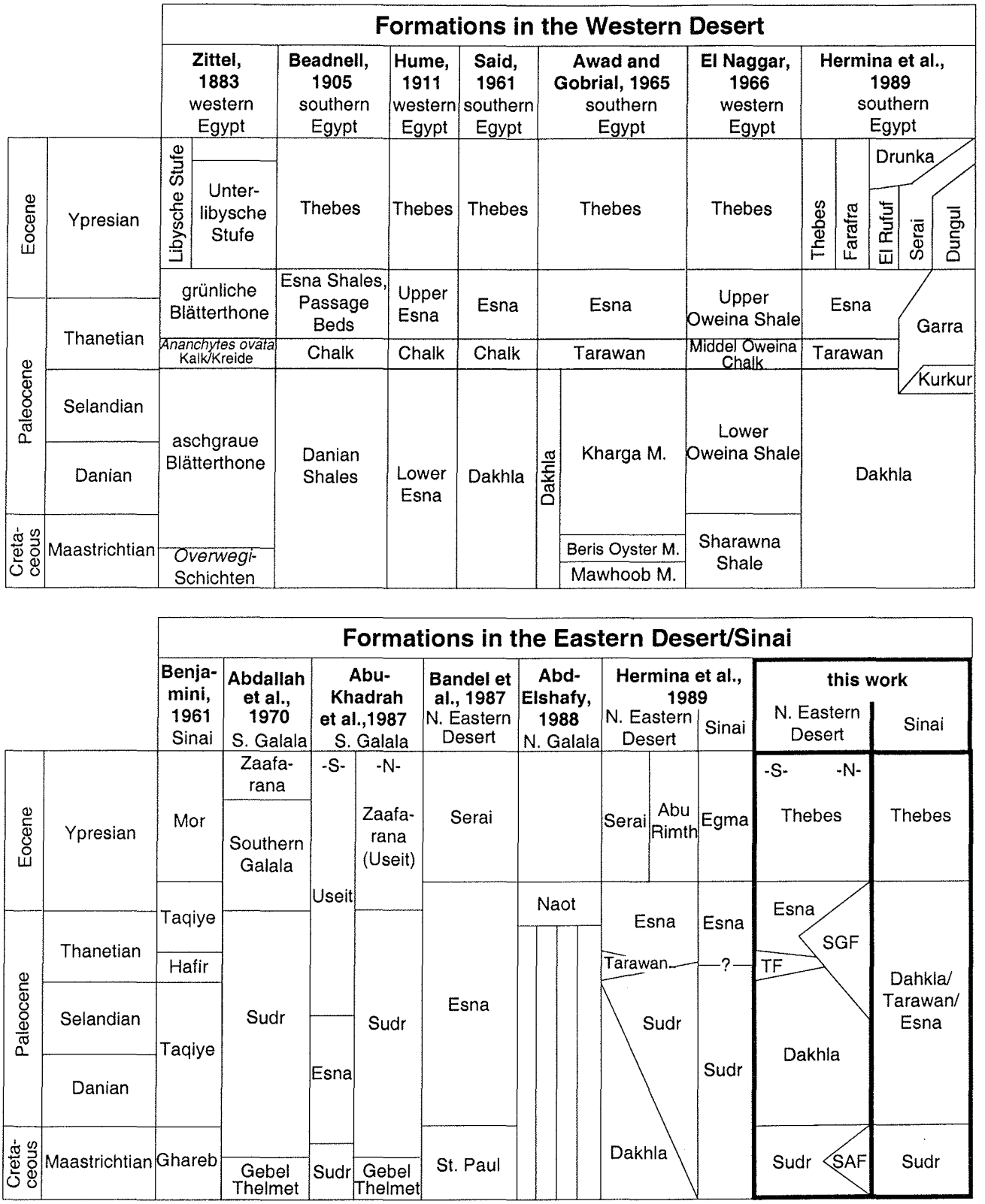

Fig. 5: *Lithostratigraphic schemes in in the Western Desert and in the Eastern Desert/Sinai. Today in southern Egypt the lithologic subdivison of Said (1961) is accepted. In northern Egypt this subdivision is not applicable due to the thin or even absent Tarawan Formation. Most authors ignore that fact and just expand the Esna Formation down to the Maastrichtian but this leads to misinterpretations. Therefore we introduced the informal Dahkla/Tarawan/Esna Formation (DTE).*

The Dakhla, Tarawan and Esna Formations and their earlier denotations are widely used in Egypt. On Sinai, however the Maastrichtian-Eocene successions were also subdivided according to the schemes for southern Israel. There the synonyms for the Sudr, Tarawan, Esna Formations and Thebes Group are Ghareb Formation, Hafir Member, Taqiye Formation and Mor Formation (Bartov and Steinitz, 1977; Romein, 1979; Benjamini, 1992). Were the chalky Tarawan Formation (Hafir Member) is missing on Sinai the entire shaley to marly formation ranging from Paleocene to Early Eocene times is referred to as Esna Formation (Said, 1990) or Taqiye Formation (e.g. Bartov and Steinitz, 1977).

Formations and their distribution within the study area:

In the following paragraph we discuss 8 formal formations (including one group) and one informal formation and their distribution within the 9 areas west (areas 1-6) and east (areas 7-9) of the Gulf of Suez (Fig. 3). The sections within the single areas are grouped together because of their stratigraphic and lithologic similarities. The stratigraphic intervals range from Maastrichtian to Lower Eocene. Areas 1-6 are located in the Eastern Desert, west of the Gulf of Suez, oriented from south (area 1) to north (area 6) (Figs. 1, 3, 4a and 6). On the eastern side of the Gulf of Suez (western-central Sinai), the areas 7-9 are also oriented from south (area 7) to north (area 9) (Fig. 4b). The transition of the Early Eocene shallow-water Southern Galala Formation to the deeper water Thebes Group in the working area is not subject of the study. Therefore the attribution of these sediments to one or the other formation is less certain. All sections studied and additional literature are listed in Table 1, the biostratigraphic and lithostratigraphic correlations of most sections are given in Fig. 4a, b. To illustrate the changing distribution of the various lithologies with time, palaeogeographic maps of the investigated area are presented for 11 Maastrichtian to Early Eocene time slices.

Sudr Formation, SF (Fig. 7c,e): most sections in Fig 4a,b:
Author and type section: Ghorab (1961); Wadi Sudr (western-central Sinai)
Stratigraphic range: Campanian-Maastrichtian (Lower Paleocene?). The contact of the Sudr Formation to the overlying Dakhla Formation is either sharp in which case it usually coincides with the Cretaceous/Palaeogene boundary or is more gradual, in which case (areas 2,7,8) the Sudr Formation terminates within late or latest Maastrichtian biozone CC25 or CC26 (Fig. 4a,b).
Lithology: Massive white and cream chalk and chalky limestone beds with thin intercalations of light grey calcareous shales and argillaceous, crystalline limestones. We studied the Sudr Formation in areas 1,2, and 3 (sections T1, D2, D3, and S1-S9) where it is composed of alternating beds of white chalk (up to 1.20 m) and thin grey marls (up to 0.10 m). In St. Paul (area 3) a 1.3 m thick shaly unit is intercalated in the upper part of biozone CC25c, which is also typical for transitional beds on Sinai.

Synonymy: Synonymous to the St. Paul Formation of Kuss (1986), Bandel et al. (1987) and Bandel and Kuss (1987) (Fig. 5).

Regional distribution: The Sudr Formation is only found in northern Egypt and Sinai.

At St. Anthony (area 4) the chalks of the Sudr Formation have a Late Campanian age. They are disconformably overlain (with an erosional surface) by the units of the St. Anthony Formation (Fig. 7d).

The stratigraphic range of the Sudr Formation at Abu Zenima/Wadi Feiran (area 8) is not clear. Most authors agree that it terminates in the Upper Maastrichtian, however, some authors indicate that the Sudr Formation continues up to the Cretaceous/Palaeogene boundary (Fig. 4b); only Ismail (1992) extended its stratigraphic range at Gebel Qabeliat to the Lower Paleocene, which seems to depend on how transitional beds are classified.

The chalks Kulbrok (1996) described at Ain Sudr (area 9) are of Upper Campanian age (*Globotruncana aegyptiaca* Zone) and those of Gebel Gindi and Hamam Faraoun are of Maastrichtian age (*Gansserina gansseri* Zone).

Both sections in Wadi Nooz (area 6) start with 25 m massive thick bedded dolomites which may be attributed to the Sudr Formation, however, dolomitisation has prohibited a conclusive stratigraphic assignment. Similar lithologies were described from the Sudr Formation of Sinai (Youssef and Shinnawi, 1954 and El-Shinnawi, 1967). Alternatively these dolomites may be attributed to the underlying Turonian strata (Abd Elshafy and Atta, 1993).

In NW-Sinai (area 9) Youssef and Shinnawi (1954) and El-Shinnawi (1967) described 175 m of pinkish white, bedded chalks and chalky limestones that change to yellowish white hard dolomitic limestone in its upper part. Samples of the upper part were thought to contain rare Maastrichtian foraminifers and *Subbotina triloculinoides* of Paleocene age (El-Shinnawi, 1967). The scarcity and the poor preservation of the foraminifers strongly puts the latter assignment into doubt although reworking may be a possible explanation. 45 m below the base of the Sudr Formation, Youssef and Shinnawi (1954) and El-Shinnawi (1967) found *Exogyra* cf. *overwegi* which correlate in area 4 (St. Anthony) to the middle/late Maastrichtian St. Anthony Formation.

Depositional setting: The Sudr Formation was deposited as basinal chalks with no shallow-water influences. Lüning et al. (1998b) discussed the depositional environment of the chalks of the Sudr Formation on E-Sinai in greater detail.

Discussion: Other authors like Abu Khadrah et al. (1987), Abdallah et al. (1970) and Abdallah and Eissa (1970), erroneously included dolomitic limestones of the white cliff (sediments of the Southern Galala Formation) above the cave of St. Anthony. Kuss and Leppig (1989) indicated a Late Paleocene age by means of planktic and benthic foraminifers for these strata and attributed them to the Southern Galala Formation.

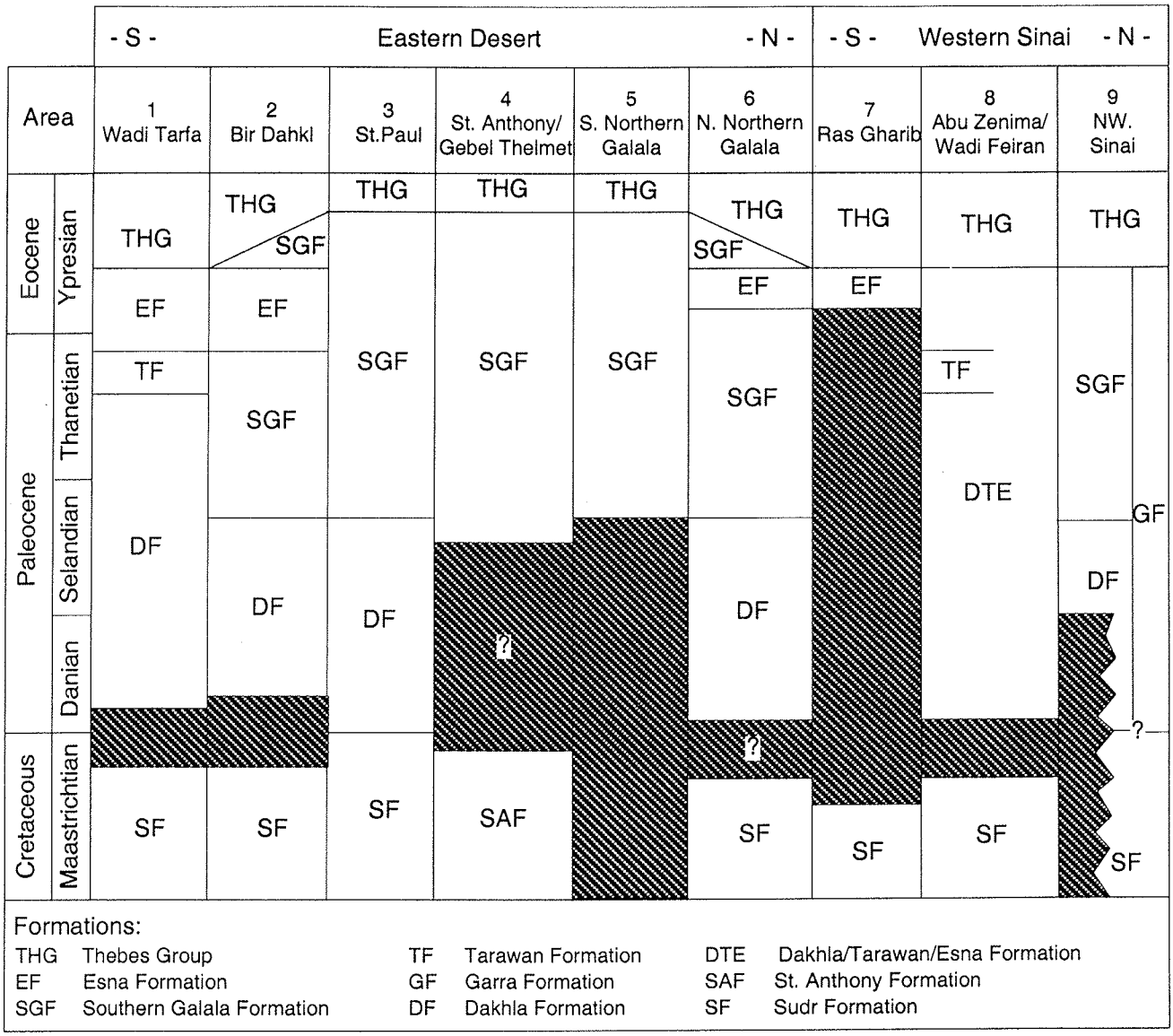

Fig. 6: *Distribution and age of foramations in the 9 investigated areas. The black units are hiatuses due to erosion or non-deposition. In area 9 on NW Sinai the stratigraphic range is uncertain because of varying stratigraphic ranges of the rock units within this area.*

St. Anthony Formation, SAF (Fig. 7d): section A1 in Fig. 4a

Authors and type section: Bandel and Kuss (1987); Monastery of St. Anthony (Eastern Desert)

Stratigraphic range: Upper Campanian-Upper Maastrichtian. The mainly carbonate lithologies of the St. Anthony Formation in the Southern Galala disconformably overlie chalks of the Sudr Formation and underlie the carbonates of the Southern Galala Formation. In the upper part of the St. Anthony Formation *Exogyra overwegi* is present. Age-equivalent sediments with *Exogyra overwegi* were first described in the Western Desert in the "*Overwegi* Layers" (Zittel, 1883), the today Beris Oyster Mudstone Member of the Dakhla Formation (Awad and Ghobrial, 1965; Luger, 1985). The base of the St. Anthony Formation is of Late Campanian age (Kuss, 1986; Kulbrok, 1996; Selima and Askalany, 1996). Although only poor biostratigraphic data is available from the

mainly sandy-dolomitic upper units a Maastrichtian age is indicated by thin-sections. Abdel-Kireem and Abdou (1979) described Upper Maastrichtian planktic foraminifers of the *Abathomphalus mayaroensis* Zone at Gebel Thelmet (GT, Fig. 4a). A possible hiatus between the Late Cretaceous and the Early Tertiary sediments in section A1 is assumed, but could not be substantiated in our sections by means of planktic foraminifers or calcareous nannoplankton.

Lithology: Chalky limestones, marls and sandstones.

Synonymy: The St. Anthony Formation corresponds to the Gebel Thelmet Formation of Abdallah and Eissa (1970) (Fig. 5). Although their term is older we follow Bandel and Kuss (1987) because Abdallah and Eissa (1970) and Abdallah et al. (1970) were apparently confused by the Cretaceous-Eocene lithologies (see discussion of Sudr Formation). Other reasons for using the term St. Anthony Formation are the accessibility and the thickness differences of the type sections. Whereas the section in Gebel Thelmet is dangerous to access (due to possible mine occurrences) and has a reduced section thickness, the section at monastery of St. Anthony is easy accessible and has a much larger thickness.

Regional distribution: The shallow-water influenced deposits of St. Anthony Formation are mapped only along the northern rim of the Southern Galala. A time equivalent formation in northern Egypt and Sinai is the Sudr Formation (Fig. 6).

Depositional setting: The sediments of the St. Anthony Formation are slope sediments of a shallow-water carbonate platform. In the lower part of the St. Anthony Formation large slumping structures occur and are well exposed. In the middle part limestones with slumping and reworked shallow-water biota such as *Orbitoides* and *Omphalocyclus* occur. In the upper part of section A3 (7 km east of St. Anthony, Fig. 1) the shallow-water bivalve *Pinna* and teeth of bony fishes were found, that thrived in calm-water-zones of reefs (pers. com. C. Werner). Kulbrok (1996) assigned the deposits of the St. Anthony Formation to a distally steepened ramp and Selima and Kerdany (1996) to shallow marine environments.

Dakhla Formation, DF (Fig. 7a, b, c, e): in most sections of Fig. 4a,b

Author and type section: Said (1961); Dakhla, north of Mut (Western Desert).

Stratigraphic range: Maastrichtian to Upper Paleocene. The lowermost occurrence of the Dakhla Formation in the Paleocene is at St. Paul (area 3) within the middle to upper foraminiferal *Parvularugoglobigerina eugubina* Zone (Pa) (Strougo et al. 1992), and respectively the middle NP 1 calcareous nannofossil zone (Girgis 1987; Faris 1997). The top of the Dakhla Formation lies in Bir Dakhl (area 2), St. Paul (area 3) and northern Northern Galala (area 6) within NP5 where it underlies the Southern Galala Formation. At Wadi Tarfa (area 1) and in W-Sinai (areas 8, 9) it occurs within NP7/8 where the Dakhla Formation underlies the Tarawan Formation. The latter is in northern Egypt and Sinai thin or even absent.

Lithology: In the studied area the Dakhla Formation consists of chalky marls in the uppermost Maastrichtian and of softer shaly grey-green marls in the Paleocene (Fig. 8). The thickness of the Dakhla Formation varies from 6.5 m (D3) to 23.5 m (T1).

Synonymy: The Dakhla Formation is synonymous to the „aschgraue Blätterthone" of Zittel (1883), the Lower Esna of Hume (1912) and the Lower Oweina Shale of El Naggar (1966) (Fig. 5).
Regional distribution: The Dakhla Formation is present in all areas except area 4, area 5 and area 7 where a stratigraphic gap occurs (Fig. 6). In contrast to our results in Bir Dakhl (area 2) Strougo and Faris (1993) attributed the whole succession sandwiched between the top of the Sudr Formation and the base of the Thebes Group to the Southern Galala Formation. But they subdivided the Southern Galala Formation into three main units, a lower light green argillaceous limestone, a middle prominent, harder bioclastic limestone with large foraminifers and thick chert bands, and an upper green-grey calcareous shale. We correlated this tripartition that is evident also in neighbouring sections to the Dakhla, Southern Galala and Esna Formations (from base to top) (Fig. 8).
In the Northern Galala (area 6) the Dakhla Formation has a thickness of 10 m and is composed of papershales and marly limestones, the latter with abundant planktic foraminifers (morozovellids) in thin-sections indicating an age of P3 and younger (section N1; Fig. 4a). We attributed these sediments to the Dakhla Formation because of their lithologic and stratigraphic similarities.
Depositional setting: The Dakhla Formation was deposited as basinal marls with no shallow-water influences. Speijer and Schmitz (1998) reported from Gebel Aweina (300 km to the south) for most of the Dakhla Formation a paleowater-depth of 200 m. Only within planktic foraminifer zone P3 the paleowater-depth decreases to lower than 100 m. Shahin (1990) described bathyal environments for the shales of the Dakhla Formation.
Discussion: In the Western Desert the Dakhla Formation was subdivided by Awad and Ghobrial (1965) into three members, the Mawhoob Shale Member, the Beris Oyster Mudstone Member and the Kharga Shale Member. The Cretaceous/Palaeogene boundary lies within the upper part of the Kharga Shale Member (Awad and Ghobrial, 1965). In contrast to southern and western Egypt where the base of the Dakhla Formation lies in the Lower Maastrichtian and exhibits the complete succession of all three members, in northern Egypt and Sinai only the equivalent of the younger Kharga Shale Member is present (Fig. 5). Here the Sudr Formation and St. Anthony Formation correlate with the Mawhoob Shale Member and the Beris Oyster Mudstone Member. In northern Egypt and Sinai the base of the Dakhla Formation lies usually at the Cretaceous/Palaeogene boundary and the top within P4/NP6 (Fig. 4a, b).

Tarawan Formation, TF (Fig. 7a, e): in all sections of area 1 in Fig. 4a; in some sections in Fig. 4b
Authors and type section: Awad and Ghobrial (1965); Gebel Tarawan, Kharga Oasis (Western Desert).
Stratigraphic range: Upper Paleocene. The base lies within NP7/8/(P4) and the top lies within lower NP9/(P5). The stratigraphic range of the Tarawan Formation comprises biozones P4/NP6 to P5/NP9. Kassab and Keheila (1994), however gave a range from zones P3/mid NP4 to P4c/lower NP9. It overlies the Dakhla Formation and underlies the Esna Formation.
Lithology: In the study area the Tarawan Formation is characterised by a 1.80 m (area1/section T1) to 2.10 m (section T2) thick chalk bed with flint, similar to the underlying Sudr Formation. In the

Kharga area it is represented by a 3 m-45 m thick chalk-unit which in places changes into chalky limestone, limestone or siliceous limestone.

Synonymy: The Tarawan Formation was described by earlier authors as Chalk (Zittel, 1883), Danian Chalk (Beadnell, 1905) or Middle Oweina Chalk Member (El-Naggar, 1966a,b) (Fig. 5).

Regional distribution: In area 1, sections WHS and WTS of Kassab and Keheila (1994) exhibit discrepancies with respect to lithology and stratigraphy. In section WHS (near to our section T1) these authors described the Dakhla Formation extending down to the Maastrichtian and no Sudr Formation, whereas in WTS (near to our section T2) the Tarawan Formation rests unconformably over Late Campanian sediments (Fig. 4a). Moreover, its thickness of 30 m to 50 m and stratigraphic range with the base lying within P3 (NP4 to NP 5) differs markedly from our observations in the neighbouring sections. Similar to the hiatuses these discrepancies may be the result of very local highs and lows controlling deposition of these different lithologies.

In section Ezz El Orban (area 7) of Ansary and Fahmy (1969) the Tarawan Formation is represented by a 43 m layer of mainly argillaceous limestone which is partly chalky in its lower part (Fig. 4b). The authors named it Middle Oweina Chalk after El-Naggar (1966) and assigned its stratigraphic range to within P4. The Tarawan Formation in Ezz El Orban is very thick in comparison to the sections of the Tarawan Formation on Sinai and in the Wadi Tarfa area. These sediments may more appropriately be assigned to the Southern Galala Formation which reaches thickness of more than 20 m in the nearby north-western Bir Dakhl area.

Depositional setting: The Tarawan Formation in the study area was deposited as basinal chalks/limestones with no shallow-water influences. Anan (1992) and Lüning et al. (1998a) concluded that the Tarawan Formation on Sinai was deposited during a period of low sea-levels. Luger (1985) and Speijer and Schmitz (1998) on the other hand reported from southern Egypt that the sediments of the Tarawan Formation were deposited during sea-level highstands.

Discussion: In northern Egypt and Sinai the Tarawan Formation has a reduced thickness or is absent (Fig. 5). But even where the Tarawan Formation is present (thin chalks or limestones at the NP6-NP9 interval) it was often not discussed by various authors, although it is visible within the respective profiles (NE-Sinai: Hewaidy 1987; Matulla: Ismail 1992; Wadi Nukhl: Marzouk and Hussein 1994; Wadi Feiran: Marzouk and Abou-El-Enein 1997; Matulla: Obaidalla 1999, Fig. 4b, Fig. 7e). The absence of the Tarawan Formation misled some authors and consequently they wrongly attributed even Maastrichtian chalks to the Tarawan Formation (e.g. Shafik and Stradner, 1971). Selima and Askalany (1996) attributed chalky limestones in Wadi Askhar (area 4) to the Tarawan Formation. In section A1 (7 km east of Wadi Askhar) these chalks contain abundant shallow-water biota (corals, coralline algae) and are attributed in our study to the Southern Galala Formation (Figs. 5, 6).

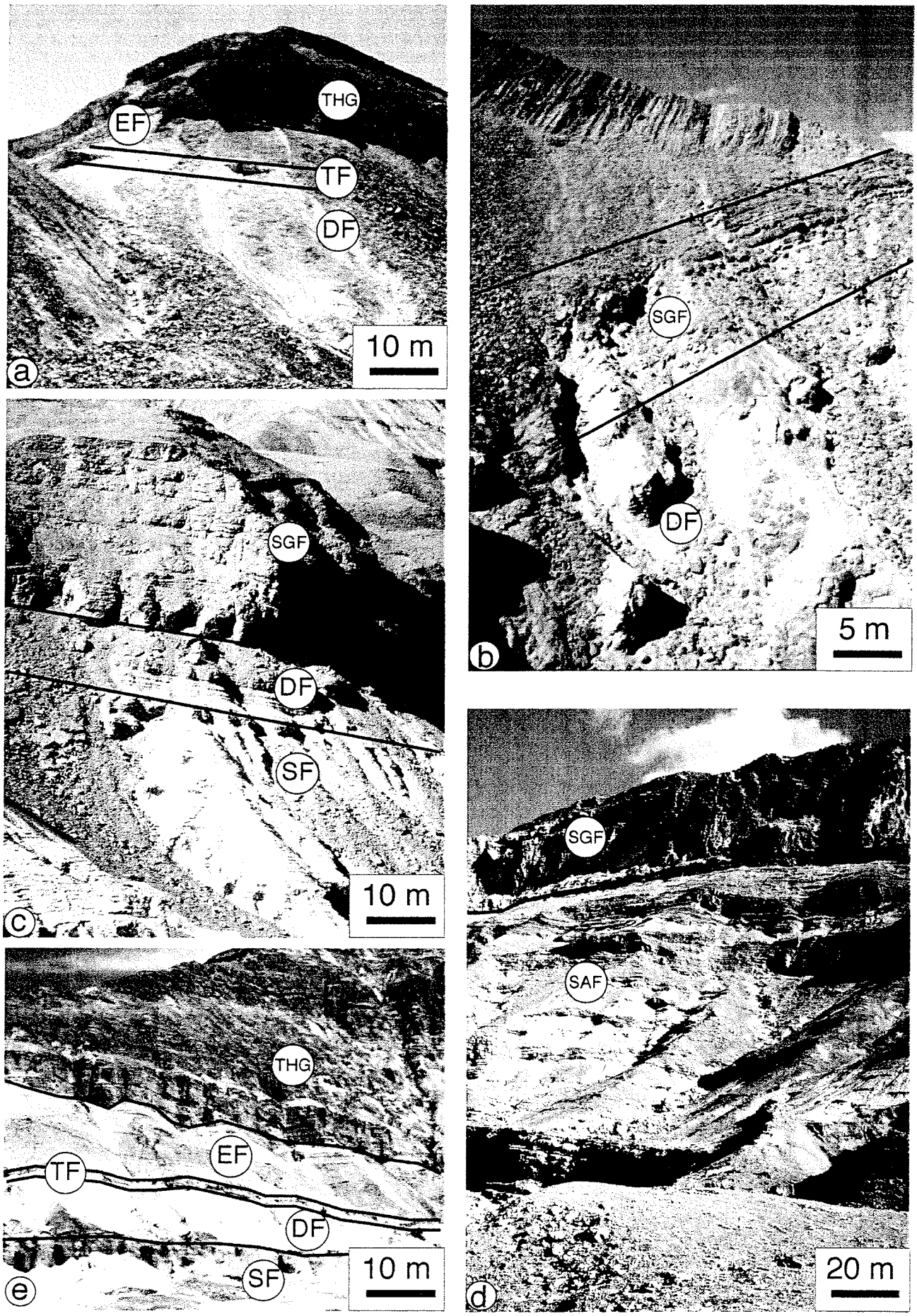
THG
EF
TF
DF
10 m
a
SGF
DF
5 m
b
SGF
DF
SF
10 m
c
SGF
SAF
20 m
d
THG
EF
TF
DF
SF
10 m
e

Fig. 7: *The Late Cretaceous - Palaeogene sediments of the western (a-d) and eastern (e) side of the Gulf of Suez. The scales are only approximations due to a distorted perspective.* **Fig. 7a:** *Section T1, the southernmost section in area 1. Chalks of the Tarawan Formation are intercalated between the marls and shales of the Dakhla Formation below and Esna Formation above. The cliff at the top is build of chalky limestones of the Serai Formation of the Thebes Group.* **Fig. 7b:** *Section D2 in area 2. Marls and shales of the Dakhla Formation are overlain by the limestones of the Southern Galala Formation with a gradual contact. The fault at the top is of younger age and due to Red Sea graben tectonics. The section continues left of the picture with the rest of the sediments of the Southern Galala Formation, the Esna Formation and the Thebes Group.* **Fig. 7c:** *Section S9 (Kuss et al. in press) in area 3. Marls and shales of the Dakhla Formation are sandwiched between chalks of the Sudr Formation below and shallow-water influenced sediments of the Southern Galala Formation above.* **Fig. 7d:** *Section A1 in area 4. The marls and sandy marls of the St.Anthony Formation are overlain by the shallow-water limestones of the Southern Galala Formation. The Southern Galala Formation forms a steep white cliff along the northern rim of the Southern Galala.* **Fig. 7e:** Wadi Nukhl on Sinai. Similar to section T1 in Fig. 7a the thin Tarawan Formation is sandwiched between the Dakhla Formation and the Esna Formation (picture courtesy R.P. Speijer).

Garra Formation, GF: present in sections Kala't al Gindi, Ras al-Giffa and Gebel Mitla in area 9 in Fig. 4b.

Author and type locality: Issawi, 1969; South of Gebel Garra, south Western Desert

Stratigraphic range: Upper Paleocene to Lower Eocene. In NW Sinai its base disconformably overlies the Sudr Formation and lies within P3a. It is overlain by the Egma Formation of the Thebes Group within P6a.

Lithology: In area 9 the Garra Formation is composed of a basal white, argillaceous limestone with chert near its top, overlain by massive limestones and thus shows similarities with the Southern Galala Formation at Bir Dakhl (area 2). In Kala't al-Gindi the Garra Formation has a maximum thickness of 49 m (Fig. 4b). At the type locality the Garra Formation is composed of well-bedded, white limestone and chalk with minor shale and marl intercalations.

Regional distribution: The Garra Formation was described only by Hamza et al. (1997) from NW and N-central Sinai.

Depositional setting: In southern Egypt the Garra Formation was deposited in the middle to inner shelf (Luger, 1985) whereas on Sinai deeper marine settings are assumed (see discussion of Southern Galala Formation, below).

Discussion: In NW Sinai (area 9) Hamza et al., (1997) described limestones of the Garra Formation (mid P3b-mid P6a), sandwiched between the chalks of the Sudr Formation and the limestones of the Thebes Group (Fig. 4b). Said and Kenawy (1956) identified a bathyal fauna in the chalky sediments. Whether these deposits are synonym to the Southern Galala Formation remains uncertain. But at least the introduction of the Garra Formation in this part of Egypt may explain earlier discrepancies in lithologic description and dating of the Sudr Formation and Thebes Group.

Hermina and Lindenberg (1989) described the Garra Formation from the southern Western Desert. It disconformably overlies the Kurkur Formation and underlies the Dungul Formation. The Garra Formation in southern Egypt is a lateral equivalent of the upper parts of the Dakhla, the Tarawan and the Esna Formations (Fig. 5).

Southern Galala Formation, SGF (Fig. 7b, c, d): present in areas 2 to 6 in Fig. 4a; in sections Hamam Faraoun and Gebel Um Makhasa in Fig. 4b.

Authors and locality: Abdallah et al. (1970); redefined by Kuss and Leppig (1989); The reference section 18/2 (Kuss and Leppig, 1989) is situated in a N-S trending wadi, 6 km W of monastery of St. Anthony

Stratigraphic range: Upper Paleocene-Lower Eocene. Our data indicate that the base of the Southern Galala Formation lies within the *Glomalveolina levis* Zone (Upper Thanetian, P4c/NP8) and the top lies within the *Alveolina dainelli* Zone (Cuisian, P9/NP13). In Bir Dakhl and St. Paul the Southern Galala Formation is overlying the Paleocene Dakhla Formation (Fig. 4a) with a stratigraphic range from middle NP5/(P3/4) to middle NP9/(P4/5). In section D2 the Southern Galala Formation interfingers with the Esna Formation and the top lies within NP10/P6 (Figs. 6, 8, 9). At St. Paul the top of the Southern Galala Formation lies within SBZ10 (NP12/P7) (Gietl, 1998). In St. Anthony the Southern Galala Formation overlies the Late Campanian-Maastrichtian St. Anthony Formation while farther north it is unconformably underlain by Turonian strata in section 20/2 (Kuss and Leppig, 1989) and other parts of the Northern Galala (Abd Elshafy and Atta, 1993) and by Campanian limestones of the Matulla Formation in Abu Darag (Abd-Elazeam and Metwally, 1998). Malchus (1990) described a hiatus ranging from Late Cenomanian to Maastrichtian in section 20/2. In the northern areas of the Northern Galala the Southern Galala Formation overlies the Paleocene Dakhla Formation (section N1 of Fig. 4a) and underlies Thebes Group.

Lithology: Massive sandy fossiliferous (alveolina, numulitids, coralline algae) limestones, limestone/sandstone intercalations, often conglomeratic with a thickness of about 250 m, in the southern parts limestones with flint.

Synonymy: Abu Khadrah et al. (1987, based on Barakat et al., 1985) introduced the Useit Formation as a junior synonym of the Southern Galala Formation. The whole Palaeogene part (P5/6; NP9/10) of section Wadi Naot (limestones and clayey siltstones) in the Northern Galala was attributed by Abd-Elshafy and Atta (1993) to the Naot Formation, which was introduced by Abd-Elshafy (1988) in Wadi Naot (Wadi Naot is a synonym of Wadi Nooz used by us). We did not employ the term Naot Formation in our study because it is possible to differentiate the Dakhla and Southern Galala Formations (Fig. 5).

Regional distribution: In sections D2 and D3 (area 2) the Southern Galala Formation starts with the first hard limestone bed and is characterised by alternating limestones (up to 1 m thick) with abundant chert layers or nodules and shaly marls (up to 0.7 m thick). The hard limestones are partly composed of bioclastic wackestones and chalky and dolomitic limestones. Fig. 9 shows the interfingering of the Southern Galala Formation and the partly overlying Esna Formation in detail (sections D2 and D3). In section D2 three limestone beds show abundant bioturbation of *Zoophycos* and *Thalassinoides*. The main part of the Southern Galala Formation unit A in sections D2 and D3 (Fig. 9) has a thickness of 17 m and 20 m, respectively. Although the Southern Galala Formation

has more or less the same thickness in these sections, the thickness of the different biozones varies (e.g. NP6 and NP7/8, Fig. 9).

At St. Paul (area 3) the Southern Galala Formation is composed of limestones with locally abundant quartz grains that were deposited as gravity flows like glides, slumps and debris flows. A few thin (max. 20 cm) marl beds are intercalated in the lower part (Scheibner et al., 2000).

The steep white cliff at St. Anthony and Gebel Thelmet (area 4) is composed of dolomitic limestones of the Southern Galala Formation (Fig. 7d). Because of its white colour and its chalky appearance that is due to diagenetic alternations several authors (Abdallah et al., 1970; Abdallah and Eissa, 1970; Abu Khadrah et al., 1987) previously misinterpreted these strata as chalks of the Sudr Formation (Fig. 5) or as chalks of the Tarawan Formation (Selima and Askalany, 1996). However, the basal conglomeratic debris flow type deposits of 0 m - 2 m thickness are overlain by white diagenetically overprinted limestones with abundant corals in the lower 15 m. In the middle part of the nearly 70 m high cliff *Hottingerina lukasi* (SBZ4/P4c) was found indicating a latest Paleocene age.

In section 20/2 (area 5) (Kuss and Leppig, 1989) the Late Paleocene-Early Eocene Southern Galala Formation is build of massive sandy limestones, limestone-sandstone intercalations and debris flows. In Wadi Nooz (area 6) it is formed of debris flows and chaotically bedded limestones. Because of lithologic similarities to the Southern Galala Formation of area 3 (St. Paul) this unit is attributed to the Southern Galala Formation. As in the underlying Dakhla Formation only morozovellids were found, indicating again an age of P3 and younger. In Hamam Faraoun, in the very south of area 9, Gietl (1998) described debris flows up to 6 m thick with siliciclastic sand and larger foraminifers, and shallow-water limestones with larger foraminifers of Early Eocene age (SBZ7-9, NP10-12). In the north of area 9 (Wadi Sudr) he found limestone/marl beds with slumps, debris flows and larger foraminifers. In Gebel Um Makhasa Kulbrok (1996) described chalky limestones of SBZ4-6 (NP8/9) with larger foraminifers and corals that may be attributed to the Southern Galala Formation.

Depositional setting: The sediments of the Southern Galala Formation are sediments of a carbonate platform and slope which were deposited on and around the NGWA high. They interfinger with basinal sediments of the Southern Galala Sub-basin in area 2 (Bir Dakhl). Kulbrok (1996), Gietl (1998) and Scheibner et al. (2000) described the carbonate platform and slope deposits of the Southern Galala Formation in more detail.

Discussion: We do not follow the classification of Abu Khadrah et al. (1987, based on Barakat et al., 1985) and Selima and Askalany (1996). The Useit Formation described by Abu Khadrah et al. (1987) was thought to overlie a unit termed Esna Formation in St. Paul, which, however, is of Early Paleocene age and therefore should be regarded as Dakhla Formation (see discussion of Abu Rimth Formation below). Moreover, the same authors correlated the Zaafarana Formation with the Useit Formation, although the first was originally described to overlie the Southern Galala Formation and is of middle Eocene age (Abdallah et al., 1970). It is not clear by the above whether the

Zaafarana Formation should be attributed to the Useit Formation and hence representing part of the Southern Galala Formation or whether it forms part of the overlying Thebes Group (Fig. 5).

Esna Formation, EF (Fig. 7a, e): many sections in Figs. 4a, b

Author and type section: Beadnell (1905); Gebel Aweina near Esna

Stratigraphic range: Late Paleocene to Early Eocene. Its stratigraphic range has been discussed intensively (El-Naggar, 1966a,b; Sabry 1968; El-Naggar, 1968; Issawi, 1972). Nowadays it is accepted in main Egypt that the Esna Formation is intercalated between two more or less chalky limestone units, the Tarawan Formation below and the Thebes Group above and thus represents Late Thanetian to Early Ypresian (P4c/lower NP9 to mid P7/NP12, Fig. 6). On Sinai, however, the term Esna Formation is quite often used to describe the whole Paleocene shales sandwiched between the Sudr Formation below and the Thebes Group above (Lüning et al., 1998a; Marzouk and Lüning, 1998; discussion see below).

Lithology: The Esna Formation is composed of green-grey shales and marls with planktic foraminifers and calcareous nannoplankton.

Synonymy: The Esna Formation is synonymous with the „grünliche Blätterthone" of Zittel (1883), the upper Esna of Hume (1912) and the Upper Oweina Shale of El Naggar (1966) (Fig. 5).

Regional distribution: In Wadi Tarfa (area 1) the Esna Formation is 10.50 m (T1) to 17.10 m (T2) thick and is composed of the same lithology as the Dakhla Formation. Nishi et al. (1994) described a section south of the Ras Gharib to El Sheikh Fadl road with only 5 m of the Esna Formation overlain by chalks of the Thebes Group whereas El Dawy (1999) reported 21 m of Esna Formation in a section south of the Ras Gharib to El Sheikh Fadl road.

Strougo and Faris (1993) in their Wadi El Dakhl section (area 2) described green-grey calcareous shales and cream to light grey laminated argillaceous limestones. In section D3 (area 2) the Esna Formation is characterised by green-grey shaly marls with abundant thin, up to 0.22 m thick sandstone layers. These sandstones are partly cross-laminated and have rip-up clasts. The sicliciclastic intercalations were interpreted as distal fan lobes, which more proximal parts at St. Paul were discussed in Scheibner et al. (2000). In Bir Dakhl (area 2) the Southern Galala Formation grades laterally into shales of the Esna Formation, best visible in section D2 and less clear in section D3 (Fig. 9). In section D2 the intimate interfingering of the Esna Formation with the Southern Galala Formation is evident (Figs. 8, 9). As a consequence this part of the section can be subdivided into 5 units. From bottom to top the following 5 units can be distinguished (Fig. 9): A) alternating limestones with abundant chert layers (see Southern Galala Formation, above), B) 2.5 m grey-green marl, C) 1.9 m alternation of silty marls and dolomitic limestone with laminations and channel structures, D) 4.4 m grey-green marl, at the base silty, E) 6 m alternation of shaly partly silty marls and dolomitic limestones with laminations, channel structures and rip-up layers, F) 5.2 m of silty marls. Within this profile units A, C and E exhibit characteristics of the Southern Galala Formation whereas units B, D and F could be attributed to the Esna Formation (Fig. 9).

In northern Northern Galala (area 6) the 15 m of the Esna Formation are of Lower Eocene age (NP11/12/P6) indicated by presence of calcareous nannofossils and planktic foraminifers. In contrast Gietl (1998) described alveolinids of SBZ5 (NP9/P5) from limestones overlying the Esna Formation which, however, may have been reworked from older carbonates.

Depositional setting: The Esna Formation was deposited as basinal marls with no shallow-water influences. Only in areas that interfinger with the Southern Galala Formation shallow-water deposits were found. Speijer and Schmitz (1998) gave a paleodepth curve from Gebel Aweina (ca. 300 km to the south) and reported paleowater-depths of about 200 m for most of the Esna Formation. Only in the uppermost part of the Esna Formation the paleowater-depth decreases to 100 m. According to Shahin (1990) the shales of the Esna Formation were deposited on Sinai in bathyal environments.

Discussion: The credit for the introduction of the Esna Formation was given to Beadnell (1905) although shales in the vicinity of Esna were mentioned earlier by Zittel (1883) and others (see El-Naggar, 1966a,b).

In northern Egypt and on Sinai the whole Paleocene shales and marls are often attributed to the Esna Formation in areas where no Tarawan Formation exists (Said, 1990) and thus having a stratigraphic range from Upper Maastrichtian to Lower Ypresian (see discussion Dakhla/Tarawan/Esna Formation, below). Even if only the lower part of the Paleocene shales are exposed, (see e.g. Abu Khadrah et al. 1987) they were quite often referred to as Esna Formation, which makes lithostratigraphic correlation very confusing (Abu Khadrah et al. 1987; Hewaidy, 1987; Said, 1990; Cherif and Ismail 1991; Marzouk and Hussein, 1994) (Fig. 5). We therefore suggest to attribute only Upper Paleocene shales to the Esna Formation, whereas Lower Paleocene shales belong to the Dakhla Formation. This bipartition is only possible in areas where either only Upper Paleocene shales or only Lower Paleocene shales were exposed or where they were separated by the Tarawan Formation. If the shales range from the Lower to the Upper Paleocene we suggest the usage of the Dakhla/Tarawan/Esna Formation (DTE) (Figs. 5, 6).

Snavely et al. (1979) stated that most authors agree with the upper portion of the Esna Formation to be assigned to the Ypresian *Morozovella subbotinae* Zone (P6/NP10/11 of Berggren et al. 1995); the transitional marly beds typical of the conformable Esna-Thebes contact were assigned to the *Morozovella aragonensis* Subzone (P7/NP12 of Berggren et al. 1995). However we found the Esna-Thebes contact in the Eastern Desert usually within NP11. In the upper part of the Esna Formation as well as in the Thebes Group *Nummulites deserti* was found (LeRoy, 1953; Hermina and Lindenberg, 1989) indicating an Ypresian age (NP11-NP12) that contrasts with the stratigraphic range of that species mentioned by Serra-Kiel et al. (1998) as SBZ4 and SBZ5, which corresponds to NP9. This discrepancy led to some confusion of the stratigraphic range of the Thebes Group. For example Gietl (1998) correlated the lower part of the Thebes Group to the *Alveolina cucumiformis* Zone (SBZ5 or NP9) which would be in disagreement to the stratigraphic range of our samples.

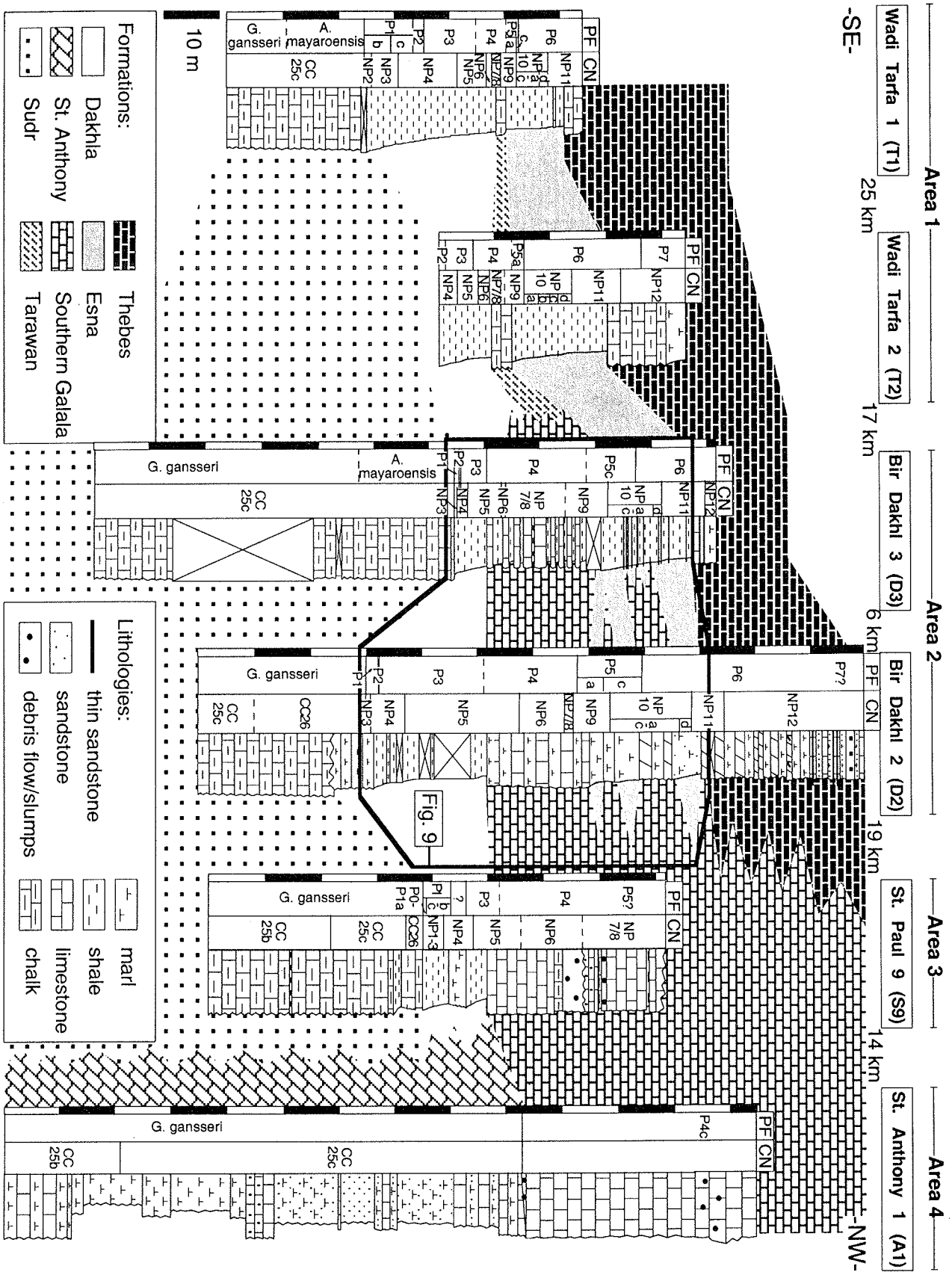

Fig. 8: *Bio- and lithostratigraphic correlation of 6 sections from area 1 to area 4 on the western side of the Gulf of Suez (Eastern Desert). Best visible is the progradation of the shallow-water sediments of the St. Anthony Formation in the Maastrichtian-Paleocene and of the Southern Galala Formation in the Paleocene-Eocene. The black rectangle in sections D3 and D2 indicates the range of the detailed correlation of Fig. 9.*

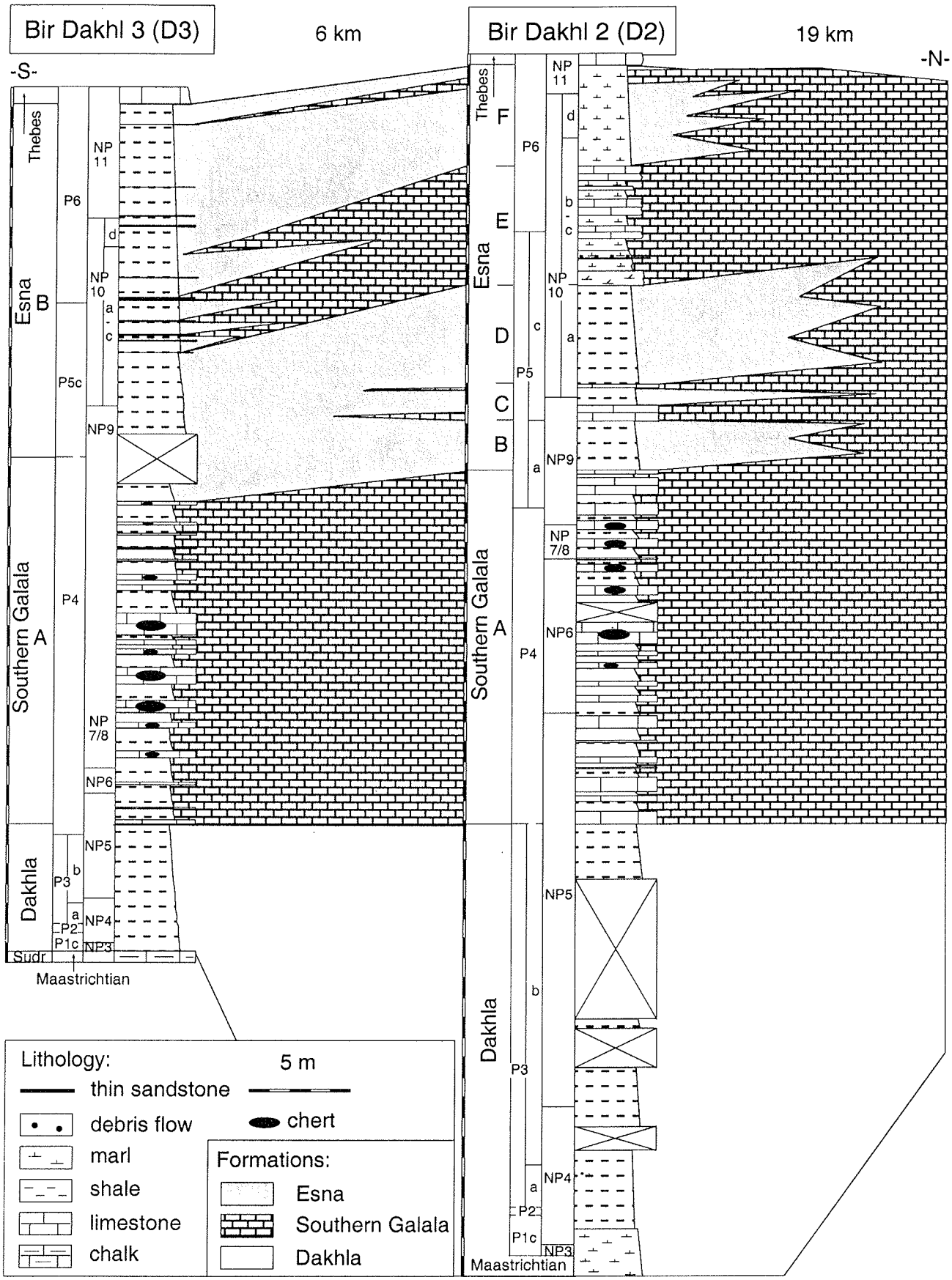

Fig. 9: *Detailed bio- and lithostratigraphic correlation of sections D3 and D2 in area 2. The letters A-F indicate different units described in the text.*

Dakhla/Tarawan/Esna Formation (DTE): some sections in Fig. 4b.

Stratigraphy: The stratigraphic range of this informal formation is Upper Maastrichtian to Lower Eocene. Because of the gradual transition from the Maastrichtian chalk to the Paleocene shales the onset of the DTE Formation in Abu Zenima/Wadi Feiran (area 8) is not clearly fixed lithologically, it varies from a level within the Upper Maastrichtian to one at the Cretaceous/Palaeogene (K/Pg) boundary. A small hiatus at the K/Pg boundary is probable (Shahin, 1992). As with the lower stratigraphic boundary, the upper boundary is not well constrained. The transition from the DTE Formation to the Thebes Group lies around P6/7, NP11/12. It overlies the Sudr Formation and underlies the Thebes Group.

Lithology: Green-grey shales and marls, similar to the Esna Formation.

Regional distribution: The DTE Formation is only present on Sinai.

Depositional setting: The DTE Formation was deposited as basinal marls similar to the Esna Formation (Shahin, 1990).

Discussion: The DTE Formation is an informal formation for the latest Cretaceous-Palaeogene grey-green shales in northern Egypt and Sinai where the Tarawan Formation cannot be identified. In most sections within the DTE Formation, at around upper P4/5, one or more limestones might be attributed to the Tarawan Formation. Masters (1984) indicated 2 limestone-beds in Wadi Feiran East which could be attributed to the Tarawan Formation and probably represent a tectonic duplication (R. P. Speijer, pers. comm.). Because of the reduced thickness of the beds probably not all authors indicated these layers as Tarawan Formation. The varying ages of the top of the DTE Formation are not due to transitional lithologies but due to the different biozonations used. Authors who worked with the calcareous nannoplankton biozonation gave older (NP11=P6) ages than authors who used the planktic foraminifer zonation (P6/7). This discrepancy probably results from the variability in the planktic foraminifers-calcareous nannoplankton correlation (Marzouk and Lüning, 1998). Another explanation may be the usage of different planktic foraminifer biozonations which were revised in time or different taxonomic concepts of the authors.

Thebes Group (THG) (Fig. 7a, e): most sections in Fig. 4a, b

Authors: Hermina and Lindenberg (1989)

Stratigraphic range: Lower Eocene (see different formations, below)

Lithology: (see different formations, below)

Synonymy: (see different formations, below)

Regional distribution: At Wadi Tarfa the base of the Thebes Group lies within NP11/P6. It is composed of chalky limestones alternating with chalky marls. Some of the chalks have layers or nodules of flint incorporated.

In Bir Dakhl (area 2) the Thebes Group is formed by chalky limestones with abundant chert layers or nodules, marly intercalations and sandstones with crossbedding, lamination and rip-ups. They may contain alternations of harder and softer marls. In the lower part of section D2 the marls are partly rich in quartz grains and *Nummulitids*. In the upper part of section D2 slumping and first

Alveolina rich sandstones occur that could belong as well to the Southern Galala Formation but this transition was not investigated in detail.

Bandel et al. (1987) described the Serai Fm. overlying the Esna Shale from the western escarpment of Wadi Tarfa. Within the upper third of the 110 m thick succession of bedded marly to platy chalks with flint intercalations, a 17 m thick unit of alveolinid-nummulitid bearing limestones aged SBZ11-14 occurs that indicate an Early Eocene age. The Thebes Group of northern Northern Galala (area 6) is composed of well bedded dolomitic limestones, partly with nummulitids, deformed alveolinids, few debris flows and quartz grains. The base lies in lower NP12. These sediments may as well belong to the Southern Galala Formation, but again were not subject of our study. The Thebes Group in area 8 is composed of a sequence of well bedded chalky limestones with intercalated chert bands (El Sheikh and El Beshtawy, 1994) or of yellowish sandy limestones followed by limestones with chert bands (Shahin, 1990, 1992). In Wadi Feiran (area 8) Eweda and El-Sorogy (1999) divided the Thebes Formation into a lower 180-190 m thick cherty chalky limestone Member and an upper 50-60 m thick calcareous claystone Member.

Depositional setting: We studied only the lower part of the Thebes Group in area 1 (Wadi Tarfa). Here the sediments were deposited in a basinal setting without any shallow-water influences. In areas 2-6 we did not investigate the transition from the Southern Galala Formation to the above lying Thebes Group. Shahin (1990) and Lüning et al. (1998a) suggested that the Thebes Group on Sinai was deposited during a time of a lowered sea level. Snavely et al. (1979) proposed the following three-stage depositional history for the Thebes Group: a) basinwide pelagic carbonate deposition with thin, shallow-water facies near the basin margins, b) gradual shallowing and c) abrupt lowering of sea-level.

Discussion: The Thebes Group was introduced by Hermina and Lindenberg (1989). It replaces the Thebes Formation of Said (1960) and is equivalent to the "Libysche Stufe" of Zittel (1883) excluding the Esna shales (Fig. 5). The Thebes Group includes the following formations (Fig. 5):

1. Farafra Fm., El Rufuf Fm., Serai Fm., Drunka Fm. and Dungul Fm., in the scarps and plateau areas south of Minia.
2. Abu Rimth Fm. in the Southern Galala
3. Egma Fm. on Sinai.

Here we focus only on the Serai, Egma and Abu Rimth Formations because they have been described in the study area of the Northern part of the Gulf of Suez. In this contribution we refer to the Thebes Group when „speaking" of Lower Eocene strata that overly the Esna Formation or DTE (except the Galala Mountains, where the Thebes Group overlies the Southern Galala Formation) and underlie the Minia Formation. In the contribution no subdivision of the different formations is done.

Serai Formation:

Authors and type section: Barron and Hume (1902); redefined by Lindenberg et al. (in Hermina and Lindenberg, 1989) as facies variation of the Thebes Group; Gebel Serai, south Wadi Qena, Eastern Desert.

Stratigraphic range: Early Eocene.

Synonymy: Synonym with the lower and middle members of the Thebes Formation by Said (1960) and the lower member of the Thebes Formation of Snavely et al. (1979).

Lithology: Fine-grained, thinly bedded micritic limestones, chalky and cherty with rare shales; grading upward into massive bioturbated beds with few allochthonous layers.

Discussion: The Serai Formation is widely developed throughout the Stable Shelf, at the plateau surface between the Nile and Kharga oasis, Wadi Qena, and the Quseir-Safaga region. A special slump facies of mixed autochthonous and allochthonous sediments is defined separately as Abu Rimth Formation in the Southern Galala (see below). The Serai Formation was described by Bandel et al. (1987) in the Wadi Tarfa area.

Egma Formation

Author and type section: Beadnell (1927) and Hermina and Lindenberg (1989) mention no type section only the type area (Egma Plateau on Sinai).

Stratigraphic range: Early Eocene

Lithology: Shallow platform deposits of medium-bedded to massive limestones with tabular chert bands, chalky, frequent turbidite layers with reworked fossils.

Discussion: The Egma Formation is present in the southern and northern Sinai. It overlies the Esna Formation, whereas the top is uncovered.

Abu Rimth Formation:

The following description is taken from Phillobbos, Lindenberg and Schmitz (in Hermina and Lindenberg, 1989)

Author and type section: Phillobbos, Lindenberg and Schmitz. (in Hermina and Lindenberg, 1989). The type area is the Wadi Abu Rimth in the Southern Galala, SSW of the monastery of St. Paul.

Stratigraphic range: Early Eocene.

Lithology: It is composed of "well-bedded open marine to shelf limestones and marls with intercalated thin turbidite and thick olistostrome layers containing abundant larger foraminifers, clasts of shallow-water carbonates, including reefal limestones, *Alveolina* limestones and displaced sand." They may have conspicuous slump structures.

Synonymy: It is synonym with the lower and middle members of the Thebes Formation by Said (1960) and the Thebes Formation of Bandel and Kuss (1987).

Discussion: The stratigraphic range of the Abu Rimth Formation (Philobbos Lindenberg and Schmitz, in Hermina and Lindenberg, 1989) collides with the stratigraphic range of the above mentioned Southern Galala Formation. Philobbos Lindenberg and Schmitz (in Hermina and Lindenberg, 1989) mentioned that the Abu Rimth Formation overlies the Esna Formation in the southern parts. But in St. Paul no Upper Paleocene shales of the Esna Formation occur but only the Lower Paleocene shales of the Dakhla Formation. As documented before the term Esna Formation is

loosely used and sometimes covers the Lower Paleocene Dakhla Formation as well. Therefore the strata overlying in St. Paul the Dakhla Formation could not belong to the Abu Rimth Formation but should be correctly attributed to the Southern Galala Formation. As a consequence the Abu Rimth Formation in the Galalas is represented by the conglomeratic sandy lithologies of the Southern Galala Formation and hence have to be attributed as a synonym of the latter. The Abu Rimth Formation is present only in the Southern Galala (Philobbos Lindenberg and Schmitz, in Hermina and Lindenberg, 1989) which corresponds to the areal extension of the Southern Galala Formation according to our results. Therefore the term Abu Rimth Formation should be abandoned.

LATERAL TRANSITIONS OF FORMATIONS

St. Anthony Formation (shallow water) and Sudr-/ Dakhla Formations (deep water)

Shallow-water carbonates and siliciclastics of the St. Anthony Formation were deposited from the late Campanian to the late Maastrichtian and are exposed only in an east-west trending belt at the northern rim of the Southern Galala. At these times no such sediments arrived 14 km to the south at St. Paul (Figs. 1, 3), where only sediments of the deeper water Sudr and Dakhla Formations accumulated. Interfingerings with the basinal Sudr and Dakhla Formations are not exposed. In St. Paul shallow-water carbonates of the Southern Galala Formation were deposited only during late Paleocene to early Eocene times. We interpret that this facies change in St. Anthony is due to the proximal position of St. Anthony to the Wadi Araba High (NGWA) in the north that shed shallow-water sediments from a carbonate platform as early as the Campanian/Maastrichtian (Kuss et al. in press).

In area 9, shallow-water sediments were deposited during the Campanian-Maastrichtian (*Exogyra* cf. *overwegi*) (Youssef and Shinnawi, 1954; El-Shinnawi, 1967), possibly equivalent to the St. Anthony Formation. In contrast to area 4 (St. Anthony) where the shallow-water Upper Cretaceous St. Anthony Formation was overlain by the shallow-water Paleocene-Eocene Southern Galala Formation, on Sinai sediments with *Exogyra* cf. *overwegi* were overlain by the deeper water chalks of the Sudr Formation. This contrast of depositional facies could be explained by differences in the vertical movements. While the Northern Galala/Wadi Araba area represents the centre of the NGWA-High, NW-Sinai (area 9) was less affected by this local high.

Southern Galala Formation (shallow water) and Dakhla-/ Esna Formations (deep water)

Similar to the St. Anthony Formation, the Southern Galala Formation is deposited in an east-west trending area in the Galalas and parts of Sinai (Hamam Faraoun). But its areal extension is far larger than that of the St. Anthony Formation. Interfingering between the deeper water deposits of the Dakhla and Esna Formations and the shallow-water limestones of the Southern Galala Formation and the lateral variations within the Dakhla and Esna Formations are best exposed at the two Bir Dakhl sections D2 and D3 (area 2) that are 6 km apart (Figs. 8, 9). In both sections the Southern Galala Formation starts in mid NP5: while the Southern Galala Formation of the

southern D3 section is represented by thin-bedded bioclastic wackestones, chalky-dolomitic limestones and thicker „Dakhla Formation" type shales, the northerly D2 section shows thicker limestones and thinner shales. We assume that this lithologic contrast in the two sections is a result of the closer position of the NGWA carbonate platform to section D2 (Kuss et al. in press) and the contemporary increase of platform-derived carbonates (Figs. 8, 9). An even more pronounced lithologic contrast is evident in the Upper Paleocene to Lower Eocene succession. In the southern D3 section distal equivalents of the Southern Galala Formation are represented only by thin siliciclastic intercalations within the Esna Formation, whereas in the northern D2 section massive siliciclastic limestones with internally reworked clasts have been deposited (units B and D) (Figs. 8, 9).

Area 3 (St. Paul) is a fine example of a ramp to basin transition. Three phases of ramp progradation were observed that are indicated by mass transport deposits of glides, slumps and debris flows. Microfacies analysis provided evidence of a change in the origin of the debris-flow deposits that reflect a transition from a basinal-to-outer-ramp setting to a middle-to-inner-ramp setting including a change in the distribution of biota (Scheibner et al., 2000).

The lithologies of the succession of the northern area of the Northern Galala (area 6) are very similar to those of areas 2 (Bir Dakhl) and 3 (St. Paul) of the Southern Galala. Allochthonous shallow-water carbonates intercalated with hemipelagic marls show the interfingering of limestones derived from the nearby shallow-water platform of the NGWA. On both sides, south and north of the NGWA, similar lithologies with slides, slumps and debris flows are present. The only biostratigraphic data from our sections of area 6 are obtained from marls of the Esna Formation. On Sinai (area 9) Gietl (1998) described similar carbonate dominated successions with debris flows, slumps, intercalated siliciclastics and larger foraminifers of the Late Paleocene-Early Eocene shallow-water Southern Galala Formation. These sedimentary textures occur in Wadi Sudr (north) and Hamam Faraoun (south) and evidence the existence of a palaeotopographic high between both areas.

Southern Galala Formation (shallow water) and Thebes Group (deep water)

The sediments attributed at Bir Dakhl (area 2) and at the northern Northern Galala (area 6) to the lower Serai Formation (Thebes Group) may also be classified as Southern Galala Formation because of basic facies similarities between both, which was not studied within our present contribution (Fig. 6). In that case again an interfingering of the deeper water Thebes Group with the shallow-water derived sediments of the Southern Galala Formation may be deduced from detailed studies on their contacts with the Thebes Group. Snavely et al. (1979) mentioned that the sediments of the lower Thebes Group were deposited as basinwide pelagic carbonates with thin, shallow-water facies near the basin margins.

HIATUSES AND SYNSEDIMENTARY TECTONICS

In the study area 4 types of hiatuses can be distinguished, characterised by variable duration and/or different trigger mechanisms.

Major hiatus from Late Cretaceous to Late Paleocene:

Together with the nowadays eroded Wadi Araba, the southern Northern Galala (area 5) represents an area affected by the Syrian Arc deformation and hence is part of Said's (1961) Unstable Shelf. In the Northern Galala compressional deformation resulted in uplift, erosion, and non-deposition during the Late Cretaceous to Late Paleocene. In the Shabraweet area approximately 70 km north of the NGWA Mohammed and Omran (1991) described a hiatus from the Campanian-Early Eocene similar to the hiatus observed in the Northern Galala. On Sinai area 7 shows similarities to area 5 (middle to south Northern Galala) where a large hiatus is evident across the Cretaceous/Palaeogene boundary as well (Fig. 4a, b). Except for section Ezz el Orban only latest Paleocene sediments occur above the K/Pg boundary. According to Said (1960) and Moustafa and Khalil (1995) the boundary between stable/unstable shelf lies at Wadi Araba and north of area 8 (north of Abu Zenima). Thus, this area shouldn't be affected by the Syrian Arc deformation. But if it was also affected, the boundary between the stable/unstable shelf should be shifted on Sinai south of the area 7.

Another possibility is the presence of a local high with non-deposition for which there is no other evidence yet. Bosworth et al. (1999) demonstrated that the Syrian Arc deformation also affected regions in stable, intraplate settings, at least as far south as the southern part of the Gulf of Suez (Esh el Mellaha Range and Gebel Zeit) due to far-field compressional stress.

In contrast to all other areas described, NW Sinai (area 9) has the most complex and inhomogenous tectonic and depositional history. Probably it could be subdivided into more areas; in areas with larger hiatuses across the K/Pg boundary and in areas with continuous sedimentation. Together with the two southern areas 7 and 8 the depositional history of central western Sinai would be even more complex. The reason for these different depositional histories may lie in the fact that these areas were differently affected by the Syrian Arc deformation. In contrast to the uplift of the NGWA high that lead to erosion and non-deposition during the Late Cretaceous-Late Paleocene in the Northern Galala, the north-western Sinai was less affected by the tectonic processes of the NGWA high (Youssef and Shinnawi, 1954; El-Shinnawi, 1967; Kulbrok, 1996; Gietl, 1998).

Hiatus across the Maastrichtian/Paleocene boundary

A hiatus across the Maastrichtian/Paleocene boundary is evident or inferred in most sections. An exception is St. Paul with the presence of the Upper Maastrichtian nannoplankton *Micula prinsii* Zone and the Lower Paleocene plankton foraminifer Pa zone. The sections in St. Paul are considered one of the most complete across the K/Pg boundary in Egypt, although they are very condensed.

Lüning et al. (1998a) also documented a very complete section ranging across the K/Pg boundary on E-Sinai.

Comparable lithologies, probably of the same stratigraphic range, to area 3 (St. Paul) (Scheibner et al., 2000) are found on Sinai in area 9 (Hamam Faraoun: Kulbrok, 1996; Gietl, 1998). Moreover, the sections Wadi El-Seig/Wadi Hialla (Abbass et al., 1994) evidenced a Late Cretaceous-Palaeogene succession with a stratigraphic range similar to section St. Paul of area 3. Elsewhere a hiatus is present at the K/Pg boundary in most of Egypt and resulted probably from a combination of low sedimentation rates, reworking, changing circulation patterns and sea-level changes (Lüning et al., 1998a).

Hiatus within the Late Paleocene (P3) of Sinai:

Some sections of Wadi Feiran/Abu Zenima (area 8) show a hiatus around P3. We assume similar reasons for this hiatus described for that of the Maastrichtian/Palaeogene boundary. Furthermore, a submarine topographic high may have influenced in combination with some of the above mentioned reasons the Late Paleocene sedimentation processes and finally resulted in the P3 hiatus.

Minor hiatuses:

Short-ranging hiatuses within single biozones are possibly present in all sections. But only in sections with exact biostratigraphic controls based on planktic foraminifers and calcareous nannoplankton these short hiatuses become evident. In sections T1 and T2 (area 1) short hiatuses between P5 and P6 occur, where parts of upper P5 and lower P6 are missing. We interpret these short hiatuses as resulting from times of non-deposition/erosion or very reduced depositional rates, that could not be mapped in detail due to larger sample spacing.

MAASTRICHTIAN TO PALAEOGENE PALAEOGEOGRAPHIC EVOLUTION OF THE NORTHERN GULF OF SUEZ

Figures 10a-10k illustrate the regional evolution of the depositional settings summarised for eleven times slices, defined for calcareous nannoplankton biozones. These time slices were chosen because they characterise the changing of the depositional environments through time best. The CC biozones represent two Maastrichtian time slices, NP1-NP9 represent the Paleocene and NP10-NP12 the Lower Eocene (compare Fig. 4 and Paleocene-Eocene boundary herein).

In areas of non-deposition or eroded areas the palaeogeographic maps illustrate only the absence of time-equivalent sediments today. Whether deposition occurred or not is not indicated because the time of erosion cannot be pinpointed accurately. For comparison of palaeogeographic maps and stratigraphy of areas of major uplift see Fig. 4. Within this stratigraphic/palaeogeographic framework, the Wadi El-Esseila succession (El-Askary and Sheeban, 1993) remains questionable because the stratigraphic subdivision here is in no concordance with the stratigraphic subdivision of the surrounding sections.

CC25 (Fig. 10a): During the middle Maastrichtian biozone CC25 the areas west and north of the northern parts of the Gulf of Suez are characterised by non-deposition that may reflect subaerial exposures or submarine swells. At the western Gulf of Suez they coincide with the NGWA (Northern Galala/Wadi Araba high). The stratigraphic range of the NGWA hiatuses may reach Turonian-Early Paleocene (Kuss and Leppig, 1987; Abd Elshafy and Atta, 1993). The eroded sediments derived from this area were mainly transported southward, where they were deposited as chalky limestones, marls and sandstones of the St. Anthony Formation in the northern parts of the Southern Galala (St. Anthony and Gebel Thelmet sections in Fig. 4a). North of the NGWA no sediments of the St. Anthony Formation are present but only the deeper water chalks of the Sudr Formation (Wadi Nooz, this work; Gebel Um Makhasa, Kulbrok, 1996). The NGWA formed an isolated island surrounded by shallow-water sediments that interfinger with chalks, marly chalks and marls of the deeper water Sudr Formation and Dakhla Formation. In addition to the uplifted area of the NGWA two local areas of non-deposition occur on Sinai (W. El-Esseila of El-Askary and Sheeban, 1993) and in the south of the investigated area (EEO, Morgan 8 and H1 of Masters, 1984). It is not clear, whether these two areas were truly exposed islands, local highs with non-deposition or only the result of later erosion.

CC26 (Fig. 10b): The regional distribution of the depositional settings is least clear within this time-slice because of the poor biostratigraphic data. On W-Sinai we rely mostly on the calcareous nannoplankton data of Abdelmalik et al. (1978) and Marzouk and Hussein (1994). The planktic foraminifers do not offer a better biostratigraphic solution as the *A. mayaroensis* Zone covers also part of CC25 and the index fossil *A. mayaroensis* is very rare in southern Egypt (Luger et al., 1998). The uppermost part of CC26 up to the early Paleocene is probably a time of non-deposition or perhaps exposure in most sections in this area as well as in most of Egypt. During the latest Maastrichtian, chalks, marly chalks and marls of the deeper water Sudr and Dakhla Formations were deposited within a basin that extends from the St. Paul/Bir Dakhl area in the west to the western-central Sinai in the east (e.g. St. Paul area, see above; Wadi El Seig/Hialla, Abbass et al, 1994; Matulla and Nuhkl, Marzouk and Hussein, 1994). It is not clear whether the shallow-water sediments of the St. Anthony Formation were deposited in the Southern Galala or not.

NP1 (Fig. 10c): The early part of NP1 is, similar to the late part of CC26, a time of non-deposition or erosion in the area of investigation (Strougo et al., 1992; Faris, 1997). The basin configuration of the Southern Galala Sub-basin is very similar to that of CC26, from the St. Paul area in the west to the western central Sinai in the east but the prevailing lithologies changed in time. Instead of chalks of the Maastrichtian Sudr Formation, marls and shales of the Dakhla and DTE Formations were deposited in the Early Paleocene.

NP2 (Fig. 10d): During NP2 times, the established basin (Southern Galala Sub-basin) with the marls and shales of the Dakhla and DTE Formations from St. Paul to the western Sinai remains in the same configuration. Additionally, marls of the Dakhla Formation were deposited in the Wadi Tarfa area. All other areas in the north-west (NGWA) and in the south-east (EEO area) are still exposed or areas of non-deposition.

NP3 (Fig. 10e): In NP3 the two isolated basins, both parts of the Southern Galala Sub-basin, with marls of the Dakhla Formation were connected though the Bir Dakhl area. Similar to NP2 the NGWA and the EEO area remain areas of non-deposition.

NP4-lower NP5 (Fig. 10f): The configuration of the Southern Galala Sub-basin remains the same. Additionally, north of the NGWA in the Wadi Nooz area (this work) marly sediments of the Dakhla and DTE Formations prevail.

Upper NP5-lower NP7/8 (Fig. 10g): During this interval, shallow-water deposits of the Southern Galala Formation prograded (Scheibner et al., 2000). Slumps and debris flows evidence the southward progradation starting from the Southern Galala towards the south to the area of Bir Dakhl; and towards the north to the area of Wadi Nooz. This ramp progradation was initiated by a main sea-level drop at the base of P4 (within NP5) as Scheibner et al. (2000) demonstrated in the area of St. Paul (area 3) and Lüning et al. (1998) on Sinai. Speijer and Schmitz (1998) reconstructed a paleodepth curve of that interval based on studies of benthic foraminifers from Gebel Aweina (ca. 300 km to the south). These authors also concluded a sea-level drop during lower P4. In the Southern Galala Sub-basin the marls and shales of the Dakhla or DTE Formations were deposited.

Upper NP 7/8-lower NP9 (Fig. 10h): During these biozones the chalks of the Tarawan Formation were deposited in the south and the east of the NGWA, although on Sinai the Tarawan Formation is very thin or even missing. Here the marly sediments of the DTE Formation were deposited. The shallow-water sediments of the Southern Galala Formation were deposited now on parts of the Northern Galala and in the south (Ras Gharib) the area of non-deposition becomes smaller. Anan (1992) and Lüning et al. (1998a) concluded that the Tarawan Formation on Sinai was deposited during a series of low sea-levels. Luger (1985) and Speijer and Schmitz (1998) on the other hand reported from southern Egypt that the sediments of the Tarawan Formation were deposited during sea-level highstands.

Upper NP 9-lower NP10 (Fig. 10i): The basin configuration of the Southern Galala Sub-basin stays the same but the lithologic character changes again. Now the marls and shales of the Esna and the DTE Formations were deposited. North of the NGWA the sediments of the Southern Galala Formation reach as far east as Gebel Um Makhasa (Kulbrok, 1996).

Upper NP 10-lower NP11 (Fig. 10j): During this interval sediments of the Southern Galala Formation dominate the areas of the NGWA. The only area of non-deposition is on the north-western Sinai (Wadi Sudr, Gietl, 1998; Ain Sudr, Kulbrok, 1996; Mitla Pass, Abdel Gawad and Zalat, 1992). For the first time sediments of the Dakhla and DTE Formations were deposited in the area of Ras Gharib which could be part of a basin Said (1990) described in the Early Eocene around Abu Zenima.

Upper NP 11-NP12 (Fig. 10k): The difference to the previous time slice is the deposition of the limestones of the Thebes Group in the Southern Galala Sub-basin instead of the marls and shales of the Esna and DTE Formations. Shahin (1990) and Lüning et al. (1998a) suggested that the Thebes Group was deposited during a time of a lowered sea level.

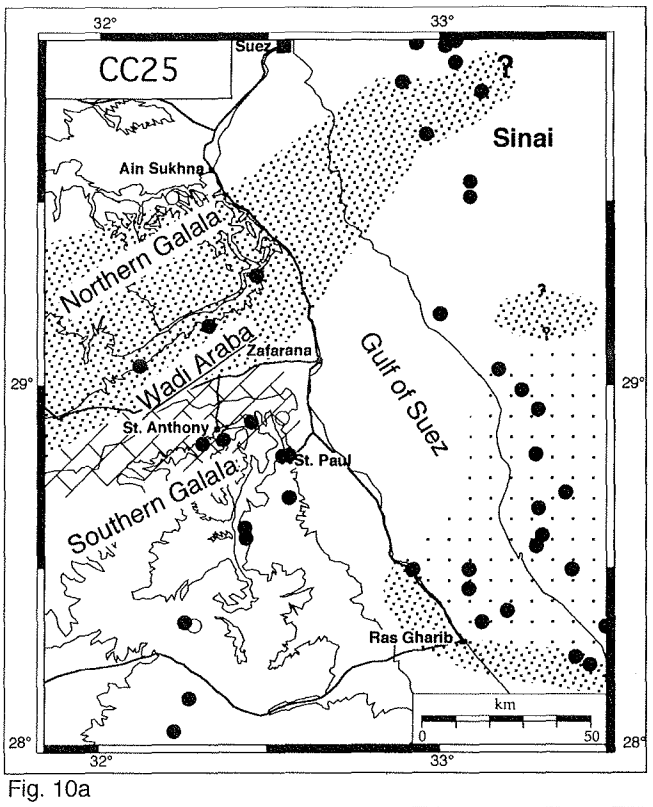

Fig. 10a

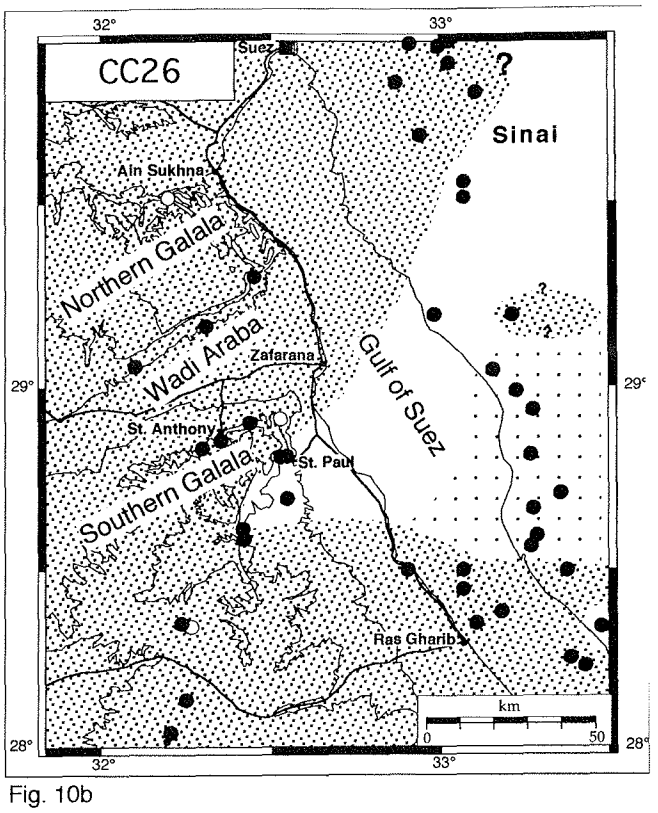

Fig. 10b

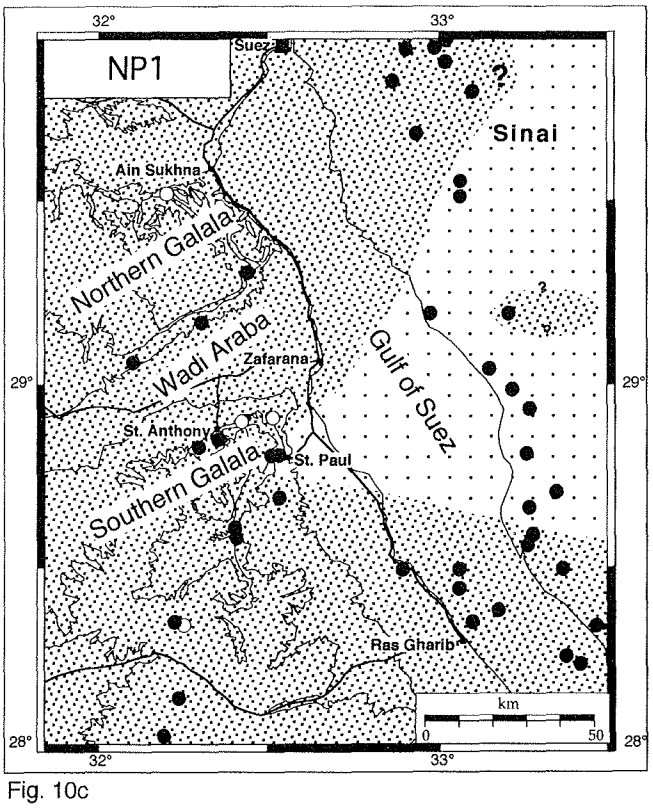

Fig. 10c

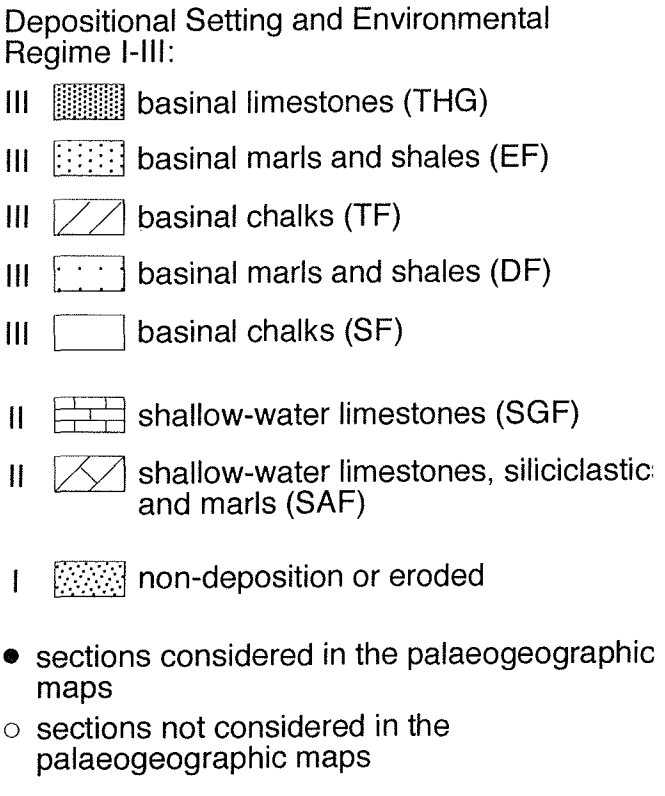

Fig. 10: *Regional palaeogeographic maps of 11 time slices from the Maastrichtian-Early Eocene. In the Maastrichtian the two calcareous nannoplankton biozones of CC25 and CC26 (Fig. 10a, b), in the Paleocene the calcareous nannoplankton biozones of NP1-N10 (Fig. 10c-i) and in the Eocene NP10-NP12 (Fig. 10j,k) were chosen. Three different environmental regimes can be distingushed (I-III). The first regime with hiatuses reflects uplift and erosion or non-depositon (I). The shallow-water influenced shelf and slope deposits of the Late Campanian-Maastrichtian St. Anthony Formation*

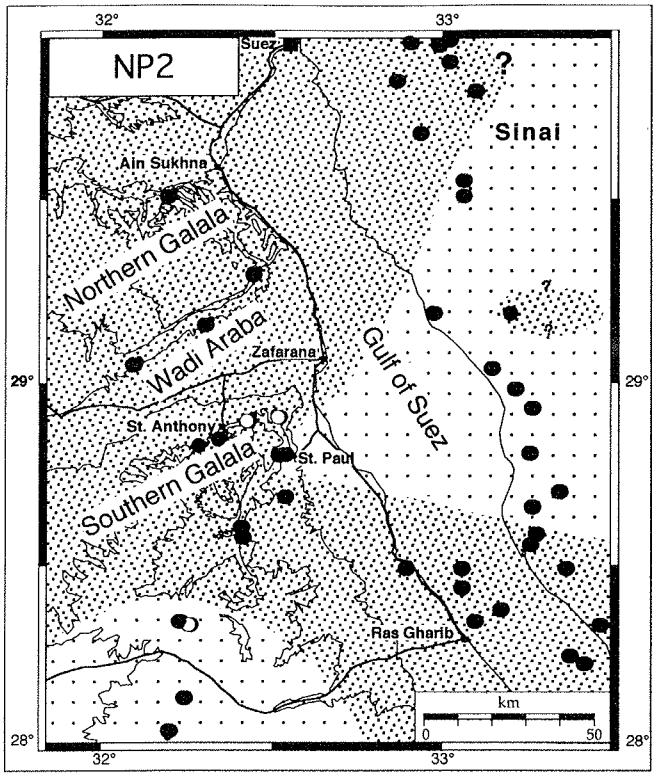

Fig. 10d

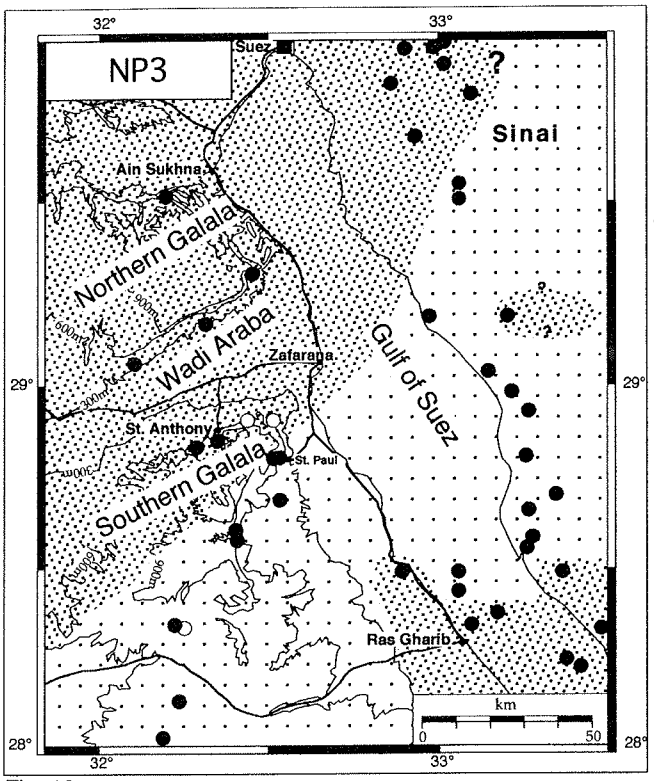

Fig. 10e

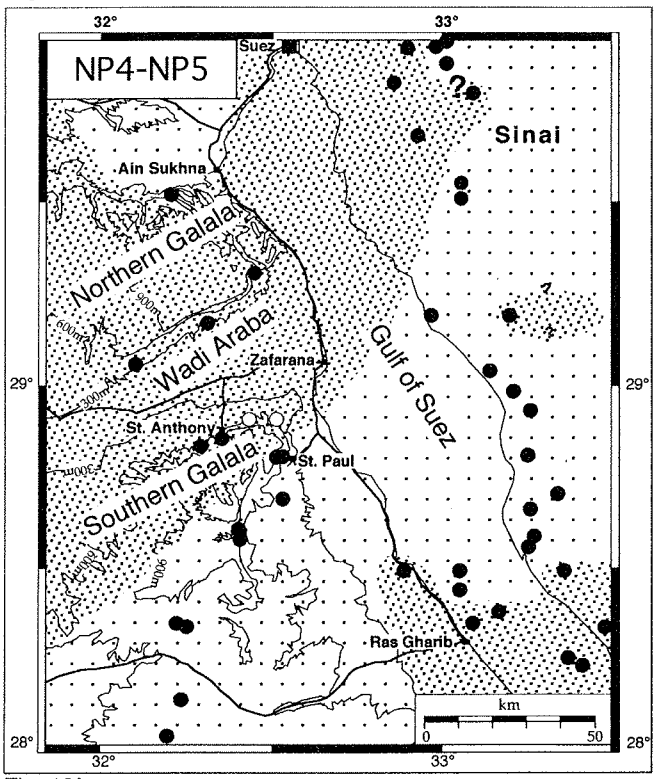

Fig. 10f

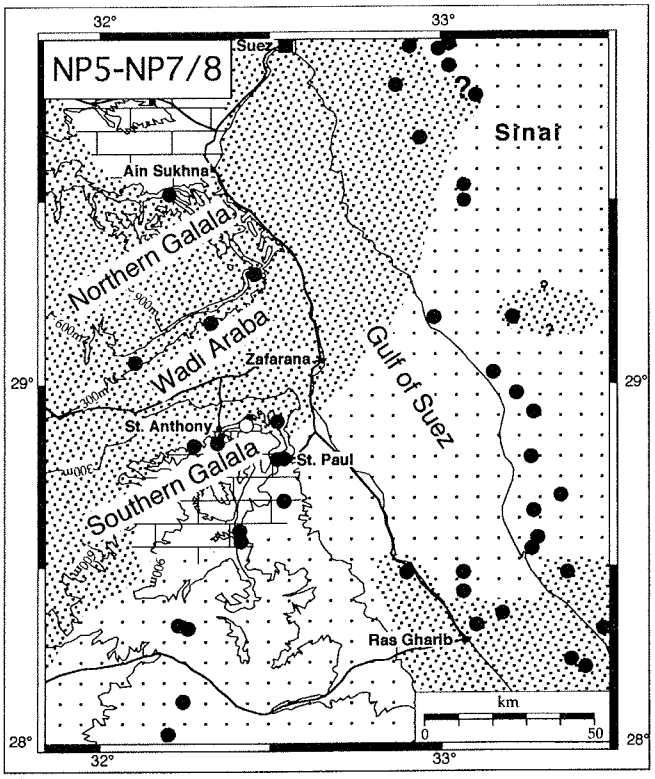

Fig. 10g

Fig. 10 continued: *and the Paleocene-Eocene Southern Galala Formation are the second environmental regime (II). The third regime is represented by the Maastrichtian Sudr Formation and the Paleocene-Eocene Dakhla, Tarawan, Esna Formations, and Thebes Group reflecting basinal lithologies (III). The topographic base-map and the location of sections (with black dots and white dots) refer to Fig. 1. Black dots indicate sections with stratigraphic information, white dots indicate sections with no stratigraphic information, due to non-exposure.*

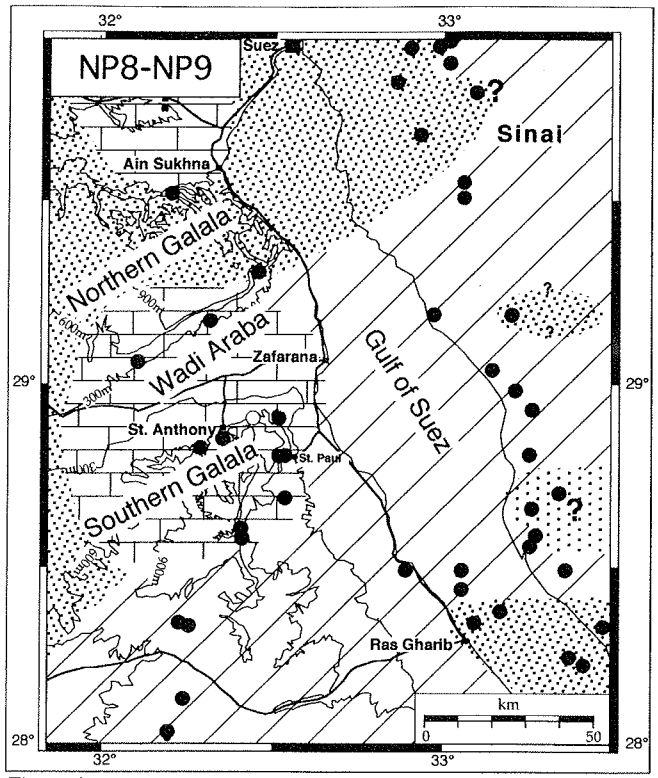

Fig. 10h

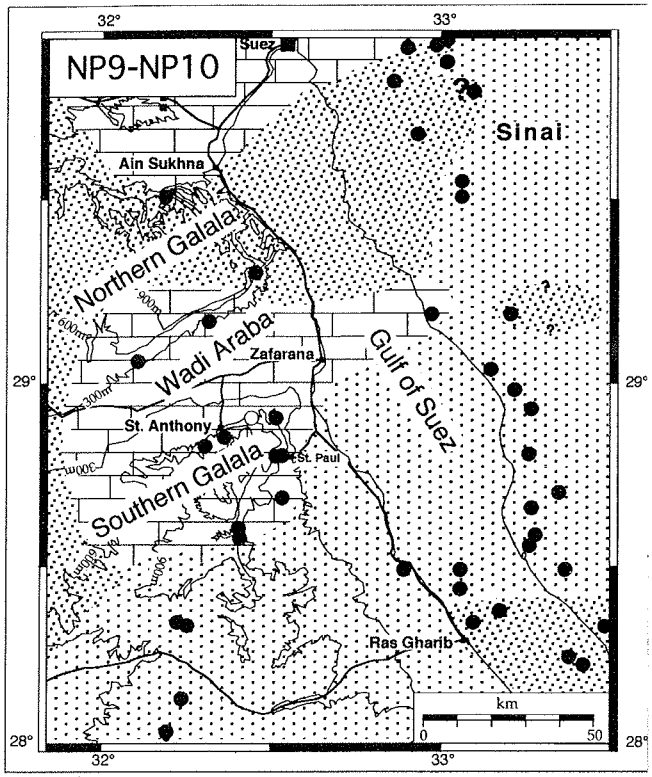

Fig. 10i

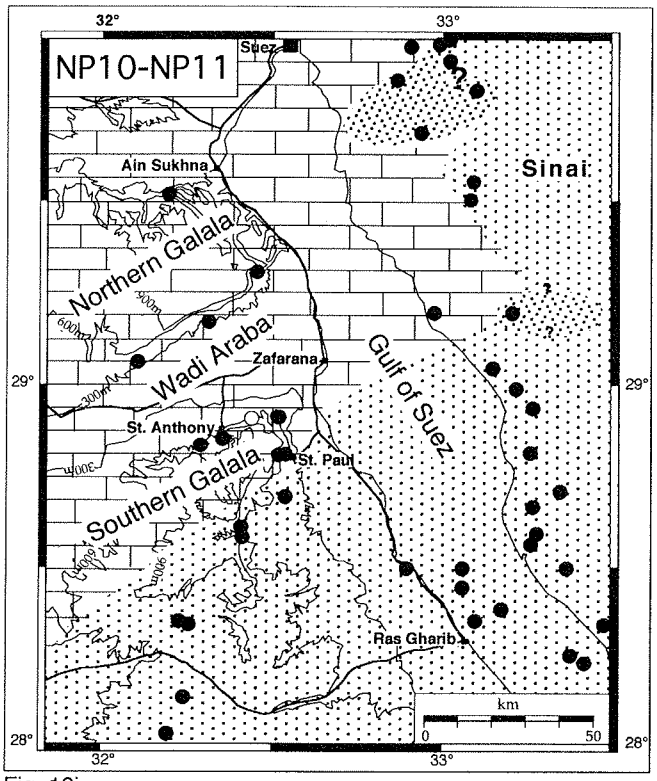

Fig. 10j

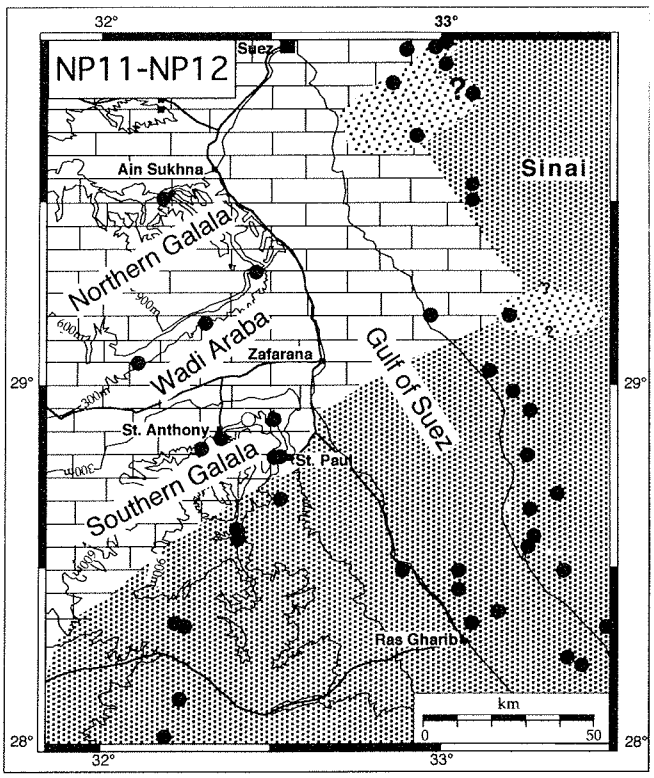

Fig. 10k

CONCLUSIONS

Palaeogeographic changes are evident in the Maastrichtian to Early Eocene deposits in the surrounding of the northern Gulf of Suez based on three environmental regimes: basinal sediments, platform-slope sediments and non-deposition. The basinal sediments include chalks of the Sudr Formation in the Maastrichtian, shaly-marly sediments of the Dakhla, Esna, and Dakhla/Tarawan/Esna (a newly introduced informal formation) Formations and chalks and limestones of the Tarawan Formation in the Paleocene to Early Eocene.

The basinal sediments of the Sudr, Dakhla and Esna Formations interfinger near the structural high of the Northern Galala/Wadi Araba high (NGWA). This high was subaerially exposed during the Late Cretaceous to Early Eocene. The shallow-water-slope deposits of the St. Anthony and Southern Galala Formations were deposited south of this high, whereas north of the high only the sediments of the Southern Galala Formation came to deposition.

Other local highs that led to non-deposition or erosion are present on NW and SW Sinai. Especially the high around Ras Gharib could indicate, that the boundary between stable and unstable Shelf on the Sinai lies farther south.

Four different types of hiatuses could be distinguished, characterised by varying duration and/or different mechanisms (e.g. sea-level changes). At least the palaeogeographical change within calcareous nannozone NP5 resulted from a main sea-level drop.

ACKNOWLEDGEMENTS:

A. M. Bassiouni (Ain Shams University) is especially thanked for many logistic supports and discussions of the stratigraphy. A. M. Morsi (Ain Shams University) is thanked for his open ear for all problems encountered during our stays in Egypt and R. P. Speijer (University of Bremen) helped with planktic foraminifers. R. P. Speijer and A. M. Morsi are also thanked for comments on a previous version of this paper. The manuscript benefited much from the thoroughly revision of S. Lüning (LASMO, London). A. Scharf, R. Bätzel and M. Brinkmann (all from the University of Bremen) helped with sample preparation. The investigations were funded by the Graduiertenkolleg „Stoff-Flüsse in marinen Geosystemen" of the University of Bremen and the German Science Foundation (DFG).

Table 1: *Newly measured sections and sections from the literature. If coordinates are given in the literature they are mentioned. Coordinates with a star do not indicate geographical points but geographical ranges given by the authors.*

Area	Profile/Location	Coordinates	Author
1	WHS/Wadi Hawashiya	without exact location	Kassab and Keheila, 1994
	WTS/Wadi Tarfa	without exact location	Kassab and Keheila, 1994
	O/Wadi Hawashiya	140 km east of El Sheikh fadl	El-Dawy, 1999
	S/Wadi Hawashiya	151 km east of El Sheikh fadl	El-Dawy, 1999
	T1/Wadi Hawashiya	N 28°13,52´; E 32°13,64´	This work
	T2/Wadi Tarfa	N 28°27,31´; E 32°13,73´	This work
	Section 11/Wadi Tarfa	without exact location	Nishi et al. 1994
	Section U/Wadi Tarfa	without exact location	Bandel et al. 1987
	Wadi Tarfa	without exact location	Tantawy et al. 2000
2	D3/Bir Dakhl	N 28°36,43´; E 32°23,77´	This work
	D2/Bir Dakhl	N 28°39,61´; E 32°23,59´	This work
	WD/Wadi Dakhl	without exact location	Strougo and Faris, 1993
	Abu Rimth 1-3	N 28°43´; E32°,30´	Gietl 1998
	Bir Dakhl	without exact location	Metwally and El Azeam, 1997
3	S9/St. Paul	N 28°50,37´; E 32°31,53´	Kuss et al. 2000
	S1-S8/St. Paul	N 28°50,72´; E 32°31,29´	Scheibner et al., 2000
	St. Paul	N 28°50,63´; E 32°32,62´	Strougo et al. 1992
	St. Paul	N 28°50,63´; E 32°32,62´	Haggag (1991)
	St. Paul	without exact location	Ismail and Abdallah, 1966; Abdou et al., 1969; Mazhar et al., 1979; Strougo, 1986; Bandel and Kuss, 1987; Girgis, 1987; Kuss and Leppig, 1989; Faris, 1997; Kulbrok, 1996; Boukhary et al., 1998
4	A1/St. Anthony	N 28°54,95´; E 32°21,21´	Kuss and Leppig, 1989; Kulbrok, 1996; this work
	A3/E of St. Anthony	N 28°56,72´; E 32°25,14´	this work
	Wadi Askhar	without exact location	Selima and Askalany, 1996
	St. Anthony	without exact location	Zittel, 1883; Awad and Abdallah, 1966; Kuss, 1986; Bandel and Kuss, 1987; Kuss and Malchus, 1989; Malchus, 1990; Kuss et al, 2000
	GT/Gebel Thelmet	without exact location	Abdel-Kireem and Abdou, 1979
	Gebel Thelmet	without exact location	Hottinger, 1960; Abdallah et al., 1970; Abdallah and Eissa, 1970; Abdel-Kireem, 1971; Mazhar et al., 1979; Kulbrok, 1996
5	20/2/S North Galala	without exact location	Kuss and Leppig, 1989; Malchus, 1990
	AD/Abu Darag	without exact location	Abd-El Azeam and Metwally, 1998
	Camp/S North Galala	without exact location	Gietl, 1998
	Several/S North Galala	without exact location	Abd-Elshafy and Atta, 1993
6	N1/Wadi Nooz	N 29°31,86´; E 32°11,24´	This work
	Wadi Nooz	without exact location	Gietl, 1998
	Wadi Noat/Wadi Nooz	without exact location	Abd Elshafy and Atta, 1993
7	EEO/Ezz-El-Orban	without exact location	Ansary and Fahmy, 1969 Barakat and Fahmy, 1969
	Qabeliat	without exact location	Marzouk and Abou-El-Enein, 1997
	J1/Gulf of Suez	without exact location	Masters, 1984 (Kerdany and Salem, 1970)
	Alef Well/Gulf of Suez	without exact location	Masters, 1984 (Kerdany and Salem, 1970)
	Morgan 8/Gulf of Suez	without exact location	Masters, 1984 (Kerdany and Salem, 1970)
	H-1 Well/Gulf of Suez	without exact location	Masters, 1984 (Kerdany and Salem, 1970)
	G. Araba/Gebel Araba	without exact location	Masters, 1984
8	AZ/Abu Zenima	without exact location	Anan, 1992
	Matulla	without exact location	Shahin, 1992; Ismail, 1992; Marzouk and Hussein 1994; Ismail, 1996; Obaidalla, 1999
	Nezzazat	without exact location	Shahin, 1992
	Nuhkl	without exact location	Marzouk and Hussein, 1994

Area	Profile/Location	Coordinates	Author
	BEM/Bir El-Markha	without exact location	Abdelmalik, 1978a,b
	Qabeliat	without exact location	Ismail, 1992
	W-Feiran	without exact location	Shahin, 1992
	W-Feiran	without exact location	Marzouk and Abou-El-Enein, 1997
	W. Feiran	without exact location	Masters, 1984
	Gebel Ekma	without exact location	Shahin, 1990
	E-Bakr Marine 1/Gulf of Suez	without exact location	Masters, 1984 (Kerdany and Salem, 1970)
	E-Feiran	without exact location	Masters, 1984
	W. Feiran	without exact location	Masters, 1984
	E. Gharib/Gulf of Suez	without exact location	Masters, 1984 (Kerdany and Salem, 1970)
	Gebel Qabeliat	without exact location	Faris et al., 1986; Allam and Khalil, 1989
	4 Sections/Abu Rudeis	without exact location	Cherif et al., 1989
	Gebel Nezzazat	without exact location	Arafa 1991
	SE Nezzazat/Wadi Feiran	without exact location	El Sheikh and El Beshtawy, 1992
	some sections/Wadi Feiran	without exact location	El Deeb and El Gammal, 1997
	Wadi Nukhl	without exact location	Monechi et al., 1999
	W. Feiran	*N 28°40´-50´; E 33°20´-30´	Eweda and El-Sorogy, 1999
9	Gindi/Gebel Gindi	without exact location	Ismail, 1992; Ismail, 1996
	Gebel Um Makhasa	without exact location	Kulbrok, 1996
	Gebel Gindi	without exact location	Kulbrok, 1996
	Wadi Sudr	N 29°50,34´; E 33°05,08´	Gietl, 1998
	Wadi Sudr	without exact location	Youssef and Shinnawi, 1954; El-Shinnawi, 1967
	Ain Sudr/Wadi Sudr	without exact location	Kulbrok, 1996
	N Ain Sudr/Wadi Sudr	without exact location	Kulbrok, 1996
	Mitla Pass	without exact location	Abdel Gawad and Zalat, 1992
	Wadi El-Seig	*N 33°00´-11´; E 29°30´-45´	Abbas et al., 1994
	Wadi Hialla	*N 33°00´-11´; E 29°30´-45´	Abbas et al., 1994
	Wadi El-Esseila	*N 33°12´-15´; E 29°10´-13´	El Askary and Shaaban, 1993
	Hamam Faraoun 1-3	N 29°11,71´; E 32°57,33´	Kulbrok, 1996; Gietl, 1998
	Kala't al Gindi/Gebel El-Raha	without exact location	Hamza et al., 1997
	Ras Al-Giffa/Gebel El-Raha	without exact location	Hamza et al., 1997
	Gebel Mitla/Gebel El-Raha	without exact location	Hamza et al., 1997

REFERENCES

Abbass, H.L., 1994. Maastrichtian-Early Eocene benthonic foraminifera from West Central Sinai and their importance to stratigraphy and paleoecology. Bulletin Faculty of Science, Assiut University 23 (2F), 11-35.

Abdallah, A.M.Eissa, A., 1970. The Campanian rocks of the Southern Galala, A.R.E. Bulletin Faculty Science, Cairo University 44, 259-271.

Abdallah, A.M., Sharkawi, M.A.E., Marzouk, A., 1970. Geology of Mersa Thelmet area, southern Galala, Eastern Desert, A.R.E. Bulletin Faculty Science, Cairo University 44, 271-280.

Abd-Elazeam, S., Metwally, M.H.M., 1998. Stratigraphy of Abu Darag Upper Cretaceous, with some regional aspects on the related sediments in the western side of the Gulf of Suez, Egypt. Middle East Research Center, Ain Shams University, Earth Science Services 12, 90-105.

Abdel-Gawad, G.I., Zalat, A., 1992. Some Upper Cretaceous macroinvertebrates from Gebel El-Hamra and Gebel Um Heriba, Mitla Pass, Western-Central Sinai, Egypt. In: Sadek, A. (Eds.), Geology of the Arab World, Cairo Univ., pp. 333-344.

Abdel-Kireem, M.A., 1971. Contributions to the stratigraphy of Gebel Thelmet area, South Galala Plateau, Eastern Desert, Egypt. Bulletin of Faculty of Science, Alexandria 11, 71-86.

Abdel-Kireem, M.R., Abdou, H.F., 1979. Upper Cretaceous-Lower Tertiary planktonic foraminifera from South Galala Plateau, Eastern Desert, Egypt. Revista Espanola de Micropaleontologica 11, 175-222.

Abdelmalik, W.M., Bassiouni, A.A., Obeid, F.L., 1978a. Biostratigraphy of Upper Cretaceous-Lower Tertiary rocks from West Central Sinai 1.- planctonic foraminifera. Actes du VI Colloque Africain de Micropaléontologie 181-215.

Abdelmalik, W.M., Bassiouni, M.A., Kerdany, M.T., Obeid, F.L., 1978b. Biostratigraphy of Upper Cretaceous-Lower Tertiary rocks from West Central Sinai 2. Calcareous Nannoplankton. Actes du VI Colloque Africain de Micropaléontologie 217-241.

Abd-Elshafy, E., 1988. On some problematic mesozoic exposures on the western side of the Gulf of Suez, Egypt. Bulletin Faculty of Science, Zagazig University 10, 61-86.

Abd-Elshafy, E., Atta, M., 1993. Cretaceous-Tertiary boundary in the Northern Galala, Gulf of Suez, Egypt. Bulletin Faculty of Science, Zagazig University 15, 246-262.

Abdou, H.F., Naim, E.M., Sultan, I.Z., 1969. Biostratigraphic studies on the Lower Tertiary rocks of Gebel Umm Rokham and Saint Paul area, Eastern Desert, Egypt. Bulletin of the Faculty of Science, Alexandria 9, 271-299.

Abu Khadrah, A.M., Darwish, M., Azabi, M.H.E., Fattah, M.A.A., 1987. Lithostratigraphy of the Upper Cretaceous-Tertiary succession in the Gulf of Suez (Southern Galala Plateau), Egypt. In: Matheis, G., Schandelmeier, H. (Eds.), Current research in African earth sciences. Balkema, pp. 171-176.

Allam, A., Khalil, H., 1989. Geology and stratigraphy of Gebel Qabeliat Area, southwestern Sinai, Egypt. Journal of African Earth Sciences 9, 59-67.

Anan, H.S., 1992. Maastrichtian to Ypresian stratigraphy of Abu Zenima section, west central Sinai, Egypt. Middle East Research Center, Ain Shams University, Earth Science Services 6, 62-68.

Ansary, S.E., Famy, S.E., 1969. Zonal stratigraphy of subsurface Paleogene deposits at Ezz El Orban Area, Gulf of Suez. J. Geol. U.A.R 13, 49-60.

Arafa, A.E.R.A., 1991. Biostratigraphic zonation of the late Cretaceous sediments of Galal Nazzazat, south-west Sinai, Egypt. Annals Geological Survey Egypt 17, 173-182.

Aubry, M.P., 1995. Towards an upper Paleocene-lower Eocene high resolution stratigraphy based on calcareous nannofossil stratigraphy. Israelian Journal of Earth Sciences 44, 239-253.

Aubry, M.P., Berggren, W.A., Cramer, B., Dupuis, C., Kent, D.V., Ouda, K., Schmitz, B., Steurbaut, E., 1999. Paleocene/Eocene boundary sections in Egypt. In: Soliman, H.A., Ouda, K.A.K. (Eds.), Symposium on Late Paleocene-Early Eocene Events from North Africa to the Middle East within The First International Conference on the Geology of Africa, Assiut, Egypt, pp. 1-11.

Awad, G.H., Ghobrial, N.G., 1965. Zonal stratigraphy of the Kharga Oasis. Geol. Surv. Egypt Paper 34, 1-77.

Awad, G.H., Abdallah, A.M., 1966. Upper Cretaceous in Southern Galala, Eastern Desert with ephasis on neighbouring areas. J. Geol. U.A.R. 10, 125-144.

Bandel, K., Kuss, J., 1987. Depositional environment of the pre-rift sediments - Galala Heights (Gulf of Suez, Egypt). Berliner geowiss. Abh. A 78, 1-48.

Bandel, K., Kuss, J., Malchus, N., 1987. The sediments of Wadi Qena (Eastern Desert, Egypt). Journal of African Earth Sciences 6, 427-455.

Barakat, M.G., Fahmy, S.E., 1969. Lithofacies and biofacies in the Lower Paleogene of Ezz El Orban Area. Proc. of the 3. African Micropal. Coll., Cairo, 107-112.

Barron, T., Hume, W.F., 1902. Topography and geology of the Eastern Desert of Egypt (Central Portion). Egyptian Survey Department, Cairo.

Bartov, Y., Steinitz, G., 1977. The Judea and Mount Scopus Groups in the Negev and Sinai with trend surface analysis of the thickness data. Israelian Journal of Earth Sciences 26, 119-148.

Beadnell, H.J.L., 1905. The relations of the Eocene and Cretaceous systems in the Esna-Aswan reach of the Nile Valley. Quart. J. geol. Soc. London 61, 667-678.

Beadnell, H.J.L., 1927. The wilderness of Sinai. Arnold, London.

Benjamini, C., 1992. The Paleocene-Eocene boundary in Israel - a candidate for the boundary stratotype. Neues Jahrbuch für Geologie und Paläontologie, Abhandlungen 186, 49-61.

Berggren, W.A., Kent, D.V., Swisher III, C.C., Aubry, M.P., 1995. A revised Cenozoic geochronology and chronostratigraphy. In: Berggren, W.A., Kent, D.V., Aubry, M.P., Hardenbol, J. (Eds.), Geochronolgy, time scales, and global stratigraphic correlation. SEPM Special Publication 54, pp. 129-212.

Bosworth, W., Guiraud, R., Kessler II, L.G., 1999. Late Cretaceous (ca. 84 Ma) compressive deformation of the stable platform of northeast Africa (Egypt): Far-field stress effects of the "Santonian event" and origin of the Syrian arc deformation belt. Geology 27, 633-636.

Boukhary, M., Abdelmalik, W., 1983. Revision of the stratigraphy of the Eocene deposits in Egypt. Neues Jahrbuch für Geologie und Paläontologie, Abhandlungen 321-337.

Boukhary, M., Kulbrok, F., Kuss, J., 1998. New nummulitids from lower Eocene limestones of Egypt (Monastery of St. Paul, Eastern Desert). Micropaleontology 44, 99-108.

Camoin, G., Bellion, Y., Dercourt, J., Guiraud, R., Lucas, J., Poisson, A., Ricou, L.E., Vielrynck, B., 1993. Late Maastrichtian Palaeoenvironments (69.5-65). In: Dercourt, J., Ricou, L.E., Vrielynck, B. (Eds.), Atlas Tethyan paleoenvironmental maps. BEICIP-FRANLAP.

Cherif, O.H., Al-Rifaiy, I.A., Al-Afifi, F.I., Orabi, O.H., 1989. Planktonic foraminifera and chronostratigraphy of Senonian exposures in wes-central Sinai, Egypt. Revue de Micropaléontologie 32, 167-184.

Cherif, O.H., Ismail, A.A., 1991. Late Senonian-Tertiary planktonic foraminiferal biostratigraphy and tectonism of the Esh-el-Mallaha and Gharamul areas, Egypt. Middle East Research Center, Ain Shams University, Earth Science Services 5, 146-159.

El Askary, M.A., Shaaban, M.N., 1993. On the geology of the Wadi El-Esseila area, western Central Sinai, Egypt. Neues Jahrbuch für Geologie und Paläontologie, Abhandlungen H 3, 181-192.

El-Dawoody, A.S., 1992. Review on the biostratigraphy of the Late Paleocene/Eocene succession in Egypt. In: Sadek, A. (Eds.), Geology of the Arab World, Cairo Univ., pp. 407-432.

El-Dawy, M.H., 1999. Paleocene benthic foraminiferal biostratigraphy an paleobathymetry in the sections between El Sheikh Fadl and Ras Gharib, Eastern Desert, Egypt. In: Soliman, H.A., Ouda, K.A.K. (Eds.), Symposium on Late Paleocene-Early Eocene Events from North Africa to the Middle East within The First International Conference on the Geology of Africa, Assiut, Egypt, pp. 24-30.

El Deeb, W.Z.M., El Gammal, R.M.H., 1997. Foraminiferal paleoecologic study of the Maastrichtian-Ypresian succession in southwest Sinai, Egypt. Middle East Research Center, Ain Shams University, Earth Science Services 11, 37-50.

El-Naggar, Z.R., 1966a. Stratigraphy and classification of type Esna Group of Egypt. Bull. Am. Assoc. Petrol. Geol. 50, 1455-1477.

El-Naggar, Z.R., 1966b. Stratigraphy and planktonic foraminifera of the upper Cretaceous-lower Tertriary succession in the Esna-Idfu region, Nile Valley, Egypt, U.A.R. Bulletin of the British Museum (natural history) Geology, London.

El-Naggar, Z.R., 1968. Stratigraphy and classification of type Esna Group of Egypt: Reply. Bull. Am. Assoc. Petrol. Geol. 52, 1794-1798.

El Sheikh, H.A., El Beshtawy, M.K., 1992. Biostratigraphic studies on the Late Cretaceous Early Tertiary between Wadi Tayiba and Wadi Feiran, West Central Sinai, Egypt. In: Sadek, A. (Eds.), Proc. 1st Int. Conf. Geology of the Arab World, Cairo Univ., pp. 395-406.

El-Shinnawi, M.A., 1967. Contributions to the stratigraphy of the white chalk formation at Wadi Sudr, western Sinai, U.A.R. Bull. Fac. of Science, Alexandria Univ. 8, 199-217.

Eweda, S., El-Sorgy, A.S., 1999. Stratigraphy and facies development of the Upper Cretaceous-Lower Tertiary succession in Wadi Feiran area, southwestern Sinai, Egypt. Neues Jahrbuch für Geologie und Paläontologie, Abhandlungen 211, 263-289.

Faris, M., Allam, A., Khalil, H.M., 1986. Early Eocene planktonic foraminifera and calcareous nannofossil biostratigraphy of Gebel Qabeliat, Southwest Sinai, Egypt. Egypt. J. Geol. 30, 71-88.

Faris, M., 1997. Late Cretaceous and Paleocene calcareous nannofossil biostratigraphy at St. Paul section, Southern Galala Plateau, Egypt. Annals Geol. Surv. Egypt 20, 527-538.

Faris, M., Strougo, A., 1998. The lower Libyan in Farafra (Western Desert) and Luxor (Nile Valley): Correlation by calcareous nannofossils. Middle East Research Center, Ain Shams University, Earth Science Services 12, 137-156.

Ghorab, M.A., 1961. Abnormal stratigraphic features in Ras Gharib oilfield. 3rd Arab Petrol. Congr., Alexandria, pp. 10.

Gietl, R., 1998. Biostratigraphie und Sedimentationsmuster einer nordostägyptischen Karbonatrampe unter Berücksichtigung der Alveolinen-Faunen. Berichte aus dem Fachbereich Geowissenschaften der Universität Bremen 112, 135.

Girgis, M.G., 1987. A morphometric analysis of the Arkhangelskiella group and its stratigraphical and palaeoenvironmental importance. In: Crux, J.A., van Heck, S.E. (Eds.), Nannofossils and their application. Ellis Horwood Ltd., pp. 327-339.

Haggag, M.A., 1991. Planktonic foraminiferal groups and zonation of the Paleocene/Eocene of the South Galala and environs. Egypt. J. Geology 35, 37-50.

Hamza, F., Ziko, A., Kamel, S., 1997. Biostratigraphical analysis of the Lower Paleogene succession in the Nort-central Sinai, Egypt. Neues Jahrbuch für Geologie und Paläontologie, Abhandlungen 204, 321-352.

Hermina, M., Lindenberg, H.G., 1989. The Tertiary. In: Hermina, M., Klitzsch, E., List, F.K. (Eds.), Stratigraphic lexicon and explanatory notes to the geological map of Egypt 1:500 000. Conoco Inc., pp. 141-217.

Hermina, M., Klitzsch, E., List, F.K., 1989. Stratigraphic lexicon and explanatory notes to the Geological Map of Egypt 1:500 000. 264. Conoco, Cairo.

Hewaidy, A., 1987. Biostratigraphy and paleobathymetry of the Esna shale in El Qusaima area, north-east Sinai, Egypt. Middle East Research Center, Ain Shams University, Earth Science Services 1, 180-206.

Hottinger, L., 1960. Recherches sur les Alvéolines du Paléocène et de l«Eocéne. Schweizerische Palaeontologische Abhandlungen 75/76, 1-243.

Hume, W.F., 1912. Explanatory notes to accompany the geological map of Egypt. Egyptian Survey Department, Cairo.

Ismail, A.A., 1992. Maastrichtian-Early Eocene benthic foraminiferal biostratigraphy and paleoecology of west central Sinai, Egypt. Middle East Research Center, Ain Shams University, Earth Science Services 6, 139-150.

Ismail, A.A., 1996. Biostratigraphy and palaeoecology of Maastrichtian-Early Eocene ostracods of west-central Sinai, Egypt. Revue de Pal_obiologie 15, 37-54.

Ismail, M.M., Abdallah, A.M., 1966. Contribution to the stratigraphy of St. Paul Monastery area by microfacies. Bulletin of the Faculty of Science, Alexandria 12, 325-334.

Issawi, B., 1969. The geology of the Kurkur-Dungul area. Annals Geological Survey Egypt 1, 53-92.

Issawi, B., 1972. Review of Upper Creatceous-Lower Tertiary Stratigraphy in Central and Southern Egypt. Bull. Am. Assoc. Petrol. Geol. 56, 1448-1463.

Issawi, B., El Hinnawi, M., Francis, M., Mazhar, A., 1999. The Phanerozoic geology of Egypt: A geodynamic approach. The Egyptian Geological Survey, Cairo.

Kassab, A.S., Keheila, E.A., 1994. Paleocene biostratigraphy and sea level changes of the northern Eastern Desert of Egypt. Newsl. Stratigr. 31, 85-100.

Kerdany, M.T., Abdel Salam, A.A., 1970. Bio- and lithostratigraphic studies of the pre-Miocene of some offshore exploration wells in the Gulf of Suez. 7th Arab Petrol. Congr., Kuwait, pp. 1-22.

Krenkel, E., 1925. Geologie Afrikas, erster Teil. Gebrüder Bornträger, Berlin.

Kulbrok, F., 1996. Biostratigraphie, Fazies und Sequenzstratigraphie einer Karbonatrampe in den Schichten der Oberkreide und des Alttertiärs Nordost-Ägyptens (Eastern Desert, N«Golf von Suez, Sinai). Berichte aus dem Fachbereich Geowissenschaften der Universität Bremen 81, 1-216.

Kuss, J., 1986. Facies develpment of Upper Cretaceous-Lower Tertiary sediments from the monastery of St. Anthony/Eastern Desert, Egypt. Facies 15, 177-194.

Kuss, J., Leppig, U., 1989. The early Tertiary (middle-late Paleocene) limestones from the western Gulf of Suez, Egypt. Neues Jahrbuch für Geologie und Paläontologie, Abhandlungen 177, 289-332.

Kuss, J., Malchus, N., 1989. Facies and composite biostratigraphy of late Cretaceous strata from northeast Egypt. In: Wiedmann, J. (Ed.), Cretaceous of the Western Tethys. Schweizerbart´sche Verlagsbuchhandlung, pp. 879-910.

Kuss, J., Scheibner, C., Gietl, R., in press. Carbonate Platform to Basin Transition along an Upper Cretaceous to Lower Tertiary Syrian Arc Uplift, Galala Plateaus, Eastern Desert, Egypt. Geoarabia 5/3.

LeRoy, L.W., 1953. Biostratigraphy of the Maqfi section, Egypt. Memoir Geological Society America 54, 1-73.

Luger, P., 1985. Stratigraphie der marinen Oberkreide und des Alttertiärs im südwestlichen Obernil-Becken (SW-Ägypten) unter besonderer Berücksichtigung der Mikropaläontologie, Palökologie und Paläogeographie. Berliner Geowissenschaftliche Abhandlungen A 63, 151.

Luger, P., El-Beshtawy, M., May, H., 1998. Maastrichtian planktonic foraminiferal biozonation and K/T boundary in central Egypt. Revista Espanola de Micropaleontología 30, 37-49.

Lüning, S., Marzouk, A.M., Kuss, J., 1998a. The Paleocene of central East Sinai, Egypt:"sequence stratigraphy" in monotonous hemipelagites. Journal of Foraminiferal Research 28, 19-39.

Lüning, S., Marzouk, A.M., Kuss, J., 1998b. Late Maastrichtian high frequency litho- and ecocycles from the hemipelagic of Eastern Sinai. Journal of African Earth Sciences 27, 373-395.

Malchus, N., 1990. Revision der Kreide-Austern (Bivalvia: Pteriomorphia) Ägyptens (Biostratigraphie, Systematik). Berliner Geowissenschaftliche Abhandlungen Reihe A, 231.

Martini, E., 1971. Standard Tertiary and Quaternary calcareous nannoplankton zonation. In: Farinacci, A. (Eds.), Proceedings of the second planktonic conference, Roma 1970. pp. 739-785.

Marzouk, A.M., Hussein, A.I.M., 1994. Carcareous nannofossil zonation of the Esna Shale in Abu Zenima Area, W. Central Sinai, Egypt. Al - Azhar Bull. Sci. 5, 157-169.

Marzouk, A.M., Abou-El-Enein, M.K., 1997. Calcareous nannofossil biostratigraphy of the Late Cretaceous-Early Tertiary of Wadi Feiran and Gebel Qabeliat, SW Sinai, Egypt. Journal of Nannoplankton Research 19, 113-121.

Marzouk, A.M., Lüning, S., 1998. Comparative biostratigraphy of calcareous nannofossils and planktonic foraminifera in the Paleocene of the Eastern Sinai, Egypt. Neues Jahrbuch für Geologie und Paläontologie, Abhandlungen 207, 77-105.

Masters, B.A., 1984. Comparison of planktonic foraminifers at the Cretaceous-Tertiary boundary from the El Haria Shale (Tunisia) and the Esna Shale (Egypt). Proceedings of the 7th Exploration Seminar, EGPC, Cairo, pp. 310-324.

Mazhar, A., Enany, N., Abdel Kader, Y., 1979. Contributions to the Cretaceous-Early Tertiary stratigraphy of El Galala El Qibliya Plateou. Annals of the Geological Survey of Egypt 9, 377-387.

Metwally, M.H.M., Abd El Azeam, S., 1997. Paleoecological analysis and environmental development of the Upper Cretaceous, Southern Galala, Gulf of Suez, Egypt. Neues Jahrbuch für Geologie und Paläontologie, Abhandlungen 203, 273-293.

Mohammad, M.H., Omran, M.A., 1991. Stratigraphy and depositional history of the sedimentary sequence and Shabraweet area, southern Ismailia, Egypt. Middle East Research Center, Ain Shams University, Earth Science Services 5, 16-30.

Monechi, S., Angori, E., Speijer, R.P., 1999. Upper Paleocene stratigraphy: northern versus southern Tethys. In: Andreasson, F.P., Schmitz, B., Thompson, E.I. (Eds.), Early Paleogene warm climates and biosphaere dynamics, Göteborg, unpaginated.

Moustafa, A.R., Khalil, M.H., 1995. Superposed deformation in the northern Suez Rift, Egypt: Relevance to hydrocarbons exploration. Journal of Petroleum Geology 18, 245-266.

Nakkady, S.E., 1950. A new foraminiferal fauna from the Esna Shales and upper Cretaceous chalk of Egypt. Journal of Paleontology 24, 675-692.

Nakkady, S.E., 1957. Biostratigraphy and inter-regional correlation of the upper Senonian and lower Paleocene of Egypt. Journal of Paleontology 31, 428-447.

Nishi, H., Elewa, A.M.T., Ishizaki, K., 1994. Planktonic foraminiferal biostratigraphy of upper Paleocene to middle Eocene sequences in the Eastern Desert Aerea, Egypt. Trans. Proc. Palaeont. Soc. Japan 175, 521-552.

Norris, R.D., Kroon, D., Klaus, A., 1998. Explanatory notes. Proceedings of the Ocean Drilling Program Initial Reports 171B, 11-44.

Obaidalla, N.A., 1999. Planktic foraminiferal biostratigraphy of the Paleocene/Eocene boundary transition in southwestern Sinai, Egypt. In: Soliman, H.A., Ouda, K.A.K. (Eds.), Symposium on Late Paleocene-Early Eocene Events from North Africa to the Middle East within The First International Conference on the Geology of Africa, Assiut, Egypt, pp. 31-37.

Perch-Nielsen, K., 1985. Mesozoic calcareous nannofossils. In: Bolli, H.M., Saunders, J.B., Perch-Nielsen, K. (Eds.), Plankton stratigraphy. Cambridge University Press, pp. 329-426.

Romein, A.J.T., 1979. Lineages in Early Paleogene calcareous nannoplankton. Utrecht Micropaleontological Bulletins 22, 1-231.

Sabry, H., 1968. Stratification and classification of type Esna Group of Egypt: Discussion. Bull. Am. Assoc. Petrol. Geol. 52, 1792-1793.

Said, R., Kenawy, A., 1956. Upper Cretaceous and Lower Tertiary foraminifera from northern Sinai, Egypt. Micropaleontology 2, 105-173.

Said, R., 1960. Planktonic foraminifera from the Thebes Formation, Luxor. Micropaleontology 6, 277-286.

Said, R., 1961. Tectonic framework of Egypt and its influence on distribution of foraminifera. Bull. Am. Assoc. Petrol. Geol. 45, 198-218.

Said, R., 1990. Cenozoic. In: Said, R. (Eds.), The geology of Egypt. Balkema, pp. 451-486.

Salvador, A. 1994. International stratigraphic guide: A guide to stratigraphic classification, terminology, and procedure. 214. The Geological Society of America, Boulder.

Scheibner, C., Kuss, J., Marzouk, A.M., 2000. Slope sediments of a Paleocene ramp-to-basin transition in NE Egypt. International Journal of Earth Sciences 88, 708-724.

Selima, A.M., Askalany, M.M., 1996. Stratigraphy and depositional environment of the Upper Cretaceous-Lower Tertiary sequence, around Wadi Askhar El Qebly South Galala, Gulf of Suez, Egypt. Bulletin Faculty of Science, Assiut University 25 (2F), 87-106.

Serra-Kiel, J., Hottinger, L., Caus, E., Drobne, K., Ferrandez, C., Jauhri, A.K., Less, G., Pavlovec, R., Pignatti, J., Samso, J.M., Schaub, H., Sirel, E., Strougo, A., Tambareau, Y., Tosquella, J., Zakrevskaya, E., 1998. Larger foraminiferal biostratigraphy of the Tethyan Paleocene and Eocene. Bulletin Society Géologie France 169, 281-299.

Shafik, S., Stradner, H., 1971. Nannofossils from the Eastern Desert, Egypt with reference to Maastrichtian Nannofossils from the USSR. Jahrb. Geol. Bundesanstalt SB17, 69-99.

Shahin, A., 1990. Late Cretaceous-Early Tertiary agglutinated benthic foraminifera and their paleoecology in the Gebel Ekma succession, southwestern Sinai, Egypt. Neues Jahrbuch für Geologie und Paläontologie, Abhandlungen 493-512.

Shahin, A., 1992. Contribution to the foraminiferal biostratigraphy and paleobathymetry of the late Cretaceous and early Tertiary in the western Central Sinai, Egytp. Revue de Micropaléontologie 35, 157-175.

Snavely, P.D., Garrison, R.E., Meguid, A.A.A., 1979. Stratigraphy and regional depositional history of the Thebes Formation (Lower Eocene), Egypt. Annals of the Geological Survey of Egypt 9, 344-362.

Speijer, R.P., Schmitz, B., 1998. A benthic foraminiferal record of Paleocene sea level and trophic/redox conditions at Gebel Aweina, Egypt. Palaeogeography, Palaeoclimatology, Palaeoecology 137, 79-101.

Speijer, R.P., Schmitz, B., Luger, P., 2000. Stratigraphy of late Palaeocene events in the Middle East: Implications for low-to middle-latitude successions and correlations. Journal of the Geological Society, London 157, 37-47.

Strougo, A., 1986. The Velascoensis Event: A significant episode of tectonic activity in the Egyptian Paleogene. Neues Jahrbuch für Geologie und Paläontologie, Abhandlungen 173, 253-269.

Strougo, A., Haggag, M.A.Y., Luterbacher, H., 1992. The basal Paleocene "Globigerina" eugubina zone in the Eastern Desert (St. Paul's Monastery, South Galala), Egypt. Neues Jahrbuch für Geologie und Paläontologie, Abhandlungen 1992, 97-101.

Strougo, A., Faris, M., 1993. Paleocene-Eocene stratigraphy of Wadi El Dakhl, Southern Galala plateou. Middle East Research Center, Ain Shams University, Earth Science Services 7, 49-62.

Tantawy, A.A., Ouda, K., von Salis, K., El-Din, M.S., 2000. Biostratigraphy of Paleocene section in Egypt. GFF 122, 163-165.

Youssef, M.I., Shinnawi, M.A., 1954. Upper Cretaceous rocks of Wadi Sudr, Western Sinai. Bull. Inst. Des. Cairo 4, 94-111.

Zittel, K.A., 1883. Beiträge zur Geologie und Palaeontologie der Lybischen Wüste und der angrenzenden Gebiete von Ägypten. Paleontographica 30, 1-147.

CHAPTER 3

Shelf architectures of an isolated Late Cretaceous platform margin, Galala Mountains (Eastern Desert, Egypt)

C. Scheibner, A.M. Marzouk and J. Kuss

published 2001
in Sedimentary Geology
Vol. 145, p. 23-43

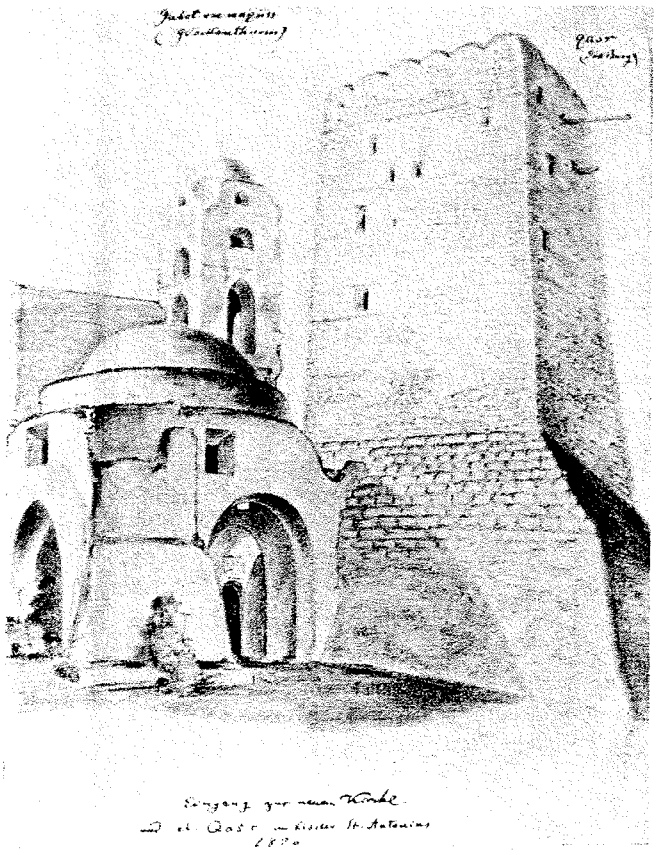

Der Burgturm in Kloster St. Antonius
(links Eingang zur neuen Kirche)

Castle tower of the monastery of St. Anthony
(on the left entrance to the new church)

Drawing by Georg Schweinfurth (1876)

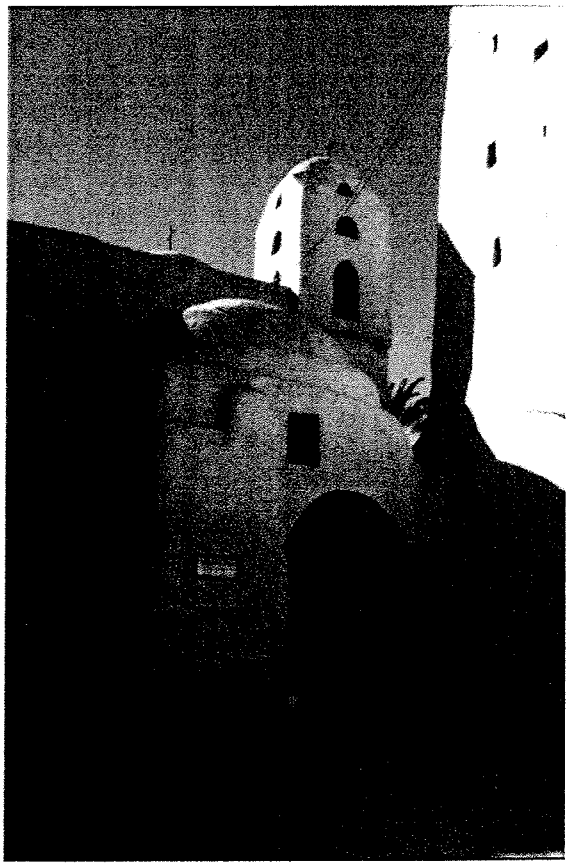

Castle tower of the monastery of St. Anthony
(on the left entrance to the new church)

Photo by Christian Scheibner (1998)

Shelf architectures of an isolated Late Cretaceous carbonate platform margin, Galala Mountains (Eastern Desert, Egypt)

Scheibner, C.[a]; Marzouk, A. M.[b]; Kuss, J.[a]

[a] Universität Bremen, FB5, P.O. Box 330440, 28334 Bremen, scheibne@uni-bremen.de, kuss@uni-bremen.de

[b] Geology Department, Faculty of Science, Tanta University, Tanta 31527, Egypt

Keywords:

Galala Mountains; Eastern Desert; Egypt; Campanian; Maastrichtian; asymmetrical carbonate platform; slope angles, sedimentary sequences; sea-level changes; biostratigraphy

Abstract:

An asymmetrical carbonate platform margin to basin transect has been investigated in the Upper Campanian-Maastrichtian succession of the Galala Mountains, northern Egypt. Identification of systems tracts and their lateral correlation was possible in slope sections only, whereas the monotonous chalk-marl alternations of the basinal sections could not be subdivided with respect to sequence stratigraphic terminology.

The platform asymmetry is expressed by varying large-scale depositional architectures exhibiting a rimmed platform with a sigmoidal slope curvature in south-easterly dip-sections and a ramp with a linear slope curvature in south-westerly dip-sections. The rimmed platform is subdivided into a gentle upper slope and a steep lower slope. The platform formed as a result of the initial topography that was controlled by the tectonic uplift of the Northern Galala/Wadi Araba Syrian Arc structure. The calculated angles of the steep lower slope of the rimmed part range from 5° to 8°, whereas the ramp part has an angle of less than 0.1°.

1. Introduction

Carbonate platforms can be differentiated into rimmed platforms and ramps. Rimmed carbonate platforms are marked by a pronounced increase in slope, whereas ramps have a gently sloping depositional surface (generally < 1°) which passes gradually offshore, with no slope break (Burchette and Wright, 1992). The terms rimmed platform and ramp not only describe the morphology of the slope but normally also imply the biology involved. Rimmed platforms are in most cases associated with „steep-sloped reefs", whereas ramps are characterised by their absence. If the inherited biology plays a minor role for description of slopes and the focus is more on the morphology or clinoforms one can more generally speak of linear, exponential and sigmoidal slope profiles (Adams et al., 1998; Adams and Schlager, 2000). The majority of the slope profiles in the

literature have a sigmoidal slope curvature, possible reasons for this can be found in (Adams et al., 1998; Adams and Schlager, 2000).

During the Campanian-Maastrichtian of the Galala Mountains, Eastern Desert, Egypt an isolated carbonate platform developed locally on top of an elongated, tectonically induced WSW-ENE striking Syrian Arc uplift (Moustafa and Khalil, 1995) (Figs. 1 and 2). In this study we focus on the description and discussion of two platform margin architecture models for this area. As most parts of the carbonate platform were deposited at the locality of today Wadi Araba (Fig. 1) we can infer information on the depositional history only from the distal parts of the carbonate platform (Kuss et al., 2000; Scheibner et al., in press.). In these and in other publications (Kuss and Leppig, 1989; Kulbrok, 1996) the terms rimmed platform and ramp were used, although, the terms sigmoidal and linear slope profile are probably more appropriate because the ecological evidence for a rimmed platform is lacking.

Sedimentological and micropaleontological studies are presented for two transects oriented parallel and perpendicular to the strike of the carbonate platform. Calculations are conducted for the varying degrees of inclination of the slope types of a rimmed carbonate platform model and an asymmetrical carbonate platform model. The latter is formed like a rimmed carbonate platform with a sigmoidal slope curvature in south-easterly directions, but like a ramp with a linear slope curvature in south-westerly directions.

2. Material and Methods

The study area extends from the northern rim of the Southern Galala approximately 70 km southwards to Wadi Tarfa (Fig. 1). We investigated in detail 11 Campanian-Maastrichtian sections in two transects: Transect A has a roughly N-S direction with the sections St. Anthony, St. Paul 9, Bir Dakhl 2-3 and Wadi Tarfa 1. Transect B is oriented in SW-NE direction along the northern rim of the Southern Galala with the sections Wadi Miraf 1, Wadi Hamada 1 and St. Anthony 1-4 (Figs. 1 and 2).

Facies and sequence stratigraphic interpretations are based on fine-scale mapping of stratigraphic sections in and along the Northern Galala/Wadi Araba High. Microscopic studies of 66 thin-sections of the Campanian-Maastrichtian interval are supplemented by analyses of 176 washed samples that formed the base for a high-resolution biostratigraphic frame mainly based on calcareous nannoplankton, supplemented by planktic and benthic foraminifera and some macrofossils. These facies and stratigraphic interpretations (chapter 5 and 6) were used as basic parameters for the development of the two platform models (chapter 7).

3. Geological Setting

Since Turonian times, the area of the Galala Mountains was influenced by vertical movements of the Syrian Arc fold belt, marking the initial stages of the collision between the African and European plates (Moustafa & Khalil, 1995). As a consequence, in northern Egypt and Sinai a system of inverted, uplifted and folded grabens was formed along the Syrian Arc, in Egypt also known as the

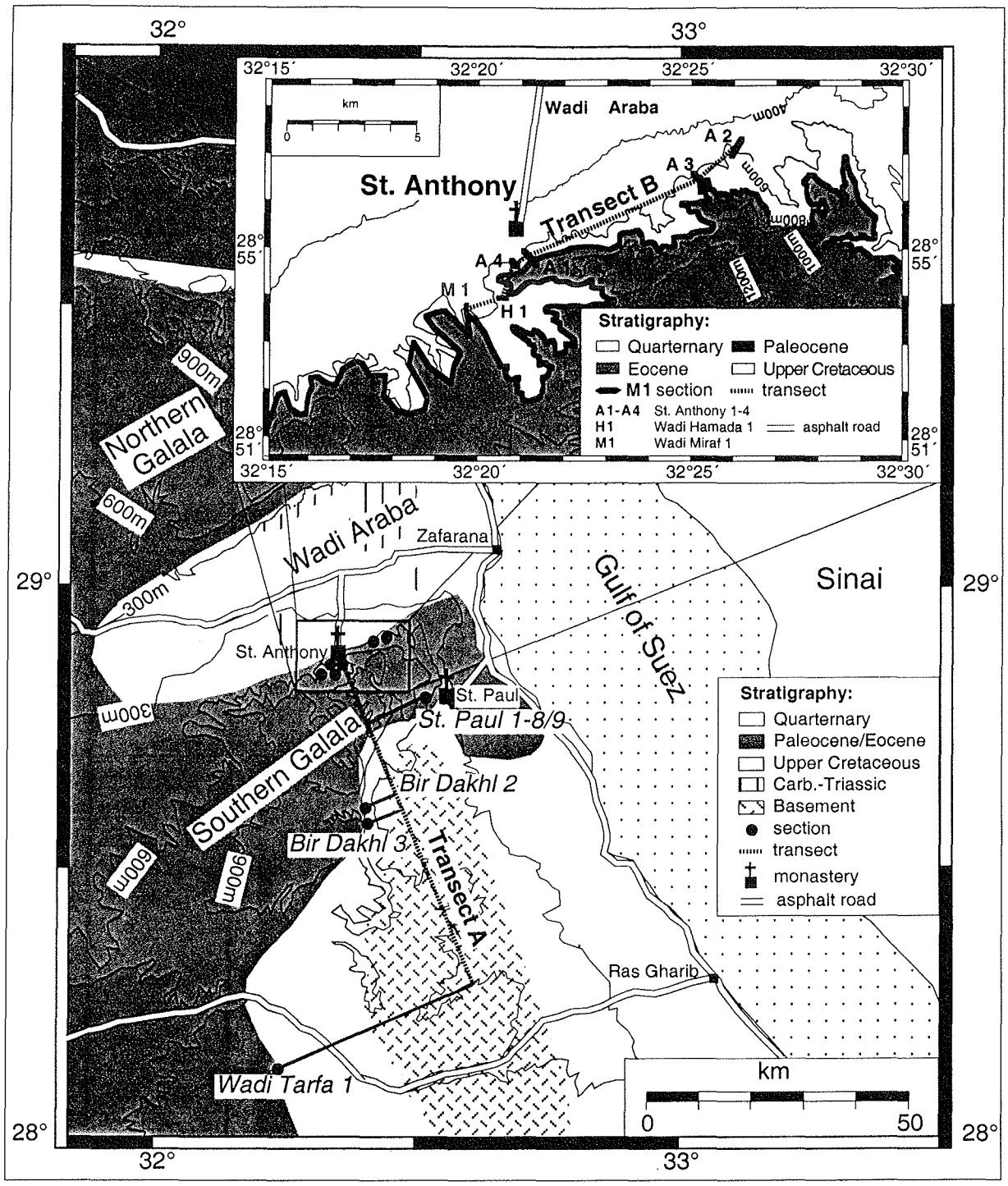

Fig. 1: *Schematic geologic map of the northern part of the Gulf of Suez with locations of sections attributing to Transect A (main map) and Transect B (inlay). The sections St. Anthony 1, St. Paul 9, Bir Dakhl 2-3 and Wadi Tarfa 1 of Transect A are projected on a NNW-SSE running line. Sections Wadi Miraf 1, Wadi Hamada 1 and St. Anthony 1-4 of Transect B (see upper inlay for detailed location) are orientated in WSW-ENE direction parallel to the northern escarpment of the Southern Galala.*

„unstable shelf" (Said 1962). In contrast to Syrian Arc Structures on Sinai like Minsherah, Magharah, Hallal, Yelleq and Areif el Naqa (Lüning et al., 1998; Kuss et al., in press.), on top of which basinal deposits were deposited during late Campanian to Paleogene times, a carbonate platform evolved on the uprising Syrian Arc structure of Northern Galala/Wadi Araba High (Fig. 2). As a consequence of the uplift of the Northern Galala/Wadi Araba High, the Southern Galala Sub-basin evolved further south, forming a part of the Eastern Desert Intrashelf Basin (Kuss et al. 2000).

The Late Cretaceous transition between the Northern Galala/Wadi Araba High and the Southern Galala Sub-basin roughly coincides with the boundary between deformed and undeformed middle-upper Campanian strata and is well exposed along the northern scarp of the Southern Galala Plateau (e.g. near St. Anthony, Fig. 1; see also Bandel & Kuss, 1987). At this locality, a major angular unconformity separates steeply south-dipping Turonian - lower Campanian units of the Northern Galala/Wadi Araba High from moderately south-dipping to nearly flat lying upper Campanian - Maastrichtian to lower Eocene strata further south (Southern Galala Sub-basin). Stratigraphic evidence of a long-term elevation in the north (Northern Galala/Wadi Araba High) is illustrated by stratigraphic gaps spanning the Coniacian to late Paleocene (Kuss et al., 2000; Scheibner et al., in press.). The WSW-ENE striking Northern Galala/Wadi Araba High strongly influenced Cretaceous-Palaeogene sedimentation processes in the studied area. This contains a gently south-dipping carbonate platform, rimming the Northern Galala/Wadi Araba High in the north and interfingering with slope sediments and hemipelagic deposits to the south. Also the siliciclastics that were shed from the platform can be explained by this structural element. During the uplift of the Northern Galala/Wadi Araba High successively older sediments were exposed and subsequently eroded (Bandel and Kuss, 1987). Based on Kulbrok (1996), three major southward prograding carbonate platform systems with different large-scale sedimentary architectures can be distinguished:

- a late Campanian/Maastrichtian rimmed shelf
- a Paleocene distally steepened ramp
- an early Eocene homoclinal ramp

In this paper we concentrate on the late Campanian/Maastrichtian rimmed shelf, whereas Scheibner et al. (2000), Kuss et al. (2000) and Scheibner et al. (in press.) further discuss the Palaeogene platform development.

4. Lithostratigraphy

The studied late Campanian-Maastrichtian sediments of the Southern Galala area (Fig. 3) consist of deposits of the shallow-water St. Anthony Formation (Transect B) and of deposits of the deep-water Sudr and Dakhla Formations (Transect A) (Figs. 3 and 4). The St. Anthony Formation, predominantly carbonates with slumping features and reworked shallow water biota, disconformably overlies basinal chalks of the Sudr Formation in the northern areas and underlies the carbonates of the Southern Galala Formation. The Sudr Formation consists of massive white and

cream coloured chalk and chalky limestone beds with thin intercalations of light greyish calcareous shales and is overlain in the southern areas (Wadi Tarfa-St. Paul) by the Dakhla Formation. The Maastrichtian part of the Dakhla Formation consists of chalky marls. A more detailed description and discussion of the biostratigraphic ranges of various Late Cretaceous-Palaeogene formations in the northern Gulf of Suez region will be found in Scheibner et al. (in press).

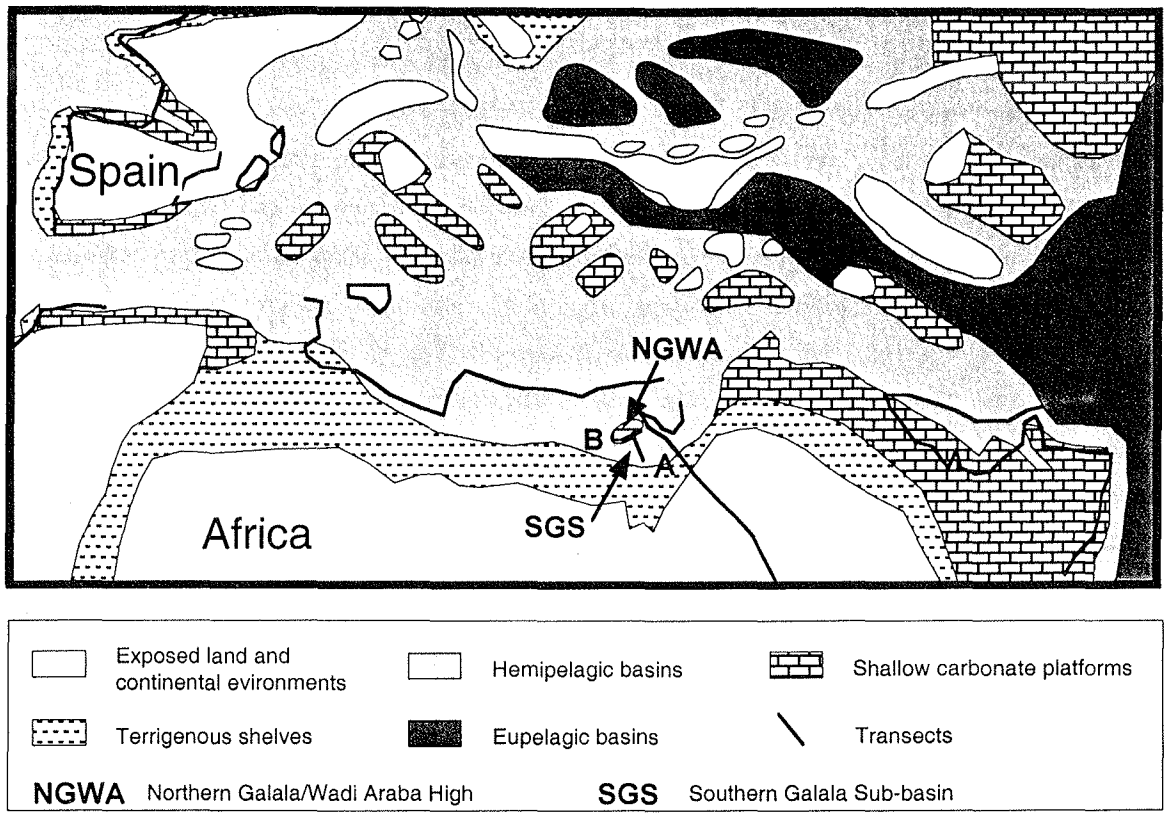

Fig. 2: *Late Campanian paleogeography of the central Tethys (modified from Camoin et al., 1993) with the location of the Northern Galala/Wadi Araba High and the Southern Galala Sub-basin.*

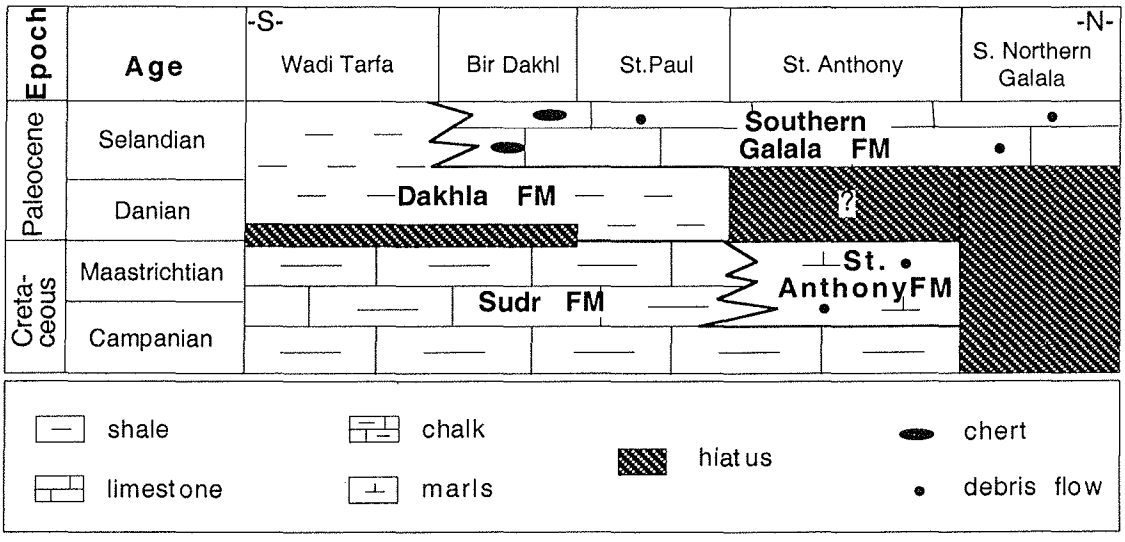

Fig. 3: *The late Campanian-Paleocene formations of the Galala Mountains to illustrate lithofacies changes throughout the working area.*

5. Biostratigraphy

The subdivision of calcareous nannoplankton biozonation into CC-zones was first established by Sissingh (1977). Comparison of the subdivisions of Norris et al. (1998) and Hardenbol et al. (1998) show clear discrepancies of the order of first and last occurrences of important calcareous nannoplankton taxa (Fig. 5). In our samples the order of first occurrences and last occurrences of calcareous nannoplankton is similar to that in the subdivision of Norris et al. (1998); therefore we follow their subdivision, including some marker levels provided by Perch-Nielsen (1985).

For planktic foraminiferal zonation we follow Caron (1985). Similar to Caron (1985) we identified the *Gansserina gansseri* Zone. Index forms of planktic foraminifera are either rare or are strongly diagenetically altered, especially in Transect B, thus limiting their use for biostratigraphy.

In addition we use *Exogyra overwegi*, benthic foraminifers (*Omphalocyclus macroporus/ Pseudomphalocyclus blumenthali, Orbitoides* sp.) and ammonites (*Discoscaphites kambysis, Saghalinites* sp.) for stratigraphic subdivision in Transect B (Fig. 4). In Transect A only calcareous nannofossils and planktic foraminifers are used for biostratigraphic correlation. For delineating the Campanian-Maastrichtian boundary and correlating zonal schemes of calcareous nannoplankton and planktic foraminifers we follow Norris et al. (1998), who correlated this stage boundary with a level in lower CC24 (Fig. 5).

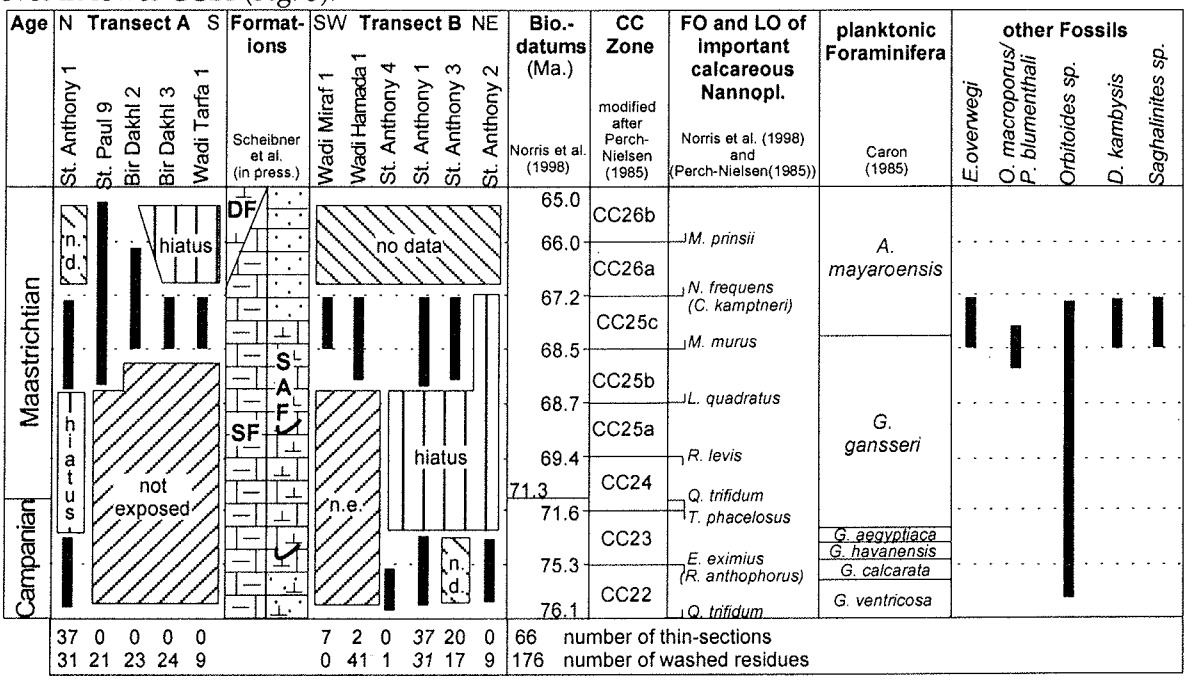

Fig. 4: *Stratigraphic ranges of the investigated sections are illustrated in columns 2 and 4 with not exposed (n.e.) lower parts of most sections of Transect A and of sections Wadi Miraf 1 and Wadi Hamada 1 of Transect B. Hiatuses occur in all St. Anthony sections, and missing of samples (no data; n.d.) or missing of biostratigraphic subdivision occur in the upper part of all sections in Transect B. Formation names of column 3 refer to a classification given by Scheibner et al. (in press.), with chalks of the Sudr Formation (SF) and marls of the Dakhla Formation (DF) occurring in Transect A and chalky limestones, marls and sandstones of the St. Anthony Formation (SAF) in all sections of Transect B (for signatures see Fig. 7). The last column gives the stratigraphic ranges of some other fossil groups: oysters (E. overwegi); large foraminifers (Omphalocyclus macroporus/Pseudomphalocyclus blumenthali, Orbitoides sp.); ammonites (Discoscaphites kambysis, Saghalinites sp.). The number of analysed thin-sections and loose samples (bottom) refer to the respective sections.*

The samples of the upper parts of the sections of Transect B allowed only preparation of thin-sections. Therefore the stratigraphic resolution is lower and often uncertain, compared to Transect A. This is evident e.g. for the hiatus across the Maastrichtian-Paleocene boundary (Scheibner et al., in press.).

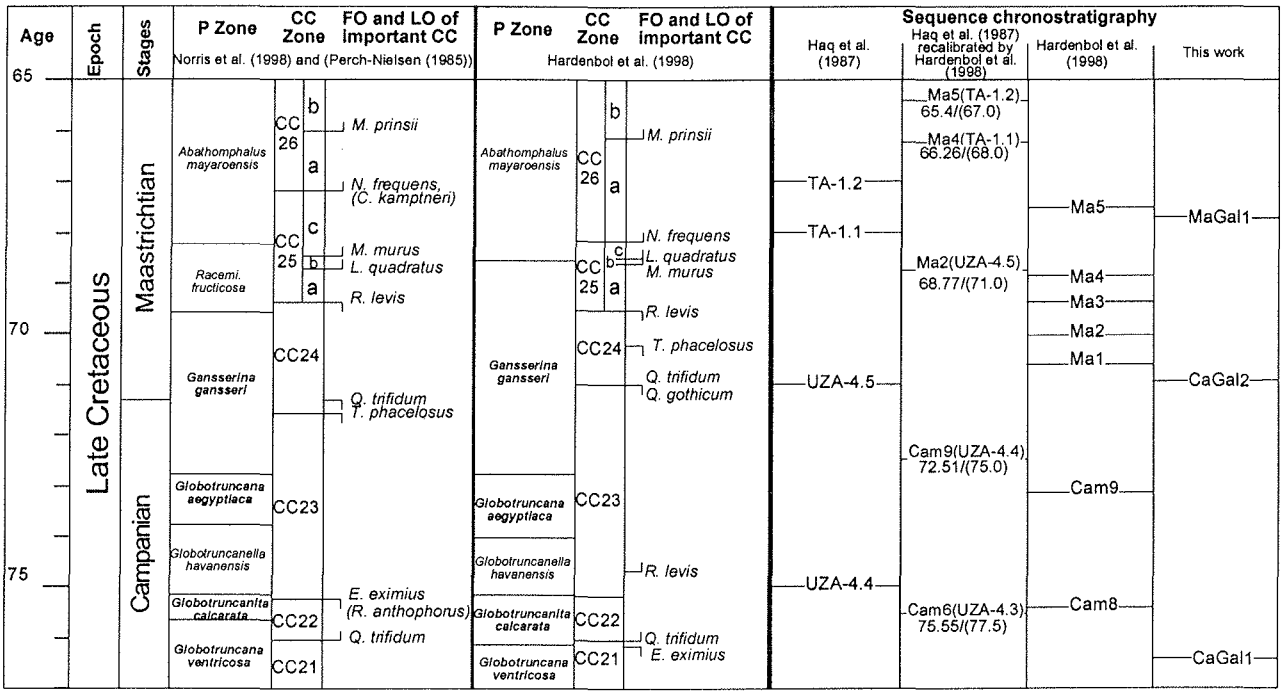

Fig. 5: *Biostratigraphy and sequence chronostratigraphy. The two biostratigraphic schemes of Norris et al. (1998)/Perch-Nielsen (1985) and Hardenbol et al. (1998) show various discrepancies of the timing of first occurrence and last occurrence of calcareous nannoplankton. In the sequence chronostratigraphic columns the sequences of Haq et al. (1987) and their recalibration by Hardenbol et al. (1998) are shown. The last column shows sequence boundaries of the Galala Mountains and their biostratigraphic position (calibrated after Norris et al., 1998).*

6. Sedimentary patterns and systems tracts:

6.1. Transect A (Fig. 7)

This ca. 70 km long transect is a projection of the sections onto a line oriented perpendicular to the strike (ENE/WSW) of the carbonate platform with section St. Anthony 1 at the northern rim of the Southern Galala and section Wadi Tarfa 1 in the Wadi Tarfa area (Figs. 1, 7). A schematic sequence stratigraphic cross-section of Transect A for the Campanian to lower Eocene can be seen in Fig. 6. In the southern basinal sections of Transect A chalk-marl alternations of the Sudr Formation (composed of up to 120 cm thick chalk-beds and up to 10 cm thick marls) prevail (Figs. 3, 7, 8k). In section St. Paul 9 they range from CC25b to CC26b, whereas in section Wadi Tarfa 1 only CC25c is present. In sections St. Paul 9 and Bir Dakhl 2 the upper parts of the Maastrichtian with alternating chalky marl beds are transitional in lithology to the overlying marls and have been partly attributed to the Dakhla Formation (Scheibner et al., in press..). Benthic foraminifera assemblages in section St. Paul 9 suggest a bathyal environment of 300-500 m (pers. comm. R.P.

Speijer). However, in section St. Paul 9 an anomalous 43 cm thick marly, bivalve-rich layer with a neritic (-200 m) benthic foraminifera assemblage has been intercalated in upper CC25b (pers. comm. R.P. Speijer). With the exception of section St. Anthony 1 a subdivision in sytems tracts is not possible. Because of its similarity to the other sections of Transect B, section St. Anthony 1 will be described in the following chapter.

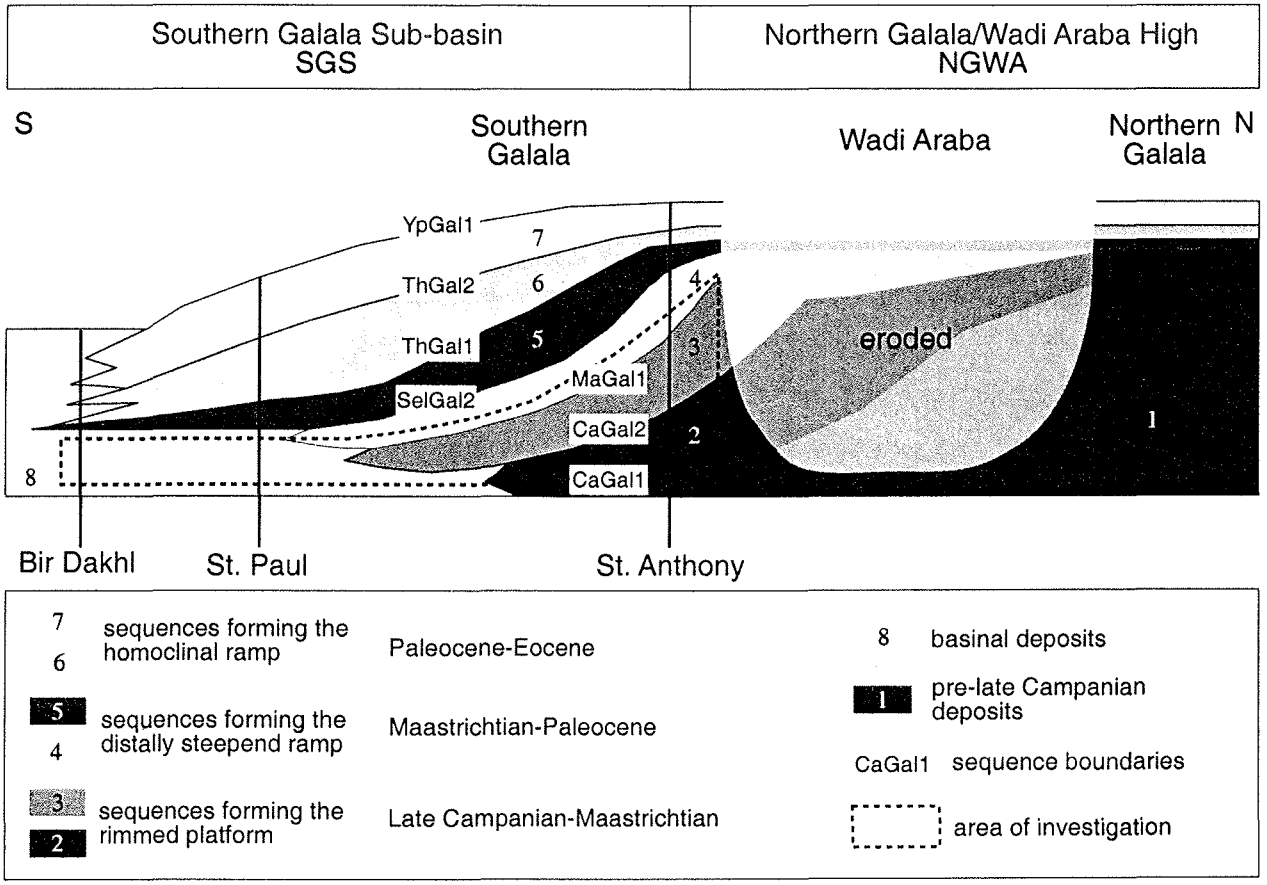

Fig. 6: *Schematic cross-section for the late Cretaceous-Paleogene sedimentary sequences to demonstrate the stratigraphic evolution of three carbonate platforms at the Northern Galala/ Wadi Araba High: (2/3) the rimmed carbonate platform, (4/5) the distally steepened ramp; (6/7) the homoclinal ramp. Modified after Kuss et al. (2000).*

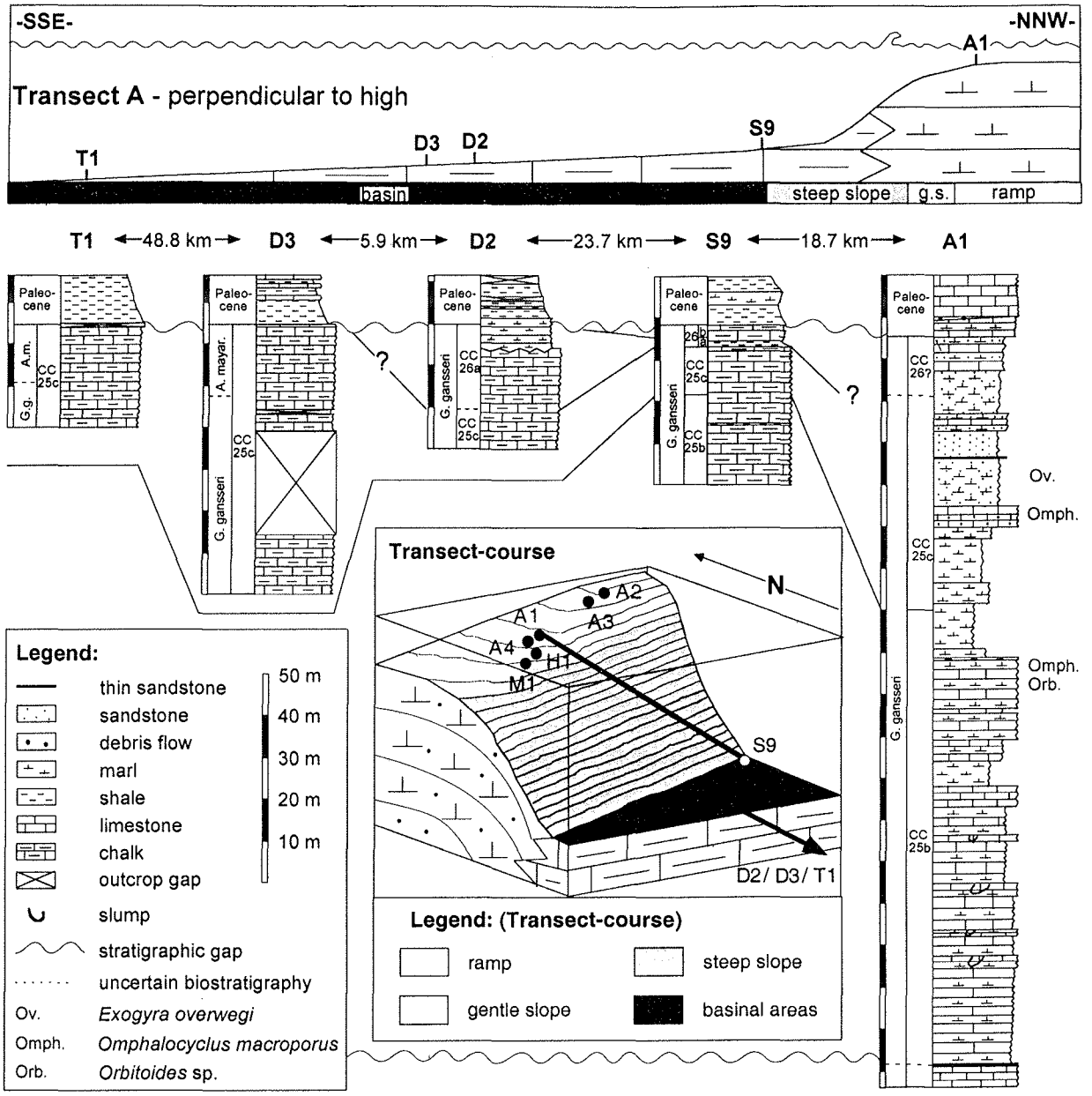

Fig. 7: *Litho- and biostratigraphic correlation of the five sections along Transect A (Fig. 1); the lower 160 m of section St. Anthony 1 are illustrated in Fig. 9. The mainly basinal chalks prevent a subdivision into systems tracts. The position of the 2D transect (top) is indicated in a 3D graph (bottom). The grey shades in the 2D and 3D graphs indicate the simplified morphology of the Maastrichtian platform margin. (T1 = Wadi Tarfa1; D2/3 = Bir Dakhl 2/3; S9 = St. Paul 9; A1 = St. Anthony 1)*

6.2. Transect B

Transect B is oriented parallel to the strike (WSW/ENE) of the carbonate platform, along the northern rim of the Southern Galala, measuring about 13 km (Figs. 1, 9). The systems tracts described below are mainly inferred from section St. Anthony 1 (Figs. 8a, 8b, 9) with additional data from the neighbouring sections of Transect B. For the Cretaceous we have found three sequences, CaGal1, CaGal2 and MaGal1. Sequence names are derived from a combination of the stage and the region

(Galala) and relate to the underlying sequence boundaries (e.g. sequence CaGal2 is located between sequence boundary CaGal2, below and sequence boundary MaGal1, above).

Sequence CaGal1: Kulbrok (1996) described a sequence boundary (UC1) in St. Anthony 3 m below the topmost chalks of the Campanian Sudr Formation at the base of a 0.5 m thick layer with siliciclastic, phosphatic pebbles, corresponding to CaGal1 of Kuss et al. (2000). Lowstand systems tracts-(LST) sediments above are characterised by silt- to sandstones and alternations of limestones and silty marls. In the upper part large-scale synsedimentary slumps with dipping directions towards the west are observed in section St. Anthony 4 (Figs. 8e, 8f). The sample below these large slumps indicate CC22. Kulbrok (1996) described *O. gruenbachensis* from these layers. Time-equivalent sediments are found only in section St. Anthony 2, composed of hard and soft marly limestones. Due to the monotonous lithology throughout section St. Anthony 2 and the poor biostratigraphic resolution, a subdivision into systems tracts is very uncertain. Only the unit with large slumping structures and channel fills around 70 m (Fig. 9) may correlate to the large synsedimentary slumpings of section St. Anthony 4 and therefore may be attributed to the LST-deposits of CaGal1 as well.

The following transgressive systems tract (TST) is best exposed in section St. Anthony 1, composed of alternating marls and carbonatic siltstones (between 110 m - 155 m of section St. Anthony 1; Kulbrok, 1996). The TST and overlying highstand systems tracts- (HST)sediments could not be biostratigraphically assigned. But in section St. Anthony 2 the sediments overlying the LST-slumps of CaGal1 can be attributed to CC22 or CC23. We therefore assume a similar age of the TST and the HST for both sections St. Anthony 1 and St. Anthony 2. The HST-deposits of section St. Anthony 1 are composed of bioclastic limestones with abundant fragments of coralline algae and shells. The top of the HST is characterised by a 0.15 m thick silty sandstone and a 0.5 m thick limestone, both with rare to abundant *Exogyra* sp.

The top of this hard limestone layer marks the sequence boundary CaGal2 (Fig. 9). We correlate the base of the debris flow in section St. Anthony 2 (around 140 m, Fig. 9) with sequence boundary CaGal2. However we cannot substantiate this correlation through independent biostratigraphic data.

Sequence CaGal2: The sediments of the CaGal2-LST can be attributed to CC25b due to the presence of *L. quadratus*. In none of the sections CC24 or CC25a was encountered; therefore we assume a stratigraphic gap for that interval coinciding with sequence boundary CaGal2 (Fig. 9).

Similar to the CaGal1-LST the CaGal2-LST is composed of marls and limestones with a subordinate siliciclastic content. Conspicuous synsedimentary slumpings occur. The top of the LST-deposits is characterised in section St. Anthony 1 by bioclastic limestones with *O. macroporus* and/or *Pseudomphalocyclus blumenthali* and in section St. Anthony 3 by a slumped limestone bed (1.40 m) with abundant bivalves, gastropods and corals.

The TST starts in sections Wadi Hamada 1 and St. Anthony 1 in the upper part of CC25b and in section St. Anthony 3 at the top of CC25b (Fig. 9), and is composed of alternating hard and soft yellow marls with a high planktic foraminiferal content (50 - 75 %). In section Wadi Hamada 1

only the middle to upper TST-sediments are exposed, compared with age-equivalent deposits of the neighbouring section St. Anthony 1 (Fig. 9). Further to the ENE, in sections St. Anthony 3 and St. Anthony 2, the stratigraphic range of the TST decreases (demonstrated by the different position of the CC25b/CC25c boundary). The lateral variations can be explained either by diachroneity of the TST-deposits („eastward onlapping") or by laterally changing sedimentation-rates.

The overlying HST is characterised either by mass flow deposits (Wadi Hamada 1) or by conglomeratic, partly bedded marls to limestones with moderate siliciclastic contents (Wadi Miraf 1, St. Anthony 1, St. Anthony 3). Increasing thicknesses of the conglomeratic/mass flow units are evident from ENE (St. Anthony 3) to WSW (Wadi Miraf 1) indicating a low angle gradient towards the west. *O. macroporus* and/or *P. blumenthali* and Lepidorbitoididae (*Praesiderolithes douvillei*?), coralline algae, gastropods and echinodermata are obvious in the HST deposits of sections Wadi Miraf 1, St. Anthony 1, St. Anthony 3. Abundant *Thalassinoides* burrows, the shallow water bivalve *Pinna*, and teeth of bony fishes, that thrived in calm-water-zones of reefs (pers. comm. C. Werner) were found in section St. Anthony 3. The top of the carbonatic mass flow unit coincides with sequence boundary MaGal1. Only in the westernmost section Wadi Miraf 1, 2.7 m thick dolomitic marls occur on top of the mass flow unit underlying sequence boundary MaGal1.

Sequence MaGal1: This sequence starts in all sections with the first *E. overwegi* beds (Figs. 8d, 8g). It overlies in section St. Anthony 2 mass flow deposits and underlies Paleocene limestones on top (Fig. 9). In all other sections (St. Anthony 3, St. Anthony 1, and Wadi Miraf 1) the MaGal1-LST-sediments exhibit a clear threefold lithologic subdivision: The reddish to yellowish siliciclastic marls at the base hold distinct layers of *E. overwegi*, *Exogyra* sp., other bivalves, gastropods (Fig. 8c) and bioturbations (Fig. 8i). Internally this unit is characterised by shallowing-up cycles of thick layers with siliciclastic marls without bivalves and by thin layers with bivalves. These shallowing-up cycles (Fig. 8h) are best visible in section St. Anthony 3 whereas in sections St. Anthony 1 and Wadi Miraf 1 the mollusc layers are less frequent and the carbonate content increases indicating again a low angle depth gradient towards the west. The middle parts of the LST contain similar sediments except for the absence of *E. overwegi*; again, an increase of the carbonate content from ENE to WSW is evident. In section St. Anthony 3 the shallowing-up cycles are emphasised by colour contrasts of red and white, where white marks the shallower bioturbated parts (Figs. 8h, 8i). In section St. Anthony 3 the upper parts of the LST are characterised by sandstones, whereas in sections St. Anthony 1 and Wadi Miraf 1 hard and soft marls and limestones alternate.

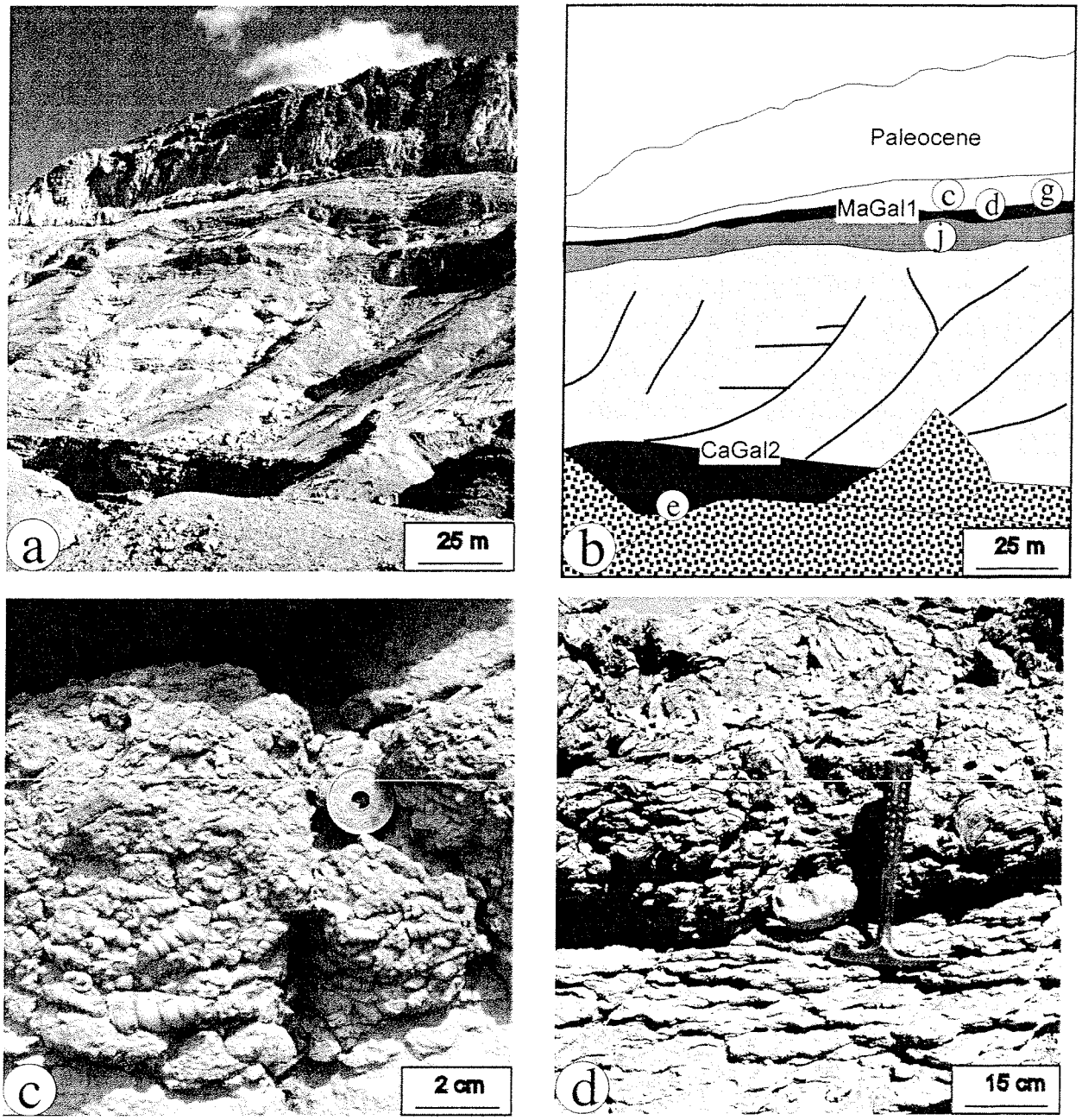

Fig. 8a, b: *Photograph and sketch of the mainly Maastrichtian-Paleocene deposits of section St. Anthony 1 with the two sequence boundaries CaGal2 and MaGal1. The encircled letters indicate the stratigraphic position (not always the location) of the appropriate photographs (Figs. 8c, 8d, 8e,8g, 8j) from different sections. Best visible are the huge LST-deposits of sequence CaGal2. The MaGal1 LST-deposits are illustrated in detail in Fig. 8g. The steep cliff on top marks the Paleocene. Compare signatures of the systems tracts to Fig. 8.*

Fig. 8c: *Accumulation of turritellid gastropods in the LST-deposits of sequence MaGal1 (section St. Anthony 1), stratigraphic position is indicated in Fig. 8g.*

Fig. 8d: *Sandy limestones with Exogyra overwegi in the HST-deposits of sequence CaGal2 (section St. Anthony 1), stratigraphic position is indicated in Fig. 8g.*

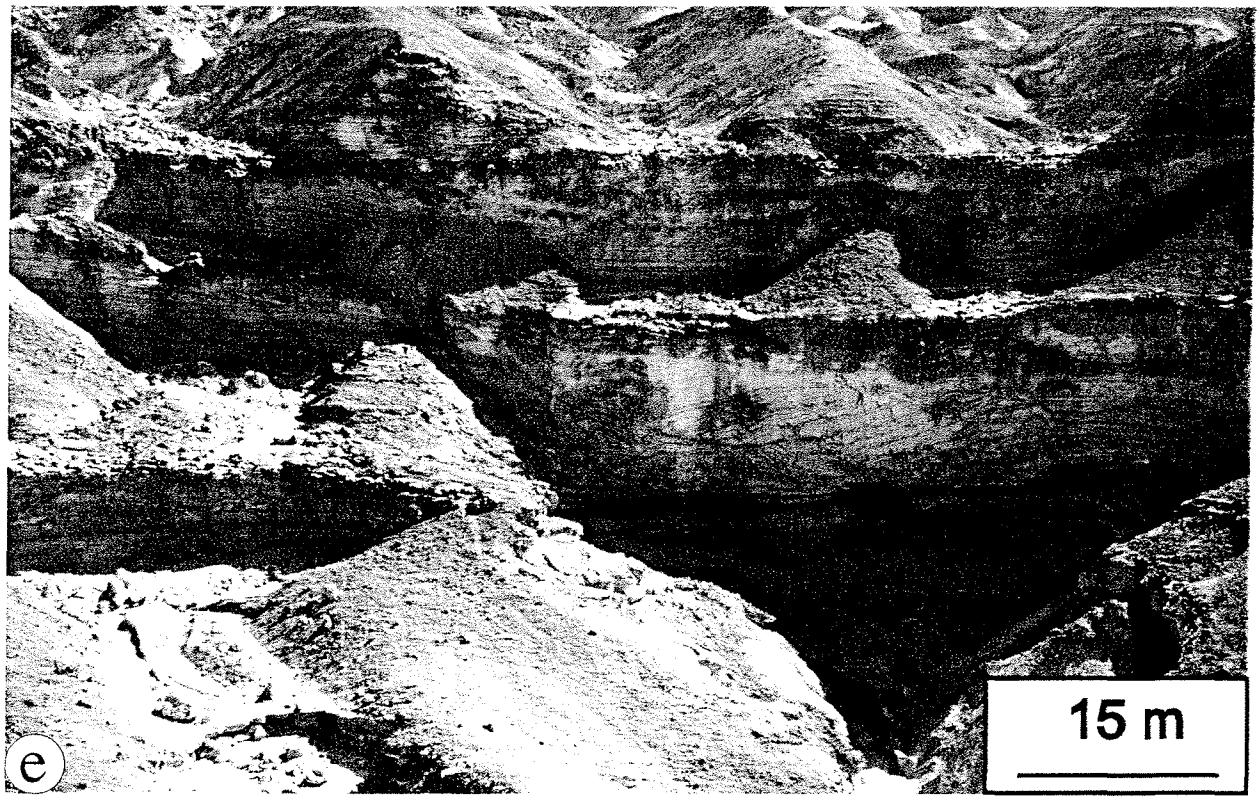

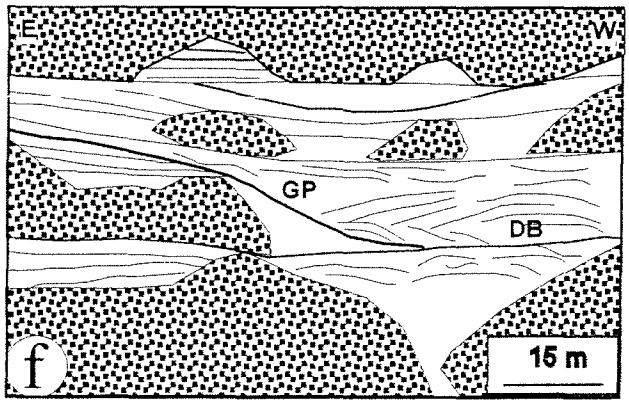

GP: gliding plane
DB: distorted beds

Fig. 8e, f: *Photograph and sketch of the synsedimentary slumpings in LST-deposits of sequence CaGal1 (section St. Anthony 4). GP represents a mayor gliding plane of the slumpings that are visible in distorted bedding planes further west.*
Fig. 8g: *The MaGal1 LST-deposits in section St. Anthony 3 (Fig. 1). The encircled letters indicate the position of Figs. 8c, 8d, 8h and 8i. The steep cliff on top represents Paleocene limestones.*
Fig. 8h: *Shallowing-up cycle within the MaGal1 LST-deposits in section St. Anthony 3. The lower massive part is characterised by red siliciclastic marls with a concentration of shells (1). The upper thin part is build of white, calcareous bioturbations (Fig. 8i).*
Fig. 8i: *Top view onto the white calcareous bioturbations of a shallowing-up cycle in the LST-deposits of MaGal 1 in section St. Anthony 3 (detail of Fig. 8h).*
Fig. 8j: *Marly TST-deposits of CaGal2 in section Wadi Hamada 1 yielding the best preserved calcareous nannoplankton and planktonic foraminifera in Transect B. The steep cliff is build of the conglomeratic carbonates of the HST-deposits of CaGal2.*
Fig. 8k: *Late Maastrichtian monotonous chalk-marl alternations of the Sudr Formation in section Bir Dakhl 2.*

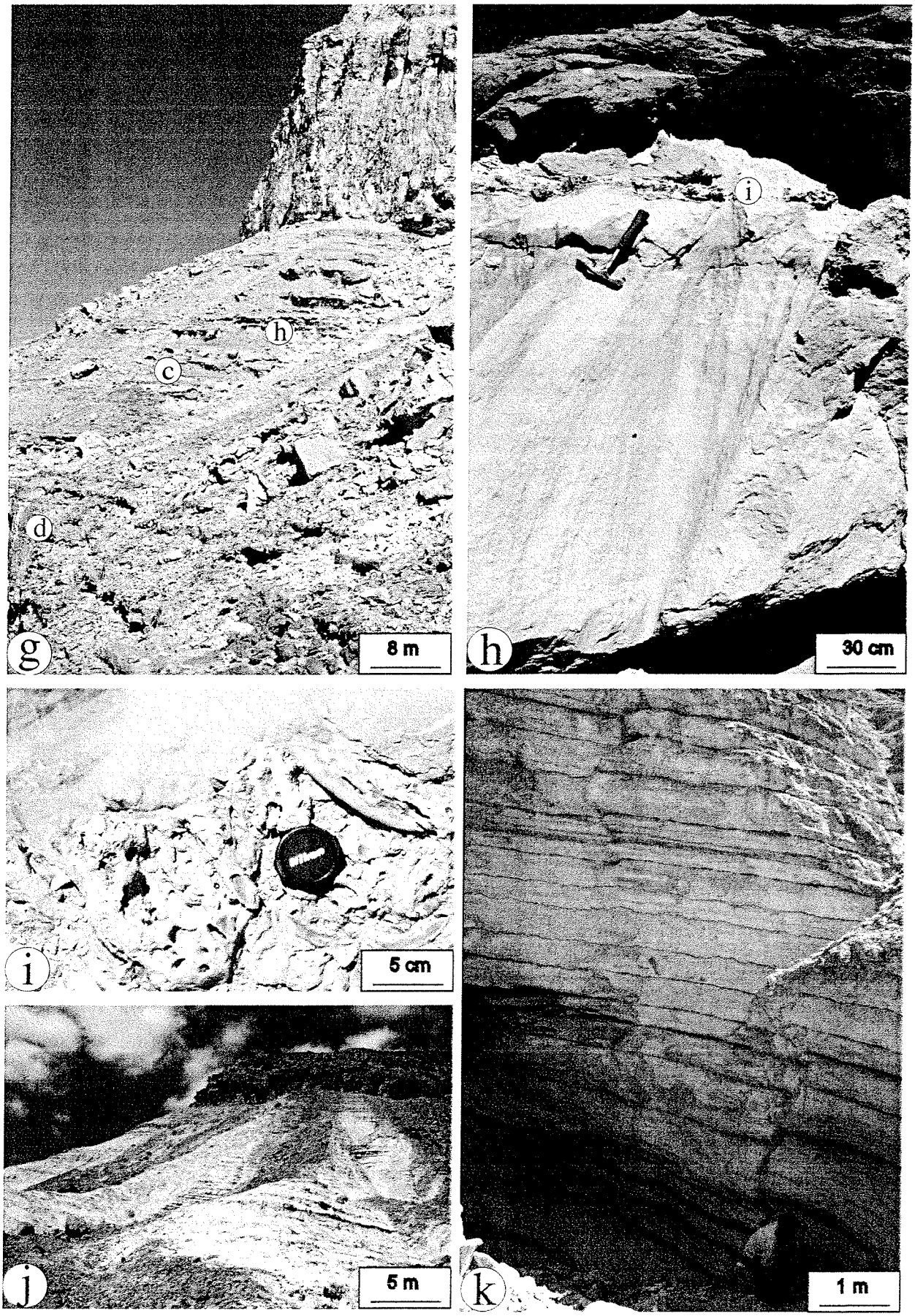
g
8 m
h
c
d
h
30 cm
i
i
5 cm
j
5 m
k
1 m

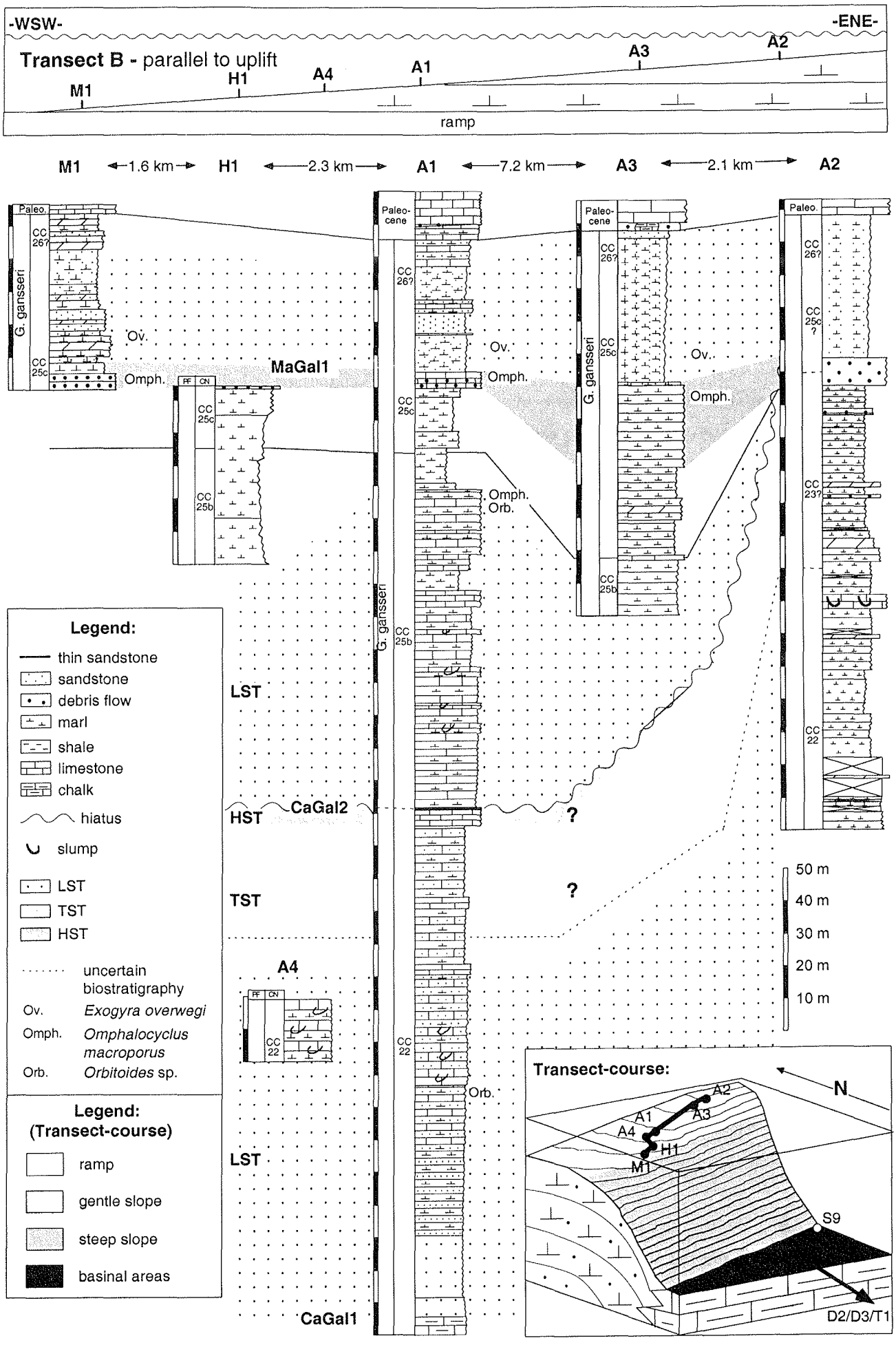
-WSW-
-ENE-
Transect B - parallel to uplift
M1
H1
A4
A1
A3
A2
ramp
M1 ←1.6 km→ H1 ←2.3 km→ A1 ←7.2 km→ A3 ←2.1 km→ A2
Paleo.
Paleo-cene
CC 26?
CC 25c
CC 25b
CC 25c ?
CC 23?
CC 22
G. gansseri
Ov.
Omph.
Orb.
MaGal1
CaGal2
CaGal1
LST
TST
HST
A4
PF
CN
?
50 m
40 m
30 m
20 m
10 m
Legend:
thin sandstone
sandstone
debris flow
marl
shale
limestone
chalk
hiatus
slump
LST
TST
HST
uncertain biostratigraphy
Ov. Exogyra overwegi
Omph. Omphalocyclus macroporus
Orb. Orbitoides sp.
Legend: (Transect-course)
ramp
gentle slope
steep slope
basinal areas
Transect-course:
N
A2
A1
A3
A4
H1
M1
S9
D2/D3/T1

Fig. 9 (previous page): *Sequence-stratigraphic correlation of the six sections of Transect B. The position of the 2D transect (top) is indicated in a 3D graph (bottom). The grey shades in the 2D and 3D graphs indicate the simplified morphology of the Maastrichtian platform margin. (M1 = Wadi Miraf 1; H1 = Wadi Hamada 1; A1-4 = St. Anthony 1-4).*

7. Carbonate platform morphology

The sedimentary patterns of the Late Campanian-Maastrichtian carbonate platform margin sediments of the Galala Mountains can be explained by two principal platform models reflecting two different platform architectures (Fig. 10);

- A: a rimmed carbonate platform with a W-E strike-direction (straight),
  A´: a rimmed carbonate platform with a ENE-WSW strike (oblique model) both with sigmoidal slope profiles and
- B: an asymmetrical carbonate platform with a gently W-dipping ramp part with a linear slope profile and a WSW-ENE striking rimmed part, also with a sigmoidal slope profile (Fig. 10).

Model parameter:

The rimmed part with the sigmoidal slope profile of both models A/A´ and B can be separated into two differently inclined slopes, an upper gentle slope and a lower steep slope. If not using this bipartition, the angle of the entire slope would be significantly higher and thus would lead to larger depth-differences between the sections in Transect B, which is not supported by the sedimentary patterns. For the following calculations the hinge-line between the gentle slope and the steep slope has been chosen close to section Wadi Miraf 1, whereas the transition from the steep slope to the basinal parts varies.

For both models we assume a paleowater-depth for section St. Anthony 2 (East) of 70 m and for section Wadi Hamada 1 (West) of 90 m; both assumptions are based on paleoecologic interpretations of benthic foraminifera assemblages in biozones CC25b and CC25c (pers. comm. K. Schnack). The difference in paleowater-depths between both sections is confirmed by sedimentary patterns (synsedimentary slumpings with a gliding plane dipping in westerly directions, more pronounced shallowing-up cycles in the easterly sections and increasing debris-flow depths in westerly directions) and paleoecologic data (findings of shallow-water biota and burrows in section St. Anthony 3) which hint to shallower water-depths in easterly directions. For the calculation of the angle of inclination, the following formula has been used (Fig. 10):

$$\tan a = WD/(D * 1000)$$

with: a = angle of inclination
WD = water depth (in m)
D = distance (in km)

Models A/A´: The rimmed carbonate platform model with a sigmoidal slope curvature assumes that the paleowater-depths of sections Wadi Miraf 1, Wadi Hamada 1, St. Anthony 4, St. Anthony 1, St. Anthony 3 and St. Anthony 2 (Transect B) were oriented in ascending order on a proximal part of

the slope (Fig. 10) while sections St. Paul 9, Bir Dakhl 2, Bir Dakhl 3 and Wadi Tarfa 1 represent the distal, basinal parts (Transect A). The strike of the slope could be oriented either in W-E direction (straight model A) or in WSW/ENE direction (oblique model A´). In both situations the slope is subdivided into a gentle and a steep part (Fig. 10). The degree of inclination of the gentle slope varies from 0.15° (model A) to 0.38° (model A´). Calculations are based on a paleowater-depth difference of 20 m between sections St. Anthony 2 and Wadi Miraf 1 and the distance between both (perpendicular to the direction of the slope). The degree of inclination of the steep slope varies between 3.1° and 8.5° (model A) and between 1.3° and 8.5° (model A´). For section St. Paul 9 we assume a water-depth of about 400 m (the bentic foraminifers assemblages suggest water-depths of 300-500m; pers. comm. R. P. Speijer), hence the water-depth difference between sections Wadi Miraf 1 and St. Paul 9 is about 300 m.

The most critical difference between the two basic models A and A´ concerns the position of the slope-basin transition. Because we do not know, whether the water-depth of 400 m is reached exactly at section St. Paul 9 or further north, we calculated the inclinations of the slope with various distances (Tab.1). By choosing a maximum distance of 5.5 km (model A) or 13 km (model A´) and a paleowater-depth difference of 300 m the inclination of the steep slope would vary between 3.1° (model A) and 1.3° (model A´). A reduction of the distance between section Wadi Miraf 1 and the slope-basin-transition would result in a steepening of the slope (for a 2 km distance the inclination would rise up to 8.5°) (Tab.1).

Model B: In this model we assume an asymmetrical carbonate platform, with a gently WSW dipping ramp with a linear slope profile and a WNW-ESE striking rimmed carbonate platform with a sigmoidal slope profile (Fig. 10). Transect B traverses the ramp part, Transect A traverses the rimmed carbonate platform part. For the ramp part we calculate an angle of inclination of 0.08°, based on assumptions of a 20 m of water-depth difference and a distance of 15 km (St. Anthony 2-Wadi Miraf 1; measured perpendicular to the isobathes). For the gentle slope and the steep slope of the rimmed carbonate platform part we assume the same angles of inclination as for the gentle and steep parts of the rimmed carbonate platform of model A´ (Tab.1). The inclination of the steep slope would also increase, if the slope-basin transition and the gentle slope-steep slope hinge-line would be closer to each other.

Fig. 10 (next page): *Comparison of different carbonate/siliciclastic platform-margin architectures based on two 3-D models and their respective top views. Location of the sections along Transect A and B are taken from GPS readings and refer to a km-grid with isobathes to illustrate different paleo-inclinations. Models A and A´ show a rimmed carbonate platform with a sigmoidal slope curvature which strike in E-W and WSW-ENE directions. Model B is an asymmetrical carbonate platform with a WSW-ENE striking rimmed carbonate platform and additionally a gentle W-dipping rim with a linear slope curvature. Section Bir Dakhl 2 lies farther south, the southernmost sections Bir Dakhl 3 and Wadi Tarfa 1 (Fig. 1) are not indicated. Within the three models a ramp part, a gentle slope and a steep slope can be distinguished based on different inclinations. Calculation of geometric relations, resulting in these different inclinations is given in Table 1.*

A/A´: rimmed carbonate platform

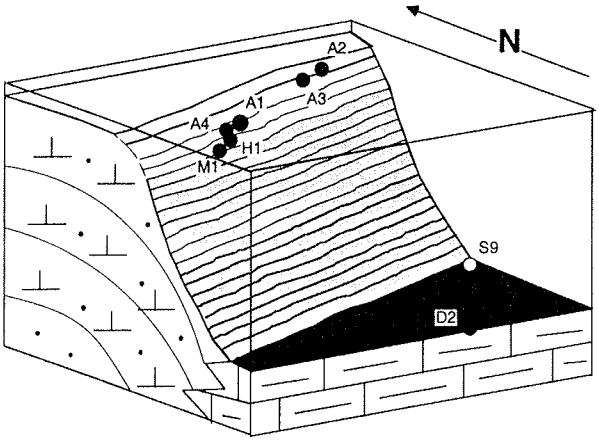

B: asymmetrical carbonate platform

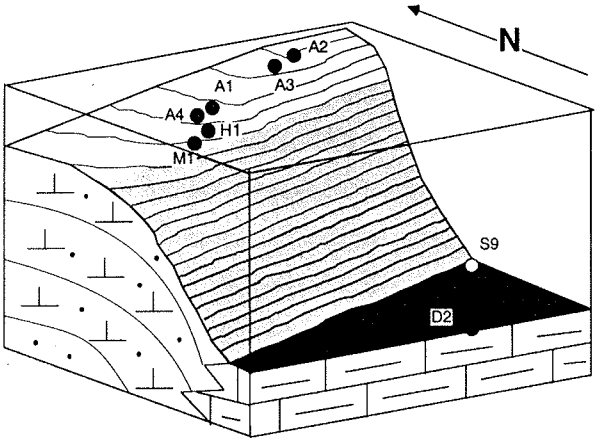

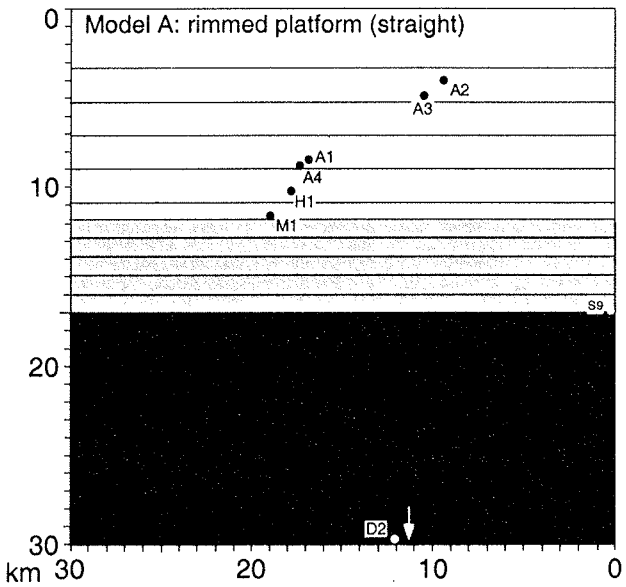

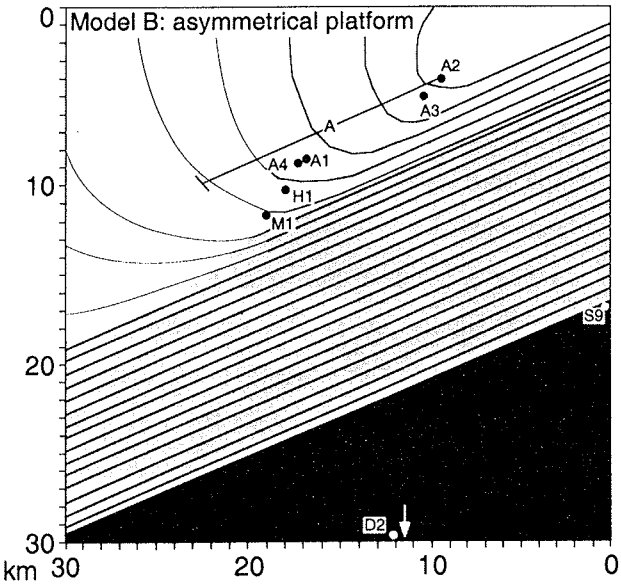

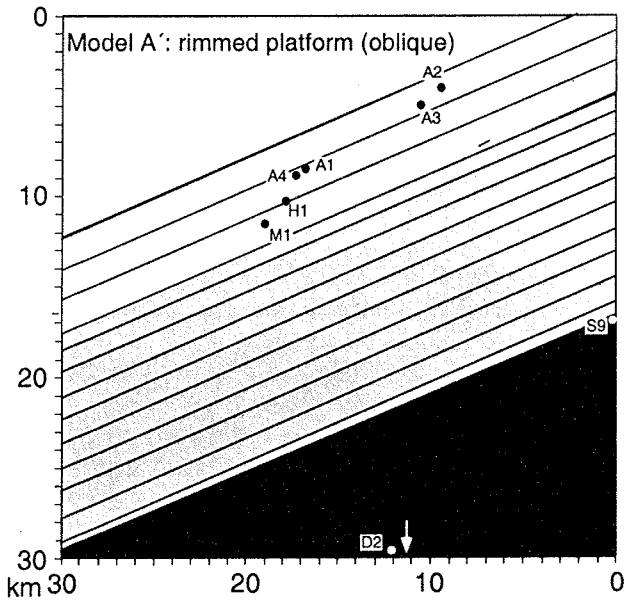

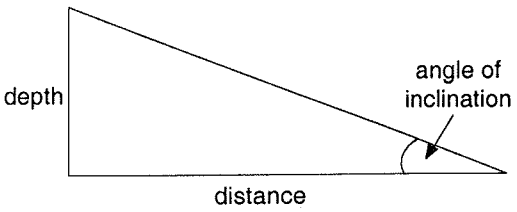

Legend:

- ramp — linear slope
- gentle slope — sigmoidal slope
- steep slope — sigmoidal slope
- basinal areas

Model A: rimmed platform (straight)										
Gentle slope:										
Water depth A2	70 m									
Distance from A2-M1 (N-S)	7,5 km									
Water-depth M1	90 m									
Angle of inclination	0,152°									
Steep slope:										
Distance from M1 to	Difference in water-depth between M1 and S9 (in m)									
Water-depth (N-S, in km)		100,00	150,00	200,00	250,00	**300,00**	350,00	400,00	450,00	500,00
WD	5,5	1,04	1,56	2,08	2,60	**3,12**	3,64	4,16	4,68	5,19
	5,0	1,15	1,72	2,29	2,86	**3,43**	4,00	4,57	5,14	5,71
	4,5	1,27	1,91	2,54	3,18	**3,81**	4,45	5,08	5,71	6,34
	4,0	1,43	2,15	2,86	3,58	**4,29**	5,00	5,71	6,42	7,13
	3,5	1,64	2,45	3,27	4,09	**4,90**	5,71	6,52	7,33	8,13
	3,0	1,91	2,86	3,81	4,76	**5,71**	6,65	7,59	8,53	9,46
	2,5	2,29	3,43	4,57	5,71	**6,84**	7,97	9,09	10,20	11,31
	2,0	2,86	4,29	5,71	7,13	**8,53**	9,93	11,31	12,68	14,04
		results = α, angle of inclination (in °)								

Model A´: rimmed platform (oblique)										
Gentle slope:										
Water-depth A2	70 m									
Distance from A2-M1 (NW-SE)	3 km									
Water-depth M1	90 m									
Angle of inclination	0,382°									
Steep slope:										
Distance from M1 to	Difference in water-depth between M1 and S9 (in m)									
Water-depth of (NW-SE, in km)		100,00	150,00	200,00	250,00	**300,00**	350,00	400,00	450,00	500,00
WD	13,0	0,44	0,66	0,88	1,10	**1,32**	1,54	1,76	1,98	2,20
	12,5	0,46	0,69	0,92	1,15	**1,37**	1,60	1,83	2,06	2,29
	12,0	0,48	0,72	0,95	1,19	**1,43**	1,67	1,91	2,15	2,39
	11,5	0,50	0,75	1,00	1,25	**1,49**	1,74	1,99	2,24	2,49
	11,0	0,52	0,78	1,04	1,30	**1,56**	1,82	2,08	2,34	2,60
	10,5	0,55	0,82	1,09	1,36	**1,64**	1,91	2,18	2,45	2,73
	10,0	0,57	0,86	1,15	1,43	**1,72**	2,00	2,29	2,58	2,86
	9,5	0,60	0,90	1,21	1,51	**1,81**	2,11	2,41	2,71	3,01
	9,0	0,64	0,95	1,27	1,59	**1,91**	2,23	2,54	2,86	3,18
	8,5	0,67	1,01	1,35	1,68	**2,02**	2,36	2,69	3,03	3,37
	8,0	0,72	1,07	1,43	1,79	**2,15**	2,51	2,86	3,22	3,58
	7,5	0,76	1,15	1,53	1,91	**2,29**	2,67	3,05	3,43	3,81
	7,0	0,82	1,23	1,64	2,05	**2,45**	2,86	3,27	3,68	4,09
	6,5	0,88	1,32	1,76	2,20	**2,64**	3,08	3,52	3,96	4,40
	6,0	0,95	1,43	1,91	2,39	**2,86**	3,34	3,81	4,29	4,76
	5,5	1,04	1,56	2,08	2,60	**3,12**	3,64	4,16	4,68	5,19
	5,0	1,15	1,72	2,29	2,86	**3,43**	4,00	4,57	5,14	5,71
	4,5	1,27	1,91	2,54	3,18	**3,81**	4,45	5,08	5,71	6,34
	4,0	1,43	2,15	2,86	3,58	**4,29**	5,00	5,71	6,42	7,13
	3,5	1,64	2,45	3,27	4,09	**4,90**	5,71	6,52	7,33	8,13
	3,0	1,91	2,86	3,81	4,76	**5,71**	6,65	7,59	8,53	9,46
	2,5	2,29	3,43	4,57	5,71	**6,84**	7,97	9,09	10,20	11,31
	2,0	2,86	4,29	5,71	7,13	**8,53**	9,93	11,31	12,68	14,04
		results = α angle of inclination (in °)								

Model B: asymmetrical platform	
Ramp part:	
Water-depth A2	70 m
Distance from A2-M1	15 km
Water-depth A2	90 m
Angle of inclination	0,076°
Gentle slope:	
same as the gentle slope of model A´	
Steep slope:	
same as the steep slope of model A´	

Table 1: *Calculation of the angle of inclination for the different parts of the platform-margin and for various water-depth differences. For the calculation of the angle of inclination the following formula has been used: tan α = WD/(D *1000) with: a = angle of inclination; WD = water depth (in m); D = distance (in km). For all calculations a water-depth of 70 m for St. Anthony 2 and of 90 m for Wadi Miraf 1 is assumed.*
In models A and A´ the gentle slope between sections St. Anthony 2 and Wadi Miraf 1 (direction measured perpendicular to the slope) vary from 0.152° (model A) to 0.382° (model A´). The steep slope of models A and A´ are calculated with different water-depth between sections Wadi Miraf 1 and St. Paul 9 and different distances from Wadi Miraf 1 to the point of the slope-basin transition. The bold characters below the number 300 (difference in water-depth between sections Wadi Miraf 1 and St. Paul 9, in m) indicate the probable angles of inclination. The smaller the distance between Wadi Miraf 1 and the slope-basin transition the steeper the slope. The ramp part of the asymmetrical carbonate platform model B has an inclination of 0.076°, whereas the gentle and the steep slope of the rimmed carbonate platform part have the same angles as the corresponding angles of the rimmed carbonate platform of model A´.
The different distances between sections St. Anthony 2 and Wadi Miraf 1 is due to the fact that these distances were measured perpendicular to the isobathes.

8. Discussion

8.1. Correlation of sequences and sea-level changes:

The correlation of our sedimentary sequences is based on biostratigraphic correlations that may cause confusion when using the Haq et al. (1987) sea-level curve. We do not refer to the general points of criticism (e.g. Miall 1992, 1997) but to the chronologies involved. The new sequence chronostratigraphic chart of Hardenbol et al. (1998) includes a recalibration of the earlier Haq et al. (1987) record (Fig. 5). With this recalibration the old sequence boundaries of Haq et al. (1987) shifted approximately 2 my upward (younger) so that e.g. the often cited sea-level fall at 71 Ma (Miller et al., 1999; Li et al., 1999) now has an age of 68.77 Ma (Hardenbol et al., 1998) and hence could not be correlated with the sea-level fall around 71 Ma (Miller et al., 1999; Li et al., 1999).

In our sections of Transect B, a hiatus spans biochrones CC24 to CC25a with a total duration of at least 3 million years from 72 Ma to 69 Ma (after Norris et al., 1998; Fig. 5). Assuming a 40 m sea-level fall around 71 Ma (Miller et al., 1999) which is in the lower part of CC24 (Norris et al., 1998) a subaerial exposure of the sediments in our sections is not realistic: no sedimentologic evidence of exposure is visible and the benthic foraminifera assemblages of the post-hiatus sediments suggest a water-depth of about 100 m what would be far more than the amount of the proposed sea-level fall and subsequent rise. If the hiatus around 71 Ma in our sections is attributed to an eustatic sea-level fall, it remains uncertain which processes led to the non-deposition and/or erosion. Possible reasons can be changed water circulation or bottom currents, condensed sections attributed to subsequent rise of sea-level or gravitational transport mechanisms like slumpings which led to the observed hiatus. In combination with eustatic sea-level changes, tectonic uplift of the Northern Galala/Wadi Araba High may have resulted in the observed hiatus. A similar hiatus was reported by Li et al. (1999) from age-equivalent sediments of Tunisia.

The sea-level fall at MaGal1 also could be the result of a eustatic sea-level fall as Haq et al. (1987) and Li et al. (1999) recorded a sea-level fall around 68 Ma. But local tectonic uplift movements of the Northern Galala/Wadi Araba High could not be ruled out because of the sudden high siliciclastic content of the whole sequence that should have their source somewhere farther north in the main regions of the Northern Galala/Wadi Araba High.

8.2. Carbonate platform models

All three models require a deepening from NE (section St. Anthony 3) to SW (section Wadi Miraf 1). This deepening can be demonstrated below and above sequence boundary MaGal1 by sedimentologic parameters like increasing carbonate contents from NE to SW, increasing thicknesses of the mass flow units from NE to SW (due to larger accommodation spaces) and in an emphasis of the shallow-up cycles in the NE section St. Anthony 3. Paleoecologic parameters like findings of shallow-water dwellers e.g. *Pinna* sp. and of teeth of bony fishes (preferring reefal environments) in calcareous nannoplankton zones CC25 of section St. Anthony 3 (NE) also suggest a shallowing towards NE. Kulbrok (1996) described sections farther in the west with depositional settings deeper than that of section St. Anthony 1. The only direct evidence for a paleoslope not only dipping in SE directions but

also in SW directions comes from the large synsedimentary slumpings visible in section St. Anthony 4 of biozone CC22 (Figs. 8e, 8f). Their gliding planes are dipping roughly E-W and thus require a paleoslope that is also oriented in E-W direction. These architecture requirements would fit with model B.

Other evidence for model B concerns the underlying structure. Many Syrian Arc structures on Sinai like Minsherah, Magharah, Hallal, Yelleq or Areif el Naqa (Moustafa and Khalil, 1995; Lüning et al. 1998; Kuss et al. in press.) exhibit double plunging anticlines, generally striking in ENE-WSW directions. Steep flanks are dipping in SE direction and gentle flanks in SW direction. This applied to the Syrian Arc Northern Galala/Wadi Araba High, representing the structural unit underneath the Late Cretaceous carbonate platform, supports the asymmetrical carbonate platform model B.

Slope angles in carbonate systems are recorded from less than 1° to up to more than 40° (Read, 1985). According to Kenter (1990) the sediment fabric is a major control on slope angles. Cohesionless sediments, such as clean sands and rubble, build up to angles over 40°, modified by shearing and avalanching. Muddy, cohesive sediments tend to maintain a low slope angle, decreasing to less than 15° for mud-supported fabrics and less than 5° for pure mud, modified by large-scale creep and rotational to translational sliding and slumping (Kenter, 1990).

The sediments of the investigated Upper Cretaceous platform margin are mainly composed of a muddy and mud-supported fabric with large-scale slumping, similar to those of the middle Miocene of the Little Bahama Bank (Kenter, 1990), where slope angles vary between 2° and 4°. As this example ranges at the lower end of the range spectrum for muddy to mud-supported sediments given by Kenter (1990), we would expect little higher values for the inclination of the Upper Cretaceous slope. Values of 5°-8° were calculated for all three models with the combination of the following parameters: a 300 m difference in water-depth between section Wadi Miraf 1 and section St. Paul 9 and a 2 km - 3 km distance between the hinge-line of the gentle/steep slope and the transition between steep slope and basin (Fig. 10; Table 1).

9. Conclusions

Systems Tracts could only be identified in the slope sections of Transect B, while the monotonous chalk-marl alternations of the basinal sections of Transect A could not be subdivided. The identified sea-level changes of sequences CaGal1, CaGal2 and MaGal1 are at least partly of eustatic origin but a tectonic component could not be ruled out, especially for the long lasting hiatus at sequence boundary CaGal2 and for the enhanced siliciclastic input of sequence MaGal1 a tectonic contribution may explain part of the sea-level changes.

We calculated the slope geometries referred to two principal carbonate platform models (rimmed platform, asymmetrical platform). Because of the initial structural topography and sedimentary patterns the model of an asymmetrical platform is favoured. This asymmetrical platform margin is formed like a rimmed platform with a sigmoidal slope profile in south-easterly direction and like a ramp with a linear slope profile in south-westerly direction. The rimmed platform can be subdivided into a gentle upper slope and a steep lower slope. The paleowater-depth between the

slope sections and the basinal sections change from 100 m (slope) to 300-500 m in the basinal sections. These differences in water-depth lead to angles of the steep slope of the rimmed part of 5° to 8°, whereas the ramp part would have an angle of less than 0.1°.

Acknowledgements:

A. M. Bassiouni (Ain Shams University) is especially thanked for many logistic supports. A. M. Morsi (Ain Shams University) is thanked for his open ear for all problems encountered during our stay in Egypt. R. P. Speijer (University of Bremen) is thanked for comments on a previous version of this paper. We thank J. A. M. Kenter, T. Aigner and B. Sellwood for their reviews and suggestions for improving the manuscript. A. Scharf, R. Bätzel and M. Brinkmann (all from University of Bremen) aided with sample preparation. The investigations were funded by the Graduiertenkolleg „Stoff-Flüsse in marinen Geosystemen" of the University of Bremen and the German Science Foundation (DFG).

References:

Abdel-Kireem, M.R. and Abdou, H.F., 1979. Upper Cretaceous-Lower Tertiary planktonic foraminifera from South Galala Plateau, Eastern Desert, Egypt. Revista Espanola de Micropaleontologica 11, 175-222.

Adams, E.W., Schlager, W. and Wattel, E., 1998. Submarine slopes with an exponential curvature. Sedimentary Geology 117, 135-141.

Adams, E.W. and Schlager, W., 2000. Basic types of submarine slope curvature. Journal of Sedimentary Research 70, 814-828.

Awad, G.H. and Ghobrial, N.G., 1965. Zonal stratigraphy of the Kharga Oasis. Geol. Surv. Egypt Paper 34, 77pp.

Bandel, K. and Kuss, J., 1987. Depositional environment of the pre-rift sediments - Galala Heights (Gulf of Suez, Egypt). Berliner geowiss. Abh. A 78, 1-48.

Burchette, T.P. and Wright, V.P., 1992. Carbonate ramp depositional systems. Sedimentary Geology 79, 3-57.

Camoin, G., Bellion, Y., Dercourt, J., Guiraud, R., Lucas, J., Poisson, A., Ricou, L.E. and Vielrynck, B., 1993. Late Maastrichtian Palaeoenvironments (69.5-65). In: Dercourt, J., Ricou, L.E. and Vrielynck, B. (Eds.), Atlas Tethyan paleoenvironmental maps. BEICIP-FRANLAP, Rueil-Malmaison.

Caron, M., 1985. Cretaceous planktic foraminifera. In: Bolli, H.M., Saunders, J.B. and Perch-Nielsen, K. (Eds.), Plankton stratigraphy. Cambridge University Press, Cambridge, pp. 17-86.

Cherif, O.H., Al-Rifaiy, I.A., Al-Afifi, F.I. and Orabi, O.H., 1989. Planktonic foraminifera and chronostratigraphy of Senonian exposures in west-central Sinai, Egypt. Revue de Micropaléontologie 32, 167-184.

Enos, P., 1991. Sedimentary parameters for computer modeling. In: Franseen, E.K., Watney, W.L., Kendall, C.G.S.C. and Ross, W. (Eds.), Sedimentary modeling: Computer simulations and methods for improved parameter definition. Kansas Geological Survey, Lawrence, pp. 63-99.

Haq, B.U., Hardenbol, J. and Vail, P., 1987. Chronology of fluctating sea levels since the triassic. Science 235, 1156-1167.

Hardenbol, J., Thierry, H., Farley, M.B., Jacquin, T., De Graciansky, P. and Vail, P.R., 1998. Mesozoic and Cenozoic sequence chronostratigraphic framework of European basins. In: de Graciansky, P.C., Hardenbol, J., Jacquin, T. and Vail, P.R. (Eds.), Mesozoic and Cenozoic sequence stratigraphy of European Basins. SEPM, Tulsa, pp. 3-13.

Kenter, J.A.M., 1990. Carbonate flanks: slope angles and sediment fabric. Sedimentology 37, 777-794.

Kuss, J., Scheibner, C. and Gietl, R., 2000. Carbonate Platform to Basin Transition along an Upper Cretaceous to Lower Tertiary Syrian Arc Uplift, Galala Plateaus, Eastern Desert, Egypt. Geoarabia 5, 405-424.

Kuss, J., Westerhold, T., Groß, U., Bauer, J. and Lüning, S., in press. Mapping of Late Cretaceous stratigraphic sequences along a Syrian Arc Uplift - examples from the Areif el Naqa/Eastern Sinai. Middle East Research Center.

Li, L., Keller, G. and Stinnesbeck, W., 1999. The Late Campanian and Maastrichtian in northwestern Tunisia: Palaeoenvironmental inferences from lithology, macrofauna and benthic foraminifera. Cretaceous Research 20, 231-252.

Luger, P., 1985. Stratigraphie der marinen Oberkreide und des Alttertiärs im südwestlichen Obernil-Becken (SW-Ägypten) unter besonderer Berücksichtigung der Mikropaläontologie, Palökologie und Paläogeographie. Berliner Geowissenschaftliche Abhandlungen A 63, 151pp.

Luger, P., El-Beshtawy, M. and May, H., 1998. Maastrichtian planktonic foraminiferal biozonation and K/T boundary in central Egypt. Revista Espanola de Micropaleontologia 30, 37-49.

Lüning, S., Kuss, J., Bachmann, M., Marzouk, A.M. and Morsi, A.M., 1998. Sedimentary response to basin inversion: Mid Cretaceous Early Tertiary pre- to syndeformational deposition at the Areif El Naqa Anticline (Sinai, Egypt). Facies 38, 103-136.

Lüning, D., Marzouk, A.M. and Kuss, J., 1998. Sequence stratigraphy of the Upper Cretaceous of central east Sinai, Egypt. Cretaceous Research 19, 153-196.

Malchus, N., 1990. Revision der Kreide-Austern (Bivalvia: Pteriomorphia) Ägyptens (Biostratigraphie, Systematik). Berliner Geowissenschaftliche Abhandlungen Reihe A, 231 pp.

Miall, A.D., 1992. Exxon global cycle chart: an event for every occasion? Geology 20, 787-790.

Miall, A.D., 1997. The geology of stratigraphic sequences. Springer, Berlin.

Miller, K.G., Barrera, E., Olsson, R.K., Sugarman, P.J. and Savin, S.M., 1999. Does ice drive early Maastrichtian eustasy? Geology 27, 783-786.

Moustafa, A.R. and Khalil, M.H., 1995. Superposed deformation in the northern Suez Rift, Egypt: Relevance to hydrocarbons exploration. Journal of Petroleum Geology 18, 245-266.

Norris, R.D., Kroon, D. and Klaus, A., 1998. Explanatory notes. Proceedings of the Ocean Drilling Program Initial Reports 171B, 11-44.

Özcan, E. and Özcan Altiner, S., 1997. Late Campanian-Maastrichtian evolution of orbitoidal foraminifera in Haymana Basin succession (Ankara, Central Turkey). Revue de Paléobiologie 16, 271-290.

Perch-Nielsen, K., 1985. Mesozoic calcareous nannofossils. In: Bolli, H.M., Saunders, J.B. and Perch-Nielsen, K. (Eds.), Plankton stratigraphy. Cambridge University Press, Cambridge, pp. 329-426.

Read, J. F., 1985. Carbonate platform facies models. AAPG Bulletin 69, 1-21.

Said, R., 1962. The geology of Egypt. Elsevier, Amsterdam.

Scheibner, C., Kuss, J. and Marzouk, A.M., 2000. Slope sediments of a Paleocene ramp-to-basin transition in NE Egypt. International Journal of Earth Sciences 88, 708-724.

Scheibner, C., Marzouk, A. M. and Kuss, J., in press. Maastrichtian-Early Eocene Lithostratigraphy and Palaeogeography of the N Gulf of Suez Region, Egypt. Journal of African Earth Sciences 32

Selima, A.M. and Askalany, M.M., 1996. Stratigraphy and depositional environment of the Upper Cretaceous-Lower Tertiary sequence, around Wadi Askhar El Qebly South Galala, Gulf of Suez, Egypt. Bulletin Faculty of Science, Assiut University 25 (2F), 87-106.

Sissingh, W., 1977. Biostratigaphy of Cretaceous nannoplankton. Geologie en Mijnbouw 56, 37-65.

Sirel, E., 1996. Description and geographic, stratigraphic distribution of the species of Laffitteina MARIE from the Maastrichtian and Paleocene of Turkey. Revue de Paléobiologie 15, 9-35.

Ward, P. D. and Kennedy, W. J., 1993. Maastrichtian ammonites from the Biscay region (France, Spain). Palaeontological Society, Memoirs 34, 1-58.

Wright, V.P. and Burchette, T.P., 1998. Carbonate Ramps: an introduction. In: Wright, V.P. and Burchette, T.P. (Eds.), Carbonate Ramps. Geological Society, London, London, pp. 1-5.

Zittel, K. A., 1883. Beiträge zur Geologie und Palaeontologie der Lybischen Wüste und der angrenzenden Gebiete von Ägypten. Paleontographica 30.

CHAPTER 4

Slope sediments of a Paleocene ramp-to-basin transition in NE Egypt

C. Scheibner, J. Kuss and A. M. Marzouk

published 2000
in the International Journal of Earth Sciences,
Vol. 88, p. 708-724.

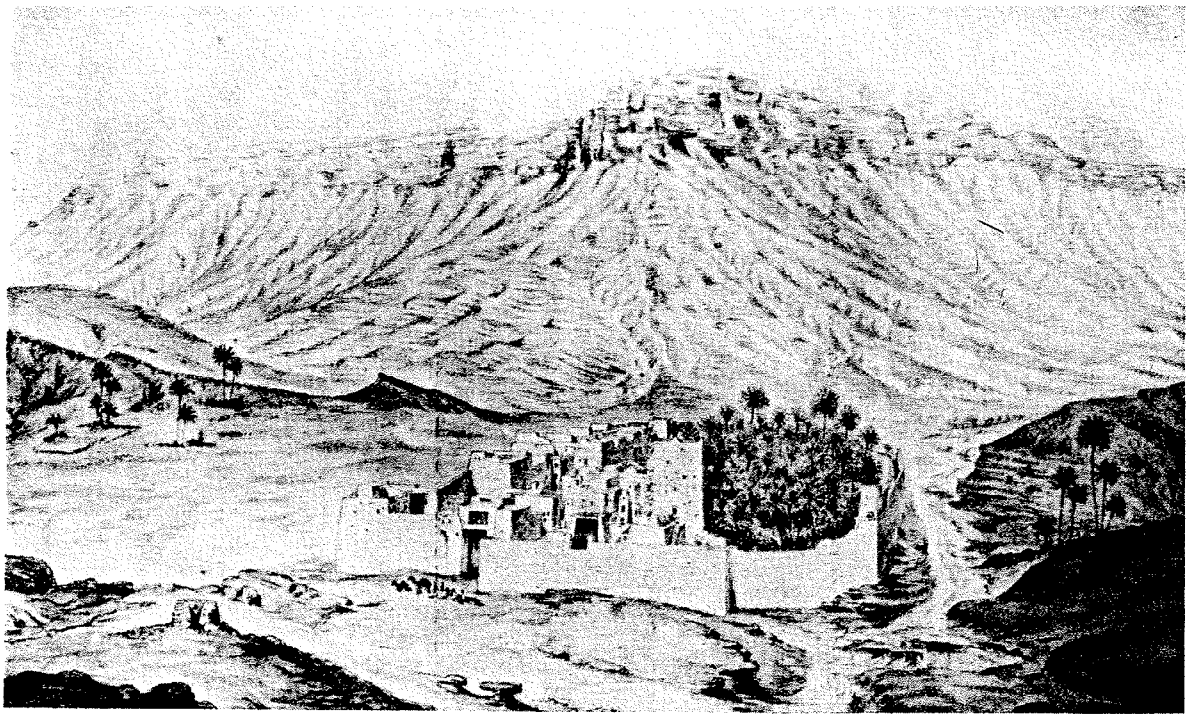

Kloster St. Paulus
von der Ringmauer auf der Ostseite aus gesehen

Monastery of St. Paul
view from the East

Drawing by Georg Schweinfurth (1876)

Slope Sediments of a Paleocene Ramp-to-Basin Transition in NE-Egypt

Christian Scheibner[a], Jochen Kuss[a] and Akmal M. Marzouk[b]

[a] Bremen University, FB 5, P.O. Box 330440, 28334 Bremen, scheibne@uni-bremen.de

[b] Geology Department, Faculty of Science, Tanta University, Tanta 31527 Egypt

Key words: Middle to Late Paleocene, glides, slumps, debris flows, microfacies analysis, algal shoals, nummulitidae shoals

Abstract:

Sedimentary structures, microfacies, and stratigraphy of a late Paleocene ramp to basin transition have been studied in the Galala Mountains in the northern part of the Eastern Desert of Egypt. Three phases of ramp progradation were observed. During non-progradation hemipelagic sediments were intercalated. These progradational phases are indicated by mass transport deposits of glides slumps and debris flows which came from different directions except from the south. At least two of these mass transport deposits may reflect deposition during sea-level lowstands, whereas the hemipelagic intercalations indicate transgressive phases. Microfacies analysis provided evidence of a change in the origin of the debris-flow deposits. They show a transition from a basinal-to-outer-ramp setting to a middle-to-inner-ramp setting and a change in organism distribution. While coralline red algae prevailed on the inner ramp in the Selandian to Thanetian, nummulitids dominated in the late Thanetian.

Introduction:

The area of the Galala mountains (Eastern Desert, Egypt) has been the focus of numerous studies mostly dealing with biostratigraphy and lithostratigraphy (Ismail and Abdallah 1966; Abdou et al. 1969; Abdel Kireem and Abdou 1979; Strougo et al. 1992; Faris, 1994). Only a few studies dealt with the overall architecture of the depositional system (Bandel and Kuss 1987; Kuss and Leppig 1989; Kulbrok 1996; Gietl 1998; Kuss et al., subm.). These authors propose a stuctural high during late Cretaceous times, situated at the central and southern parts of the North Galala including the Wadi Araba area to the south. Late Cretaceous slope deposits of the mid-outer ramp are exposed at the monastery of St. Anthony (Fig. 1). However, they are not present further south at the monastery of St. Paul where only their basinal equivalents occur (Kuss and Kulbrok, 1995). Ramp progradation continued during the Paleogene. The first ramp-derived allochthonous sediments were transported during the Selandian from northerly directions to the St. Paul area. The sections studied, west of the monastery of St. Paul, represent a segment of a ramp to basin transition within that southward-prograding ramp system.

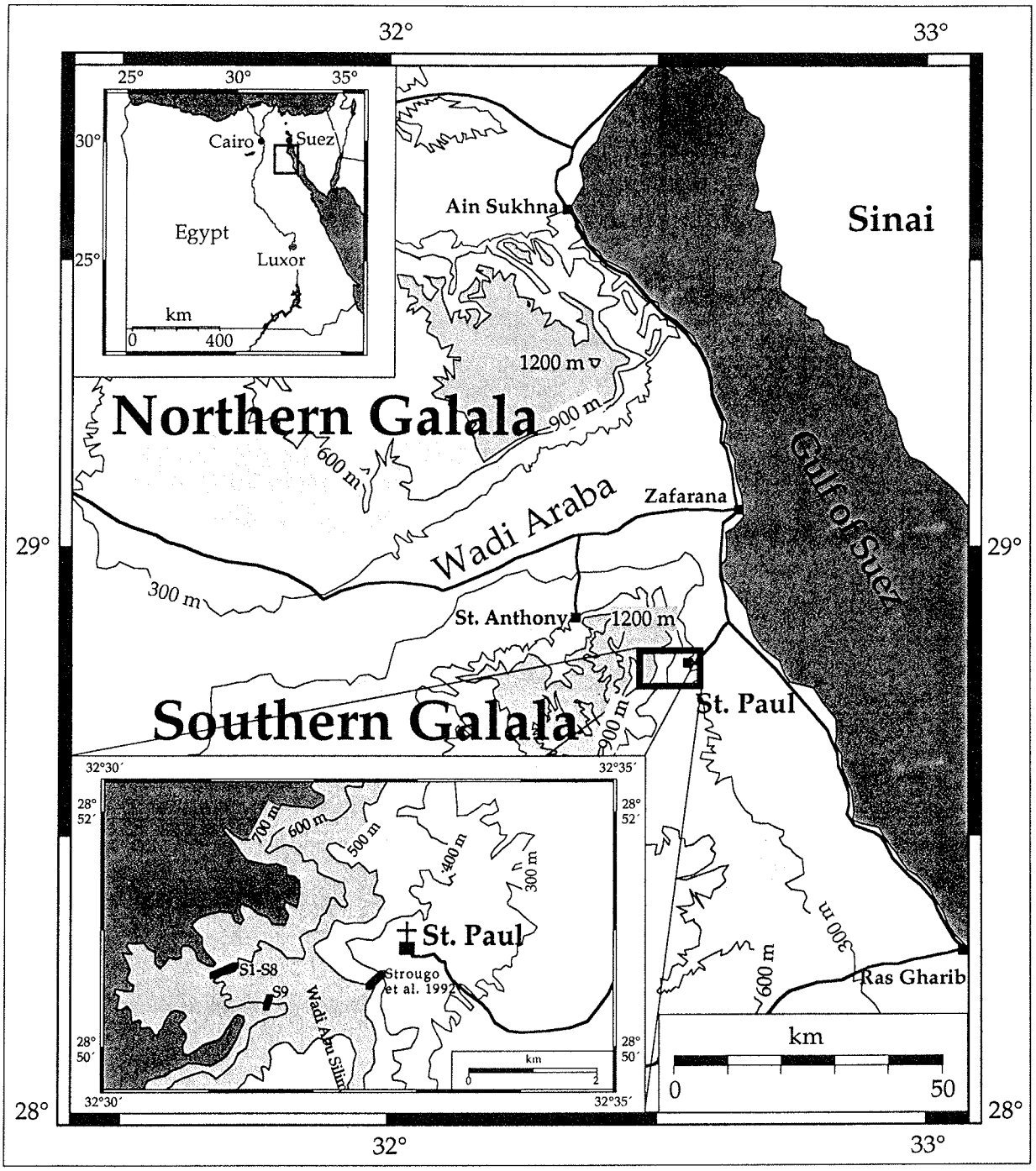

Fig. 1: *Topography of the Galala Mountains, Eastern Desert, Egypt, with insert maps of Egypt and the vicinity of the monastery St. Paul. Sections are indicated.*

This paper concentrates on an excellent, continuous outcrop near the monastery of St. Paul, 360 m wide and 50 m high, including a massive layer (20 m) composed of various units of mass transport sediments (Figs. 1, 3). They exhibit multiple transitions between glides and debris flows, mainly composed of carbonates with only minor contents of quartz. Thin section analysis of allochthonous carbonates indicates a wide spectrum of components originally formed in different environments of the Paleogene carbonate ramp situated further north. Many limestones within the different allochthonous units are comparable with shallow-water autochthonous ramp environments described earlier by Gietl (1998); moreover, we discuss various stages of ramp progradation during the late Paleocene.

Geological Setting:

During Maastrichtian to early Eocene times, a south dipping carbonate ramp evolved in the northern parts of the Eastern Desert of Egypt (Galala Heights, Fig. 1). Predominantly carbonate sediments were deposited along an E-W running tectonically induced uplift that covered parts of today's North Galala and Wadi Araba. This uplift represents the southernmost area affected by the Syrian Arc fold belt (Moustafa, 1995). It was formed as a consequence of the closing Tethys since Turonian times (Lüning et al., 1998).

The lower to upper Paleocene strata in the area of St. Paul reflect a transition from distal ramp settings, with basinal hemipelagic sediments, to settings influenced by carbonate mass transport deposits and shallow-water limestones. The Danian to Selandian (Planktic Foraminifers P1-P3 biochrons) basinal marls overlie upper Cretaceous (Maastrichtian) basinal chalks with marly intercalations of up to 12 cm thickness, whereas the chalky layers reach maximum thicknesses of 75 cm. In the upper part of the upper Maastrichtian succession, a few thin black shale intervals are intercalated.

A biostratigraphically continuous record across the K/T boundary is well documented in most sections of the St. Paul area, where sediments of the upper Maastrichtian calcareous nannoplankton *Micula prinsii* zone are overlain by Paleocene strata of the planktic foraminifer P1a zone (middle part of calcareous nannoplankton zone NP1, Strougo et al., 1992; Faris, 1994).

Marls prevail up to zone P3b (Fig. 3), and are disconformably overlain by limestones. Carbonate deposition was interrupted by two prominent marly intercalations during late NP5 and NP6 (Figs. 2, 5).

Few shallow-water communities of organic buildups recovered from the late Maastrichtian to early Paleocene biotic crisis (Schuster 1996). Diversity of carbonate communities began to increase again during the late Paleocene. Organic buildups were mainly composed of corals and red algae, although bryozoans are also reported locally (Bryan, 1991; Vecsei and Moussavian, 1997). The Eocene, however, was a time when larger foraminifers (mainly *nummulites*) thrived in shallow-water environments (Aigner, 1983). An overview of the paleoecology of reefal foraminifers and algae in the Cenozoic is given by Ghose (1977).

Material and Methods:

The ramp to basin transition was studied along a roughly WSW-ENE striking wadi ridge within the foothills south of the rising escarpment of the South Galala heights (Fig. 1) situated 2,5 km W of the monastery of St. Paul (E 32°31,288´; N 28°50,718´). The outcrop was subdivided into 6 distinct lithostratigaphic units.

The study is based on a detailed facies analysis (macro- and microscale) of eight vertical sections (S1-S8), taken along a lateral profile. 87 limestone samples were studied through thin-section analyses and 42 marly-shale samples for micropaleontologic studies (Fig. 2). A detailed mapping of all sedimentologic and structural features along the outcrop was supported by a photomosaic (Figs. 3, 4). Additionally, one parallel section (S9) was taken about 1 km to the SE of the profile presented here(Fig. 1) and covers the uppermost Cretaceous to lower Eocene succession. 60 washed samples and 15 thin-section samples were studied from this section and yield supporting data but will be discussed in Kuss et al. (subm.).

Biostratigraphy:

The biostratigraphic framework is based on both planktic and larger foraminifers, and calcareous nannoplankton. The biozonal and chronostratigraphic standards of Berggren et al. (1995) and Olsson et al. (1999) are used for planktic foraminifers, Martini (1971) for calcareous nannoplankton biozonation, and Hottinger et al. (1964), Serra-Kiel et al. (1998), and Gietl (1998) for larger foraminifers biozonation (Fig. 2).

Planktic foraminifers were found in marls of Units A, B, C, and E. A well preserved assemblage of *Acarinina strabocella, Morozovella angulata, M. conicotruncata, Igorina albeari, Globanomalina chapmani, Gl. haunsbergensis* occurs in Unit A. *Globanomalina pseudomenardii, Acarinina subsphaerica* and *A. mackanni* were not found in this unit, indicating biozone P3b. Forms morphologically similar to *M. acuta* were found as well but may belong to *M. conicotruncata*. Two samples of Unit B contain poorly preserved planktics, which could not support a biostratigraphic assessment.

A similar assemblage of planktic foraminifers as in Unit A was observed in Unit C. Moreover, the first specimens of *M. velascoensis* were found, which could be attributed to biozone P4 (Fig. 5).

Unit E was also attributed to biozone P4, suggested by typical *M. velascoensis* with well pronounced decoration, and the first occurrence of *Acarinina* sp. The index fossil *G. pseudomenardii* was not found. Luger (1985) indicated that *G. pseudomenardii* is seldom found in Egypt.

Larger foraminifers: Several index species were identified in thin sections: *Glomalveolina* sp., *Hottingerina lukasi* and the two conical species *Fallotella kochanskae persica* and *F. alavensis*. According to Drobne (1975), *H. lukasi* ranges within the *A. (G.) primaeva* biozone in Slovenia. However, White (1994) demonstrated this species ranging from *A. (G.) primaeva* to *A. (A.) ellipsoidalis* zones in Oman. Serra-Kiel et al. (1998) described it as index fossil of shallow benthic zone SBZ 4. Gietl (1998) and Kuss and Leppig (1989) described *H. lukasi* in the Galala Mountains

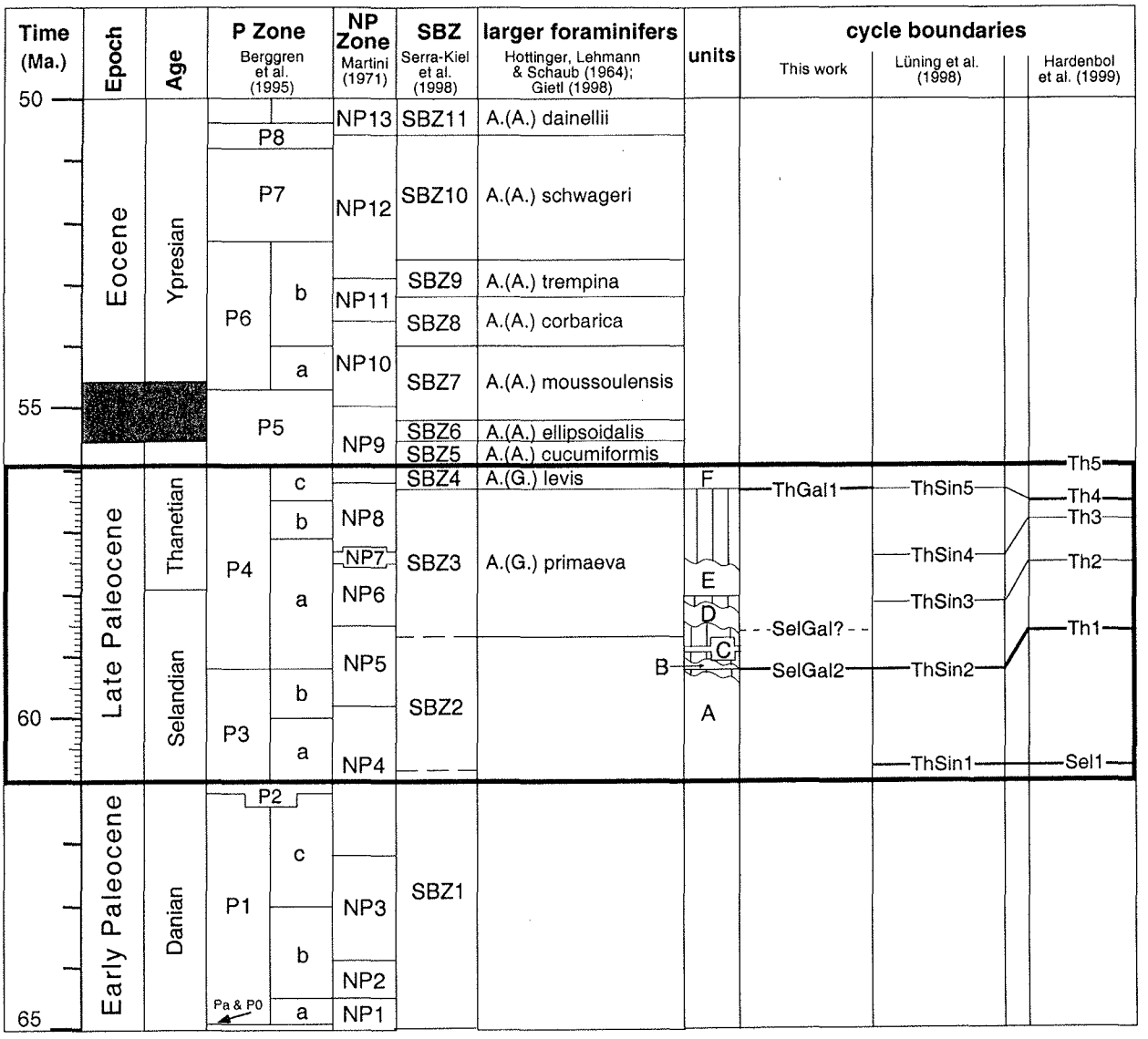

Fig. 2: *Paleocene to Eocene time scale. The time (Ma), epoch, age and planktonic foraminifers zonation are from Berggren et al. (1995). Calcareous nannoplankton zonation is from Martini (1971), the shallow benthic zonation (SBZ) is from Serra-Kiel et al. (1998) and the larger foraminifer zonation is from Hottinger et al. (1964) and Gietl (1998). The broad grey band reflects the current opinion on the position of the Paleocene/Eocene boundary. The black rectangle marks the stratigraphic interval investigated in sections S1-S8. Within the rectangle the units described and cycle boundaries are marked. Comparisons of cycle-boundaries are based on absolute ages. Mismatches are due to different biostratigraphic concepts used by the authors.*

from the *A. (G.) levis* biozone. *Fallotella alavensis* was found by Leppig (1987) in Spain coinciding with the A. (G.) *primaeva* biozone, and according to Hottinger and Drobne (1980) and Serra-Kiel (1998) this species is restricted to the *A. (G.) primaeva* biozone; the same is true for *F. kochanskae persica* (Hottinger and Drobne, 1980). In contrast, Gietl (1998) and Kuss and Leppig (1989) found this species in the *A. (G.) levis* biozone from the Galala Mountains. On the basis of this classification, the association of *H. lukasi, F. kochanskae persica, F. alavensis, Mis. rhomboidea,* Discocyclinidae,

Broeckinella, A (G.) dachelensis, Ranikothalia and *Archeolithothamnium* has been used to define the *A. (G.) levis* biozone, coinciding with SBZ 4 of Serra-Kiel et al. (1998).

Small larger foraminifers were also found within the hemipelagic marls of Unit E.

Benthic foraminifers: Whereas the benthic foraminifers of Unit A indicate a position on the deeper shelf, the samples of Units C and E contain a mixture of autochthonuous deeper (mixed Midway and Velasco Fauna, indicating a water depth of about 500 m) and allochthonous shallower shelf forms (Speijer et al., 1994, pers. com; R.P. Speijer, 1999).

Calcareous nannoplankton: Well preserved microfloras have been identified in marls of Units A, B, C, and E. Unit A was attributed to biozones NP4 (S2-1 - 8) with *Markalius inversus, Chiasmolithus tenius, Ellipsolithus macellus* (index form) and *Coccolithus pelagicus*. Units B and C have been attributed to NP5 (Fig. 5). NP5 (S1-1 - 3; S2-9 - 13, S4-5 - 7; S7-1 - 4; S8-1 - 7) is characterised by the above mentioned species and *Fasciculithus tympaniformis* (index form), *F. janii, F. bitectus* and *Chiasmolithus consuetus*. Samples S4-20 and S4-21 of Unit E hold specimens of NP6 with the index form *Heliolithus kleinpellii*.

Lithostratigraphic Units:

Unit A (thickness: 5 m - 10 m) consists of marls at the base which are of early to early late Paleocene (P1-P3) age disconformably overlain by limestones of Unit B. The sharp contact between both units, which is often covered by alluvial gravel (Figs. 3a, b), is well exposed in sections S1, S2, S8, and S9. Following the contact laterally from S1 in the west to S8 in the east, its erosive character becomes obvious: several incisions of Unit B into the soft lithologies of Unit A form a conspicuous large-scale undulating boundary along the profile (Fig. 3).

Unit B (thickness: 4 m - 6 m) is characterised by hard, massive carbonates with various textural characteristics. Peloidal micrites prevail together with a varying degree of quartz. The latter is also frequent in washed samples (S1-5 and S2-14).

The carbonates include undisturbed horizontally to eastward dipping bedding planes, glides and slumps. The intensity of disturbance within this unit decreases from west to east. At the western end of the profile (lateral distance (ld) 1 m -10 m; Fig. 3), a chaotic melange occurs with only few slumped beds that exhibit an S-shape; next to this, an area of slumped beds occurs that are still in original sedimentary contact (ld 15 m, Fig. 4g). A little further to the east (ld 30 m), no obvious slumps occur but the beds are dipping at a maximum angle of 20° to the east. Dipping is best visible in the upper parts of Unit B due to its constant bed thickness. But a few basal beds exhibit changing thicknesses (Fig. 4h). Here, the younger limestone beds clearly show onlap patterns. Further to the east, slumping ceases (ld 85 m) and the strata dip to the east with less and less inclination. East of ld 270 m (Fig. 3), no onlap is visible but all beds have a smooth waveform appearence. Abundant *Thalassinoides* burrows were found at the top of Unit B in sections S3, S5, and S6 (Fig. 5).

Unit B is mainly composed of glides and slumps except one debris flow at the easternmost part of the profile between sections S7 and S8 (Figs. 3b, 4l). Prather et al. (1998) classified slope deposits from

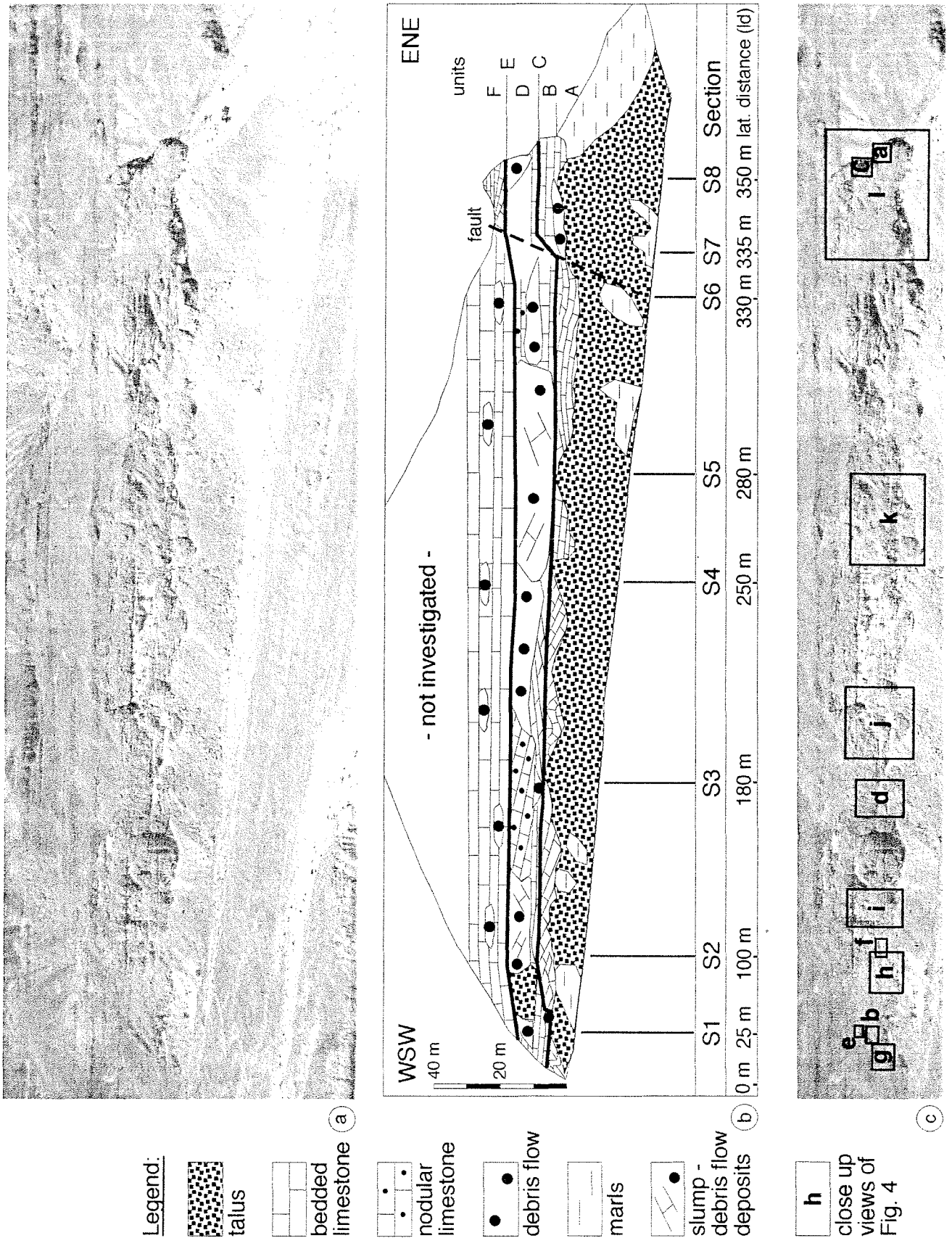

Fig. 3: a) *Investigated outcrop.* 3b) *Sketch of outcrop with sedimentological features and location of sections. c) Outcrop with location of close-up photographs shown in Fig. 4.*

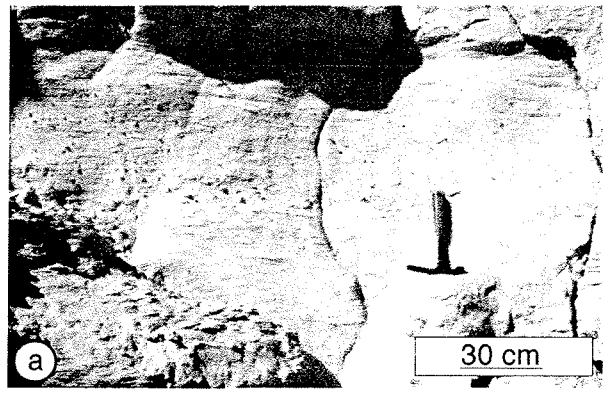
a
30 cm

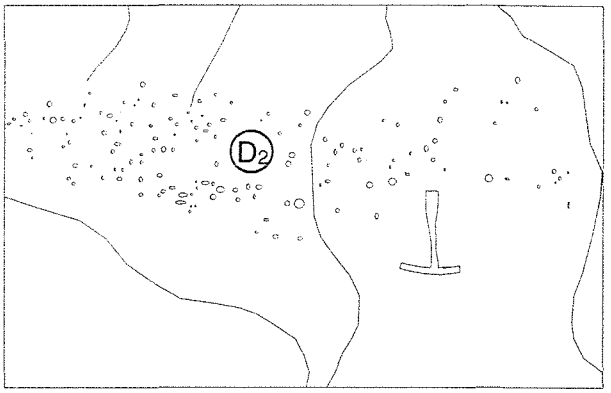
D2


b
60 cm


c
60 cm


d
2 m

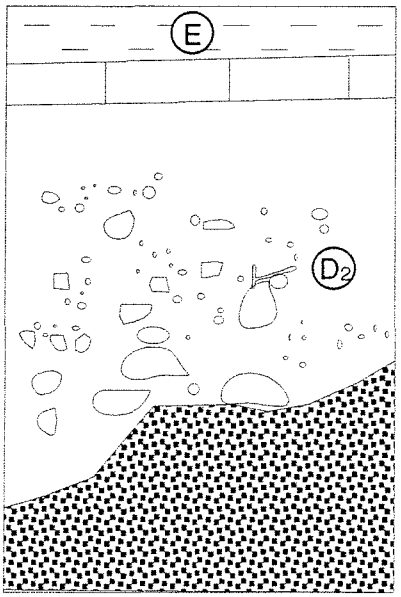
E
D2

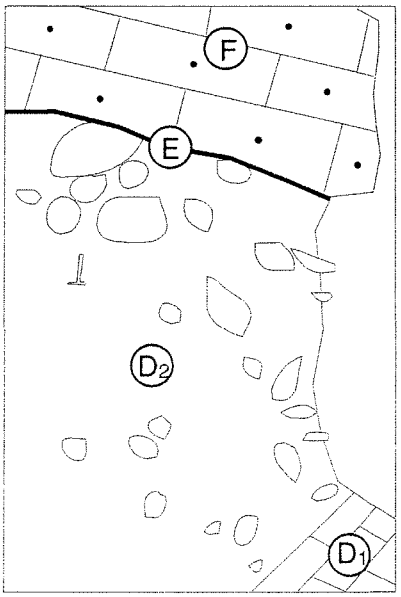
F
E
D2
D1

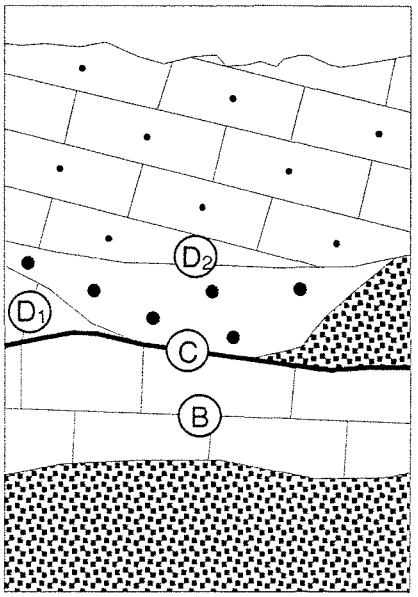
D2
D1
C
B

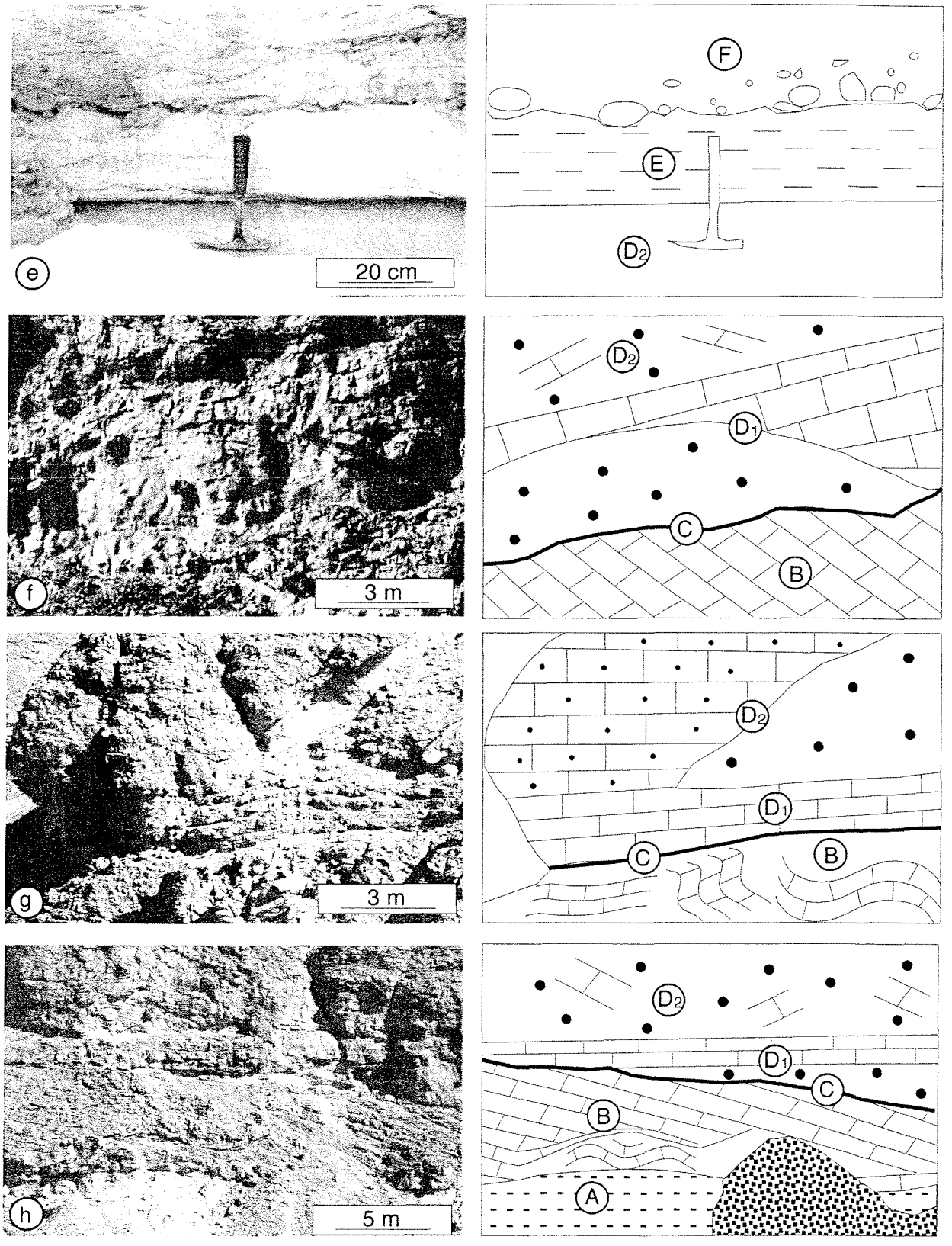
e
20 cm
F
E
D2
f
3 m
D2
D1
C
B
g
3 m
D2
D1
C
B
h
5 m
D2
D1
C
B
A

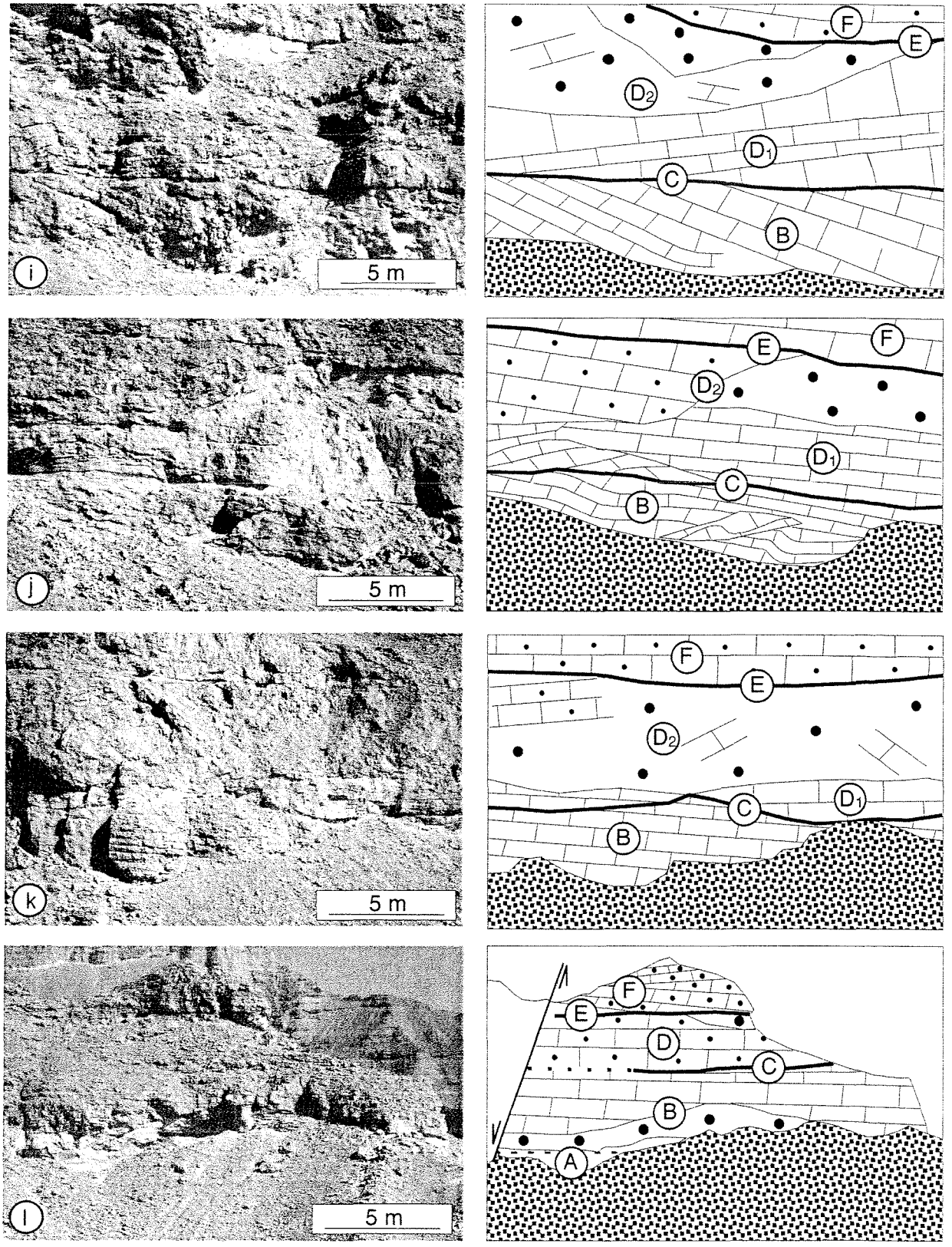
i
5 m
F
E
D2
D1
C
B
j
5 m
E
F
D2
D1
C
B
k
5 m
F
E
D2
C
D1
B
l
5 m
F
E
D
C
B
A

Fig. 4 (previous 3 pages): *Photographs (left side or upper side) and illustrated sketchs (right side or lower side) of close ups. For location and legend of close ups see Fig. 3. Scale is in the lower right corner of the photographs. The letters within the sketches indicate the units present.*
Figs. a-c illustrate the different types of debris flows (df) present.
a) *df 1a, with very small clasts of about 1 cm is present in one debris flow east of section S8.*
b) *df 1 with heterogeneous size distribution ranging between df 1a and df 1b. This is the most common debris flow type.*
c) *df 1b with very large clasts of 25 - 50 cm is present in one debris flow in section S8.*
Figs. d-l are close ups of the outcrop.
d) *In contrast to all other debris flows which are shaped convex-upward this one is shaped convex-downward. Probably it was deposited within a channel.*
e) *Erosional contact of hemipelagic marly chalks of Unit E and a debris flow of Unit F (profile S1).*
f) *Typical convex-upward shaped debris flow. The surrounding strata show onlap structures.*
g) *Western end of lateral profile. Here Unit B is composed of heavily slumped beds which are disconformably overlain by Unit D. The more or less horizontal carbonate layers of Unit D_1 are overlain on the left by a massive slightly layered nodular limestone and on the right by a debris flow (for detail see Fig. 4b).*
h) *Generally east dipping beds of Unit B. Note the wavy bed thinning to the left. Here one of the two debris flows within Unit D_1 is seen. The horizontal layers of D_1 are onlapping Unit B. On top a typical slump to debris flow deposit is visible.*
i) *The contrast of the east dipping beds of Unit B (20°) and the west dipping, partly thinning beds of Unit D_1 is clearly visible. The top is composed of slump to debris flow deposits and a debris flow.*
j) *Onlap pattern of massive, slightly bedded nodular limestone on a debris flow in Unit D_2. Note the slumps in Units B and D_1. The hemipelagic marly chalk deposits of Unit E clearly separate the shallower deposits of Units D and F.*
k) *Nearly horizontal layers of Unit B are overlain by a slump to debris flow. Again Unit E separates Unit D and F.*
l) *The eastern end of the lateral profile. A fault and debris on the left side make the correlation to the rest of the profile difficult. Note the debris flow in Unit B with typical onlap structures of surrounding sediments. The debris flow of Unit D is characterised by debris flow type 1b with large clasts. For detail see Fig. 4c. Unit F here is composed of slightly layered nodular limestones with changing inclination.*

the Gulf of Mexico on the basis of seismic facies; their facies A + Bl of chaotic rotated slump blocks exhibit similar characteristics of the slumps, submarine slides, and debris flow described here.

Unit C (thickness: 5 cm-8 cm) consists of a few centimeters thick marly intercalation exposed in sections S3 and S5 only. Units B and D overlie one another disconformably in all other sections without exposing Unit C. The correlation of Unit C with a 20 cm thick chalk layer in section S8 is based on lithostratigraphy only, and could not be confirmed due to a fault and gravel cover between sections S7 and S8 (Fig. 4l).

Unit D (thickness: ~ 10 m) forms a steep cliff, and allows detailed mapping of the internal sedimentologic architecture based on both, field observations and the use of a photomosaic. The prevailing debris flows and slump deposits in the upper part of the unit (D_2) conformably overlie nearly horizontally bedded, slightly W-dipping deposits of the lower parts (D_1). These are composed of mainly well bedded carbonates with a large-scale undulating lower boundary and small slumping structures. In contrast to Unit B with a general eastward dipping direction (maximum inclination of 20°), the strata of Unit D_1 dip to the west (maximum inclination of 10°). A few small-scale debris flows with a maximum width of 20 m and a height of 2 m directly overlie Unit C (Fig.

5f) and, moreover, onlap patterns are obvious. In section S6 a 2 m thick stratified sand layer at the base of D_1 disconformably overlies Unit B (Fig. 5); small bivalves are oriented horizontally in several layers of that carbonate-cemented sandstone.

At the western end of Unit D_2, the lateral profile consists of poorly bedded to massive carbonates clearly onlapping a debris flow from west to east (Fig. 4g). East to this debris flow, a 25 m wide, poorly exposed area was mapped, followed by a 40 m wide unit (ld 90 m) of a slump to debris flow, exhibiting both partly stratified beds and true debris flow deposits. Within the next 70 m (ld 150 m), poorly bedded nodular limestones occur dipping to the east with an inclination of 10° (Fig. 4j). Onlapping patterns are discernible where these poorly bedded layers overlie a 50 m wide true debris flow, laterally grading into a slump to debris flow unit of 70 m width. Further to the east (ld 300 m), another 30 m wide debris flow continues. Fine gravel covers Unit D_2 in the eastern parts of the profile, where prevailing bedded strata have been discerned. At the easternmost end of the lateral profile, again a small debris flow has been mapped, unconformably overlain by bedded nodular limestones of Unit F (Fig. 4l). Similar to Unit B *Thalassinoides* burrows were found at the top. Carbonates of Unit D_1 reflect deeper shelf to shallow slope deposits, compared to hemipelagic drape deposits on slopes (Prather et al., 1998). The intercalated sandstone layer (section S6) reflects a discontinuous channelized body that has been interpreted as sediment derived from submarine canyons. Unit D_2 comprises all lateral and vertical transitions from slumps to debris flows; a clear separation between them is not always possible (see discussion for Unit B).

Unit E (thickness: 20 cm - 40 cm) unconformably overlying Unit D consists of a thin chalk-marl couplet. It could be traced from east to west throughout the entire profile and was also identified in section S9 (Fig. 1).

Unit F (thickness: 10 m - 12 m) couldn't be mapped in detail neither in the field nor with the photo-mosaic because of the poor exposure and strong weathering of this topmost Unit F. Two macroscopically determined facies have been distinguished; bedded carbonates and debris flows. The debris flows of Unit F mainly consist of clasts with only little surrounding matrix, in contrast to the debris flows from the lower units (B and D) with a minor volume of clasts. Few of the bedded carbonates show internally nodular structures. In section S1, the overlying Unit F is composed of a small debris flow with single to few clasts (Fig. 4e), here with a clearly visible erosive contact between them.

While the debris flows of Unit F exhibit a plastic internal mechanical behaviour, the nodular limestones argue for an elastic behaviour, formed within translational slides (glides sensu Cook and Mullins, 1983).

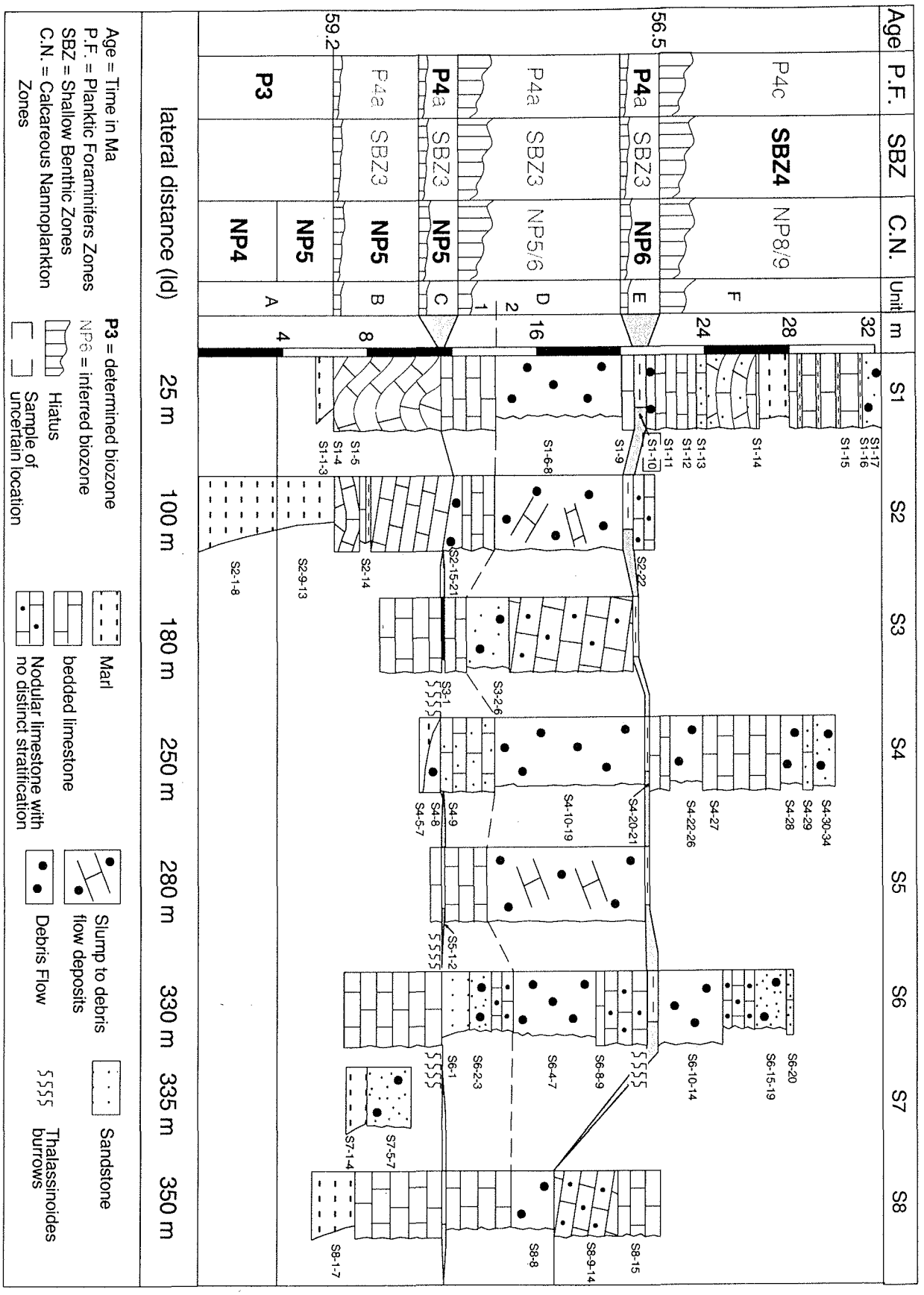

Fig. 5: *Stratigraphic correlation of sections S1 to S8 with their typical sedimentologic features. Sample numbers are indicated.*

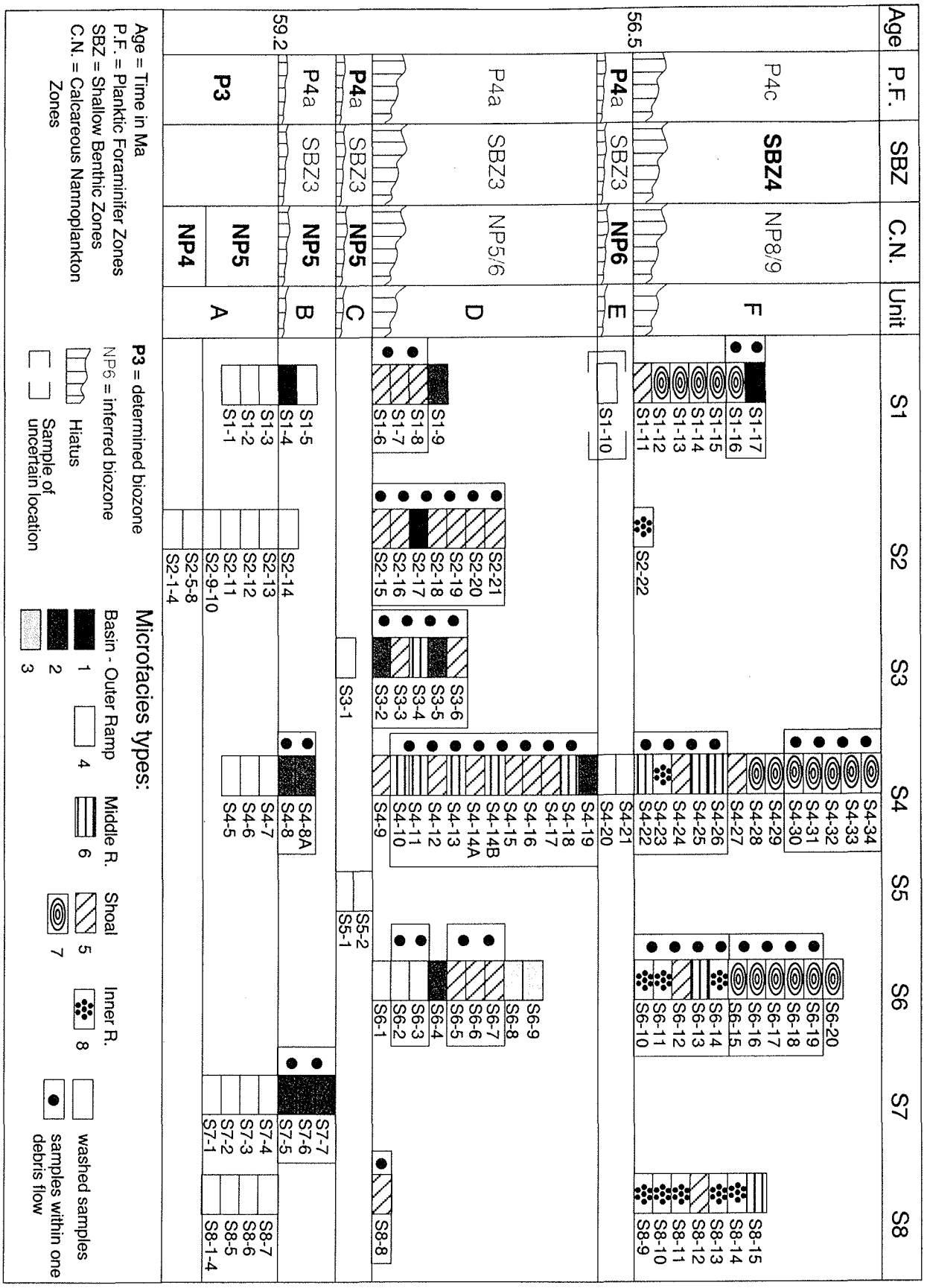

Fig. 6: *Microfacies type distribution throughout sections S1 to S8 with stratigraphic correlation. The samples grouped together with dots are from one debris flow. Note, that the debris flows are quite often formed by only one microfacies type.*

Microfacies Types:

In Table 1 the important components are listed and their distribution within the microfacies types is marked. Fig. 6 shows the microfacies type distribution throughout sections S1 to S8 with stratigraphic correlation.

MFT1 Planktic foraminifers micrite: It was formed as hemipelagic mud in deeper shelf areas, not or only slightly influenced by nearby shallow-water deposits. The relatively high quartz content may be derived from submarine canyons and reflects sediment bypassing (Fig. 7).

MFT2 Micrite with quartz: The co-occurrence of planktic foraminifers, filaments, and further small bioclasts in MFT2 combined with the absence of shallow-water biota is interpreted as being characteristic of outer ramp environments, again influenced by siliciclastic sediment bypassing.

MFT3 *Discocyclina* micrite: Bryan (1991) described *Discocyclina* from deep fore-reef and upper basin slope environments similarly to Ghose (1976), who described long, flat *Discocyclina* from the fore-reef. Gietl (1998) reported *Discocylina* from the middle ramp facies of the Galala areas. MFT3 was attributed to autochthonous middle to outer ramp environments because of the abundance of long, flat *Discocyclina* and *Asterocyclina* and the small quantity of other biota.

MFT4 Micritic sandstone: The quartz grains are derived from siliciclastic shoals of the shallow ramp (Gietl, 1998). We interpret their occurrence in section S6 as a result of transportation downslope via submarine canyons. An amalgamation with debris flows cannot be excluded due to their similarities to MFT2.

MFT5 Corallinacean nummulitid micrite to sparite: The coralline algae can be used for paleobathymetric interpretations. According to Bosence (1991) small solitary and branching forms occur in medium energy reefs and buildups such as maerl or back-reef mounds. Autochthonous floatstones with coralline algae have been described by Gietl (1998) from upper Paleocene limestones of the North Galala, where they occur in deeper environments of the inner ramp. This interpretation is in good concordance with observations by Buchbinder (1977), who described similar algal deposits of Miocene back-reef platform areas in Israel.

MFT6 Coral micrite: The allochthonous coral fragments dominate this MFT that was originally formed as talus of coral algal reefs, although a reef belt has not been reported by previous authors from the areas further north, our observations suggest at least broader patch reefs. Similar small-scale Early Paleocene coral algal reefs have been reported by e.g. Vecsei and Moussavian (1997) from the Maiella Platform (Italy) and Schuster (1996) from the Abu Tartur Plateau (Western Egypt).

MFT7 Nummulitid micrite to sparite: The limestones of MFT 7 were originally formed close to nummulitic shoal environments situated near inner to middle ramp positions (Gietl, 1998). Allochthonous alveolinids and dasycladaceans demonstrate inner ramp influences. The two subtypes reflect no true nummulitid shoal deposits as described by Gietl (1998), but are deposited in back- or fore-shoal areas.

MFT8 Miliolid biopel sparite to micrite: This MFT reflects inner ramp environments and includes reworked particles from restricted areas, documented by the high amounts of miliolids and endolithic algae. This is also indicated by the occurrence of conical imperforate foraminifers (Hottinger and Drobne, 1980). The high content of nummulitids is interpreted as a result of redeposition.

MF-types	number of thinsections	Dunham-Classification	components	matrix: micrite	matrix: sparite	biogene components: planktic foraminifers	biogene components: discocyclinidae	biogene components: nummulitidae	biogene components: *miscellanea*	biogene components: *glomalveolina*	biogene components: conical foraminifers	biogene components: miliolids	biogene components: *Hottingerina lukasi*	biogene components: coralline algae	biogene components: corals	biogene components: dasycladaceans	biogene components: echinoderms	abiogene components: peloids	abiogene components: intraclasts	abiogene components: quartz	occurance:clast(c)/bed(b)	prevailing in unit	interpretation
1-Planktic foraminifers micrite	3	w																			c,b	all	hemipelagic mud
2-Micrite with quartz	10	w,p																			c,b	B,D	outer ramp
3-Discocyclina micrite	2	w,p																			b	D	outer to middle ramp
4-Micritic sandstone	3	p																			c,b	D	outer ramp
5-Corallinacean nummulitid micrite to sparite	26	p																			c,b	D,F	shoal, middle to inner ramp
6-Coral micrite	11	p																			c,b	D,F	coral-algal reef
7-Nummulitid micrite to sparite	18	p																			c,b	F	nummulitid shoal, middle to inner ramp
8-Miliolid biopel sparite to micrite	10	p																			c,b	F	inner ramp

— rare — common ▬ abundant ▬ very abundant

Table 1: *Distribution of components in the MF-types. Within the table only the most important components are mentionend. Gastropods, shell fragments, bioclasts, etc. are of minor importance.*

Discussion:

The lateral and vertical distribution of the studied late Paleocene sediments allowed to reconstruct the sedimentation processes of a ramp to basin transition during seven successive stages (Fig. 8A-F). On the basis of all sedimentologic and stratigraphic data, the progradation of mainly allochthonous carbonate ramp deposits (of outer-mid ramp to mid-shallow ramp origin) and their interfingering with autochthonous basin sediments will be illustrated.

Types of Mass Transport

The main transport mechanisms of the sediments described here are mass transport processes due to gravity forces. Einsele (1991) summarized many descriptions of prevailing siliciclastic mass transport deposits. Carbonate-dominated mass transport processes have been subdivided by Cook and Mullins (1983) into three types: rockfall, slides and sediment gravity flows (Table 2). Slides can furthermore be divided into translational (glide) and rotational (slump) types. The shear plane of glides is parallel to the underlying beds, whereas in slumps the shear planes are concave-upward with a backward rotation of the slumped body (Cook and Mullins, 1983). Middleton and Hampton (1976) defined the term sediment gravity flow as "flows consisting of sediment moving downslope under the action of gravity". They distinguished four subtypes that differ in the support mechanisms of the single grains within the flow: debris flow, grain flow, fluidized sediment flow and turbidity current. Lowe (1976) added the liquefied sediment flow to these four subtypes. These classifications represent idealized members of sediment gravity flows, and real flows can show all transitions between the grain support mechanisms (Middleton and Hampton, 1976). Along a lateral transect, one subtype may also induce the other, e.g. a glide may induce a debris flow which itself could induce a turbidity current. Thus they might evolve during downslope transport, when the rheologic (Prior and Coleman, 1984) or relief parameters (Piper et al., 1999) change. Within the gravity flow processes, debris flows (cohesive) and turbidites are the main mechanisms for sediment transport (Mutti, 1992), whereas the others like grain flows, liquefied flows and fluidized flows represent transient conditions that occur within gravity flows during transport. Further details about flow regimes in sediment gravity flows are found in Postma (1986), Fisher (1983), Enos (1977), and Einsele (1991). In the lateral profile studied, slides (represented by glides and slumps) and sediment gravity flows (represented by debris flows) including transitions between both are most frequent.

Debris Flow Deposits

They vary in size and shape, both vertically and horizontally. Moreover, they contain different types of clasts also varying in size. The following short description summarizes major differences of debris flows observed macroscopically.

All debris flows vary in thickness between 0.5 m to 7 m and in width between 10 m to 50 m; however, originally greater thickness values may have been reduced by subsequent erosion. The most common debris flow shape is represented by convex-upward lenses often visible only at one side of a debris flow cross-section (Figs. 4f, 4g, 4j, 4l; see also Mutti, 1992) with onlap patterns of the younger sediments. Few debris flows exhibit convex-downward shapes (Fig. 4d) with sharp contacts to the overlying layers. Sharp straight contacts can also be seen in convex-upward debris flows, especially the large ones of Unit D which are directly overlain by Unit E (Fig. 5). This contact is probably an erosional feature (Fig. 4j).

Two main groups of debris flows (df) have been distinguished, matrix supported (df 1) and clast supported (df 2). Within the first containing well-sorted clasts (all within a fine matrix), two

different subtypes have been established (df 1a, b) ranging from small clasts with a maximum diameter of 1 cm (df 1a, Fig. 4a) to large clasts of 25-50 cm diameter (df 1b, Fig. 4c). Both subtypes of well-sorted debris flows are only found in the vicinity of section S8, while all the other matrix supported debris flow deposits are characterised by a lesser sorting of clasts (Fig. 4b). 33 clasts of df 1 deposits have been sampled for the detailed descriptions of microfacies types (MFT) given above. We selected fossil-bearing clasts without macroscopically discernible diagenetic overprints. Therefore, the MFT distribution shown for the entire outcrop (Fig. 6) reflects a non-statistical distribution (over-representation). Micrites with planktic foraminifers (MFT1) are present in all debris flows in varying amounts, only few micritic samples were taken, resulting in an under-representation in Fig. 6.

Clast-supported debris flows (df 2) have been observed only in Unit F, often with transition to nodular limestones. This type of debris flow has little or no matrix, and in contrast to df 1, all the 22 clast samples taken contain mainly fossil-bearing MFTs. Most debris flows found are composed of only one MFT, e.g. Unit D_2 of MFT5 or Unit F of MFT7 (Fig. 6).

Types of mass transport		Transport mechanism and dominant sediment support
Rockfall		Freefall and rolling single blocks along steep slopes
Slide	translational (Glide)	Shear failure along discrete shear planes subparalell to underlying bed
	rotational (Slump)	Shear failure along discrete concave-up shear planes accompanied by rotation of slide
Sediment gravity flow	Debris flow or Mud flow	Shear distributed throughout the sediment mass. Clasts supported above base of bed by cohesive strength of mud matrix and clast buoyancy. Can be initiated and move long distances along very low angle slopes
	Grain flow	Cohesionless sediment supported by dispersive pressure. Usually requires steep slopes for initiation and sustained downslope movement
	Liquefied flow	Cohesionless sediment supported by upward displacement of fluid. Requires slopes > 3°
	Fluidized flow	Cohesionless sediment supported by upward motion of escaping pore fluid. Thin and short lived
	Turbidity current flow	Clasts supported by fluid turbulence. Can move long distances along low angle slopes

Table 2: *Mayor types of submarine mass transport on slopes and their transport mechanism and dominant sediment support (modified after Cook and Mullins, 1983)*

Evolution of Units:

The upper Maastrichtian hemipelagic chalk-marl deposits of the area south of the South Galala continue in marly lower Paleocene sediments (**Unit A**). While the stratigraphic succession of the lateral profile spans from zone P3 (NP4) upwards, the neighbouring section S9 (Fig. 1) spans an upper Maastrichtian - Paleocene succession. In section S9 zones P1 - P4 and NP1 - NP5 were encountered. Benthic foraminiferal assemblage, including *Gavelinella beccariformis* and *Nuttallides truempyi*, indicate "bathyal" deposition (pers. com. R.P. Speijer, 1999).

Unit B was formed during late NP5 times, but a short-term hiatus is indicated by the basal erosive contact with the underlying Unit A (Figs. 2, 5). The carbonates of Unit B originated from distal ramp settings and represent the first phase of early late Paleocene ramp progradation onto hemipelagic sediments. Here, glides and slumps are obvious (Fig. 4g - 4k), and even few small-scale debris flows occur (Fig. 4l). Prevailing eastward dipping directions of glides and slumps indicate a west-east direction of transport (Fig. 8). We assume that these mass transport deposits were formed in outer ramp environments, as indicated by characteristic MFTs determined in clasts that were derived from the internal parts of debris flows in sections S4 and S7.

Prior to the onset of Unit C, the carbonate sedimentation of Unit B ceases as evidenced by the occurrence of decimeters thick *Thalassinoides* burrows at the top. Formed within aerobic environments (Zhou Zhicheng et al., 1997), these *Thalassinoides* burrows indicate a decrease of sedimentation rates during late Unit B times and the top the burrows may represent a flooding surface.

The soft hemipelagic marls of **Unit C** (NP5) disconformably overlie the limestones of Unit B. The benthic foraminifers show a mixture of autochthonous deeper (mixed Midway and Velasco Fauna) and allochthonous shallower shelf forms (Speijer et al., 1994, pers. com. R.P. Speijer, 1999). Unit C was possibly deposited under rising sea-level conditions and marks the transgressive part of the sea-level curve.

The exact stratigraphic position of **Unit D** remains questionable: a latest NP5 or early NP6 age is possible, because Unit D is sandwiched between upper NP5 deposits of Unit C and NP6 deposits of Unit E (Fig. 2). Sedimentologically, these carbonates represent the second phase of ramp progradation and can be subdivided in a lower Unit D_1 and an upper Unit D_2. The first is composed of mainly well bedded carbonates with onlap patterns towards the west onto Units B or C, clearly indicating transport directions from the east (Fig. 8D). Slumpings may occur (Fig. 4j) and few debris flows are present (Fig. 4h). In contrast to the debris flows of Unit B (where all clasts are composed of micrite with abundant quartz grains), debris flows here contain clasts exhibiting various microfacies types. Those of section S2 consist of corallinacean-nummulitid micrite to sparite (MFT5) indicating shallow-water shoal deposition of the inner to middle ramp. In contrast, debris flows (and also the well bedded carbonates) of section S6 are dominated by micritic sandstones, whereas all other bedded sediments of Unit D_1 are composed of micrite-dominated limestones without fossils. We interpret the siliciclastic layer as being transported via submarine canyons that cut through the slope transect and thus reflect siliciclastic sediment bypassing (Fig. 7). An amalgamation of these

with various facies types originally formed in different ramp environments has been assumed. Similarities of D_1-limestones to those of Unit B are obvious, both originally deposited at the outer ramp. The first, however, exhibiting a stronger influence of shallow-water deposition.

The upper Unit D_2 is characterised by large-scale debris flows and slump to debris flow deposits with inter-debris flow deposits of weakly stratified nodular limestones (section S3, Fig. 5). Most clasts of the debris flows here represent deposits of the middle to inner ramp, which originally consisted of mainly corallinacean-dominated microfacies types with abundant nummulitids. In contrast to Units D_1 and B, bedded limestones with deep-water microfacies types are rarely present. The quartz content of these sediments is low. Because of dominating shallow-water MFTs, a more proximal outer to middle ramp position is proposed. Only the nodular limestones of section S3 indicate transport directions from west to east, while debris flows and slump to debris flow deposits exhibit no transport directions. Similar to Unit B, sedimentation on top of Unit D ceased, as documented by *Thalassinoides* burrows (section S6), and subsequent erosion occurred. This may represent a flooding surface. The debris flows and slump to debris flow deposits are here truncated at the top. Usually, debris flows are characterised by convex-upward shapes (Mutti, 1985), but this feature was observed only at their sides, whereas their tops end with sharp contacts towards the overlying Unit E.

The marly chalky sediments of **Unit E** in all sections disconformably overlie the limestones of Unit D (Fig. 4e). Unit E represents a second short intercalation of hemipelagic basinal sediments formed during an interval when the export of carbonates from the ramp was interrupted by rising sea-level conditions. Similar to Unit C this marks the transgressive part of the sea-level curve. Nannofossils indicate a late Paleocene age of biozone NP6, however, the duration of the hiatus at the disconformable boundary to Unit D below cannot be estimated. The exact position of the NP5-NP6 boundary lies within Unit D or the hiatus thereafter (Fig. 2). The hiatus-surface at the top of Unit E separates shallow-water deposits of the mid to inner ramp (Unit F) from hemipelagic marls of Unit E. Similar to Unit C benthic foraminifers show a mixture of autochthonous deeper (mixed Midway and Velasco Fauna) and allochthonous shallower shelf forms (Speijer et al., 1994, pers. com. R.P. Speijer, 1999). Small larger forminifers were found as well (pers. com. R.P. Speijer, 1999).

Unit F has been assigned to SBZ4. According to the shallow benthic zonation (Fig. 2) given by Serra-Kiel (1998), these sediments have been correlated with the plankton/nannoplankton chronology of Berggren et al. (1995) and Martini (1971) and correlate to P4c/NP8/9. Unit F represents the third phase of ramp progradation characterised by small-scale debris flows and nodular limestones (without distinct stratification), both lithofacies are often hard to differentiate. Similar to Units B and D, reworking of sediments originating from different facies zones was evident in Unit F, with prevailing shallow-water deposits from mid to inner ramp settings. Imprints of the shallowest inner ramp deposits (miliolid biopel sparite to micrite) are observed. In contrast to the shoal deposits of Unit D (composed of corallinacean-nummulitid micrite to sparite) nummulitid micrite to sparite prevail here. As indicated in Fig. 8F, no dominant transport direction occurs: dipping directions vary

from west, south to east, suggesting a general southward directed transport. The deposits of Unit F reflect middle to inner ramp environments.

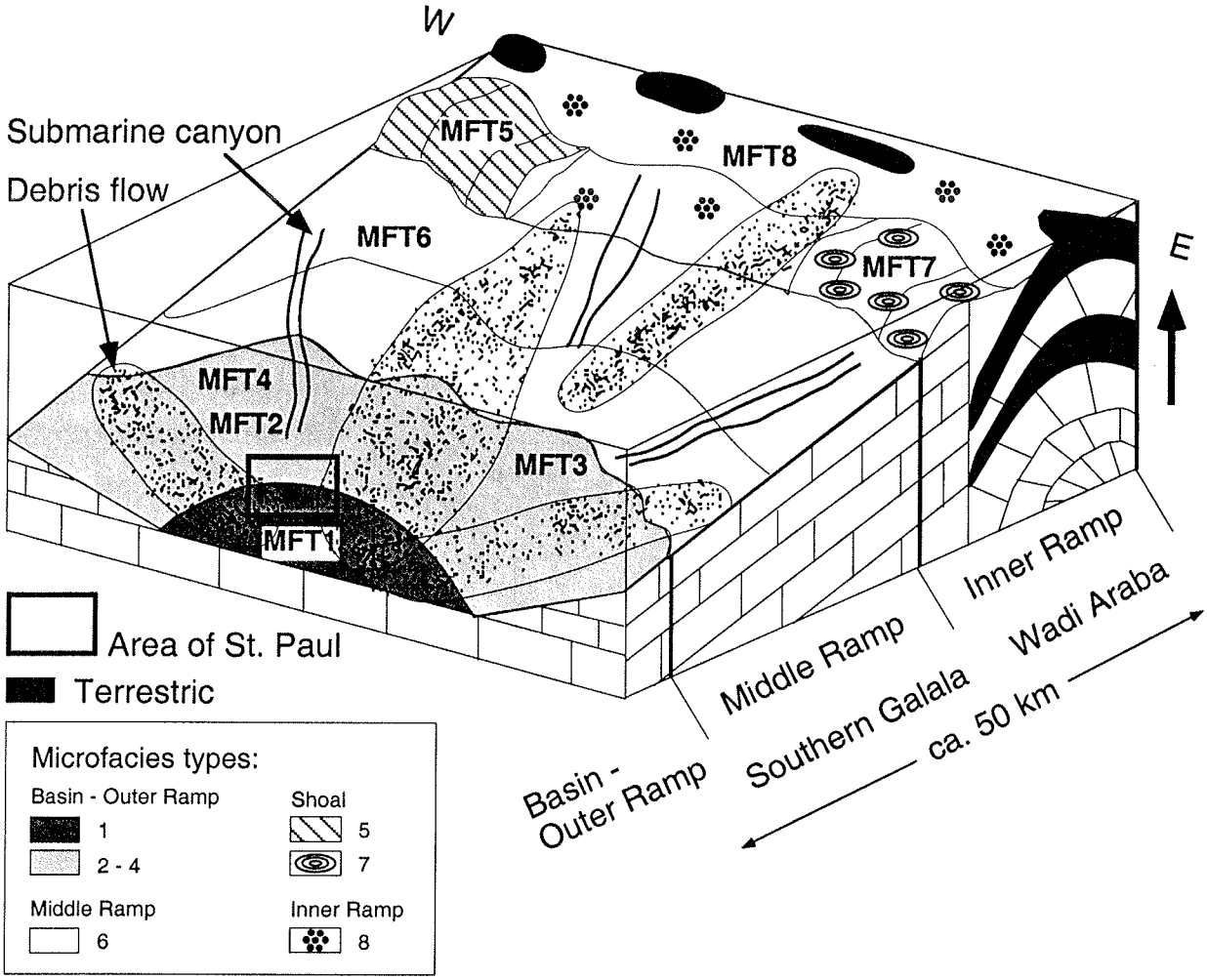

Fig. 7: *Schematic model of the southward dipping ramp of the Galala Mountains. Microfacies type distribution is inferred from the debris flows of the investigated lateral profile by the monastery of St. Paul.*

Sea-level as trigger mechanism for mass transport deposition

The two factors responsible for initiation of mass transports are strength reduction and stress increase (Prior and Coleman, 1984). Strength reduction is essentially a product of internal sediment variations of water content, pore water, and gas pressure. They can be changed by sedimentary loading, pressure from surface waves during storms, sea-level changes, and pore-gas generation due to internal geochemical and bacteriological processes. A gravitational stress increase might be induced by tectonics, localized sea-floor erosion, waves, and sedimentation (Prior and Coleman, 1984). Debris flows are deposited when the gravitational force decreases below the strength of the debris and a sudden "freezing" occurs (Middleton and Hampton, 1976).

Among the various factors and mechanisms that control the slope sedimentation, we discuss the mass transport deposits of St. Paul in the light of fluctuations of the relative sea-level that may

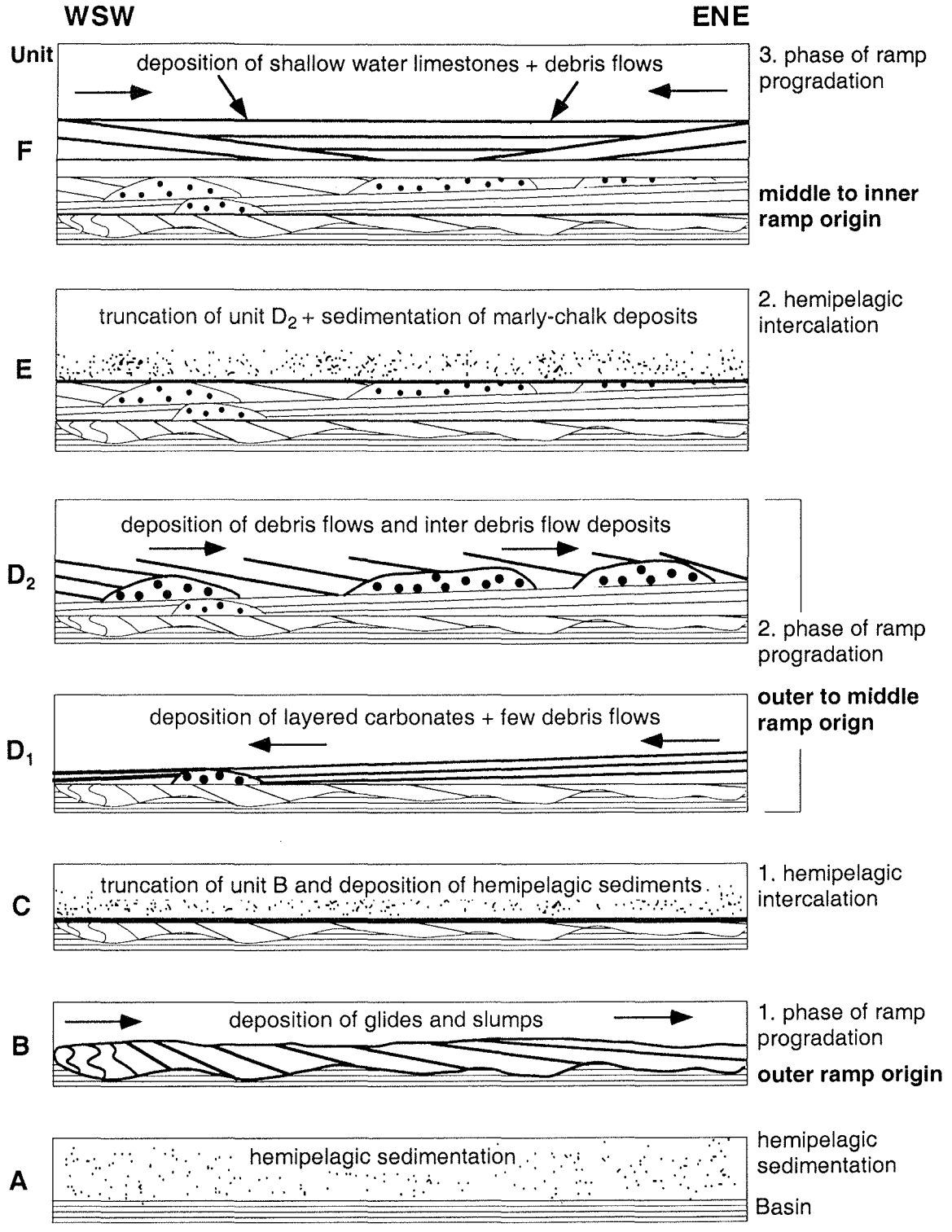

Fig. 8: *Deposition mode of the units indicating the different phases of ramp progradation and location of deposition.*
Unit A: hemipelagic sedimentation. Unit B: first phase of ramp progradation with deposition of glides and slumps from westerly directions, the samples are indicating an outer ramp origin. Unit C: truncation of Unit B and first hemipelagic intercalation. Unit D_1: second phase of ramp progradation with deposition of layered carbonates and few debris flows from easterly directions. Unit D_2: deposition of debris flows and inter debris flow sediments from westerly directions, the samples of Unit D are indicating an outer to middle ramp origin. Unit E: truncation of Unit D_2 and second hemipelagic intercalation. Unit F: third phase of ramp progradation with deposition of shallow water limestones and debris flows from all directions except the south, the samples are indicating a middle to inner ramp origin.

influence accommodation space at the ramp: sea-level drops initiate ramp progradation. Recent studies on the Paleocene sea-level history of the Sinai (Lüning et al., 1998) suggest a main sea-level drop at the base of P4 (within NP5) and subsequent sea-level oscillations during P4, similar to the cycle boundaries of Hardenbol et al. (1999). Speijer and Schmitz (1998) reconstructed a paleodepth curve of that interval based on studies of benthic foraminifers from Gebel Aweina (about 300 km to the south). These authors also concluded a sea-level drop during lower P4 (upper part of NP5), matching TH 1 of Hardenbol et al. (1999) and probably TH Sin2 of Lüning et al. (1998). If the mass transport deposits of Unit B and D and the respective cycle boundaries SelGal2 and SelGal? would be considered as lowstand deposits this would fit in the sequence stratigraphic frame of Lüning et al. (1998) and Hardenbol et al. (1999). However, if both mass transport deposits would be attributed to the same sea level lowstand the duration of unit C would be very short. Another possibilty is the non-correlation of one of the two cycle boundaries with any known lowstand. This might have one of two reasons: the local character of the lowstand, or the mass transport deposits of one of the units are not related to a sea-level lowstand but triggered by other mechanisms, e.g. tectonics. However, the onset of the mass transport deposits of Unit F (due to ramp progradation and regional lowstand) coincides with cycle boundary ThGal1 (Fig. 2), as per TH Sin5 (Lüning et al., 1998) and TH 4 (Hardenbol et al., 1998) and a sea-level drop in Speijer and Schmitz (1998).

Conclusions:

During the late Paleocene (P3 - P4) interval, three phases of carbonate ramp progradation and three hemipelagic units have been differentiated at the southern Galala (St. Paul). The three prograding phases are indicated by increased mass transport deposition composed of glides, slumps, and debris flows which came from different directions excluding the south. Each subsequent advance of ramp progradation was more pronounced. Microfacies investigations (mainly deduced from clasts in the debris flow deposits) highlight the changing depositional origins from a basinal-outer ramp setting to a middle-inner ramp setting at the end of the Paleocene. Moreover, changes of organism composition with time were evidenced: During early P4, corallinacean algae thrived on the ramp (especially at the inner-middle ramp transition and the shoal area), whereas during late P4, these areas were dominated by nummulitids.

Sea-level changes are a likely trigger for the onset of mass transport deposition. Comparisons with regional cycle boundary interpretations led to the attribution of at least two mass transport deposits to lowstands. The two older mass transport deposits (Unit B/D) either reflect one event (attributed to a single sea-level drop) or one of them reflects a local lowstand or have been triggered by other mechanisms independent of sea-level change, e.g. tectonics. Both show on top of the strata abundant *Thalassinoides* burrows followed by hemipelagic marly intercalations that are probably indications for a flooding surface indicating a subsequent transgressive phase.

In contrast to the carbonate mass transport deposits, siliciclastic sediments are of minor importance in the investigated area. They are probably sourced via submarine canyons and reflect sediment

bypassing. While the transport mechanism of siliciclastic deposits has a point source character, carbonate deposits are dominated by a line source character.

Acknowledgements

Prof. A. M. Bassiouni (Ain Shams University) is especially thanked for the logistical support and making work in Egypt possible for us (organisation of permits), Dr. A. Mohsen Morsi (Ain Shams Univ.) is equally thanked for logistical support, for providing his room for the washing of samples, and an open ear for all problems encountered during our stay in Egypt. All other colleagues of the Geology Department of Ain Shams University and the monks of the monastery of St. Paul are thanked for their hospitality. Robert Speijer (Univ. Bremen) is thanked for help with the planktic foraminifers and comments on an earlier version of the paper. Anja Scharf, Ralf Bätzel and Markus Brinkmann (all Univ. of Bremen) helped with the sample preparation. Erna Friedel read and corrected the manuscript. The manuscript was improved by reviews of J. Grötsch, T. Bechstedt and G. Einsele. The investigations were funded by the Graduiertenkolleg "Stoff-Flüsse in marinen Geosystemen" of the University of Bremen and the German Science Foundation (DFG)

References

Abdel-Kireem MR and Abdou HF (1979) Upper Cretaceous-Lower Tertiary planktonic foraminifera from South Galala Plateau, Eastern Desert, Egypt. Revista Espanola de Micropaleontologica 11: 175-222

Abdou HF, Naim EM and Sultan IZ (1969) Biostratigraphic studies on the Lower Tertiary rocks of Gebel Umm Rokham and Saint Paul area, Eastern Desert, Egypt. Bulletin of the Faculty of Science, Alexandria 9: 271-299

Aigner T (1983) Facies and origin of nummulitic buildups: an example from the Giza Pyramids Plateau (Middle Eocene, Egypt). N. Jh. Geol. Paläont. Abh. 166: 347-368

Bandel K and Kuss J (1987) Depositional environment of the pre-rift sediments - Galala Heights (Gulf of Suez, Egypt). Berliner geowiss. Abh. A 78: 1-48

Berggren WA, Kent DV, Swisher III CC and Aubry MP (1995) A revised Cenozoic geochronology and chronostratigraphy. In: Berggren WA, Kent KV, Aubry MP and Hardenbol J (eds) Geochronolgy, time scales, and global stratigraphic correlation. SEPM, Special publication 54, pp 129-212

Bosence DWJ (1991) Coralline algae: mineralization, taxonomy, and palaeoecology. In: Riding, R Calcareous algae and stromatolites. Springer, pp 98-113

Bryan JR (1991) A Paleocene coral-algal-sponge reef from southwestern Alabama and the ecology of Early Tertiary reefs. Lethaia 24: 423-438

Buchbinder B (1977) The coralline algae from the Miocene Ziqlag Formation in Israel and their environmental significance. In: Flügel E (eds) Fossil algae: recent results and developments. Springer, 279-285

Cook HE and Mullins HT (1983) Basin margin environment. In: Scholle PA, Bebout DG and Moore CH (eds) Carbonate depositional environments. AAPG Mem. 33, pp 539-617

Drobne K (1975) *Hottingerina lukasi* n.gen., n.sp. (Foraminiferida) iz srednjega paleocena v severozahodni jugoslaviji. Radzprave 18: 242-253

Einsele G (1991) Submarine mass flow deposits and turbidites. In: Einsele G, Ricken W and Seilacher A (eds) Cycles and events in stratigraphy. Springer, pp 313-339

Enos P (1977) Flow regimes in debris flow. Sedimentology 24: 133-142

Faris M (1994-1995) Late Cretaceous and Paleocene calcareous nannofossil biostratigraphy at St. Paul section, Southern Galala Plateau, Egypt. Annals Geol. Surv. Egypt 20: 527-538

Fisher RV (1983) Flow transformations in sediment gravity flows. Geology 11: 273-274
Ghose BK (1977) Paleoecology of the Cenozoic reefal foraminifers and algae-a brief review. Palaeogeography, Palaeoclimatology, Palaeoecology 22: 231-356
Gietl R (1998) Biostratigraphie und Sedimentationsmuster einer nordostägyptischen Karbonatrampe unter Berücksichtigung der Alveolinen-Faunen. Berichte aus dem Fachbereich Geowissenschaften der Universität Bremen 112: 1-135
Hardenbol J, Thierry J, Farley MB, Jacquin T, de Graciansky PC and Vail PR (1999) Mesozoic-Cenozoic sequence chronostratigraphic framework of European Basins. In: de Graciansky PC, Hardenbol J, Jacquin T, Vail PR and Farley MB (eds) Sequence Stratigraphy of European Basins. SEPM, Spec. Publ. 60, pp
Hottinger L, Lehmann R and Schaub H (1964) Donèes actuelles sur la biostratigraphie du Nummulitique Méditerranéen. Mém. Bur. Rech. Geol. Min (Colloque Paléogène, Bordeaux) 28: 611-652
Hottinger L and Drobne K (1980) Early Tertiary conical imperforate foraminifera. Radzprave 22: 188-276
Ismail MM and Abdallah AM (1966) Contribution to the stratigraphy of St. Paul Monastery area by microfacies. Bulletin of the Faculty of Science, Alexandria 12: 325-334
Kulbrok F and Kuss J (1995) Sedimentary sequences of the Late Cretaceous/early Tertiary succession in NE Egypt. Terra Nostra 1/95: 28-29
Kulbrok F (1996) Biostratigraphie, Fazies und Sequenzstratigraphie einer Karbonatrampe in den Schichten der Oberkreide und des Alttertiärs Nordost-Ägyptens (Eastern Desert, N'Golf von Suez, Sinai). Berichte aus dem Fachbereich Geowissenschaften der Universität Bremen 81: 1-216
Kuss J and Leppig U (1989) The early Tertiary (middle-late Paleocene) limestones from the western Gulf of Suez, Egypt. N. Jb. Geol. Paläont. Abh. 177: 289-332
Kuss J and Scheibner C and Gietl R (subm.) Late Cretaceous - early Tertiary platform to basin transitions along a Syrian Arc Uplift (Eastern Desert, Egypt)
Leppig U (1987) Biostratigraphy of larger foraminifera and facies development from the Upper Albian to the Middle Paleocene in the Sierra de Cantabria and the Montes Obarenes (Northwestern Spain). N. Jb. Geol. Paläont. Mh. 1987: 647-666
Lowe DR (1976) Subaqueous liquefied and fluidized sediment flows and their deposits. Sedimentology 23: 285-308
Lüning S, Marzouk AM and Kuss J (1998) The Paleocene of central East Sinai, Egypt:"sequence stratigraphy" in monotonous hemipelagites. Journal of Foraminiferal Research 28: 19-39
Luger P (1985) Stratigraphie der marinen Oberkreide und des Alttertiärs im südwestlichen Obernil-Becken (SW-Ägypten) unter besonderer Berücksichtigung der Mikropaläontologie, Palökologie und Paläogeographie. Berliner Geowissenschaftliche Abhandlungen A 63: 1-151
Martini E (1971) Standard Tertiary and Quaternary calcareous nannoplankton zonation. In: Farinacci A (ed) Proceedings of the second planktonic conference, Roma 1970. pp 739-785
Middleton GV and Hampton MA (1976) Subaqueous sediment transport and deposition by sediment gravity flows. In: Stanley DJ and Swift DJP (eds) Marine sediment transport and environmental managment. Wiley, New York, pp 197-218
Moustafa AR and Khalil MH (1995) Superposed deformation in the northern Suez Rift, Egypt: Relevance to hydrocarbons exploration. Journal of Petroleum Geology 18: 245-266
Mutti E (1992) Turbidite sandstones. Agip S.p.A., Milan, pp 1-275
Olsson RK, Hemleben C, Berggren WA and Huber BT (1999) Atlas of Paleocene planktonic foraminifera. Smithsonian Institution Press, Washington, D.C., pp 1-252
Piper DJW, Cochonat P and Morrison ML (1999) The sequence of events around the epicentre of the 1929 Grand Banks earthquake: initiation of debris flows and turbidity current inferred from sidescan sonar. Sedimentology 46: 79-97
Postma G (1986) Classification for sediment gravity-flow deposits based on flow conditions during sedimentation. Geology 14: 291-294
Prather BE, Booth JR, Steffens GS and Craig PA (1998) Classification, lithologic calibration, and stratigraphic succession of seismic facies of intraslope basins, deep-water Gulf of Mexico. AAPG Bulletin 82: 701-728
Prior DB and Coleman JM (1984) Submarine slope instability. In: Brunsden D and Prior DB (eds) Slope instability. pp 419-455

Schuster F (1996) Paleoecology of Paleocene and Eocene corals from the Kharga and Farafra Oases (Western Desert, Egypt) and the depositional history of the Paleocene Abu Tartur carbonate platform, Kharga Oasis. Tübinger Geowissenschaftliche Arbeiten A 31: pp 1-96

Serra-Kiel J, Hottinger L, Caus E, Drobne K, Ferrandez C, Jauhri AK, Less G, Pavlovec R, Pignatti J, Samso JM, Schaub H, Sirel E, Strougo A, Tambareau Y, Tosquella J and Zakrevskaya E (1998) Larger foraminiferal biostratigraphy of the Tethyan Paleocene and Eocene. Bull. Soc. géol. France 169: 281-299

Speijer RP (1994) The late Paleocene benthic foraminiferal extinction as observed in the Middle East. Bulletin de la Société belge de Géologie 103: 267-280

Speijer RP and Schmitz B (1998) A benthic foraminiferal record of Paleocene sea level and trophic/redox contitions at Gebel Aweina, Egypt. Palaeogeography, Palaeoclimatology, Palaeoecology 137: 79-101

Strougo A, Haggag MAY and Luterbacher H (1992) The basal Paleocene "*Globigerina*" *eugubina* zone in the Eastern Desert (St. Paul's Monastery, South Galala), Egypt. N. Jb. Geol. Paläont. Mh. 1992: 97-101

Vecsei A and Moussavian E (1997) Paleocene Reefs on the Maiella platform margin, Italy: an example of the effects of the Cretaceous/Tertiary boundary events on reefs and carbonate platforms. Facies 36: 123-140

White MR (1994) Foraminiferal biozonation of the northern Oman Tertiary carbonate succession. In: Simmons MD (eds) Micropaleontology and hydrocarbon exploration in the Middle East. Chapman and Hall, London, pp 309-332

Zhicheng Z, Willems H and Binggao Z (1997) Marine Cretaceous-Paleogene biofacies and ichnofacies in southern Tibet, China, and their sedimentary significance. Marine Micropaleontology 32: 3-2

CHAPTER 5

Carbonate platform to basin transition along an Upper Cretaceous to Lower Tertiary Syrian Arc Uplift, Galala Plateaus, Eastern Desert, Egypt

J. Kuss, C. Scheibner and R. Gietl

published 2000
in GeoArabia
Vol. 5, p. 405-424

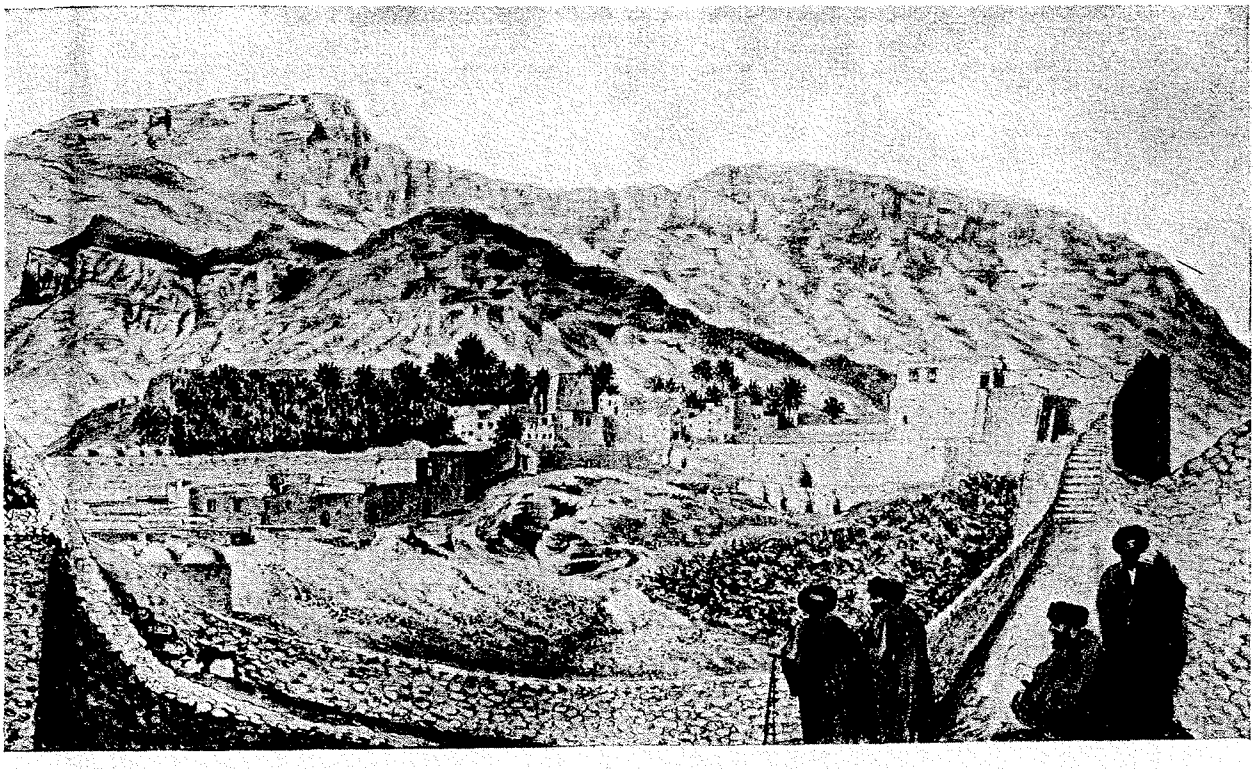

Kloster St. Antonius
von der Ringmauer auf der Nordseite aus gesehen (rechts 4 Mönche, unten die Holzvorräte)

Monastery of St. Anthony
view from the North (on the right 4 monchs, below wood supply)

Drawing by Georg Schweinfurth (1876)

Carbonate Platform to Basin Transition along an Upper Cretaceous to Lower Tertiary Syrian Arc Uplift, Galala Plateaus, Eastern Desert of Egypt

Jochen Kuss, Christian Scheibner, and Ralf Gietl

Universität Bremen, FB5, P.O. Box 330440, 28334 Bremen, scheibne@uni-bremen.de

Abstract: Biostratigraphy and facies analysis on Upper Campanian to Lower Eocene strata along a 58-kilometer-long dip transect between the Northern and Southern Galala Plateaus, west of the Gulf of Suez. The analyses enabled us to reconstruct the evolution of a platform-slope-basin transition that is roughly parallel with the trend of the plateaus. We interpret individual sedimentary cycles as processes of a southward prograding carbonate platform that developed along a branch of the Syrian Arc Fold Belt. The Northern Galala area was a structural high as shown by hiatuses spanning the Late Cretaceous (Coniacian) to Early Paleocene times. To the south, carbonate platform progradation is evident from the Late Campanian onward. Late Cretaceous platform-derived slope deposits interfinger with basinal chalks and calcareous shales farther south. Early Tertiary carbonates were deposited in platform, slope, and basin settings. The evolution of the platform-slope-basin transition is documented by the changing large-scale depositional geometries. The evolution occurs within sedimentary sequences that are interpreted by means of a high-resolution biostratigraphic framework. The facies architecture reflects the evolution from a rimmed shelf (Late Cretaceous) to a distally steepened ramp (latest Cretaceous to Paleocene) and eventually to a homoclinal ramp (Early Eocene). The reconstruction of the imprint of fluctuating sea levels on the sedimentary record has been used to establish comparisons with age-equivalent cycles from neighbouring regions.

1. Introduction

Several authors have studied the stratigraphy and sedimentology of the outcropping Upper Cretaceous - Lower Tertiary surface successions in the Eastern Desert (e.g. Awad and Abdallah, 1966; Abdel Kireem and Abdou, 1979; Bandel and Kuss, 1987; Bandel et al., 1987; Hendriks et al., 1987; Kuss and Leppig, 1989). Interpretations of synsedimentary tectonics of the Upper Cretaceous - Paleocene carbonate-dominated strata in the northern part (Galala area) are found in Kuss (1992) and Moustafa and Khalil (1995) and form the basis for further detailed investigations by Kulbrok (1996), Gietl (1998), Scheibner et al. (2000), and Scheibner et al. (in press). This study summarises the results of biostratigraphic and lithofacies investigations of the carbonate-dominated Upper Campanian - Lower Eocene strata along a shelf-slope-basin transect across the Galala plateaus west of the Gulf of Suez (Figure 1). It also evaluates the implications for deposition along a structural uplift and reconstructs the cyclic organisation of the sedimentary successions within the time-slices of the Late Cretaceous and the Paleocene to Early Eocene. Several factors controlled sedimentation

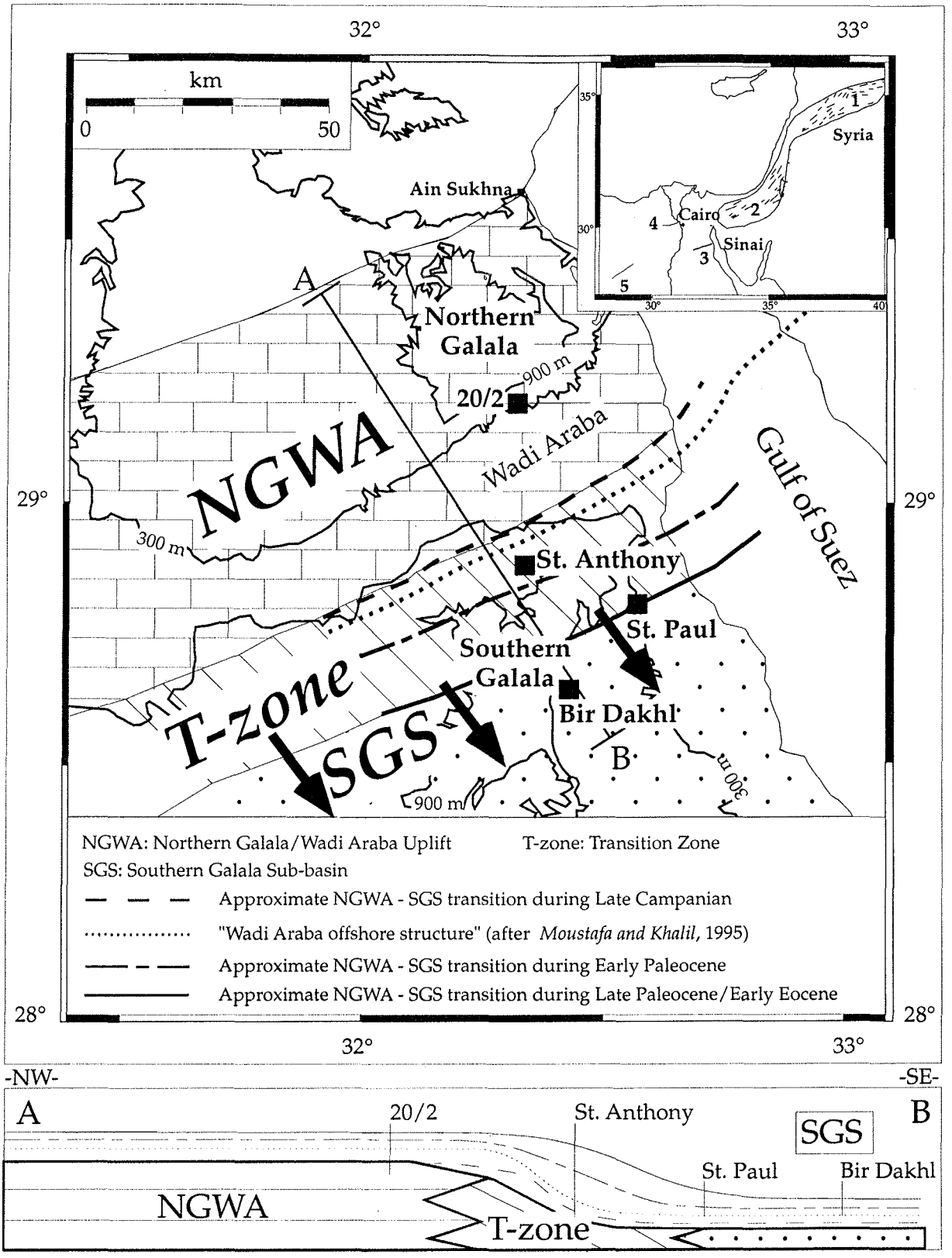

Fig. 1: *The Galala area, part of a Syrian Arc fold in the Eastern Desert near the western coast of the Gulf of Suez (Inset shows Syrian Arc and location of Galala area: 1 = Palmyrid Fold Belt; 2 = Areif el Naqa anticline in the Negev-Sinai Fold Belt; 3 = Northern Galala/Wadi Araba Uplift; 4 = Abu Roash; 5 = Bahariya Uplift/Western Desert). During Late Cretaceous–Paleogene times, the platform (**NGWA**) to basin (**SGS**) transitions (**T-zone**) were formed approximately parallel to the Galala trend and shifted southward, as indicated by the time-lines along transect A – B (below). Black squares show the locations of the four key-sections (Figure 5).*

on the shallow-water shelves in the north and in the slope-transitions to an adjacent basin farther south. The most important are erosion of elevated areas (siliciclastic input), carbonate platform sedimentation (biosedimentary input), and sea-level fluctuation (accommodation space). They vary in time and space and interact to have diverse depositional effects. In contrast to the pre-Upper Campanian and post-Paleocene successions, sediments of the studied Late Cretaceous – Paleocene-Early Eocene interval may not have been influenced by synsedimentary tectonic processes. This hypothesis is supported by sequence stratigraphic interpretations of age-equivalent strata from a Syrian Arc uplift in neighbouring Sinai (Lüning et al., 1998a).

The north-northwest-trending Gulf of Suez developed as a result of Miocene rifting. It is bordered by sharp scarps. The younger tectonic structures crosscut the depositional architecture and sedimentary structures of the Cretaceous-Palaeogene sediments along faults that extend farther west for several tens of kilometres. Rift-related tectonism has been the cause of local weathering and alteration of the underlying Palaeogene strata. For example, Miocene salts favour the dolomitisation of the older strata and may leach away microfossils. Major rift-related and rotated fault blocks characterise the present-day geomorphology today of plateaus, plains and wadis (Figure 1).

2. Material and Methods

During several field seasons in northeastern Egypt between 1993 and 1998, about 45 stratigraphic sections were logged on either side of the Gulf of Suez, most of them along the northern, eastern, and southern rims of the Galala Plateaus. The work has been documented by Kulbrok (1996), Gietl (1998) and Scheibner et al. (2000). About 550 hand specimens of limestones for thin-section studies and 600 samples of chalk and calcareous shales (for investigations on washed microfossil) were collected. In this study, we concentrate on four key-sections (Figure 1) to demonstrate the lithologic and stratigraphic variations from north to south (Figure 2) that reflect a platform-slope-basin transition in the Eastern Desert (Figure 4). The key sections are:

- *Section 20/2:* Late Cretaceous uplift and Paleocene platform sedimentation of the Southern Galala Formation.
- *St. Anthony Section*: southward prograding slope deposition of the Late Cretaceous St. Anthony Formation and Paleocene platform-to-slope deposits of the Southern Galala Formation
- *St. Paul Section*: Late Cretaceous basinal sediments of the uppermost Sudr Formation and the Dakhla Formation and Paleocene slope-to-basin deposits of the Southern Galala Formation.
- *Bir Dakhl Section*: Paleocene basin sediments of the Dakhla Formation, Sudr Formation, and Late Paleocene – Early Eocene slope-to-basin deposits of the Southern Galala Formation interfingering with the basinal Esna Formation.

The biostratigraphic and lithostratigraphic data are used to correlate these sections and to illustrate the large-scale depositional architecture of the sedimentary sequences. These data form the basis of our regional interpretations of uplift, erosion, sedimentation, and renewed subsidence, marked by the southward shifting Transition zone (**T-zone**, Figure 1). Cycle-boundaries are

indicated by variations in water depths and allow for reconstruction of relative changes in sea-level. They form the basis for sequence stratigraphic interpretations combined with the evaluation of facies and microfacies, field observations of sedimentary structures, vertical stacking patterns, and microfaunal compositions. For more details, refer to Gietl (1998), Scheibner et al. (2000), and Scheibner et al. (in press).

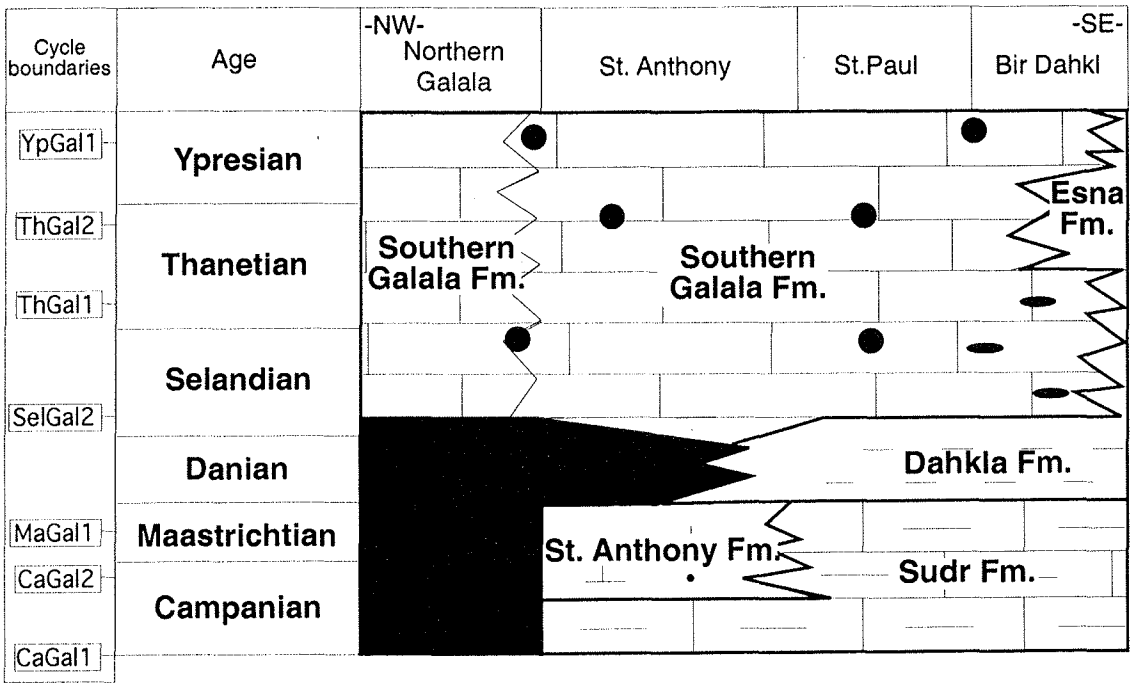

Fig. 2: *The Late Campanian–Early Eocene formations of the four key-sections to illustrate lithofacies changes from NW to SE within a stratigraphic frame. The chronostratigraphic and biostratigraphic ranges of the cycle boundaries (left column) are indicated in Figure 5 and discussed in the text. Compared with Figure 1, the blue colour represents basin deposits of the SGS (Sudr, Dakhl and Esna Formations), while the orange colour stands for slope deposits of the T-zone (St. Anthony and Southern Galala Formations), or for platform deposits of the NGWA Uplift (yellow colour).*

3. Geologic Setting

Surface sections on the Northern and Southern Galala Plateaus consists mainly clastic sedimentary rocks of late Palaeozoic to Early Cretaceous age, and predominantly carbonate strata of the Late Cretaceous to Palaeogene (Bandel and Kuss, 1987). Their gross architecture reflects a southward-thinning, wedge-like pile of sediments that were deposited during marine transgressions that came mainly from the north onto the African-Arabian Shelf (Kuss and Bachmann, 1996). Locally, in the Late Cretaceous, structural highs affected the sedimentary successions to form islands along the Northern Galala/Wadi Araba Uplift.

The complex uplifts and domal anticlines of the Syrian Arc Fold Belt were formed during the closure of the Neo-Tethys (Stampfli et al., 1995), as a consequence of the convergence of the African and Eurasian Plates. Northeastern Egypt, situated at the northern edge of the African-Arabian Craton, was affected during Late Cretaceous to Early Tertiary times, by east-northeast-oriented dextral wrench faulting. This resulted in transpressive movements and the inversion of the Late Triassic-

Liassic half-grabens, which cut east-northeastward across the northern rim of the African-Arabian Plate.

The Syrian Arc can be traced from Syria to the central Western Desert of Egypt, via Sinai and the northern part of the Eastern Desert (Figure 1, inset). It is composed of the Palmyride and the Sinai-Negev Fold Belts, both having similar lithologic and structural characteristics (Shahar, 1994). The Galala Plateaus represent a major branch of the Syrian Arc in the Eastern Desert, characterised by Late Cretaceous uplifting in the north and subsidence farther to the south (Figure 1). In contrast to various Syrian Arc localities in Egypt and neighbouring areas, the Galala Plateaus exhibit a unique Late Cretaceous to Early Palaeogene carbonate-dominated platform-to-slope succession. This is comparable to other island-like Tethyan elevations rimmed by carbonate platforms, such as the Bakony Mountains of Hungary (Haas, 1999), Maiella in Italy (Eberli et al., 1994), and Sicily (Camoin et al., 1988).

Folding and/or uplift of the Syrian Arc began in post-Cenomanian times (Aal and Lelek, 1994) and reached its acme during the Late Cretaceous. However, diverse ages for the peak deformation exist based on studies in other regions. For example: Moustafa and Khalil (1995) reported an early Late Senonian age of major uplift as indicated by surface and subsurface data from localities in northeast Egypt. Lüning et al. (1998a) gave evidence of a major Late Campanian - Early Maastrichtian uplift, based on micropaleontologic studies on exposures in Sinai, while Bosworth et al. (1999) assumed a major pre-Campanian compressive deformation event based on surface and subsurface data from the southern Gulf of Suez.

We cannot define exactly the onset of uplift in the two Galalas because of later erosion, but their rise is obvious during pre-Late Campanian times when the uplift affected the depositional processes on their southern flank.

The area under investigation can roughly be subdivided into three east-northeast-striking facies belts (Figure 1):

- The **Northern Galala/Wadi Araba Uplift (NGWA)** in the north is characterised by long-lasting hiatuses (if Upper Cretaceous deposits are present at all, they are mainly dolomitised). The overlying carbonate platform deposits of latest Paleocene age interfinger with slope deposits of the Transition Zone (T-zone) farther south (Figure 1).
- The **Transition Zone (T-zone)** is characterised by Upper Cretaceous to Paleogene slope deposits. It is composed of the Upper Campanian-Lower Paleocene St. Anthony Formation and the Late Paleocene to Early Eocene Southern Galala Formation (see Figures 1 and 2, and discussion in Scheibner et al. (in press)). The slope sediments were formed in the transition to the Southern Galala Sub-basin (SGS, Figures 1, 3).
- The **Southern Galala Sub-basin (SGS)** is formed in the Late Campanian by the Northern Galala/Wadi Araba Uplift and represents the northern part of the Eastern Desert Intrashelf Basin (EDIB – Figure 3). The interfingering of Late Paleocene – Early Eocene slope and basin deposits is seen in the Southern Galala Sub-basin (Bir Dakhl Section – Figure 2, and Scheibner et al., in press). Sedimentary wedges prograding southward from the Northern Galala/Wadi

Araba Uplift led to an increase in loading and subsidence in the SGS. The Late Cretaceous to Early Tertiary evolution of the SGS was closely connected to the development of the Eastern Desert Intrashelf Basin. The SGS's configuration became apparent in the Paleocene, as shown by palaeobathymetric estimates (Speijer and van der Zwaan, 1994; Scheibner et al., 2000).

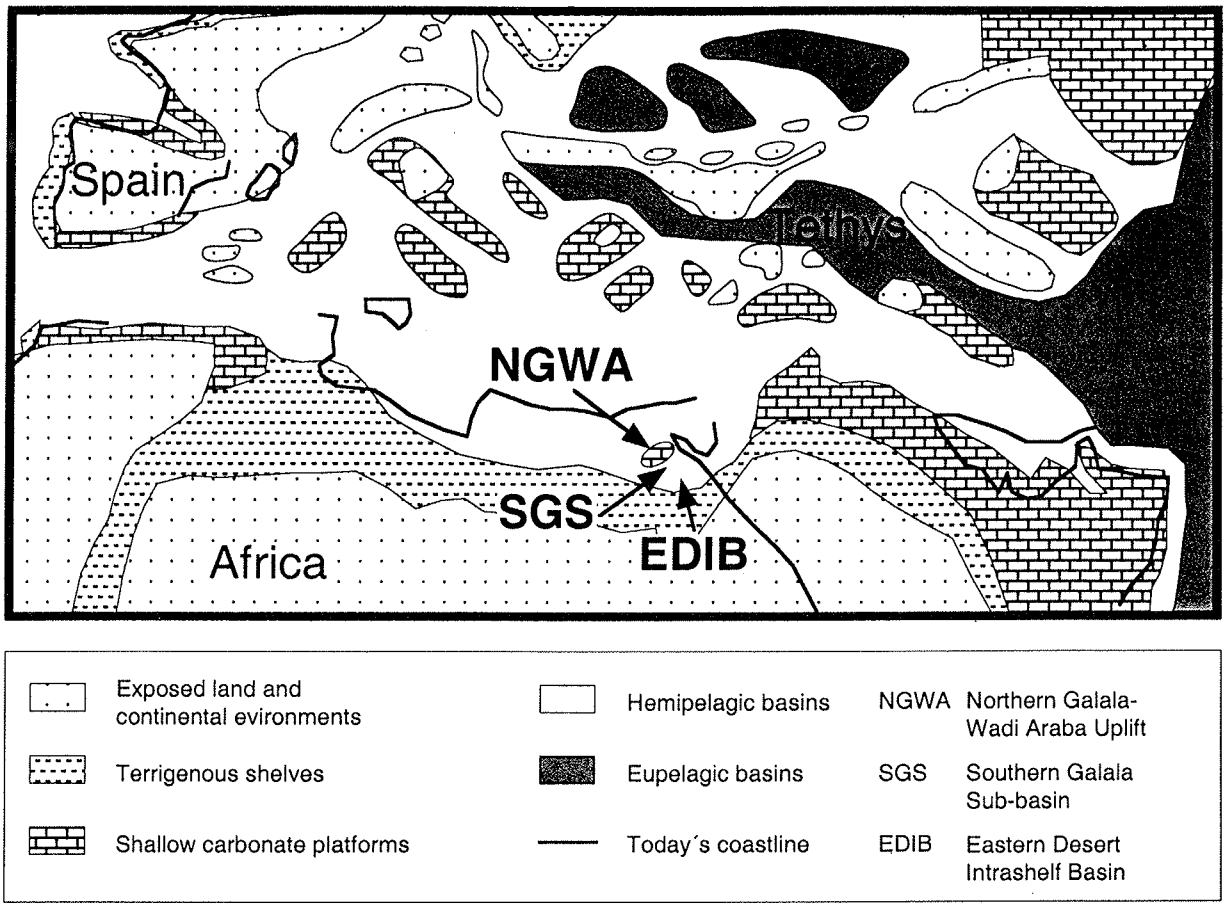

Fig. 3: *Late Campanian paleogeography of the central Tethys and the puzzling islands of its southern margin (modified from Camoin et al., 1993). The Eastern Desert Intrashelf Basin (EDIB) was probably formed as a consequence of Late Cretaceous-Paleogene uplift and subsidence.*

The Late Cretaceous **NGWA/SGS** boundary coincides with the separation between deformed/undeformed pre-Campanian strata. It is well exposed along the northern scarp of the Southern Galala Plateau, for example near the St. Anthony section (Figure 1; see also Bandel and Kuss, 1987). At this location, an angular unconformity separates steeply south-dipping Turonian-Lower Campanian units of the Northern Galala/Wadi Araba uplift from moderately south-dipping to nearly horizontally bedded Upper Campanian-Maastrichtian to Lower Eocene strata of the Southern Galala Sub-basin. Biostratigraphic evidence of a palaeostructural elevation in the north (NGWA) and its long duration is illustrated by hiatuses, ranging in age from post-Turonian to Late Paleocene (see section 20/2, Figure 6). The east-northeast-trending NGWA influenced the Late Cretaceous-Paleogene sedimentation processes in the area. Consequently, they are characterised by a gently south-dipping carbonate platform that rims the NGWA in the north and interfingers with transitional slope sediments and with hemipelagic deposits of the SGS farther south. Based on the

work of Kuss and Kulbrok (1995), the following three major southward-prograding carbonate-platform systems can be distinguished with respect to their large-scale sedimentary architecture (Figure 4):

- The Late Campanian/Maastrichtian rimmed shelf
- The Paleocene distally steepened ramp
- The Early Eocene homoclinal ramp

Late Cretaceous Platform-to-Basin Configuration

The tectonically induced topography strongly affected sedimentation during the Late Cretaceous. Whereas long intervals of non-deposition prevailed in the central part of the Northern Galala/Wadi Araba Uplift, Upper Campanian fine-grained mixed siliciclastic and carbonate sediments of the St. Anthony Formation accumulated in the Transition Zone. The sediments represent the foreslope of a rimmed carbonate shelf that fringed the NGWA (Figure 4). Carbonate-secreting shallow-water benthic organisms are present in proximal slope deposits on the southern edge of the NGWA. They occur in a Late Campanian lowstand wedge and in Early Maastrichtian shallow-water limestones within the St. Anthony Formation at the St. Anthony Section (see Figures 6 and 7a, here inlays a2 and a3). The regional distribution of these slope deposits follows an east-northeast trend parallel to the "Wadi Araba offshore structure" of Moustafa and Khalil (1995). This structure has been mapped farther east from subsurface data and coincides with the southern boundary of the NGWA (Figure 1). "Syrian Arc" inversion tectonics in this area resulted in a steeply south-dipping margin that reflects the topography of a Late Campanian-Early Maastrichtian rimmed carbonate shelf (compare platform models of Burchette and Wright, 1992 and Handford and Loucks, 1993).

The succeeding Maastrichtian units of the St. Anthony Formation are composed of siliciclastic carbonates. They correlate with major areas of non-deposition to the north (NGWA) and open marine chalk-calcareous shale intercalations of the Sudr Formation farther south in the Southern Galala Sub-basin (Figure 4). The lateral extent and duration of the Late Cretaceous carbonate shelf that rimmed the NGWA and extended into the SGS is difficult to estimate because of its later erosion. Moreover, a more than 10-kilometer-wide segment of the former platform is missing due to subsequent erosion of the present-day Wadi Araba (Figures 1 and 4). However, the lowstand deposits of the St. Anthony Formation in the St. Anthony Section and age-equivalent basinal sedimentary rocks of the Sudr Formation farther south enable rough estimates to be made. The lowstand deposits are about 180 m thick and consist of wedge-like sediments that include slumps and slides (Figure 7a, inlay a3). They pass into chalks and calcareous shales that are about 60 m thick in the St. Paul Section 14 km farther south (Figures 6, 7b) where no imprints of major sedimentary disturbances were observed. A stratigraphic model predicts a Late Cretaceous carbonate shelf more than 100 m thick that may have rimmed the southern edge of the Northern Galala/Wadi Araba Uplift (Figure 4). The model assumes a time interval of 2.3 to 2.5 my and a shelf-to-basin profile inclined 1.3° to 8.5° to the south.

There is little evidence of any latest Maastrichtian-Early Paleogene shallow-water carbonates in the Transition Zone. Their absence might be due to the mainly siliciclastic lithologies and a latest Maastrichtian-Early Paleocene marine regression.

Paleogene Platform to Basin Configuration

The gross architecture of the Late Cretaceous rimmed platform gradually changed to a Paleogene ramp-basin transition, seen as stepwise, southward-prograding successions (Figure 4). The distally steepened Paleocene carbonate ramp evolved into an Early Eocene homoclinal ramp (Gietl, 1998). Shallow-water limestones of the Southern Galala Formation were deposited on a gently south-dipping carbonate ramp. They crop out on the NGWA and interfinger with slope deposits in the Transition Zone and basinal sediments (Esna Formation) of the Southern Galala Sub-basin (Figure 2). Evidence for these transitions is found in planktic foraminiferal zone P4/P5 (Figure 5). In this interval the proximal slope deposits of the Southern Galala Formation in the St. Anthony Section include debris flows (see Figure 7a) and interfinger with slope deposits about 14 km to the south (near St. Paul, Figure 7b). They also have intertonguing relationships with basin sediments of the Esna Formation in the in Bir Dakhl Section, 12 km farther south (Figure 7c). The distribution and facies of the Lower Eocene carbonates in the Northern Galala/Wadi Araba Uplift and the Transition Zone indicate a homoclinal ramp morphology (Figure 4). The morphological model is also supported by evidence of thickness changes, the sequence geometries and coevally increasing occurrences of local build-ups and shoals in the shallow ramp areas (Kuss, 1992; Kulbrok, 1996; Gietl, 1998).

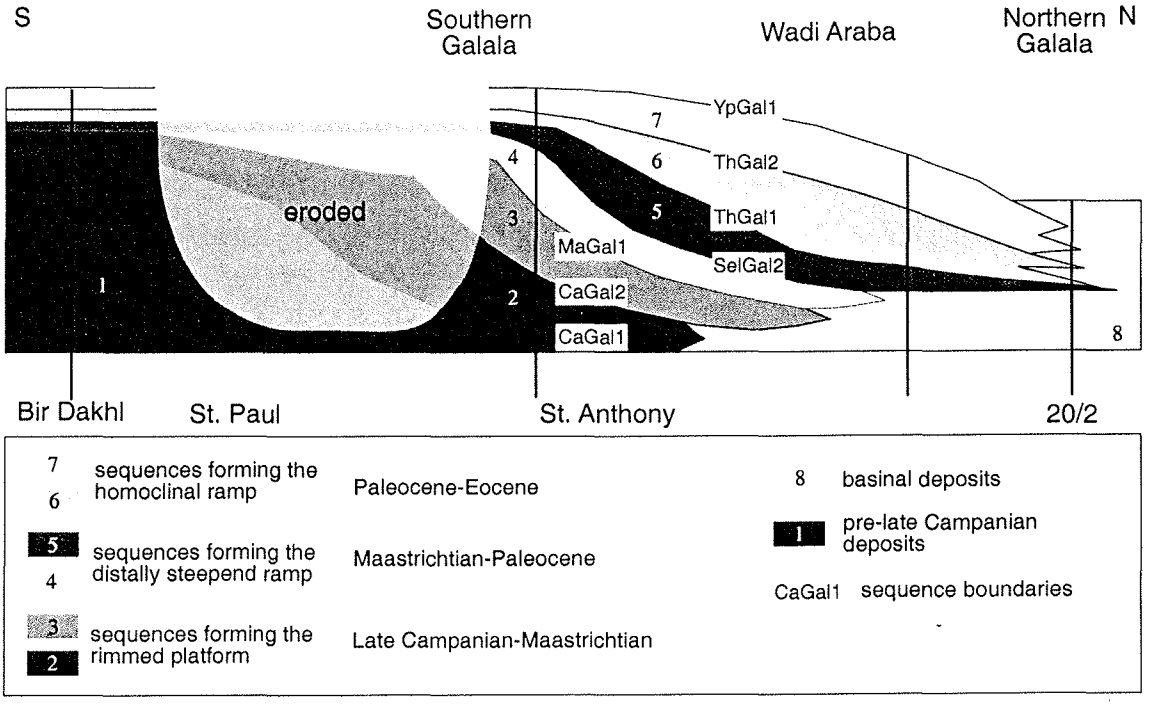

Fig. 4: *Schematic cross-sections of Late Cretaceous–Paleogene sedimentary sequences to demonstrate the stratigraphic evolution of three carbonate platforms at the NGWA-uplift: (1) the rimmed shelf; (2) the distally steepened ramp; and (3) the homoclinal ramp.*

4. Biostratigraphy

Late Campanian - Maastrichtian

Biostratigraphic subdivisions of the Late Cretaceous deposits in the study area (Figure 5) are mainly based on planktic (Norris et al., 1998) and benthic foraminifera (Caus et al., 1996). Supplementary data are provided by a few ammonites and are compared with range-zones given by Ward and Kennedy (1993). Detailed descriptions and illustrations of the local biozones are given by Abdel Kireem and Abdou (1979), Kuss (1986) and Kulbrok (1996).

The lack of Late Cretaceous biostratigraphic data for most of the Northern Galala/Wadi Araba Uplift is either due to the absence of strata of that age or, if they do exist, to strong diagenetic alteration. Only at its southernmost edge in the Transition Zone to the Southern Galala Sub-zone, are mainly hemipelagic sediments present (St. Anthony Section). The isolated microfossils are for the most part poorly preserved owing to the presence of silty-sandy intercalations and frequent dolomitisation (Abdallah and Eissa, 1966; Kuss, 1986). Microfossil preservation improves southward and Maastrichtian planktonic foraminifera occur in the mostly hemipelagic succession of chalk and calcareous shales of the Southern Galala Sub-basin at St. Paul. According to the biozonal scheme given by Kulbrok (1996), the Upper Cretaceous succession in the St. Anthony Section of the Transition Zone starts with Campanian chalk of the late *G. ventricosa - Gita. calcarata*-zones (*G. havanensis*). The chalk is overlain by dolomitic calcareous shale of the Upper Campanian *Globotruncanella havanensis* to *Globotruncana aegyptiaca* zones intercalated with several silt-/sandstone and marly-limestone units. They contain larger benthic foraminifera of *Orbitoides gruenbachensis* together with *Siderolites calcitrapoides* from the lower part of the *G. aegyptiaca* biozone, and *O.* cf. *apiculata* from the lower part of the *Gansserina gansseri* zone (Figure 5). However, no evidence exists for age-equivalent calcareous shales to the south in the St. Paul and Bir Dakhl Sections. In this areas, the Upper Cretaceous calcareous shales hold planktonic microfaunas of the late *G. gansseri* zone to *A. mayaroensis* zone.

Limestones intercalated with calcareous shales of the lower part of the *G. gansseri*-zone are found only in the St. Anthony section. They contain the larger benthic foraminifera of *Orbitoides* sp. and *Omphalocyclus macroporus*. In this section, the overlying marly siltstones contain the ammonite taxa *Saghalinites* sp. and *Discoscaphites kambysis* together with the baculite *Eobaculites* cf. *simplex* (J.K. Kennedy, oral comm.). *Saghalinites* sp. indicates a Late Maastrichtian age (Ward and Kennedy, 1993). The zonal marker-species of the latest Maastrichtian *A. mayaroensis* biozone is missing in from most of northeastern Egypt (see discussion in Luger et al., 1998), including the St. Anthony Section. However, evidence for the *Kassabiana falsocalcarata* subzone is found in several sections of the Southern Galala Sub-basin (Masters, 1984). The subzone coincides with the upper part of the *A. mayaroensis* biozone according to Luger et al. (1998).

Paleocene – Early Eocene

Most biostratigraphic studies of the Paleocene-Early Eocene succession in the Galala were made on the mainly chalky and shaly facies from the southern part of the Southern Galala Sub-basin.

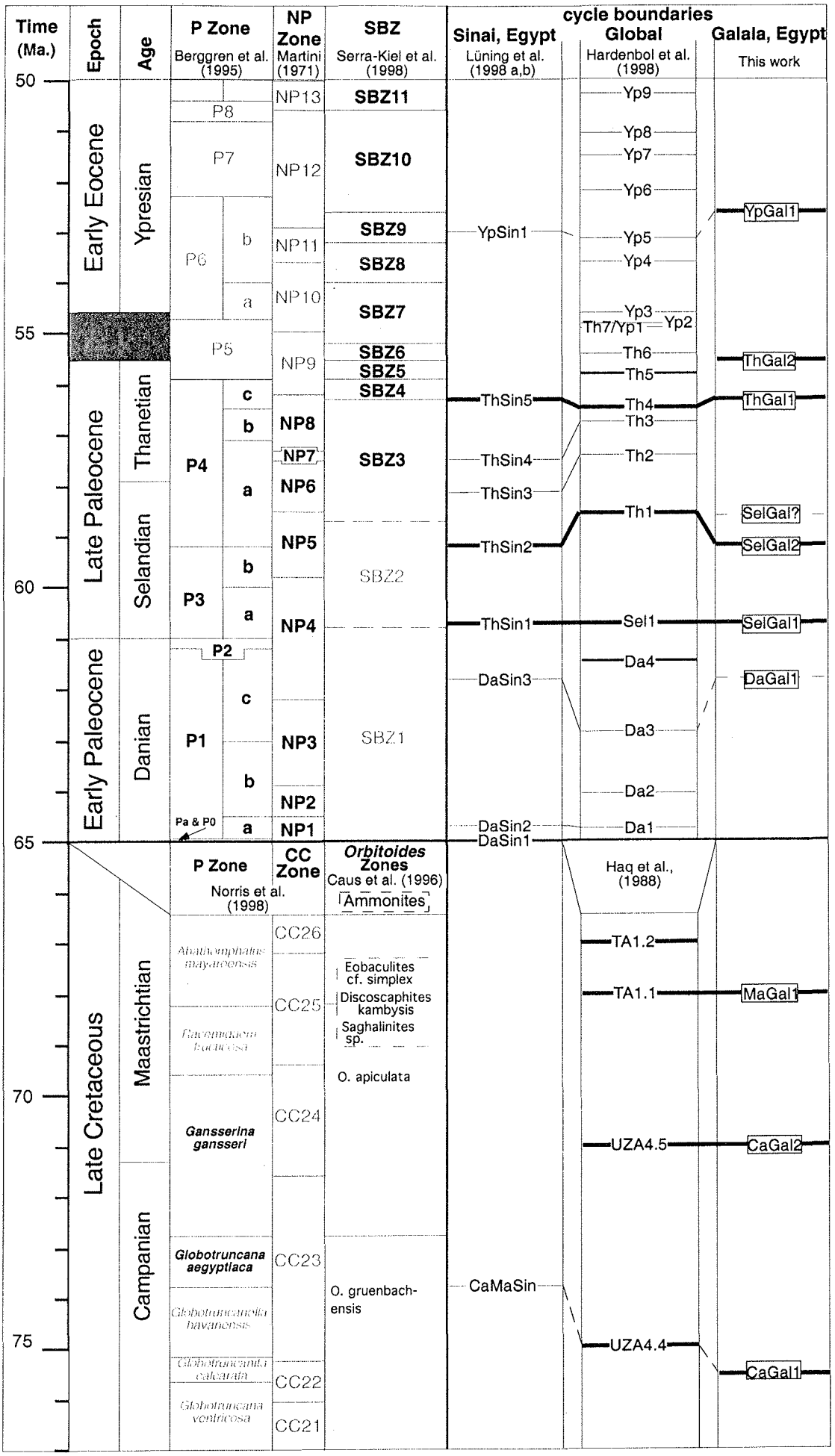
Time (Ma.)
Epoch
Age
P Zone Berggren et al. (1995)
NP Zone Martini (1971)
SBZ Serra-Kiel et al. (1998)
cycle boundaries
Sinai, Egypt Lüning et al. (1998 a,b)
Global Hardenbol et al. (1998)
Galala, Egypt This work
50
55
60
65
70
75
Early Eocene
Late Paleocene
Early Paleocene
Late Cretaceous
Ypresian
Thanetian
Selandian
Danian
Maastrichtian
Campanian
P8
P7
P6
P5
P4
P3
P2
P1
NP13
NP12
NP11
NP10
NP9
NP8
NP7
NP6
NP5
NP4
NP3
NP2
NP1
SBZ11
SBZ10
SBZ9
SBZ8
SBZ7
SBZ6
SBZ5
SBZ4
SBZ3
SBZ2
SBZ1
Pa & P0
YpSin1
ThSin5
ThSin4
ThSin3
ThSin2
ThSin1
DaSin3
DaSin2
DaSin1
CaMaSin
Yp9
Yp8
Yp7
Yp6
Yp5
Yp4
Yp3
Th7/Yp1
Yp2
Th6
Th5
Th4
Th3
Th2
Th1
Sel1
Da4
Da3
Da2
Da1
YpGal1
ThGal2
ThGal1
SelGal?
SelGal2
SelGal1
DaGal1
P Zone Norris et al. (1998)
CC Zone
Orbitoides Zones Caus et al. (1996)
Ammonites
Haq et al., (1988)
CC26
CC25
CC24
CC23
CC22
CC21
Eobaculites cf. simplex
Discoscaphites kambysis
Saghalinites sp.
O. apiculata
O. gruenbach-ensis
TA1.2
TA1.1
UZA4.5
UZA4.4
MaGal1
CaGal2
CaGal1

Fig. 5: *Stratigraphy and cycle boundaries of Late Campanian to Early Eocene strata in the Galala area. The time scale adopted in the three left hand columns is based on Norris et al. (1998) and relies on the time scales of Gradstein et al. (1995) for the Cretaceous datums and of Berggren et al. (1995) for the Paleocene-Eocene datums. Age estimates for most of the Late Cretaceous calcareous nannofossil and planktonic foraminiferal datums were taken from Erba et al. (1995). Black characters and numbers in the fourth, fifth, and sixth columns refer to determined biozones - grey characters and numbers relate to inferred biozones. Comparisons of cycle boundaries are based on absolute ages; mismatches are due to different biostratigraphic concepts used by various authors (see discussion in the text). Colours as for Figure 2.*

Examples are in Strougo et al. (1992), Faris (1994), Kulbrok (1996), Scheibner et al. (2000) and Scheibner et al. (in press). Biozones are based on planktonic foraminifera (P-Zones) by Berggren et al. (1995) and nannoplankton (NP-Zones) by Martini (1971) (Figure 5). Only a few contributions deal with the shallow-water calcareous shales and limestones of the Transition Zone and the NGWA area farther north. In these areas, work by Kuss and Leppig (1989), Gietl (1998), and Boukhary et al. (1998), are based on larger foraminifera using criteria by Hottinger (1960) for alveolinids and by Schaub (1981) for nummulitids. Serra-Kiel et al. (1998) revised the correlation of Palaeogene planktonic and shallow-water benthic zones and introduced the concept of "shallow benthic zones" (SBZ of Figure 5). In Figure 5, following zonation was used for the units of the four key sections:

- Biozones P1-P4 of the standard Paleocene-Early Eocene biozones (Berggren et al., 1995) are determined from hemipelagic deposits of St. Paul Section and Bir Dakhl sections, in accordance with data of Strougo et al. (1992). The biostratigraphic record of shallow-water deposits commences with redeposited limestones of the latest SBZ2, sandwiched between calcareous shales of the P3 - P4 boundary interval (Scheibner et al., 2000).
- First occurrences of autochthonous ramp carbonates are evidenced at the NGWA only locally for the late SBZ3 (Gietl, 1998), but in most areas their deposition began in SBZ4 or P4c. Shallow-water limestones of the SBZ5 - SBZ10 (equivalent to basin sediments of P5 - P6) are present at several localities on the NGWA (Kuss and Leppig, 1989; Gietl, 1998) and in the Transition Zone farther south (St. Anthony Section, Figure 6).

5. Sedimentary Facies, Cycles, and Sea-Level Changes

The integration of the sedimentologic and stratigraphic data from the four sections has enabled us to attribute the vertical and horizontal facies distribution to changing environments that are essentially controlled by variations in water depths. Comparisons with regional age-equivalent sea-level fluctuations occur in Sinai (Lüning et al., 1998 a,b), and Israel (Lewy, 1990). They support the definition and correlation of lithofacies along the transect from the NGWA in the north to the SGS in the south. They enable the reconstruction of the internal geometries and architectures of the lithofacies with respect to changes in depositional conditions (Figures 4 and 7). Detailed descriptions of Late Cretaceous-Palaeogene macro- and microfacies, including descriptions of shallow-water biota are found in Bandel and Kuss (1987), Kuss and Leppig (1989), Kuss (1986; 1992), Kuss and Herbig (1993), Kulbrok (1996) and Gietl (1998). Cretaceous-Palaeogene sea-level

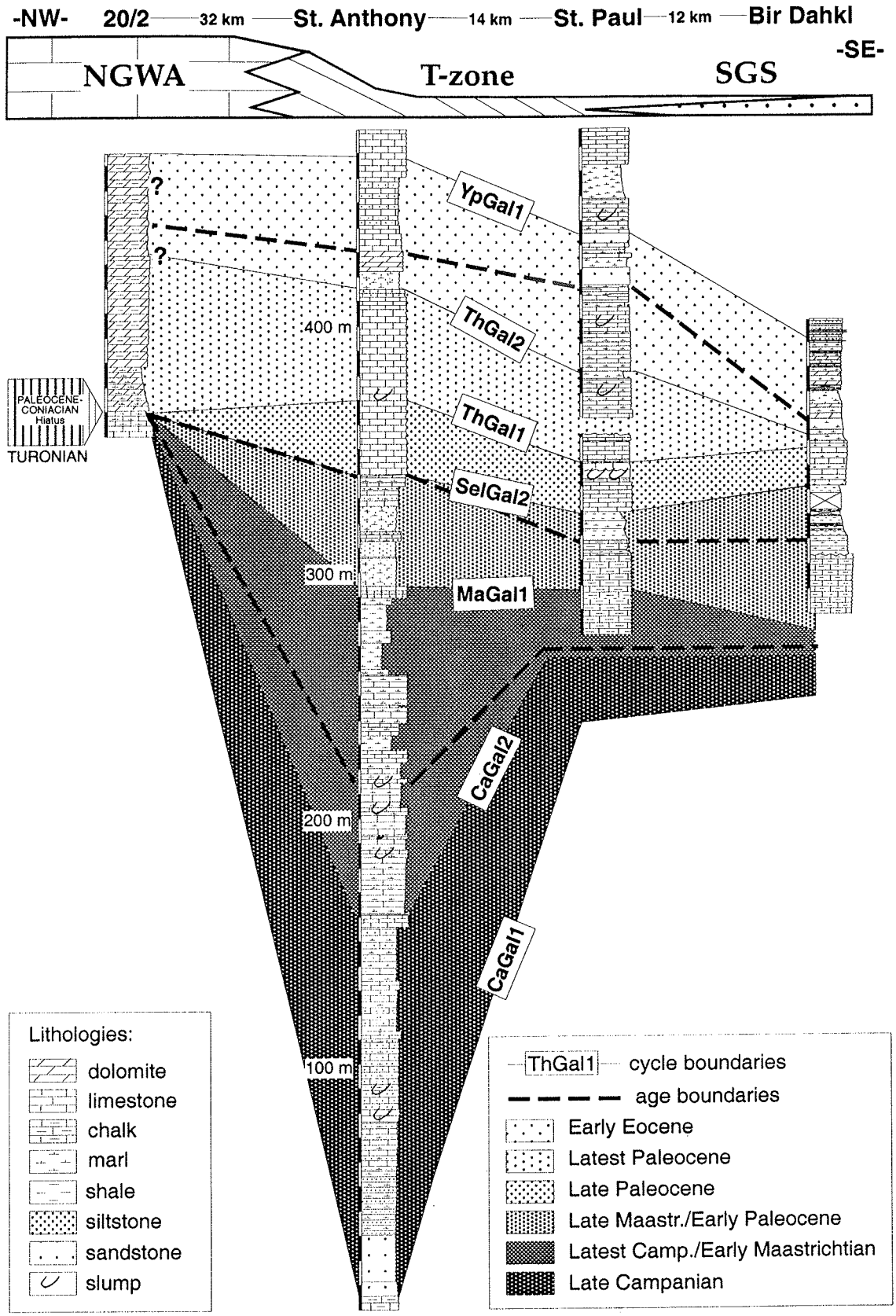

Fig. 6: *Stratigraphic correlation and cycle boundaries of the four Late Cretaceous-Paleogene key-sections (key section St. Paul is a composite profile). Hiatuses, lithologic variations, and thickness variations are due to palaeogeographic differences of the Uplift, Transition Zone, and Sub-basin (see schematic section on top). The distances between sections refer to their position on transect-line A – B (Figure 1).*

fluctuations from deeper ramp-basinal areas of the Southern Galala were reported by Kulbrok (1996) and recently re-studied by Scheibner et al. (2000). We concentrated on characteristics, such as foraminiferal data (P/B ratio) or sedimentologic interpretations that are relevant to water-depth estimates and the reconstruction of regional fluctuations in sea-level fluctuations.

Paraconformities and discontinuities occur at various levels within each section and are used for the interpretation of sequence boundaries. A major hiatus is present in section 20/2 (Figure 6) spanning the Coniacian to Late Paleocene interval. Although we cannot estimate the lower and upper boundaries of this hiatus on an exact biostratigraphic scale, a long-lasting period of non-deposition and/or erosion due to uplift is concluded from regional observations. Another important hiatus is possibly present in the St. Anthony Section near the Maastrichtian-Paleocene boundary, but again the exact biostratigraphic evidence is missing. Discontinuities of much shorter duration in slope-areas are indicated by the penecontemporaneous reworking of sediments (Scheibner et al., 2000). The same is true in areas that are more basinal where the absence of individual sub-zones suggest an incomplete stratigraphic record.

Upper Cretaceous

Upper Cretaceous rocks are exposed only on the southernmost edge of the Northern Galala/Wadi Araba Uplift (St. Anthony Section, Figure 6). The basal part of the St. Anthony Section consists of Campanian chalk-calcareous shale intercalations and massive chalks that reflect deep-neritic outer-shelf. Farther north, there is no stratigraphic evidence of any Upper Cretaceous rocks, which suggests that most parts of the Northern Galala were above sea level in Late Campanian - Early Maastrichtian times. Similarly, no age-equivalent sediments are to be found in outcrops to the south.

The Campanian chalk in the St. Anthony Section is truncated disconformably by the chaotic Upper Campanian units of the St. Anthony Formation. The Formation contains olistoliths, south-verging slumps, and debris flows composed of intercalations of bioclastic limestone, sandstone, and siltstone (Figures 6, 7a, inlay a3). We interpret the base of this unit to be a sequence boundary (CaGal1, Figure 5). It may be correlated with CaMaSin boundary in southeastern Sinai (Lüning et al., 1998a) and with unconformities in the vicinity of the Campanian-Maastrichtian boundary described from Israel (Almogi-Labin et al., 1990; Lewy, 1990). These Upper Campanian strata contain redeposited shallow-water biota, such as orbitoids and green algae together with corallinaceans and planktonic foraminifera. This assemblage of organisms that originally living in shallow-platform to deeper-shelf environments favours the model of a rimmed carbonate shelf situated at the southern edge of the elevated Norther Galala/Wadi Araba swell (Figure 4). The platform morphology can also be deduced from the sedimentary structures, facies characteristics, and the relatively short distance between platform (NGWA) and slope deposits (T-zone). In the St. Anthony Section, the reworked sediments sandwiched between CaGal1 and CaGal2 (Figure 6) are interpreted as a southward prograding low-stand wedge (Figure 7a3) resulting from falling sea level during the Late Campanian (lowermost *G. aegyptiaca*-zone (Figure 5). We assume that the subaerial exposure of the

elevated areas farther north, hitherto covered by the sea included the Northern Galala/Wadi Araba Uplift. This uplifted area formed an island with (at present unexposed) Upper Cretaceous carbonate platform deposits that prograded southward along its southern coast (Figure 4). In the St. Paul and Bir Dakhl Sections rocks of that age are also not exposed (Figure 6). However, there is evidence of correlation with hemipelagic chalk/marl successions in the Eastern Desert Intrashelf Basin(Figure3) to the south (Bandel et al., 1987).

In the St. Anthony Section and farther south, a Late Campanian rise of sea level is indicated by the presence of hemipelagic calcareous shales of the upper *G. aegyptiaca* zone (Kulbrok, 1996). Conspicuous facies changes characterise the cycle boundary CaGal2 (comparable to UZA4.5 of Haq et al., 1988). Mixed siliciclastic limestones containing omphalocyclids and reworked shallow-water biota occur above the CaGal2 boundary. They indicate a second interval of southward prograding shallow-water deposits (Figure 7a2), originally formed on the northerly carbonate platform. They are overlain by neritic carbonates of the latest Campanian (*G. gansseri*-zone) and by calcareous shales of the Lower Maastrichtian (late *G. gansseri* – *A. mayaroensis*-zones, Kulbrok, 1996). Cycle boundary MaGal1 (equivalent to TA1.1 of Haq et al., 1988) coincides with the onset of siliciclastic-dominated sediments. In contrast, there is no evidence of shallow-water deposition in the Upper Maastrichtian chalk of the Sudr Formation in the Southern Galala Sub-basin (St. Paul and Bir Dakhl Sections, Figure 6).

The exact reconstruction of the Late Cretaceous uplift history of the Northern Galala/Wadi Araba area is further complicated by the poor stratigraphic record (section 20/2, Figure 4). Nevertheless, we can assume a longer interval of uplift on the basis of hiatuses (also reported in neighbouring areas), that range from post-Turonian to pre-Late Paleocene times (see Shahar, 1994).

Paleocene - Lower Eocene

Evidence of regional fluctuations in sea-level is present in sediments of the Palaeogene ramp that covered parts of the Northern Galala/Wadi Araba area, as well as in slope-basin successions farther south.

The first lowstand of the Early Paleocene sea level and its corresponding sequence boundary DaGal1 (Figure 5) were interpreted by Kulbrok (1996) and may coincide with DaSin-3 of east Sinai (Lüning et al., 1998b). The same authors reported two earlier Paleocene sea-level falls also known from outcrops in the Nile Valley (Speijer and Schmitz, 1998) but not discernible in the Galala Plateaus (Figure 5). Cycle boundary SelGal1 was recognised to the northeast of the Gulf of Suez on sedimentologic evidence (Kulbrok, 1996). It may coincide with a mid-NP4 benthic peak described from Gebel Oweina by Speijer and Schmitz (1998) and from east Sinai (ThSin1) by Lüning et al. (1998b), and may be comparable with Sel1 of Hardenbol et al. (1998).

The Late Paleocene (NP 5 - NP9) slope section of the northern Southern Galala Sub-basin (St. Paul Section) provides evidence of three phases of ramp progradation. At least two of the phases can be equated with falls in sea level (Scheibner et al., 2000). In the Bir Dakhl Section, thin equivalents of the prograding ramp deposits interfinger with basinal calcareous shales of the Dakhla Formation

NW
St. Anthony(a)
St. Paul(b)
Bir Dahkl(c)
SE
Southern Galala Fm.
platform/ slope depos.
St. Anthony Formation
marls, limestones and siltstones
slumps
ThGal1
SelGal2
MaGal1
CaGal2
a2
a3
a
25m
Southern Galala Fm.
debris flows
a1
1m
Southern Galala Formation
debris flows and layered limestones
debris flows
slides, slumps, and debris flows
Dahkla Fm.
basinal marls
ThGal1
SelGal?
SelGal2
b
3m
a2
10m
Southern Galala Formation
distal fan lobes
Dahkla Fm.
basinal marls
SelGal2
c
1m
St. Anthony Formation
a3
3m

Fig. 7: *Lithologic characteristics, formations and cycle boundaries of three key section (a) St. Anthony, (b) St. Paul and (c) Bir Dakhl. Details of St. Anthony Section are illustrated in the figures: (a1) debris flows of the Southern Galala Formation, composed of shallow water limestone clasts (up to several dm thick); (a2) well-bedded shallow water limestones of the St. Anthony Formation; a3 Late Campanian limestones and sandstones of the St. Anthony Formation, exhibiting slumps, olistolithes, and debris flows that are formed at the proximal slopes of the Late Cretaceous Transition Zone.*

(Figure 7c). The succession indicates that the Sub-basin was fed with carbonates derived from the south-prograding Paleogene ramp (Figures 3 and 4). A pronounced fall in sea level in middle of the NP5 zone (SelGal2) correlates with a sequence boundary recognised from the northern Gulf of Suez (Kulbrok, 1996) and from Sinai (ThSin2 of Lüning et al., 1998b). Furthermore, Lüning et al. (1998b) gave evidence of its synchroneity with Th1 from Hardenbol et al. (1998), which suggests that SelGal2 may be a candidate for a global cycle boundary (Figure 5). A second phase of ramp progradation described from the northern South Galala Sub-basin by Scheibner et al. (in press) could reflect a cycle boundary. However, it cannot be correlated with other regional descriptions and it may be related to the sea-level fall that caused SelGal2 (Figure 5). Cycle boundary ThGal1 coincides with a phase of ramp progradation in the northern part of the Southern Galala Sub-basin, interpreted as being the result of a major fall in sea-level. Evidence comes from the relationship of the SBZ4 interval (Scheibner et al., 2000) with the ThSin5 boundary of Lüning et al. (1998b) from east Sinai and Th4 of Hardenbol et al. (1998). In contrast, it was not possible to prove the presence of sequence boundaries ThSin3 and ThSin4 of Lüning et al. (1998b) in the Sub-basin or in the Oweina area (Speijer and Schmitz, 1998) to the south.

Fluctuations in sea level on the latest Paleocene - Early Eocene ramp are indicated by lateral and vertical facies changes supported by the distribution of facies-relevant alveolinids (Gietl, 1998). Cycle boundary ThGal2 from the basal SBZ6 may correspond to a mid-NP9 sea-level signal from the same interval in eastern Sinai. Productivity controls or hiatuses, however, cannot be excluded here as possible causes of variations in planktonic-benthonic foraminifera ratios (Lüning et al., 1998b). The exact age of the later YpGal1 cycle boundary (basal SBZ10 - P6/P7 boundary interval) is difficult to determine because of poor stratigraphic resolution based on alveolinids in the ramp carbonates. YpGal1 may be equivalent to the YpSin-1 sequence boundary, the determination of which, however, is also difficult (Lüning et al., 1998b) because of the diachronous character of lithologic boundaries.

6. Comparison with other regions of Syrian Arc Deformation

The deformational history of the Syrian Arc is difficult to unravel because of the marked changes in the intensities of deformation in time and space. For example, few major phases of uplift represent peaks of deformation that are comparable from one area to another. Nevertheless, they help in understanding the geodynamic processes that acted along the northern rim of the African-Arabian Plate, and give clues that help in the elucidation of the neighbouring southeastern Mediterranean Plate puzzle. Shahar (1994) estimated a 400- to 600-m uplift during the Late

Turonian-Eocene in the Sinai-Negev Fold Belt. Hirsch et al. (1995) reconstructed initial, main, and late phases of compression pulses for the Negev Fold Belt from the Coniacian to the Miocene. Based on continent-wide comparisons, Guiraud and Bosworth (1996) assume several Late Cretaceous compressive events but they rejected the model of a long-lasting compressional regime. Their interpretation was of Late Santonian deformation and Campanian rifting, followed by compression phases during the Late Maastrichtian and in the Miocene (Aquitanian-Burdigalian and Tortonian times). On a wider regional scale, the relationship of Syrian Arc tectonics to Late Cretaceous African deformational events is presently unknown (Bosworth et al., 1999), because of the absence of exact stratigraphic evidence of the respective intervals of deformation.

First evidences of Late Cenomanian-Turonian compression between the northeastern part of the African-Arabian Plate and the Eurasian Plate seems to predate initial uplift in the Syrian Arc. The collision zone is flanked by an ophiolite belt of Upper Cretaceous ages that extends from Cyprus to Oman. Post-Cenomanian compressional regimes are described from Turkey and Oman by Collins and Robertson (1997) and by Patton and O'Connor (1988). The compressions correlate with the first inversion movements in the Syrian Arc system (Moustafa, 1988) that began in Early Turonian times along older deep-seated extensional faults. An example is at Abu Roash in Egypt (location 4 on inset map, Figure 1). In the Negev, Honigstein et al. (1988) reconstructed a major Late Turonian–Early Santonian tectonic phase based on short-distance thickness changes and biostratigraphically well constrained onlap patterns.

A good reference area for several Late Cretaceous–Palaeogene uplift phases is the Areif el Naqa anticline (location 2 on inset map, Figure1). The anticline is part of the southern branch of the Syrian Arc (Lüning et al., 1998a). Lateral facies changes and thickness changes are linked to the anticlinal geometry and reflect Coniacian–Santonian basin inversion (Bartov et al., 1980). Age-equivalent tectonic activity was described from other localities of northern Sinai, where Upper Coniacian sediments are missing (Lewy, 1975) while, at the same time, central Sinai was covered by the sea. Similar results (although poorly constrained by biostratigraphy) are based on interpretations of seismic profiles. The profiles show evidence of Late Cretaceous to Oligocene onlap against synsedimentary rising anticlines in the Negev-Sinai Fold Belt (Ayyad and Darwish, 1996) and the Palmyride Fold Belt (Chaimov et al., 1992).

The culmination of Syrian Arc movements at Areif el Naqa during Late Campanian – Early Maastrichtian times may be coeval with uplift in the Northern Galala area. The movements are documented by reworked sandstones and silicified limestones that accumulated at the anticlinal flanks of the Areif el Naqa anticline, while the crest was exposed above the level of the Late Cretaceous sea. In contrast, the Late Campanian to Maastrichtian deposits of the Northern Galala/Wadi Araba were formed in an adjacent carbonate platform setting (Figures 3 and 4).

Similar carbonate platforms rimmed the Northern Galala/Wadi Araba Uplift during Paleocene to Eocene times (Figure 3). Age-equivalent rocks of the Areif el Naqa anticline are composed of hemipelagic marls and chalks gently inclined relative to the underlying folded Late Cretaceous deposits (Lüning et al., 1998a). This Late Paleocene angular unconformity is present elsewhere in

Sinai (Moustafa and Khalil, 1995) and in northern Negev (Zur et al., 1995). A major uplift phase in the Gulf of Suez region was described by Patton et al. (1994). It commenced in the Late Paleocene and it may be coeval with the second phase of ramp progradation at sequence boundary SelGal? (Figure 5) of the Northern Galala Wadi Araba Uplift.

7. Implications for the Hydrocarbon Potential

The Late Campanian to Early Eocene shallow-water limestones of the Galala plateaus contrast with age-equivalent lithologies described from most of the other areas of uplift in the Syrian Arc. For example, chalky, shaley and marly rocks occur at. Abu Roash near Cairo (Moustafa, 1988), at Areif el Naqa in eastern Sinai (Lüning et al., 1998a), and are interpreted from subsurface seismic data (Ayyad and Darwish, 1996). Slumps, thin silt-sand intercalations, stratigraphic discontinuities or onlap patterns indicate gravity flows from submarine slopes or island that, however, are not rimmed by Galala-type carbonate platforms.

Cretaceous–Tertiary platform carbonates that were deposited on the southern shores of the Neo-Tethyan Ocean contain significant hydrocarbon resources. Many of the carbonates important reservoirs with porosities due to the interplay of primary, secondary and later diagenetic alternations, or they are source rocks formed mainly during transgressions. Kerogen-rich limestones often develop in intrashelf basins, such as the Late Aptian–Cenomanian Sinai ramp (Kim et al., 1999) or the productive Cenomanian-Turonian platform deposits of the Arabian Gulf (Alsharhan and Nairn, 1994). Similarly, the Late Cretaceous – Early Tertiary carbonates of the Northern Galala/Wadi Araba contain source-rock facies that are characterised by laminated argillaceous and shaley lime-mudstones and wackestones. If the down-faulted Galala-type sediments in the Gulf of Suez are similar, we may expect to find mature organic-rich carbonate deposits there that were formed in intrashelf basins of the Late Campanian-Eocene carbonate platforms. for example, the source rock of the Zafarana field in the Gulf of Suez is probably composed of organic-rich Senonian-Eocene carbonate deposits.

8. Conclusions

The stratigraphic evolution of the Upper Cretaceous–Paleogene succession of the Galala Plateaus in the Eastern Desert of Egypt was controlled by a Syrian Arc Uplift that defined the subsequent basin-and-swell morphology. During Late Campanian times, the Northern Galala/Wadi Araba Uplift (NGWA) was formed, as indicated by southward-prograding slope deposits of a Transition Zone (T-zone) that links the Uplift with the Southern Galala Sub-basin of the Eastern Desert Intrashelf Basin (Figure1). The Sub-basin is the result of the southward prograding Late Cretaceous - Palaeogene sedimentary wedges of the Transition Zone causing loading and subsequent subsidence. The slope deposits of the Transition Zone interfinger with neritic and hemipelagic sediments of the Sub-basin. The successive Paleogene sequences are evidence for a gradual southward movement of the Transition Zone (Figure 1).

The platform to basin transition of the Galala area is reflected in the facies architecture (Figure 4) and the sedimentologic and palaeoecologic variations. It is mainly controlled by the interplay of uplift and subsequent erosion, re-deposition, biogenic sedimentation, and sea-level changes. An analysis of the prograding depositional geometry of the Uplift margin and of the slope deposits of the Transition Zone reveal changing margin morphologies that evolved spatially and temporally into each other. Consequently the Late Cretaceous rimmed platform is followed by a Paleocene distally steepened ramp and overlain by an Early Eocene homoclinal ramp (Figure 4). Only the slope deposits of the Transition Zone give evidence of the now eroded Upper Cretaceous carbonate shelf. On a regional scale, rare occurrences of well-bedded shallow-water carbonates may be equivalent to the Early Paleocene carbonate platform in the Galala area. Carbonate production resumed in most areas of the Northern Galala/Wadi Araba Uplift during Late Paleocene times and resulted in the deposition of massive carbonates.

9. Acknowledgement

Funding by the German Research Foundation (DFG-Graduiertenkolleg: Stoff-Flüsse in marinen Geosystemen) and Bremen University allowed fieldwork and other investigations to be made. Ain Shams University, Cairo gave much valuable logistical support. Special thanks for helpful discussions and advice are due to Professor Dr. M.A.A. Bassiouni (Ain Shams University), Dr. P. Luger (Technical University Berlin), Dr. R. Speijer (Bremen University), and Dr. S. Lüning (Lasmo,London). Dr. E. Caus (Barcelona University) helped with the identification of the orbitoids. We thank E. Friedel (Bremen) for reading and correcting several versions of the manuscript and four anonymous reviewers for their valuable comments.

10. References

Aal, A.A and J.J. Lelek 1994. *Structural development of the northern Sinai, Egypt and its implications on the hydrocarbon prospectivity of the Mesozoic.* In GEO'94, Proceedings of the Middle East Geoscience Conference: Bahrain, GeoArabia, v. 1, p. 15-30.

Abdallah, A. M. and A. Eissa 1966. *The Campanian rocks of the southern Galala.* A.R.E. Bulletin, Faculty of Sciences, University of Cairo, v. 44, p. 259-271.

Abdel Kireem, M. R. and H. F. Abdou 1979. *Upper Cretaceous - Lower Tertiary planktonic foraminifera from South Galala Plateau, Eastern Desert, Egypt.* Revista Española Micropaleontologia, v. XI(2), p. 175-222.

Almogi-Labin, A., A. Flexer, A. Honigstein, A. Rosenfeld and E. Rosenthal 1990. *Biostratigraphy and tectonically controlled sedimentation of the Maastrichtian in Israel and adjacent countries.* Revista Española Paleontologia, v. 5, p. 41-52.

Alsharhan, A. S and A.E.M. Nairn 1994. *Carbonate Platform Models of Arabian Cretaceous Reservoirs.* In J. A. T. Simo et al. (Eds.) Cretaceous Carbonate Platforms American Association of Petroleum Geologists Memoirs, v. 56, p. 173-184.

Awad, G. H. and A. M. Abdallah 1966. *Upper Cretaceous in Southern Galala, Eastern Desert with emphasis on neighbouring areas.* Journal of Geology U.A.R., v. 10, No. 2, p. 125-144

Ayyad, M. H. and M. Darwish 1996. *Syrian Arc Structures: a unifying model of inverted basins and hydrocarbon occurrences in North Egypt.* Egyptian Geolgogical Petroleum Company Seminar, November 1996, Cairo, 19 p.

Bandel K. and J. Kuss 1987. *Depositional environment of the pre-rift sediments of the Galala heights (Gulf of Suez, Egypt).* Berliner geowissenschaftliche Abhandlungen (A), v. 78, p. 1-48.

Bandel K., J.Kuss and N. Malchus 1987. *The sediments of Wadi Qena (Eastern Desert, Egypt).* Journal of African Earth Science, v. 6(4), p. 427-455.

Bartov, Y., Z. Lewy, G. Steinitz and I. Zak 1980. *Mesozoic and structural history of the Gebel Areif El Naqa area, Eastern Sinai.* Israel Journal of Earth-Science, v. 29, p. 114-139.

Berggren, W.A., D.V. Kent, I.C.C., Swisher and M.-P. Aubry 1995. *A revised geochronology and chronostratigraphy.* In W. A. Berggren et al. (Eds.) Geochronology, Time Scales and Global Stratigraphic Correlation, Society of Economic Paleontologists and Mineralogists Special Publications, v. 54, p. 129-212.

Bosworth, W., R. Guiraud and L.G. Kessler 1999. *Late Cretaceous (ca. 84 Ma) compressive deformation of the stable platform of northeast Africa(Egypt): Far-field stress effects of the "Santonian event" and origin of the Syrian arc deformation belt.* Geology, v. 27/7, p. 633-636.

Boukhary, M., F. Kulbrok and J. Kuss 1998. *New nummulitids from lower Eocene limestones of Egypt (Monastery of St. Paul, Eastern Desert).* Micropaleontology, v. 44/1, p. 99-108.

Burchette, T. P. and V. P. Wright 1992. *Carbonate ramp depositional systems.* Sedimentary Geology, v. 79, p. 3-57.

Camoin, G., M.C. Bernet-Rollande and J.Philip 1988. *Rudist-coral frameworks associated with submarine volcanism in the Maastrichtian of the Pachino area (Sicily).* Sedimentology v. 35, p. 123-138.

Camoin, G., Y. Bellion, J. Dercourt, R Guiraud, J. Lucas, A. Poisson, L.E. Ricou and B. Vrielynck. 1993. *Late Maastrichtian (69.5 – 65 Ma).* In J. Dercourt, L.E. Ricou and B. Vrielynck (Eds.), Atlas Tethys Palaeoenvironmental Maps p. 179-196. Gauthier-Villars, Paris.

Caus, E., J. M. Bernaus and A. Gomez-Garrido 1996. *Biostratigraphic utility of the genus Orbitoides.* Journal of foraminiferal Research, v. 26/2, p. 124-136.

Chaimov, T.A., Barazangi, M., Al-Saad, D., Sawaf, T. and A. Gebran 1992. *Mesozoic and Cenozoic deformation inferred from seismic stratigraphy in the southwestern intracontinental Palmyride fold-thrust belt, Syria.* Geological Society of America, Bulletin, 104, p. 704-715.

Collins, A.S. and A.H.F. Robertson 1997. *Lycian melange, southwestern Turkey: An emplaced Late Cretaceous accretionary complex*: Geology, v. 25 (3), p. 255-258.

Eberli, G. P., D. Bernoulli, D. Sanders and A. Vecsei 1994. *From Aggradation to Progradation: The Maiella Platform, Abbruzi, Italy.* In J. A. T. Simo et al. (Eds.) Cretaceous Carbonate Platforms American. Association of Petroleum Geologists Memoirs, v. 56, p. 213-232.

Erba, E., Premoli Silva, I. and D.K. Watkins, 1995. *Cretaceous calcareous plankton biostratigraphy of Sites 872 through 879.* In J.A. Haggerty, I. Premoli Silva, F. Rack and M.K. McNutt (Eds.) Proceedings of the Ocean Drilling Program, Scientific Results, p. 157-169.

Faris, M. 1994. *Late Cretaceous and Paleocene calcareous nannofossils Biostratigraphy at St. Paul. Southern Galala Plateau.* Annals of the Geological Survey Egypt, v. 20, p. 585-601.

Gietl, R. 1998. *Biostratigraphie und Sedimentationsmuster einer nordostägyptischen Karbonatrampe unter Berücksichtigung der Alveolinen-Faunen.* Berichte aus dem Fachbereich Geowissenschaften der Universität Bremen, v. 112, p. 1-135.

Gradstein, F.M., Agterberg, F.P., Ogg, J.G., Hardenbol, J., van Veen, P., Thierry, J. and Z. Huang 1995. *A Triassic, Jurassic and Cretaceous time scale.* In Berggren, et al. (Eds.), Geochronology, time scales and global stratigraphic correlation , 95-126

Guiraud, R. and W. Bosworth 1996. *Senonian basin inversion and rejuvenation of rifting in Africa and Arabia: implications to models of plate boundary-intra plate dynamics* [abstr.]: IGCP 369 "Comparative Evolution of PeriTethyan Rift Basins", 3rd Ann. Meeting, 19-24 Nov. 1996, Cairo, Egypt.

Haas, J. 1996. *Genesis of Late Cretaceous toe-of-slope breccias in the Bakony Mts., Hungary.* Sedimentary Geology, v. 128, p. 51-66.

Handford, C. R. and R. G. Loucks 1993. *Carbonate depositional sequences and systems tracts. Responses of Carbonate Platforms to relative sea-level changes.* In R. G. Loucks and F. Sarg (Eds.), Carbonate sequence stratigraphy. American Association of Petroleum Geologists Memoirs, v. 57, p. 3-41.

Haq, B. U., J. Hardenbol and P. R. Vail 1988. *Mesozoic and Cenozoic chronostratigraphy and cycles of sea-level change.* In C.K. Wilgus, B.C. Hastings, C.A. Ross, H. Posamentier, J. van Wagoner and C.G.St.C Kendall (Eds.), Sea-level changes – an integrated approach. Society of Economic Palaeontologists and Mineralogists, Special Publications, v. 42, p. 71-108.

Hardenbol, J., J. Thierry, M.B. Farley, T. Jacquin, P.-C. De Graciansky and P.R. Vail 1998. *Mesozoic-Cenozoic sequence chronostratigraphy framework of European Basins.* In P.-C. de Graciansky et

al. (Eds.), Sequence Stratigraphy of European Basins. Society of Economic Palaeontologists and Mineralogists, Special Publications.

Hendriks, F., P. Luger, J., Bowitz and H. Kallenbach 1987. *Evolution of the depositional environment of SE-Egypt during the Cretaceous and Tertiary*. Berliner geowissenschaftliche Abhandlungen (A), v. 75.1, p. 49-82.

Hirsch, F., Flexer, A., Ilani, S., Rosenfeld, A., Roded, R. and A. Yelin-Dror 1995. *The Levantides Folding Belt*. "The Geology of the Eastern Mediterranean Region" Jerusalem, Aug. 27 – Sep. 1, 1995, Abstract Volume, p. 6.

Honigstein, A. Flexer, A. and A. Rosenfeld 1988. *Tectonic activity in the Syrain Arc in Israel, as indicated by Senonian ostracodes*. Neues Jahrbuch Geologie Paläontologie Monatshefte, 3, p. 173-183.

Hottinger, L. 1960. *Über paleozäne und eozäne Alveolinen*. Eclogae Geologicae Helvetiae, v. 53/1, p. 256-284.

Kim, Y., T. Wagner, M.Bachmann and J. Kuss 1999. *Organic facies and thermal maturity of Late Aptian to Early Cenomanian shelf deposits, Northern Sinai (Egypt)*. International Journal of Coal Geology, v. 39, p. 251-278.

Kulbrok, F. 1996. *Biostratigraphie, Fazies und Sequenzstratigraphie einer Karbonatrampe in den Schichten der Oberkreide und des Alttertiärs Nordost-Ägyptens (Eastern Desert, N' Golf von Suez, Westsinai)*. Berichte aus dem Fachbereich Geowissenschaften der Universität Bremen, v. 81, p. 1-153.

Kuss, J. 1986. *Facies development of Upper Cretaceous-Lower Tertiary sediments of monastery of St. Anthony, Eastern Desert, Egypt*. Facies, v. 15, p. 177-194.

Kuss, J. 1992. *The Aptian-Paleocene shelf carbonates of Northeastern Egypt and Southern Jordan: Establishment and break-up of carbonate platfoms along the southern Tethyan shores*. Zeitschrift der deutschen geologischen Gesellschaft, v. 143, p. 107-132.

Kuss, J. and U. Leppig 1989. *The Early Tertiary (middle-late Paleocene) limestones from the western Gulf of Suez, Egypt*. Neues Jahrbuch für Geologie und Paläontologie, Monatshefte, v. 177(3), p. 289-332.

Kuss, J. and H.-G. Herbig 1993. Biogeography, Facies, and Taxonomy of Early Tertiary Green Algae from Egypt and Morocco. In F. Barattolo et al. (Eds.), Studies on Fossil Benthic Algae. Bolletino della Società Paleontologica Italiana, Special Volume 1, p. 249-280.

Kuss, J. and F. Kulbrok 1995. *Pre-rift Strata and Syntectonic Sedimentation in the Gulf of Suez Area*. "Rift Sedimentation and Tectonics in the Red Sea – Gulf of Aden Region" Sana´a, Yemen, 23-31.October 1995, Abstract Volume, p. 34.

Kuss, J. and M. Bachmann 1996. *Cretaceous paleogeography of the Sinai Peninsula and neighbouring areas*. Comptes Rendus Académie des Sciences Paris, v. 322/ser.IIa, p. 915-933.

Lewy, Z. 1975. *The geological history of Southern Israel and Sinai during the Coniacian*.- Israel Journal of Earth-Science, v. 24, p. 19-43.

Lewy, Z. 1990. *Transgressions, regressions and relative sea-level changes on the Cretaceous shelf of Israel and adjacent countries. A critical evaluation of Cretaceous global sea-level correlations*. Paleoceanography, v. 5/4, p. 619-637.

Lüning, S., J. Kuss, M. Bachmann, A. Marzouk and A. M. Morsi 1998a. *Sedimentary response to Basin Inversion: Mid Cretaceous Early Tertiary Pre- to Syndeformational Deposition at the Areif El Naqa Anticline (Sinai, Egypt)*. Facies, v. 38, p. 103-136.

Lüning, S., A. Marzouk and J. Kuss 1998b. *The Paleocene of Central East Sinai, Egypt: 'Sequence Stratigraphy' in Monotonous Hemipelagites*. Journal of Foraminiferal Research, v. 28/1, p. 19-39.

Luger, P., M. El-Beshtawy and H. Mai 1998. *Maastrichtian Planktonic Foraminiferal Biozonation and K/T Boundary in Central Egypt*. Revista Española de Micropaleontologia, v. 30(2), p. 37-49.

Martini, E. 1971. *Standard Tertiary and Quaternary calcareous nannoplankton zonation*. In A. Farinacci (Ed.), Proceedings of II Planktonic Conference, Roma 1970, Proceedings II Planktonic Conference , v. 2, p. 739-785.

Masters, B.A., 1984 *Comparison of Planktonic Foraminifers at the Cretaceous-Tertiary Boundary from the El Haria Shale (Tuninisa) and the Esna Shale (Egypt)*. Proceedings of the 7th Exploration Seminar, Egyptian Petroleum Company, Cairo, p. 310-324

Moustafa, A. 1988. *Wrench tectonics in the north Western Desert of Egypt (Abu Roash area, southwest of Cairo)*. Middle East Research Center, Ain Shams University, Earth Sciences Series, v. 2, p. 1-16.

Moustafa, A. and H. M. Khalil 1995. *Superposed Deformation in the Northern Suez Rift, Egypt: Relevance to Hydrocarbons Exploration.* Journal of Petroleum Geologists, v. 18/3, p. 245-266.

Norris, R.D., D. Kroon , A. Klaus et al. 1998. *Explanatory Notes.* In R.D. Norris, D. Kroon, A. Klaus et al. (Eds.), Proceedings of the Ocean Drilling Program, Proc. ODP Initial Reports, v. 160, p. 11-42.

Patton, T. L. and S.J. O'Connor 1988. *Cretaceous flexural history of northern Oman mountain foredeep, United Arab Emirates.* American Association of Petroleum Geologists Bulletin, v. 72 (7), p. 797-809.

Patton, T. L., A. R. Moustafa, R. A. Nelson and S. A. Abdine 1994. Tectonic evolution and structural setting of the Suez Rift. In S. M. Landon (Ed.), Interior Rift Basins, American Association of Petroleum Geologists Memoir, v. 59, p. 9-55.

Schaub, H. 1981. *Nummulites et Assilines de la Téthys paléogène. Taxinomie, phylogenèse et biostratigraphie.* Schweizerische Paläontologische Abhandlungen, v. 104-106, p. 1-236.

Scheibner, C., J. Kuss and A. Marzouk 1999. *Slope sediments of a Paleocene ramp-to- basin transition on NE Egypt.* International Journal of Earth Science (in press).

Scheibner, C., A. Marzouk and J. Kuss in press. *Bio- and lithostratigraphy of the Maastrichtian – Early Eocene deposits of NE- Egypt/Sinai.* Journal of African Earth-Sciences.

Serra-Kiel, J., L. Hottinger, E. Caus, K. Drobne, C. Ferrandez, A.K. Jauhri, R. Pavlovec, J. Pignatti, J. M. Samso, H. Schaub, E. Sirel, A. Strougo, Y. Tambareau, J. Tosquella and E. Zakrevskaya 1999. *Larger Foraminiferal Biostratigraphy of the Tethyan Paleocene and Eocene.* Bulletin de la Société Géologique de France, v. 169, p. 281-299.

Shahar, J. 1994. *The Syrian arc system: an overview.* Palaeogeography, Palaeoclimatology, Palaeoecology, v. 112, p. 125-142.

Speijer, R. P. and B. Schmitz 1998. *A benthic foraminiferal record of Paleocene sea level and trophic/redox conditions at Gebel Aweina, Egypt.* Palaeogeography, Palaeoclimatology, Palaeoecology, v. 137, p. 79-101.

Speijer, R. P. and G. J. van der Zwaan 1994. *The differential effect of the Paleocene-Eocene boundary event: Extinction and survivorship in shallow to deep-water Egyptian benthic foraminiferal assemblages from Egypt.* In R. P. Speijer (Ed.), Extinction and Recovery Patterns in Benthic Foraminiferal Paleocommunities across the Cretaceous/Palaeogene and Paleocene/Eocene Boundaries, Geologica Ultraiectina, v. 124, p. 121-168.

Stampfli, G., P. Favre, A.Pillevuit and J.C. Vannay 1995. *The Neotethys-East Mediterranean basin connection.* Program 2nd International Symposium: The Geology of the Eastern Mediterranean Region, Jerusalem, 1995, Abstract Volume, p. 17.

Strougo, A., M.A.I. Haggag and H. Luterbacher 1992. *The basal paleocene 'Globigerina eugubina' zone in the Eastern desert (St. Pauls Monastery, South Galala), Egypt.* Neues Jahrbuch für Geologie und Paläontologie, Monatshefte, v. 2, p. 97-101.

Ward, P.D. and W. J. Kennedy 1993. *Maastrichtian ammonites from the Biscay region (France, Spain).* Palaeontological Society, Memoirs, v. 34, p. 1-58.

Zur, Y. Eyal, Y. and G. Shamir 1995. *Unconformities associated with the development of the Syrian Arc Fold System in the Giva`t Mador area.*- 2nd International Symposium "The Geology of the Eastern Mediterranean Region" Jerusalem, Aug. 27 – Sep. 1, 1995, Abstract Volume, p. 27.

CHAPTER 6

Stratigraphic modelling of carbonate platform-to-basin sediments (Maastrichtian to Paleocene) in the Eastern Desert, Egypt

submitted to
Paleogeography, Palaeoclimatology, Palaeoecology

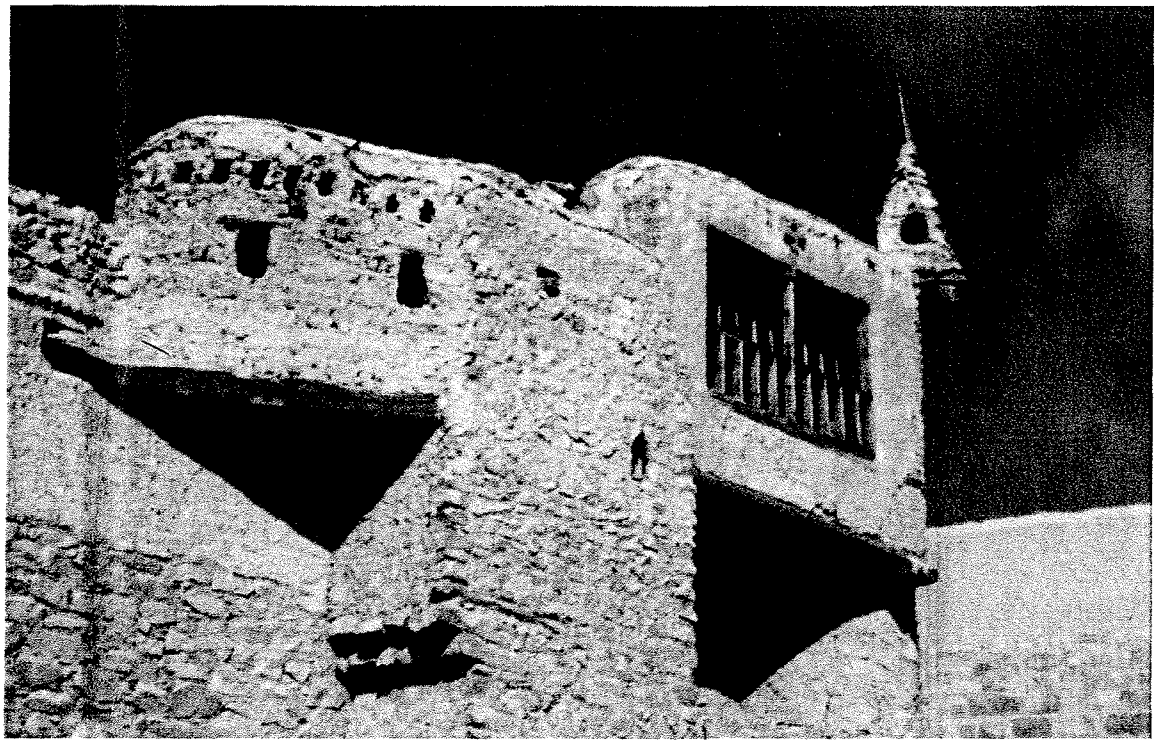

Besides the main entrance of the monastery of St. Paul
(on the right the small bell tower)

Photo by Christian Scheibner (1998)

Stratigraphic modelling of carbonate platform-to-basin sediments (Maastrichtian to Paleocene) in the Eastern Desert, Egypt

C. Scheibner, J. Kuss and R. P. Speijer

Bremen University, FB 5, P.O. Box 330440, 28334 Bremen, scheibne@uni-bremen.de

Keywords

Galala Mountains, Egypt, Maastrichtian, Paleocene, sedimentation rates, stratigraphic modelling, platform-basin transition

Abstract

In the Galala Mountains of the Eastern Desert, Egypt, carbonate platform and basin deposits are excellently exposed. These exposures show a late Campanian-early Paleocene rimmed platform evolving to a late Paleocene distally steepened ramp. We modelled the evolution of the platform-basin transition during the Maastrichtian and Paleocene (using the stratigraphic simulation program PHIL) and compared the results with outcrop sections. All stratigraphic, facies, and environmental data are summarised and operate as input and control parameters for the computer simulation. The most important parameters that control the depositional geometries of the late Cretaceous mixed carbonate siliciclastic platform and the Paleogene carbonate platform are changes in relative sea-level, sediment flux and initial topography. The simulation provides understanding on areas of the platform that are poorly exposed or have been eroded. Moreover, the simulated geologic parameters like lithology, overall thickness and paleowater-depth very closely resemble field and laboratory measurements of the individual sections. In an earlier study the timing of the transition from a rimmed platform to a distally steepened ramp was during latest Maastrichtian-early Paleocene: This study shows that the rimmed platform persists at least until the late Paleocene (59 Ma), documented by the relatively high slope angles of 6°. The Maastrichtian slope angle, calculated earlier to be 5°-8° are confirmed by the results of this study which proposes an angle of 8°.

Introduction

The area of the Galala mountains (Eastern Desert, Egypt, Fig. 1) has been in the focus of numerous studies mostly dealing with biostratigraphy and lithostratigraphy (Abdel Kireem and Abdou, 1979; Strougo et al., 1992; Strougo and Faris, 1993; Faris, 1995). A number of studies have dealt with the overall architecture of the depositional system (Bandel and Kuss, 1987; Kuss and Leppig, 1989; Kulbrok, 1996; Gietl, 1998; Kuss et al., 2000; Scheibner et al., 2001). These authors proposed a carbonate platform depositional system evolving on a Syrian Arc high with a generally southward progradation direction since Campanian times. Recently, studies dealing with individual

biosedimentary processes and their controlling parameters of this platform have started (Scheibner et al., 2000; Scheibner et al., in press).

In this study, we concentrate on a stratigraphic computer simulation of depositional sequences and on their lithostratigraphic properties performed in two models with time-slices for the Maastrichtian and for the Paleocene. In the first part all geological data like stratigraphy, depositional setting, slope architecture, paleobathymetry, sedimentation rates and sea-level changes are summarised. Special emphasis has been put on the interpretation of the extremly varying sedimentatation rates. In the second part the forward computer modelling program PHIL is used to simulate the depositional sequences and the lithostratigraphic properties of the Maastrichtian and Paleocene. One fraction of the geological data will serve as input data while other fractions act as a control data set for the simulation results.

The purpose of this study are i) to reconstruct the depositional history of the platform-basin transect in the Galala Mountains, ii) to obtain information on areas of the carbonate platform that are not or only poorly exposed and iii) to provide general insights into the processes and factors controlling the growth of carbonate platforms.

Geological setting

The investigated area represents a segment of the northern passive margin of the Afro-Arabian Plate, formed during the late Triassic/Jurassic opening of the Neotethys with the activation of half-grabens. Beginning with the initial stages of the collision between the African and European plates during Turonian times, a dextral transpressive reactivating of the half-grabens took place along the North African-Arabian plate boundary (e.g. Moustafa and Khalil, 1995). As a consequence, a system of inverted, uplifted and folded grabens was formed along the Syrian Arc System. In Egypt this area is also known as "unstable shelf" (Said, 1962). It contrasts with the tectonically little affected area further south ("stable shelf"). While the latter is characterised by laterally rather uniform marine strata, formed on a gently north-dipping shelf, pronounced small-scale facies variations characterize the basin-swell-morphologies of the unstable shelf area (Kuss et al., 2000).

The Galala mountains in the Eastern Desert together with areas on W-Sinai represent a southern branch of the Syrian Arc, called Northern Galala/Wadi Araba High (NGWA High) (Kuss et al. 2000). The upper Cretaceous-Paleogene carbonate dominated successions of a south and north-dipping carbonate platform prograde from the NGWA High. During the late Campanian-Maastrichtian large masses of shallow-water sediments (carbonates, marls and siliciclastics) were shed from the NGWA High, mainly in southerly directions. These sediments accumulated on the slope of a carbonate platform evidenced within a very narrow belt at the northern rim of the Southern Galala (sections around St. Anthony, Fig. 1). Further south, at the southern rim of the Southern Galala age equivalent basinal chalks were deposited (Scheibner et al. in press). In contrast to the small area of late Cretaceous platform and slope deposition, the Paleogene platform and slope deposits have a much wider areal distribution. The facies-transitions between the Paleocene

shallow-water ramp carbonates and deeper-water marls of the Southern Galala Sub-basin farther south have been studied in sections along the dip direction (Scheibner et al. 2001). The slope sediments are often characterised by mass transport deposits like slides, slumps, and debris-flows that have been investigated in detail for an upper Paleocene section (Scheibner et al. 2000).

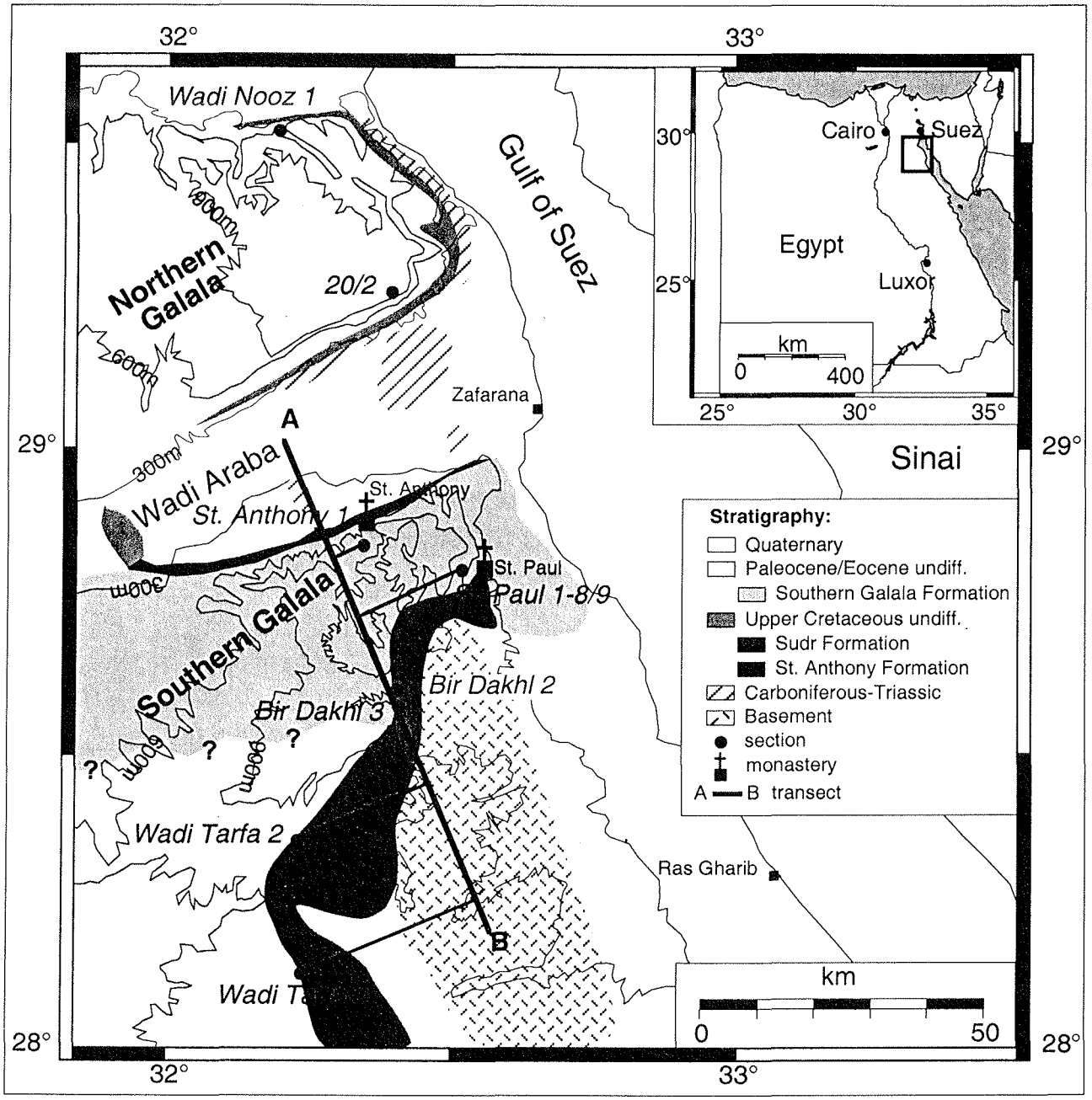

Fig.1: Schematic geological map of the Galala Mountains in the Eastern Desert, west of the Gulf of Suez (see upper inlay) with locations of sections projected on line A-B which runs in NNW-SSE direction, perpendicular to the Northern Galala/Wadi Araba High. The zero point of profil line A-B lies within the Wadi Araba. Sections 20/2 and Wadi Nooz 1 in the Northern Galala were only used for bio- and lithostratigraphic comparisons and not for the stratigraphic simulation. The exact stratigraphic range of the individual formations is indicated in Fig. 2

Material and Methods

The study area extends from the Northern Galala approximately 100 km southwards to Wadi Tarfa (Fig. 1). The following six sections are considered for the stratigraphic simulation: Section St. Anthony 1 is located along the northern rim of the Southern Galala while sections St. Paul 9, Bir Dakhl 2, 3 and Wadi Tarfa 1, 2 are located further south (Fig. 1). Additional stratigraphic data, from Kuss (1986), Bandel and Kuss (1987), Kuss and Leppig (1989), Kulbrok (1996), and Gietl (1998) have been incorporated.

Facies interpretations are based on fine scale mapping of stratigraphic sections of the carbonate platform. Microscopic studies of 181 thin-sections of the Campanian-Eocene interval are supplemented by analyses of washed residues of 533 marl samples that formed the base for a high-resolution biostratigraphic frame based on calcareous nannoplankton and planktic foraminifers. For stratigraphic modelling, the forward stratigraphic simulation program PHIL (see below) has been used on a Macintosh computer.

INPUT DATA

In the following paragraphs the geographical and geological data serving as input and control parameters for the stratigraphic simulation program PHIL are documented. For detailed data, interpretation and discussion refer to Kuss et al. (2000) and Scheibner et al. (2000, 2001, in press).

Location of sections

The locations of all sections that are considered as relevant for obtaining the input parameters were measured by GPS (global positioning system). The exact positions of the locations were projected on a line that runs perpendicular to the strike of the carbonate platform. The zero point (A) of the profile line A-B is assumed in Wadi Araba, the former central part of the NGWA High (Fig. 1). The assumed position of the starting point defines in turn the relative positions of the individual sections, located at the following distances from the zero point: section St. Anthony 1/16 km; section St. Paul 9/32 km; section Bir Dakhl 2/42 km; section Bir Dakhl 3/48 km; section Wadi Tarfa 2/62 km; section Wadi Tarfa 1/82 km (Fig. 1).

Biostratigraphy

For the Campanian and Maastrichtian, we follow the biostratigraphic scheme of Caron (1985) for planktic foraminifers, of Perch-Nielsen (1985) and Norris et al. (1998) for calcareous nannoplankton (CC-zones) and Caus et al. (1996) for *Orbitoides* (Fig. 2). The biostratigraphic schemes of Berggren et al. (1995) for planktic foraminifers (P-zones), of Martini (1971) and Aubry (1995) for calcareous nannoplankton (NP-zones) and of Serra-Kiel et al. (1998) for shallow benthic foraminifers (SB-zones) are used for the Paleocene and early Eocene (Fig. 2). The calibration of planktic foraminifers and calcareous nannoplankton and the absolute numeric age of biochronal and stage boundaries is from Norris et al. (1998) for the Cretaceous and from Berggren et al. (1995) for the Paleogene. More

information about the biostratigraphy of the area and the sections used in this manuscript can be found in Kuss et al. (2000), Scheibner et al. (2000, 2001, in press) and Marzouk and Scheibner (subm.).

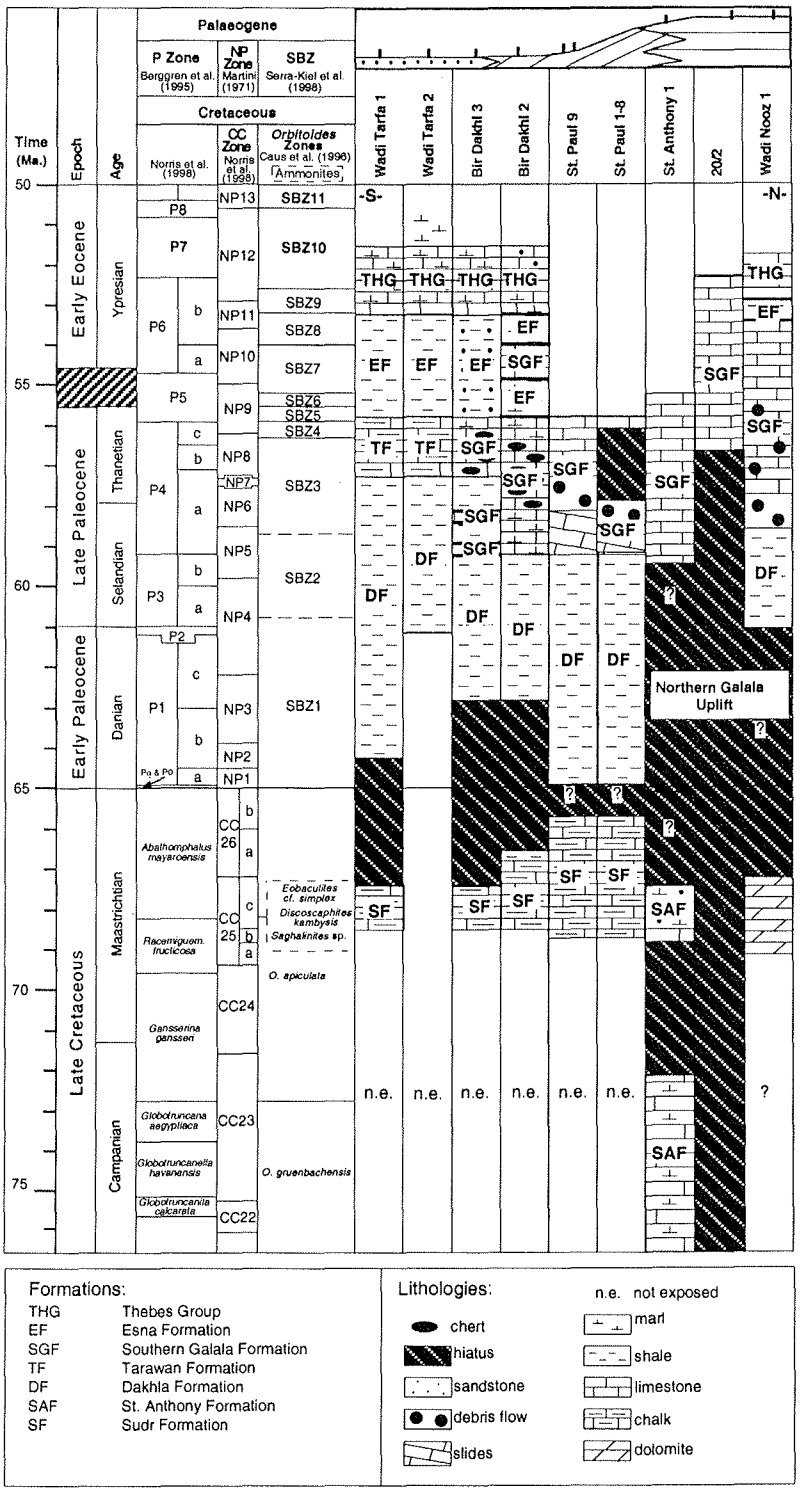

Fig.2: Bio- and lithostratigraphic correlation of 9 measured sections arranged along a transect across the Northern Galala/Wadi Araba High. The broad grey band (left column) reflects the current opinion on the position of the Paleocene-Eocene boundary. The biozonations of planktonic foraminifers (P zones), calcareous nannoplankton (NP zones for Paleogene and CC zones for Maastrichtian) and shallow benthic foraminifers (SBZ) are listed. Black areas indicate hiatuses, due to erosion or non-deposition. Question marks indicate uncertain stratigraphic ranges. On top is a 2-D transect of the platform-to-basin architecture, where the individual sections are indicated.

Lithostratigraphy, depositional setting and lateral transitions

The Campanian-Eocene sediments of the Galala area can be subdivided into three different environmental regimes of deposition or non-deposition/erosion (Fig. 2; Scheibner et al., 2001). The first regime is characterised by uplift and erosion or non-deposition resulting mostly from the uplift of the Northern Galala/Wadi Araba High (NGWA High) structure, a branch of the Syrian Arc foldbelt. The shallow-water carbonate platform and slope deposits of the late Campanian-Maastrichtian St. Anthony Formation and the Paleocene-lower Eocene Southern Galala Formation represent the second regime and are found north and south of the NGWA High. The third regime is represented by basinal chalks, marls and shales of the Campanian-Maastrichtian Sudr Formation and of the Paleocene-Eocene Dakhla, Tarawan, Esna Formations and the Thebes Group (Fig. 2). The distribution and lateral interfingering of the above mentioned environmental regimes reflect different tectonic movements, changing basin morphology, sea-level changes and progradation of shallow-water sediments (Scheibner et al., 2001).

Shallow-water carbonates and siliciclastics of the St. Anthony Formation were deposited during the late Campanian to late Maastrichtian and are exposed only in an east-west trending belt at the northern rim of the Southern Galala. Simultaneously basinal sediments sediments of the Sudr and Dakhla Formations accumulated 14 km to the south at St. Paul (Fig. 3). The interfingering between the St. Anthony Formation and the basinal Sudr and Dakhla Formations is not exposed.

Similar to the St. Anthony Formation, the sediments of the Paleogene Southern Galala Formation were deposited in an east-west trending area in the Galalas and parts of Sinai. But its areal outcrop extension is far larger than that of the St. Anthony Formation (Fig. 1).

Interfingering between deeper water deposits of the Dakhla and Esna Formations and shallow-water limestones of the Southern Galala Formation (including lateral variations within the Dakhla and Esna Formations) are best exposed at sections Bir Dakhl 2 and Bir Dakhl 3 (Figs. 3). In both sections the base of the Southern Galala Formation is situatated in mid NP5 biozone.

Sections St. Paul 1-8 and St. Paul 9 illustrate a good example of a ramp to basin transition (Scheibner et al., 2000). Three phases of ramp progradation were observed in the Paleocene that are indicated by mass transport deposits of glides, slumps and debris flows. Microfacies analysis provided evidence of a change in the origin of the debris-flow deposits. This change reflect a transition from a basinal-to-outer-ramp setting to a middle-to-inner-ramp setting, including a change in the distribution of biota.

Slope architecture

Scheibner et al. (in press) calculated the slope geometries of the late Maastrichtian (CC25) carbonate platform margin of the Galala Mountains. Because of initial structural topography and sedimentary patterns the model of an asymmetrical platform is favoured. This asymmetrical platform margin is formed like a rimmed platform in south-easterly direction and like a ramp in south-westerly direction. The rimmed platform is subdivided into a gentle upper slope and a steep lower slope. with slope angles of the rimmed part of 5° to 8°, whereas the ramp part would have an

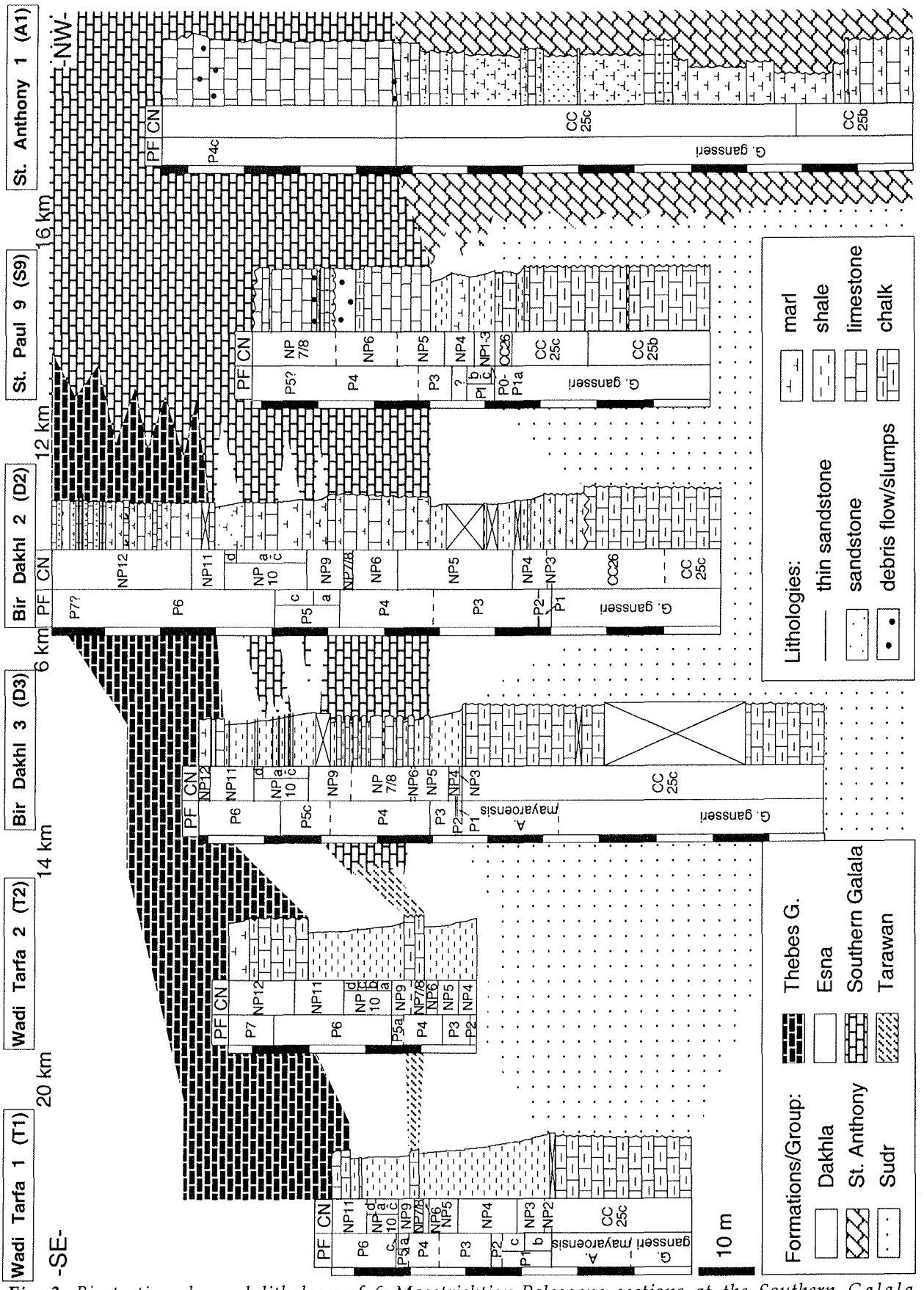

Fig. 3: Biostratigraphy and lithology of 6 Maastrichtian-Paleogene sections at the Southern Galala to illustrate the field-based depositional architectures. Best visible is the progradation of the shallow-water sediments of the Southern Galala Formation in the Paleocene-Eocene. Left to the sections the biozones of planktic foraminifers (PF) and calcareous nannoplankton (CN) are plotted.

angle of less than 0.1°. The relatively steep slope explains the narrow depositional belt of Campanian to Maastrichtian carbonate platform-slope sediments. For the Paleocene no such detailed calculations exist but from investigations of the depositional settings a more gentle inclined slope is assumed (Kulbrok, 1996; Kuss et al. 2000) which fits well with a much broader depositional belt of the Paleogene slope deposits.

Paleobathymetry

The chalky and marly hemipelagic sediments deposited in the area of St Paul's monastery and further southwards yield rich and diverse foraminiferal assemblages. These are dominated by planktic foraminifera and indicate open marine conditions and good connections to the Tethys ocean. Analysis of benthic foraminiferal assemblages is a powerful and widely-used tool to estimate depositional depths (e.g. Culver, 1993). In the study area, we observed Maastrichtian and Paleocene assemblages which have previously been described from Israel, Sinai, and northern Tunisia (Reiss, 1952; Said and Kenawy, 1956; Speijer, 1995; Speijer and van der Zwaan, 1996; Widmark and Speijer, 1997b). Maastrichtian and Paleocene assemblages have a significant component of typical neritic taxa in common. This component is characterized by various species of *Anomalinoides*, *Bulimina*, *Lenticulina*, and *Cibicidoides*, taxa that are generally more abundant in neritic deposits of central Egypt (e.g. LeRoy, 1953; Luger, 1985; Speijer and van der Zwaan, 1996; Speijer and Schmitz, 1998; Schnack, 2000). Another large component constituting Maastrichtian and Paleocene benthic foraminiferal assemblages is composed of various bathyal and deep-sea species. Typical Maastrichtian representatives of this are *Eouvigerina subsculptura*, *Sliteria varsoviensis*, *Bolivinoides draco* and *Sitella* spp. (Widmark and Speijer, 1997a; Widmark, 2000; Alegret and Thomas, in press), which all became extinct at the K/P boundary (Speijer and van der Zwaan, 1996). In the Paleocene these taxa with deep water affinity were replaced by other typical deep-sea taxa, known as Velasco type taxa, like *Gavelinella beccariiformis*, the most abundant one, and *Gyroidinoides globosus*, *Pullenia coryelli*, *Cibicidoides hyphalus*, *Bulimina trinitatensis*, and *Nuttallides truempyi* (e.g. Van Morkhoven et al., 1986 and references therein). The combination of typical deep-sea taxa co-occurring with shelf taxa and the similarity with foraminiferal faunas from Sinai, Israel and northern Tunisia, indicates deposition at depths of ~400 m during the Maastrichtian, deepening to ~500 m during the early Paleocene. We could observe no significant down-slope differences in the benthic assemblages between St. Paul's and Wadi Tarfa, the reason for this being that the bathymetric extent of the biofacial units at these depths is supposed to have been much larger than those in neritic environments.

Sedimentation rates

The late Cretaceous - Paleogene sedimentation rates of the Galala mountains and the adjacent areas show a high variability within the different depositional settings and the different time slices and are therefore presented in detail. Furthermore, late Cretaceous - Paleogene sedimentation rates of

the area have not been published before. The sedimentation rates are calculated for 5 CC-zones (Campanian-Maastrichtian) and 11 NP-zones (Paleogene) for two basinal sections, two basinal-distal slope sections and two proximal slope-platform sections (Fig. 4).

To calculate the duration of the individual biozones we used the timescale of Norris et al. (1998). Sedimentation rates are considered true sedimentation rates, if both the bottom and the top of a stratigraphic interval are marked by a biostratigraphic datum. In contrast, minimum sedimentation rates refer to stratigraphic intervals with only one or no biostratigraphic datum. All sedimentation rates are calculated for compacted sediments and are illustrated for: i) three different depositional settings, each represented by two sections (Fig. 4a), ii) individual biozones of each section (Fig. 4b) and iii) time versus thickness (Figs. 5a-5f). Sedimentation rates are given in Bubnoffs (1 Bubnoff = 1 mm/ky).

Cretaceous:

The late Campanian-Maastrichtian sedimentation rates show the greatest variability with values ranging from 2.1 B up to 432 B (Fig. 4). In contrast to the better biostratigraphic resolution during the Paleogene, the less well constrained late Cretaceous biostratigraphic resolution allows calculations of sedimentation rates only for a few biozones. Highest values are obtained in subzone CC25b both for the basinal settings (87 B in section St. Paul 9, Fig. 5b) and for the proximal slope settings (432 B in section St. Anthony 1, Fig. 5a). According to Norris et al. (1998) subzone CC25b (biostratigraphic interval between the FO of *L. quadratus* and the FO of *M. murus*) has a duration of 225.000 years. Either the high sedimentation rates in subzone CC25b are considered realistic or the FOs of either *L. quadratus* or *M. murus* (or both) are diachronous and therefore cannot be used for the absolute timescale. Diachroneity has been suggested by Norris et al. (1998) for *M. murus*, *N. frequens* and *M. prinsii*, but even diachroneity may not explain the extremely high values of sedimentation rates in section St. Anthony 1. Enos (1991) compiled sedimentation rates of terrigenous shelf deposits of the North American shelf ranging from 0-400 B and of hemipelagic deposits ranging of up to 500 B, which are in good concordance with the high sedimentation rates in subzone CC25b.

Paleogene:

The sedimentation rates of the Paleogene range from 0.3 B up to 16.1 B (Fig. 4). In contrast to the higher late Cretaceous sedimentation rates, those of the early Paleocene reach only values of 4.3 B. With the onset of prograding debris-flows and calciturbidites within biozone NP5 the sedimentation rates of the slope (St. Paul 9, Fig. 5b) and of the mass flow influenced basinal sections (Bir Dakhl 2+3, Figs. 5c, 5d) show slightly higher values in comparison to the basinal sections (Wadi Tarfa 1+2, Figs. 5e, 5f). From the Eocene onwards the sedimentation rates in the basinal sections begin to rise as well.

The differences between Maastrichtian and Paleogene sedimentation rates may be partly explained by local factors. However, we cannot exclude an overall world-wide trend during that interval. Hay et al. (1981) reported very high average sedimentation rates for the world ocean (estimated from the data of the Deep Sea Drilling Project) during Maastrichtian times, whereas during Paleocene times they dropped to one of the lowest levels in the Phanerozoic.

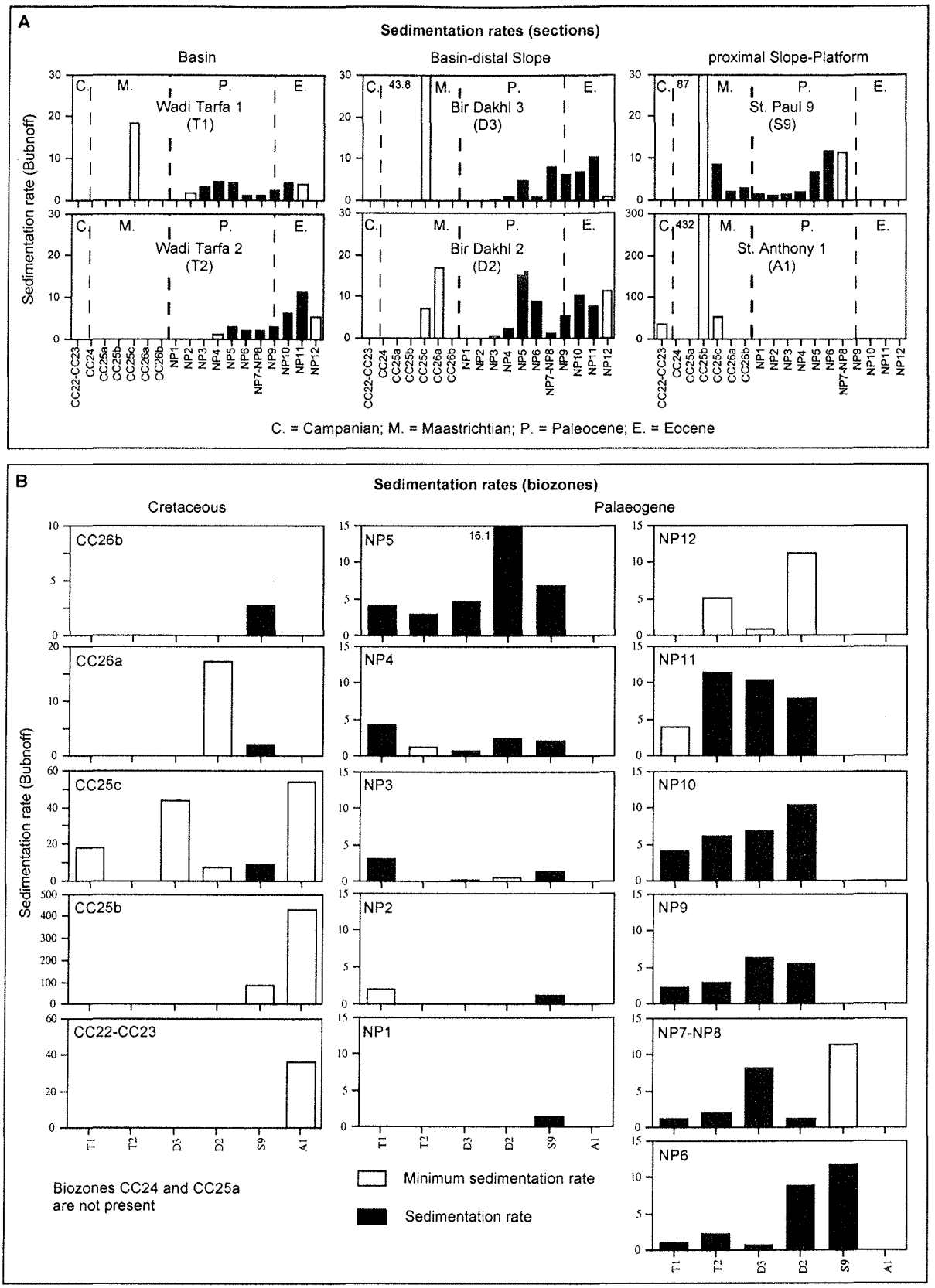

Fig. 4: Sedimentation rates of 6 sections. The missing of values in all biozones is either due to non-exposition or hiatuses.
a) Sedimentation rates plotted against the individual biozones. Note the different scale in section St. Anthony 1.
b) Sedimentation rates of the individual biozones, plotted against different sections. Note the varying scales for the Cretaceous sedimentation rate plots.

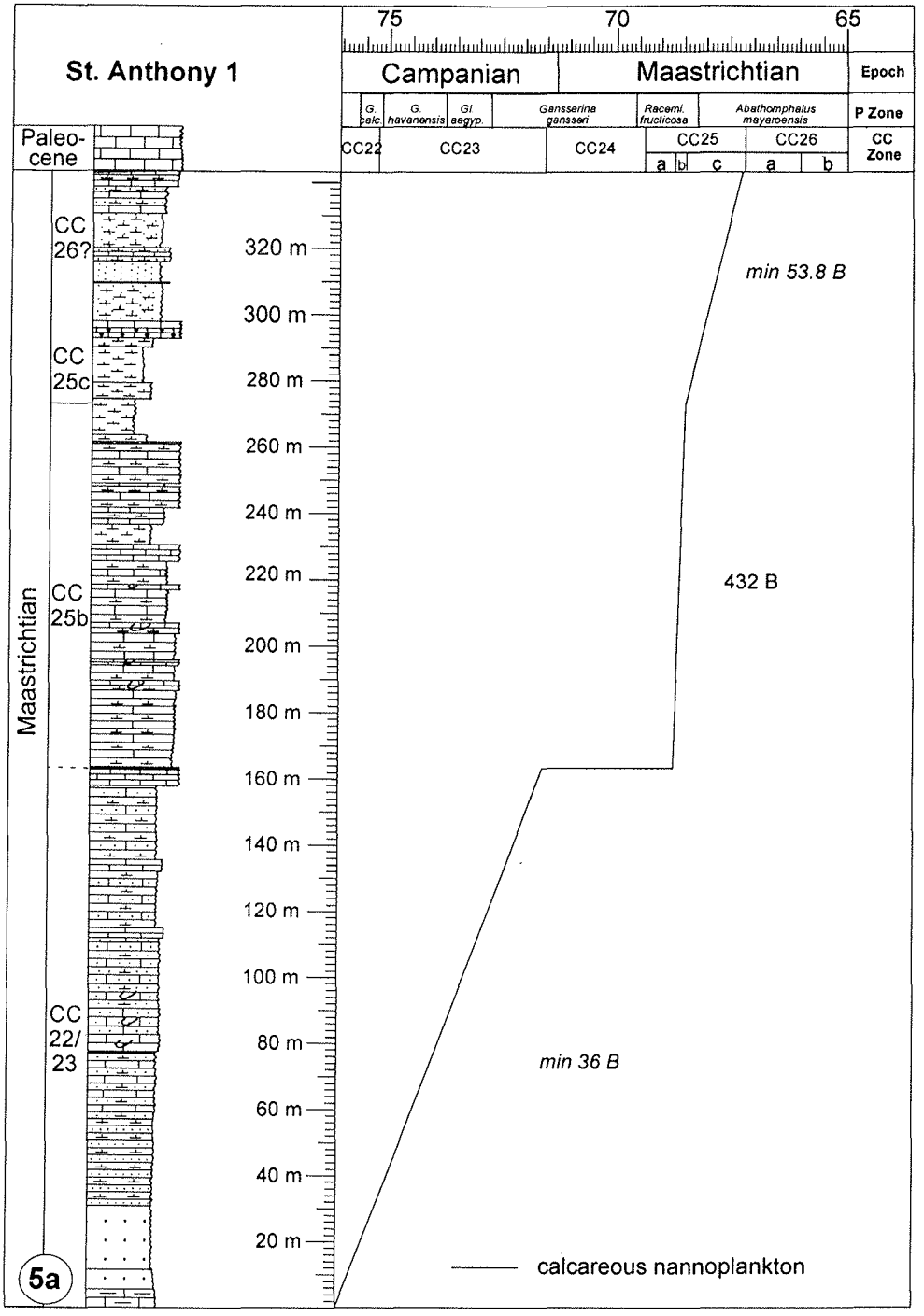

Fig. 5: Sedimentation rate plots calculated from the Late Cretaceous-Paleogene successions of 6 sections from the western side of the Gulf of Suez (Eastern Desert) with no correction for compaction. Note the differences in the individual plots, regarding either planktic foraminifera or calcareous nannoplankton (all values left of the curves are for planktic foraminifera, all values right of the curves are for calcareous nannoplankton; at the bottom and at the top the values for sedimentation rates are minimum sedimentation rates).

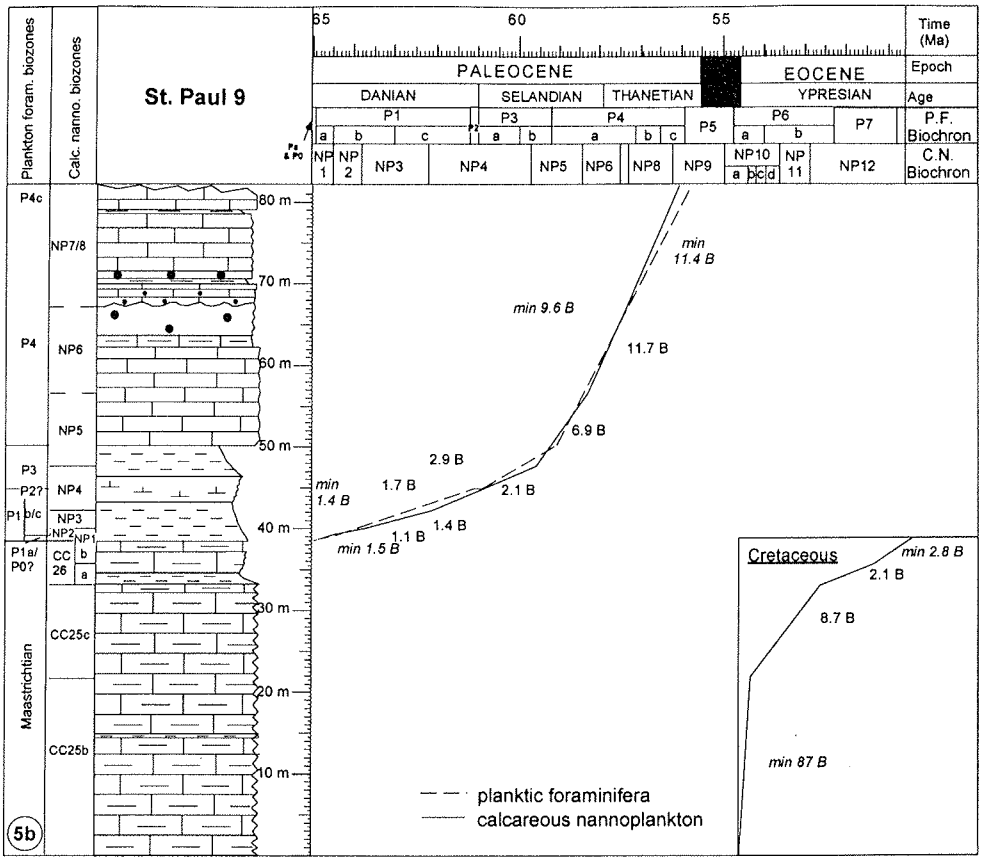
St. Paul 9
Plankton foram. biozones
Calc. nanno. biozones
65
60
55
Time (Ma)
PALEOCENE
EOCENE
Epoch
DANIAN
SELANDIAN
THANETIAN
YPRESIAN
Age
P.F. Biochron
C.N. Biochron
80 m
70 m
60 m
50 m
40 m
30 m
20 m
10 m
Maastrichtian
min 11.4 B
min 9.6 B
11.7 B
6.9 B
2.9 B
2.1 B
1.7 B
min 1.4 B
1.4 B
1.1 B
min 1.5 B
Cretaceous
min 2.8 B
2.1 B
8.7 B
min 87 B
planktic foraminifera
calcareous nannoplankton
5b

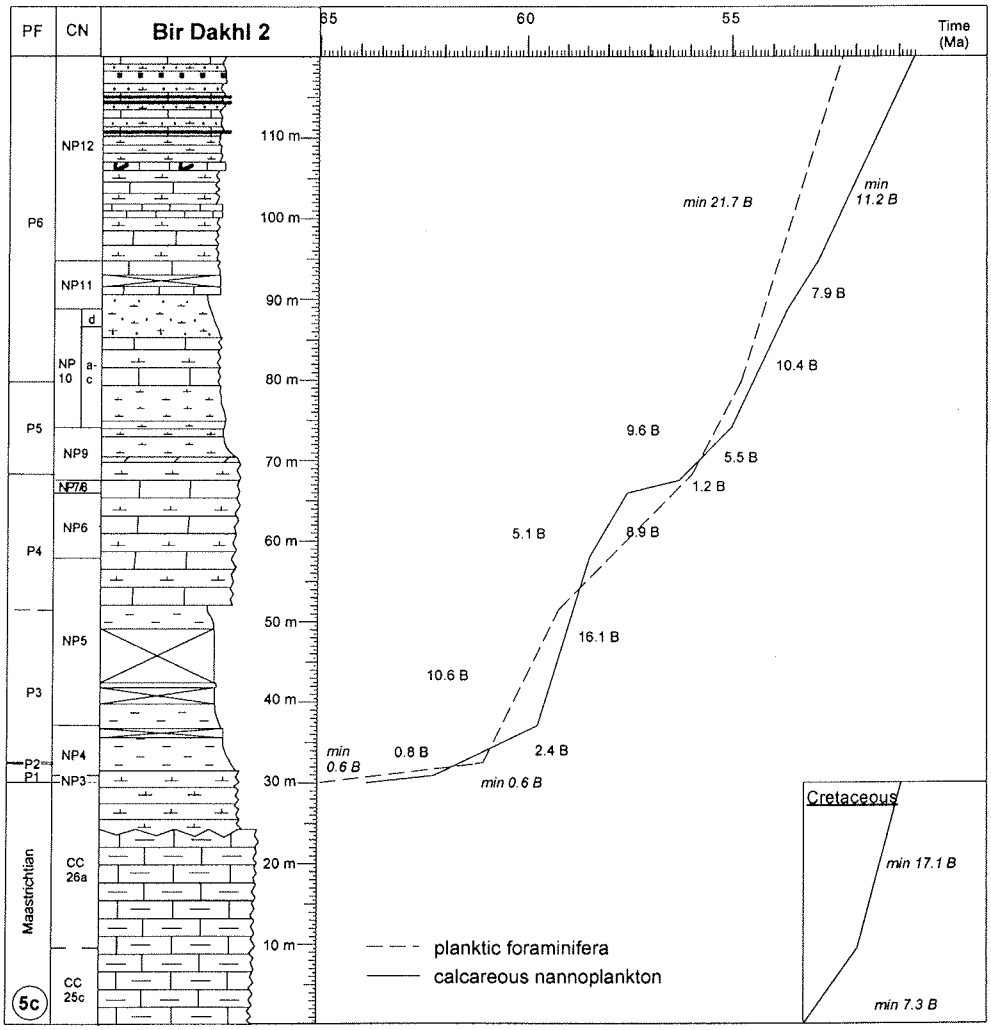
Bir Dakhl 2
PF
CN
65
60
55
Time (Ma)
110 m
100 m
90 m
80 m
70 m
60 m
50 m
40 m
30 m
20 m
10 m
Maastrichtian
min 21.7 B
min 11.2 B
7.9 B
10.4 B
9.6 B
5.5 B
1.2 B
5.1 B
8.9 B
16.1 B
10.6 B
min 0.6 B
0.8 B
2.4 B
min 0.6 B
Cretaceous
min 17.1 B
min 7.3 B
planktic foraminifera
calcareous nannoplankton
5c

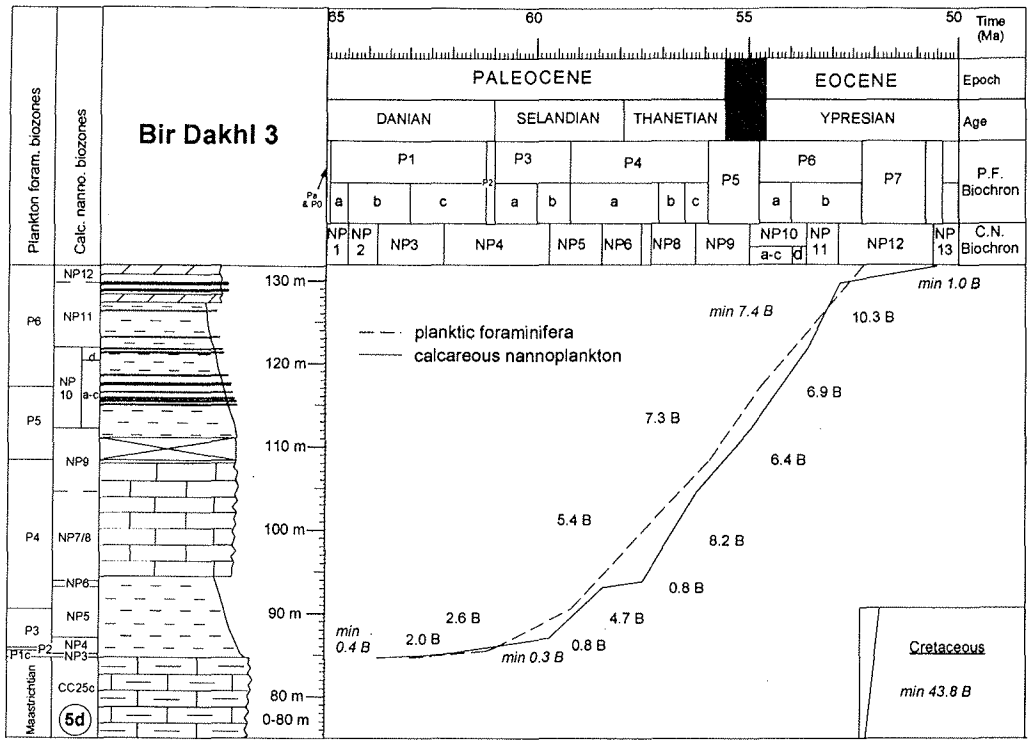
Bir Dakhl 3
Plankton foram. biozones
Calc. nanno. biozones
65
60
55
50
Time (Ma)
PALEOCENE
EOCENE
Epoch
DANIAN
SELANDIAN
THANETIAN
YPRESIAN
Age
P.F. Biochron
C.N. Biochron
130 m
120 m
110 m
100 m
90 m
80 m
0-80 m
planktic foraminifera
calcareous nannoplankton
min 1.0 B
min 7.4 B
10.3 B
6.9 B
7.3 B
6.4 B
5.4 B
8.2 B
0.8 B
2.6 B
4.7 B
min 0.4 B
2.0 B
min 0.3 B
0.8 B
Cretaceous
min 43.8 B
5d

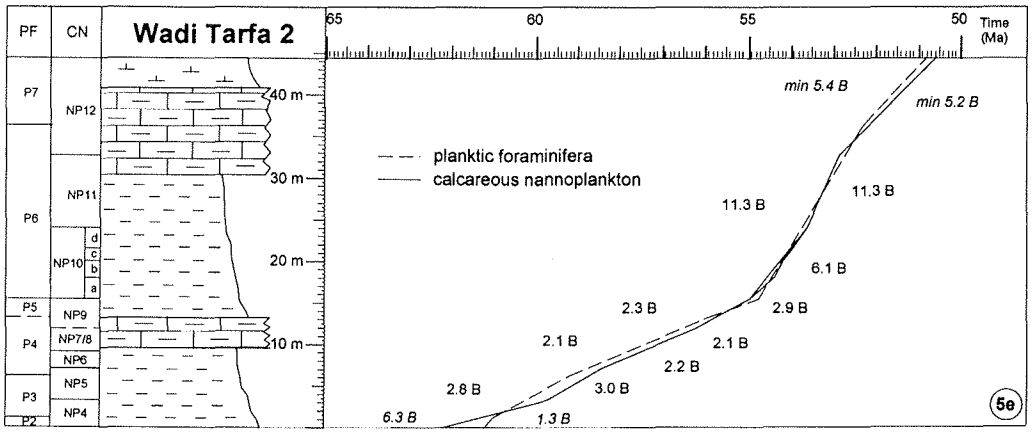
Wadi Tarfa 2
PF
CN
65
60
55
50
Time (Ma)
40 m
30 m
20 m
10 m
planktic foraminifera
calcareous nannoplankton
min 5.4 B
min 5.2 B
11.3 B
11.3 B
6.1 B
2.3 B
2.9 B
2.1 B
2.1 B
2.2 B
2.8 B
3.0 B
6.3 B
1.3 B
5e

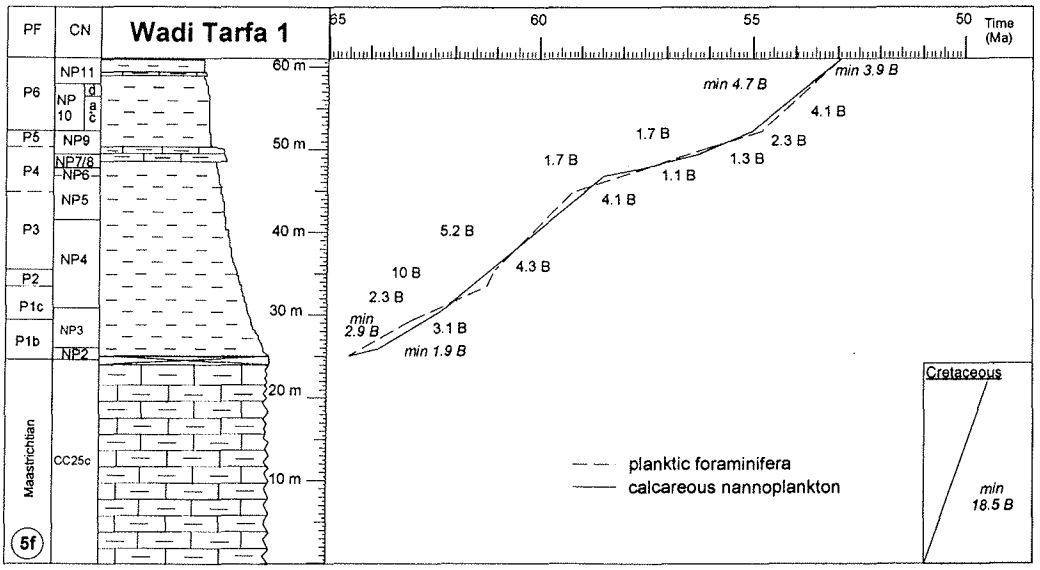
Wadi Tarfa 1
PF
CN
65
60
55
50
Time (Ma)
60 m
50 m
40 m
30 m
20 m
10 m
min 4.7 B
min 3.9 B
4.1 B
1.7 B
2.3 B
1.7 B
1.3 B
1.1 B
4.1 B
5.2 B
10 B
4.3 B
2.3 B
min 2.9 B
3.1 B
min 1.9 B
Cretaceous
min 18.5 B
planktic foraminifera
calcareous nannoplankton
5f

Sea-level changes

Maastrichtian:

A lowering of the upper Maastrichtian sea-level (biozone CC25c) is proposed by Kuss et al. (2000) and Scheibner et al. (in press). For modelling purposes we used the sea-level curve of Hardenbol et al. (1998) for the Maastrichtian.

Paleogene:

Scheibner et al. (2000) documented in a detailed study the interrelationship of two late Paleocene mass-flow units with sea-level drops that coincide with those from Sinai (Lüning et al., 1998), from Gebel Aweina (ca. 300 km to the south, Speijer and Schmitz, 1998) and with those from Hardenbol et al. (1998). For modelling purposes we combined the Paleocene sea-level curves of Lüning et al. (1998) and Hardenbol et al. (1998).

STRATIGRAPHIC MODELLING

General concepts

Computer simulation models have been developed since the late 1940´s (Watney et al., 1999) for all kinds of depositional settings. For general discussions and examples of stratigraphic modelling refer to the articles in Franseen et al. (1991) and Harbaugh et al. (1999). The main reasons for using stratigraphic computer programs to analyse sedimentary successions are: first, the evaluation of depositional processes and their controlling parameters and, second, the prediction of lithostratigraphic properties away from points of control (Perlmutter et al. 1999). The programs may help to describe depositional records that have been eroded or that are covered by younger sediments.

Modelling may be either forward or inverse. Forward models simulate sedimentary processes by using a preliminary set of input parameters. After each computer run the output is compared with the geological data set and subsequently the input parameters are modified to adjust the computer output to the real world. Inverse models, in comparison, use the structure of a forward model to simulate a specific result (Miall, 1997).

Numerous types of data are used as input parameters for computer models. Most of these parameters can be lumped into one of the following four categories, a) accommodation, including changes in sea level and tectonics, b) sediment supply, c) sediment redeposition and d) initial depositional profile (Watney et al., 1999). Enos (1991) presented a review of the most important input parameters.

In the study presented here we use PHIL (Process- and History- Integrated Layers) as the modelling program (Marco Polo Software Inc. 1995). According to Bowman and Vail (1999) this program is one of the most complete models to date. In recent years, PHIL has been used to model various settings in different times. For example, Read (1998) modelled ramp development and architecture during greenhouse, transitional and icehouse intervals whereas Leyrer et al. (1999) used the program to model two platform-slope-basin configurations of the Stassfurth Carbonate (Zechstein, late

Permian) in Germany. Finally, Bowman and Vail (1999) documented the history of the Baltimore Canyon Trough, offshore New Jersey from 30 Ma. onwards.

Functionality of PHIL

The following paragraph shortly explains the functionality of PHIL. For detailed description and discussion refer to Bowman and Vail (1999) and Leyrer et al. (1999). The overall modelling approach of PHIL incorporates the principles employed in cellular automata. In this framework, one of the most important assumptions is that each cell is only dependant upon the conditions in the neighbouring cell (Marco Polo Software Inc., 1995). The input parameters of PHIL can be pooled in the following parameter-groups: Spatial and time dimensions editor, basin editor, siliciclastic, carbonate and pelagic sediment editor, evaporites, organic carbon, erosion, slumping and gravity flow editor (Table 1). Within each group several single parameters can be adjusted, maintained in the default mode or can be deactivated. In the spatial and time dimensions editor the number of cells and time-layers used for the stratigraphic model are defined. The number of cells controls the lateral resolution of the model. The chosen time-steps have to be set short enough to resolve the details of the process of interest. The best results are obtained by choosing a time increment of 1/2 or 1/4 of the shortest periodicity involved (Emery and Myers, 1996; Bowman and Vail, 1999). The basin editor allows to change bathymetry, water level, subsidence, compaction, flexural loading and marine currents. In the sediment editors the sedimentation rates and degrees of various depositonal settings can be changed. Additionally, several input parameters can be modelled cyclic-, time- or spatial-dependant. The results of the modelling can be displayed either as depth-distance (depth plot) or time-distance plots (chrono plot/Wheeler diagram) (Figs. 6, 7). Furthermore, PHIL can produce stratigraphic columns for every distance. For the three plot types a variety of coloured graphic displays exist, e.g. depositional systems, chronostratigraphy, lithology, systems tracts and paleobathymetry.

Modelling procedure applied in this study

A Macintosh G3/300 MHz with 320 MB RAM has been used for the modelling. The input parameter refer to geologic data and interpretations from Kuss et al. (2000) and Scheibner et al. (2000, 2001, in press). They form the first set of input data for modelling the evolution of depositional cycles in two separate simulations covering intervals in the upper Maastrichtian and in the Paleocene. The spatial and time dimensions of the two models are specified in the following. For the Maastrichtian the starting point is defined for 68.7 Ma. (onset of CC25b after Norris et al., 1998). This run terminates with the Cretaceous/Paleogene boundary at 65 Ma. The Paleocene run is modelled from 65 Ma to 56 Ma (latest Thanetian). For both models the maximum spatial extension of 100 km coincides with the transect A-B (Fig. 1). The sections of St. Anthony 1, St. Paul 9, Bir Dakhl 2+3 and Wadi Tarfa 2+1 are projected onto this line and are considered reference positions from north to south. The depositional gross architecture of the study area with transitions from a rimmed platform during the upper Cretaceous to a distally steepened ramp during the Paleocene serves as

one basic input parameter to define the bottom topography. Furthermore, an angle of 8° is used as the angle of the depositional front for the Maastrichtian (Scheibner et al., in press) (Table 1). For the Paleocene distally steepened ramp no such calculations exist and an angle of 1.5° is assumed, that is slightly higher than the angle of homoclinal ramps, according to general carbonate ramp models (Burchette and Wright, 1992). Sedimentation rates for the different depositional settings were assumed as constant though time and derived from calculations described before. The sea-level curves of Hardenbol et al. (1998) for the Maastrichtian and Lüning et al (1998) and Hardenbol et al. (1998) for the Paleocene were incorporated into the program. The default mode is used for subsidence values for the first simulation because a subsidence analysis has not been applied to the data. Other parameters were left in the default mode or switched off, like evaporites or organic carbon that are of no interest in this study. After this basic set-up of the program, an appropriate time step is chosen for the first run. The output, graphic displays of various parameters, of this initial run are checked against the geologic data and parameters are adjusted in subsequent runs, until an acceptable match is produced. Several tens of runs are necessary to produce the results presented in this study. Table 1 lists all input parameters that were used for the final simulation runs and indicates their mode (personal, default or switched off).

Editor	Parameters	Maastrichtian	Paleocene	Mode
spatial dimensions	depositional dimension	0-100.000 m	0-100.000 m	personal
	cells	500	500	personal
	cell spacing	200 m	200 m	default
	grid	0-32.000 m	0-32.000 m	personal
time dimensions	beginning	68.7 Ma	65 Ma	personal
	final	65 Ma	56 Ma	personal
	time intervall	100.000 y	250.000 y	personal
	layers	37	37	personal
basin	bathymetry	personal	personal	personal
	water level	*	*	personal
	subsidence	1-5.5 m/My	default	personal /default
	compaction	over compressior	over compressior	default
	flexural loading	default	default	default
	marine currents	default	default	default
siliciclastic sediment	sedimentation rate	default	switched off	default/switched off
	depositional front (°)	8°	switched off	personal/switched off
carbonate sediment	sed. rate shelf margin	200 m/My (B)	70 m/My (B)	personal
	sed. rate shelf	130 m/My (B)	70 m/My (B)	personal
	sed. rate suspension	200 m/My (B)	40 m/My (B)	personal
	fore slope (°)	8°	6°	personal
pelagic	sedimentation rate	15 m/My (B)	3 m/My (B)	personal
erosion	various parameters	default	default	default
slumping	deposition rate	default	default	default
gravity flow	various parameters	default	default	default

Table 1: *The individual parameters for the Maastrichtian and Paleocene simulations with PHIL. In the first row the different editors of PHIL are listed, the second row names the most important parameters used in the two runs, the third and fourth row list the individual parameters of the two runs and in the fifth row the mode of the parameters is indicated. The asterisks in the table (water level) refer to the modified sea-level curves of Hardenbol et al. (1998) for the Maastrichtian and of*

Hardenbol et al. (1998) and Lüning et al. (1998) for the Paleocene. Bathymetry in the basin editor is the parameter for the initial setting of the bottom topography. The sedimentation rates in PHIL are given in m/My which equates 1 Bubnoff (B).

Results of the stratigraphic modelling with PHIL

For both modelled time-slices (late Maastrichtian and Paleocene) the results are displayed in 8 different plots. The graphic output comprises 4 depth and 4 chrono plots (Wheeler diagram) of the absolute age, the paleowater-depth, the lithology, and the depositional setting (Figs. 6, 7). Furthermore, the modified sea-level curves of Hardenbol et al. (1998) for the Maastrichtian, and of Hardenbol et al. (1998) and Lüning et al. (1998) for the Paleocene are given in Fig. 8. In Figs. 6 and 7 only the first 32 km of the totally 100 km long transect are displayed to emphasise the processes on the carbonate platform-slope transition. The basinal areas exhibit no major changes of lithologies (Fig. 6g small inlay). Therefore only the locations of sections St. Anthony 1 at 16 km and St. Paul 9 at 32 km are visualised, whereas the more basinward sections of Bir Dakhl 2+3 and Wadi Tarfa 1+2 are neglected. The overall geometry of the modelled transect A-B can be seen in the inlay of Fig. 6g. Due to the different depth and distance scales a vertical exaggeration of 40 times is generated. The steepest parts of the slope have only angles of 8° during the Maastrichtian and of 6° during the Paleocene.

Maastrichtian:

The stratigraphic simulation of the upper Maastrichtian (from 68.7 Ma to 65 Ma) covers a time interval of 3.7 My. More than 200 m of sediments were deposited on the carbonate platform (eroded today, Fig. 1), contrasting with only about 60 m in the basin (Fig. 6). Between 66 Ma and 67 Ma the model predicts a hiatus on the most proximal parts of the carbonate platform with a duration of about 0.9 My (Fig. 6b). Two smaller hiatuses occur at 68.5 Ma and 65.5 Ma. While the two older hiatuses can be attributed to a lowering of the sea level (Fig. 8), the youngest hiatus around 14 km represents a combination of rising sea-level and oversteepened slope. The slope reached the maximum angle of 8° and consequently no sediments were deposited near the platform-break but were transported into the basin (Fig. 6).

The proximal platform-sediments are mainly composed of silt and clay (Fig. 6c) and the central platform areas are mainly represented by tidal algal laminates, with minor portions of mudstones and quartz-poor marine mud. The distal platform near the transition to the slope mainly contains bioclastic boundstones and bioclastic coarse grainstones with minor percentages of quartz-poor marine mud (Fig. 6c). During some intervals peloidal packstones dominate these environments. The sediments of the upper part of the slope are dominated by bioclastic fine wackestones with portions of mudstones and quartz-poor marine mud. Basinwards the bioclastic fine wackestones diminish and reach the same proportion as the mudstones, whereas the quartz-poor marine mud still occurs with minor percentages. The sediment distribution on the carbonate platform is mainly controlled by

variations of relative sea-level (Fig. 6) and by variations of sedimentation rates within different areas of the carbonate platform (Tab. 1).

On the carbonate platform the paleowater-depth normally does not exceed 10 m. Only at times of a fast rising sea level the distal parts of the platform are covered by nearly 50 m of water (Figs. 6e, 6f).

The depositional setting plots (Fig. 6g, 6h) show that the proximal parts of the platform are mainly covered by siliciclastics of the coastal plain and shoreface. Most carbonate environments belong to the depositonal setting of slumps and suspension. Even where tidal algal laminates and bioclastic boundstones and coarse bioclastic wackestones occur and tidal flats or reef environments should be expected, slumps and suspension deposits are simulated. At 50 km this depositional setting is replaced by calciturbidites (see inlay of Fig. 6g).

Fig. 6 a-h: *Graphical display of the Late Maastrichtian (69 Ma-65 Ma) simulation results for the profile line A-B (Fig. 1). For better resolution only the first 32 km are displayed, an overview of the whole modelled area is shown in the inlay of figure 6g. The horizontal scales of each depth and chrono plot indicate the distance (from 0-32 km), while the vertical scales refer to the depth (depth plots) or to the time (chrono plots). The vertical exaggeration of the depth plots is 40 fold. The legends for the chrono plots are the same as for the depth plots.*

6 a, b) Depth plot and time plot (Wheeler diagramm) of the absolute age. The colours from red to blue indicate successively younger ages. In the depth plot the overall thickness of the individual time slices are visible. The black colours in the time plot show the distribution of hiatuses. The large hiatus between 67 Ma and 66 Ma in the proximal areas of the platform (0 m-12.000 m) is due to a lowering in sea level (Fig. 8) whereas the small hiatus around 65.8 Ma is caused by an oversteepened slope and sedimentary bypass.

6 c, d) Depth plot and time plot of the lithology. The colours indicate different lithologies that are explained in the depth plot (Fig. 6c). On the proximal platform silt, clay, medium to fine sand and tidal algal laminates have been deposited. The shelf break is characterised by bioclastic boundstones whereas the slope is dominated by bioclastic fine wackestones and marine mud.

6 e, f) Depth plot and time plot of the paleowater-depth. From red to blue the colours indicate a deepening in paleowater-depth. During the first 2 - 3 Ma the platform architecture is characterized by aggradation. Around 66 Ma a tongue of shallow-water deposits is prograding to a position close to 15.000 m that is followed by rapid retrogradation which in turn is followed by another progradation. The combination of a changing sea-level, sediment supply and subsidence is responsible for the change in the depositional modus.

6 g, h) Depth plot and time plot of the depositional setting. The colours indicate different depositional settings that are explained in the depth plot (Fig. 6g). Except of the proximal platform the depositional setting is characterized by slumps and suspension.

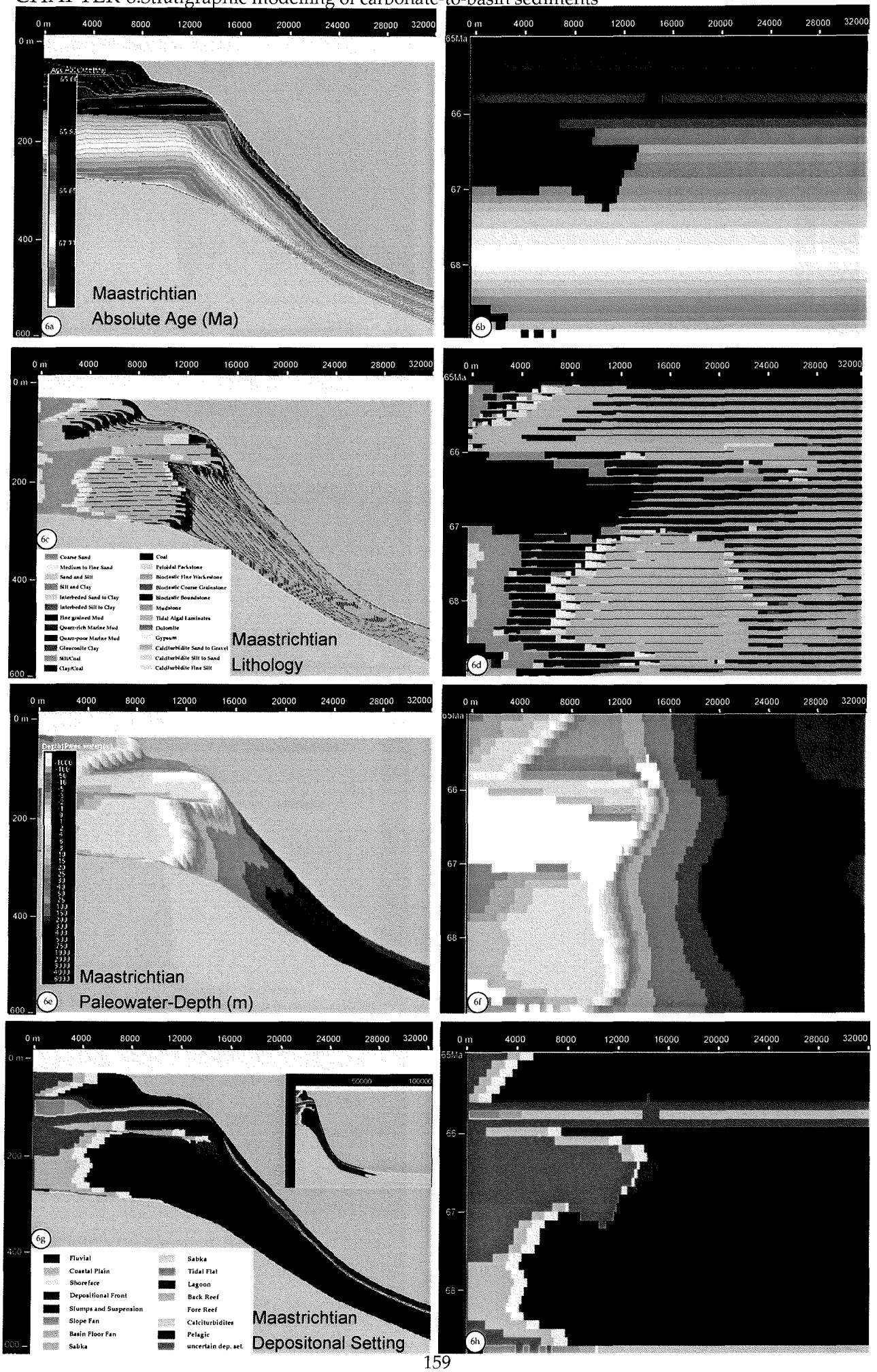
0 m
4000
8000
12000
16000
20000
24000
28000
32000
200
400
600
65Ma
66
67
68
Maastrichtian
Absolute Age (Ma)
6a
6b
Maastrichtian
Lithology
6c
6d
Coarse Sand
Medium to Fine Sand
Sand and Silt
Silt and Clay
Interbedded Sand to Clay
Interbedded Silt to Clay
Fine grained Mud
Quarz-rich Marine Mud
Quarz-poor Marine Mud
Glauconite Clay
Silt/Coal
Clay/Coal
Coal
Peloidal Packstone
Bioclastic Fine Wackestone
Bioclastic Coarse Grainstone
Bioclastic Boundstone
Mudstone
Tidal Algal Laminates
Dolomite
Gypsum
Calciturbidite Sand to Gravel
Calciturbidite Silt to Sand
Calciturbidite Fine Silt
Maastrichtian
Paleowater-Depth (m)
6e
6f
Maastrichtian
Depositonal Setting
6g
6h
Fluvial
Coastal Plain
Shoreface
Depositional Front
Slumps and Suspension
Slope Fan
Basin Floor Fan
Sabka
Sabka
Tidal Flat
Lagoon
Back Reef
Fore Reef
Calciturbidites
Pelagic
uncertain dep. set.

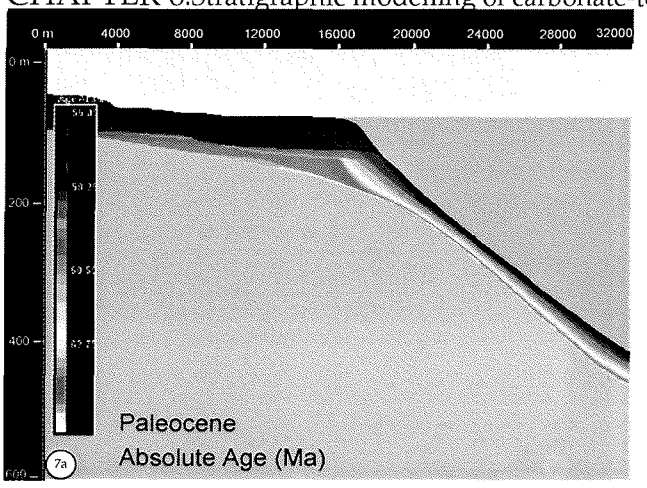
0 m
4000
8000
12000
16000
20000
24000
28000
32000
0 m
200
400
600
Paleocene
Absolute Age (Ma)
7a

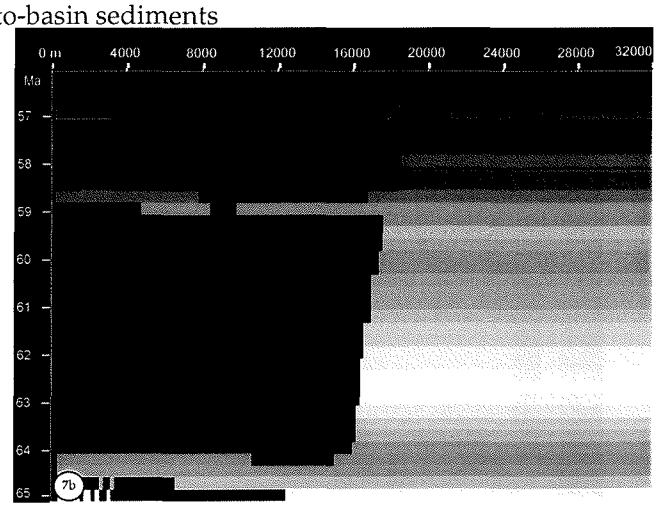
0 m
4000
8000
12000
16000
20000
24000
28000
32000
Ma
57
58
59
60
61
62
63
64
65
7b

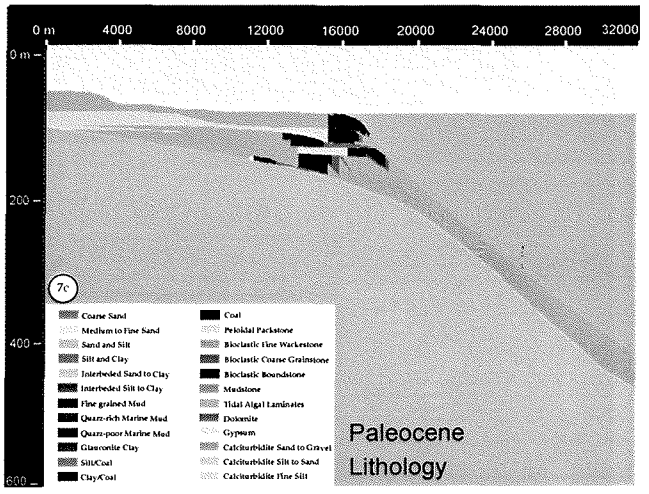
0 m
4000
8000
12000
16000
20000
24000
28000
32000
0 m
200
400
600
7c
Coarse Sand
Medium to Fine Sand
Sand and Silt
Silt and Clay
Interbeded Sand to Clay
Interbeded Silt to Clay
Fine grained Mud
Quarz-rich Marine Mud
Quarz-poor Marine Mud
Glauconite Clay
Silt/Coal
Clay/Coal
Coal
Peloidal Packstone
Bioclastic Fine Wackestone
Bioclastic Coarse Grainstone
Bioclastic Boundstone
Mudstone
Tidal Algal Laminates
Dolomite
Gypsum
Calciturbidite Sand to Gravel
Calciturbidite Silt to Sand
Calciturbidite Fine Silt
Paleocene
Lithology

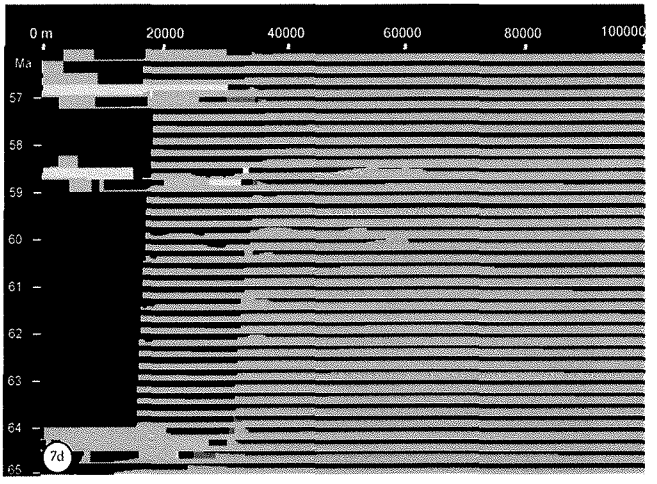
0 m
20000
40000
60000
80000
100000
Ma
57
58
59
60
61
62
63
64
65
7d

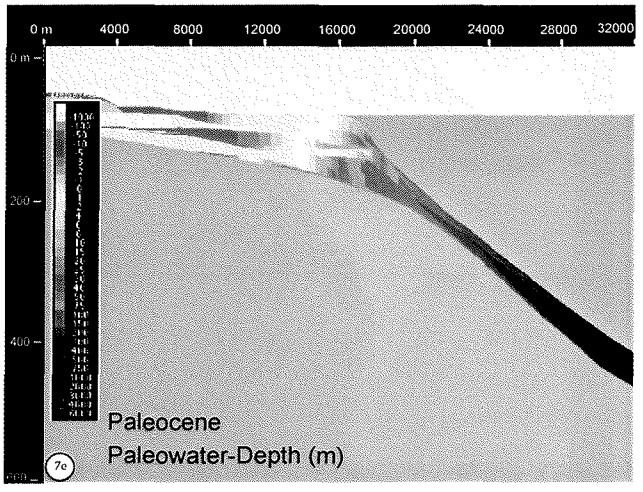
0 m
4000
8000
12000
16000
20000
24000
28000
32000
0 m
200
400
600
Paleocene
Paleowater-Depth (m)
7e

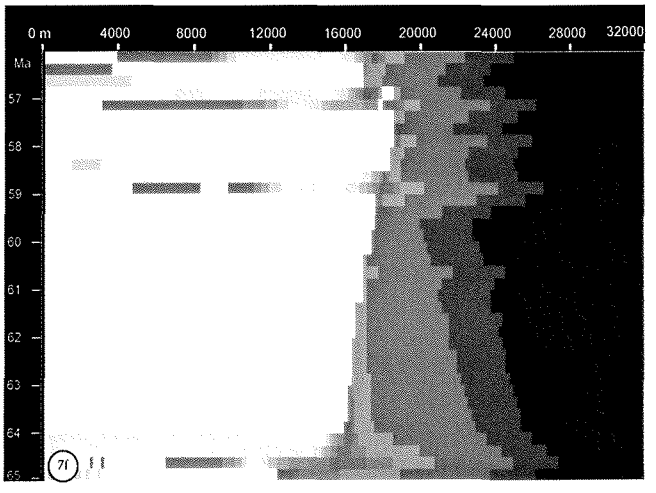
0 m
4000
8000
12000
16000
20000
24000
28000
32000
Ma
57
58
59
60
61
62
63
64
65
7f

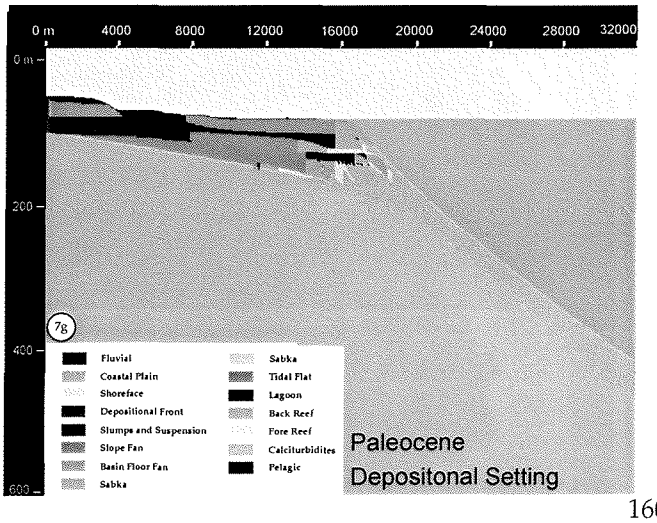
0 m
4000
8000
12000
16000
20000
24000
28000
32000
0 m
200
400
600
7g
Fluvial
Coastal Plain
Shoreface
Depositional Front
Slumps and Suspension
Slope Fan
Basin Floor Fan
Sabka
Sabka
Tidal Flat
Lagoon
Back Reef
Fore Reef
Calciturbidites
Pelagic
Paleocene
Depositonal Setting

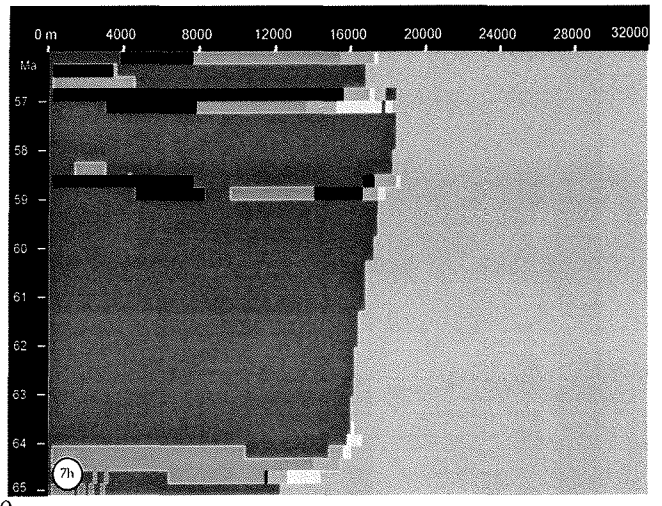
0 m
4000
8000
12000
16000
20000
24000
28000
32000
Ma
57
58
59
60
61
62
63
64
65
7h

Fig. 7 a-h: Graphical display of the Paleocene (65 Ma-56 Ma) simulation results. For better resolution only the first 32 km are displayed. The horizontal scales of each depth and chrono plot indicate the distance (from 0-32 km), while the vertical scales refer to the depth (depth plots) or to the time (chrono plots). The vertical exaggeration of the depth plots is 40 fold. The legends for the chrono plots are the same as for the depth plots.
7a, b) Depth plot and time plot of the absolute age. The colours from red to blue indicate successively younger ages. The black colours in the time plot show the distribution of hiatuses. Deposition on the platform occurs only during three distinctive time slices.
7c, d) Depth plot and time plot of the lithology. The time plot (7d) covers the whole profile line A-B from 0 to 100 km (Fig. 1). The colours indicate different lithologies that are explained in the depth plot (Fig. 7c). On the proximal platform peloidal packstone and tidal algal laminates have been deposited. Siliciclastic deposits do not occure because the siliciclastic sediment editor is switched off. The shelf break is characterised by bioclastic boundstones whereas the slope is dominated by bioclastic fine wackestones and marine mud.
7e, f) Depth plot and time plot of the paleowater-depth. From red to blue the colours indicate a deepening in paleowater-depth. The sediments are characterised by a change in progradation and retrogradation. The combination of a strong changing sea-level, sediment supply and subsidence is responsible for the change in the depositional modus and in the preservation of sediments on the platform and on the slope.
7g, h) Depth plot and time plot of the depositional setting. The colours indicate different depositional settings that are explained in the depth plot (Fig. 7g). The Paleocene platform is characterized by tidal flats and lagoons, whereas at the shelf break reefs accumulated. The slope is characterized by calciturbidites.

Paleocene:

The stratigraphic simulation of the Paleocene started at 65 Ma at the K/P boundary and finished at 56 Ma. During this time interval of 9 My less than 100 m of sediments were deposited on the carbonate platform, whereas in the basin thicknesses of only about 40 m occur (Fig. 7). Reasons for the reduced thicknesses (compared to the Maastrichtian) are: first, the low sedimentation rates that effect thicknesses in both settings, and second, long-lasting stratigraphic gaps that occur on most parts of the platform (Fig. 7b). Deposition on the carbonate platform is evidenced only for three short time-intervals around 65 Ma, 59 Ma and 57 Ma (Figs. 7a, 7b). The long lasting hiatuses in between are due to the oscillating relative sea level and an abrupt fall in sea level at around 59 Ma. This sea-level fall is accompanied with severe erosion on the subaerially exposed platform while sedimentation continues in the slope and basinal areas.

Field observations indicate prevailing carbonate sedimentation on the Paleocene platform with very little siliciclastic input: the modelling program was therefore run with the siliciclastic editor switched off. The carbonate platform is dominated by tidal algal laminates and peloidal packstones (Fig. 7c). At the transition to the slope bioclastic boundstones and bioclastic coarse grainstones dominate. The deeper slope and basinal settings are composed of bioclastic fine wackestones and mudstones. Sedimentation is mainly controlled by the changing relative sea-level (Fig. 8) and the sedimentation rates of the carbonate platform (Table 1).

The paleowater-depth on the Paleocene carbonate platform does not exceed 10 m, similar to the paleowater-depth on the Cretaceous platform. Due to the prominent fall of sea level at 59 Ma a tongue of shallow-water deposits reaches into the basin (Figs. 7 e, f).

The depositional plots (Figs. 7 g, h) of the pure carbonate lithologies show a variety of carbonate depositional settings. On the platform tidal flats and lagoons dominate while at the platform-slope transition back reefs and fore reefs are located. The slope and the basin are covered by calciturbidites.

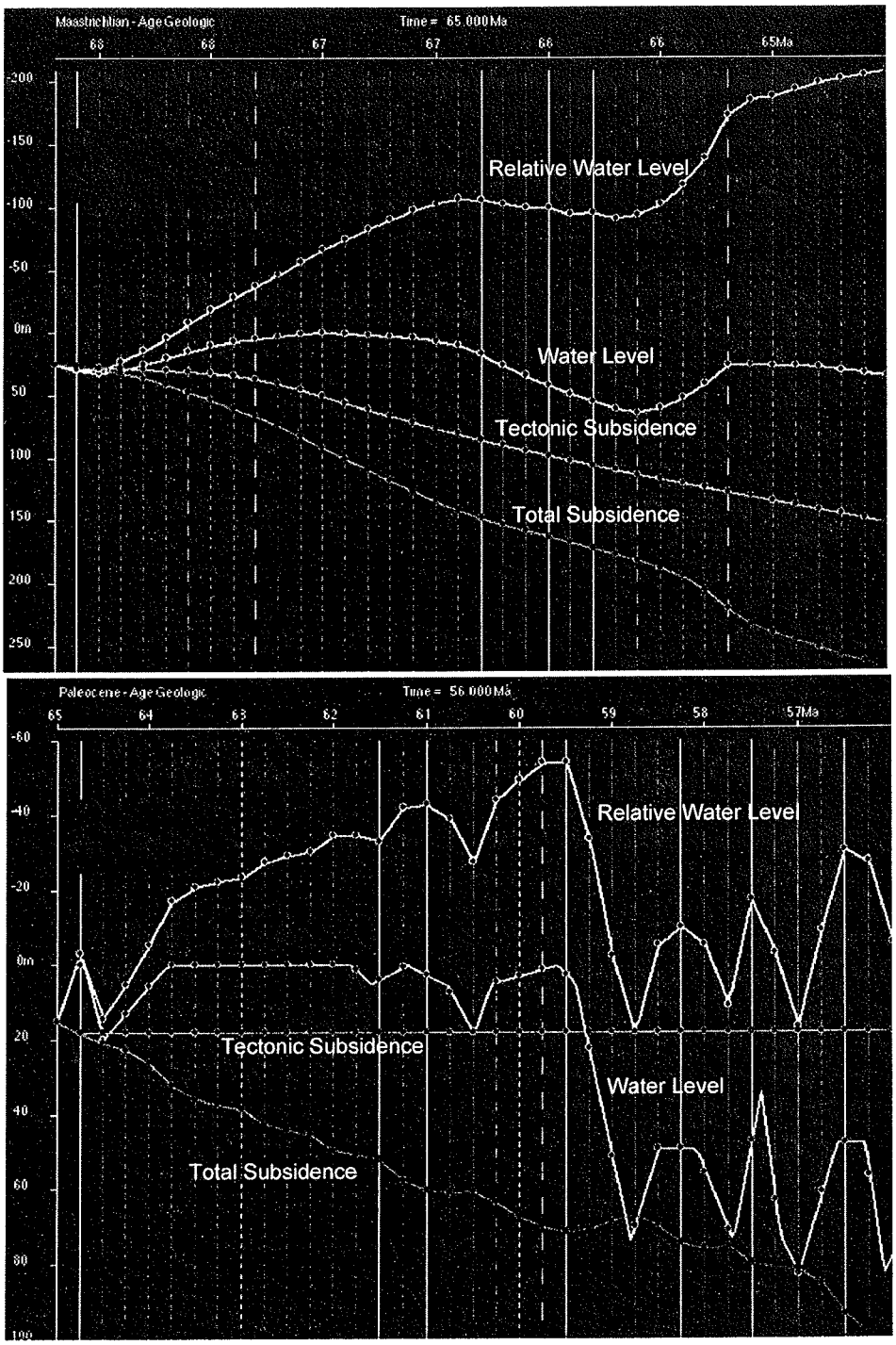

Fig. 8: Computer plots of the relative water level, the water level, the tectonic subsidence and the total subsidence of the Maastrichtian (top) and the Paleocene (bottom). The horizontal scales indicate the absolute ages, whereas the vertical scales indicate the spatial display in meters with a supposed zero level. Subsidence and lowering of sea level are positive, while uplift and rise in sea level are negative. The vertical lines indicate systems tracts that are not considered in this work.

Similarities and differences of the Maastrichtian and the Paleocene models:

When comparing the plots of the Maastrichtian and the Paleocene platforms, the most striking discrepancy concerns their thicknesses. Although the Maastrichtian platform built up during only 3.7 My, its thickness is more than double than that for the Paleocene platform that was built up during 9 My which makes sense considering the different sedimentation rates. For the Maastrichtian the maximum sedimentation rates for carbonates on the platform range between 130 and 200 B, whereas during the Paleocene they range only from 40 to 70 B (Table 1). Average sedimentation rates of the Maastrichtian pelagic setting are 15 B , that is 5 times higher than those of the Paleocene with only 3 B. In addition to the low Paleocene sedimentation rates, platform sediments are preserved only during 3 distinct time-slices due to large hiatuses (Fig. 7b). The combination of the overall low sedimentation rates and the stratigraphic gaps leads to a reduced thickness of the Paleocene carbonate platform.

The lithologies and depositional settings of strata within both time-slices are different. In the Maastrichtian a mixed siliciclastic-carbonate system is present (Figs. 6c, 6d), whereas the Paleocene platform sediments are entirely composed by carbonates (Figs. 7c, 7d). These differences in lithology result in rather different depositional settings. Siliciclastic lithologies dominate the proximal Maastrichtian platform and interfinger with mainly carbonate sediments of the distal platform. Apparently the admixtures of siliciclastic sediments prohibit the formation of tidal flats and reefs. Instead of pure and uniform carbonate depositional systems the Maastrichtian platform sediments exhibit a slump and suspension derived succession. Preliminary studies suggest that siliciclastic admixtures will reduce the productivity of the carbonate system (Mount, 1984; Cortes and Risk, 1985; from Bowman and Vail, 1999).

Comparison between simulated stratigraphies and field data

As the simulations are based also on real geologic data, both model results and field data are compared. We concentrate on the locations of the individual sections, especially the most proximal sections of St. Anthony 1 at 16 km and St. Paul 9 at 32 km (Figs. 6, 7). As mentioned above the most important difference between simulation and outcrop is the absence of a large part of the carbonate platform due to late Cenozoic erosion (today Wadi Araba, Fig. 1).

Maastrichtian:

Sedimentation rates:

The sedimentary sequences and the gross architecture of the upper Cretaceous platform are investigated by Kuss et al. (2000) and Scheibner et al. (2001, in press). In section St. Anthony 1 sedimentation rates are very high for subzone CC25b (Figs. 4, 5a) whereas the younger subzones yield significantly lower sedimentation rates. A similar trend is visible in the sedimentation rates at section St. Paul 9, although here the absolute values are lower (Figs. 4, 5b). These oscillating sedimentation rates can not be reproduced with the set of input parameters used in the model. Instead, the sedimentary sequences are reproduced with a constant sedimentation rate through time that model the absolute thicknesses of the sections very well. By using constant sedimentation rates

it is not possible to simulate stratigraphic gaps in areas that are not subaerially exposed. Hence, the stratigraphic gap around the K/T boundary or even smaller gaps within individual biozones are not reproducible. On the other hand the model predicts a stratigraphic gap due to morphological reasons in the area where the oversteepened slope occurs (Fig. 6).

Slope architecture:

In Scheibner et al. (in press) a slope angle of 5°-8° is calculated for the Maastrichtian rimmed platform. Our model uses an angle of 8° for the depositional front which fits very well with the calculated one.

Lithology:

In section St. Anthony 1 the sediments of the upper Cretaceous St. Anthony Formation are composed of chalky limestones, marls and sandstones (Scheibner et al., 2001). At 16 km (section St. Anthony 1) the model simulates deposition of mainly bioclastic fine wackestones with minor percentages of mudstones and quartz-poor marine mud. In the basinal sections St. Paul 9 to Wadi Tarfa 1 chalk-marl couplets with thick chalk beds and thin marl beds dominate that were modelled as bioclastic fine wackestones and mudstones with minor percentages of quartz-poor marine mud.

Paleowater-depth:

Scheibner et al. (in press) assume paleowater-depths of about 100 m for section St. Anthony 1 and of about 400 for section St. Paul 9. The computer model calculates paleowater-depths of 100-150 m at 16 km (section St. Anthony 1) and of 400-500 m at 32 km (section St. Paul 9) that fit both well within the assumed range. In section St. Paul 9 (Fig. 4) a thin marly bed with an admixture of neritic benthic foraminifers is deposited that may coincide with the lowermost drop in sea level. In the upper part of section St. Anthony 1 siliciclastic sediments with *Exogyra overwegi* occur that should be deposited at shallower water-depths (Fig. 5a). This may correlate with the drop in relative sea-level around 66-67 Ma (Fig. 8).

Paleocene:

Sedimentation rates:

Similar to the Maastrichtian the calculated thicknesses of the Paleocene succession very well resemble the measured thicknesses. In contrast to the high sedimentation rates during the Maastrichtian low sedimentation rates prevail during the Paleocene. Again, stratigraphic gaps in the basin are not reproducible with the constant sedimentation rates of the computer model.

Slope architecture:

For the Paleocene, a distally steepened ramp is proposed (Kuss et al., 2000) contrasting with the rimmed platform of the upper Cretaceous with angles of 8°. The slope angle for the distally steepened ramp should be a little higher than 1° as ramps normally exhibit slope angles of less than 1° (Ahr, 1973) or even less than 0.1° (Wright and Burchette, 1998). For the simulation of the sedimentary processes of the Paleocene only a relatively high slope angle of 6° reproduces the measured sediment thicknesses. Simulations with lower slope angles will shed more sediments into the basin because they reach their stability threshold during a shorter time span and cannot accumulate large quantities of sediment. Consequently, the sections of the platform-basin transect

would have similar thicknesses. But this is not observed in the field. So, at least for the lower Paleocene a rimmed platform architecture is still valid.

Lithology:

The Southern Galala Formation of section St. Anthony 1 characterized by abundant corals and other shallow-water bioclasts are found (Scheibner et al., 2001). The computer model associates bioclastic boundstones, bioclastic coarse grainstones and bioclastic fine wackestones with the position of St. Anthony section at 16 km that fits well with our field observations (Figs. 7c, 7d). In the lower Paleocene, hemipelagic shales of the Dakhla Formation prevail at sections St. Paul 9, Bir Dakhl 2+3 and Wadi Tarfa1+2. These lithologies are modelled as bioclastic fine wackestones and mudstones. In the upper Paleocene, slides and debris flows with partly high contents of quartz are deposited at St. Paul 9 (Scheibner et al., 2000). These depositional features are not displayed neither in the lithology nor in the depositional plot of the computer model. Scheibner et al. (2000) observed that the siliciclastic sediments are of minor importance and were probably transported via submarine canyons, reflecting bypassing. During the whole Paleocene the model proposes that calciturbidites are deposited on the slope and in the basin. The onset of the slides, debris flows, and calciturbidites of the Southern Galala Formation at section St. Paul 9 and sections Bir Dakhl 2 and 3 during the upper NP5 biozone (59Ma) correlates with lowered values for the paleowater-depth calculated by the computer model (Fig. 7e, 7f).

Paleowater-depth:

The benthic foraminiferal assemblages found in the sediments of section St. Paul, located at 32 km were deposited during the Paleocene at paleowater-depths around 500 m, which is in good concordance with the simulated paleowater-depths.

Conclusions

The two stratigraphic simulations of the Maastrichtian to Paleocene sediments of the Galala Mountains in the Eastern Desert of Egypt are conducted with the forward stratigraphic modelling program PHIL. The model results lead to the following conclusions:

- the highly varying sedimentation rates of the Maastrichtian and Paleocene are discussed but can not be modelled because constant sedimentation rates through time for the Maastrichtian and Paleocene are chosen as input parameters.
- the most important parameters that control stratigraphic geometry of carbonate or mixed carbonate siliciclastic platforms are changes in relative sea-level, the sediment flux and the initial topography.
- the timing of the earlier proposed transition from a Maastrichtian rimmed platform to a Paleocene distally steepened ramp can be improved. The rimmed platform persists at least until the late Paleocene what is documented by slope angles of 6°.
- Earlier calculated Maastrichtian slope angles of 5°-8° are confirmed by the computer model that uses an angle of 8°.

- the computer model proposes a mixed siliciclastic-carbonate platform with thicknesses of more than 200 m for the Maastrichtian and a carbonate platform with thicknesses of about 100 m for the Paleocene that today is completely eroded (today's Wadi Araba).
- the simulated geologic parameters lithology, overall thickness and paleowater-depth resemble very well field and laboratory measurements of the individual sections.

Acknowledgements

A. M. Bassiouni (Ain Shams University) is especially thanked for many logistic supports. A. M. Morsi (Ain Shams University) is thanked for his open ear for all problems encountered during our stays in Egypt. T. Wagner (Bremen) improved parts of the manuscript. The investigations were funded by the Graduiertenkolleg „Stoff-Flüsse in marinen Geosystemen" of the University of Bremen and the German Science Foundation (DFG).

References

Ahr, W.M., 1973. The carbonate ramp: an alternative to the shelf model. Transactions, Gulf Coast Association of Geological Societies, 23: 221-225.

Alegret, L. and Thomas, E., in press. Upper Cretaceous and lower Paleogene benthic foraminifera from around the Gulf of Mexico. Micropaleontology.

Aubry, M.P., 1995. Towards an upper Paleocene-lower Eocene high resolution stratigraphy based on calcareous nannofossil stratigraphy. Israel Journal of Earth Sciences, 44: 239-253.

Bandel, K. and Kuss, J., 1987. Depositional environment of the pre-rift sediments - Galala Heights (Gulf of Suez, Egypt). Berliner geowissenschaftliche Abhandlungen A, 78: 1-48.

Berggren, W.A., Kent, D.V., Swisher III, C.C. and Aubry, M.P., 1995. A revised Cenozoic geochronology and chronostratigraphy. In: Berggren, W.A., Kent, D.V., Aubry, M.P. and Hardenbol, J. (Eds.), Geochronolgy, time scales, and global stratigraphic correlation, SEPM Spec. Publ. 54, Tulsa, pp. 129-212.

Bowman, S.A. and Vail, P.R., 1999. Interpreting the stratigraphy of the Baltimore Canyon section, offshore New Jersey with Phil, a stratigraphic simulator. In: Harbaugh, J.W., Watney, W.L., Rankey, E.C., Slingerland, R., Goldstein, R.H. and Franseen, E.K. (Eds.), Numerical experiments in stratigraphy: Recent advances in stratigraphic and sedimentologic computer simulations, SEPM Spec. Publ. 62, Tulsa, pp. 117-138.

Burchette, T.P. and Wright, V.P., 1992. Carbonate ramp depositional systems. Sedimentary Geology, 79: 3-57.

Caron, M., 1985. Cretaceous planktic foraminifera. In: Bolli, H.M., Saunders, J.B. and Perch-Nielsen, K. (Eds.), Plankton stratigraphy, Cambridge University Press, Cambridge, pp. 17-86.

Caus, E., Bernaus, J.M. and Gomez-Garrido, A., 1996. Biostratigraphy utility of species of the Genus Orbitoides. Journal of Foraminiferal Research, 26: 124-136.

Cortes, J. and Risk, M.J., 1985. A reef under siltation stress: Cahuita, Costa Rica. Bulletin of Marine Science, 36: 339-356.

Culver, S.J., 1993. Foraminifera. In: Lipps, J.H. (Ed.), Fossil Prokaryotes and Protists. Blackwell, Oxford, pp. 203-247.

Emery, D. and Myers, K.J., 1996. Sequence stratigraphy. Blackwell, Oxford.

Enos, P., 1991. Sedimentary parameters for computer modeling. In: Franseen, E.K., Watney, W.L., Kendall, C.G.S.C. and Ross, W. (Eds.), Sedimentary modeling: Computer simulations and methods for improved parameter definition, Kansas Geological Survey, Lawrence, pp. 63-99.

Faris, M., 1995. Late Cretaceous and Paleocene calcareous nannofossil biostratigraphy at St. Paul section, Southern Galala Plateau, Egypt. Annals Geol. Surv. Egypt, 20: 527-538.

Franseen, E.K., Watney, W.L., Kendall, C.G.S.C. and Rose, W., 1991. Sedimentary modeling: Computer simulations and methods for improved parameter definition. Kansas Geological Survey, Lawrence.

Gietl, R., 1998. Biostratigraphie und Sedimentationsmuster einer nordostägyptischen Karbonatrampe unter Berücksichtigung der Alveolinen-Faunen. Berichte aus dem Fachbereich Geowissenschaften der Universität Bremen, 112: 1-135.

Harbaugh, J.W., Watney, W.L., Rankey, E.C., Slingerland, R., Goldstein, R.H. and Franseen, E.K., 1999. Numerical experiments in stratigraphy: Recent advances in stratigraphic and sedimentologic computer simulation. SEPM Spec Publ. 62, Tulsa.

Hardenbol, J., Thierry, H., Farley, M.B., Jacquin, T., De Graciansky, P. and Vail, P.R., 1998. Mesozoic and Cenozoic sequence chronostratigraphic framework of European basins. In: de Graciansky, P.C., Hardenbol, J., Jacquin, T. and Vail, P.R. (Eds.), Mesozoic and Cenozoic sequence stratigraphy of European Basins, SEPM Spec Publ. 60, Tulsa, pp. 3-13.

Hay, W.W., Barron, E.J., Sloan, J.L., Southam, J.R., 1981. Continental drift and the global pattern of sedimentation. Geologische Rundschau, 70: 302-315.

Kulbrok, F., 1996. Biostratigraphie, Fazies und Sequenzstratigraphie einer Karbonatrampe in den Schichten der Oberkreide und des Alttertiärs Nordost-Ägyptens (Eastern Desert, N'Golf von Suez, Sinai). Berichte aus dem Fachbereich Geowissenschaften der Universität Bremen, 81: 216.

Kuss, J., 1986. Facies development of Upper Cretaceous-Lower Tertiary sediments from the monastery of St. Anthony/Eastern Desert, Egypt. Facies, 15: 177-194.

Kuss, J. and Leppig, U., 1989. The early Tertiary (middle-late Paleocene) limestones from the western Gulf of Suez, Egypt. Neues Jahrbuch für Geologie und Paläontologie, Abhandlungen, 177: 289-332.

Kuss, J., Scheibner, C. and Gietl, R., 2000. Carbonate Platform to Basin Transition along an Upper Cretaceous to Lower Tertiary Syrian Arc Uplift, Galala Plateaus, Eastern Desert, Egypt. GeoArabia, 5: 405-424.

LeRoy, L.W., 1953. Biostratigraphy of the Maqfi section, Egypt. Geol. Soc. Amer., Mem., 54: 73 pp.

Leyrer, K., Strohmenger, C., Rockenbauch, K. and Bechstaedt, T., 1999. High-resolution formward stratigraphic modeling of Ca2-carbonate platforms and off-platform highs (Upper Permian, Northern Germany). In: Harff, J., Lemke, W. and Stattegger, K. (Eds.), Computerized modeling of sedimentary systems, Springer, Berlin, pp. 307-339.

Luger, P., 1985. Stratigraphie der marinen Oberkreide und des Alttertiärs im südwestlichen Obernil-Becken (SW-Ägypten) unter besonderer Berücksichtigung der Mikropaläontologie, Palökologie und Paläogeographie. Berl. Geowiss. Abh., Rh. A: Geol. Paläontol., 63: 151 pp.

Lüning, S., Marzouk, A.M. and Kuss, J., 1998. The Paleocene of central East Sinai, Egypt:"sequence stratigraphy" in monotonous hemipelagites. Journal of Foraminiferal Research, 28: 19-39.

Marco Polo Software Inc., 1995. PHILTM 1.5 Manual. Houston.

Martini, E., 1971. Standard Tertiary and Quaternary calcareous nannoplankton zonation. In: Farinacci, A. (Ed.), Proceedings of the second planktonic conference, Roma 1970, Tecnoscienza, 739-785.

Marzouk, A.M. and Scheibner, C., subm. Calcareous nannofossil biostratigraphy and paleoenvironment of the late Cretaceous-Paleogene of the Galala Mountains, Eastern Desert, Egypt. Courier Forschungsinstitut Senckenberg,

Miall, A.D., 1997. The geology of stratigraphic sequences. Springer, Berlin.

Mount, J.F., 1984. Mixing of siliciclastic and carbonate sediments in shallow shelf environments. Geology, 12: 432-435.

Moustafa, A.R. and Khalil, M.H., 1995. Superposed deformation in the northern Suez Rift, Egypt: Relevance to hydrocarbons exploration. Journal of Petroleum Geology, 18: 245-266.

Norris, R.D., Kroon, D. and Klaus, A., 1998. Explanatory notes. In: Proceedings of the Ocean Drilling Program, Texas A & M University, Ocean Drilling Program. College Station, TX, 11-44.

Perch-Nielsen, K., 1985. Mesozoic calcareous nannofossils. In: Bolli, H.M., Saunders, J.B. and Perch-Nielsen, K. (Eds.), Plankton stratigraphy, Cambridge University Press, Cambridge, pp. 329-426.

Perlmutter, M.A., De Boer, P.L. and Syvitski, J.R.L., 1999. Geological observations and parameterizations. In: Harbaugh, J.W., Watney, W.L., Rankey, E.C., Slingerland, R., Goldstein, R.H. and Franseen, E.K. (Eds.), Numerical experiments in stratigraphy: Recent advances in stratigraphic and sedimentologic computer simulation, SEPM, Spec. Publ. 62, Tulsa, pp. 25-28.

Read, J.F., 1998. Phanerozoic carbonate ramps from greenhouse, transitional and ice-house worlds: clues from field and modelling studies. In: Wright, V.P. and Burchette, T.P. (Eds.), Carbonate ramps, Geological Society, London, pp. 107-135.

Reiss, Z., 1952. On the upper Cretaceous and lower Tertiary microfaunas of Israel. Res. Counc. Isr., Bull., 2: 37-50.

Said, R. and Kenawy, A., 1956. Upper Cretaceous and lower Tertiary foraminifera from northern Sinai, Egypt. Micropaleontology, 2: 105-173.

Said, R., 1962. The geology of Egypt. Elsevier, Amsterdam.

Scheibner, C., Kuss, J., Marzouk, A.M., 2000. Slope sediments of a Paleocene ramp-to-basin transition in NE Egypt. International Journal of Earth Sciences, 88: 708-724.

Scheibner, C., Marzouk, A.M., Kuss, J., 2001. Maastrichtian-Early Eocene litho- biostratigraphy and Palaeogeography of the northern Gulf of Suez region, Egypt. Journal of African Earth Sciences, 32: 223-255.

Scheibner, C., Marzouk, A.M., Kuss, J., in press. Shelf architectures of an isolated Late Cretaceous carbonate platform margin, Galala Mountains (Eastern Desert, Egypt). Sedimentary Geology,

Serra-Kiel, J., Hottinger, L., Caus, E., Drobne, K., Ferrandez, C., Jauhri, A.K., Less, G., Pavlovec, R., Pignatti, J., Samso, J.M., Schaub, H., Sirel, E., Strougo, A., Tambareau, Y., Tosquella, J., Zakrevskaya, E., 1998. Larger foraminiferal biostratigraphy of the Tethyan Paleocene and Eocene. Bulletin Société Géologique de France, 169: 281-299.

Schnack, K., 2000. Biostratigraphie und fazielle Entwicklung in der Oberkreide und im Alttertiär im Bereich der Kharga Schwelle, Westliche Wüste, SW Ägypten., Berichte, Fachbereich Geowissenschaften, Universität Bremen, 151: 1-142.

Speijer, R.P., 1995. The late Paleocene benthic foraminiferal extinction as observed in the Middle East. In: P. Laga (Ed.), Paleocene-Eocene Boundary Events. Bull. Soc. Belge Géol., 103: 267-280. (Volume year 1994, Published 1995)

Speijer, R.P. and Van der Zwaan, G.J., 1996. Extinction and survivorship of southern Tethyan benthic foraminifera across the Cretaceous/ Palaeogene boundary. In: M.B. Hart (Ed.), Biotic recovery from mass extinction events. Geol. Soc., Lond., Spec. Publ., 102: 343-371.

Speijer, R.P., Schmitz, B., 1998. A benthic foraminiferal record of Paleocene sea level and trophic/redox conditions at Gebel Aweina, Egypt. Palaeogeography, Palaeoclimatology, Palaeoecology, 137: 79-101.

Strougo, A., Haggag, M.A.Y., Luterbacher, H., 1992. The basal Paleocene "Globigerina" eugubina zone in the Eastern Desert (St. Paul's Monastery, South Galala), Egypt. Neues Jahrbuch für Geologie und Paläontologie, Monatshefte, 1992: 97-101.

Strougo, A., Faris, M., 1993. Paleocene-Eocene stratigraphy of Wadi El Dakhl, Southern Galala plateou. Middle East Research Center, Ain Shams University, Earth Science Services, 7: 49-62.

Van Morkhoven, F.P.C.M., Berggren, W.A. and Edwards, A.S., 1986. Cenozoic Cosmopolitan Deep-Water Benthic Foraminifera. Bulletin des Centres de Rechèrches Exploration-Production Elf-Aquitaine, Memoir, 11. Elf Aquitaine, Pau, 421 pp.

Watney, W.L., Rankey, E.C., Harbaugh, J., 1999. Perspectives on stratigraphic simulation models: Current approaches and future opportunities. In: Harbaugh, J.W., Watney, W.L., Rankey, E.C., Slingerland, R., Goldstein, R.H., Franseen, E.K. (Eds.), Numerical experiments in stratigraphy: Recent advances in stratigraphic and sedimentologic computer simulation, SEPM, Spec. Publ. 62, Tulsa, pp. 3-21.

Widmark, J.G.V., 2000. Biogeography of terminal Cretaceous benthic foraminifera: Deep-water circulation and trophic gradients in the deep South Atlantic. Cret. Res., 21: 367-379.

Widmark, J.G.V. and Speijer, R.P., 1997a. Benthic foraminiferal ecomarker species of the terminal Cretaceous (late Maastrichtian) deep-sea Tethys. Mar. Micropaleontol., 31: 135-155.

Widmark, J.G.V. and Speijer, R.P., 1997b. Benthic foraminiferal faunas and trophic regimes at the terminal Cretaceous Tethyan seafloor. Palaios, 12: 354-371.

Wright, V.P., Burchette, T.P., 1998. Carbonate Ramps: an introduction. In: Wright, V.P., Burchette, T.P. (Eds.), Carbonate Ramps, Geological Society, London, London, pp. 1-5.

CHAPTER 7

Conclusions and Perspectives

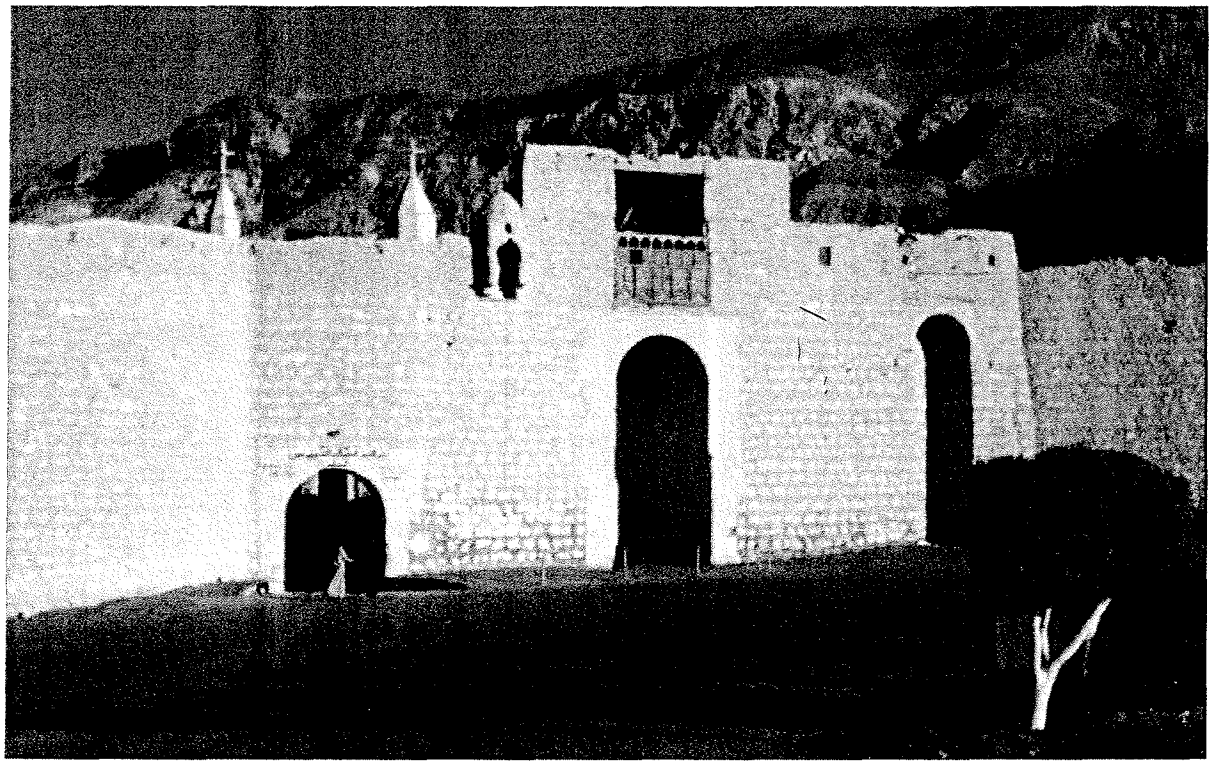

The main entrance to the monastery of St. Anthony

Photo by Christian Scheibner (1998)

Conclusion and Perspectives

Conclusions:

Campanian to Early Eocene deposits from the carbonate platform of the Galala Mountains, Eastern Desert (Egypt) and the adjacent transitional and basinal settings farther south have been studied in detail using data from field geology, paleontology and sedimentology. The research mainly focussed on the evaluation of the depositional processes on and from the carbonate platform and their controlling parameters. Of special interest was the transitional zone between shallow-water limestones and deep-water marls, shales and chalks as this zone reveals information from both settings and enables to build an integrated stratigraphic framework.

The main results of this study are:

- High resolution biostratigraphy is a principal requirement for the estimation of any event or process in the stratigraphic record. Calcareous nannoplankton and planktic foraminifers are used here to obtain two separate independently biozonations.
- On the basis of new measured sections and isolated local and regional studies published in the literature, the Maastrichtian to Early Eocene deposits of the northern Gulf of Suez can be divided into three environmental regimes. The results of this facies investigation in combination with the different types of hiatuses observed in the area enabled to reconstruct a detailed evolution of palaeogeography throughout the Maastrichtian to Early Eocene, as documented in 11 palaeogeographic maps.
- The facies architecture of the platform-basin transect reflects the evolution from a rimmed shelf (Late Cretaceous) to a distally steepened ramp (latest Cretaceous to Paleocene) and eventually to a homoclinal ramp (Early Eocene)
- For the Maastrichtian, an asymmetrical platform margin is proposed. It is formed like a rimmed platform in southeasterly direction and like a ramp in southwesterly direction with slope angles of 5° to 8° for the rimmed part and slope angle of less than 0.1° for the ramp part.
- During the late Paleocene, three phases of carbonate ramp progradation and three intercalated hemipelagic units were differentiated at St. Paul at the southern rim of the Southern Galala. The three prograding phases are indicated by increased mass-transport deposition of glides, slumps and debris flows.
- Using allochthonous sediments, like debris flows and a computer simulation it was possible to obtain a perception of the areas of the carbonate platform that are not or only poorly exposed. This enabled us to propose a facies model for the Paleocene.
- The computer simualation with the chosen input parameter reflects the field data well.

Perspectives:

The present PhD thesis discusses the controlling parameters of the depositional processes on and from the carbonate platform of and from the Galala Mountains during the Campanian to Early Eocene. However, the accuracy of estimation of the various parameters discussed in the previous

chapters is not equivilant for all time-slices studied what leaves the opportunity for further studies. In the following paragraph several research possibilites are discussed.

For the Upper Cretaceous, slope settings are found only at the northern rim of the Southern Galala in the vicinity of St. Anthony. Farther south at St. Paul only chalks of basinal settings are exposed. Further field-campaigns can investigate the area between St. Paul and St. Anthony for Upper Cretaceous transitional settings to compare them with the well-studied Paleocene slope-basin transitions. Expanding the time-slice from the Campanian-Early Eocene to the Eocene provides another target for future research, as for this time-slice there exist numerous well-exposed sections from shallow-water to basinal settings in the Galala Mountains.

Apllications of supplementary methods like gamma-ray measurements offer the possibility to establish an independent correlation-tool for platform to basin sediments. On the platform gamma-ray measurements may also reveal small-scaled cycles which are well discussed for rimmed platforms but remain relatively unexplained for ramps.

For the Palaeogene ramp, the calculation of the slope angles are still missing. Until now, the main focus of investigation was on the interpretation of the architecture of the carbonate platform-basin transition and their controlling factors. Paleoceanographic topics that include the effects of more regional or global processes and events during the Late Cretaceous and Palaeogene have not been put forward and should be included in future research. All the below mentioned processes and events are documented in deep-water settings but their effectiveness within the shallower carbonate slope and platform settings still remains uncertain. The well-exposed transitional zone between deep-water and shallow-water settings of the carbonate platform of the Galala mountains provides excellant conditions to study

- To what extent are changes in paleoproductivity effective on the slope and the shallow-water settings of the Late Cretaceous carbonate platform?
- Were Tethyan carbonate platforms unaffected by the Late Paleocene Thermal Maximum, although associated environmental perturbations disturbed the geobiosphere worldwide?

Appendix

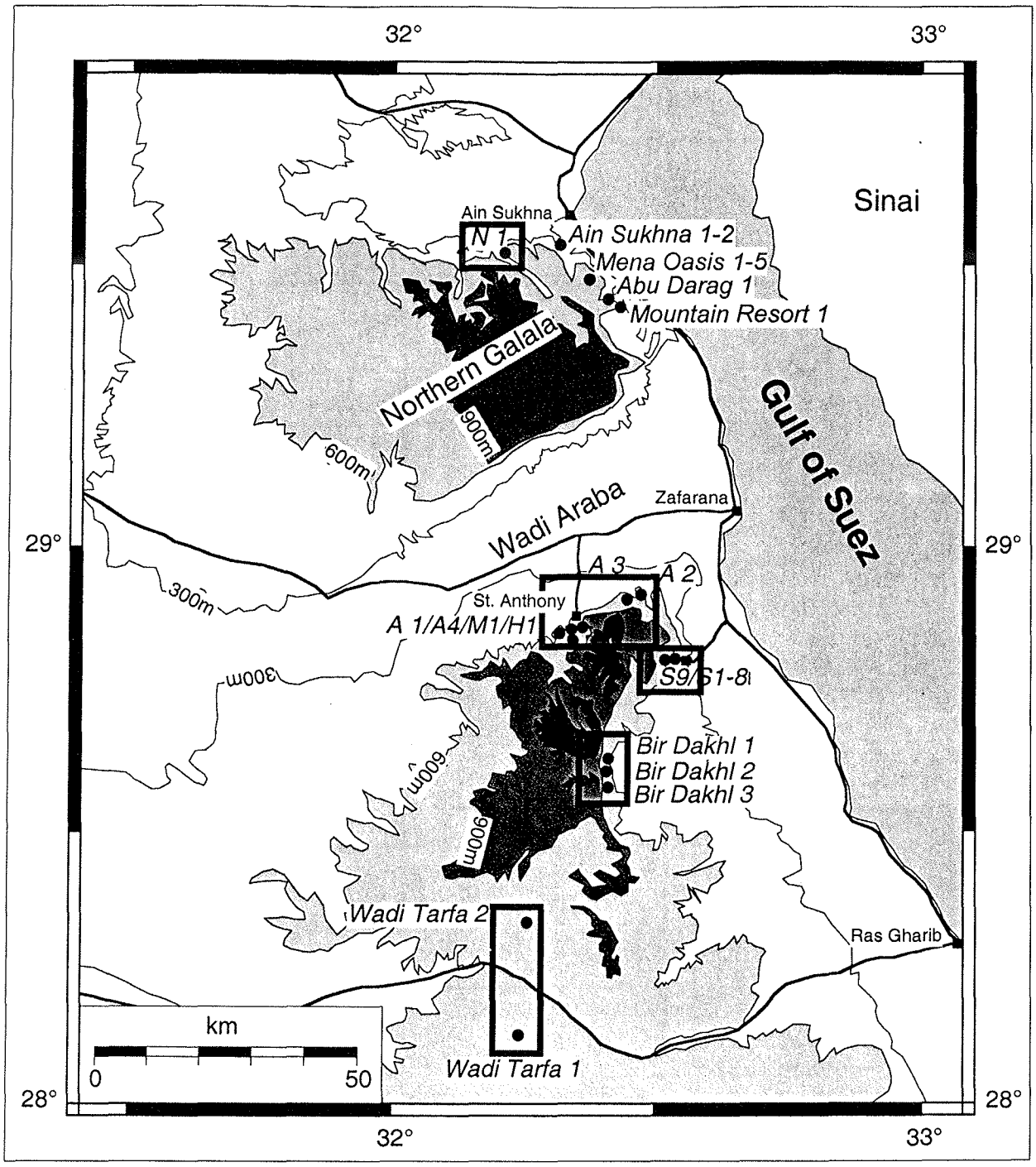

Topographic map of the Galalas with the individual sections, rectangles indicate detailed topographic maps.

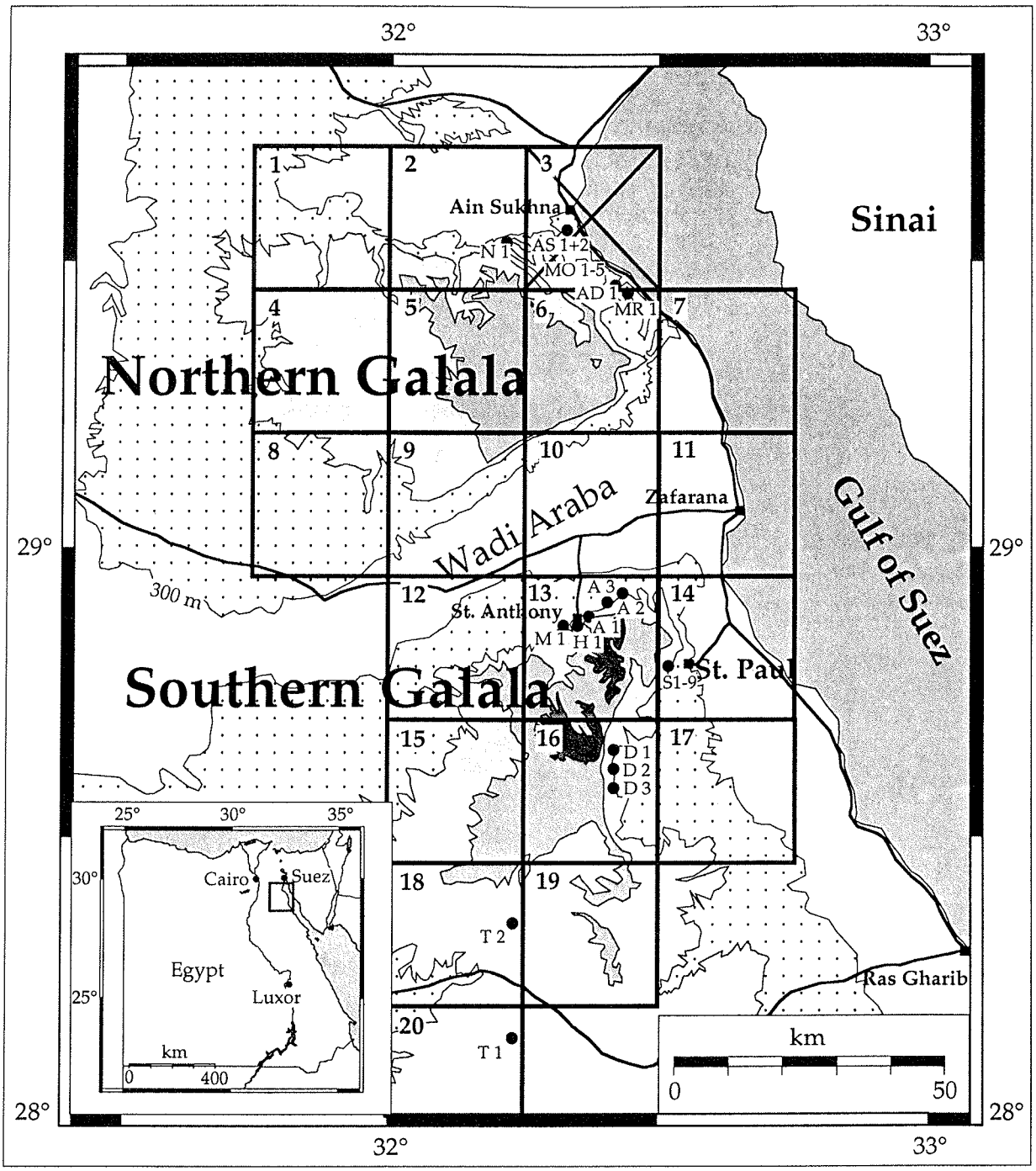

1) NH36F4b: Bir Al-Airamiyyah
2) NH36F5a: Gabal Umm Risay (N1)
3) NH36F5b: not available (Mo1-Mo5, As1-As2)
4) NH36F1d: Wadi Al-Khalal
5) NH36F2c: Wadi Al Abyad
6) NH36F2d: abal al Jalalah Al-Bahariyyah
7) NH36F3c: Ras Abu Daraj
8) NH36F1b: Wadi Abu Risha
9) NH36F2a: Bir Bardah
10) NH36F2b: Wadi Ad-Dayr
11) NH36F3a: Az-za Faranah
12) NH36B5c: Bir Buwayrat
13) NH36B5d: Dayr St. Anthony (M1, H1, A1-A4)
14) NH36B6c: Dayr St. Paul (S1-S9)
15) NH36B5a: Wadi Arkas
16) NH36B5b: Bir Ad-Dahal (D1-D3)
17) NH36B6a: Wadi Ad-Dahal
18) NH36B2c: Wadi Muhir at Tarfah (T2)
19) NH36B2d: Wadi Al-Murr
20) NH36B2a: East Sikkat Al-Ajal (T1)

Topographic basemaps (1:50.000, published by the Egyptyian General Survey Authority) with location of the individual sections.

Samples Scheibner (1997/98):

Profile		Thickness	Thin-sections	Loose samples	Samples (total)
Wadi Nooz 1	(N 1)	112,23 m	16	30	46
Ain Suhkna 1	(AS 1)	102,16 m	2	0	2
Ain Suhkna 2	(AS 2)	121,65 m	8	0	8
Mena Oasis 1	(MO 1)	115,65 m	15	0	15
Mena Oasis 2	(MO 2)	61,72 m	15	0	15
Mena Oasis 3	(MO 3)	57,54 m	10	0	10
Mena Oasis 4	(MO 4)	82,56 m	10	4	14
Mena Oasis 5	(MO 5)	70,69 m	15	3	18
Abu Darag 1	(AD 1)	29,30 m	1	0	1
Mountain Resort 1	(MR 1)	129,24 m	19	25	44
Wadi Araba					
St. Anthony 1	(A 1)	196,98 m	37	31	68
St. Anthony 2	(A 2)	144,18 m	0	9	9
St. Anthony 3	(A3)	119,78 m	20	17	37
St. Anthony 4	(A4)	15,00 m	0	1	1
Wadi Hamada 1	(H 1)	53,53 m	2	41	43
Wadi Miraf 1	(M 1)	53,63 m	7	0	7
St. Paul 1	(P0/S1)	25,76 m	15	6	21
St. Paul 2	(P1/S2)	20,71 m	8	14	22
St. Paul 4	(P2/S4)	19,31 m	28	5	33
St. Paul 3	(P3/S3)	7,01 m	5	1	6
St. Paul 5	(P4/S5)	2,01 m	0	2	2
St. Paul 8	(P5/S8)	16,13 m	8	7	15
St. Paul 7	(P6/S7)	3,00 m	3	4	7
St. Paul 6	(P7/S6)	20,95 m	20	0	20
St. Paul 8	(P8/S9)	80,71 m	15	60	75
Bir Dahkl 1	(D 1)	29,48 m	0	24	24
Bir Dahkl 2	(D2)	119,56 m	9	104	113
Bir Dahkl 3	(D3)	131,45 m	4	82	86
Wadi Tarfa 1	(T 1)	60,71 m	0	62	62
Wadi Tarfa 2	(T 2)	44,17 m	0	63	63
Samples without rectangles		**1993,27 m**	**292**	**595**	**887**
Rectangles in MO	(MO1-2)		38	0	38
Samples with rectangles			**330**	**595**	**925**
Single samples of Wadi Abyad			3	0	3
Total samples			**333**	**595**	**928**

GPS Coordinates Egypt

Profile	Abb.	Name/Year	UTM Coordinates (m)	Lat/Lon Minutes
Northern Galala				
Wadi Nooz 1	N 1	Scheibner/97	E 421249	N 29°31,863´
			N 3266920	E 32°11,239´
Wadi Abyad 1	WA	Scheibner/97	E 415795	N 29°30,789´
			N 3264977	E 32°07,871´
Ain Sukhna 1	AS 1	Scheibner/97	E 435806	N 29°34,409´
			N 3271530	E 32°20,235´
Ain Sukhna 2	AS 2	Scheibner/97	E 436639	N 29°33,756´
			N 3270320	E 32°20,755´
Mena Oasis 1	MO 1	Scheibner/97	E 438341	N 29°31,642´
			N 3266406	E 32°21,823´
Mena Oasis 2	MO 2	Scheibner/97	50 m north of MO 1	
Mena Oasis 3	MO 3	Scheibner/97	1,5 km sw of MO 1	
Mena Oasis 4	MO 4	Scheibner/97	3 km sw of MO 1	
Mena Oasis 5	MO 5	Scheibner/97	E 437799	N 29°32,009´
			N 3267087	E 32°21,485´
Abu Darag 1	AD 1	Scheibner/97	E 441906	N 29°27,706´
			N 3259119	E 32°24,053´
Mountain Resort 1	MR 1	Scheibner/97	E 447003	N 29°26,564´
			N 3256985	E 32°27,213´
Northern escarpment of the Southern Galala				
St. Anthony 1	A 1	Scheibner/97	E 436984	N 28°54,952´
			N 3198660	E 32°21,214´
St. Anthony 2	A 2	Scheibner/97	E 444974	N 28°57,452´
			N 3203237	E 32°26,118´
St. Anthony 3	A 3	Scheibner/98	E 443379	N 28°56,723´
			N 3201898	E 23°25,140´
St. Anthony 4	A 4	Scheibner/98	E 436399	N 28°54,755´
			N 3198300	E 32°20,855´
Wadi Hamada 1	H 1	Scheibner/97	E 435829	N 28°53,939´
			N 3196797	E 32°20,509´
Wadi Miraf 1	M 1	Scheibner/97	E 434758	N 28°53,848´
			N 3196635	E 32°19,851´
Wadi Miraf		Gietl/95	E 434449	N 28°53,306´
			N 3195635	E 32°19,664´
Umm Jiraf 1		Gietl/95	E 433061	N 28°52,959´
			N 3195002	E 32°18,812´
Umm Jiraf 2		Gietl/95	E 433048	N28°52,964´
			N 3195011	E 32°18,812´

GPS Coordinates Egypt

Profile	Abb.	Name/Year	UTM Coordinates (m)	Lat/Lon Minutes
Southern escarpment of the Southern Galala				
St. Paul	S	Strougo/91	E 455480 N 3190600	N 28°50,633´ E 32°32,617´
St. Paul 0	P0/S1	Scheibner/98	325 m west of P5	lateral distance 25 m
St. Paul 1	P1/S2	Scheibner/98	250 m west of P5	lateral distance 100 m
St. Paul 2	P2/S4	Scheibner/98	100 m west of P5	lateral distance 250 m
St. Paul 3	P3/S3	Scheibner/98	170 m west of P5	lateral distance 180 m
St. Paul 4	P4/S5	Scheibner/98	70 m west of P5	lateral distance 280 m
St. Paul 5	P5/S8	Scheibner/98	E 453321 N 3190766	N 28°50,718´ E 32°31,288´ lateral distance 350 m
St. Paul 6	P6/S7	Scheibner/98	15 m west of P5	lateral distance 335 m
St. Paul 7	P7/S6	Scheibner/98	20 m west of P5	lateral distance 330 m
St. Paul 8	P8/S9	Scheibner/98	E 453715 N 3190121	N 28°50,370´ E 32°31,532´
Abu Rimth 1		Gietl/95	E 452611 N 3178117	N 28°42,867´ E 32°30,867´
Abu Rimth 2		Gietl/95	E 452576 N 3176271	N 28°43,867´ E 32°30,883´
Bir Dahkl 1	D 1	Scheibner/97	E 440954 N 3174355	N 28°41,801´ E 32°23,745´
Bir Dahkl 2	D 2	Scheibner/98	E 440692 N 3170303	N 28°39,605´ E 32°23,585´
Bir Dahkl 3	D 3	Scheibner/98	E 440969 N 3164430	N 28°36,425´ E 32°23,773´
Wadi Tarfa 1	T 1	Scheibner/97	E 424192 N 3122223	N 28°13,515´ E 32°13,644´
Wadi Tarfa 2	T 2	Scheibner/97	E 424498 N 3147700	N 28°27,313´ E 32°13,732´
Profile U Coordinates estimated	U	Kuss/Bandel 87		N 28°35,5´ E 32°22,5´
Profile V Coordinates estimated	V	Kuss/Bandel 87		N 28°24,5´ E 32°,10´

Legend:

Lithology:

 limestone

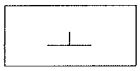 marl

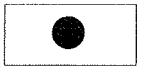 nodular limestone debris flow

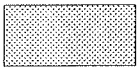 siltstone

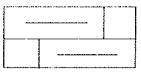 chalk

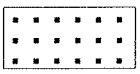 sandstone

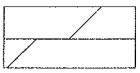 dolomite

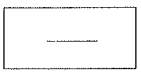 shale

Biogenes:

N	Nummulites	Omph	Omphalocyclus
A	Alveolinids	C	Coral
T	Thalassinoides	Bio	Bioturbation
Z	Zoophycos	Ex	Exogyra
Ov	Exogyra overwegi	Oy	Oyster
G	Gastropods		

Calcareous nannoplankton:

Abundance:

- ■ abundant
- ▮ common
- ❙ few
- | rare

Preservation:

- ● good
- • moderate
- · poor

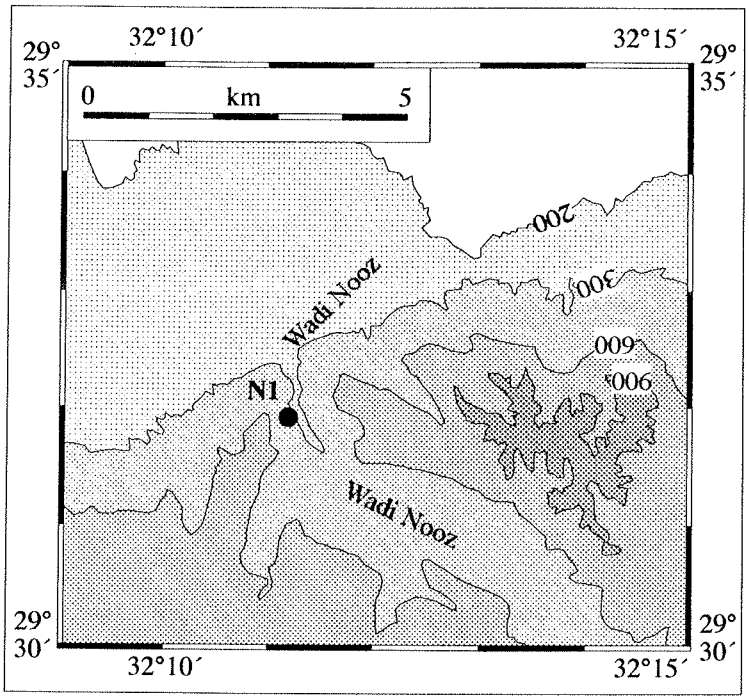
29° 35´
32°10´
32°15´
29° 35´
0
km
5
200
300
600
900
Wadi Nooz
N1
Wadi Nooz
29° 30´
32°10´
32°15´
29° 30´

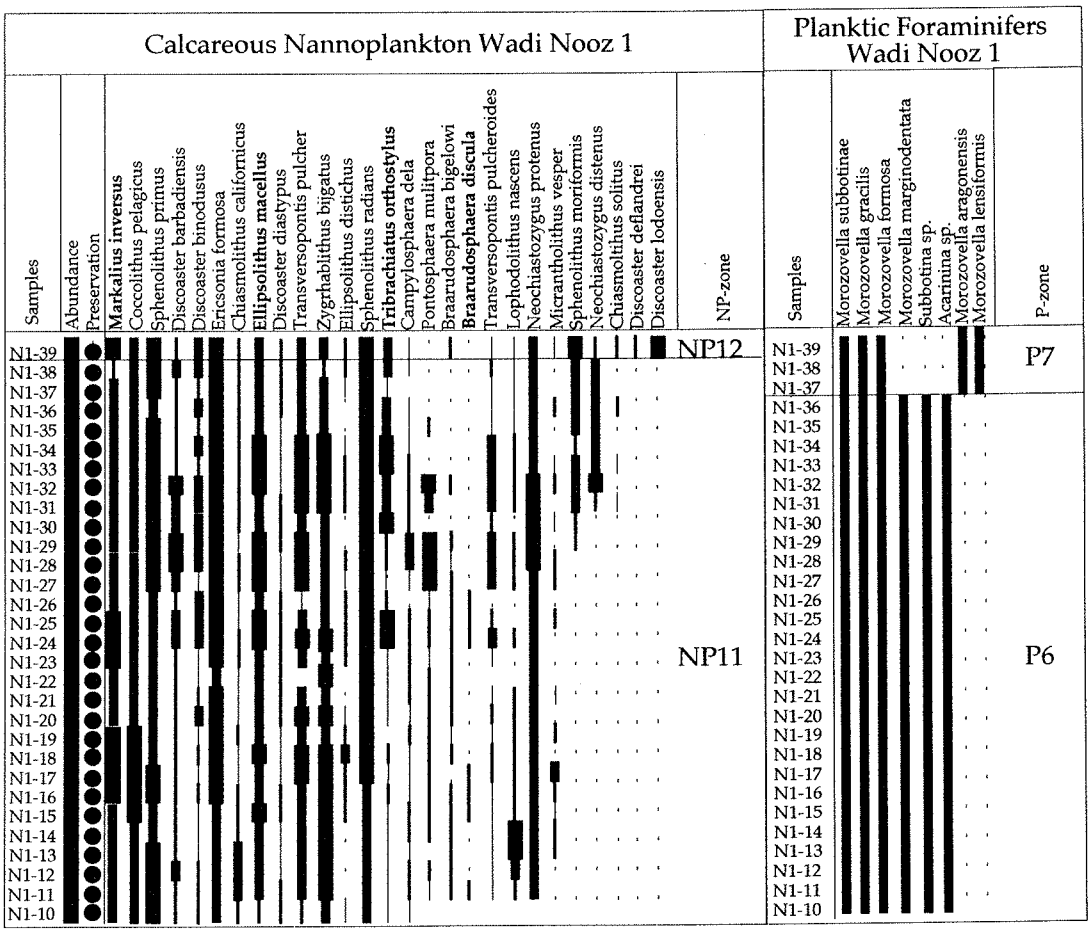
Calcareous Nannoplankton Wadi Nooz 1
Planktic Foraminifers Wadi Nooz 1
Samples
Abundance
Preservation
Markalius inversus
Coccolithus pelagicus
Sphenolithus primus
Discoaster barbadiensis
Discoaster binodusus
Ericsonia formosa
Chiasmolithus californicus
Ellipsolithus macellus
Discoaster diastypus
Transversopontis pulcher
Zygrhablithus bigatus
Ellipsolithus distichus
Sphenolithus radians
Tribrachiatus orthostylus
Campylosphaera dela
Pontosphaera multipora
Braarudosphaera bigelowi
Braarudosphaera discula
Transversopontis pulcheroides
Lophodolithus nascens
Neochiastozygus protenus
Micrantholithus vesper
Sphenolithus moriformis
Neochiastozygus distenus
Chiasmolithus solitus
Discoaster deflandrei
Discoaster lodoensis
NP-zone
Samples
Morozovella subbotinae
Morozovella gracilis
Morozovella formosa
Morozovella marginodentata
Subbotina sp.
Acarinina sp.
Morozovella aragonensis
Morozovella lensiformis
P-zone
N1-39
N1-38
N1-37
N1-36
N1-35
N1-34
N1-33
N1-32
N1-31
N1-30
N1-29
N1-28
N1-27
N1-26
N1-25
N1-24
N1-23
N1-22
N1-21
N1-20
N1-19
N1-18
N1-17
N1-16
N1-15
N1-14
N1-13
N1-12
N1-11
N1-10
NP12
NP11
P7
P6

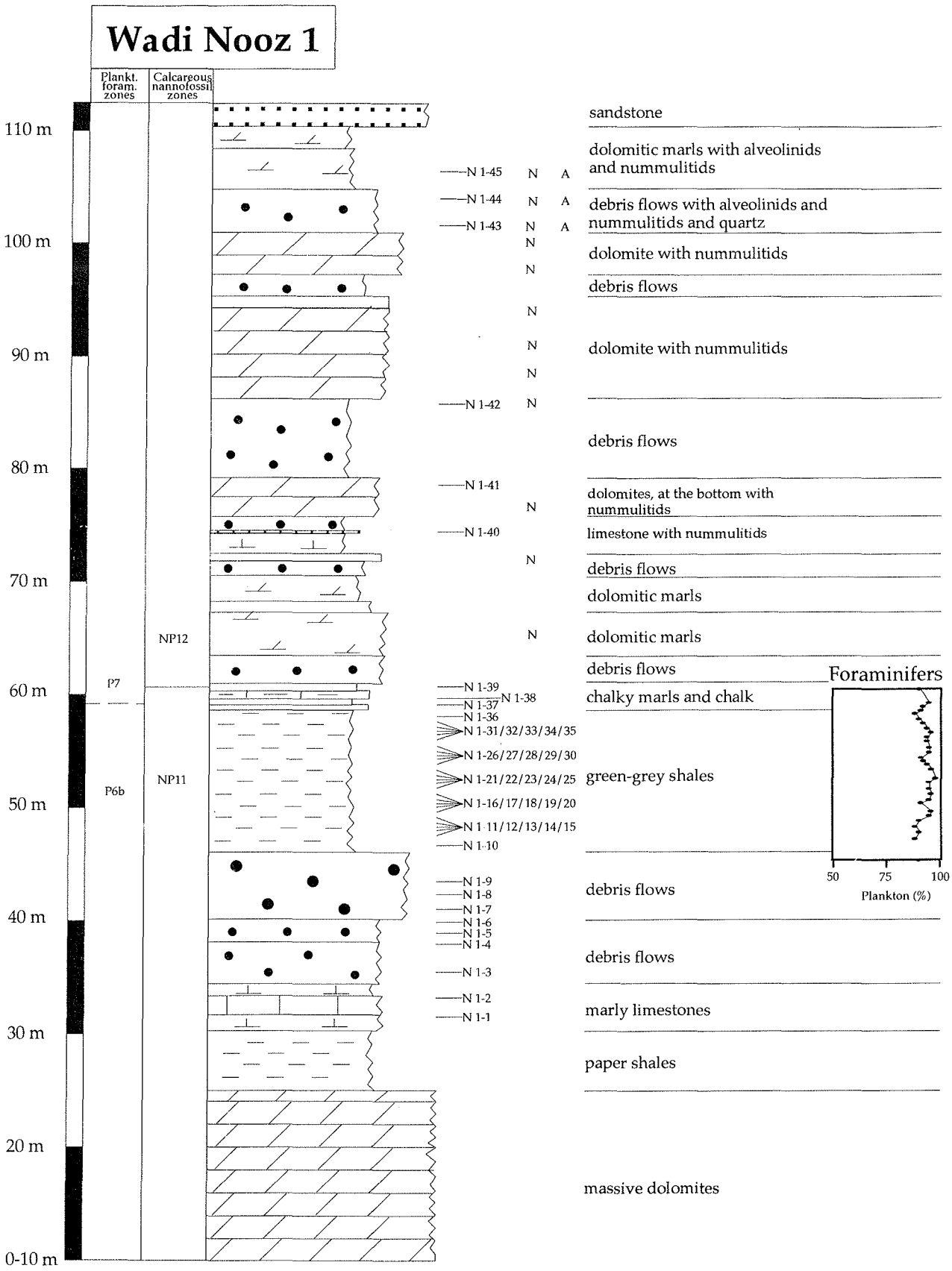
Wadi Nooz 1
Plankt. foram. zones
Calcareous nannofossil zones
110 m
100 m
90 m
80 m
70 m
60 m
50 m
40 m
30 m
20 m
0-10 m
P7
P6b
NP12
NP11
N 1-45 N A
N 1-44 N A
N 1-43 N A
N
N
N
N
N
N 1-42 N
N 1-41
N
N 1-40
N
N
N 1-39
N 1-38
N 1-37
N 1-36
N 1-31/32/33/34/35
N 1-26/27/28/29/30
N 1-21/22/23/24/25
N 1-16/17/18/19/20
N 1-11/12/13/14/15
N 1-10
N 1-9
N 1-8
N 1-7
N 1-6
N 1-5
N 1-4
N 1-3
N 1-2
N 1-1
sandstone
dolomitic marls with alveolinids and nummulitids
debris flows with alveolinids and nummulitids and quartz
dolomite with nummulitids
debris flows
dolomite with nummulitids
debris flows
dolomites, at the bottom with nummulitids
limestone with nummulitids
debris flows
dolomitic marls
dolomitic marls
debris flows
chalky marls and chalk
green-grey shales
debris flows
debris flows
marly limestones
paper shales
massive dolomites
Foraminifers
50
75
100
Plankton (%)

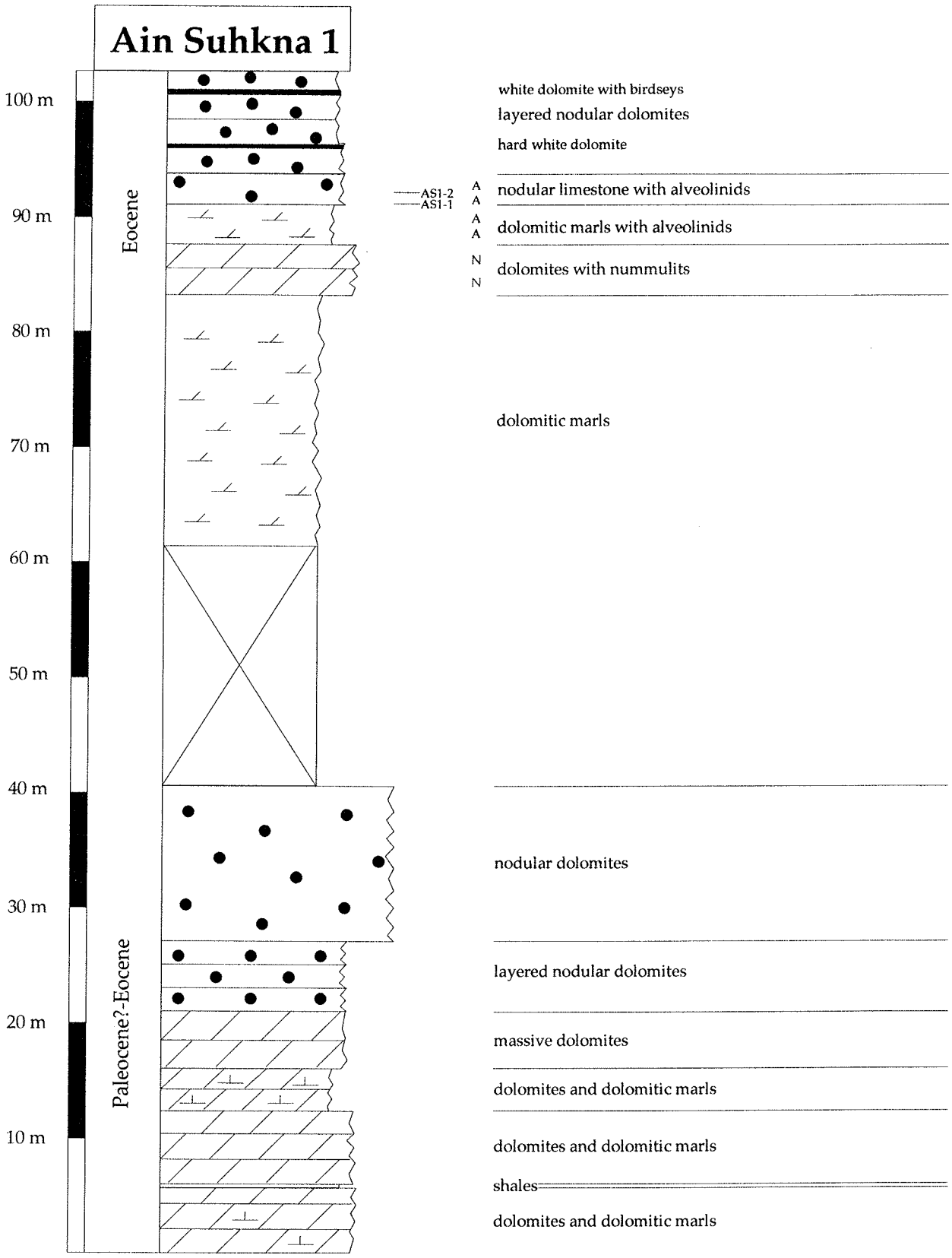
Ain Suhkna 1
100 m
90 m
80 m
70 m
60 m
50 m
40 m
30 m
20 m
10 m
Eocene
Paleocene?-Eocene
AS1-2
AS1-1
white dolomite with birdseys
layered nodular dolomites
hard white dolomite
nodular limestone with alveolinids
dolomitic marls with alveolinids
dolomites with nummulits
dolomitic marls
nodular dolomites
layered nodular dolomites
massive dolomites
dolomites and dolomitic marls
dolomites and dolomitic marls
shales
dolomites and dolomitic marls

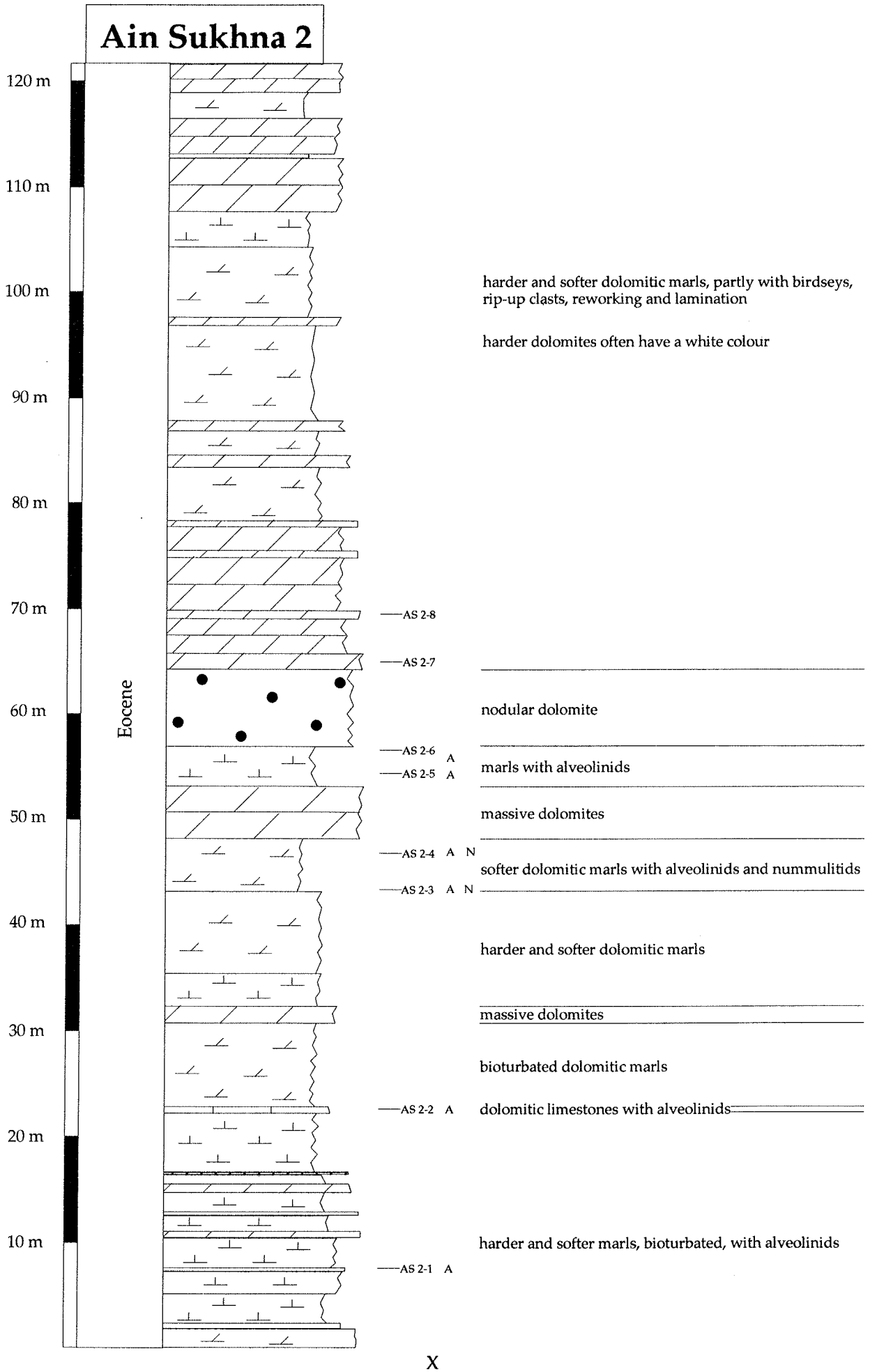
Ain Sukhna 2
120 m
110 m
100 m
90 m
80 m
70 m
60 m
50 m
40 m
30 m
20 m
10 m
Eocene
AS 2-8
AS 2-7
AS 2-6 A
AS 2-5 A
AS 2-4 A N
AS 2-3 A N
AS 2-2 A
AS 2-1 A
harder and softer dolomitic marls, partly with birdseys, rip-up clasts, reworking and lamination
harder dolomites often have a white colour
nodular dolomite
marls with alveolinids
massive dolomites
softer dolomitic marls with alveolinids and nummulitids
harder and softer dolomitic marls
massive dolomites
bioturbated dolomitic marls
dolomitic limestones with alveolinids
harder and softer marls, bioturbated, with alveolinids

X

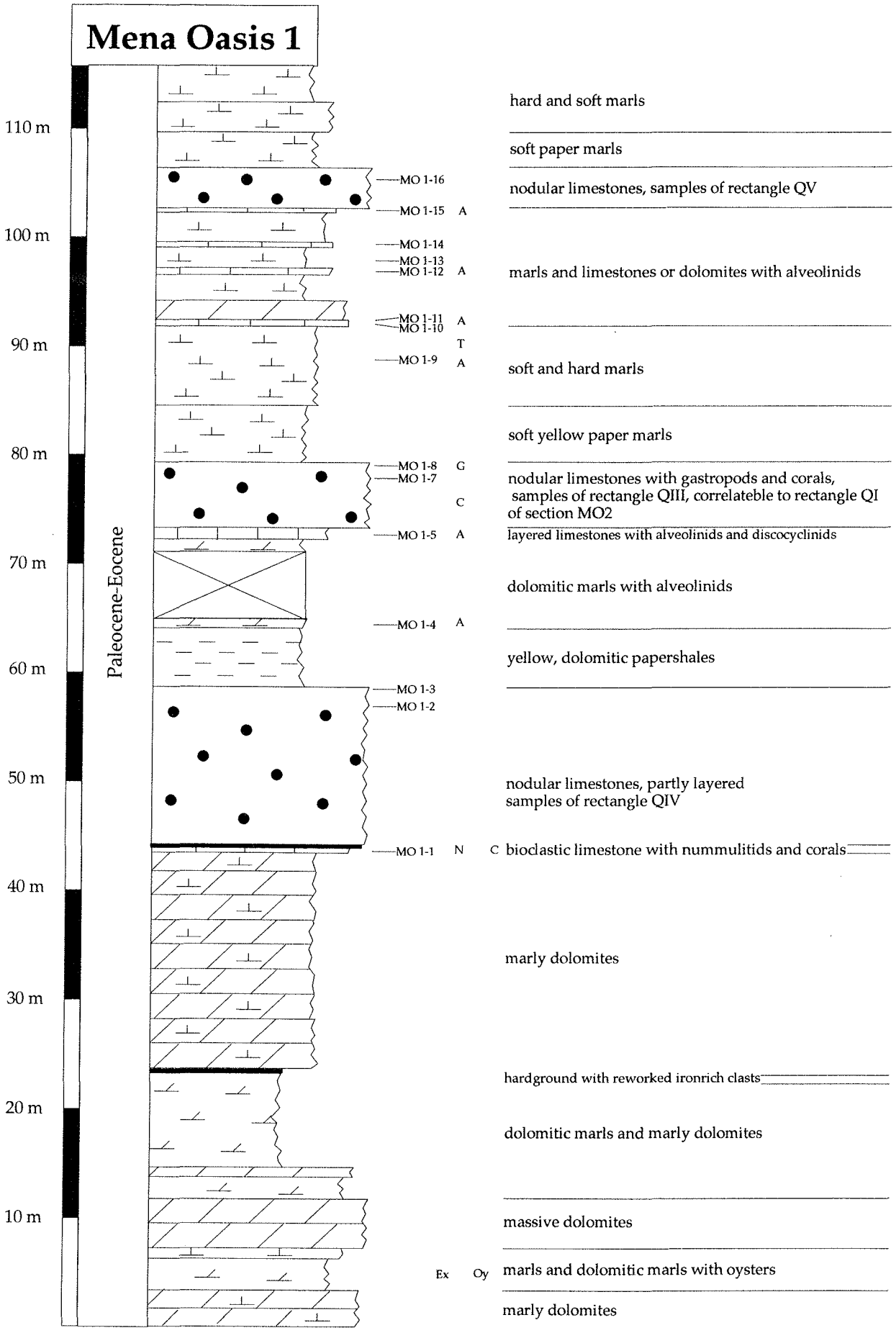
Mena Oasis 1
110 m
100 m
90 m
80 m
70 m
60 m
50 m
40 m
30 m
20 m
10 m
Paleocene-Eocene
MO 1-16
MO 1-15 A
MO 1-14
MO 1-13
MO 1-12 A
MO 1-11 A
MO 1-10
T
MO 1-9 A
MO 1-8 G
MO 1-7
C
MO 1-5 A
MO 1-4 A
MO 1-3
MO 1-2
MO 1-1 N C
Ex Oy
hard and soft marls
soft paper marls
nodular limestones, samples of rectangle QV
marls and limestones or dolomites with alveolinids
soft and hard marls
soft yellow paper marls
nodular limestones with gastropods and corals, samples of rectangle QIII, correlateble to rectangle QI of section MO2
layered limestones with alveolinids and discocyclinids
dolomitic marls with alveolinids
yellow, dolomitic papershales
nodular limestones, partly layered samples of rectangle QIV
bioclastic limestone with nummulitids and corals
marly dolomites
hardground with reworked ironrich clasts
dolomitic marls and marly dolomites
massive dolomites
marls and dolomitic marls with oysters
marly dolomites

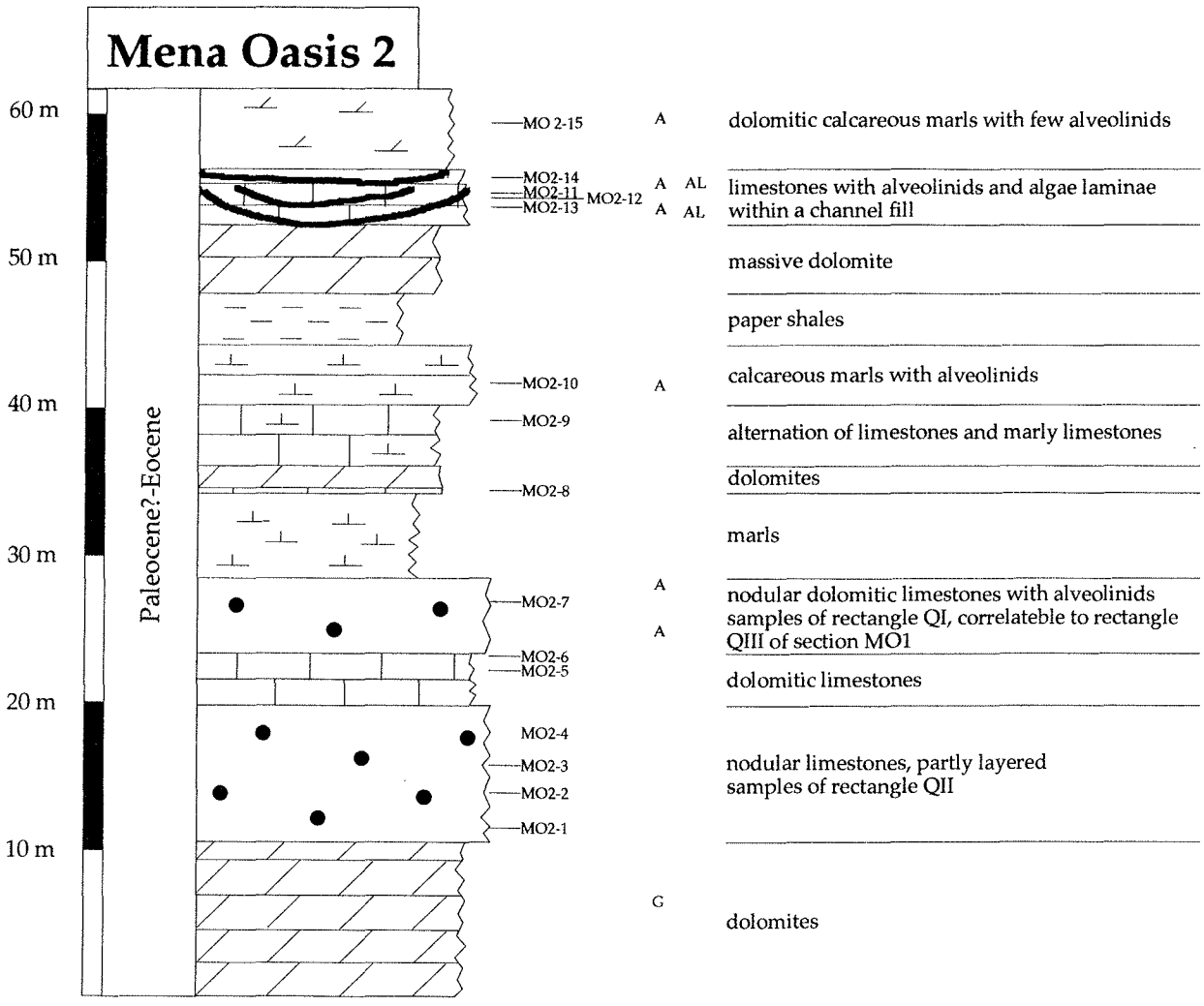
Mena Oasis 2
60 m
50 m
40 m
30 m
20 m
10 m
Paleocene?-Eocene
MO 2-15
MO2-14
MO2-11
MO2-12
MO2-13
MO2-10
MO2-9
MO2-8
MO2-7
MO2-6
MO2-5
MO2-4
MO2-3
MO2-2
MO2-1
A
A AL
A AL
A
A
A
G
dolomitic calcareous marls with few alveolinids
limestones with alveolinids and algae laminae within a channel fill
massive dolomite
paper shales
calcareous marls with alveolinids
alternation of limestones and marly limestones
dolomites
marls
nodular dolomitic limestones with alveolinids samples of rectangle QI, correlateble to rectangle QIII of section MO1
dolomitic limestones
nodular limestones, partly layered samples of rectangle QII
dolomites

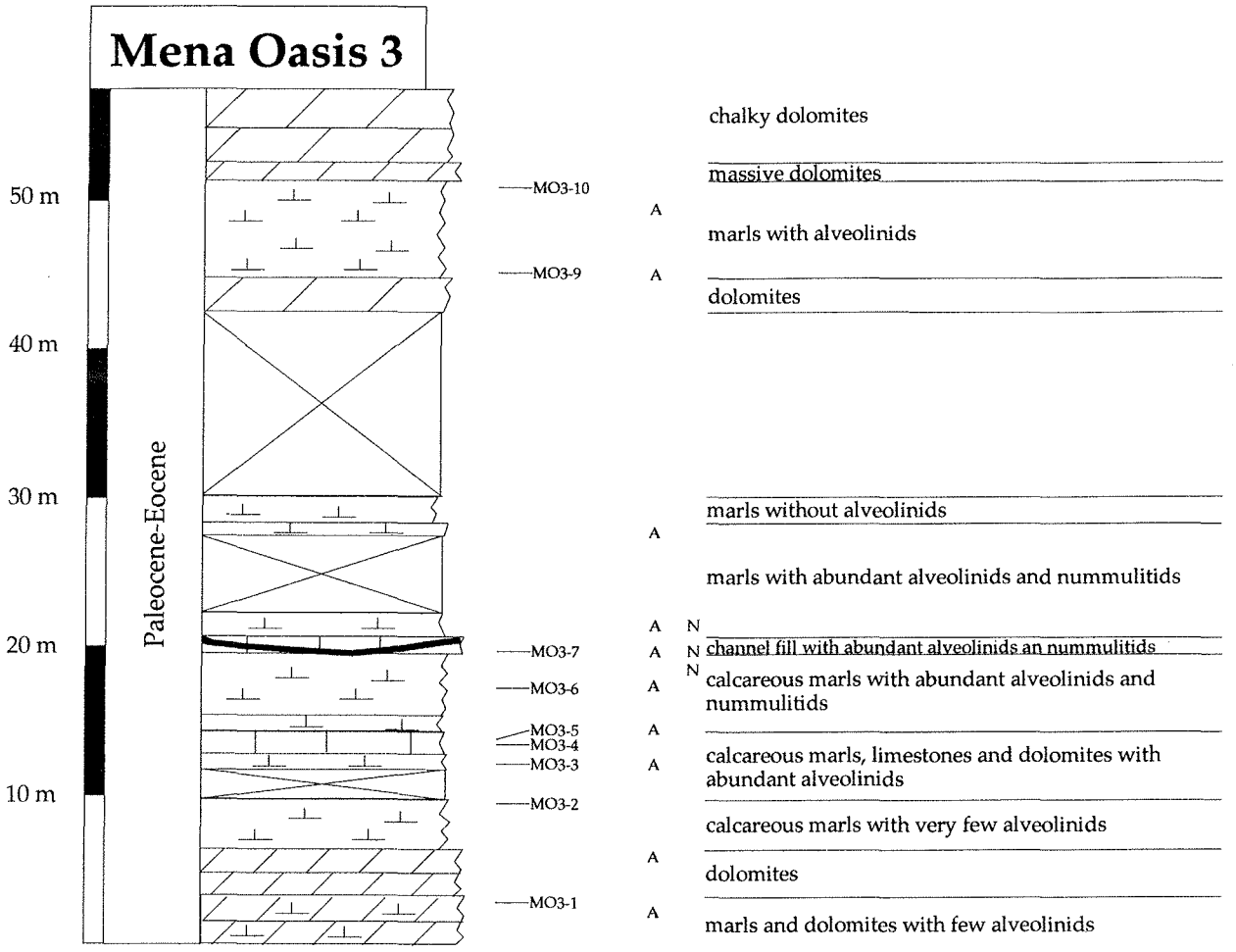
Mena Oasis 3
50 m
40 m
30 m
20 m
10 m
Paleocene-Eocene
MO3-10
MO3-9
MO3-7
MO3-6
MO3-5
MO3-4
MO3-3
MO3-2
MO3-1
A
A
A
A
A
A
A
A
N
N
N
chalky dolomites
massive dolomites
marls with alveolinids
dolomites
marls without alveolinids
marls with abundant alveolinids and nummulitids
channel fill with abundant alveolinids an nummulitids
calcareous marls with abundant alveolinids and nummulitids
calcareous marls, limestones and dolomites with abundant alveolinids
calcareous marls with very few alveolinids
dolomites
marls and dolomites with few alveolinids

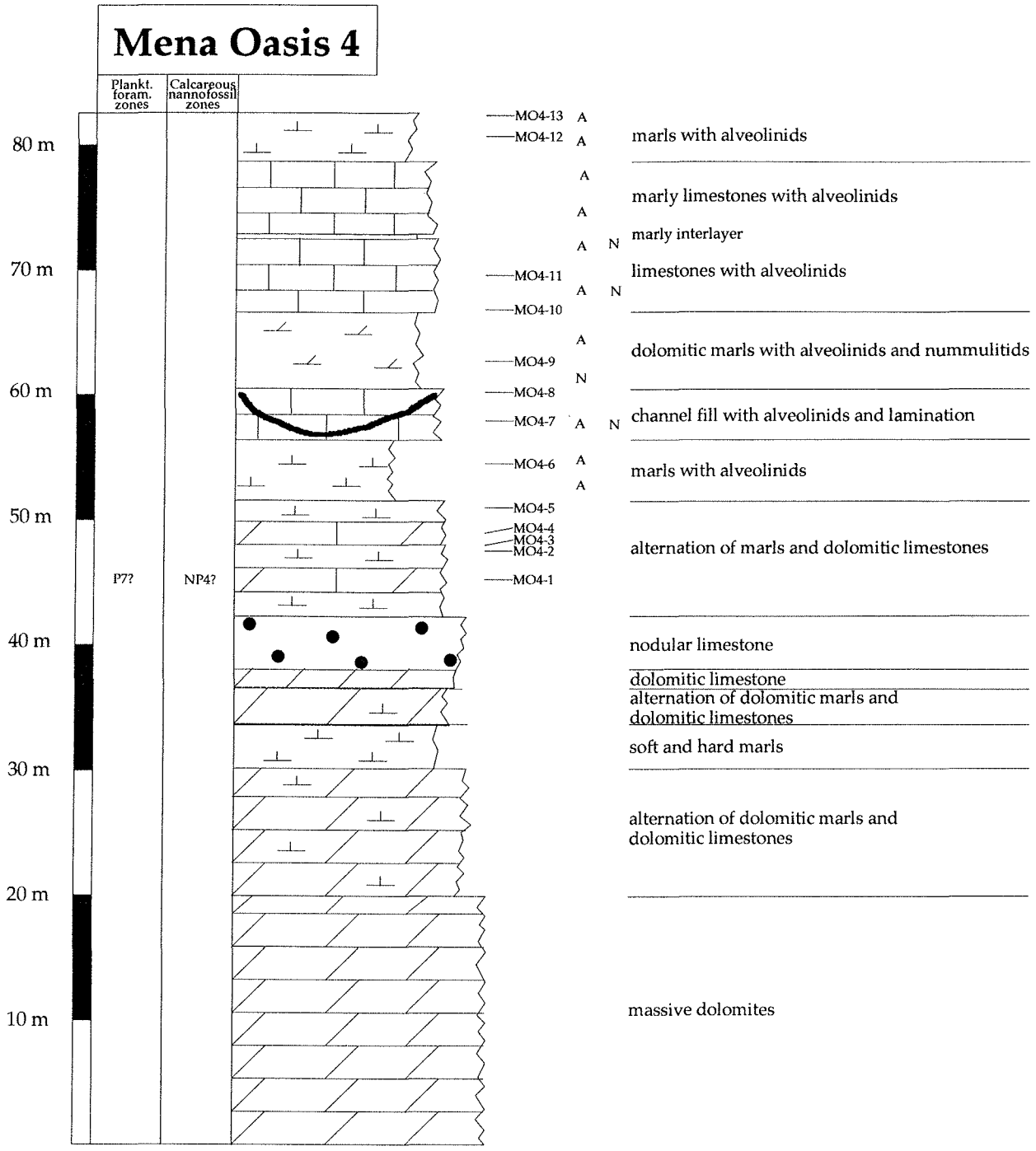
Mena Oasis 4
Plankt. foram. zones
Calcareous nannofossil zones
80 m
70 m
60 m
50 m
40 m
30 m
20 m
10 m
P7?
NP4?
MO4-13
MO4-12
MO4-11
MO4-10
MO4-9
MO4-8
MO4-7
MO4-6
MO4-5
MO4-4
MO4-3
MO4-2
MO4-1
A
N
marls with alveolinids
marly limestones with alveolinids
marly interlayer
limestones with alveolinids
dolomitic marls with alveolinids and nummulitids
channel fill with alveolinids and lamination
marls with alveolinids
alternation of marls and dolomitic limestones
nodular limestone
dolomitic limestone
alternation of dolomitic marls and dolomitic limestones
soft and hard marls
alternation of dolomitic marls and dolomitic limestones
massive dolomites

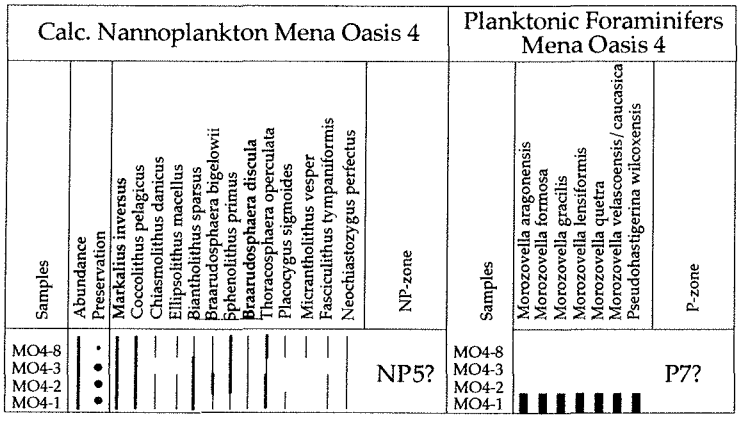
Calc. Nannoplankton Mena Oasis 4
Samples
Abundance
Preservation
Markalius inversus
Coccolithus pelagicus
Chiasmolithus danicus
Ellipsolithus macellus
Biantholithus sparsus
Braarudosphaera bigelowii
Sphenolithus primus
Braarudosphaera discula
Thoracosphaera operculata
Placocygus sigmoides
Micrantholithus vesper
Fasciculithus tympaniformis
Neochiastozygus perfectus
NP-zone
MO4-8
MO4-3
MO4-2
MO4-1
NP5?
Planktonic Foraminifers Mena Oasis 4
Samples
Morozovella aragonensis
Morozovella formosa
Morozovella gracilis
Morozovella lensiformis
Morozovella quetra
Morozovella velascoensis/caucasica
Pseudohastigerina wilcoxensis
P-zone
MO4-8
MO4-3
MO4-2
MO4-1
P7?

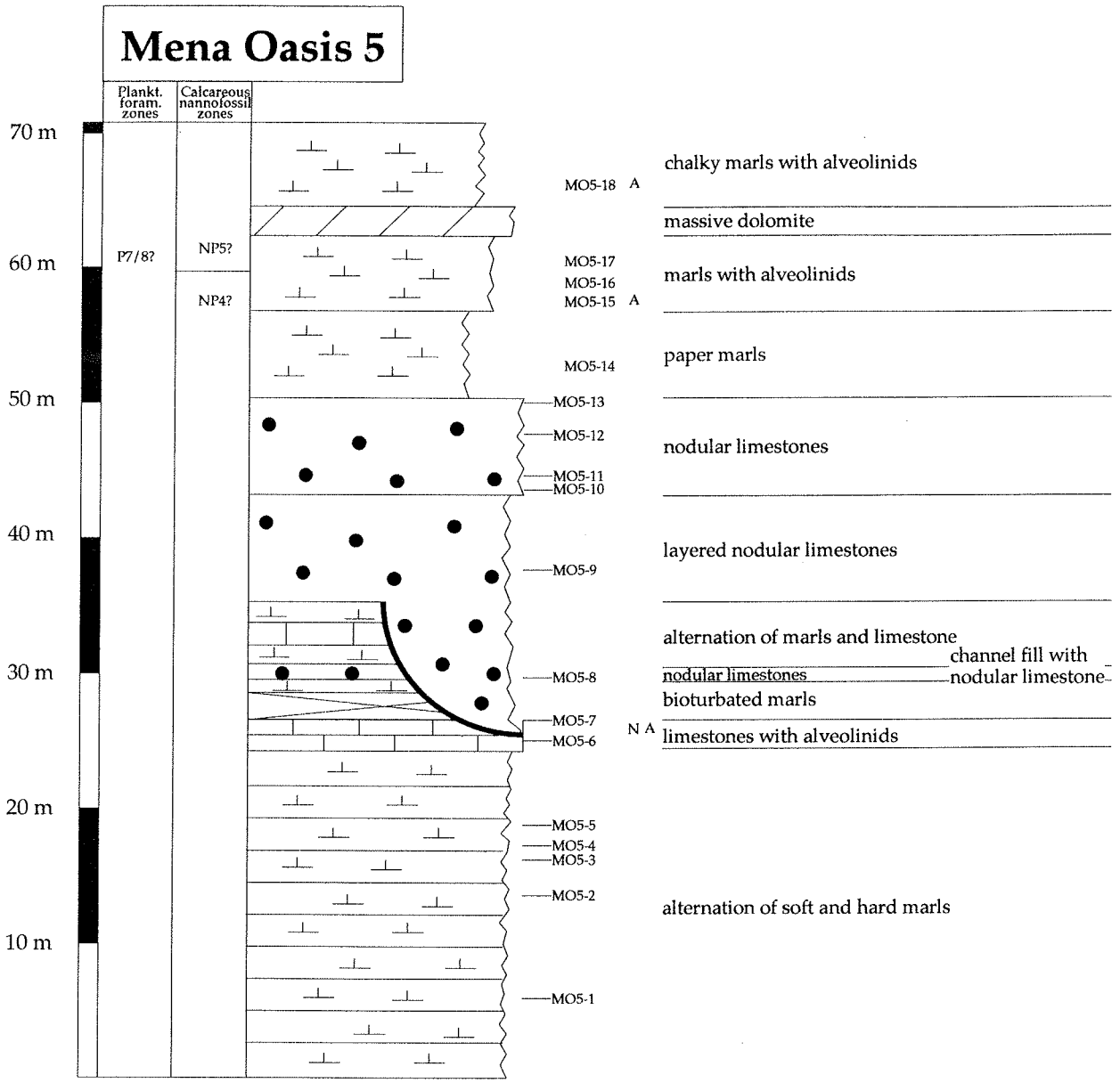
Mena Oasis 5
Plankt. foram. zones
Calcareous nannofossil zones
70 m
60 m
50 m
40 m
30 m
20 m
10 m
P7/8?
NP5?
NP4?
MO5-18 A
MO5-17
MO5-16
MO5-15 A
MO5-14
MO5-13
MO5-12
MO5-11
MO5-10
MO5-9
MO5-8
MO5-7
MO5-6
MO5-5
MO5-4
MO5-3
MO5-2
MO5-1
N A
chalky marls with alveolinids
massive dolomite
marls with alveolinids
paper marls
nodular limestones
layered nodular limestones
alternation of marls and limestone
channel fill with nodular limestone
nodular limestones
bioturbated marls
limestones with alveolinids
alternation of soft and hard marls

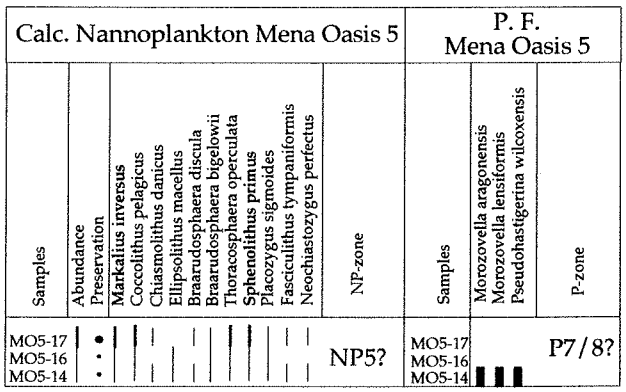
Calc. Nannoplankton Mena Oasis 5
P. F. Mena Oasis 5
Samples
Abundance
Preservation
Markalius inversus
Coccolithus pelagicus
Chiasmolithus danicus
Ellipsolithus macellus
Braarudosphaera discula
Braarudosphaera bigelowii
Thoracosphaera operculata
Sphenolithus primus
Placozygus sigmoides
Fasciculithus tympaniformis
Neochiastozygus perfectus
NP-zone
MO5-17
MO5-16
MO5-14
NP5?
Samples
Morozovella aragonensis
Morozovella lensiformis
Pseudohastigerina wilcoxensis
P-zone
MO5-17
MO5-16
MO5-14
P7/8?

Abu Darag 1

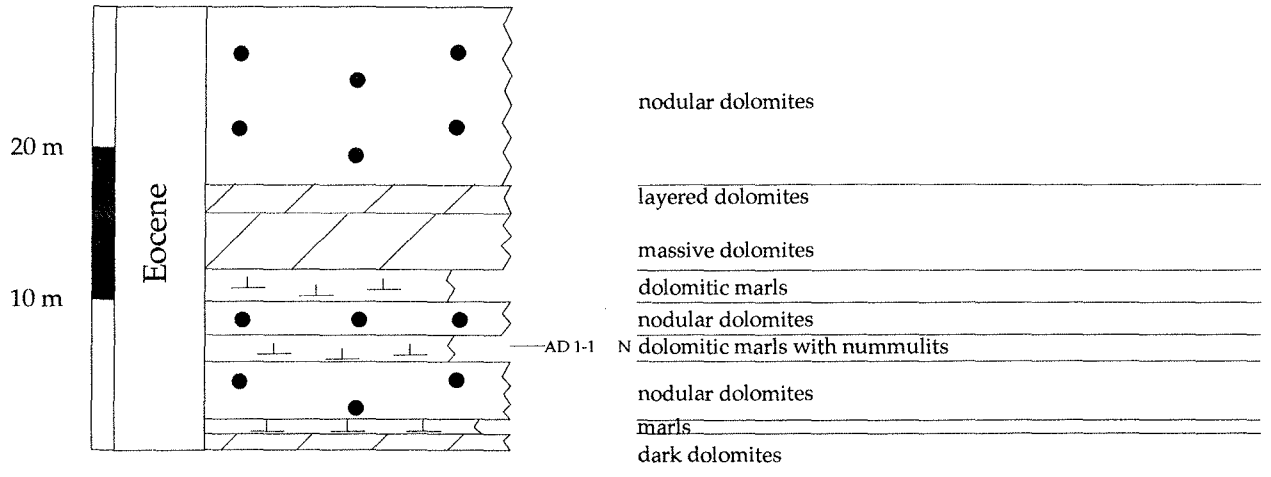
20 m
10 m
Eocene
AD 1-1
N
nodular dolomites
layered dolomites
massive dolomites
dolomitic marls
nodular dolomites
dolomitic marls with nummulits
nodular dolomites
marls
dark dolomites

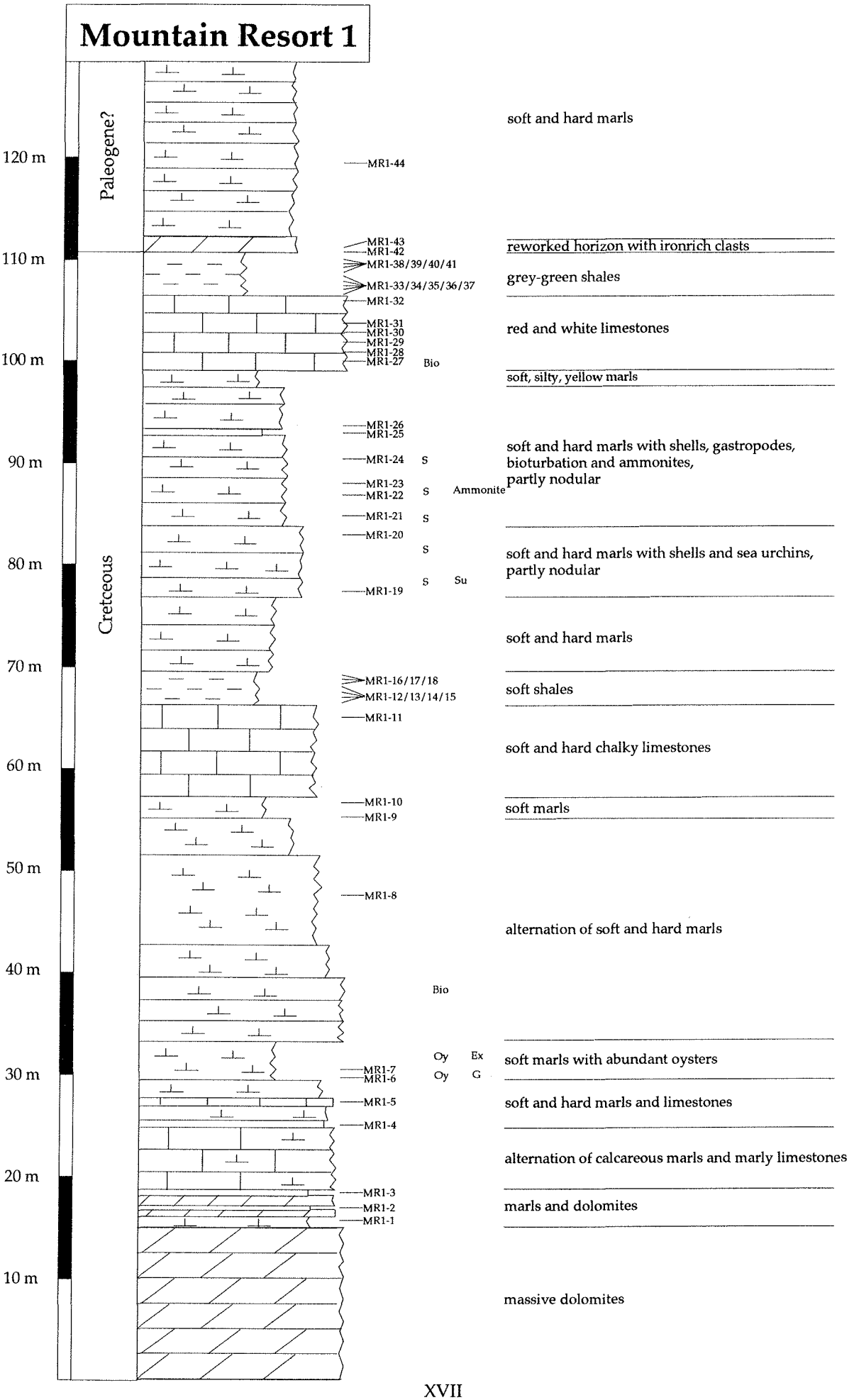
Mountain Resort 1
Paleogene?
Cretceous
120 m
110 m
100 m
90 m
80 m
70 m
60 m
50 m
40 m
30 m
20 m
10 m
MR1-44
MR1-43
MR1-42
MR1-38/39/40/41
MR1-33/34/35/36/37
MR1-32
MR1-31
MR1-30
MR1-29
MR1-28
MR1-27
Bio
MR1-26
MR1-25
MR1-24
S
MR1-23
MR1-22
S
Ammonite
MR1-21
S
MR1-20
S
S
Su
MR1-19
MR1-16/17/18
MR1-12/13/14/15
MR1-11
MR1-10
MR1-9
MR1-8
Bio
Oy
Ex
MR1-7
Oy
G
MR1-6
MR1-5
MR1-4
MR1-3
MR1-2
MR1-1
soft and hard marls
reworked horizon with ironrich clasts
grey-green shales
red and white limestones
soft, silty, yellow marls
soft and hard marls with shells, gastropodes, bioturbation and ammonites, partly nodular
soft and hard marls with shells and sea urchins, partly nodular
soft and hard marls
soft shales
soft and hard chalky limestones
soft marls
alternation of soft and hard marls
soft marls with abundant oysters
soft and hard marls and limestones
alternation of calcareous marls and marly limestones
marls and dolomites
massive dolomites

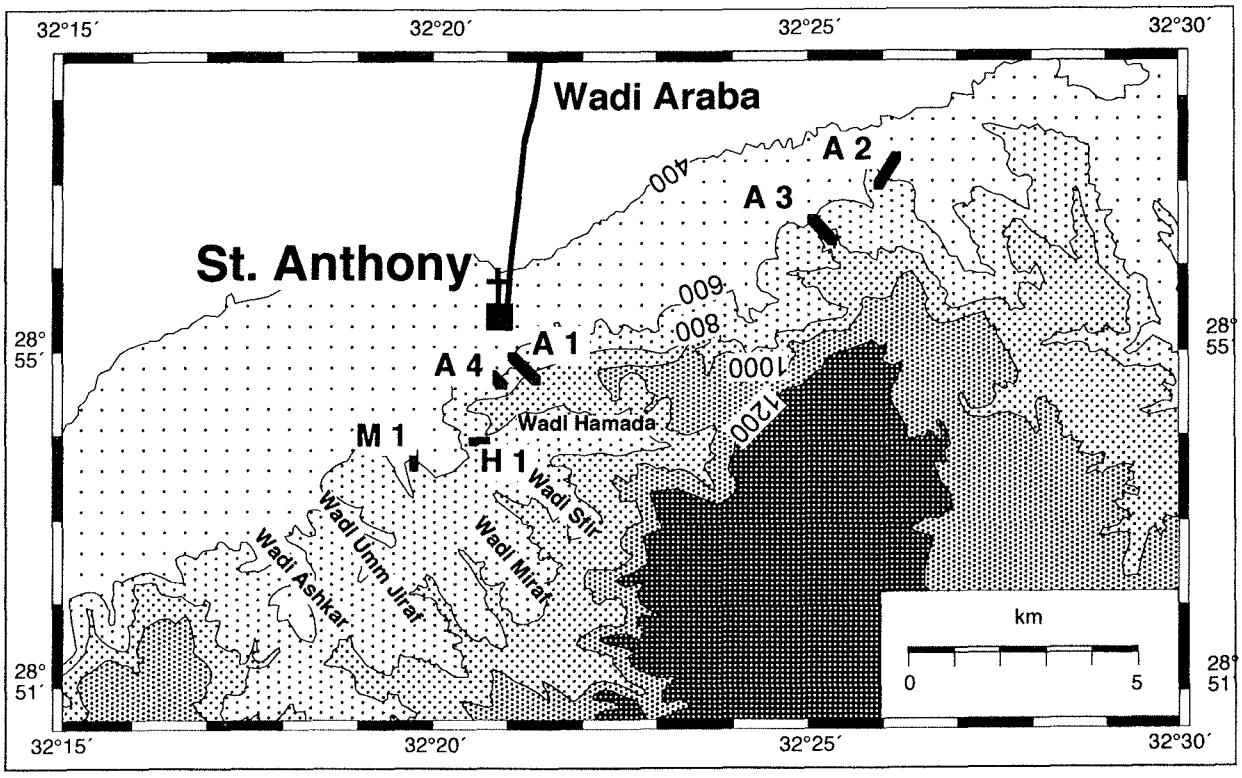
32°15´
32°20´
32°25´
32°30´
Wadi Araba
St. Anthony
A 2
A 3
A 1
A 4
M 1
H 1
Wadi Hamada
Wadi Stir
Wadi Mirat
Wadi Umm Jirat
Wadi Ashkar
400
600
800
1000
1200
28° 55´
28° 51´
km
0
5

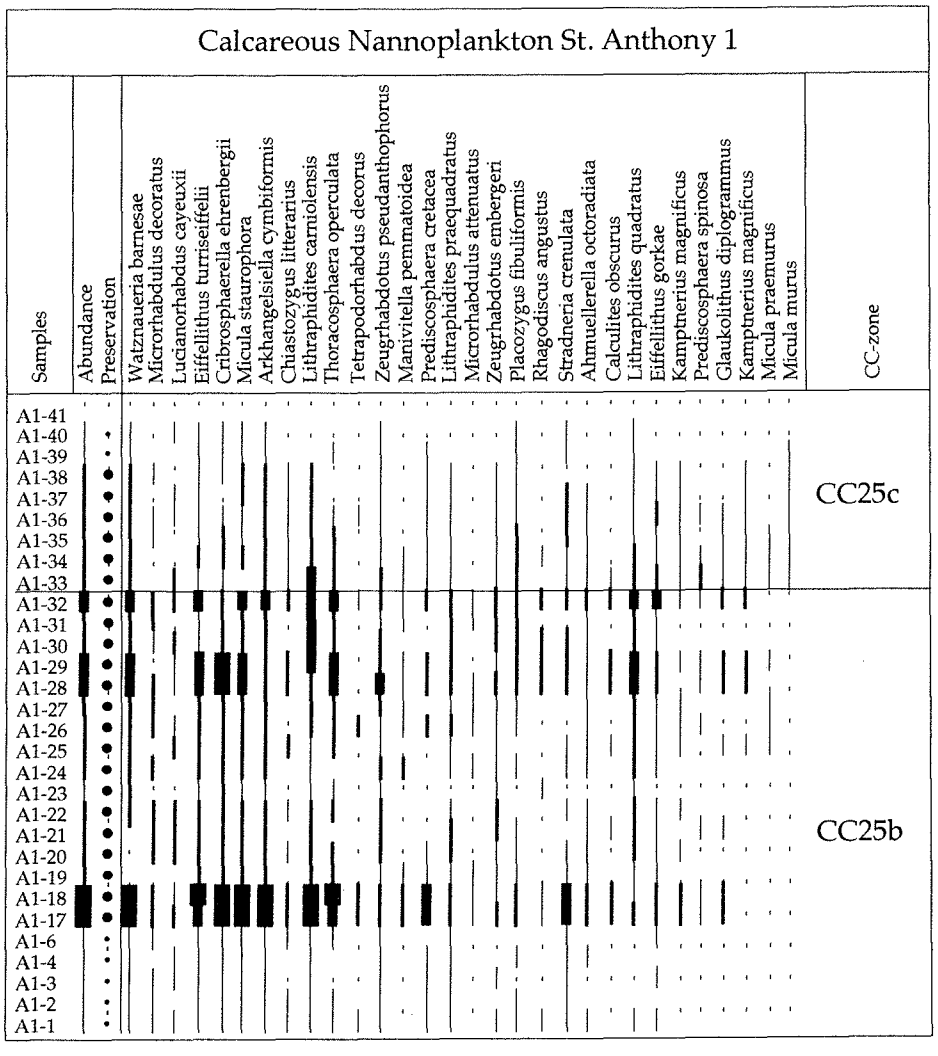
Calcareous Nannoplankton St. Anthony 1
Samples
Abundance
Preservation
Watznaueria barnesae
Microrhabdulus decoratus
Lucianorhabdus cayeuxii
Eiffellithus turriseiffelii
Cribrosphaerella ehrenbergii
Micula staurophora
Arkhangelsiella cymbiformis
Chiastozygus litterarius
Lithraphidites carniolensis
Thoracosphaera operculata
Tetrapodorhabdus decorus
Zeugrhabdotus pseudanthophorus
Manivitella pemmatoidea
Prediscosphaera cretacea
Lithraphidites praequadratus
Microrhabdulus attenuatus
Zeugrhabdotus emberger
Placozygus fibuliformis
Rhagodiscus angustus
Stradneria crenulata
Ahmuellerella octoradiata
Calculites obscurus
Lithraphidites quadratus
Eiffellithus gorkae
Kamptnerius magnificus
Prediscosphaera spinosa
Glaukolithus diplogrammus
Kamptnerius magnificus
Micula praemurus
Micula murus
CC-zone
A1-41
A1-40
A1-39
A1-38
A1-37
A1-36
A1-35
A1-34
A1-33
A1-32
A1-31
A1-30
A1-29
A1-28
A1-27
A1-26
A1-25
A1-24
A1-23
A1-22
A1-21
A1-20
A1-19
A1-18
A1-17
A1-6
A1-4
A1-3
A1-2
A1-1
CC25c
CC25b

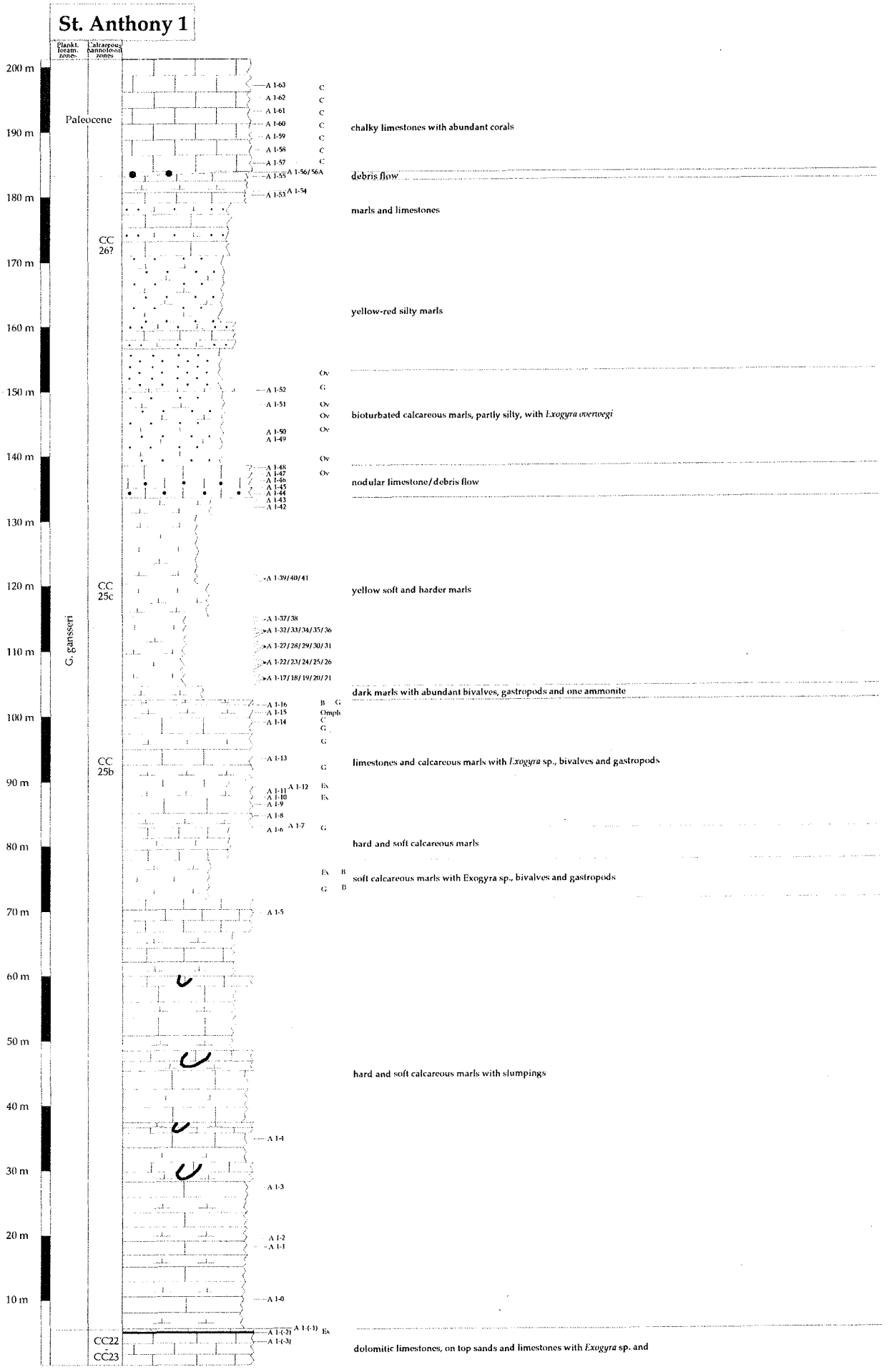
St. Anthony 1
Plankt. foram. zones
Calcareous nannofossil zones
200 m
190 m
180 m
170 m
160 m
150 m
140 m
130 m
120 m
110 m
100 m
90 m
80 m
70 m
60 m
50 m
40 m
30 m
20 m
10 m
Paleocene
G. gansseri
CC 26?
CC 25c
CC 25b
CC22
CC23
A 1-63
A 1-62
A 1-61
A 1-60
A 1-59
A 1-58
A 1-57
A 1-56/56A
A 1-55
A 1-54
A 1-53
A 1-52
A 1-51
A 1-50
A 1-49
A 1-48
A 1-47
A 1-46
A 1-45
A 1-44
A 1-43
A 1-42
A 1-39/40/41
A 1-37/38
A 1-32/33/34/35/36
A 1-27/28/29/30/31
A 1-22/23/24/25/26
A 1-17/18/19/20/21
A 1-16
A 1-15
A 1-14
A 1-13
A 1-12
A 1-11
A 1-10
A 1-9
A 1-8
A 1-7
A 1-6
A 1-5
A 1-4
A 1-3
A 1-2
A 1-1
A 1-0
A 1(-1)
A 1(-2)
A 1(-3)
chalky limestones with abundant corals
debris flow
marls and limestones
yellow-red silty marls
bioturbated calcareous marls, partly silty, with Exogyra overwegi
nodular limestone/debris flow
yellow soft and harder marls
dark marls with abundant bivalves, gastropods and one ammonite
limestones and calcareous marls with Exogyra sp., bivalves and gastropods
hard and soft calcareous marls
soft calcareous marls with Exogyra sp., bivalves and gastropods
hard and soft calcareous marls with slumpings
dolomitic limestones, on top sands and limestones with Exogyra sp. and

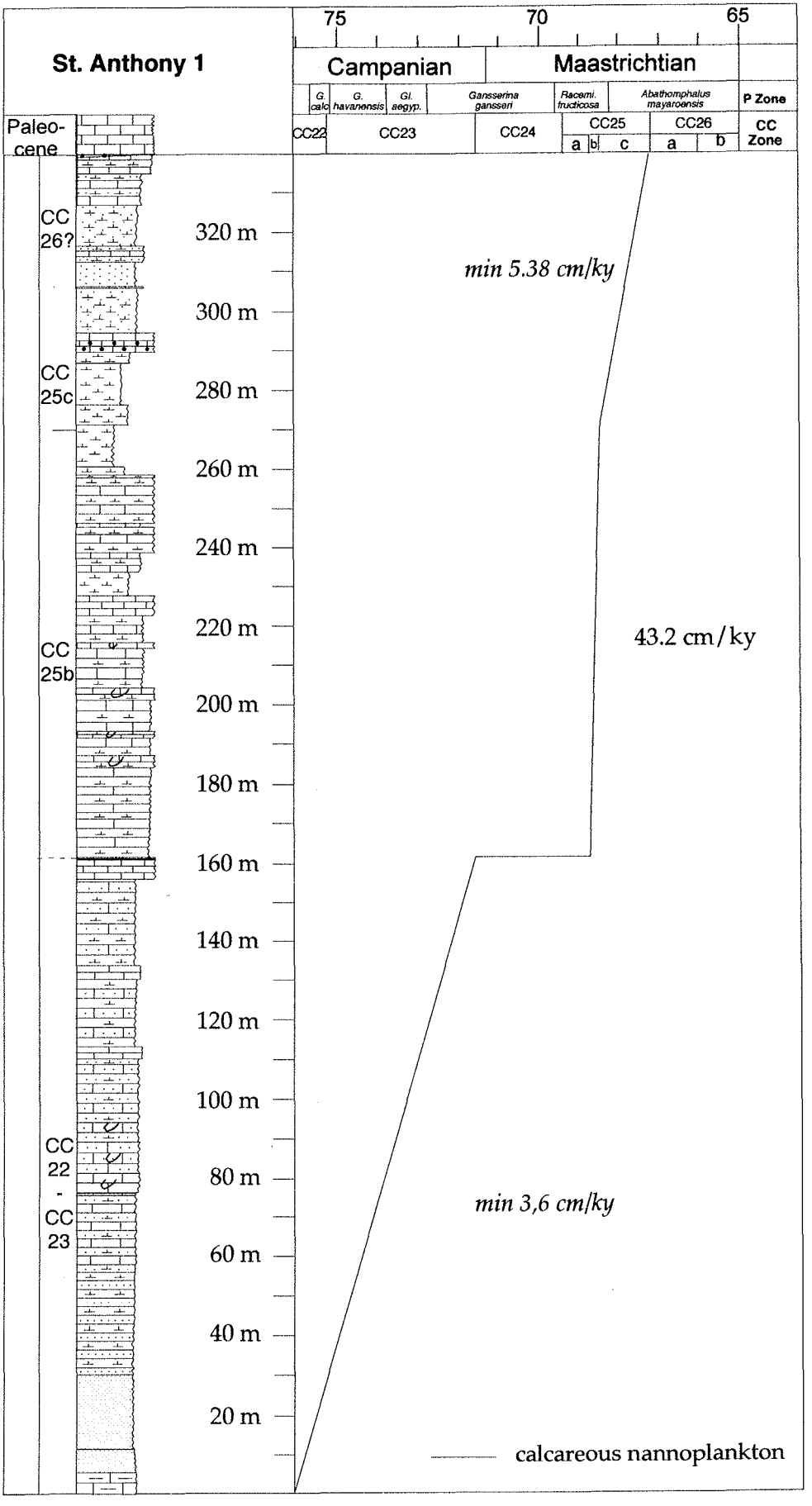
St. Anthony 1
75
70
65
Campanian
Maastrichtian
G. calc
G. havanensis
Gl. aegyp.
Gansserina gansseri
Racemi. fructicosa
Abathomphalus mayaroensis
P Zone
Paleo-cene
CC22
CC23
CC24
CC25
a
b
c
CC26
a
b
CC Zone
CC 26?
CC 25c
CC 25b
CC 22 - CC 23
320 m
300 m
280 m
260 m
240 m
220 m
200 m
180 m
160 m
140 m
120 m
100 m
80 m
60 m
40 m
20 m
min 5.38 cm/ky
43.2 cm/ky
min 3,6 cm/ky
calcareous nannoplankton

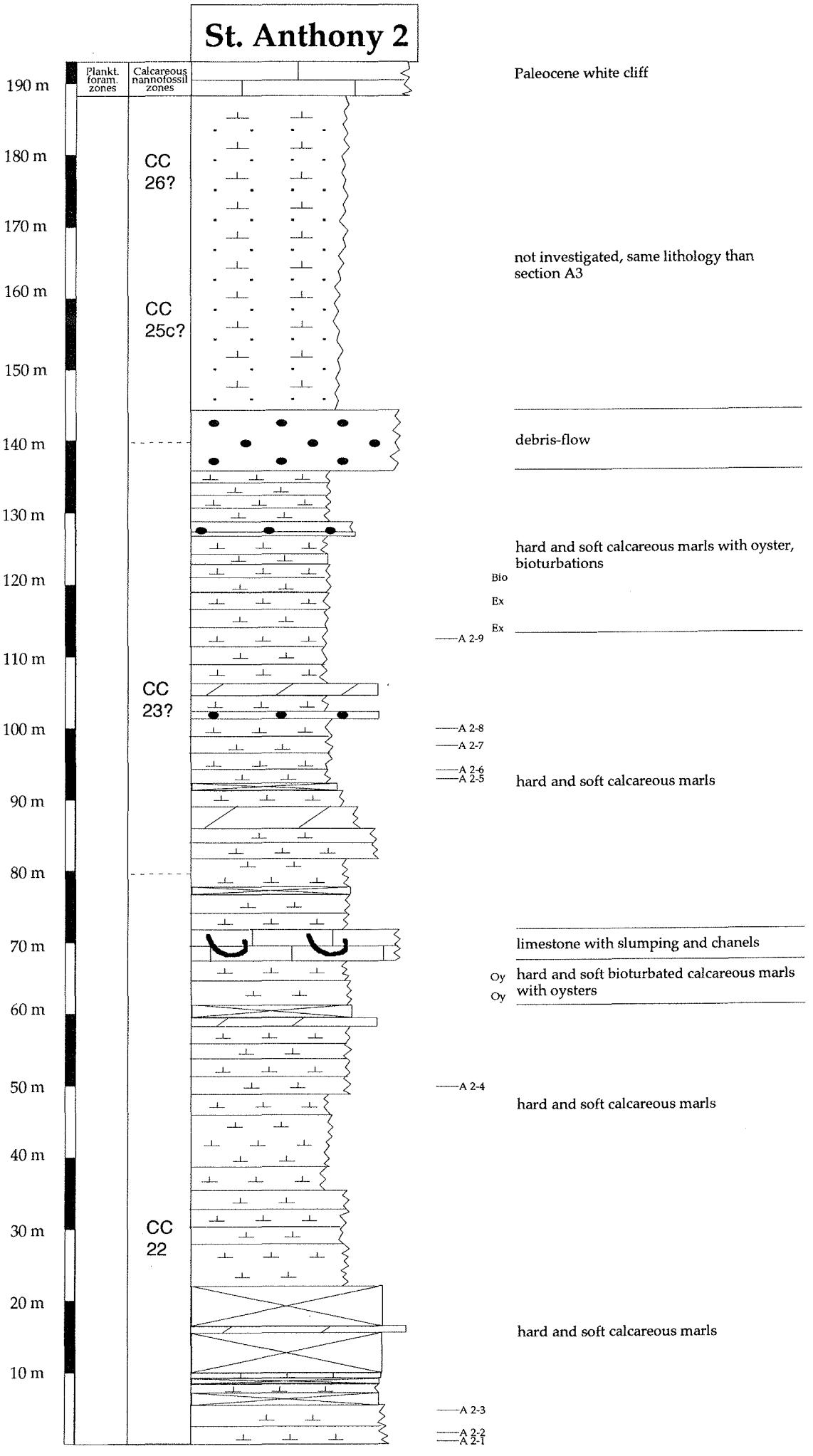
St. Anthony 2
Plankt. foram. zones
Calcareous nannofossil zones
190 m
180 m
170 m
160 m
150 m
140 m
130 m
120 m
110 m
100 m
90 m
80 m
70 m
60 m
50 m
40 m
30 m
20 m
10 m
CC 26?
CC 25c?
CC 23?
CC 22
Paleocene white cliff
not investigated, same lithology than section A3
debris-flow
hard and soft calcareous marls with oyster, bioturbations
Bio
Ex
Ex
A 2-9
A 2-8
A 2-7
A 2-6
A 2-5
hard and soft calcareous marls
limestone with slumping and chanels
Oy
hard and soft bioturbated calcareous marls with oysters
Oy
A 2-4
hard and soft calcareous marls
hard and soft calcareous marls
A 2-3
A 2-2
A 2-1

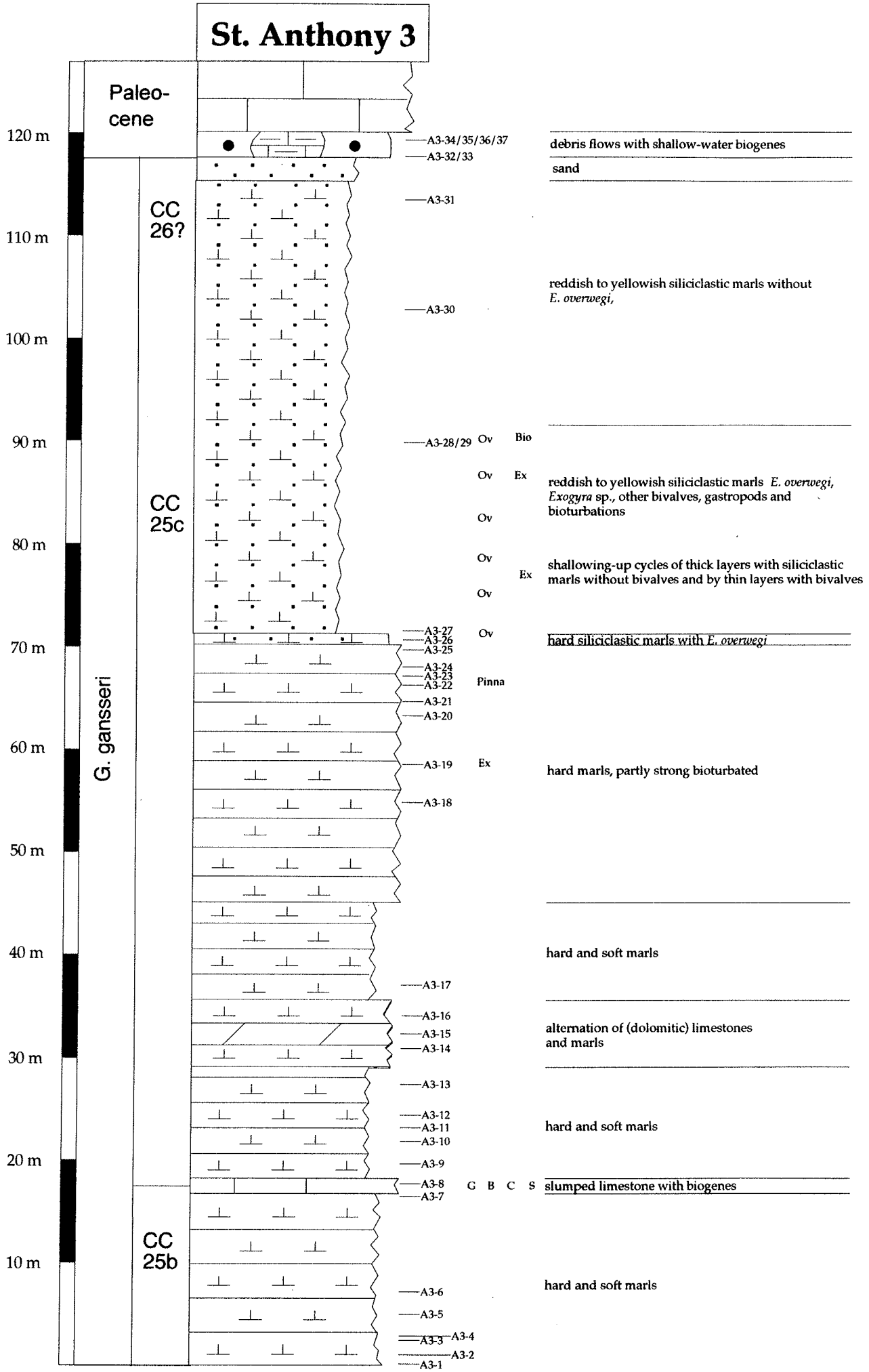
St. Anthony 3
Paleo-
cene
CC
26?
CC
25c
CC
25b
G. gansseri
120 m
110 m
100 m
90 m
80 m
70 m
60 m
50 m
40 m
30 m
20 m
10 m
A3-34/35/36/37
A3-32/33
A3-31
A3-30
A3-28/29
A3-27
A3-26
A3-25
A3-24
A3-23
A3-22
A3-21
A3-20
A3-19
A3-18
A3-17
A3-16
A3-15
A3-14
A3-13
A3-12
A3-11
A3-10
A3-9
A3-8
A3-7
A3-6
A3-5
A3-4
A3-3
A3-2
A3-1
Ov
Bio
Ex
Pinna
G B C S
debris flows with shallow-water biogenes
sand
reddish to yellowish siliciclastic marls without E. overwegi,
reddish to yellowish siliciclastic marls E. overwegi, Exogyra sp., other bivalves, gastropods and bioturbations
shallowing-up cycles of thick layers with siliciclastic marls without bivalves and by thin layers with bivalves
hard siliciclastic marls with E. overwegi
hard marls, partly strong bioturbated
hard and soft marls
alternation of (dolomitic) limestones and marls
hard and soft marls
slumped limestone with biogenes
hard and soft marls

Calcareous Nannoplankton St. Anthony 2
Samples
A2-1
A2-2
A2-3
A2-4
A2-5
A2-6
A2-7
A2-8
A2-9
Abundance
Preservation
Watznaueria barnesae
Micula starurophora
Zeugrhabdotus pseudanthophorus
Microrhabdulus decoratus
Cribrosphaerella ehrenbergii
Lucianorhabdulus cayeuxii
Eiffellithus turriseiffelii
Tetrapodorhabdus decorus
Manivitella pemmatoidea
Arkhangelskiella cymbiformis
Lithraphidites carniolensis
Prediscosphaera cretacea
Eiffellithus eximus
Aspidolithus parcus constrictus
Reinhardtites anthophorus
Rhagodiscus angustus
Stradneria crenulata
Chiastozygus litterarius
Thoracosphaera operculata
Reinhardtites levis
Tranolithus manifestus
Micula concava
Quadrum gothicum
CC22
CC-zone
Planktic Foraminifers St. Anthony 2
Samples
Globotruncana arca
Globotruncana insignis
Globotruncana linneiana
Globotruncana mariei
Globotruncana orientalis
Globotruncana rosetta
Rosita fornicata
Globotruncanita stuartiformis
G. falsostuarti
G. elevata
Plankton-zone
Calcareous Nannoplankton St. Anthony 3
Samples
A3-1
A3-2
A3-3
A3-4
A3-5
A3-6
A3-7
A3-9
A3-10
A3-11
A3-12
A3-13
A3-14
A3-15
A3-16
A3-17
A3-30
Abundance
Preservation
Watznaueria barnesae
Arkhangelskiella cymbiformis
Cribrosphaerella ehrenbergii
Micula staurophora
Prediscoshaera cretacea
Lucianorhabdus cayeuxii
Microrhabdulus decoratus
Thoracosphaera operculata
Lithraphidites carniolensis
Eiffellithus turriseiffelii
Zeugrhabdotus pseudanthophorus
Tetrapodorhabdus decorus
Chiastozygus litteraius
Kamptnerius magnificus
Stradneria crenulata
Prediscospaera spinosa
Lithraphidites quadratus
Ahmuellerella octoradiata
Eiffellithus gorkae
Micula praemurus
Micula murus
Placozygus fibuliformis
CC25b
CC25c
CC-zone
Calcareous Nannoplankton St. Anthony 4
Samples
A4-1
Abundance
Preservation
Arkhangelskiella cymbiformis
Watznaueria barnesae
Lithraphidites carniolensis
Cribrosphaerella ehrenbergii
Eiffellithus turriseiffelii
Zeugrhabdotus pseudanthophorus
Prediscosphaera cretacea
Lucianorhabdulus cayeuxii
Micula staurophora
Reinhardtites anthophorus
Rhagodiscus angustus
Tranolithus manifestus
Tranolithus phacelosus
Microrhabdulus decoratus
Tetrapodorhabdus decorus
Aspidolithus parcus constrictus
Manivitella pemmatoidea
Thoracosphaera operculata
Chiastozygus litterarius
Stradneria crenulata
Glaukolithus diplogrammus
Quadrum trifidum
Micula concava
Calculites obscurus
Reinhardtites levis
Quadrum gothicum
CC22
CC-zone

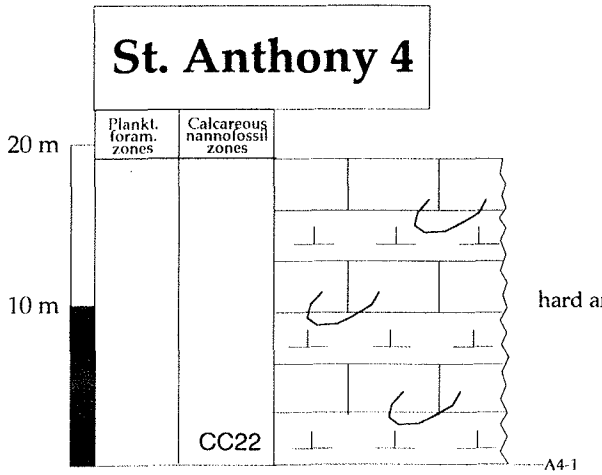

hard and soft marls with large synsedimentary slumps

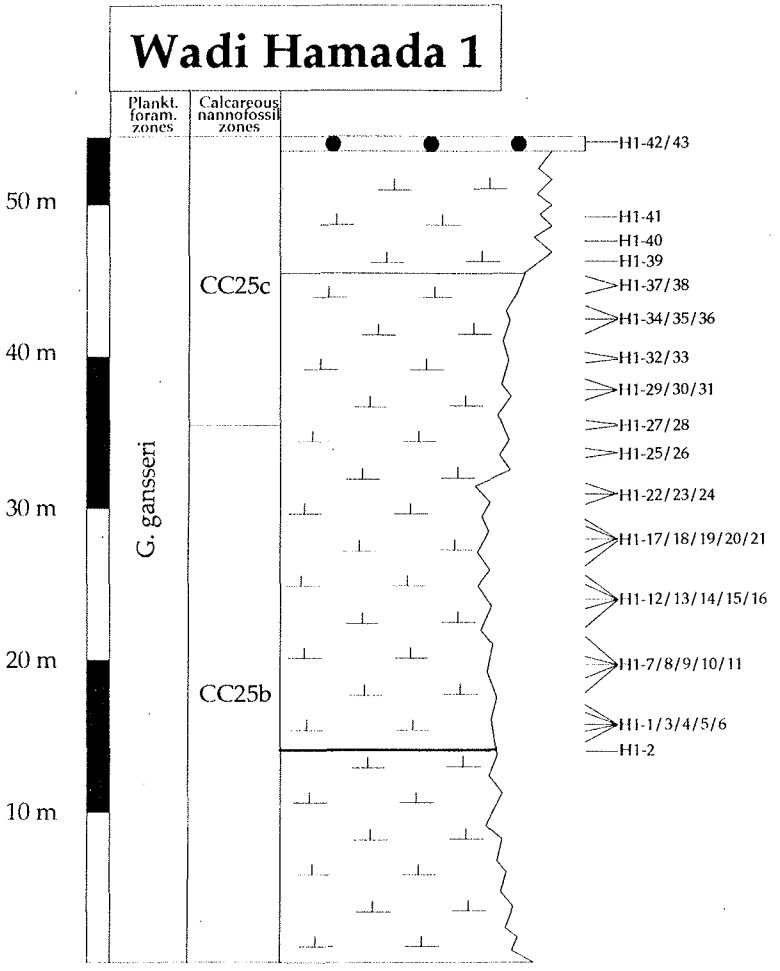

massive marls with debris flows

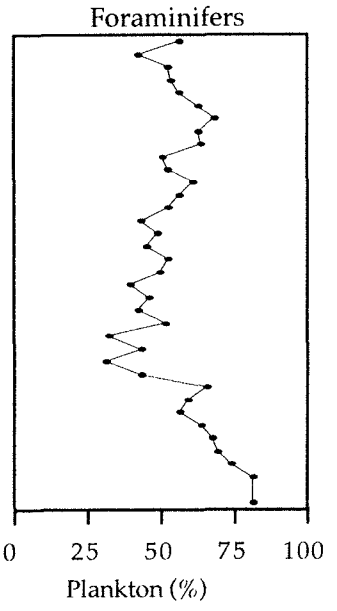

alternation of hard and soft marls

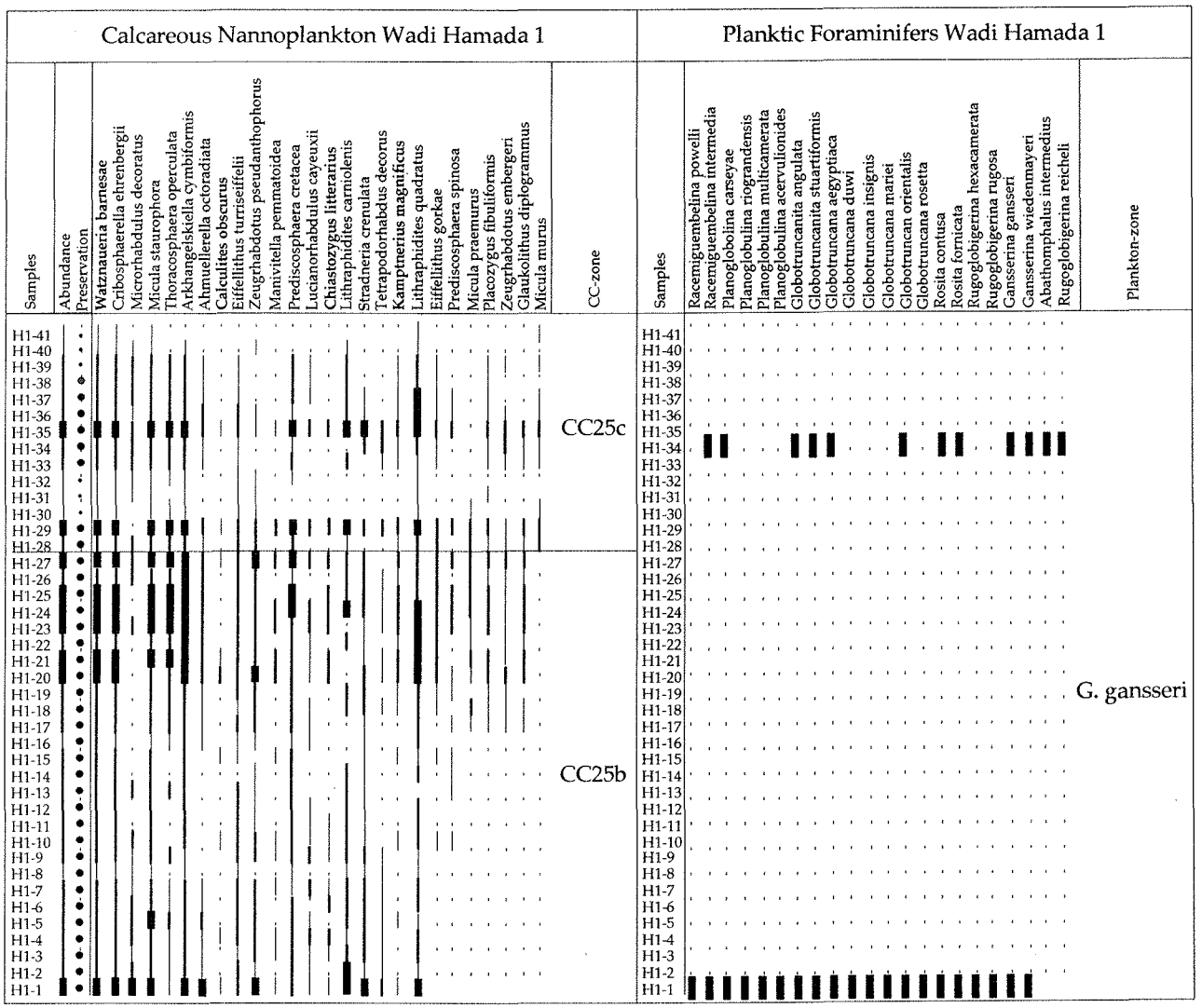
Calcareous Nannoplankton Wadi Hamada 1
Planktic Foraminifers Wadi Hamada 1
Samples
Abundance
Preservation
Watznaueria barnesae
Cribosphaerella ehrenbergii
Microrhabdulus decoratus
Micula staurophora
Thoracosphaera operculata
Arkhangelskiella cymbiformis
Ahmuellerella octoradiata
Calculites obscurus
Eiffellithus turriseiffelii
Zeugrhabdotus pseudanthophorus
Manivitella pemmatoidea
Prediscosphaera cretacea
Lucianorhabdus cayeuxii
Chiastozygus litterarius
Lithraphidites carniolenis
Stradneria crenulata
Tetrapodorhabdus decorus
Kamptnerius magnificus
Lithraphidites quadratus
Eiffellithus gorkae
Prediscosphaera spinosa
Micula praemurus
Placozygus fibuliformis
Zeugrhabdotus embergeri
Glaukolithus diplogrammus
Micula murus
CC-zone
CC25c
CC25b
Racemiguembelina powelli
Racemiguembelina intermedia
Planoglobolina carseyae
Planoglobulina riograndensis
Planoglobulina multicamerata
Planoglobulina acervulinoides
Globotruncanita angulata
Globotruncanita stuartiformis
Globotruncana aegyptiaca
Globotruncana duwi
Globotruncana insignis
Globotruncana marei
Globotruncan orientalis
Globotruncana rosetta
Rosita contusa
Rosita fornicata
Rugoglobigerina hexacamerata
Rugoglobigerina rugosa
Gansserina gansseri
Gansserina wiedenmayeri
Abathomphalus intermedius
Rugoglobigerina reicheli
Plankton-zone
G. gansseri

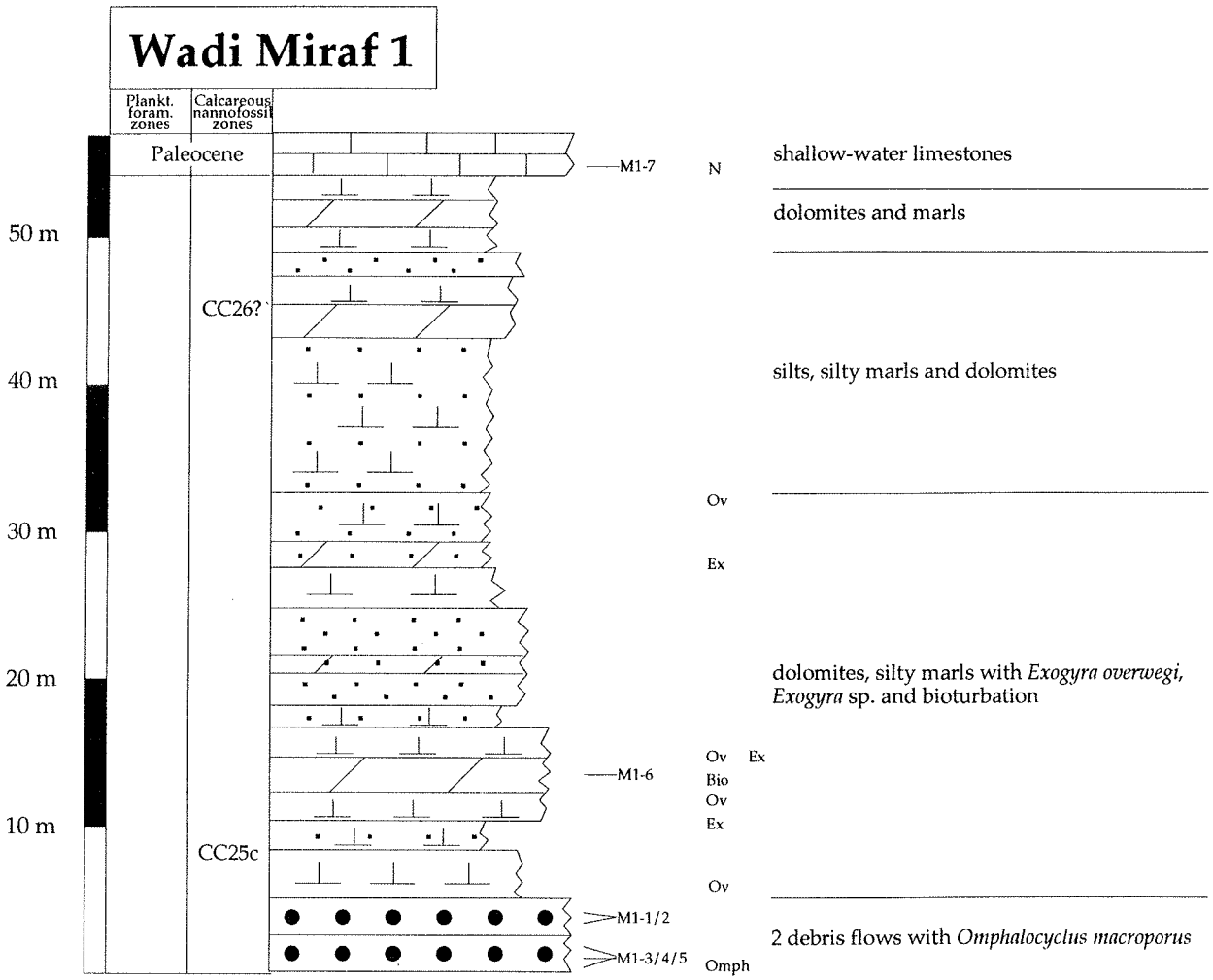
Wadi Miraf 1
Plankt. foram. zones
Calcareous nannofossil zones
Paleocene
CC26?
CC25c
50 m
40 m
30 m
20 m
10 m
M1-7
M1-6
M1-1/2
M1-3/4/5
N
Ov
Ex
Ov Ex
Bio
Ov
Ex
Ov
Omph
shallow-water limestones
dolomites and marls
silts, silty marls and dolomites
dolomites, silty marls with Exogyra overwegi, Exogyra sp. and bioturbation
2 debris flows with Omphalocyclus macroporus

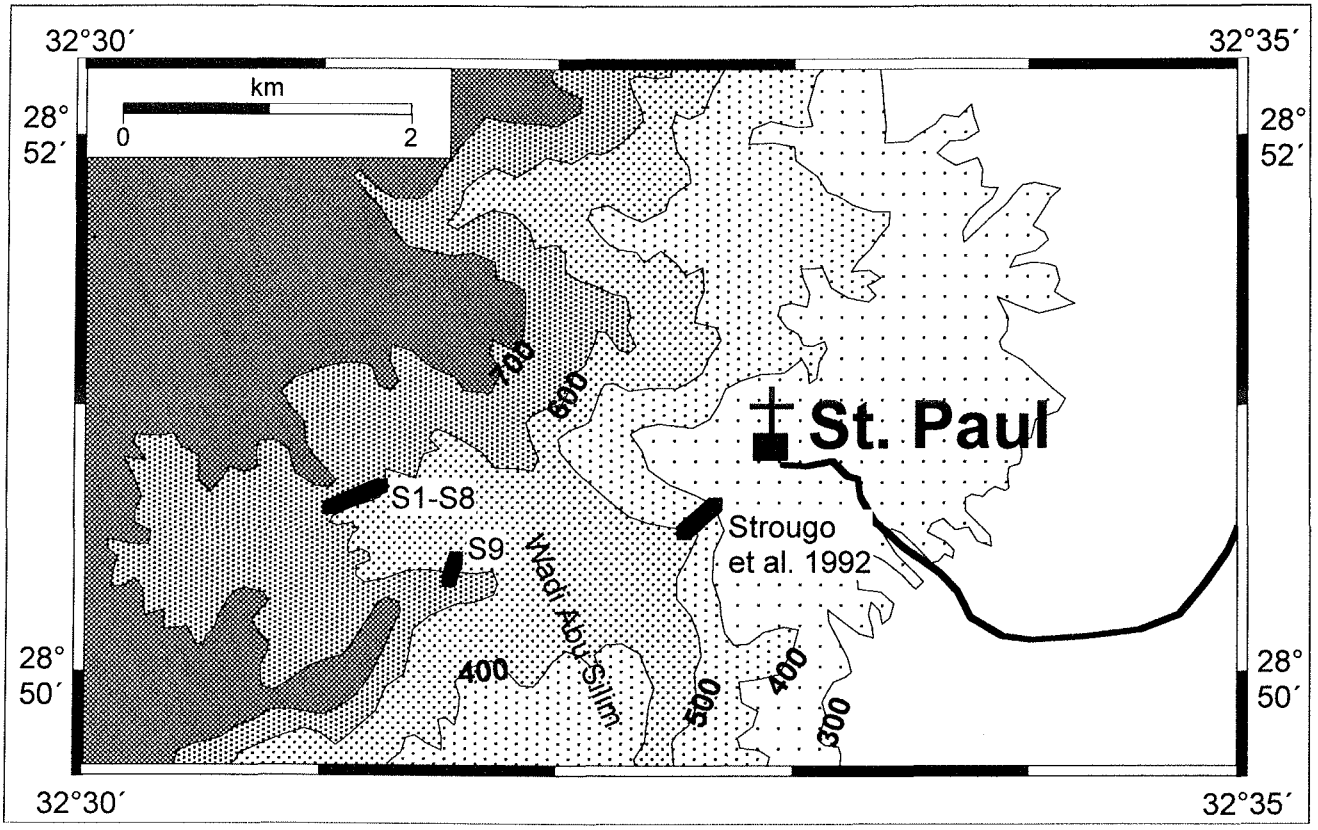
32°30′
32°35′
28°
52′
28°
50′
km
0
2
700
600
St. Paul
S1-S8
S9
Wadi Abu Silim
Strougo
et al. 1992
400
500
400
300

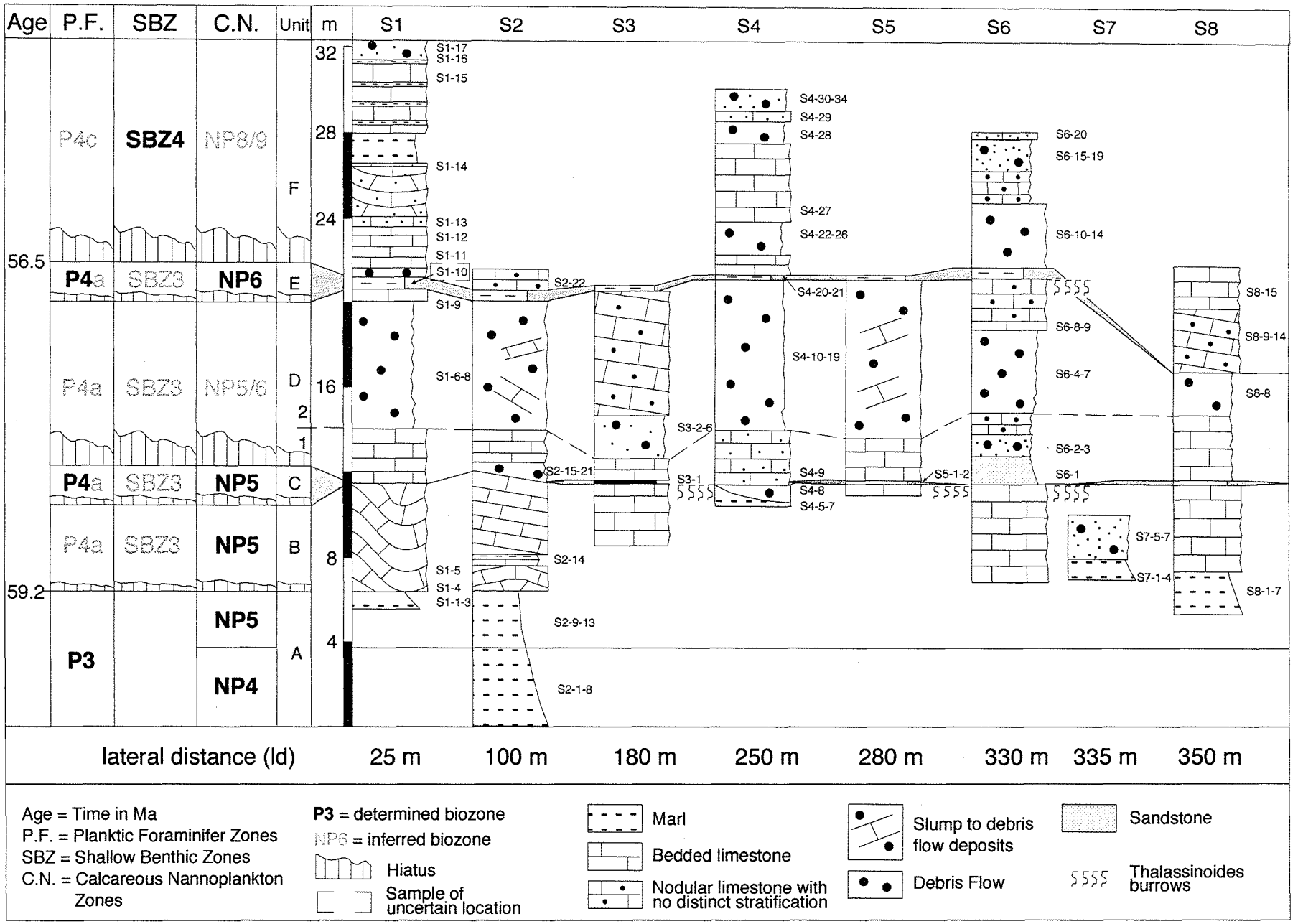
Age
P.F.
SBZ
C.N.
Unit
m
S1
S2
S3
S4
S5
S6
S7
S8
32
28
24
16
8
4
56.5
59.2
P4c
SBZ4
NP8/9
F
P4a
SBZ3
NP6
E
P4a
SBZ3
NP5/6
D
2
1
P4a
SBZ3
NP5
C
P4a
SBZ3
NP5
B
NP5
P3
NP4
A
S1-17
S1-16
S1-15
S1-14
S1-13
S1-12
S1-11
S1-10
S1-9
S1-6-8
S1-5
S1-4
S1-1-3
S2-22
S2-15-21
S2-14
S2-9-13
S2-1-8
S3-2-6
S3-1
S4-30-34
S4-29
S4-28
S4-27
S4-22-26
S4-20-21
S4-10-19
S4-9
S4-8
S4-5-7
S5-1-2
S6-20
S6-15-19
S6-10-14
S6-8-9
S6-4-7
S6-2-3
S6-1
S7-5-7
S7-1-4
S8-15
S8-9-14
S8-8
S8-1-7
lateral distance (ld)
25 m
100 m
180 m
250 m
280 m
330 m
335 m
350 m
Age = Time in Ma
P.F. = Planktic Foraminifer Zones
SBZ = Shallow Benthic Zones
C.N. = Calcareous Nannoplankton Zones
P3 = determined biozone
NP6 = inferred biozone
Hiatus
Sample of uncertain location
Marl
Bedded limestone
Nodular limestone with no distinct stratification
Slump to debris flow deposits
Debris Flow
Sandstone
Thalassinoides burrows

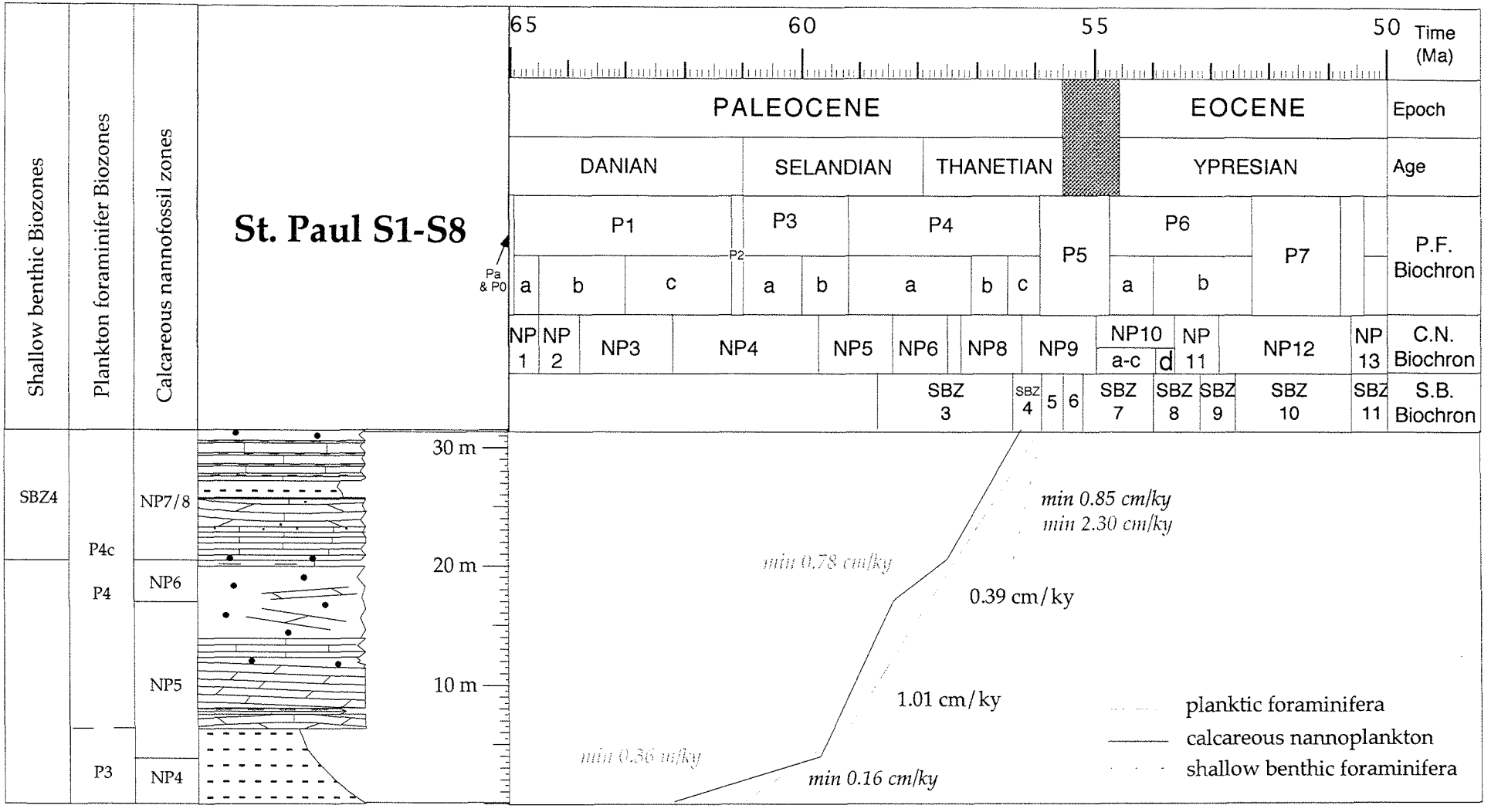
St. Paul S1-S8
Shallow benthic Biozones
Plankton foraminifer Biozones
Calcareous nannofossil zones
65
60
55
50
Time (Ma)
PALEOCENE
EOCENE
Epoch
DANIAN
SELANDIAN
THANETIAN
YPRESIAN
Age
P1
P2
P3
P4
P5
P6
P7
Pa & P0
a
b
c
P.F. Biochron
NP 1
NP 2
NP3
NP4
NP5
NP6
NP8
NP9
NP10
a-c
d
NP 11
NP12
NP 13
C.N. Biochron
SBZ 3
SBZ 4
5
6
SBZ 7
SBZ 8
SBZ 9
SBZ 10
SBZ 11
S.B. Biochron
SBZ4
P4c
P4
P3
NP7/8
NP6
NP5
NP4
30 m
20 m
10 m
min 0.85 cm/ky
min 2.30 cm/ky
min 0.78 cm/ky
0.39 cm/ky
1.01 cm/ky
min 0.36 m/ky
min 0.16 cm/ky
planktic foraminifera
calcareous nannoplankton
shallow benthic foraminifera

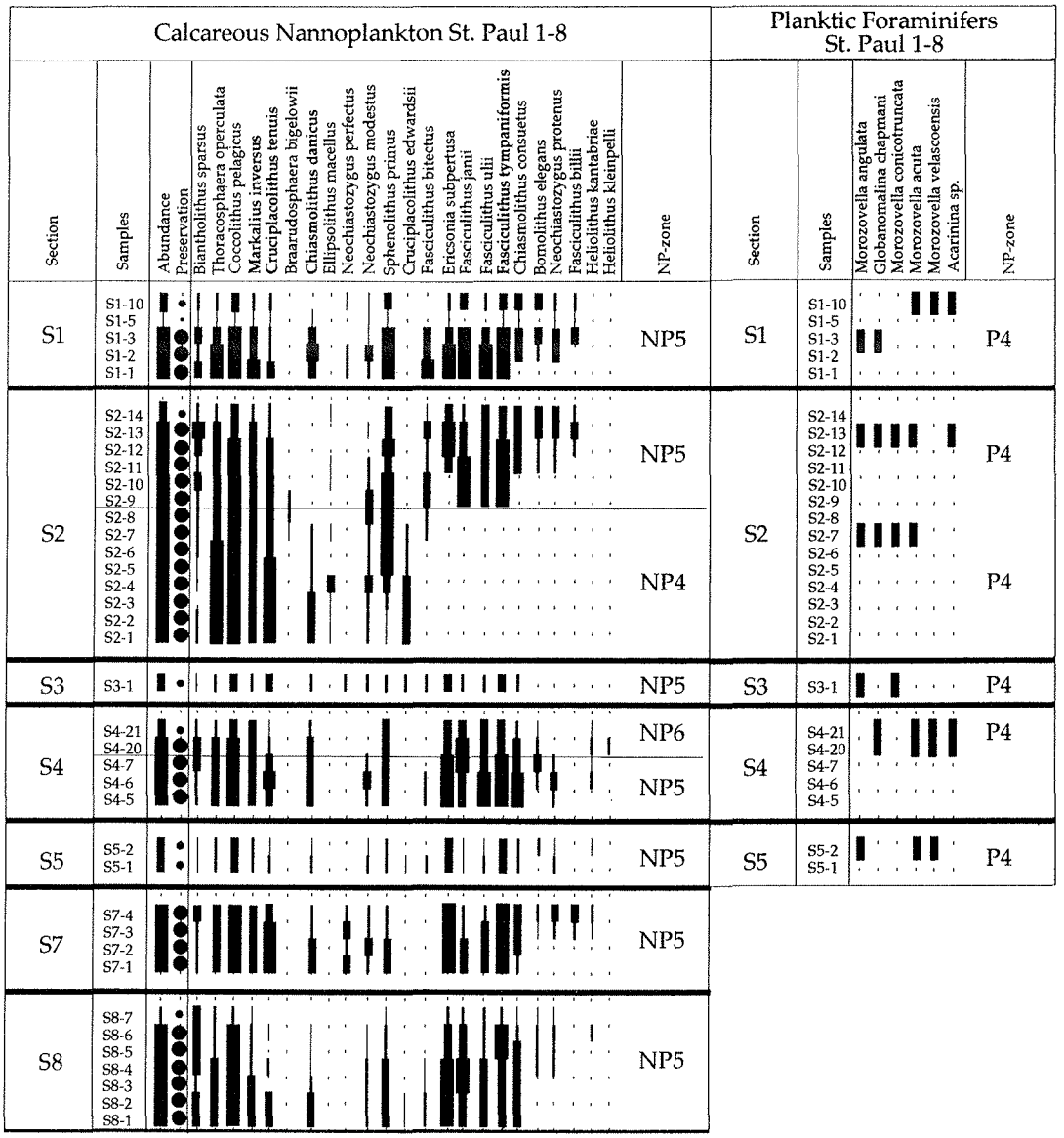
Calcareous Nannoplankton St. Paul 1-8
Planktic Foraminifers St. Paul 1-8
Section
Samples
Abundance
Preservation
Biantholithus sparsus
Thoracosphaera operculata
Coccolithus pelagicus
Markalius inversus
Cruciplacolithus tenuis
Braarudosphaera bigelowii
Chiasmolithus danicus
Ellipsolithus macellus
Neochiastozygus perfectus
Neochiastozygus modestus
Sphenolithus primus
Cruciplacolithus edwardsii
Fasciculithus bitectus
Ericsonia subpertusa
Fasciculithus janii
Fasciculithus ulii
Fasciculithus tympaniformis
Chiasmolithus consuetus
Bomolithus elegans
Neochiastozygus protenus
Fasciculithus billii
Heliolithus kantabriae
Heliolithus kleinpelli
NP-zone
Morozovella angulata
Globanomalina chapmani
Morozovella conicotruncata
Morozovella acuta
Morozovella velascoensis
Acarinina sp.
P4
NP5
NP4
NP6
S1
S1-10
S1-5
S1-3
S1-2
S1-1
S2
S2-14
S2-13
S2-12
S2-11
S2-10
S2-9
S2-8
S2-7
S2-6
S2-5
S2-4
S2-3
S2-2
S2-1
S3
S3-1
S4
S4-21
S4-20
S4-7
S4-6
S4-5
S5
S5-2
S5-1
S7
S7-4
S7-3
S7-2
S7-1
S8
S8-7
S8-6
S8-5
S8-4
S8-3
S8-2
S8-1

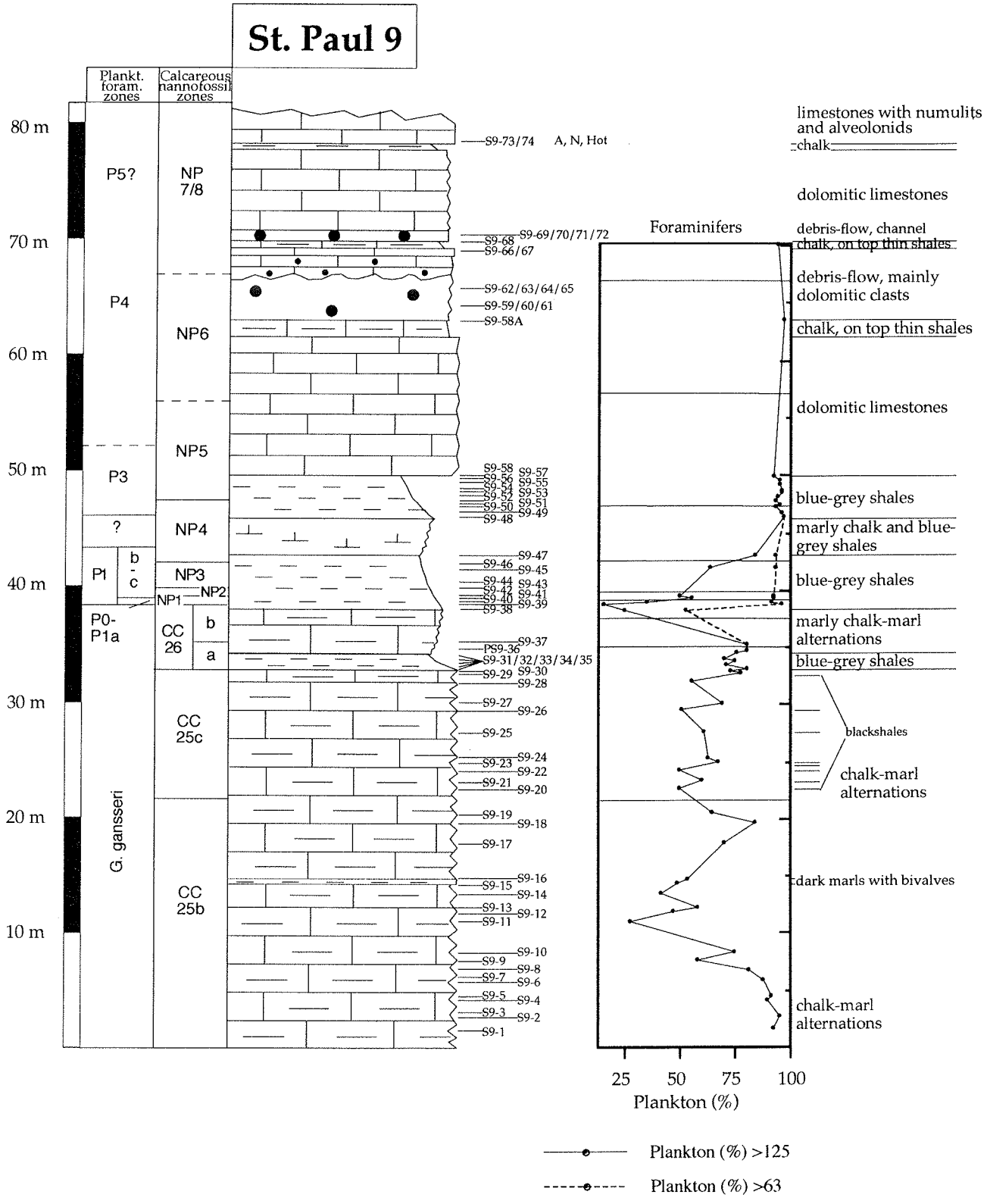
St. Paul 9
Plankt. foram. zones
Calcareous nannofossil zones
80 m
70 m
60 m
50 m
40 m
30 m
20 m
10 m
P5?
P4
P3
?
P1
b
c
P0-
P1a
G. gansseri
NP 7/8
NP6
NP5
NP4
NP3
NP2
NP1
CC 26
b
a
CC 25c
CC 25b
S9-73/74 A, N, Hot
S9-68
S9-69/70/71/72
S9-66/67
S9-62/63/64/65
S9-59/60/61
S9-58A
S9-58
S9-57
S9-56
S9-55
S9-54
S9-53
S9-52
S9-51
S9-50
S9-49
S9-48
S9-47
S9-46
S9-45
S9-44
S9-43
S9-42
S9-41
S9-40
S9-39
S9-38
S9-37
PS9-36
S9-31/32/33/34/35
S9-29
S9-30
S9-28
S9-27
S9-26
S9-25
S9-24
S9-23
S9-22
S9-21
S9-20
S9-19
S9-18
S9-17
S9-16
S9-15
S9-14
S9-13
S9-12
S9-11
S9-10
S9-9
S9-8
S9-7
S9-6
S9-5
S9-4
S9-3
S9-2
S9-1
Foraminifers
limestones with numulits and alveolonids
chalk
dolomitic limestones
debris-flow, channel
chalk, on top thin shales
debris-flow, mainly dolomitic clasts
chalk, on top thin shales
dolomitic limestones
blue-grey shales
marly chalk and blue-grey shales
blue-grey shales
marly chalk-marl alternations
blue-grey shales
blackshales
chalk-marl alternations
dark marls with bivalves
chalk-marl alternations
25
50
75
100
Plankton (%)
Plankton (%) >125
Plankton (%) >63

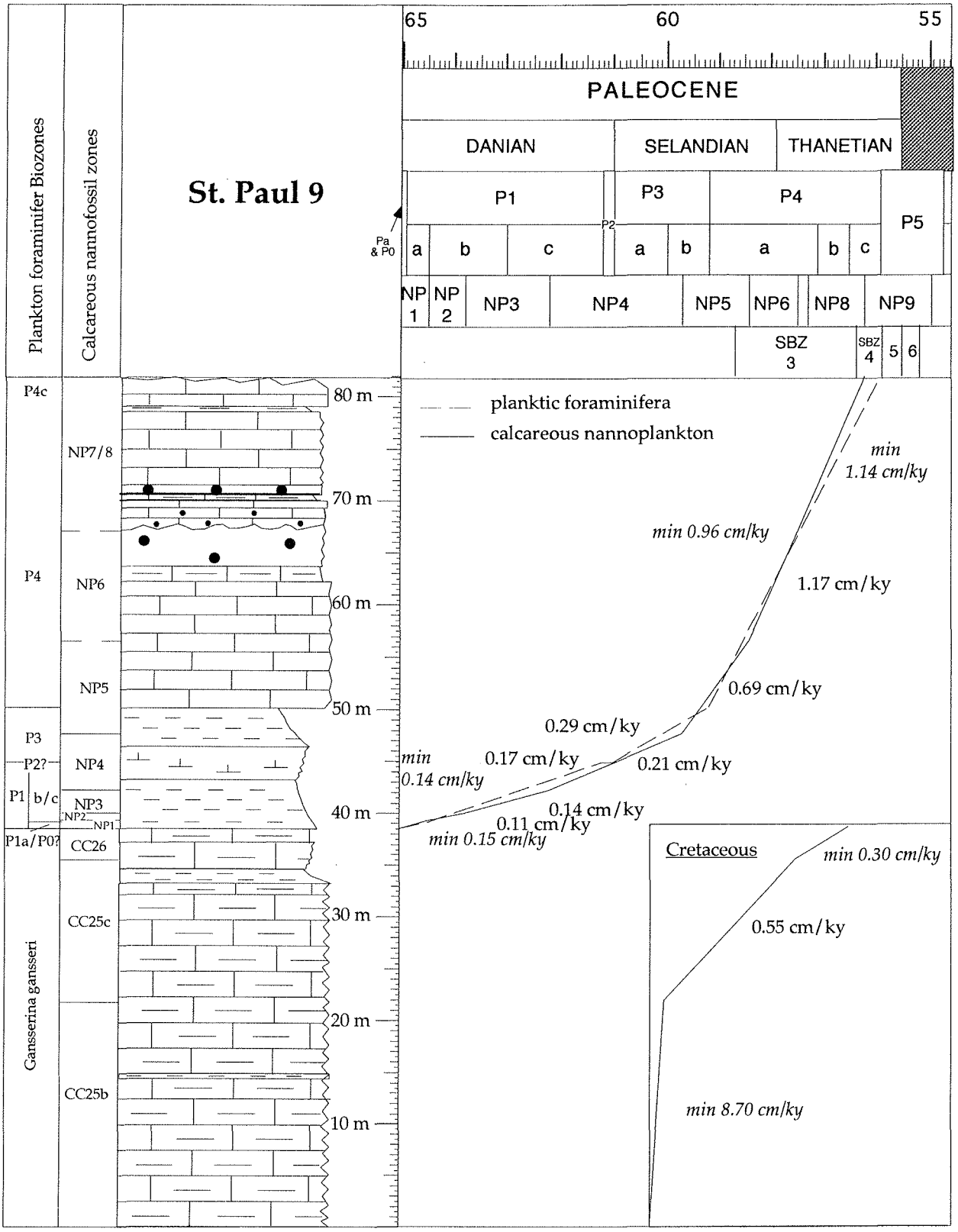
St. Paul 9
Plankton foraminifer Biozones
Calcareous nannofossil zones
65
60
55
PALEOCENE
DANIAN
SELANDIAN
THANETIAN
P1
P2
P3
P4
P5
Pa & P0
a
b
c
NP 1
NP 2
NP3
NP4
NP5
NP6
NP8
NP9
SBZ 3
SBZ 4
5
6
P4c
P4
P3
P2?
P1
b/c
P1a/P0?
NP7/8
NP6
NP5
NP4
NP3
NP2
NP1
CC26
CC25c
CC25b
Gansserina gansseri
80 m
70 m
60 m
50 m
40 m
30 m
20 m
10 m
planktic foraminifera
calcareous nannoplankton
min 1.14 cm/ky
min 0.96 cm/ky
1.17 cm/ky
0.69 cm/ky
0.29 cm/ky
min 0.14 cm/ky
0.17 cm/ky
0.21 cm/ky
0.14 cm/ky
0.11 cm/ky
min 0.15 cm/ky
Cretaceous
min 0.30 cm/ky
0.55 cm/ky
min 8.70 cm/ky

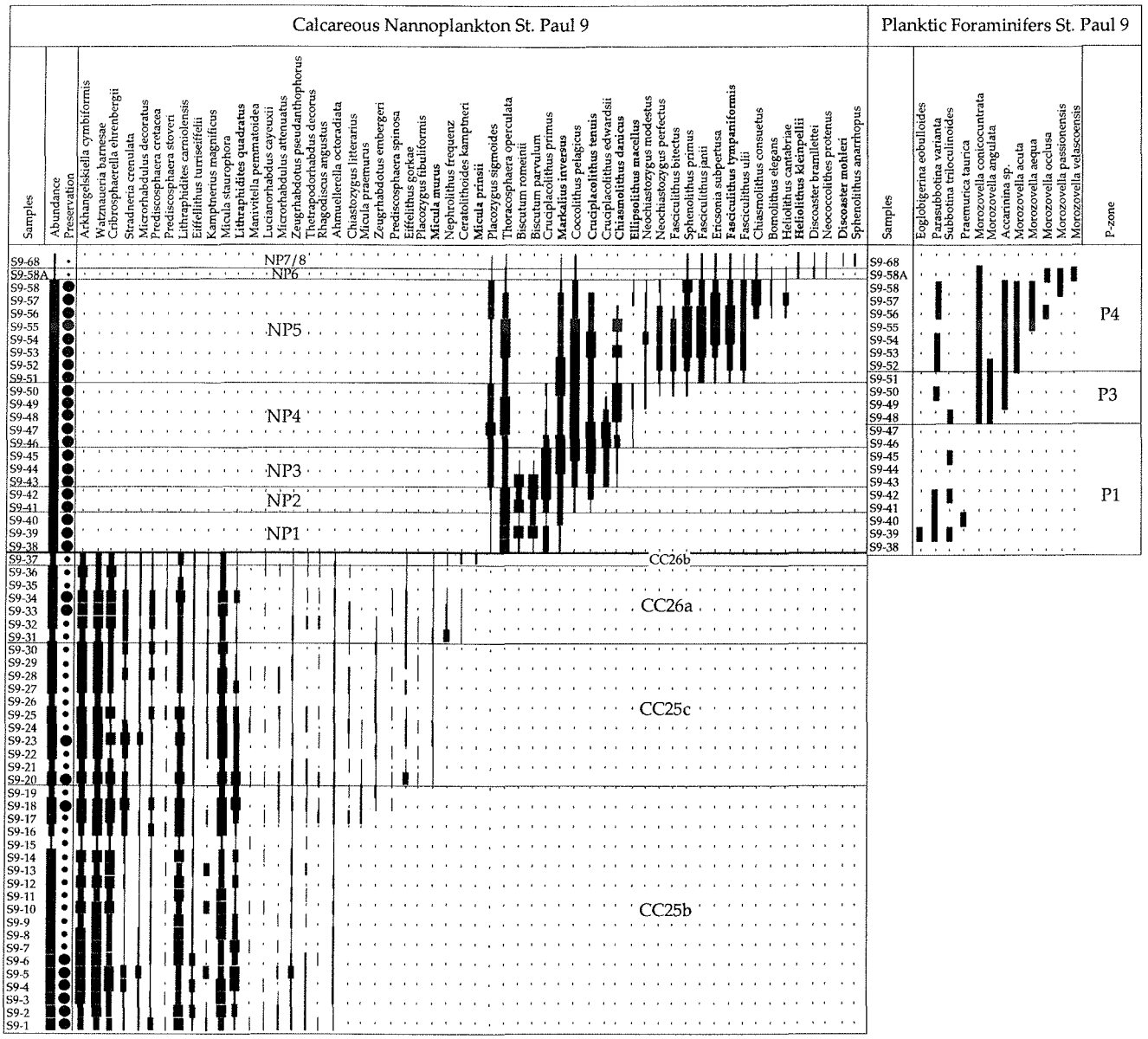
Calcareous Nannoplankton St. Paul 9
Planktic Foraminifers St. Paul 9
Samples
Abundance
Preservation
Arkhangelskiella cymbiformis
Watznaueria barnesae
Cribrosphaerella ehrenbergii
Stradneria crenulata
Microrhabdulus decoratus
Prediscosphaera cretacea
Prediscosphaera stoveri
Lithraphidites carniolensis
Eiffellithus turriseiffelii
Kamptnerius magnificus
Micula staurophora
Lithraphidites quadratus
Manivitella pemmatoidea
Lucianorhabdus cayeuxii
Microrhabdulus attenuatus
Zeugrhabdotus pseudanthophorus
Thetrapodorhabdus decorus
Rhagodiscus angustus
Ahmuellerella octoradiata
Chiastozygus litterarius
Micula praemurus
Zeugrhabdotus embergeri
Prediscosphaera spinosa
Eiffellithus gorkae
Placozygus fibuliformis
Micula murus
Nephrolithus frequenz
Ceratolithoides kamptneri
Micula prinsii
Placozygus sigmoides
Thoracosphaera operculata
Biscutum romeinii
Biscutum parvulum
Cruciplacolithus primus
Markalius inversus
Coccolithus pelagicus
Cruciplacolithus tenuis
Cruciplacolithus edwardsii
Chiasmolithus danicus
Ellipsolithus macellus
Neochiastozygus modestus
Neochiastozygus perfectus
Fasciculithus bitectus
Sphenolithus primus
Fasciculithus janii
Ericsonia subpertusa
Fasciculithus tympaniformis
Fasciculithus ulii
Chiasmolithus consuetus
Bomolithus elegans
Heliolithus cantabriae
Heliolithus kleinpellii
Discoaster bramlettei
Neococcolithes protenus
Discoaster mohleri
Sphenolithus anarrhopus
NP7/8
NP6
NP5
NP4
NP3
NP2
NP1
CC26b
CC26a
CC25c
CC25b
Samples
Eoglobigerina eobulloides
Parasubbotina varianta
Subbotina triloculinoides
Praemurica taurica
Morozovella conicocuntrata
Morozovella angulata
Accarinina sp.
Morozovella acuta
Morozovella aequa
Morozovella occlusa
Morozovella passionensis
Morozovella velascoensis
P-zone
P4
P3
P1

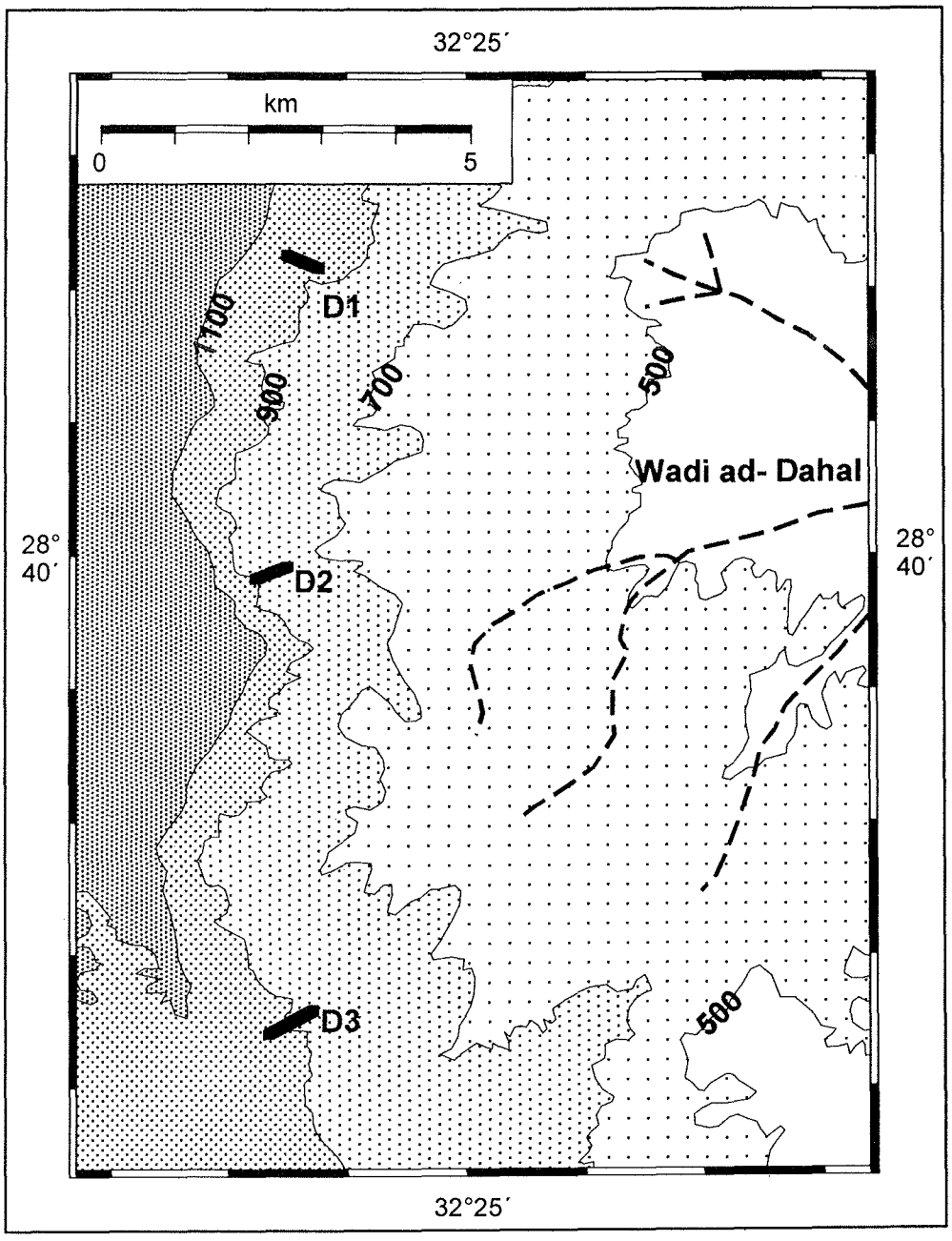

Bir Dakhl 1

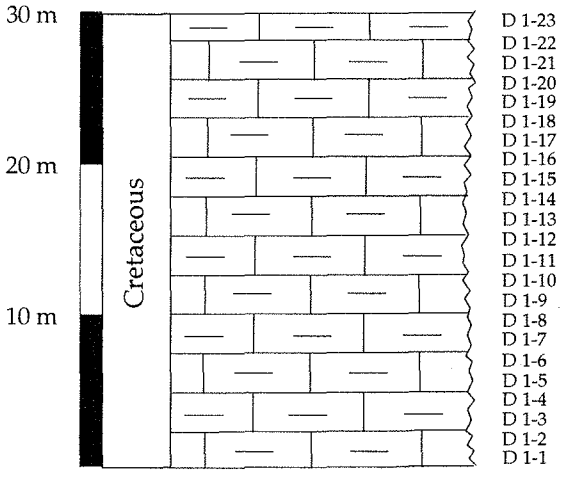

chalk-marl alternations
preservation of microfossils very poor

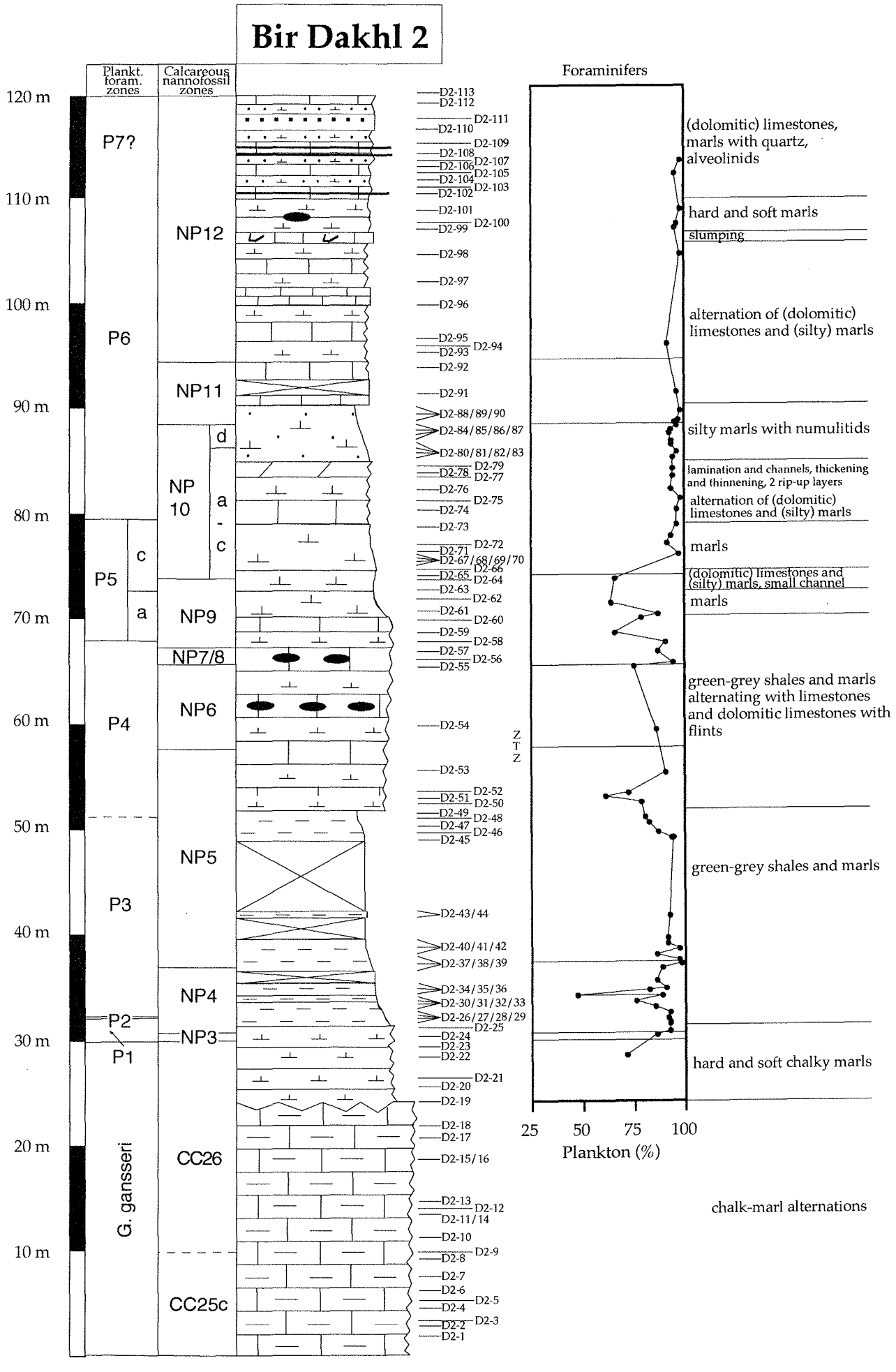
Bir Dakhl 2
Plankt. foram. zones
Calcareous nannofossil zones
Foraminifers
120 m
110 m
100 m
90 m
80 m
70 m
60 m
50 m
40 m
30 m
20 m
10 m
P7?
P6
P5
P4
P3
P2
P1
G. gansseri
NP12
NP11
NP 10
d
a - c
c
a
NP9
NP7/8
NP6
NP5
NP4
NP3
CC26
CC25c
D2-113
D2-112
D2-111
D2-110
D2-109
D2-108
D2-107
D2-106
D2-105
D2-104
D2-103
D2-102
D2-101
D2-100
D2-99
D2-98
D2-97
D2-96
D2-95
D2-94
D2-93
D2-92
D2-91
D2-88/89/90
D2-84/85/86/87
D2-80/81/82/83
D2-79
D2-78
D2-77
D2-76
D2-75
D2-74
D2-73
D2-72
D2-71
D2-67/68/69/70
D2-66
D2-65
D2-64
D2-63
D2-62
D2-61
D2-60
D2-59
D2-58
D2-57
D2-56
D2-55
D2-54
D2-53
D2-52
D2-51
D2-50
D2-49
D2-48
D2-47
D2-46
D2-45
D2-43/44
D2-40/41/42
D2-37/38/39
D2-34/35/36
D2-30/31/32/33
D2-26/27/28/29
D2-25
D2-24
D2-23
D2-22
D2-21
D2-20
D2-19
D2-18
D2-17
D2-15/16
D2-13
D2-12
D2-11/14
D2-10
D2-9
D2-8
D2-7
D2-6
D2-5
D2-4
D2-3
D2-2
D2-1
ZTZ
(dolomitic) limestones, marls with quartz, alveolinids
hard and soft marls
slumping
alternation of (dolomitic) limestones and (silty) marls
silty marls with numulitids
lamination and channels, thickening and thinnening, 2 rip-up layers
alternation of (dolomitic) limestones and (silty) marls
marls
(dolomitic) limestones and (silty) marls, small channel
marls
green-grey shales and marls alternating with limestones and dolomitic limestones with flints
green-grey shales and marls
hard and soft chalky marls
chalk-marl alternations
25
50
75
100
Plankton (%)

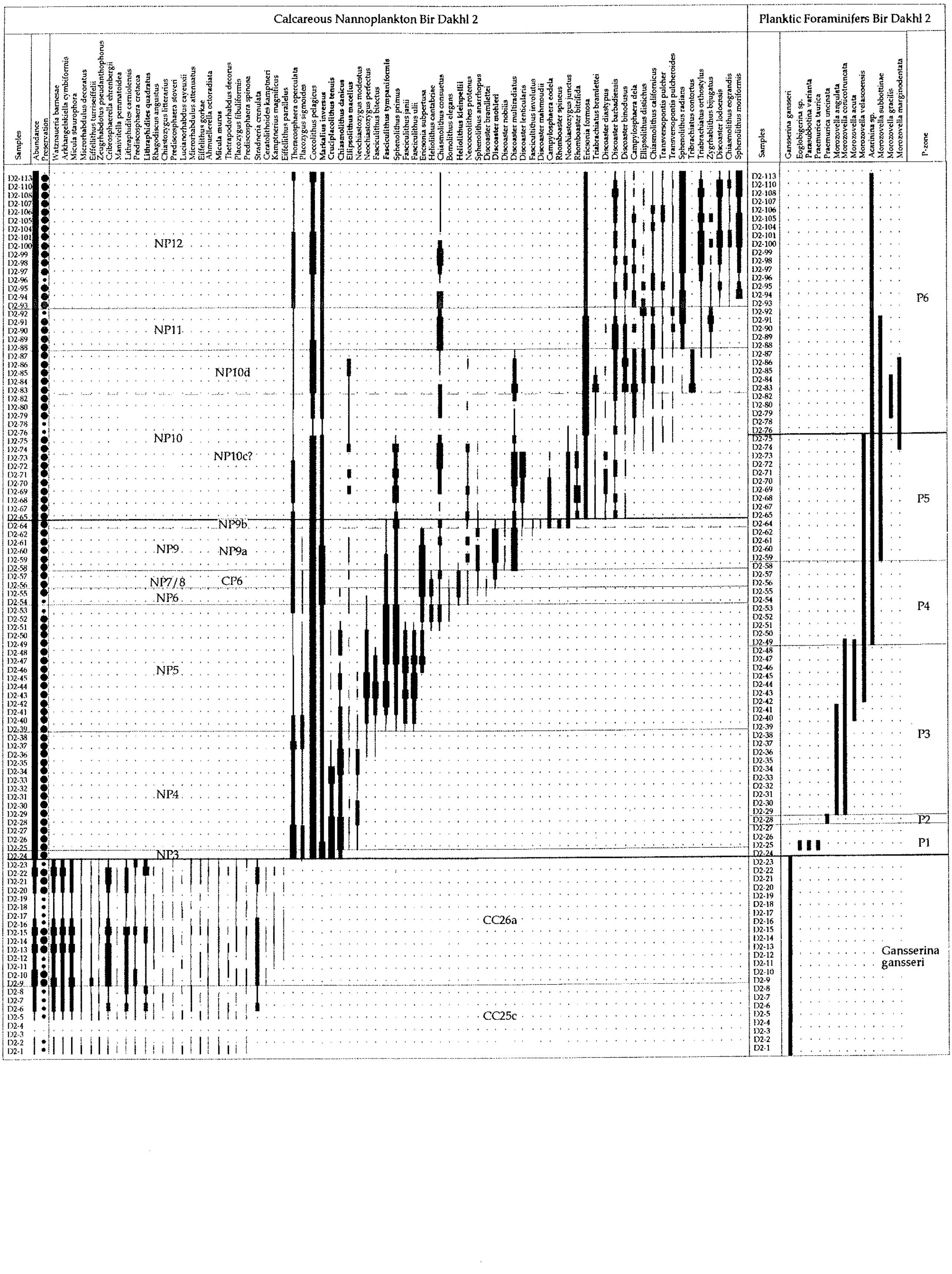
Calcareous Nannoplankton Bir Dakhl 2
Planktic Foraminifers Bir Dakhl 2
Samples
Abundance
Preservation
NP12
NP11
NP10d
NP10
NP10c?
NP9b
NP9
NP9a
NP7/8
CP6
NP6
NP5
NP4
NP3
CC26a
CC25c
P-zone
P6
P5
P4
P3
P2
P1
Gansserina gansseri

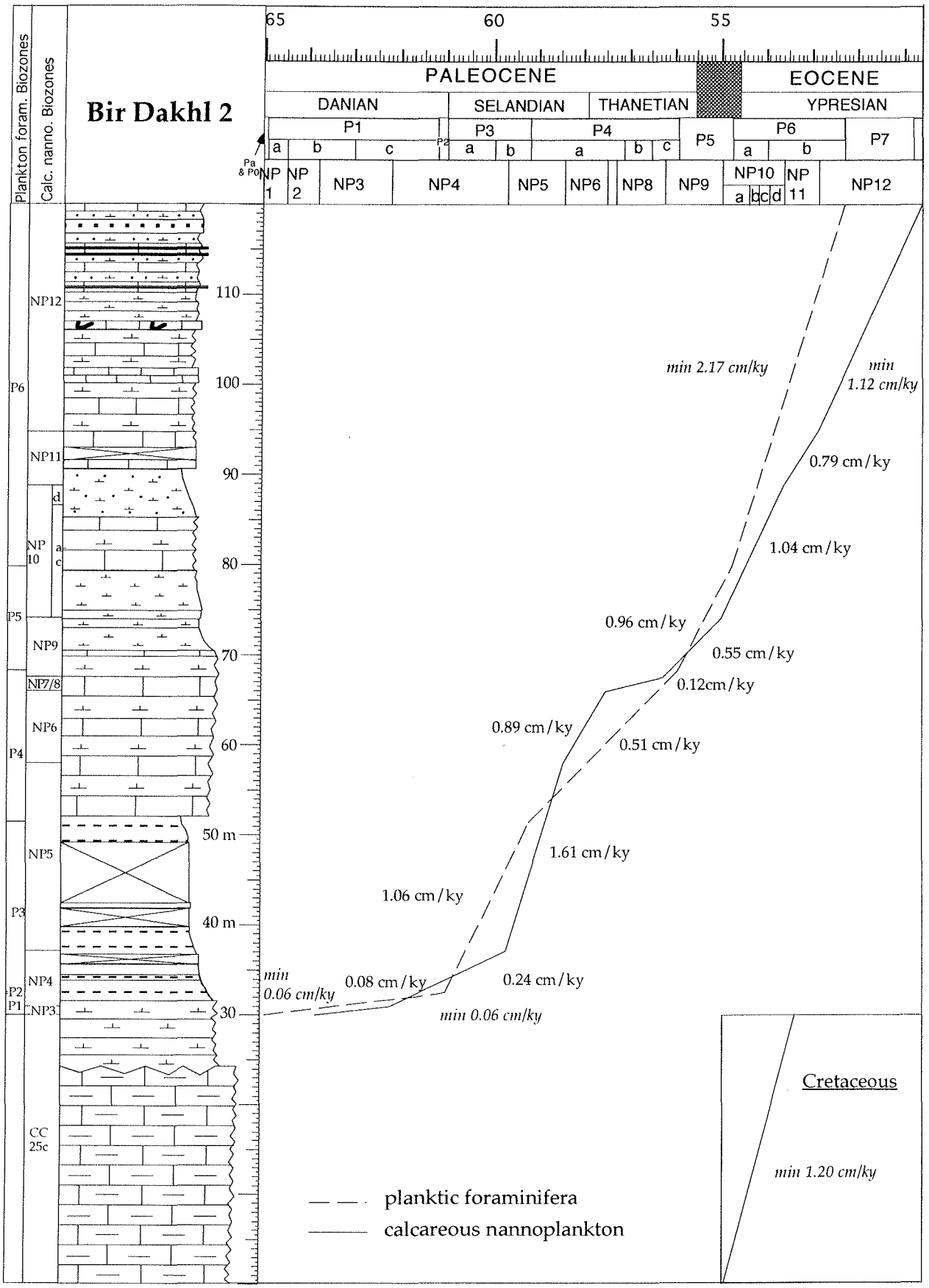
Bir Dakhl 2
Plankton foram. Biozones
Calc. nanno. Biozones
65
60
55
PALEOCENE
EOCENE
DANIAN
SELANDIAN
THANETIAN
YPRESIAN
P1
P2
P3
P4
P5
P6
P7
a
b
c
Pa & Po
NP 1
NP 2
NP3
NP4
NP5
NP6
NP8
NP9
NP10
NP 11
NP12
110
100
90
80
70
60
50 m
40 m
30
min 2.17 cm/ky
min 1.12 cm/ky
0.79 cm/ky
1.04 cm/ky
0.96 cm/ky
0.55 cm/ky
0.12cm/ky
0.89 cm/ky
0.51 cm/ky
1.61 cm/ky
1.06 cm/ky
min 0.06 cm/ky
0.08 cm/ky
0.24 cm/ky
min 0.06 cm/ky
Cretaceous
min 1.20 cm/ky
planktic foraminifera
calcareous nannoplankton

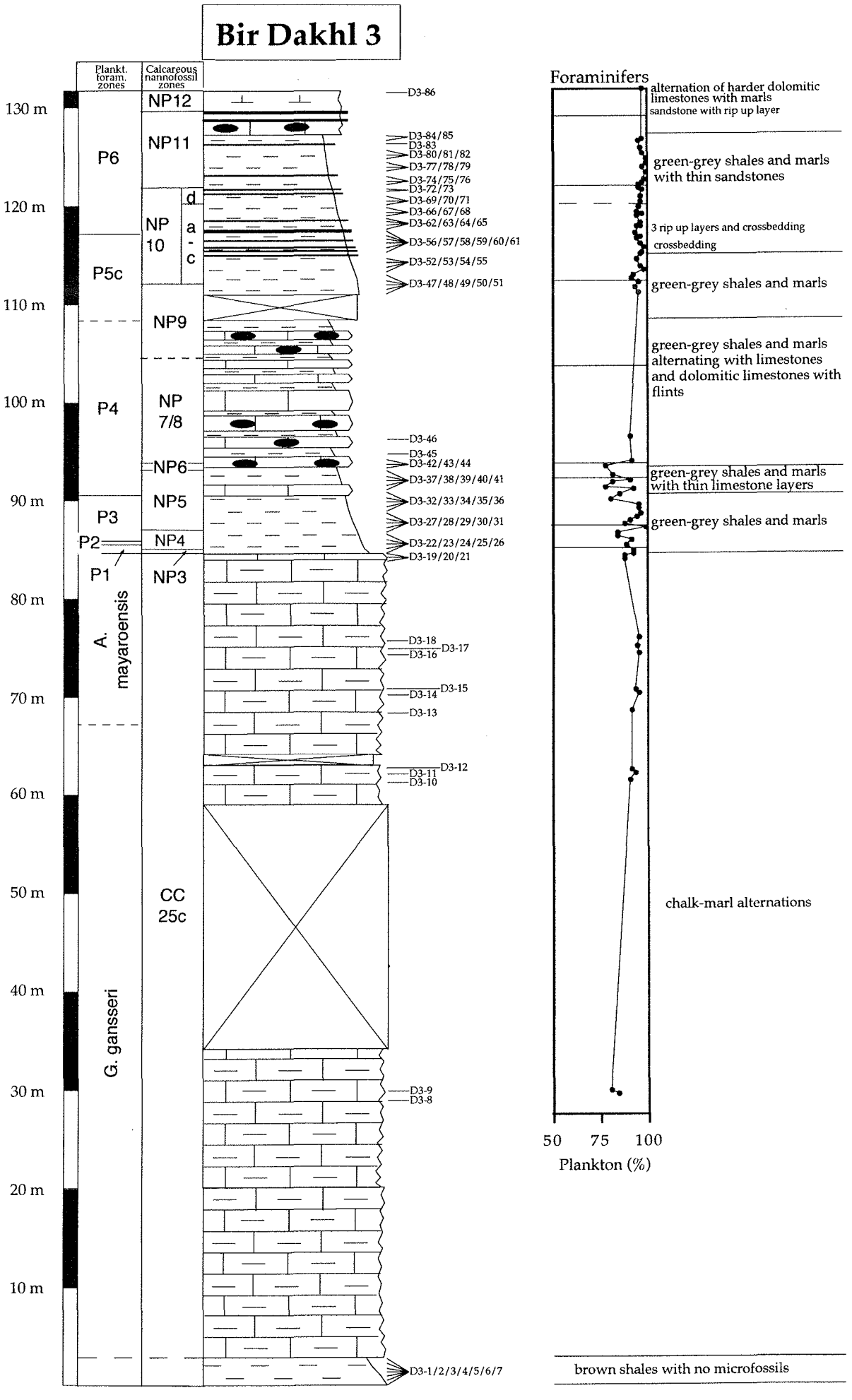
Bir Dakhl 3
Plankt. foram. zones
Calcareous nannofossil zones
130 m
120 m
110 m
100 m
90 m
80 m
70 m
60 m
50 m
40 m
30 m
20 m
10 m
P6
P5c
P4
P3
P2
P1
NP12
NP11
NP 10
d
a
-
c
NP9
NP 7/8
NP6
NP5
NP4
NP3
A. mayaroensis
G. gansseri
CC 25c
D3-86
D3-84/85
D3-83
D3-80/81/82
D3-77/78/79
D3-74/75/76
D3-72/73
D3-69/70/71
D3-66/67/68
D3-62/63/64/65
D3-56/57/58/59/60/61
D3-52/53/54/55
D3-47/48/49/50/51
D3-46
D3-45
D3-42/43/44
D3-37/38/39/40/41
D3-32/33/34/35/36
D3-27/28/29/30/31
D3-22/23/24/25/26
D3-19/20/21
D3-18
D3-17
D3-16
D3-15
D3-14
D3-13
D3-12
D3-11
D3-10
D3-9
D3-8
D3-1/2/3/4/5/6/7
Foraminifers
alternation of harder dolomitic limestones with marls
sandstone with rip up layer
green-grey shales and marls with thin sandstones
3 rip up layers and crossbedding
crossbedding
green-grey shales and marls
green-grey shales and marls alternating with limestones and dolomitic limestones with flints
green-grey shales and marls with thin limestone layers
green-grey shales and marls
chalk-marl alternations
brown shales with no microfossils
50
75
100
Plankton (%)

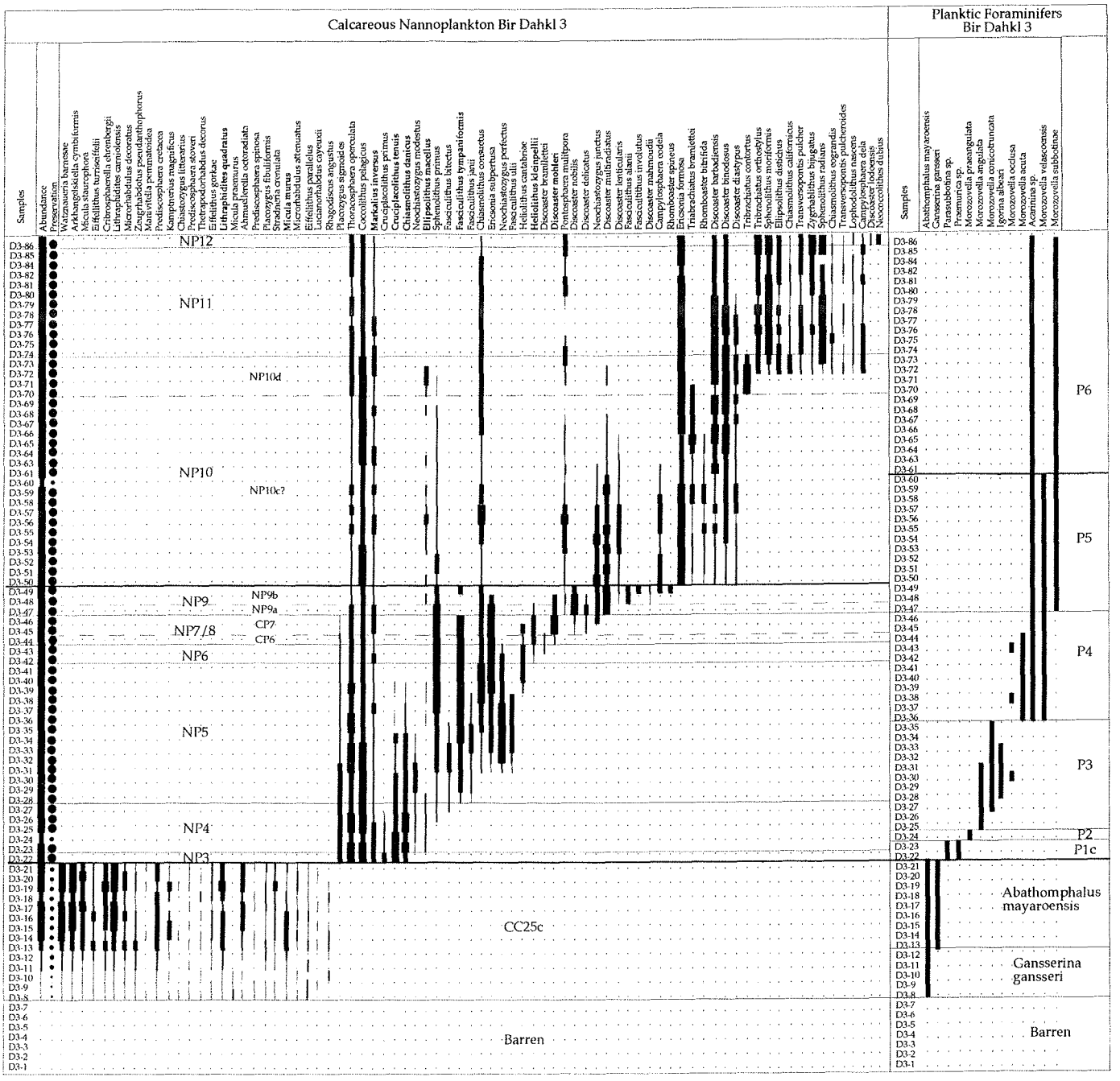
Calcareous Nannoplankton Bir Dahkl 3
Planktic Foraminifers Bir Dahkl 3
Samples
Abundance
Preservation
Watznaueria barnesae
Arkhangelskiella cymbiformis
Micula staurophora
Eiffellithus turriseiffelii
Cribrosphaerella ehrenbergii
Lithraphidites carniolensis
Microrhabdulus decoratus
Zeugrhabdotus pseudanthophorus
Manivitella pemmatoidea
Prediscosphaera cretacea
Kamptnerius magnificus
Prediscosphaera stoveri
Prediscosphaera columnata
Thoracosphaera deflandrei
Eiffellithus gorkae
Lithraphidites quadratus
Micula praemurus
Ahmuellerella octoradiata
Prediscosphaera spinosa
Placozygus fibuliformis
Stradnerita crenulata
Micula murus
Microrhabdulus attenuatus
Eiffellithus parallelus
Lucianorhabdus cayeuxii
Rhagodiscus angustus
Placozygus sigmoides
Thoracosphaera operculata
Coccolithus pelagicus
Markalius inversus
Cruciplacolithus primus
Cruciplacolithus tenuis
Chiasmolithus danicus
Neochiastozygus modestus
Ellipsolithus macellus
Sphenolithus primus
Fasciculithus tympaniformis
Fasciculithus janii
Chiasmolithus consuetus
Ericsonia subpertusa
Neochiastozygus perfectus
Fasciculithus ulii
Heliolithus cantabriae
Heliolithus kleinpellii
Discoaster brainiformis
Discoaster mohleri
Discoaster multiradiatus
Discoaster nobilis
Discoaster deflandrei
Discoaster delicatus
Neochiastozygus junctus
Discoaster multiradiatus
Discoaster lenticularis
Fasciculithus alanii
Fasciculithus involutus
Discoaster mahmoudii
Campylosphaera eodela
Rhomboaster spineus
Ericsonia formosa
Trabrachiatus bramlettei
Rhomboaster bitrifida
Discoaster barbadiensis
Discoaster binodosus
Discoaster diastypus
Tribrachiatus contortus
Tribrachiatus orthostylus
Sphenolithus moriformis
Ellipsolithus macellus
Ellipsolithus distichus
Chiasmolithus californicus
Transversopontis pulcher
Zygrhablithus bijugatus
Sphenolithus radians
Chiasmolithus oamaruensis
Transversopontis pulcheroides
Lophodolithus nascens
Campylosphaera dela
Discoaster lodoensis
Neococcolithes dubius
NP12
NP11
NP10d
NP10
NP10c?
NP9
NP9b
NP9a
NP7/8
CP7
CP6
NP6
NP5
NP4
NP3
CC25c
Barren
Abathomphalus mayaroensis
Gansserina gansseri
Parasubbotina sp.
Praemurica sp.
Morozovella praeangulata
Morozovella angulata
Morozovella conicotruncata
Igorina albeari
Morozovella occlusa
Morozovella acuta
Acarinina sp.
Morozovella velascoensis
Morozovella subbotinae
P6
P5
P4
P3
P2
P1c
Abathomphalus mayaroensis
Gansserina gansseri
Barren

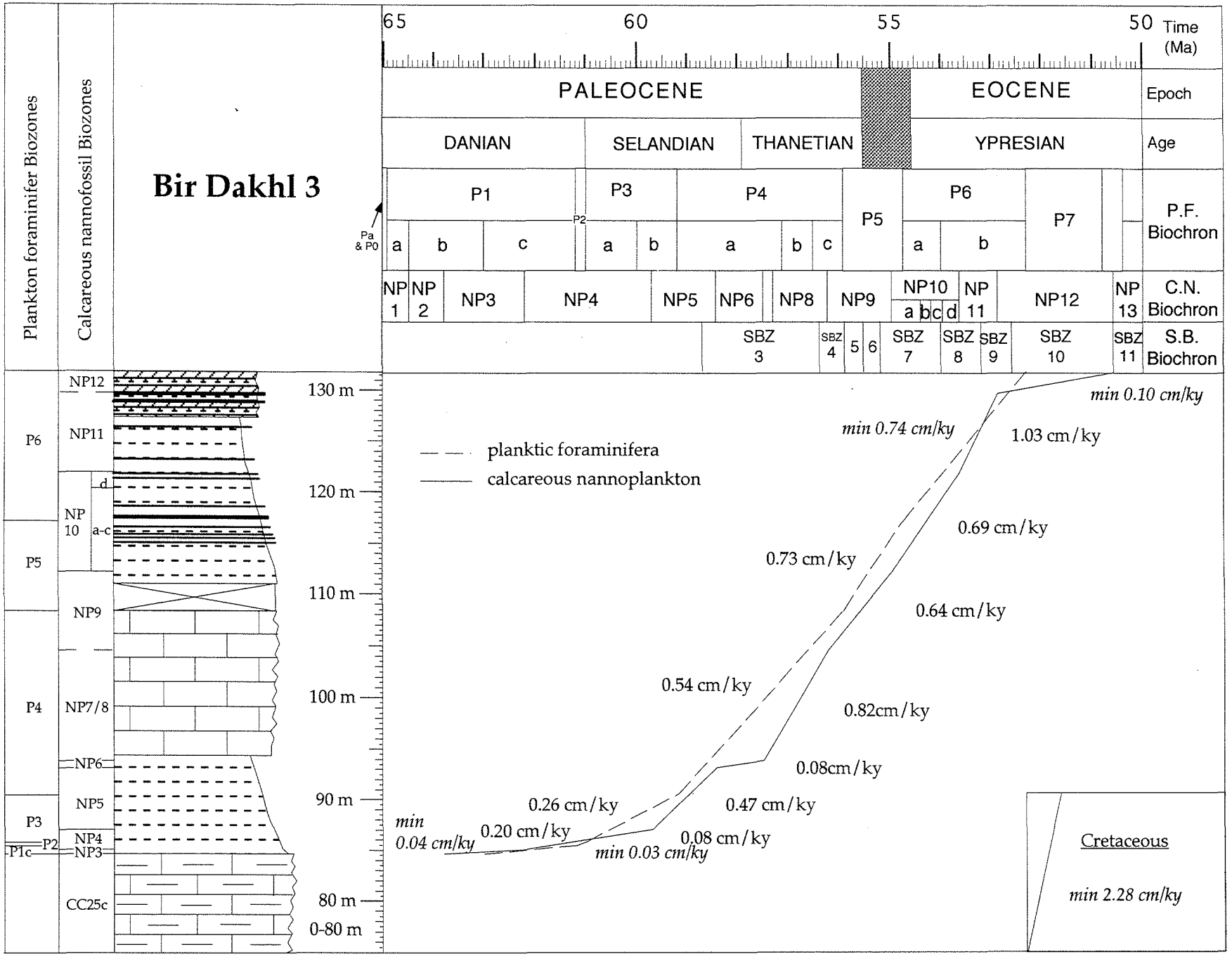
Bir Dakhl 3
Plankton foraminifer Biozones
Calcareous nannofossil Biozones
65
60
55
50
Time (Ma)
PALEOCENE
EOCENE
Epoch
DANIAN
SELANDIAN
THANETIAN
YPRESIAN
Age
P1
P2
P3
P4
P5
P6
P7
Pa & P0
a
b
c
P.F. Biochron
NP 1
NP 2
NP3
NP4
NP5
NP6
NP8
NP9
NP10
a b c d
NP 11
NP12
NP 13
C.N. Biochron
SBZ 3
SBZ 4
5
6
SBZ 7
SBZ 8
SBZ 9
SBZ 10
SBZ 11
S.B. Biochron
NP12
NP11
NP 10
a-c
d
NP9
NP7/8
NP6
NP5
NP4
NP3
P1c
CC25c
130 m
120 m
110 m
100 m
90 m
80 m
0-80 m
planktic foraminifera
calcareous nannoplankton
min 0.10 cm/ky
min 0.74 cm/ky
1.03 cm/ky
0.69 cm/ky
0.73 cm/ky
0.64 cm/ky
0.54 cm/ky
0.82cm/ky
0.08cm/ky
0.26 cm/ky
0.47 cm/ky
min 0.04 cm/ky
0.20 cm/ky
0.08 cm/ky
min 0.03 cm/ky
Cretaceous
min 2.28 cm/ky

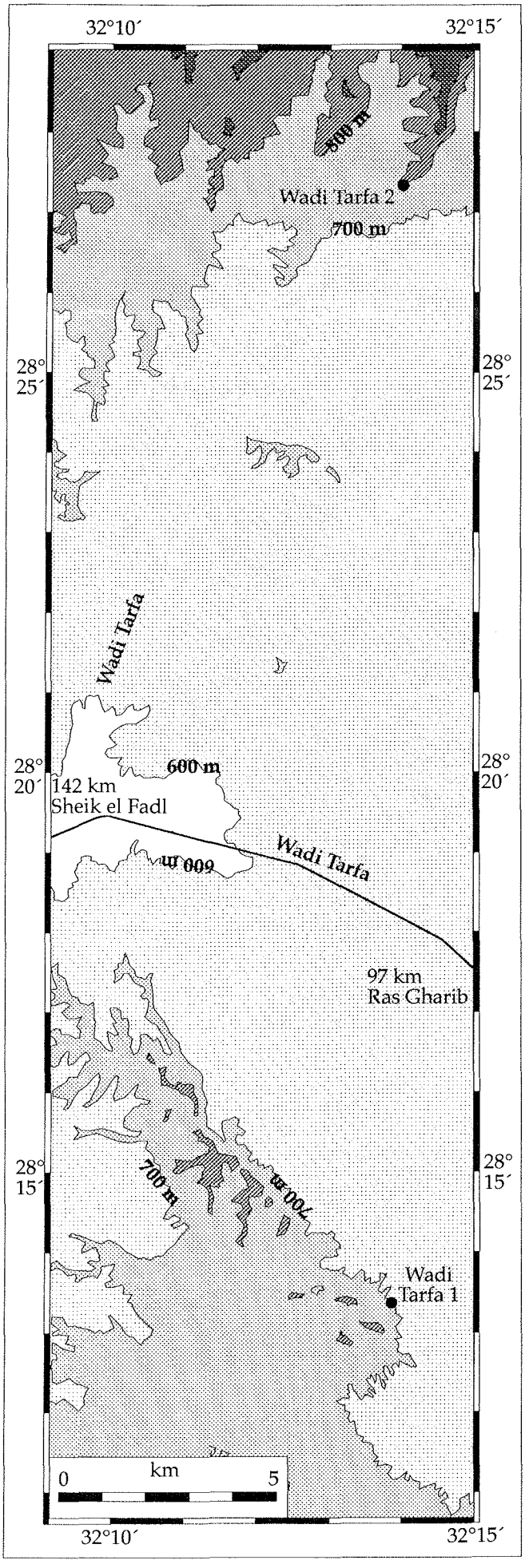
32°10´
32°15´
Wadi Tarfa 2
700 m
28°
25´
Wadi Tarfa
28°
20´
600 m
142 km
Sheik el Fadl
Wadi Tarfa
97 km
Ras Gharib
28°
15´
700 m
Wadi
Tarfa 1
0
km
5
32°10´
32°15´

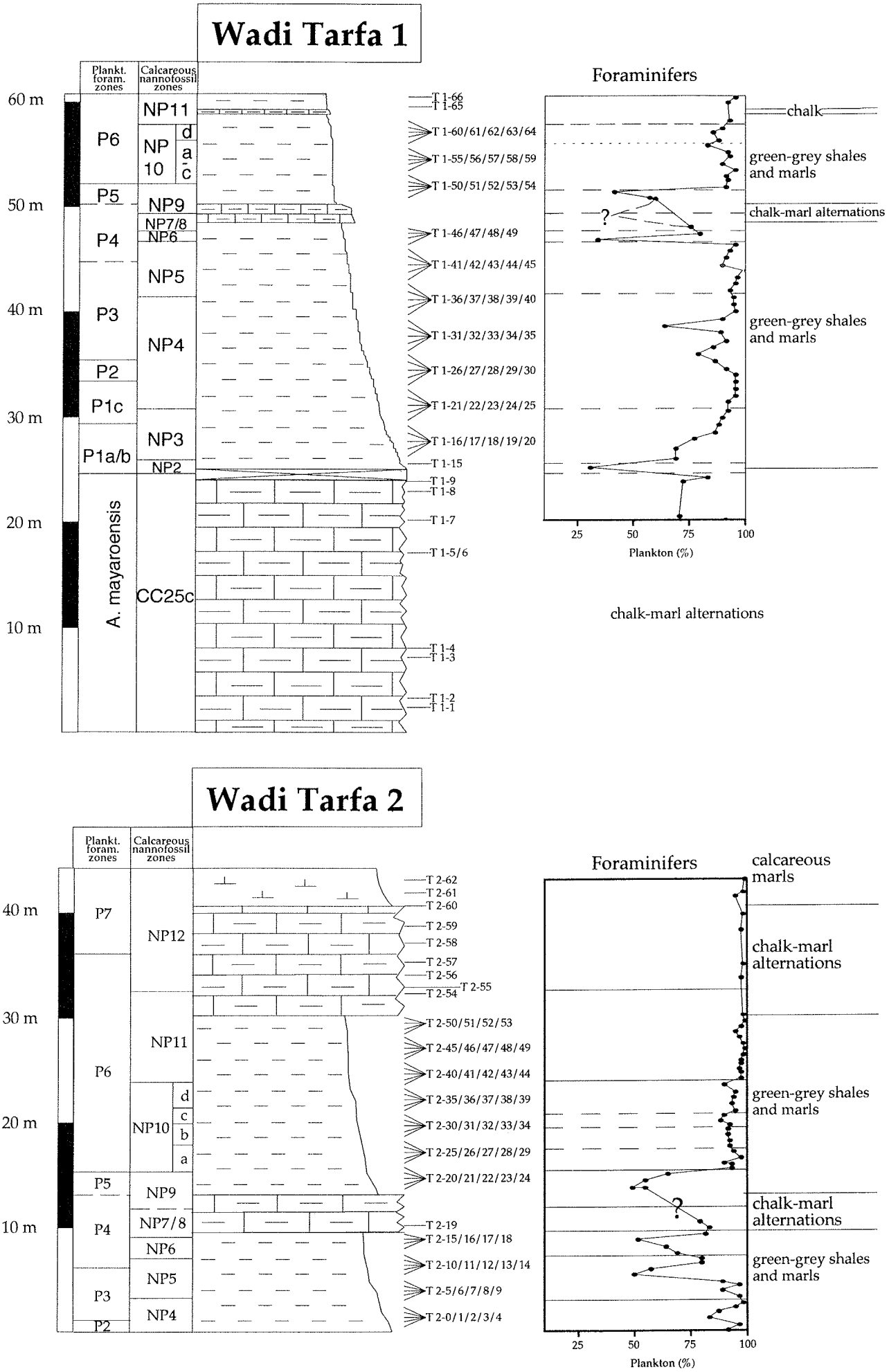
Wadi Tarfa 1
Plankt. foram. zones
Calcareous nannofossil zones
60 m
50 m
40 m
30 m
20 m
10 m
P6
P5
P4
P3
P2
P1c
P1a/b
NP11
NP 10 d a c
NP9
NP7/8
NP6
NP5
NP4
NP3
NP2
A. mayaroensis
CC25c
T 1-66
T 1-65
T 1-60/61/62/63/64
T 1-55/56/57/58/59
T 1-50/51/52/53/54
T 1-46/47/48/49
T 1-41/42/43/44/45
T 1-36/37/38/39/40
T 1-31/32/33/34/35
T 1-26/27/28/29/30
T 1-21/22/23/24/25
T 1-16/17/18/19/20
T 1-15
T 1-9
T 1-8
T 1-7
T 1-5/6
T 1-4
T 1-3
T 1-2
T 1-1
Foraminifers
chalk
green-grey shales and marls
chalk-marl alternations
?
green-grey shales and marls
25
50
75
100
Plankton (%)
chalk-marl alternations
Wadi Tarfa 2
Plankt. foram. zones
Calcareous nannofossil zones
40 m
30 m
20 m
10 m
P7
P6
P5
P4
P3
P2
NP12
NP11
NP10 d c b a
NP9
NP7/8
NP6
NP5
NP4
T 2-62
T 2-61
T 2-60
T 2-59
T 2-58
T 2-57
T 2-56
T 2-55
T 2-54
T 2-50/51/52/53
T 2-45/46/47/48/49
T 2-40/41/42/43/44
T 2-35/36/37/38/39
T 2-30/31/32/33/34
T 2-25/26/27/28/29
T 2-20/21/22/23/24
T 2-19
T 2-15/16/17/18
T 2-10/11/12/13/14
T 2-5/6/7/8/9
T 2-0/1/2/3/4
Foraminifers
calcareous marls
chalk-marl alternations
green-grey shales and marls
?
chalk-marl alternations
green-grey shales and marls
25
50
75
100
Plankton (%)

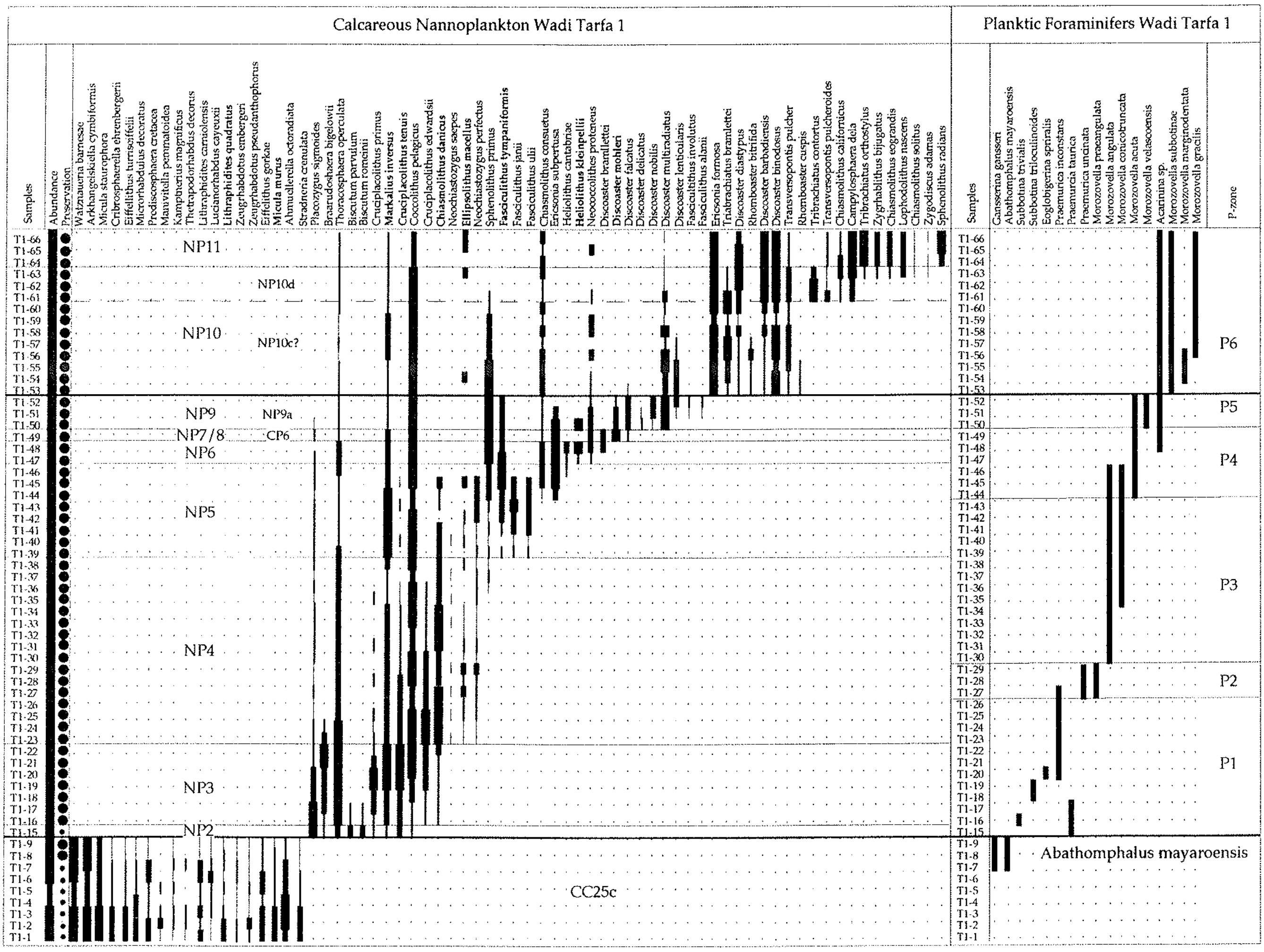
Calcareous Nannoplankton Wadi Tarfa 1
Planktic Foraminifers Wadi Tarfa 1
Samples
Abundance
Preservation
Watznaueria barnesae
Arkhangelskiella cymbiformis
Micula staurophora
Cribrosphaerella ehrenbergerii
Eiffellithus turriseiffelii
Microrhabdulus decoratus
Prediscosphaera cretacea
Manivitella pemmatoidea
Kamptnerius magnificus
Thetrapodorhabdus decorus
Lithraphidites carniolensis
Lucianorhabdus cayeuxii
Lithraphidites quadratus
Zeugrhabdotus embergeri
Zeugrhabdotus pseudanthophorus
Eiffellithus gorkae
Micula murus
Ahmuellerella octoradiata
Stradneria crenulata
Placozygus sigmoides
Braarudoshaera bigelowii
Thoracosphaera operculata
Biscutum parvulum
Biscutum romeinii
Cruciplacolithus primus
Markalius inversus
Cruciplacolithus tenuis
Coccolithus pelagicus
Cruciplacolithus edwardsii
Chiasmolithus danicus
Neochiastozygus saepes
Ellipsolithus macellus
Neochiastozygus perfectus
Sphenolithus primus
Fasciculithus tympaniformis
Fasciculithus janii
Fasciculithus ulii
Chiasmolithus consuetus
Ericsonia subpertusa
Heliolithus cantabriae
Heliolithus kleinpellii
Neococcolithes protenus
Discoaster bramlettei
Discoaster mohleri
Discoaster falcatus
Discoaster delicatus
Discoaster nobilis
Discoaster multiradiatus
Discoaster lenticularis
Fasciculithus involutus
Fasciculithus alanii
Ericsonia formosa
Triabrachiatus bramlettei
Discoaster diastypus
Rhomboaster bitrifida
Discoaster barbadiensis
Discoaster binodosus
Transversopontis pulcher
Rhomboaster cuspis
Tribrachiatus contortus
Transversopontis pulcheroides
Chiasmolithus californicus
Campylosphaera dela
Tribrachiatus orthostylus
Zygrhablithus bijugatus
Chiasmolithus eograndis
Lophodolithus nascens
Chiasmolithus solitus
Zygodiscus adamas
Sphenolithus radians
NP11
NP10d
NP10
NP10c?
NP9
NP9a
NP7/8
CP6
NP6
NP5
NP4
NP3
NP2
CC25c
Gansserina gansseri
Abathomphalus mayaroensis
Subbotina trivialis
Subbotina triloculinoides
Eoglobigerina spriralis
Praemurica inconstans
Praemurcia taurica
Praemurica uncinata
Morozovella praeangulata
Morozovella angulata
Morozovella conicotruncata
Morozovella acuta
Morozovella velascoensis
Acarinina sp.
Morozovella subbotinae
Morozovella marginodentata
Morozovella gracilis
P-zone
P6
P5
P4
P3
P2
P1
Abathomphalus mayaroensis

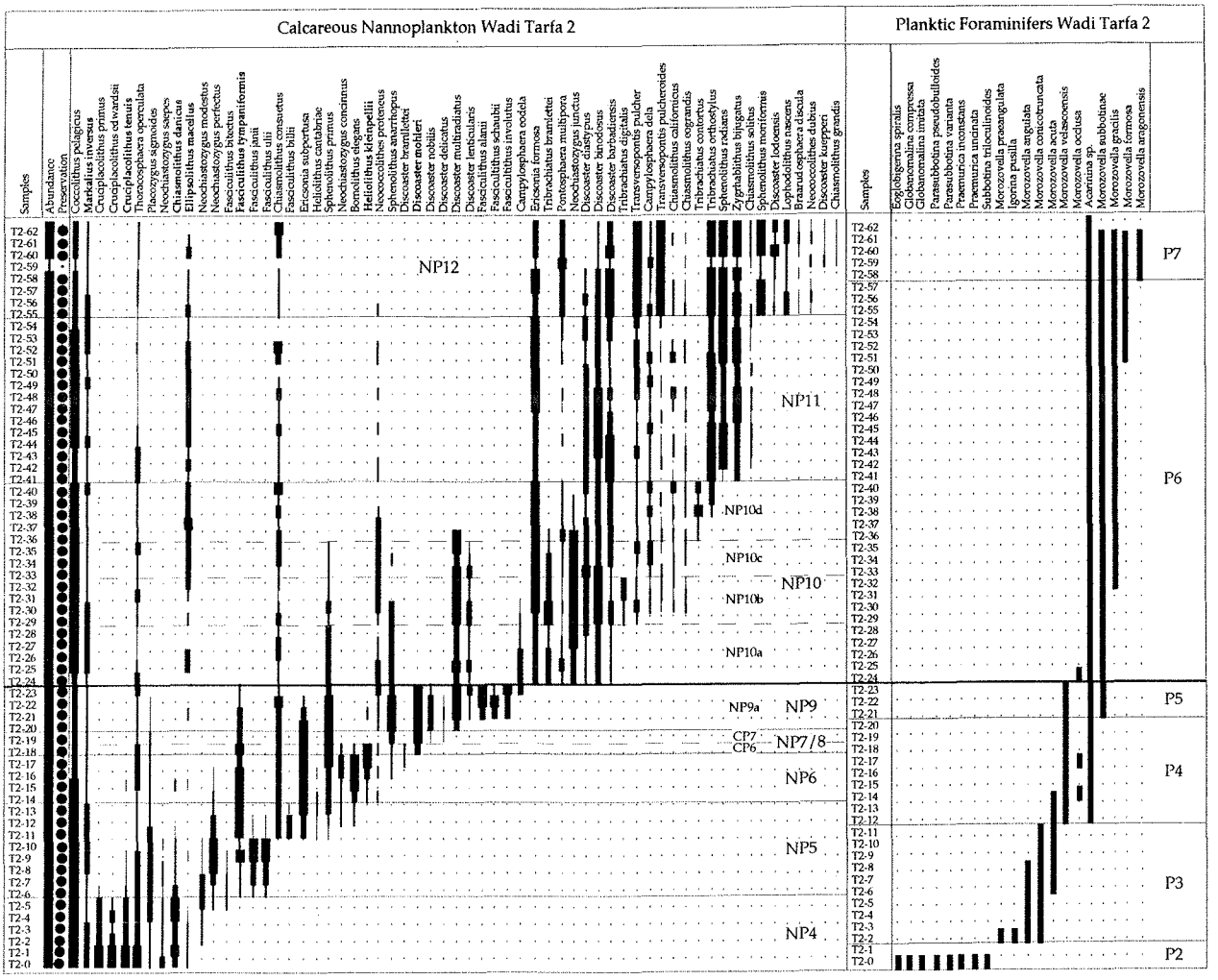
Calcareous Nannoplankton Wadi Tarfa 2
Planktic Foraminifers Wadi Tarfa 2
Samples
Abundance
Preservation
Coccolithus pelagicus
Markalius inversus
Cruciplacolithus primus
Cruciplacolithus edwardsii
Cruciplacolithus tenuis
Thoracosphaera operculata
Placozygus sigmoides
Neochiastozygus saepes
Chiasmolithus danicus
Ellipsolithus macellus
Neochiastozygus modestus
Neochiastozygus perfectus
Fasciculithus bitectus
Fasciculithus tympaniformis
Fasciculithus janii
Fasciculithus ulii
Chiasmolithus consuetus
Fasciculithus billii
Ericsonia subpertusa
Heliolithus cantabriae
Sphenolithus primus
Neochiastozygus concinnus
Bomolithus elegans
Heliolithus kleinpellii
Neococcolithes protenus
Sphenolithus anarrhopus
Discoaster bramlettei
Discoaster mohleri
Discoaster nobilis
Discoaster delicatus
Discoaster multiradiatus
Discoaster lenticularis
Fasciculithus alanii
Fasciculithus schaubii
Fasciculithus involutus
Campylosphaera eodela
Ericsonia formosa
Tribrachiatus bramlettei
Pontosphaera multipora
Neochiastozygus junctus
Discoaster diastypus
Discoaster binodosus
Discoaster barbadiensis
Tribrachiatus digitalis
Transversopontis pulcher
Campylosphaera dela
Transversopontis pachecoides
Chiasmolithus solitus
Chiasmolithus oamaruensis
Chiasmolithus expansus
Tribrachiatus contortus
Tribrachiatus orthostylus
Sphenolithus radians
Zygrhablithus bijugatus
Chiasmolithus solitus
Sphenolithus moniformis
Discoaster lodoensis
Lophodolithus nascens
Braarudosphaera discula
Neococcolithes dubius
Discoaster kuepperi
Chiasmolithus grandis
NP12
NP11
NP10d
NP10c
NP10b
NP10a
NP10
NP9a
NP9
CP7
CP6
NP7/8
NP6
NP5
NP4
Samples
Eoglobigerina spiralis
Globanomalina compressa
Globanomalina imitata
Parasubbotina pseudobulloides
Parasubbotina varianta
Praemurica inconstans
Praemurica uncinata
Subbotina trilocullinoides
Morozovella praeangulata
Igorina pusilla
Morozovella angulata
Morozovella conicotruncata
Morozovella acuta
Morozovella velascoensis
Acarinina sp.
Morozovella subbotinae
Morozovella gracilis
Morozovella formosa
Morozovella aragonensis
P7
P6
P5
P4
P3
P2

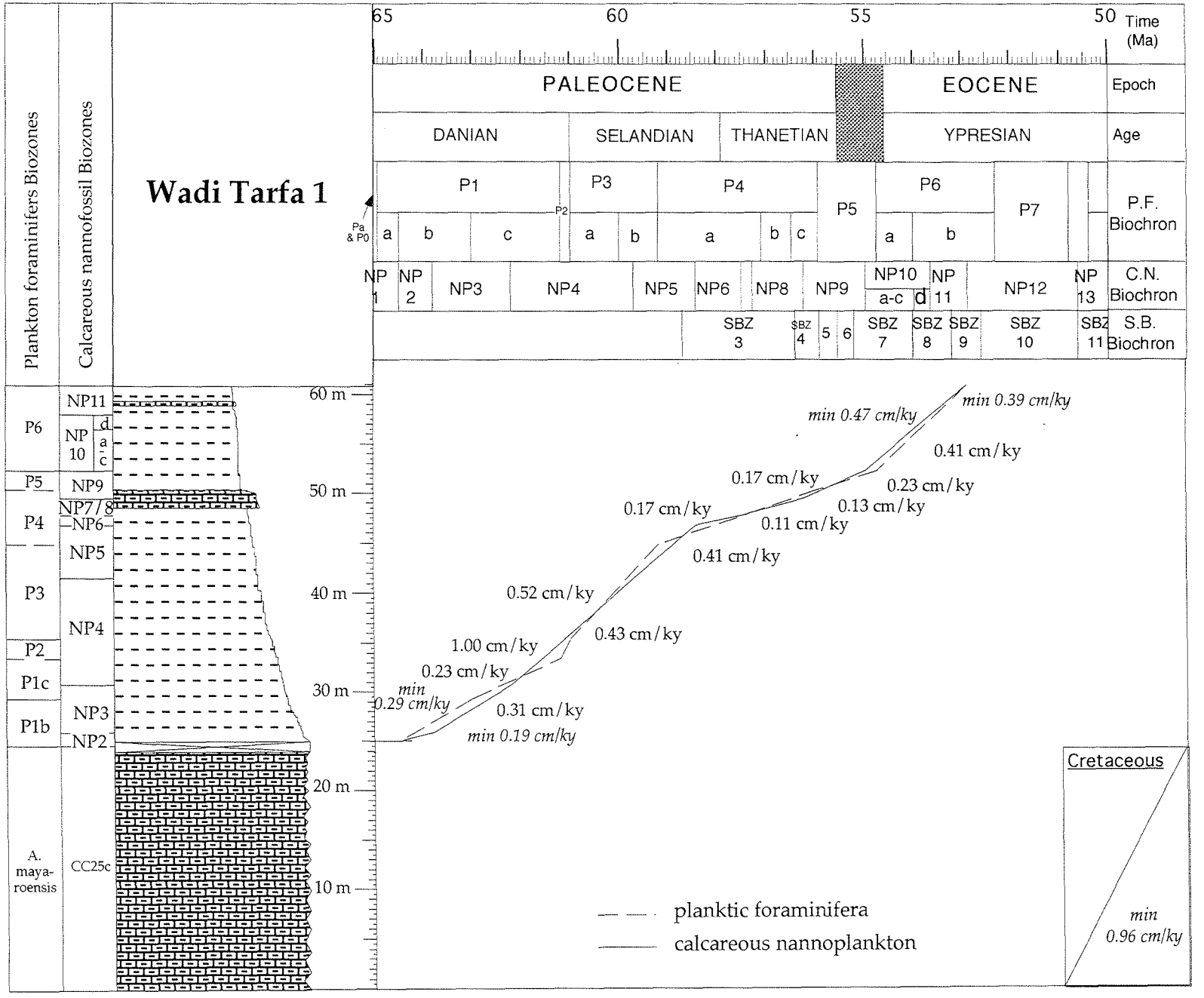
Wadi Tarfa 1
Plankton foraminifers Biozones
Calcareous nannofossil Biozones
65
60
55
50
Time (Ma)
PALEOCENE
EOCENE
Epoch
DANIAN
SELANDIAN
THANETIAN
YPRESIAN
Age
P1
P2
P3
P4
P5
P6
P7
Pa & P0
a
b
c
P.F. Biochron
NP 1
NP 2
NP3
NP4
NP5
NP6
NP8
NP9
NP10
a-c
d
NP 11
NP12
NP 13
C.N. Biochron
SBZ 3
SBZ 4
5
6
SBZ 7
SBZ 8
SBZ 9
SBZ 10
SBZ 11
S.B. Biochron
NP11
NP 10
NP9
NP7/8
NP6
NP5
NP4
NP3
NP2
P6
P5
P4
P3
P2
P1c
P1b
A. maya-roensis
CC25c
60 m
50 m
40 m
30 m
20 m
10 m
min 0.47 cm/ky
min 0.39 cm/ky
0.41 cm/ky
0.17 cm/ky
0.23 cm/ky
0.17 cm/ky
0.13 cm/ky
0.11 cm/ky
0.41 cm/ky
0.52 cm/ky
0.43 cm/ky
1.00 cm/ky
0.23 cm/ky
min 0.29 cm/ky
0.31 cm/ky
min 0.19 cm/ky
planktic foraminifera
calcareous nannoplankton
Cretaceous
min 0.96 cm/ky

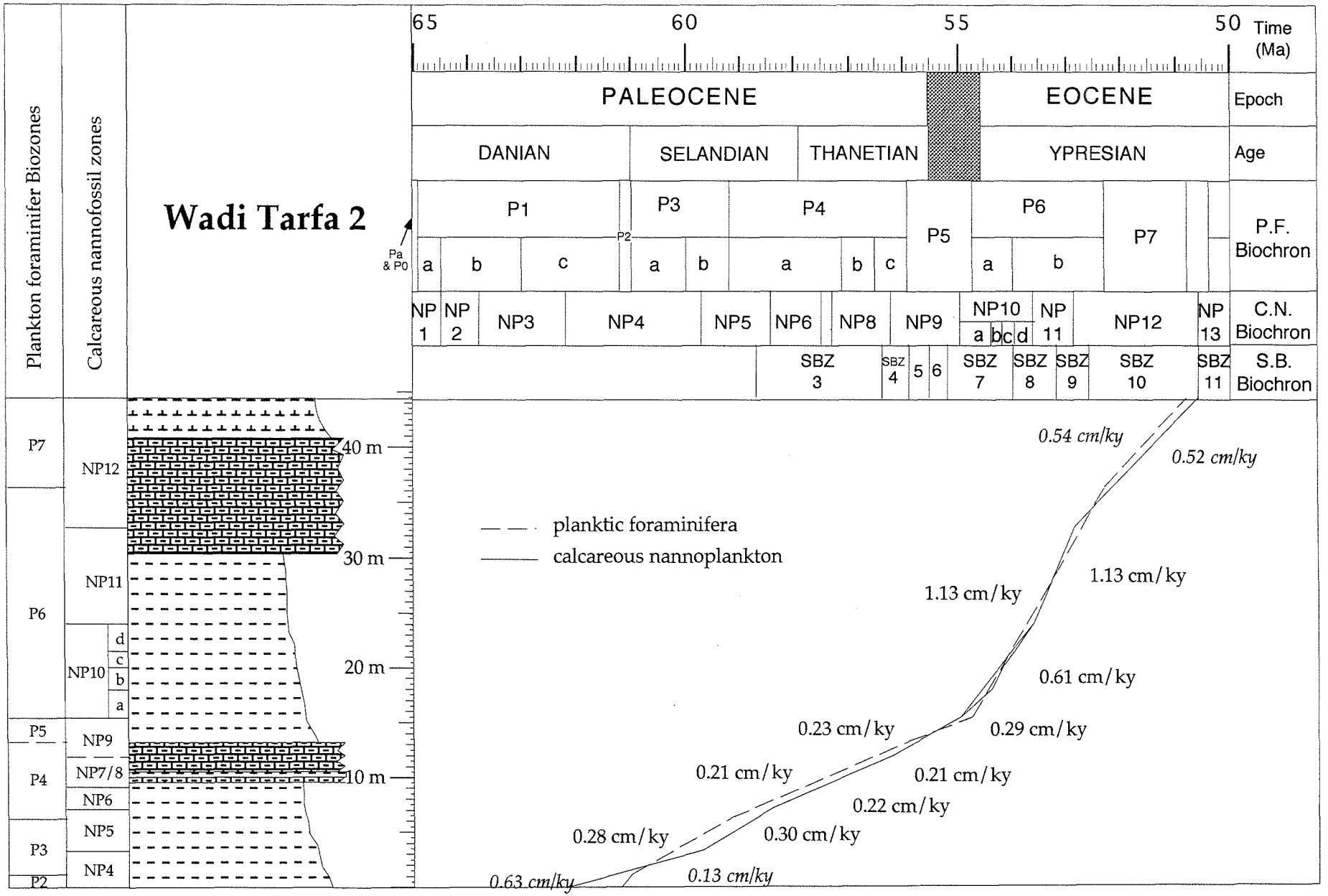
Wadi Tarfa 2
Plankton foraminifer Biozones
Calcareous nannofossil zones
65
60
55
50
Time (Ma)
PALEOCENE
EOCENE
Epoch
DANIAN
SELANDIAN
THANETIAN
YPRESIAN
Age
P1
P2
P3
P4
P5
P6
P7
Pa & P0
a
b
c
P.F. Biochron
NP 1
NP 2
NP3
NP4
NP5
NP6
NP8
NP9
NP10
NP 11
NP12
NP 13
C.N. Biochron
SBZ 3
SBZ 4
5
6
SBZ 7
SBZ 8
SBZ 9
SBZ 10
SBZ 11
S.B. Biochron
40 m
30 m
20 m
10 m
d
c
b
a
planktic foraminifera
calcareous nannoplankton
0.54 cm/ky
0.52 cm/ky
1.13 cm/ky
1.13 cm/ky
0.61 cm/ky
0.23 cm/ky
0.29 cm/ky
0.21 cm/ky
0.21 cm/ky
0.22 cm/ky
0.28 cm/ky
0.30 cm/ky
0.63 cm/ky
0.13 cm/ky

Publications of this series:

No. 1 **Wefer, G., E. Suess and cruise participants**
Bericht über die POLARSTERN-Fahrt ANT IV/2, Rio de Janeiro - Punta Arenas, 6.11. - 1.12.1985.
60 pages, Bremen, 1986.

No. 2 **Hoffmann, G.**
Holozänstratigraphie und Küstenlinienverlagerung an der andalusischen Mittelmeerküste.
173 pages, Bremen, 1988. (out of print)

No. 3 **Wefer, G. and cruise participants**
Bericht über die METEOR-Fahrt M 6/6, Libreville - Las Palmas, 18.2. - 23.3.1988.
97 pages, Bremen, 1988.

No. 4 **Wefer, G., G.F. Lutze, T.J. Müller, O. Pfannkuche, W. Schenke, G. Siedler, W. Zenk**
Kurzbericht über die METEOR-Expedition No. 6, Hamburg - Hamburg, 28.10.1987 - 19.5.1988.
29 pages, Bremen, 1988. (out of print)

No. 5 **Fischer, G.**
Stabile Kohlenstoff-Isotope in partikulärer organischer Substanz aus dem Südpolarmeer (Atlantischer Sektor). 161 pages, Bremen, 1989.

No. 6 **Berger, W.H. and G. Wefer**
Partikelfluß und Kohlenstoffkreislauf im Ozean.
Bericht und Kurzfassungen über den Workshop vom 3.-4. Juli 1989 in Bremen.
57 pages, Bremen, 1989.

No. 7 **Wefer, G. and cruise participants**
Bericht über die METEOR - Fahrt M 9/4, Dakar - Santa Cruz, 19.2. - 16.3.1989.
103 pages, Bremen, 1989.

No. 8 **Kölling, M.**
Modellierung geochemischer Prozesse im Sickerwasser und Grundwasser.
135 pages, Bremen, 1990.

No. 9 **Heinze, P.-M.**
Das Auftriebsgeschehen vor Peru im Spätquartär. 204 pages, Bremen, 1990. (out of print)

No. 10 **Willems, H., G. Wefer, M. Rinski, B. Donner, H.-J. Bellmann, L. Eißmann, A. Müller, B.W. Flemming, H.-C. Höfle, J. Merkt, H. Streif, G. Hertweck, H. Kuntze, J. Schwaar, W. Schäfer, M.-G. Schulz, F. Grube, B. Menke**
Beiträge zur Geologie und Paläontologie Norddeutschlands: Exkursionsführer.
202 pages, Bremen, 1990.

No. 11 **Wefer, G. and cruise participants**
Bericht über die METEOR-Fahrt M 12/1, Kapstadt - Funchal, 13.3.1990 - 14.4.1990.
66 pages, Bremen, 1990.

No. 12 **Dahmke, A., H.D. Schulz, A. Kölling, F. Kracht, A. Lücke**
Schwermetallspuren und geochemische Gleichgewichte zwischen Porenlösung und Sediment im Wesermündungsgebiet. BMFT-Projekt MFU 0562, Abschlußbericht. 121 pages, Bremen, 1991.

No. 13 **Rostek, F.**
Physikalische Strukturen von Tiefseesedimenten des Südatlantiks und ihre Erfassung in Echolotregistrierungen. 209 pages, Bremen, 1991.

No. 14 **Baumann, M.**
Die Ablagerung von Tschernobyl-Radiocäsium in der Norwegischen See und in der Nordsee.
133 pages, Bremen, 1991. (out of print)

No. 15 **Kölling, A.**
Frühdiagenetische Prozesse und Stoff-Flüsse in marinen und ästuarinen Sedimenten.
140 pages, Bremen, 1991.

No. 16 **SFB 261 (ed.)**
1. Kolloquium des Sonderforschungsbereichs 261 der Universität Bremen (14.Juni 1991):
Der Südatlantik im Spätquartär: Rekonstruktion von Stoffhaushalt und Stromsystemen.
Kurzfassungen der Vorträge und Poster. 66 pages, Bremen, 1991.

No. 17 **Pätzold, J. and cruise participants**
Bericht und erste Ergebnisse über die METEOR-Fahrt M 15/2, Rio de Janeiro - Vitoria,
18.1. - 7.2.1991. 46 pages, Bremen, 1993.

No. 18 **Wefer, G. and cruise participants**
Bericht und erste Ergebnisse über die METEOR-Fahrt M 16/1, Pointe Noire - Recife,
27.3. - 25.4.1991. 120 pages, Bremen, 1991.

No. 19 **Schulz, H.D. and cruise participants**
Bericht und erste Ergebnisse über die METEOR-Fahrt M 16/2, Recife - Belem, 28.4. - 20.5.1991.
149 pages, Bremen, 1991.

No. 20 **Berner, H.**
Mechanismen der Sedimentbildung in der Fram-Straße, im Arktischen Ozean und in der Norwegischen See. 167 pages, Bremen, 1991.

No. 21 **Schneider, R.**
Spätquartäre Produktivitätsänderungen im östlichen Angola-Becken: Reaktion auf Variationen im Passat-Monsun-Windsystem und in der Advektion des Benguela-Küstenstroms.
198 pages, Bremen, 1991. (out of print)

No. 22 **Hebbeln, D.**
Spätquartäre Stratigraphie und Paläozeanographie in der Fram-Straße. 174 pages, Bremen, 1991.

No. 23 **Lücke, A.**
Umsetzungsprozesse organischer Substanz während der Frühdiagenese in ästuarinen Sedimenten.
137 pages, Bremen, 1991.

No. 24 **Wefer, G. and cruise participants**
Bericht und erste Ergebnisse der METEOR-Fahrt M 20/1, Bremen - Abidjan, 18.11.- 22.12.1991.
74 pages, Bremen, 1992.

No. 25 **Schulz, H.D. and cruise participants**
Bericht und erste Ergebnisse der METEOR-Fahrt M 20/2, Abidjan - Dakar, 27.12.1991 - 3.2.1992.
173 pages, Bremen, 1992.

No. 26 **Gingele, F.**
Zur klimaabhängigen Bildung biogener und terrigener Sedimente und ihrer Veränderung durch die Frühdiagenese im zentralen und östlichen Südatlantik. 202 pages, Bremen, 1992.

No. 27 **Bickert, T.**
Rekonstruktion der spätquartären Bodenwasserzirkulation im östlichen Südatlantik über stabile Isotope benthischer Foraminiferen. 205 pages, Bremen, 1992. (out of print)

No. 28 **Schmidt, H.**
Der Benguela-Strom im Bereich des Walfisch-Rückens im Spätquartär. 172 pages, Bremen, 1992.

No. 29 **Meinecke, G.**
Spätquartäre Oberflächenwassertemperaturen im östlichen äquatorialen Atlantik.
181 pages, Bremen, 1992.

No. 30 **Bathmann, U., U. Bleil, A. Dahmke, P. Müller, A. Nehrkorn, E.-M. Nöthig, M. Olesch, J. Pätzold, H.D. Schulz, V. Smetacek, V. Spieß, G. Wefer, H. Willems**
Bericht des Graduierten Kollegs. Stoff-Flüsse in marinen Geosystemen.
Berichtszeitraum Oktober 1990 - Dezember 1992. 396 pages, Bremen, 1992.

No. 31 **Damm, E.**
Frühdiagenetische Verteilung von Schwermetallen in Schlicksedimenten der westlichen Ostsee.
115 pages, Bremen, 1992.

No. 32 **Antia, E.E.**
Sedimentology, Morphodynamics and Facies Association of a mesotidal Barrier Island Shoreface (Spiekeroog, Southern North Sea). 370 pages, Bremen, 1993.

No. 33 **Duinker, J. and G. Wefer (ed.)**
Bericht über den 1. JGOFS-Workshop. 1./2. Dezember 1992 in Bremen. 83 pages, Bremen, 1993.

No. 34 **Kasten, S.**
Die Verteilung von Schwermetallen in den Sedimenten eines stadtbremischen Hafenbeckens.
103 pages, Bremen, 1993.

No. 35 **Spieß, V.**
Digitale Sedimentographie. Neue Wege zu einer hochauflösenden Akustostratigraphie.
199 pages, Bremen, 1993.

No. 36 **Schinzel, U.**
Laborversuche zu frühdiagenetischen Reaktionen von Eisen (III) - Oxidhydraten in marinen Sedimenten.189 pages, Bremen, 1993.

No. 37 **Sieger, R.**
CoTAM - ein Modell zur Modellierung des Schwermetalltransports in Grundwasserleitern.
56 pages, Bremen, 1993. (out of print)

No. 38 **Willems, H. (ed.)**
Geoscientific Investigations in the Tethyan Himalayas. 183 pages, Bremen, 1993.

No. 39 **Hamer, K.**
Entwicklung von Laborversuchen als Grundlage für die Modellierung des Transportverhaltens von Arsenat, Blei, Cadmium und Kupfer in wassergesättigten Säulen. 147 pages, Bremen, 1993.

No. 40 **Sieger, R.**
Modellierung des Stofftransports in porösen Medien unter Ankopplung kinetisch gesteuerter Sorptions- und Redoxprozesse sowie thermischer Gleichgewichte. 158 pages, Bremen, 1993.

No. 41 **Thießen, W.**
Magnetische Eigenschaften von Sedimenten des östlichen Südatlantiks und ihre paläozeanographische Relevanz. 170 pages, Bremen, 1993.

No. 42 **Spieß, V. and cruise participants**
Report and preliminary results of METEOR-Cruise M 23/1, Kapstadt - Rio de Janeiro, 4.-25.2.1993. 139 pages, Bremen, 1994.

No. 43 **Bleil, U. and cruise participants**
Report and preliminary results of METEOR-Cruise M 23/2, Rio de Janeiro - Recife, 27.2.-19.3.1993 133 pages, Bremen, 1994.

No. 44 **Wefer, G. and cruise participants**
Report and preliminary results of METEOR-Cruise M 23/3, Recife - Las Palmas, 21.3. - 12.4.1993 71 pages, Bremen, 1994.

No. 45 **Giese, M. and G. Wefer (ed.)**
Bericht über den 2. JGOFS-Workshop. 18../19. November 1993 in Bremen. 93 pages, Bremen, 1994.

No. 46 **Balzer, W. and cruise participants**
Report and preliminary results of METEOR-Cruise M 22/1, Hamburg - Recife, 22.9. - 21.10.1992. 24 pages, Bremen, 1994.

No. 47 **Stax, R.**
Zyklische Sedimentation von organischem Kohlenstoff in der Japan See: Anzeiger für Änderungen von Paläoozeanographie und Paläoklima im Spätkänozoikum. 150 pages, Bremen, 1994.

No. 48 **Skowronek, F.**
Frühdiagenetische Stoff-Flüsse gelöster Schwermetalle an der Oberfläche von Sedimenten des Weser Ästuares. 107 pages, Bremen, 1994.

No. 49 **Dersch-Hansmann, M.**
Zur Klimaentwicklung in Ostasien während der letzten 5 Millionen Jahre: Terrigener Sedimenteintrag in die Japan See (ODP Ausfahrt 128). 149 pages, Bremen, 1994.

No. 50 **Zabel, M.**
Frühdiagenetische Stoff-Flüsse in Oberflächen-Sedimenten des äquatorialen und östlichen Südatlantik. 129 pages, Bremen, 1994.

No. 51 **Bleil, U. and cruise participants**
Report and preliminary results of SONNE-Cruise SO 86, Buenos Aires - Capetown, 22.4. - 31.5.93 116 pages, Bremen, 1994.

No. 52 **Symposium: The South Atlantic: Present and Past Circulation.**
Bremen, Germany, 15 - 19 August 1994. Abstracts. 167 pages, Bremen, 1994.

No. 53 **Kretzmann, U.B.**
^{57}Fe-Mössbauer-Spektroskopie an Sedimenten - Möglichkeiten und Grenzen. 183 pages, Bremen, 1994.

No. 54 **Bachmann, M.**
Die Karbonatrampe von Organyà im oberen Oberapt und unteren Unteralb (NE-Spanien, Prov. Lerida): Fazies, Zyklo- und Sequenzstratigraphie. 147 pages, Bremen, 1994. (out of print)

No. 55 **Kemle-von Mücke, S.**
Oberflächenwasserstruktur und -zirkulation des Südostatlantiks im Spätquartär. 151 pages, Bremen, 1994.

No. 56 **Petermann, H.**
Magnetotaktische Bakterien und ihre Magnetosome in Oberflächensedimenten des Südatlantiks. 134 pages, Bremen, 1994.

No. 57 **Mulitza, S.**
Spätquartäre Variationen der oberflächennahen Hydrographie im westlichen äquatorialen Atlantik. 97 pages, Bremen, 1994.

No. 58 **Segl, M. and cruise participants**
Report and preliminary results of METEOR-Cruise M 29/1, Buenos-Aires - Montevideo, 17.6. - 13.7.1994
94 pages, Bremen, 1994.

No. 59 **Bleil, U. and cruise participants**
Report and preliminary results of METEOR-Cruise M 29/2, Montevideo - Rio de Janiero 15.7. - 8.8.1994. 153 pages, Bremen, 1994.

No. 60 **Henrich, R. and cruise participants**
Report and preliminary results of METEOR-Cruise M 29/3, Rio de Janeiro - Las Palmas 11.8. - 5.9.1994. Bremen, 1994. (out of print)

No. 61 **Sagemann, J.**
Saisonale Variationen von Porenwasserprofilen, Nährstoff-Flüssen und Reaktionen in intertidalen Sedimenten des Weser-Ästuars. 110 pages, Bremen, 1994. (out of print)

No. 62 **Giese, M. and G. Wefer**
Bericht über den 3. JGOFS-Workshop. 5./6. Dezember 1994 in Bremen.
84 pages, Bremen, 1995.

No. 63 **Mann, U.**
Genese kretazischer Schwarzschiefer in Kolumbien: Globale vs. regionale/lokale Prozesse.
153 pages, Bremen, 1995. (out of print)

No. 64 **Willems, H., Wan X., Yin J., Dongdui L., Liu G., S. Dürr, K.-U. Gräfe**
The Mesozoic development of the N-Indian passive margin and of the Xigaze Forearc Basin in southern Tibet, China. – Excursion Guide to IGCP 362 Working-Group Meeting "Integrated Stratigraphy". 113 pages, Bremen, 1995. (out of print)

No. 65 **Hünken, U.**
Liefergebiets - Charakterisierung proterozoischer Goldseifen in Ghana anhand von Fluideinschluß - Untersuchungen. 270 pages, Bremen, 1995.

No. 66 **Nyandwi, N.**
The Nature of the Sediment Distribution Patterns in ther Spiekeroog Backbarrier Area, the East Frisian Islands. 162 pages, Bremen, 1995.

No. 67 **Isenbeck-Schröter, M.**
Transportverhalten von Schwermetallkationen und Oxoanionen in wassergesättigten Sanden. - Laborversuche in Säulen und ihre Modellierung -. 182 pages, Bremen, 1995.

No. 68 **Hebbeln, D. and cruise participants**
Report and preliminary results of SONNE-Cruise SO 102, Valparaiso - Valparaiso, 95.
134 pages, Bremen, 1995.

No. 69 **Willems, H. (Sprecher), U.Bathmann, U. Bleil, T. v. Dobeneck, K. Herterich, B.B. Jorgensen, E.-M. Nöthig, M. Olesch, J. Pätzold, H.D. Schulz, V. Smetacek, V. Speiß. G. Wefer**
Bericht des Graduierten-Kollegs Stoff-Flüsse in marine Geosystemen.
Berichtszeitraum Januar 1993 - Dezember 1995.
45 & 468 pages, Bremen, 1995.

No. 70 **Giese, M. and G. Wefer**
Bericht über den 4. JGOFS-Workshop. 20./21. November 1995 in Bremen. 60 pages, Bremen, 1996. (out of print)

No. 71 **Meggers, H.**
Pliozän-quartäre Karbonatsedimentation und Paläozeanographie des Nordatlantiks und des Europäischen Nordmeeres - Hinweise aus planktischen Foraminiferengemeinschaften.
143 pages, Bremen, 1996. (out of print)

No. 72 **Teske, A.**
Phylogenetische und ökologische Untersuchungen an Bakterien des oxidativen und reduktiven marinen Schwefelkreislaufs mittels ribosomaler RNA. 220 pages, Bremen, 1996. (out of print)

No. 73 **Andersen, N.**
Biogeochemische Charakterisierung von Sinkstoffen und Sedimenten aus ostatlantischen Produktions-Systemen mit Hilfe von Biomarkern. 215 pages, Bremen, 1996.

No. 74 **Treppke, U.**
Saisonalität im Diatomeen- und Silikoflagellatenfluß im östlichen tropischen und subtropischen Atlantik. 200 pages, Bremen, 1996.

No. 75 **Schüring, J.**
Die Verwendung von Steinkohlebergematerialien im Deponiebau im Hinblick auf die Pyritverwitterung und die Eignung als geochemische Barriere. 110 pages, Bremen, 1996.

No. 76 **Pätzold, J. and cruise participants**
Report and preliminary results of VICTOR HENSEN cruise JOPS II, Leg 6, Fortaleza - Recife, 10.3. - 26.3. 1995 and Leg 8, Vitoria - Vitoria, 10.4. - 23.4.1995.
87 pages, Bremen, 1996.

No. 77 **Bleil, U. and cruise participants**
Report and preliminary results of METEOR-Cruise M 34/1, Cape Town - Walvis Bay, 3.-26.1.1996.
129 pages, Bremen, 1996.

No. 78 **Schulz, H.D. and cruise participants**
Report and preliminary results of METEOR-Cruise M 34/2, Walvis Bay - Walvis Bay, 29.1.-18.2.96
133 pages, Bremen, 1996.

No. 79 **Wefer, G. and cruise participants**
Report and preliminary results of METEOR-Cruise M 34/3, Walvis Bay - Recife, 21.2.-17.3.1996.
168 pages, Bremen, 1996.

No. 80 **Fischer, G. and cruise participants**
Report and preliminary results of METEOR-Cruise M 34/4, Recife - Bridgetown, 19.3.-15.4.1996. 105 pages, Bremen, 1996.

No. 81 **Kulbrok, F.**
Biostratigraphie, Fazies und Sequenzstratigraphie einer Karbonatrampe in den Schichten der Oberkreide und des Alttertiärs Nordost-Ägyptens (Eastern Desert, N'Golf von Suez, Sinai). 153 pages, Bremen, 1996.

No. 82 **Kasten, S.**
Early Diagenetic Metal Enrichments in Marine Sediments as Documents of Nonsteady-State Depositional Conditions. Bremen, 1996.

No. 83 **Holmes, M.E.**
Reconstruction of Surface Ocean Nitrate Utilization in the Southeast Atlantic Ocean Based on Stable Nitrogen Isotopes. 113 pages, Bremen, 1996.

No. 84 **Rühlemann, C.**
Akkumulation von Carbonat und organischem Kohlenstoff im tropischen Atlantik: Spätquartäre Produktivitäts-Variationen und ihre Steuerungsmechanismen. 139 pages, Bremen, 1996.

No. 85 **Ratmeyer, V.**
Untersuchungen zum Eintrag und Transport lithogener und organischer partikulärer Substanz im östlichen subtropischen Nordatlantik. 154 pages, Bremen, 1996.

No. 86 **Cepek, M.**
Zeitliche und räumliche Variationen von Coccolithophoriden-Gemeinschaften im subtropischen Ost-Atlantik: Untersuchungen an Plankton, Sinkstoffen und Sedimenten. 156 pages, Bremen, 1996.

No. 87 **Otto, S.**
Die Bedeutung von gelöstem organischen Kohlenstoff (DOC) für den Kohlenstoffffluß im Ozean. 150 pages, Bremen, 1996.

No. 88 **Hensen, C.**
Frühdiagenetische Prozesse und Quantifizierung benthischer Stoff-Flüsse in Oberflächensedimenten des Südatlantiks. 132 pages, Bremen, 1996.

No. 89 **Giese, M. and G. Wefer**
Bericht über den 5. JGOFS-Workshop. 27./28. November 1996 in Bremen. 73 pages, Bremen, 1997.

No. 90 **Wefer, G. and cruise participants**
Report and preliminary results of METEOR-Cruise M 37/1, Lisbon - Las Palmas, 4.-23.12.1996. 79 pages, Bremen, 1997.

No. 91 **Isenbeck-Schröter, M., E. Bedbur, M. Kofod, B. König, T. Schramm & G. Mattheß**
Occurrence of Pesticide Residues in Water - Assessment of the Current Situation in Selected EU Countries. 65 pages, Bremen 1997.

No. 92 **Kühn, M.**
Geochemische Folgereaktionen bei der hydrogeothermalen Energiegewinnung. 129 pages, Bremen 1997.

No. 93 **Determann, S. & K. Herterich**
JGOFS-A6 "Daten und Modelle": Sammlung JGOFS-relevanter Modelle in Deutschland. 26 pages, Bremen, 1997.

No. 94 **Fischer, G. and cruise participants**
Report and preliminary results of METEOR-Cruise M 38/1, Las Palmas - Recife, 25.1.-1.3.1997, with Appendix: Core Descriptions from METEOR Cruise M 37/1. Bremen, 1997.

No. 95 **Bleil, U. and cruise participants**
Report and preliminary results of METEOR-Cruise M 38/2, Recife - Las Palmas, 4.3.-14.4.1997. 126 pages, Bremen, 1997.

No. 96 **Neuer, S. and cruise participants**
Report and preliminary results of VICTOR HENSEN-Cruise 96/1. Bremen, 1997.

No. 97 **Villinger, H. and cruise participants**
Fahrtbericht SO 111, 20.8. - 16.9.1996. 115 pages, Bremen, 1997.

No. 98 **Lüning, S.**
Late Cretaceous - Early Tertiary sequence stratigraphy, paleoecology and geodynamics of Eastern Sinai, Egypt. 218 pages, Bremen, 1997.

No. 99 **Haese, R.R.**
Beschreibung und Quantifizierung frühdiagenetischer Reaktionen des Eisens in Sedimenten des Südatlantiks. 118 pages, Bremen, 1997.

No. 100 **Lührte, R. von**
Verwertung von Bremer Baggergut als Material zur Oberflächenabdichtung von Deponien - Geochemisches Langzeitverhalten und Schwermetall-Mobilität (Cd, Cu, Ni, Pb, Zn). Bremen, 1997.

No. 101 **Ebert, M.**
Der Einfluß des Redoxmilieus auf die Mobilität von Chrom im durchströmten Aquifer. 135 pages, Bremen, 1997.

No. 102 **Krögel, F.**
Einfluß von Viskosität und Dichte des Seewassers auf Transport und Ablagerung von Wattsedimenten (Langeooger Rückseitenwatt, südliche Nordsee). 168 pages, Bremen, 1997.

No. 103 **Kerntopf, B.**
Dinoflagellate Distribution Patterns and Preservation in the Equatorial Atlantic and Offshore North-West Africa. 137 pages, Bremen, 1997.

No. 104 **Breitzke, M.**
Elastische Wellenausbreitung in marinen Sedimenten - Neue Entwicklungen der Ultraschall Sedimentphysik und Sedimentechographie. 298 pages, Bremen, 1997.

No. 105 **Marchant, M.**
Rezente und spätquartäre Sedimentation planktischer Foraminiferen im Peru-Chile Strom. 115 pages, Bremen, 1997.

No. 106 **Habicht, K.S.**
Sulfur isotope fractionation in marine sediments and bacterial cultures. 125 pages, Bremen, 1997.

No. 107 **Hamer, K., R.v. Lührte, G. Becker, T. Felis, S. Keffel, B. Strotmann, C. Waschkowitz, M. Kölling, M. Isenbeck-Schröter, H.D. Schulz**
Endbericht zum Forschungsvorhaben 060 des Landes Bremen: Baggergut der Hafengruppe Bremen-Stadt: Modelluntersuchungen zur Schwermetallmobilität und Möglichkeiten der Verwertung von Hafenschlick aus Bremischen Häfen. 98 pages, Bremen, 1997.

No. 108 **Greeff, O.W.**
Entwicklung und Erprobung eines benthischen Landersystemes zur *in situ*-Bestimmung von Sulfatreduktionsraten mariner Sedimente. 121 pages, Bremen, 1997.

No. 109 **Pätzold, M. und G. Wefer**
Bericht über den 6. JGOFS-Workshop am 4./5.12.1997 in Bremen. Im Anhang: Publikationen zum deutschen Beitrag zur Joint Global Ocean Flux Study (JGOFS), Stand 1/1998. 122 pages, Bremen, 1998.

No. 110 **Landenberger, H.**
CoTReM, ein Multi-Komponenten Transport- und Reaktions-Modell. 142 pages, Bremen, 1998.

No. 111 **Villinger, H. und Fahrtteilnehmer**
Fahrtbericht SO 124, 4.10. - 16.10.199. 90 pages, Bremen, 1997.

No. 112 **Gietl, R.**
Biostratigraphie und Sedimentationsmuster einer nordostägyptischen Karbonatrampe unter Berücksichtigung der Alveolinen-Faunen. 142 pages, Bremen, 1998.

No. 113 **Ziebis, W.**
The Impact of the Thalassinidean Shrimp *Callianassa truncata* on the Geochemistry of permeable, coastal Sediments. 158 pages, Bremen 1998.

No. 114 **Schulz, H.D. and cruise participants**
Report and preliminary results of METEOR-Cruise M 41/1, Málaga - Libreville, 13.2.-15.3.1998. Bremen, 1998.

No. 115 **Völker, D.J.**
Untersuchungen an strömungsbeeinflußten Sedimentationsmustern im Südozean. Interpretation sedimentechographischer Daten und numerische Modellierung. 152 pages, Bremen, 1998.

No. 116 **Schlünz, B.**
Riverine Organic Carbon Input into the Ocean in Relation to Late Quaternary Climate Change. 136 pages, Bremen, 1998.

No. 117 **Kuhnert, H.**
Aufzeichnug des Klimas vor Westaustralien in stabilen Isotopen in Korallenskeletten. 109 pages, Bremen, 1998.

No. 118 **Kirst, G.**
Rekonstruktion von Oberflächenwassertemperaturen im östlichen Südatlantik anhand von Alkenonen. 130 pages, Bremen, 1998.

No. 119 **Dürkoop, A.**
Der Brasil-Strom im Spätquartär: Rekonstruktion der oberflächennahen Hydrographie während der letzten 400 000 Jahre. 121 pages, Bremen, 1998.

No. 120 **Lamy, F.**
Spätquartäre Variationen des terrigenen Sedimenteintrags entlang des chilenischen Kontinentalhangs als Abbild von Klimavariabilität im Milankoví- und Sub-Milankoví-Zeitbereich. 141 pages, Bremen, 1998.

No. 121 **Neuer, S. and cruise participants**
Report and preliminary results of POSEIDON-Cruise Pos 237/2, Vigo – Las Palmas, 18.3.-31.3.1998. 39 pages, Bremen, 1998

No. 122 **Romero, O.E.**
Marine planktonic diatoms from the tropical and equatorial Atlantic: temporal flux patterns and the sediment record. 205 pages, Bremen, 1998.

No. 123 **Spiess, V. und Fahrtteilnehmer**
Report and preliminary results of RV SONNE Cruise 125, Cochin – Chittagong, 17.10.-17.11.1997. 128 pages, Bremen, 1998.

No. 124 **Arz, H.W.**
Dokumentation von kurzfristigen Klimaschwankungen des Spätquartärs in Sedimenten des westlichen äquatorialen Atlantiks. 96 pages, Bremen, 1998.

No. 125 **Wolff, T.**
Mixed layer characteristics in the equatorial Atlantic during the late Quaternary as deduced from planktonic foraminifera. 132 pages, Bremen, 1998.

No. 126 **Dittert, N.**
Late Quaternary Planktic Foraminifera Assemblages in the South Atlantic Ocean: Quantitative Determination and Preservational Aspects. 165 pages, Bremen, 1998.

No. 127 **Höll, C.**
Kalkige und organisch-wandige Dinoflagellaten-Zysten in Spätquartären Sedimenten des tropischen Atlantiks und ihre palökologische Auswertbarkeit. 121 pages, Bremen, 1998.

No. 128 **Hencke, J.**
Redoxreaktionen im Grundwasser: Etablierung und Verlagerung von Reaktionsfronten und ihre Bedeutung für die Spurenelement-Mobilität. 122 pages, Bremen 1998.

No. 129 **Pätzold, J. and cruise participants**
Report and preliminary results of METEOR-Cruise M 41/3, Vitoria, Brasil – Salvador de Bahia, Brasil, 18.4. - 15.5.1998. Bremen, 1999.

No. 130 **Fischer, G. and cruise participants**
Report and preliminary results of METEOR-Cruise M 41/4, Salvador de Bahia, Brasil – Las Palmas, Spain, 18.5. – 13.6.1998. Bremen, 1999.

No. 131 **Schlünz, B. und G. Wefer**
Bericht über den 7. JGOFS-Workshop am 3. und 4.12.1998 in Bremen. Im Anhang: Publikationen zum deutschen Beitrag zur Joint Global Ocean Flux Study (JGOFS), Stand 1/ 1999. 100 pages, Bremen, 1999.

No. 132 **Wefer, G. and cruise participants**
Report and preliminary results of METEOR-Cruise M 42/4, Las Palmas - Las Palmas - Viena do Castelo; 26.09.1998 - 26.10.1998. 104 pages, Bremen, 1999.

No. 133 **Felis, T.**
Climate and ocean variability reconstructed from stable isotope records of modern subtropical corals (Northern Red Sea). 111 pages, Bremen, 1999.

No. 134 **Draschba , S.**
North Atlantic climate variability recorded in reef corals from Bermuda. 108 pages, Bremen, 1999.

No. 135 **Schmieder, F.**
Magnetic Cyclostratigraphy of South Atlantic Sediments. 82 pages, Bremen, 1999.

No. 136 **Rieß, W.**
In situ measurements of respiration and mineralisation processes – Interaction between fauna and geochemical fluxes at active interfaces. 68 pages, Bremen, 1999.

No. 137 **Devey, C.W. and cruise participants**
Report and shipboard results from METEOR-cruise M 41/2, Libreville – Vitoria, 18.3. – 15.4.98. 59 pages, Bremen, 1999.

No. 138 **Wenzhöfer, F.**
Biogeochemical processes at the sediment water interface and quantification of metabolically driven calcite dissolution in deep sea sediments. 103 pages, Bremen, 1999.

No. 139 **Klump, J.**
Biogenic barite as a proxy of paleoproductivity variations in the Southern Peru-Chile Current. 107 pages, Bremen, 1999.

No. 140 **Huber, R.**
Carbonate sedimentation in the northern Northatlantic since the late pliocene. 103 pages, Bremen, 1999.

No. 141 **Schulz, H.**
Nitrate-storing sulfur bacteria in sediments of coastal upwelling. 94 pages, Bremen, 1999.

No. 142 **Mai, S.**
Die Sedimentverteilung im Wattenmeer: ein Simulationsmodell. 114 pages, Bremen, 1999.

No. 143 **Neuer, S. and cruise participants**
Report and preliminary results of Poseidon Cruise 248, Las Palmas - Las Palmas, 15.2.-26.2.1999.
45 pages, Bremen, 1999.

No. 144 **Weber, A.**
Schwefelkreislauf in marinen Sedimenten und Messung von *in situ* Sulfatreduktionsraten.
122 pages, Bremen, 1999.

No. 145 **Hadeler, A.**
Sorptionsreaktionen im Grundwasser: Unterschiedliche Aspekte bei der Modellierung des Transportverhaltens von Zink. 122 pages, 1999.

No. 146 **Dierßen, H.**
Zum Kreislauf ausgewählter Spurenmetalle im Südatlantik: Vertikaltransport und Wechselwirkung zwischen Partikeln und Lösung. 167 pages, Bremen, 1999.

No. 147 **Zühlsdorff, L.**
High resolution multi-frequency seismic surveys at the Eastern Juan de Fuca Ridge Flank and the Cascadia Margin – Evidence for thermally and tectonically driven fluid upflow in marine sediments. 118 pages, Bremen 1999.

No. 148 **Kinkel, H.**
Living and late Quaternary Coccolithophores in the equatorial Atlantic Ocean: response of distribution and productivity patterns to changing surface water circulation. 183 pages, Bremen, 2000.

No. 149 **Pätzold, J. and cruise participants**
Report and preliminary results of METEOR Cruise M 44/3, Aqaba (Jordan) - Safaga (Egypt) – Dubá (Saudi Arabia) – Suez (Egypt) - Haifa (Israel), 12.3.-26.3.-2.4.-4.4.1999. 135 pages, Bremen, 2000.

No. 150 **Schlünz, B. and G. Wefer**
Bericht über den 8. JGOFS-Workshop am 2. und 3.12.1999 in Bremen. Im Anhang:
Publikationen zum deutschen Beitrag zur Joint Global Ocean Flux Study (JGOFS), Stand 1/ 2000.
95 pages, Bremen, 2000.

No. 151 **Schnack, K.**
Biostratigraphie und fazielle Entwicklung in der Oberkreide und im Alttertiär im Bereich der Kharga Schwelle, Westliche Wüste, SW-Ägypten. 142 pages, Bremen, 2000.

No. 152 **Karwath, B.**
Ecological studies on living and fossil calcareous dinoflagellates of the equatorial and tropical Atlantic Ocean. 175 pages, Bremen, 2000.

No. 153 **Moustafa, Y.**
Paleoclimatic reconstructions of the Northern Red Sea during the Holocene inferred from stable isotope records of modern and fossil corals and molluscs. 102 pages, Bremen, 2000.

No. 154 **Villinger, H. and cruise participants**
Report and preliminary results of SONNE-cruise 145-1 Balboa – Talcahuana, 21.12.1999 – 28.01.2000.
147 pages, Bremen, 2000.

No. 155 **Rusch, A.**
Dynamik der Feinfraktion im Oberflächenhorizont permeabler Schelfsedimente. 102 pages, Bremen, 2000.

No. 156 **Moos, C.**
Reconstruction of upwelling intensity and paleo-nutrient gradients in the northwest Arabian Sea derived from stable carbon and oxygen isotopes of planktic foraminifera. 103 pages, Bremen, 2000.

No. 157 **Xu, W.**
Mass physical sediment properties and trends in a Wadden Sea tidal basin. 127 pages, Bremen, 2000.

No. 158 **Meinecke, G. and cruise participants**
Report and preliminary results of METEOR Cruise M 45/1, Malaga (Spain) - Lissabon (Portugal),
19.05. - 08.06.1999. 39 pages, Bremen, 2000.

No. 159 **Vink, A.**
Reconstruction of recent and late Quaternary surface water masses of the western subtropical Atlantic Ocean based on calcareous and organic-walled dinoflagellate cysts. 160 pages, Bremen, 2000.

No. 160 **Willems, H. (Sprecher), U. Bleil, R. Henrich, K. Herterich, B.B. Jørgensen, H.-J. Kuß, M. Olesch, H.D. Schulz,V. Spieß, G. Wefer**
Abschlußbericht des Graduierten-Kollegs Stoff-Flüsse in marine Geosystemen.
Zusammenfassung und Berichtszeitraum Januar 1996 - Dezember 2000. 340 pages, Bremen, 2000.

No. 161 **Sprengel, C.**
Untersuchungen zur Sedimentation und Ökologie von Coccolithophoriden im Bereich der Kanarischen Inseln: Saisonale Flussmuster und Karbonatexport. 165 pages, Bremen, 2000.

No. 162 **Donner, B. and G. Wefer**
Bericht über den JGOFS-Workshop am 18.-21.9.2000 in Bremen:
Biogeochemical Cycles: German Contributions to the International Joint Global Ocean Flux Study.
87 pages, Bremen, 2000.

No. 163 **Neuer, S. and cruise participants**
Report and preliminary results of Meteor Cruise M 45/5, Bremen – Las Palmas, October 1 – November 3, 1999. 93 pages, Bremen, 2000.

No. 164 **Devey, C. and cruise participants**
Report and preliminary results of Sonne Cruise SO 145/2, Talcahuano (Chile) - Arica (Chile), February 4 – February 29, 2000. 63 pages, Bremen, 2000.

No. 165 **Freudenthal, T.**
Reconstruction of productivity gradients in the Canary Islands region off Morocco by means of sinking particles and sediments. 147 pages, Bremen, 2000.

No. 166 **Adler, M.**
Modeling of one-dimensional transport in porous media with respect to simultaneous geochemical reactions in CoTReM. 147 pages, Bremen, 2000.

No. 167 **Santamarina Cuneo, P.**
Fluxes of suspended particulate matter through a tidal inlet of the East Frisian Wadden Sea (southern North Sea). 91 pages, Bremen, 2000.

No. 168 **Benthien, A.**
Effects of CO_2 and nutrient concentration on the stable carbon isotope composition of C37:2 alkenones in sediments of the South Atlantic Ocean. 104 pages, Bremen, 2001.

No. 169 **Lavik, G.**
Nitrogen isotopes of sinking matter and sediments in the South Atlantic. 140 pages, Bremen, 2001.

No. 170 **Budziak, D.**
Late Quaternary monsoonal climate and related variations in paleoproductivity and alkenone-derived sea-surface temperatures in the western Arabian Sea. 114 pages, Bremen, 2001.

No. 171 **Gerhardt, S.**
Late Quaternary water mass variability derived from the pteropod preservation state in sediments of the western South Atlantic Ocean and the Caribbean Sea. 109 pages, Bremen, 2001.

No. 172 **Bleil, U. and cruise participants**
Report and preliminary results of Meteor Cruise M 46/3, Montevideo (Uruguay) – Mar del Plata (Argentina), January 4 – February 7, 2000. Bremen, 2001.

No. 173 **Wefer, G. and cruise participants**
Report and preliminary results of Meteor Cruise M 46/4, Mar del Plata (Argentina) – Salvador da Bahia (Brazil), February 10 – March 13, 2000. With partial results of METEOR cruise M 46/2. 136 pages, Bremen, 2001.

No. 174 **Schulz, H.D. and cruise participants**
Report and preliminary results of Meteor Cruise M 46/2, Recife (Brazil) – Montevideo (Uruguay), December 2 – December 29, 1999. 107 pages, Bremen, 2001.

No. 175 **Schmidt, A.**
Magnetic mineral fluxes in the Quaternary South Atlantic: Implications for the paleoenvironment.
97 pages, Bremen, 2001.

No. 176 **Bruhns, P.**
Crystal chemical characterization of heavy metal incorporation in brick burning processes.
93 pages, Bremen, 2001.

No. 177 **Karius, V.**
Baggergut der Hafengruppe Bremen-Stadt in der Ziegelherstellung. 131 pages, Bremen, 2001.

No. 178 **Adegbie, A. T.**
Reconstruction of paleoenvironmental conditions in Equatorial Atlantic and the Gulf of Guinea Basins for the last 245,000 years. 113 pages, Bremen, 2001.

No. 179 **Spieß, V. and cruise participants**
Report and preliminary results of R/V Sonne Cruise SO 149, Victoria - Victoria, 16.8. - 16.9.2000.
100 pages, Bremen, 2001.

No. 180 **Kim, J.-H.**
Reconstruction of past sea-surface temperatures in the eastern South Atlantic and the eastern South Pacific across Termination I based on the Alkenone Method. 114 pages, Bremen, 2001.

No. 181 **von Lom-Keil, H.**
Sedimentary waves on the Namibian continental margin and in the Argentine Basin – Bottom flow reconstructions based on high resolution echosounder data. 126 pages, Bremen, 2001.

No. 182 **Hebbeln, D. and cruise participants**
PUCK: Report and preliminary results of R/V Sonne Cruise SO 156, Valparaiso (Chile) - Talcahuano (Chile), March 29 - May 14, 2001. 195 pages, Bremen, 2001.

No. 183 **Wendler, J.**
Reconstruction of astronomically-forced cyclic and abrupt paleoecological changes in the Upper Cretaceous Boreal Realm based on calcareous dinoflagellate cysts. 149 pages, Bremen, 2001.

No. 184 **Volbers, A.**
Planktic foraminifera as paleoceanographic indicators: production, preservation, and reconstruction of upwelling intensity. Implications from late Quaternary South Atlantic sediments. 122 pages, Bremen, 2001.

No. 185 **Bleil, U. and cruise participants**
Report and preliminary results of R/V METEOR Cruise M 49/3, Montevideo (Uruguay) - Salvador (Brasil), March 9 - April 1, 2001. Bremen, 2001.